

4

**AD-A196 157**

**DTIC FILE COPY**

**DASIAC-TN-87-35-V1**

**TECHNICAL PAPERS PRESENTED AT THE DEFENSE  
NUCLEAR AGENCY GLOBAL EFFECTS  
REVIEW—7 - 9 APRIL 1987**

**Volume I**

**Kaman Sciences Corporation  
Tempo Division  
Alexandria Office  
Huntington Building, Suite 500  
2560 Huntington Avenue  
Alexandria, VA 22303-1410**

**30 April 1987**

**DTIC  
SERIALIZED  
JUN 28 1988  
S H D**

**Technical Report**

**CONTRACT No. DNA 001-82-C-0274**

**Approved for public release;  
distribution is unlimited.**

**THIS WORK WAS SPONSORED BY THE DEFENSE NUCLEAR AGENCY  
UNDER RDT&E RMSS CODE B331086466 P99QMXDC00003 H2590D.**

**Prepared for  
Director  
DEFENSE NUCLEAR AGENCY  
Washington, DC 20305-1000**

**88 6 28 164**

## DISTRIBUTION LIST UPDATE

This mailer is provided to enable DNA to maintain current distribution lists for reports. We would appreciate your providing the requested information.

- Add the individual listed to your distribution list.
- Delete the cited organization/individual.
- Change of address.

NAME: \_\_\_\_\_

ORGANIZATION: \_\_\_\_\_

**OLD ADDRESS**

**CURRENT ADDRESS**

\_\_\_\_\_  
\_\_\_\_\_  
\_\_\_\_\_

\_\_\_\_\_  
\_\_\_\_\_  
\_\_\_\_\_

TELEPHONE NUMBER: ( ) \_\_\_\_\_

SUBJECT AREA(S) OF INTEREST:

\_\_\_\_\_  
\_\_\_\_\_  
\_\_\_\_\_

\_\_\_\_\_  
\_\_\_\_\_  
\_\_\_\_\_

DNA OR OTHER GOVERNMENT CONTRACT NUMBER: \_\_\_\_\_

CERTIFICATION OF NEED-TO-KNOW BY GOVERNMENT SPONSOR (if other than DNA):

SPONSORING ORGANIZATION: \_\_\_\_\_

CONTRACTING OFFICER OR REPRESENTATIVE: \_\_\_\_\_

SIGNATURE: \_\_\_\_\_

CUT HERE AND RETURN



Director  
Defense Nuclear Agency  
ATTN: [REDACTED] TITL  
Washington, DC 20305-1000

Director  
Defense Nuclear Agency  
ATTN: [REDACTED] TITL  
Washington, DC 20305-1000

UNCLASSIFIED

SECURITY CLASSIFICATION OF THIS PAGE

## REPORT DOCUMENTATION PAGE

1a REPORT SECURITY CLASSIFICATION <b>UNCLASSIFIED</b>		1b RESTRICTIVE MARKINGS	
2a SECURITY CLASSIFICATION AUTHORITY <b>N/A since Unclassified</b>		3 DISTRIBUTION/AVAILABILITY OF REPORT  Approved for public release; distribution is unlimited.	
2b DECLASSIFICATION/DOWNGRADING SCHEDULE <b>N/A since Unclassified</b>		5 MONITORING ORGANIZATION REPORT NUMBER(S)  DASIAC-TN-87-35-V1	
4 PERFORMING ORGANIZATION REPORT NUMBER(S)		7a NAME OF MONITORING ORGANIZATION Director Defense Nuclear Agency	
6a NAME OF PERFORMING ORGANIZATION Kaman Sciences Corp., Tempo Div., Alexandria Office	6b OFFICE SYMBOL (if applicable)	7b ADDRESS (City, State, and ZIP Code)  Washington DC 20305-1000	
6c ADDRESS (City, State, and ZIP Code) Huntington Building, Suite 500 2560 Huntington Avenue Alexandria, VA 22303-1410		9 PROCUREMENT INSTRUMENT IDENTIFICATION NUMBER  DNA 001-82-C-0274	
8a NAME OF FUNDING/SPONSORING ORGANIZATION	8b OFFICE SYMBOL (if applicable) RARP/Auton	10 SOURCE OF FUNDING NUMBERS	
8c ADDRESS (City, State, and ZIP Code)		PROGRAM ELEMENT NO 62715H	PROJECT NO P99QMXD
		TASK NO C	WORK UNIT ACCESSION NO DH008684
11 TITLE (Include Security Classification) TECHNICAL PAPERS PRESENTED AT THE DEFENSE NUCLEAR AGENCY GLOBAL EFFECTS REVIEW—7 - 9 APRIL 1987, Volume I			
12 PERSONAL AUTHOR(S) Various (Alderson, D. M. (Compiler))			
13a TYPE OF REPORT Technical	13b TIME COVERED FROM 860407 TO 860409	14 DATE OF REPORT (Year, Month, Day) 870430	15 PAGE COUNT 404
16 SUPPLEMENTARY NOTATION This work was sponsored by the Defense Nuclear Agency under RDT&E RMSS Code B331086466 P99QMXDC00003 H2590D.			
17 COSATI CODES		18 SUBJECT TERMS (Continue on reverse if necessary and identify by block number)	
FIELD	GROUP	SUB-GROUP	
4	1	Nuclear War	
15	6	Global Climate Effects	
19 ABSTRACT (Continue on reverse if necessary and identify by block number)  This document contains technical papers presented at the Defense Nuclear Agency Review of Global Effects held at Mission Research Corporation, Santa Barbara, CA 7 - 9 April 1987.			
20 DISTRIBUTION/AVAILABILITY OF ABSTRACT <input type="checkbox"/> UNCLASSIFIED/UNLIMITED <input checked="" type="checkbox"/> SAME AS RPT <input type="checkbox"/> DTIC USERS		21 ABSTRACT SECURITY CLASSIFICATION UNCLASSIFIED	
22a NAME OF RESPONSIBLE INDIVIDUAL Sandra E. Young		22b TELEPHONE (Include Area Code) (202) 325-7042	22c OFFICE SYMBOL DNA/CSTI

DD FORM 1473, 84 MAR

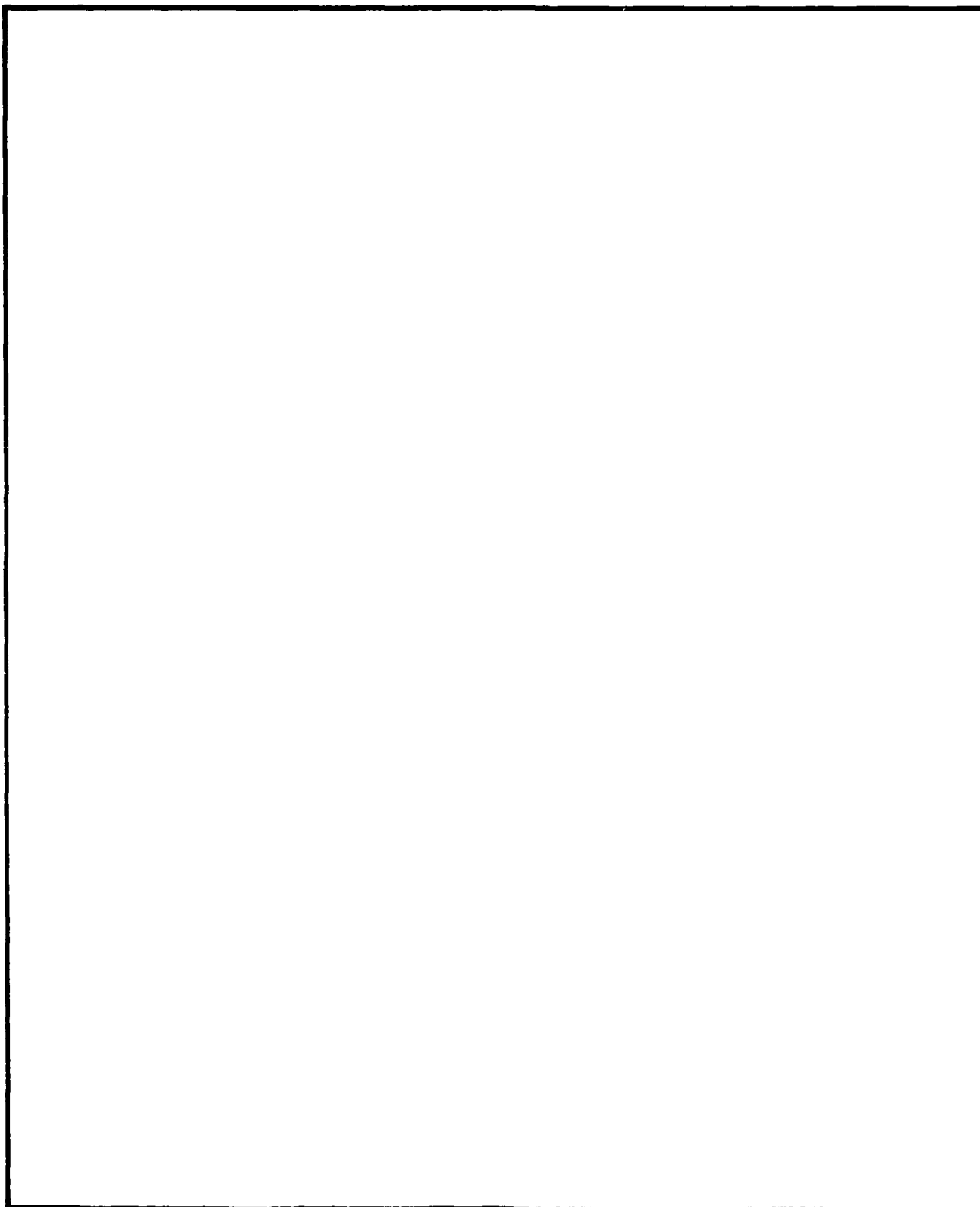
83 APR edition may be used until exhausted

All other editions are obsolete

SECURITY CLASSIFICATION OF THIS PAGE

UNCLASSIFIED

UNCLASSIFIED  
SECURITY CLASSIFICATION OF THIS PAGE



## SUMMARY

### NUCLEAR WINTER: WHERE DO WE STAND?

R. P. Turco

Four years of research on nuclear winter has greatly improved our understanding of this complex phenomenon. Studies have confirmed the possibility of significant temperature decreases and other severe environmental perturbations following a nuclear war, with potentially critical implications for human survival. Nevertheless, important uncertainties remain to be resolved. The major issues and their present research status are reviewed.

o Fuel Inventories: Fuel burdens in rural and urban settings appear to be known to within a factor of 2, and are lower than earlier estimates by a factor of 2 or so.

o Fuel Impaction: The quantities of fuels affected by nuclear explosions are sensitive to the scenario adopted, although definitive targeting analyses are forthcoming, issues of targeting policy may never be fully resolved and must necessarily remain uncertain; ignition and burning of rubblized fuels, while likely after a nuclear attack, may be of lower intensity; it is presently understood that a major nuclear attack against identified military/industrial targets would cause extensive collateral damage in urban areas;

o Smoke Emission Factor: Burning petroleum, plastics and related materials can emit 5% or more of their mass as soot; recent experiments reveal that the combustion of wood, under restricted ventilation, can convert up to 2% to soot; such emission factors imply blacker smoke than has been presumed in most existing studies; soot emission factors for large scale nuclear-induced oil refinery and urban fires are still uncertain, but have more likely been underestimated than overestimated;

o Plume Heights: Simulations and observations indicate initial smoke injection as high as 15 kilometers; soot generated under intense flaming conditions is likely to be injected into the middle and upper troposphere, while smoke produced by lower intensity combustion would be deposited in the middle and lower troposphere;

o Prompt Scavenging: The immediate rainout of the sooty component of smoke emissions is probably less than 50%, because of its poor nucleation properties relative to other materials, and because of the likely overseeding and reduced precipitation efficiencies of smoke clouds; actual scavenging processes remain to be tested in full-scale field tests;

o Mesoscale Dispersion: Observations of large smoke plumes caused by fire complexes suggest rapid regional dispersion; the role of water vapor in modifying soot properties and initiating precipitation requires investigation; smoke aging by coagulation and chemical reaction must also be carefully defined in this regime;

o Acute Climate Change: The extent of land surface cooling for a specific smoke injection can presently be estimated to within a factor of 2; the primary unknowns concern the surface boundary layer response to a sudden loss of solar energy, including the formation of fogs and inversion layers; critical changes in precipitation rates may also occur, but are currently less well understood;

o Long-term Climate Change: Preliminary investigations show important couplings between smoke injections, oceanic responses, ice formation and other processes that drive persistent climate fluctuations over periods of years; residual stabilized smoke layers could greatly enhance these effects; uncertainty about the long-term chemical interaction between soot and ozone must be resolved;

o Other Environmental Effects: Substantial ozone layer depletions are expected following a nuclear war due to smoke-induced perturbations in atmospheric temperatures, composition and circulation, but the effect has not been quantified; radiological impacts would be severe over large areas because of local fallout, although global health effects need to be more clearly defined; release of chemical toxins leading to hazardous local pollution of air, soil and water must be quantified;

o Biological Impacts: The human consequences of nuclear war as described in the SCOPE Report must be extended and refined; an organized research program should be developed in the U.S. to place the biological conclusions on a firmer analytical foundation.

PREFACE

The Defense Nuclear Agency has collected and printed the attached papers from the April 7-9 1987 Global Effects review as a service to the community. The Defense Nuclear Agency takes this opportunity to express its gratitude to the numerous participants in the Global Effects review.

The technical papers enclosed include all those which were received by DNA prior to the closing date of 15 May 1987. Where papers are missing their place is occupied by the abstract received prior to the meeting.

The inclusion of a paper in this proceedings does not imply endorsement of the results of the research reported or conclusions which might be drawn from that research. It is the position of the Defense Nuclear Agency that, while progress is being made in improving our understanding of Global Effects, the results to date are tentative and preliminary and should not be used for planning purposes beyond the planning of future research.



Accession For	
NTIS GRA&I	<input checked="" type="checkbox"/>
DTIC TAB	<input type="checkbox"/>
Unannounced	<input type="checkbox"/>
Justification	
By _____	
Distribution/	
Availability Codes	
Dist	Avail and/or Special
A-1	



## TABLE OF CONTENTS

	Page
SUMMARY	v
PREFACE	vii
SECTION 1 <u>Fuel Inventory and Fires</u>	1
1. Estimation of the Magnitude and Spatial Distribution of Combustible Materials in the San Jose Area, California - Simonett	2
2. Estimation of Urban Fuel Loadings for NATO and Warsaw Pact Countries - Veregin	6
3. Smoke Production by a Nuclear Attack on the United States - Anno, Bush, Dore, Small	12
4. Code For Early-Time Fire Phenomenology - Martin	35
5. Large Pool Fires in Nuclear Winter Studies - Keltner	51
6. Large Fires and Australia- Pyne	63
7. Atmospheric Chemistry Following a Nuclear War - Birks, Stephens	68
SECTION 2 <u>Smoke Emissions</u>	88
8. Effect of Radiant Flux on Smoke Emission - Mulholland, Henzel, Babrauskas	89
9. Smoke Emission Factors From Burning Wood and Asphalt - Williamson, Brown, Novakov	105
10. Preliminary Measurements of the Absorption Properties of the Smoke from Burning Plastic Materials - Patterson	121
11. Room-Scale Smoke Characterization Testing at Sandia National Laboratories - Nowlen, Williams, Einfeld	122
12. JP-4 Pool Fires: Preliminary Data on Scaling - Zak, Einfeld, Mokler, Morrison, Nowlen	160
13. Smoke Particle Emission Factors and Optical Characteristics of the Smoke from the Lodi Canyon Burn - Radke, Lyons	169

14.	Characteristics of Particles Generated by an Urban Fire Storm - Fields, Yalcintas, Crenshaw	170
15.	Chemical Reactivity of Smoke Particles with Ozone - Silver, deHaas, Fristrom, Linevsky	171
16.	The Heterogeneous Reaction of Ozone on Carbonaceous Surfaces - Stephens, Rossi, Golden	189
17.	Nuclear Winter: Global Consequences of Multiple Nuclear Explosions Turco, Toon, Akerman, Pollack, Sagan	203
18.	Consequences of Large-Scale Nuclear War for Ecological Systems, and Proposed Research Needs - Grover	227
SECTION 3 <u>Microphysics</u>		246
19.	How Motions Influence Aerosol Scavenging in Clouds - Hallett	247
20.	Potential Nucleation Scavenging of Smoke Particles Over Large Fires, A Parametric Study - Edwards, Penner	248
21.	Scavenging of Aerosol Particles by Ice Crystals - Miller, Wang	264
22.	Characterization of Combustion Aerosol for Haze and Cloud Formation - Hallett, Hudson, Rogers	265
23.	UMR Combustion Aerosol Facility - Hagen, Trueblood, White	286
24.	A Laboratory Cloud Chamber for Testing Some Nuclear Winter Hypotheses - Carrier, Fendell, Lake, Kwoh, Beach, Wagner	309
SECTION 4 <u>Plume Dynamics</u>		327
25.	Surface Vector Wind Fields in Fires - Palmer	328
26.	Fire Plume-Surface Interactions - Porch	331
27.	The Effects of Turbulence and Swirl on Plume Rise from Large-Area Fires - Marcus, Gaj, Rosenblatt	336
28.	Clouds Formed by Large Area Fires - Heikes, Ransohoff, Small	337
29.	Smoke Injection into the Atmosphere from Large Area Fires - Bacon, Sarma	349
30.	Numerical Simulation of Nucleation Scavenging Within Smoke Plumes above Large Fires - Bradley	375
31.	A Numerical Simulation of the Smoke Plume Generated by a Hypothetical Urban Fire Near Jan Jose, California - Tripoli, Kang	388

## Estimation of the Magnitude and Spatial Distribution of Combustible Materials in the San Jose Area, California

David S. Simonett  
Department of Geography  
UC Santa Barbara  
Santa Barbara CA 93106  
(805) 961-2013

Accurate urban fuel loading data are an important prerequisite in examining the global climatic consequences of nuclear war, since the dynamics of large urban fires such as those that might occur as a result of a nuclear exchange are sensitive to variations in the magnitude and spatial distribution of combustible materials over urban areas. Methods currently used to estimate fuel loadings rely on gross approximations and simplifying assumptions that severely limit the accuracy and usefulness of the results. For example, such methods are often based on the use of global production statistics for various combustible materials which, when combined with assumptions regarding the lifetimes of such materials, enable the calculation of the total weight of combustible materials for those cities assumed to be involved in a nuclear attack. These studies also rely on the assumption that combustible materials are distributed uniformly in urban areas or as a simple step function in which city centers have a higher fuel loading than the remainder of the city. This latter assumption is clearly unrealistic since it ignores local concentrations of combustible material associated with areas of high building density, and discontinuities in fuel loadings corresponding to parks, streets, freeways, rivers, reservoirs and undeveloped land.

This research project is concerned with the collection of detailed, micro-scale fuel loading data using a methodology based on the measurement of building parameters from aerial photographs covering a single urban area. Fuel loading data for the metropolitan area of San Jose have been collected under funding from Lawrence Livermore National Laboratory and the Institute on Global Conflict and Cooperation at UC San Diego. The methodology employed in the collection of these data is based on the measurement of building parameters, including types, numbers, sizes and heights, from 1:26,794-scale USGS black and white panchromatic aerial photographs. To preserve the spatial distribution of fuel loadings, the study area was first divided into a 111 by 153 matrix of grid cells having ground dimensions 1000 by 1000 ft. This matrix was drawn onto mylar sheets on which major streets were also located. The aerial photographs were registered to the matrix using streets and street intersections as ground control points. A total of 5843 cells were located within the built-up area of the city and therefore had to be inventoried.

For each cell, building parameters were measured for each of eight building categories: residential (single-family detached dwellings), apartments, mobile homes, commercial, school/institutional, offices, and light and heavy industry. These categories were interpreted from the aerial photographs with the aid of ancillary data including land use and zoning maps. The following parameters were measured for each cell: the number of buildings in each category; the average basal area of buildings in each category; and the average number of stories per building in each category. The total floor area for all categories in each cell was computed as the product of these three parameters. The total fuel loading of each building category was then calculated as the product of the total floor area of the category and the average fuel loading (or weight of combustible materials per unit of floor area) of the category. The total fuel loading per cell was obtained by summing the total fuel loading of each building category present in the cell. Table 1 summarizes the building parameters collected by this procedure. Table 2 gives the average fuel loadings for the different building categories, which were obtained from published sources. A more detailed explanation of this methodology can be found in Simonett et al (1986).

As Table 1 shows, residential buildings represent 87.6 percent of all buildings in the study area, but due to their relatively small size, they account for a smaller percentage of the total floor area and total fuel loading. Combined, residential buildings, apartments and mobile homes account for 96.3 percent of all buildings, 68.6 percent of the total floor area and 82.4 percent of the total fuel loading of the city. The total floor area of all buildings is  $67.24 \times 10^6$  m<sup>2</sup>, yielding an average of 11,507.79 m<sup>2</sup> per cell and  $12.37 \times 10^{-2}$  m<sup>2</sup> per m<sup>2</sup> of ground area (i.e., the average built-upness of the city is approximately 12 percent). The total fuel

SECTION 1

FUEL INVENTORY AND FIRES

loading of the city is  $4566.54 \times 10^6$  kg, yielding an average of 781,540 kg per cell and  $8.40 \text{ kg/m}^2$  of ground area.

The latter figure is considerably smaller than most other estimates (Turco et al 1983, Crutzen et al 1984, NRC 1985). Several factors account for this difference, one of which is the fact that we did not include fuel loadings for oil, gas and coal storage, oil and gas in pipelines, gasoline stored in underground tanks of secondary storage facilities (including gas stations), asphaltic surfaces on roofs, roads and parking lots, live vegetation, and major wood and plastics storage areas. Crutzen et al (1984) and the National Research Council (1985) indicate that oil and asphalt comprise between 10 and 22 percent of the total fuel loading. In the present case, this represents a value of between  $0.9$  and  $2.4 \text{ kg/m}^2$ , raising our partial estimate of  $8.4 \text{ kg/m}^2$  to between  $9.3$  and  $10.8 \text{ kg/m}^2$ . These estimates may increase by an additional 1 to 2  $\text{kg/m}^2$  by the inclusion of major raw materials storage areas. We realise that these estimates are crude, but as yet have no basis for an alternate judgement.

The sensitivity of our results to variations in average fuel loadings for different building categories is also shown in Table 3, which retabulates the figures in Table 1 substituting Bing's (1986) estimate of the average fuel loading of single-family residential buildings for our original figure (Table 2). The use of Bing's estimate results in a 37 percent increase in average fuel loadings, raising our previous estimate of  $8.4 \text{ kg/m}^2$  to  $11.5 \text{ kg/m}^2$ .

Our current research effort focusses on the accuracy of the collected data. Errors in the data may derive from two main sources: misclassification of building categories; and systematic over- or underestimation of building parameters from the aerial photographs. The latter source arises from the methods used to measure building parameters from the photographs, which were based on the use of photo interpretation keys. These keys were designed for visual estimation of parameters in order to speed the data collection procedure. In order to assess accuracy, a sample of 1000-ft cells was selected for which building parameters were measured meticulously using ground-based data collection techniques, and a combination of vertical and oblique aerial photograph interpretation. Results are as yet incomplete but suggest that errors due to misclassification have a smaller effect on the net error in fuel loading than errors in measured building parameters. This is due in part to the fact that San Jose is dominated by single-family residential structures, which are almost always interpreted correctly, and may not hold for other cities which contain a more heterogeneous mixture of buildings. Assessment of these errors is important, not only to bound the level of error in the San Jose data set, but to devise suitable methodologies to apply to other cities which realise cost savings without significantly affecting accuracy.

**Table 1: Building Parameters by Building Type, San Jose**

Building Type	Number of Buildings		Average Number of Floors	Average Basal Area (m <sup>2</sup> )	Total Floor Area		Total Fuel Loading	
	(number)	(%)			(10 <sup>6</sup> m <sup>2</sup> )	(%)	(10 <sup>6</sup> kg)	(%)
Residential	235,343	87.6	1.03	143.90	34.91	51.9	3001.93	65.7
Apartments	14,496	5.4	1.54	368.00	10.28	15.3	678.66	14.9
Mobile Homes	8907	3.3	1.00	96.62	0.96	1.4	84.13	1.8
Commercial	3792	1.4	1.22	1045.44	5.83	8.7	291.49	6.4
School/Institutional	1853	0.7	1.35	1420.48	3.92	5.8	176.16	3.9
Offices	474	0.2	2.33	2130.85	2.41	3.6	96.27	2.1
Light Industry	3103	1.2	1.07	1728.28	5.94	8.8	178.09	3.9
Heavy Industry	764	0.3	1.09	3762.82	2.99	4.5	59.81	1.3
<b>Total</b>	<b>268,732</b>	<b>100.0</b>	<b>1.06</b>	<b>208.03</b>	<b>67.24</b>	<b>100.0</b>	<b>4566.54</b>	<b>100.0</b>

**Table 2: Average Fuel Loadings for Building Categories**

Building Type	Average Fuel Loading (kg/m <sup>2</sup> )
Residential	86
Apartments	66
Mobile Homes	88
Commercial	50
School/Institutional	45
Office	40
Light Industry	30
Heavy Industry	20

**Table 3: Building Parameters by Building Type, San Jose\***

Building Type	Number of Buildings		Average Number of Floors	Average Basal Area (m <sup>2</sup> )	Total Floor Area		Total Fuel Loading	
	(number)	(%)			(10 <sup>6</sup> m <sup>2</sup> )	(%)	(10 <sup>6</sup> kg)	(%)
Residential	235,343	87.6	1.03	143.90	34.91	51.9	4677.94	74.9
Apartments	14,496	5.4	1.54	368.00	10.28	15.3	678.66	10.9
Mobile Homes	8907	3.3	1.00	96.62	0.96	1.4	84.13	1.3
Commercial	3792	1.4	1.22	1045.44	5.83	8.7	291.49	4.7
School/Institutional	1853	0.7	1.35	1420.48	3.92	5.8	176.16	2.8
Offices	474	0.2	2.33	2130.85	2.41	3.6	96.27	1.5
Light Industry	3103	1.2	1.07	1728.28	5.94	8.8	178.09	2.9
Heavy Industry	764	0.3	1.09	3762.82	2.99	4.5	59.81	1.0
Total	268,732	100.0	1.06	208.03	67.24	100.0	6242.55	100.0

\* This Table uses Bing's estimate of average fuel loading for residential buildings.

#### References

- Bing, George, *Estimates of Total Combustible Material in NATO and Warsaw Pact Countries*, UCRL-93192, Lawrence Livermore National Laboratory, Livermore, CA, 1986.
- Crutzen, P.J., I.E. Galbally and C. Bruhl, "Atmospheric Effects from Post Nuclear Fires," *Climatic Change*, vol. 6, pp. 323-365, 1984.
- National Research Council (NRC), *The Effects on the Atmosphere of a Major Nuclear Exchange*, National Academy Press, Washington DC, 1985.
- Simonett, D.S., T.N. Barrett, S. Gopal, F.J. Holsmuller, G.-Q. Sun and H. Veregin, *Magnitude and Spatial Distribution of Urban Flammable Materials in the San Jose Area, California*, UCRL-15794, Lawrence Livermore National Laboratory, Livermore, CA, 1986.
- Turco, R.P., O.B. Toon, T.P. Ackermann, J.B. Pollack and C. Sagan, "Nuclear Winter: Global Consequences of Multiple Nuclear Explosions," *Science*, vol. 222, pp. 1283-1292, 1983.

## Estimation of Urban Fuel Loadings for NATO and Warsaw Pact Countries

Howard Veregin  
Department of Geography  
University of California  
Santa Barbara CA 93106  
(805) 961-3663

This paper concerns a fundamental issue in the nuclear winter debate — the accuracy of urban fuel loading estimates. These estimates are needed to calculate the total amount of smoke and soot injected into the atmosphere from large urban fires, one of the main factors determining the net reduction in global temperatures that might result from a large nuclear exchange. In previous studies urban fuel loading estimates vary by as much as a factor of 2, and there appears to be little consensus as to the actual fuel loading for any specific set of cities. The objective of this paper is to present some preliminary findings concerning the accuracy of previous fuel loading estimates, based on more recent data and alternate methods of measuring the parameters required for fuel loading calculation.

Average urban fuel loading can be defined simply as the ratio of the total weight of combustible materials in a specific city or group of cities to the total area of the city or cities. Calculation of average urban fuel loading enables total urban smoke and soot production to be computed as the product of the average fuel loading, the total megatonnage detonated, the average urban area ignited per megaton, the proportion of available fuel expected to burn and the average urban smoke emission factor. This approach assumes that fuel is spread uniformly across cities, an assumption which is not overly realistic, especially in large, sprawling cities of the American West. In practice, researchers have often employed simplified models of urban morphology in which the city center has a higher average fuel loading than the remainder of the city. Use of this step-function requires a slightly different method of fuel loading calculation, involving the separate estimation of average fuel loadings in different regions of the city.

The TTAPS study (Turco et al 1983) for example, employed such a step-function approach to calculate the average urban fuel loading for NATO and Warsaw Pact cities with populations of 100,000 or more (hereafter "major" cities). They assumed that the total area of these cities was approximately 480,000 km<sup>2</sup>. Average fuel loadings of 100 kg/m<sup>2</sup> in city centers and 30 kg/m<sup>2</sup> in suburbs were employed. The former region was assumed to account for 5 percent of the total urban land area, giving an average urban fuel loading of 33.5 kg/m<sup>2</sup>. The NRC (1985) report employed similar parameter values and arrived at an average fuel loading of 40 kg/m<sup>2</sup>. The total area of major NATO and Warsaw Pact cities was assumed to be 500,000 km<sup>2</sup>. Crutzen et al (1984) computed the fuel loading for 300 cities, primarily in the NATO and Warsaw Pact nations. They assumed that these cities occupied a total land area of 250,000 km<sup>2</sup>. Average fuel loadings were calculated as 40 kg/m<sup>2</sup>, as in the NRC report. The latter group of researchers obtained a second, independent estimate for the same group of cities, but based on a different methodology using global production rates and assumed lifetimes for various combustible materials. The average urban fuel loading thus calculated was 21.6 kg/m<sup>2</sup>, a bit more than half of their original figure.

We have recomputed these average fuel loadings using more current and accurate estimates of the parameters required for their calculation. Of particular importance is the estimate of the total land area of those cities assumed to be involved in the exchange. This figure was recalculated using the well-known relationship between the population and built-up area of cities known as the law of allometric growth (Nordbeck 1965). This law expresses the relationship between area and population as:  $A = a P^b$  where  $A$  is the area,  $P$  is the population, and  $a$  and  $b$  are estimated coefficients where  $b < 1$ . This relationship accounts for the fact that larger cities tend to have higher population densities than smaller ones. Empirical research over the last 35 years in Europe, North America and Asia indicates that this relationship is consistently strong, with a correlation coefficient on the order of 0.9. Table 1 gives the various countries and dates for which this relationship has been evaluated, as well as the estimated values of the  $a$  and  $b$  coefficients.

The area of each major NATO and Warsaw Pact city was calculated by applying this relationship, using population data from the 1984 UN Demographic Yearbook. These are rough estimates of actual population since there is little consistency among countries in terms of the criteria used to delineate cities,



whether the legal boundary, the limits of the built-up area, or the zone of social and economic interdependence. Table 2 shows the figures obtained by this procedure. Note that the total area of all major NATO and Warsaw Pact cities is 175,000 km<sup>2</sup>, considerably less than the figure of 500,000 km<sup>2</sup> employed in some previous studies.

Calculation of average fuel loadings also requires an estimate of the total weight of combustible materials assumed to be involved in a nuclear exchange. To date, the most thorough assessment of this parameter has been carried out by Bing (1986), who obtained separate estimates for residential and non-residential buildings, petroleum and petroleum products, asphalt, plastics, synthetic fibers and rubber tires. This procedure yielded a total weight of combustible materials in the NATO and Warsaw Pact countries of 7700 Tg. Assuming similar fuel loadings per capita in residential and non-residential areas (which may be unrealistic), this yields a total weight of about 3600 Tg for major cities (as Table 2 shows, major cities account for about 46 percent of the total population).

The average urban fuel loading obtained by dividing the latter figure by the total land area of these cities (as computed with the law of allometric growth) is 20.31 kg/km<sup>2</sup>. This figure is in agreement with the most recent value obtained for San Jose (Simonett et al 1986) in the sense that both values suggest that previous studies have overestimated average urban fuel loadings to a considerable degree. Obviously, San Jose is somewhat anomalous, both in the American setting and in the context of Europe, where cities tend to be more compact. One would not therefore expect the value for San Jose to match those for the NATO and Warsaw Pact countries as a whole.

The implications of the above findings are shown in Table 3, which presents original and modified urban fuel loading estimates for the three studies examined here. The main features of this Table are as follows:

- (1) The total urban area ignited has been overestimated by as much as a factor of 2.
- (2) As a result of errors in area and weight, average urban fuel loadings have been overestimated by as much as a factor of 2.
- (3) Total urban smoke emission has been overestimated by as much as a factor of 4 due to these errors.

Note that total urban smoke emission is dependent, not only on average urban fuel loadings, but on the total urban area ignited. This is because in all studies the total urban area ignited, expressed as the total megatonnage detonated times the average urban area ignited per megaton, is actually larger than the total urban land area which actually exists.

For a number of reasons, these new results should not be considered as robust and unequivocal:

- (1) The method of land area calculation for cities is based on coefficients obtained as much as 35 years ago. Moreover, these coefficients have never been obtained for certain NATO and Warsaw Pact countries.
- (2) There are likely to be errors in other parameters required for smoke and soot production estimates, which have not been addressed here.
- (3) The validity of the whole approach to the estimation of smoke and soot production, which relies on the extensive use of average values in place of detailed, micro-scale data, remains to be established.

**Table 1**  
**Relationship Between Population and Built-Up Area**

Researcher	Region and Year	Sample Size	Coefficient a	Coefficient b	Correlation Coefficient
Stewart and Warntz (1958)	USA 1940	412	$7.255 \times 10^{-3}$	0.75	-
Stewart and Warntz (1958)	UK 1951	157	$5.385 \times 10^{-3}$	0.75	0.87
Boyce (1963)	USA 1950	-	$3.422 \times 10^{-3}$	0.857	0.84
Boyce (1963)	USA 1960	-	$4.595 \times 10^{-3}$	0.863	0.87
Nordbeck (1965)	USA 1950	155	$3.263 \times 10^{-3}$	0.86	0.928
Nordbeck (1965)	USA 1960	213	$3.911 \times 10^{-3}$	0.876	0.922
Nordbeck (1965)	Sweden 1960	70	$8.5 \times 10^{-3}$	0.664	0.976
Nordbeck (1965)	Japan 1960	518	$2.81 \times 10^{-4}$	0.915	0.967
Maher and Bourne (1969) <sup>[1]</sup>	Canada 1960	51	$2.679 \times 10^{-3}$	0.874	0.987
Welch (1980)	China 1953	124	$1.882 \times 10^{-7}$	1.380 <sup>[2]</sup>	0.75
Welch (1980)	China 1970	10	$1.304 \times 10^{-13}$	2.417 <sup>[2]</sup>	0.82

[1] Cited in Tobler (1969).

[2] Note that, in theory, these coefficients should be < 1. The source of this discrepancy is unclear.

**Table 2**  
**Population and Area Statistics for Major Cities**

Country	Total Population <sup>(1)</sup> (000s)	Number of Cities <sup>(1)</sup>	Population of Cities <sup>(1)</sup> (000s)	Population of Cities <sup>(1)</sup> (% of total)	Area of Cities (km <sup>2</sup> )
<b>NATO</b>					
Belgium	9849	8	2168	22.0	500 <sup>(2)</sup>
Canada	24,343	24	13,979	57.4	6600 <sup>(3)</sup>
Denmark	5124	4	1807	35.3	200 <sup>(4)</sup>
France	54,335	57	23,342	43.0	4200 <sup>(2)</sup>
Germany (West)	60,651	65	20,270	33.4	4300 <sup>(2)</sup>
Greece	9740	5	4101	42.1	600 <sup>(2)</sup>
Iceland	205	1	128	62.4	0 <sup>(6)</sup>
Italy	56,557	48	15,769	27.9	3200 <sup>(2)</sup>
Luxembourg	365	0	0	0.0	0
Netherlands	13,061	16	5780	44.3	1200 <sup>(2)</sup>
Norway	4091	3	985	24.1	100 <sup>(4)</sup>
Portugal	9833	2	2927	29.8	500 <sup>(2)</sup>
Spain	37,746	50	15,863	42.0	3300 <sup>(2)</sup>
Turkey	44,737	25	14,447	32.3	2600 <sup>(2)</sup>
United Kingdom	55,678	56	18,292	32.9	3500 <sup>(2)</sup>
USA	226,546	254	175,409	77.4	116,800 <sup>(5)</sup>
<b>Total NATO</b>	<b>612,861</b>	<b>618</b>	<b>315,267</b>	<b>51.4</b>	<b>147,600</b>
<b>Warsaw Pact</b>					
Bulgaria	8730	8	2461	28.2	500 <sup>(2)</sup>
Czechoslovakia	15,283	7	2772	18.1	600 <sup>(2)</sup>
Germany (East)	16,706	15	4410	26.4	1000 <sup>(2)</sup>
Hungary	10,709	8	3180	29.7	600 <sup>(2)</sup>
Poland	35,061	38	10,873	31.0	2400 <sup>(2)</sup>
Romania	21,560	20	5991	27.8	1300 <sup>(2)</sup>
USSR	262,436	280	106,709	40.7	21,000 <sup>(2)</sup>
<b>Total Warsaw Pact</b>	<b>370,485</b>	<b>376</b>	<b>136,396</b>	<b>36.8</b>	<b>27,400</b>
<b>Total NATO and Warsaw Pact</b>	<b>983,346</b>	<b>994</b>	<b>451,663</b>	<b>45.9</b>	<b>175,000</b>
<p>(1) Source: United Nations (1984).                  (2) Source: Coefficients for the United Kingdom in 1951 [Stewart and Warrtz (1958)].                  (3) Source: Coefficients for Canada in 1960 [Maher and Bourne (1969)].                  (4) Source: Coefficients for Sweden in 1960 [Nordbeck (1965)].                  (5) Source: Coefficients for the United States in 1960 [Nordbeck (1965)].                  (6) Less than 100 km<sup>2</sup>.</p>					

**Table 3**  
**Original and Modified Fuel Loading Estimates**

Researchers	Modification	Total Number of Cities Examined	Total Urban Area Ignited (km <sup>2</sup> )	Average Urban Fuel Loading (kg/m <sup>2</sup> )	Total Urban Smoke Emission (10 <sup>9</sup> kg)
TTAPS	Original	1000	240,000	33.5	116
	Modified	994	175,000	20.31	51.4
NRC	Original	1100	250,000	40	150
	Modified	994	175,000	20.31	53.3
Crutzen et al	Original	300	250,000	40	149
	Modified	300	126,000	20.31	38.1
Crutzen et al <sup>[1]</sup>	Original	300	250,000	21.6	80.5
	Modified	300	126,000	20.31	38.1

[1] Alternate method of fuel loading calculation.

### References

- Bing, George, "Estimates of Total Combustible Material in NATO and Warsaw Pact Countries," UCRL-93192, Lawrence Livermore National Laboratory, Livermore, CA, 1986.
- Boyce, Ronald R., "Changing Patterns of Urban Land Consumption," *The Professional Geographer*, vol. 25, no. 2, pp. 19-24, 1963.
- Crutzen, P.J., I.E. Galbally and C. Bruhl, "Atmospheric Effects from Post Nuclear Fires," *Climatic Change*, vol. 6, pp. 323-365, 1984.
- Maher, C. and L. Bourne, *Land Use Structure and City Size: an Ontario Example*, Centre for Urban and Community Studies, University of Toronto, 1969.
- National Research Council (NRC), *The Effects on the Atmosphere of a Major Nuclear Exchange*, National Academy Press, Washington DC, 1985.
- Nordbeck, Stig, *The Law of Allometric Growth*, Discussion Paper Number 7, Michigan Inter-University Community of Mathematical Geographers, 1965.
- Simonett, D.S., T.N. Barrett, S. Gopal, F.J. Holsmuller, G.-Q. Sun and H. Veregin, "Magnitude and Spatial Distribution of Urban Flammable Materials in the San Jose Area, California," UCRL-15794, Lawrence Livermore National Laboratory, Livermore, CA, 1986.
- Stewart, John Q. and William Warntz, "Physics of Population Distribution," *Journal of Regional Science*, vol. 1, no. 1, pp. 99-123, 1958.
- Tobler, Waldo R., "Satellite Confirmation of Settlement Size Coefficients," *Area*, pp. 30-34, 1969.
- Turco, R.P., O.B. Toon, T.P. Ackermann, J.B. Pollack and C. Sagan, "Nuclear Winter: Global Consequences of Multiple Nuclear Explosions," *Science*, vol. 222, pp. 1283-1292, 1983.
- United Nations (Department of International Economic and Social Affairs), *Demographic Yearbook 1984*, United Nations, New York, 1986.
- Welch, R., "Monitoring Urban Population and Energy Utilization Patterns from Satellite Data," *Remote Sensing of Environment*, vol. 9, pp. 1-9, 1980.

**SMOKE PRODUCTION BY A NUCLEAR ATTACK  
ON THE UNITED STATES**

**G. H. ANNO, B. W. BUSH, M. A. DORE, R. D. SMALL**

**PACIFIC-SIERRA RESEARCH CORP.**

**A SUBSIDIARY OF EATON CORPORATION**

**LOS ANGELES, CALIFORNIA**

**PRESENTED AT THE  
DEFENSE NUCLEAR AGENCY  
GLOBAL EFFECTS PROGRAM TECHNICAL MEETING**

**APRIL 7-9, 1987**

**SANTA BARBARA, CALIFORNIA**

# URBAN AREA ANALYSIS

- CITY, SUBURBAN, AND RURAL AREAS MAPPED
- TARGETS LOCATED WITHIN URBAN AREAS
- CITIES GROUPED ACCORDING TO BURNABLE DENSITIES
- URBAN STRUCTURE AND TARGET AREAS CHARACTERIZED
- FUEL TYPES AND LOADINGS DETERMINED FOR EACH CITY SECTION
- SMOKE GENERATION ESTIMATED BY FUEL TYPE
- FIRE PLUME AND SMOKE CLOUD CALCULATED

# ASSUMED TARGETS AND DISTRIBUTION

## CONTINENTAL UNITED STATES

TARGET CATEGORY	W	NW	SW	N	S	NE	TOTAL
<b>INDUSTRIAL</b>							
REFINERIES	49	30	84	54	88	16	321
MILITARY WEAPON PRODUCTION	5	0	15	28	15	13	76
NUCLEAR WEAPON PRODUCTION	1	2	4	4	5	0	16
SELECTED DOD CONTRACTORS	72	11	40	60	32	111	326
<b>COMMERCIAL</b>							
POLITICAL CENTERS	2	6	9	11	9	17	54
PORTS	12	15	4	11	33	34	109
HYDROELECTRIC FACILITIES	57	109	46	27	122	30	391
FOSSIL FUEL POWER PLANTS	45	44	232	395	283	182	1181
NUCLEAR POWER PLANTS	3	6	8	23	24	21	85
<b>AIR FORCE FACILITIES</b>							
OPERATING BASES	10	8	27	9	20	12	86
STATIONS	7	11	3	6	10	7	44
NATIONAL GUARD BASES	7	11	11	31	25	23	108
<b>ARMY FACILITIES</b>							
FORTS	7	4	12	7	16	23	69
DEPOTS	3	1	6	6	4	4	24
TRAINING CENTERS	1	1	0	2	5	7	16
R&D CENTERS	0	0	6	1	0	9	16
<b>NAVY FACILITIES</b>							
OPERATING BASES	9	4	0	1	4	10	28
SHIPYARDS	3	1	0	0	1	3	8
AIR STATIONS	6	1	5	1	9	5	27
TRAINING BASES	11	3	1	3	5	14	37
DEPOTS	2	0	0	0	2	4	8
<b>MISSILE FIELDS</b>							
ICBM SILOS	13	650	236	145	23	0	1067
LAUNCH CONTROL FACILITIES	7	65	56	15	18	0	161
<b>TOTAL</b>	<b>332</b>	<b>983</b>	<b>805</b>	<b>840</b>	<b>753</b>	<b>545</b>	<b>4258</b>



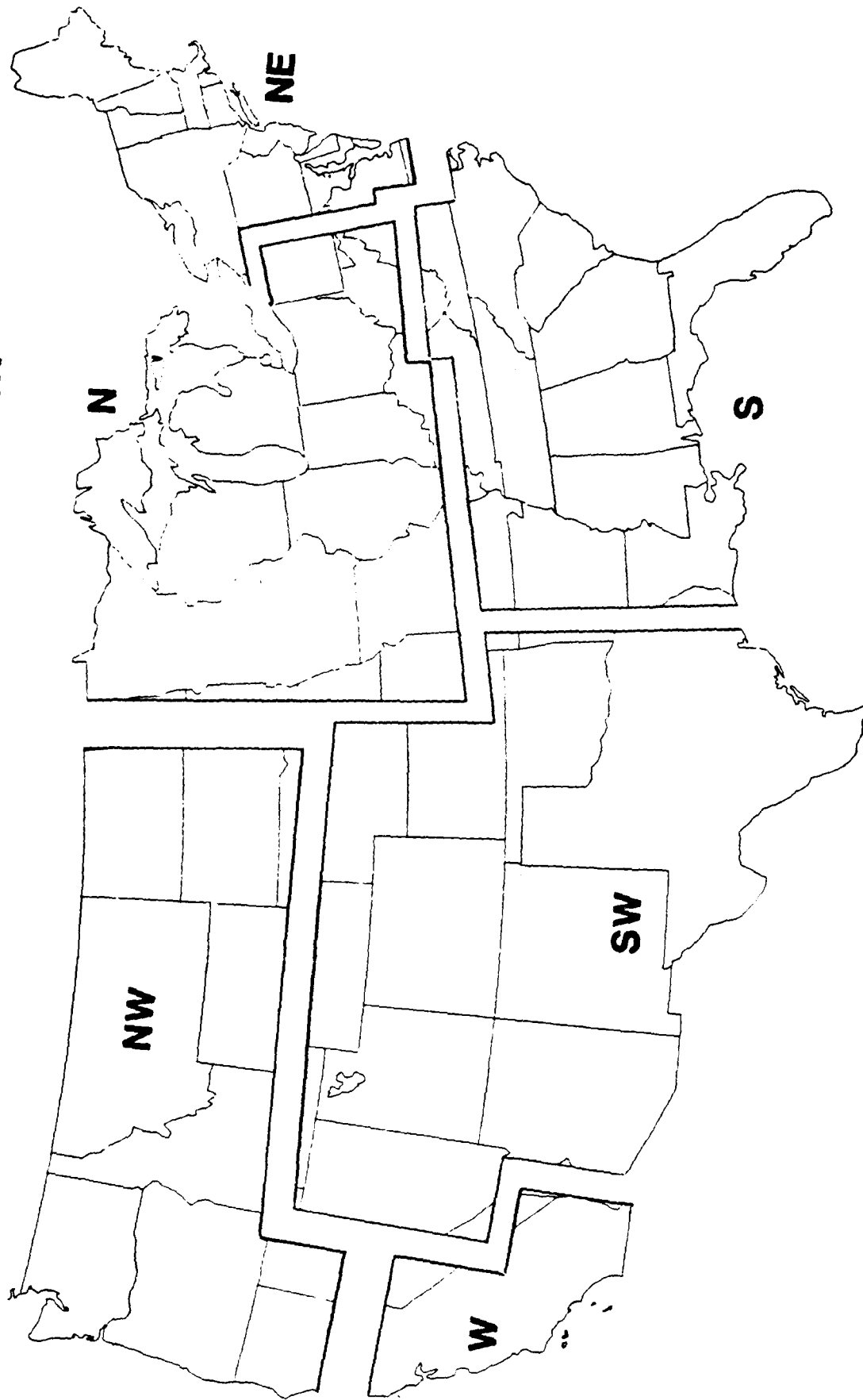
## URBAN TARGET AREAS BY REGION

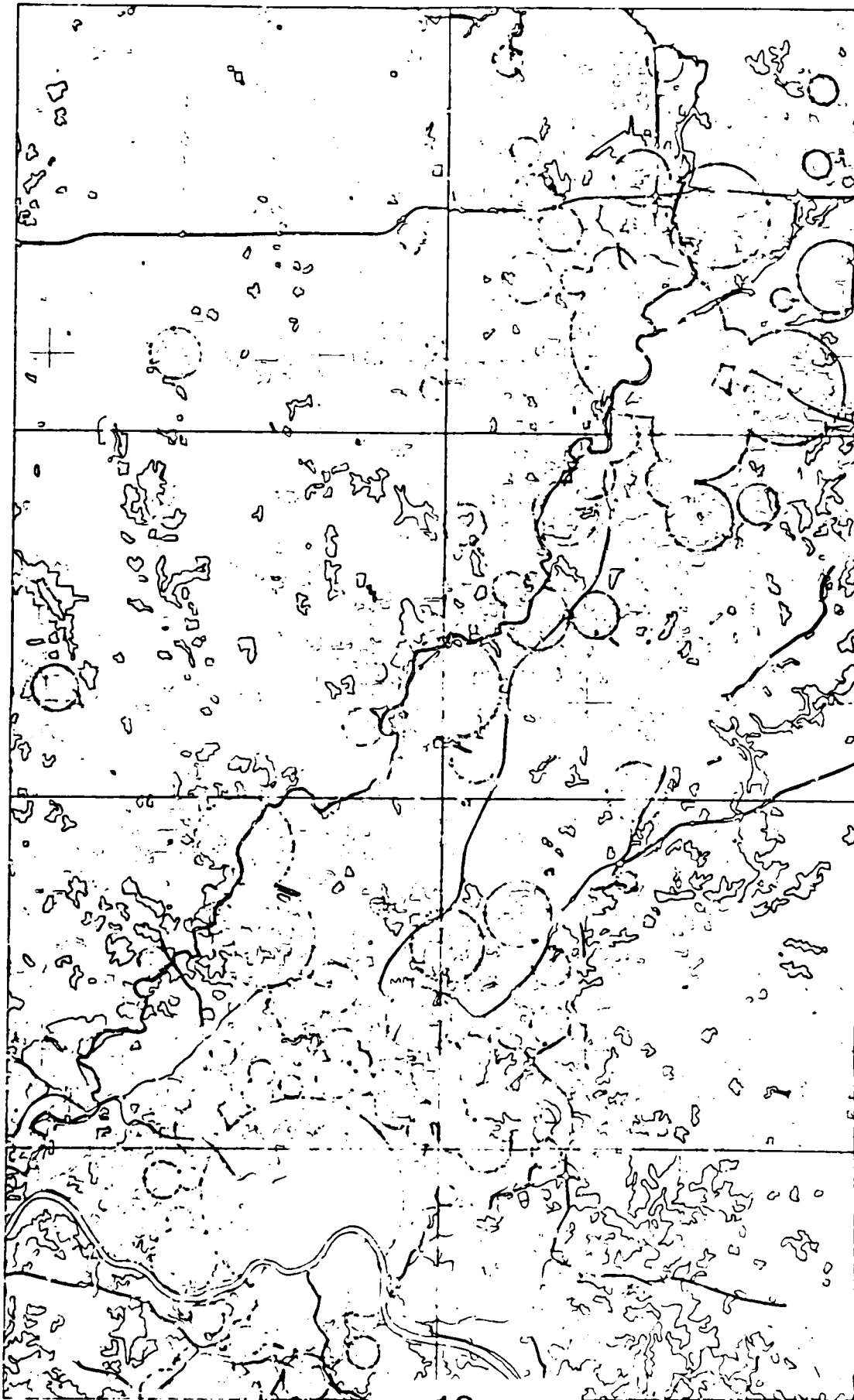
GEOGRAPHIC ZONE	URBAN AREA (KM <sup>2</sup> )	POPULATION	COLOCATED TARGET- URBAN AREA (KM <sup>2</sup> )	NONURBAN TARGET AREA (KM <sup>2</sup> )
CALIFORNIA (W)	14,108	20,553,740	7,900	26,679
NORTHWEST (NW)	6,952	6,321,264	3,237	138,055
SOUTHWEST (SW)	23,556	18,782,320	12,258	108,249
NORTH (N)	39,171	41,794,620	18,004	114,713
SOUTH (S)	37,681	27,689,520	16,646	112,929
NORTHEAST (NE)	25,689	37,073,220	15,620	54,776
	147,853	152,214,700	73,665	555,401

## 6-CLASS BREAKDOWN

GEOGRAPHIC REGION	W	NW	SW	N	S	NE
SINGLE FAMILY AREA PER DEVELOPED AREA	37.4	38.9	35.6	35.0	40.3	26.4
MULTIPLE FAMILY AREA PER DEVELOPED AREA	9.25	2.69	2.71	4.74	3.66	10.01
COMMERCIAL AREA PER DEVELOPED AREA	6.08	4.73	5.17	5.17	7.09	7.87
INDUSTRIAL AREA PER DEVELOPED AREA	5.93	4.80	6.09	12.00	5.92	9.14
STREET AREA PER DEVELOPED AREA	22.9	33.8	24.7	25.0	24.0	21.2
SEMI-PUBLIC AREA PER DEVELOPED AREA	18.4	15.1	25.7	18.1	19.0	25.3

# CONUS REGIONAL BREAKDOWN





# LAND USE IN URBAN TARGET AREAS

## LAND USE IN BUILT-UP AREAS

LAND USE	REGION						
	W	NW	SW	N	S	NE	CONUS
RESIDENTIAL	0.573	0.718	0.563	0.590	0.690	0.572	0.610
COMMERCIAL, SERVICES AND MIXED	0.186	0.129	0.160	0.204	0.145	0.202	0.178
INDUSTRIAL AND MIXED	0.126	0.035	0.049	0.066	0.064	0.080	0.072
COMMUNICATIONS, TRANSPORTATION AND UTILITIES	0.056	0.033	0.151	0.095	0.071	0.079	0.086
OTHER	<u>0.059</u>	<u>0.085</u>	<u>0.077</u>	<u>0.045</u>	<u>0.030</u>	<u>0.067</u>	<u>0.054</u>
	1.000	1.000	1.000	1.000	1.000	1.000	1.000

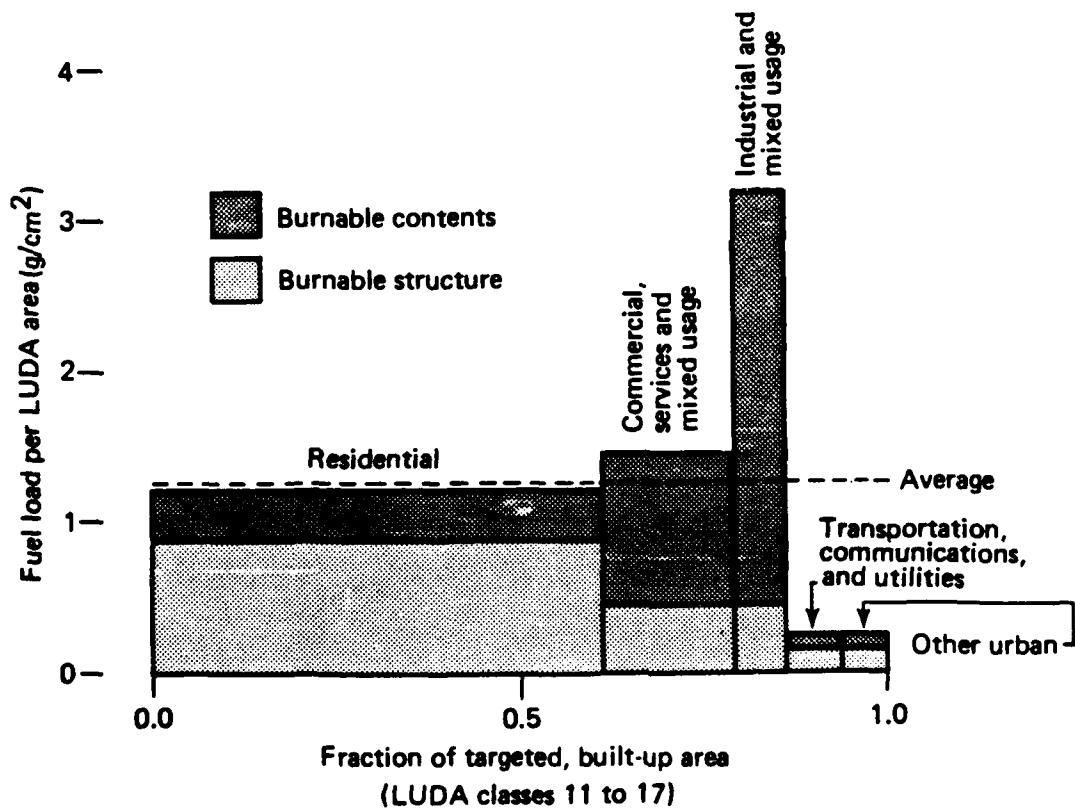
## LAND USE IN OPEN URBAN AREAS

LAND USE	REGION						
	W	NW	SW	N	S	NE	CONUS
WATER	0.571	0.599	0.091	0.030	0.144	0.339	0.194
AGRICULTURE	0.008	0.048	0.641	0.769	0.452	0.268	0.494
FOREST	-	0.340	0.145	0.161	-	0.350	0.168
OTHER	<u>0.421</u>	<u>0.013</u>	<u>0.123</u>	<u>0.013</u>	<u>0.404</u>	<u>0.043</u>	<u>0.144</u>
	1.000	1.000	1.000	1.000	1.000	1.000	1.000

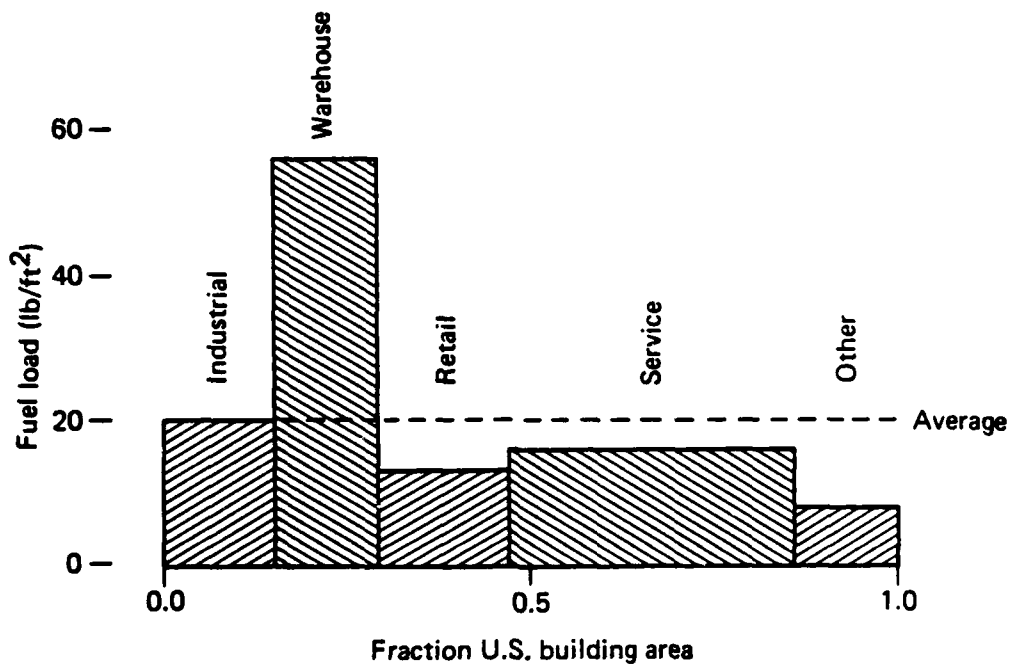
## BUILT-UP FRACTION IN URBAN AREAS

LAND USE	REGION						
	W	NW	SW	N	S	NE	CONUS
BUILT-UP	0.827	0.790	0.592	0.800	0.819	0.793	0.770
OPEN	<u>0.173</u>	<u>0.210</u>	<u>0.408</u>	<u>0.200</u>	<u>0.181</u>	<u>0.207</u>	<u>0.230</u>
	1.000	1.000	1.000	1.000	1.000	1.000	1.000

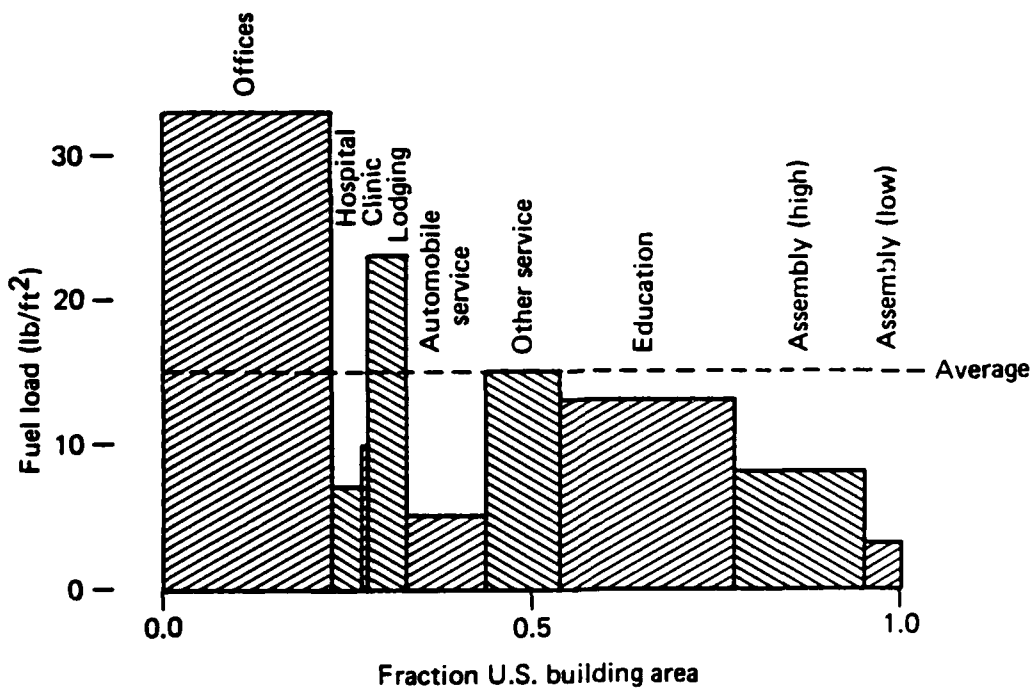
# TARGET AREA BUILDING CLASSES AND FUEL LOADINGS



# NONRESIDENTIAL FUEL-LOAD DISTRIBUTION

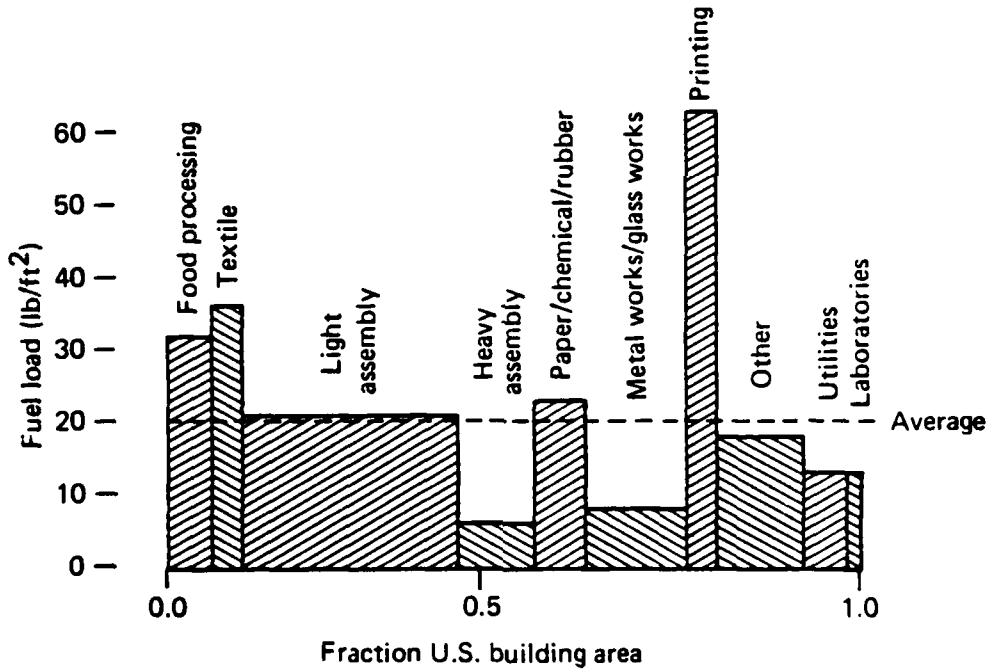


# SERVICE FUEL-LOAD DISTRIBUTION

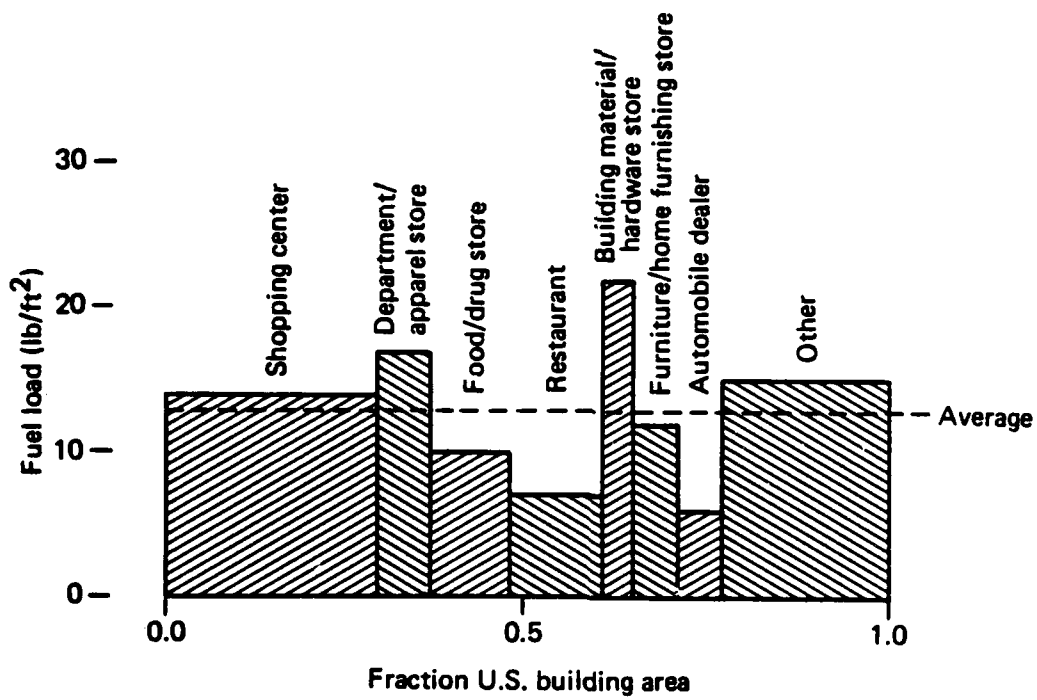




# INDUSTRIAL FUEL-LOAD DISTRIBUTION



# RETAIL FUEL-LOAD DISTRIBUTION



# COMMERCIAL AND INDUSTRIAL FUEL LOADING

## CLASSIFICATION (33 CATEGORIES)

- 10 INDUSTRY (FOOD, TEXTILE, ASSEMBLY, ...)
- 2 WAREHOUSE (HIGH RACK, MULTISTORY)
- 8 RETAIL (SHOPPING CENTER, RESTAURANT, FURNITURE, ...)
- 9 SERVICE (OFFICE, MEDICAL, SCHOOL, ASSEMBLY, ...)
- 4 OTHER (AGRICULTURE, VACANT, RESIDENTIAL, ...)

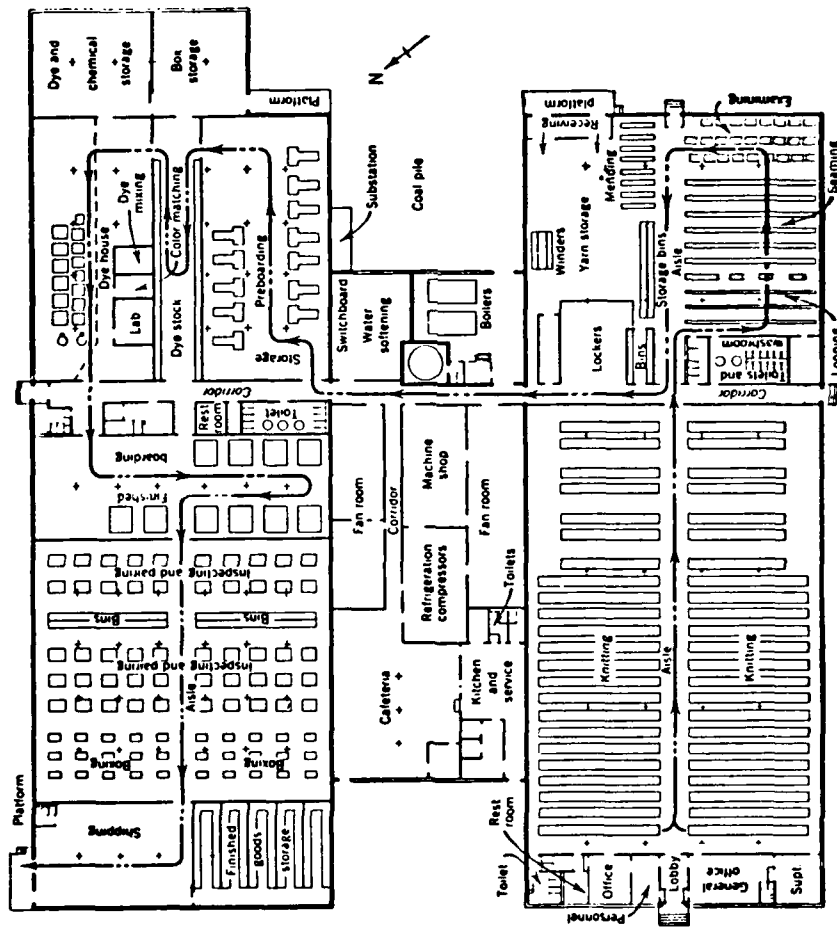
## FACILITY STATISTICS

- NUMBERS AND TYPES OF BUILDINGS IN 33 CATEGORIES
- BUILDING CHARACTERISTICS (LAYOUT, USAGE, NUMBER OF FLOORS, AREA, CONSTRUCTION)
- LOT SIZE/BUILDING DENSITY
- GEOGRAPHIC DISTRIBUTION

## COMBUSTIBLE CONTENTS DETERMINED FOR EACH CATEGORY

## FUEL LOADINGS CALCULATED FOR EACH LAND USE CATEGORY

# INDUSTRIAL LAYOUT-HOSIERY MILL



SOURCE: MALLICK AND GAUDREAU, 1951.

# AVERAGED URBAN AREA FUEL LOADS AND EMISSION FACTORS

LAND USE	FUEL LOAD PER FOUNDATION AREA (g/cm <sup>2</sup> )		EMISSION FACTOR (PERCENT)	FRACTION OF GROUND COVERED (PERCENT)	FUEL LOADING (g/cm <sup>2</sup> )	AVERAGE EMISSION FACTOR (PERCENT)
	STRUCTURE CONTENTS	STRUCTURE CONTENTS				
RESIDENTIAL	6.8	2.4	1.3	13	1.2	1.8
COMMERCIAL, SERVICE <sup>a</sup> AND MIXED USAGE	2.9	6.8	1.7	15	1.5	3.3
INDUSTRIAL AND MIXED USAGE <sup>b</sup>	2.9	18.6	1.7	15	3.2	3.7
TRANSPORTATION	2.9	2.0	1.7	5	0.2	2.6
OTHER	2.9	2.0	1.7	5	0.2	2.6

<sup>a</sup>INCLUDES ONE-HALF OF ALL "LOW" WAREHOUSES.

<sup>b</sup>INCLUDES ALL "HIGH" WAREHOUSES AND ONE-HALF OF "LOW" WAREHOUSES.

## VEGETATION IN URBAN TARGET AREAS

LAND USE	FRACTION COVERED WITH VEGETATION (PERCENT)	FUEL LOAD (g DRY MATTER /cm <sup>2</sup> )
<b>BUILT-UP</b>		
RESIDENTIAL	40	0.5
COMMERCIAL,SERVICES, AND MIXED	10	0.5
INDUSTRIAL AND MIXED	5	0.5
TRANSPORTATION, COMMUNICATIONS AND UTILITIES	15	0.5
OTHER	50	0.5
<b>OPEN</b>		
WATER	0	0
AGRICULTURE	70	0.25
FOREST	100	1.0
OTHER	90	0.25

## FUEL LOADINGS (g/cm<sup>2</sup>) DISTRIBUTED BY REGION

	W	NW	SW	N	S	NE	TOTAL
<b>BUILT-UP</b>	0.14	0.17	0.15	0.15	0.16	0.15	0.15
<b>OPEN</b>	0.13	0.34	0.28	0.30	0.20	0.40	0.24
<b>URBAN AVERAGE</b>	0.14	0.21	0.20	0.18	0.16	0.20	0.18
<b>TOTAL (Tg)</b>	5.3	3.2	12.0	15.4	13.1	15.3	64.3

# TARGETED HYDROCARBON STORAGE IN Tg CONTINENTAL UNITED STATES

	GEOGRAPHIC REGION							EMISSION FACTOR PERCENT
	W	NW	SW	N	S	NE	U.S. TOTAL	
PRIMARY STOCKS <sup>a</sup>	18.3	11.2	31.4	20.2	32.8	6.0	119.8	8.0
SECONDARY/TERTIARY STOCKS <sup>b</sup>	2.0	0.8	3.1	4.6	4.2	4.0	18.7	5.0
CHEMICALS <sup>c</sup>	0.5	0.2	0.7	1.1	1.1	0.9	4.4	5.0
NATURAL GAS <sup>d</sup>	7.2	3.0	11.2	16.5	15.3	14.3	67.5	1.0
COAL <sup>e</sup>	2.6	2.5	13.3	22.6	16.2	10.4	67.5	8.0
TOTAL	30.6	17.7	59.7	65.0	69.5	35.6	278.1	
AVERAGE EMISSION FACTOR (PERCENT)	6.1	6.6	6.5	6.0	6.2	4.8	6.0	

<sup>a</sup>INCLUDES ALL PRIMARY STOCKS (CRUDE OIL AND PRODUCTS) IN REFINERIES, 1% OF STRATEGIC PETROLEUM RESERVE, AND 50% OF CRUDE IN PIPELINES.

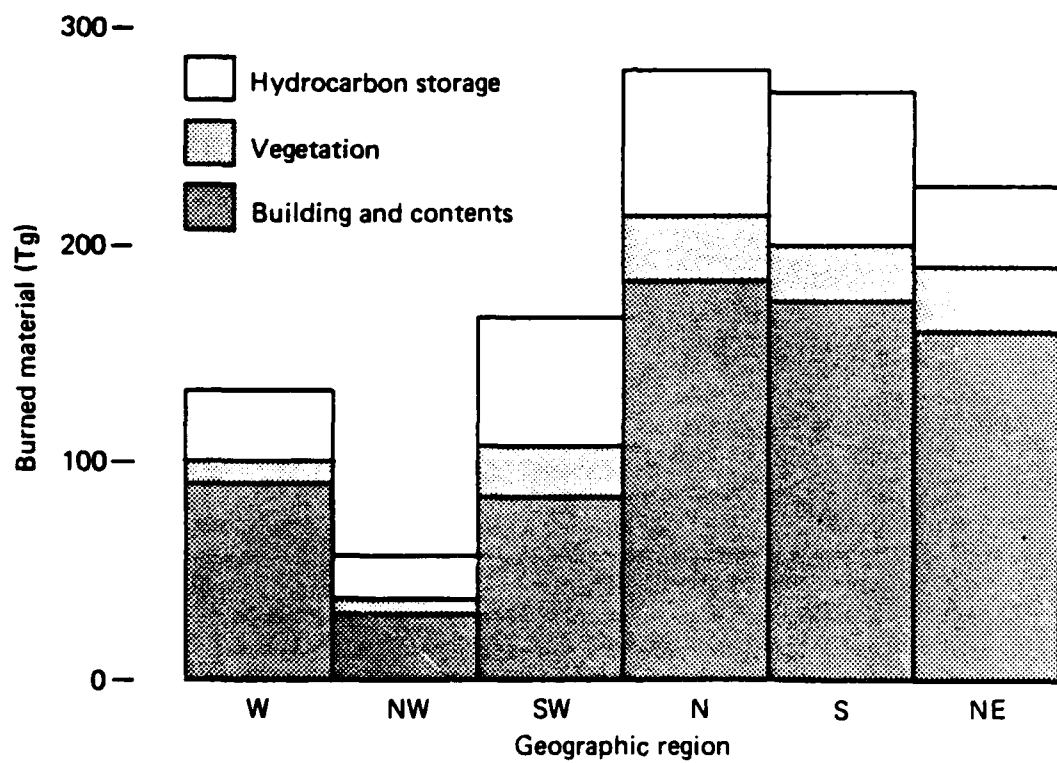
<sup>b</sup>SECONDARY/TERTIARY STOCKS DISTRIBUTED UNIFORMLY IN URBAN AREA; ALL TARGETED FRACTIONS BURN.

<sup>c</sup>ALL TARGETED CHEMICAL STOCKS BURN.

<sup>d</sup>ASSUMES 50% OF U.S. INVENTORY BURNS.

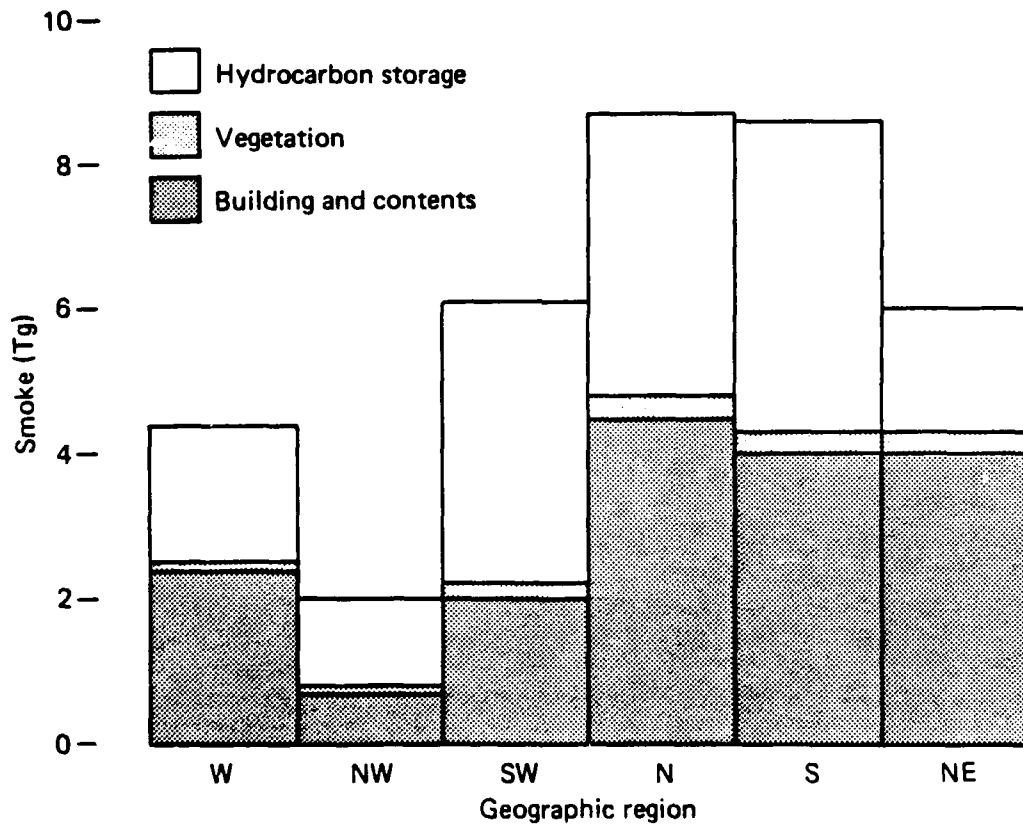
<sup>e</sup>ONE-THIRD OF INVENTORY AT COAL-FIRED UTILITIES BURNS.

# URBAN FUEL BURNED





# URBAN SMOKE PRODUCTION

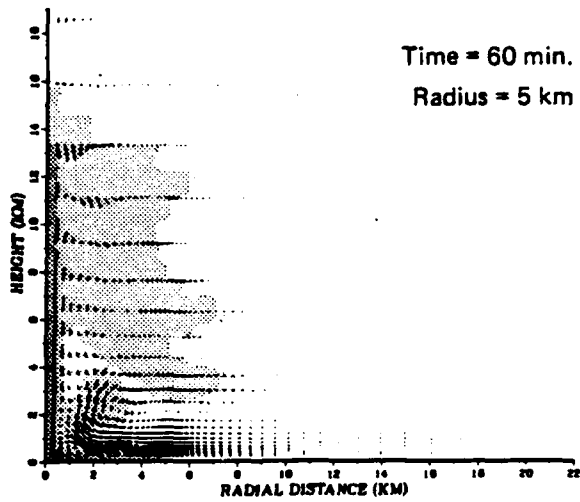


# SUMMARY U.S. URBAN SMOKE PRODUCTION

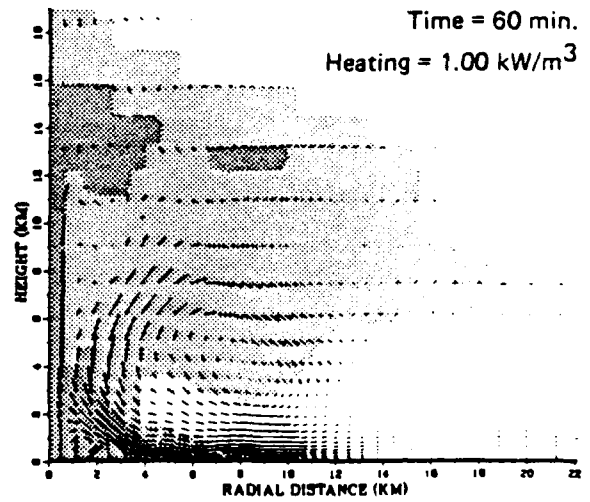
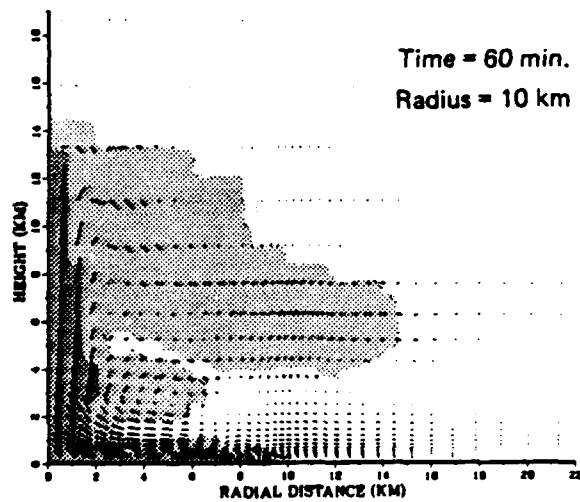
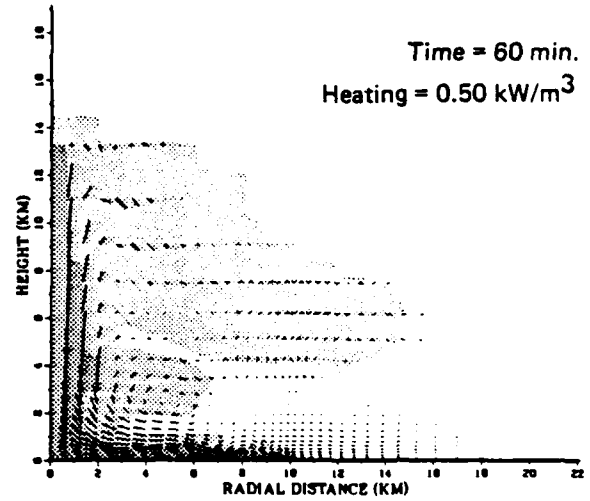
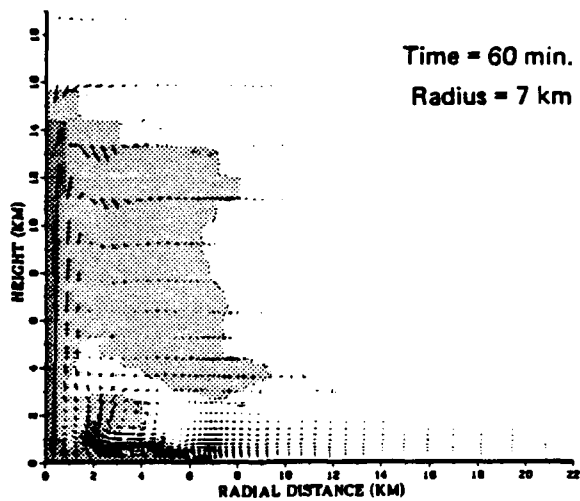
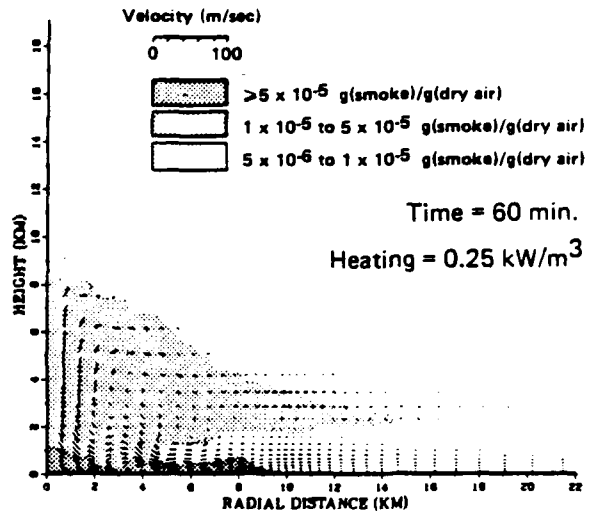
DATA DESCRIPTION	GEOGRAPHIC REGION								U.S. TOTAL
	W	NW	SW	N	S	NE			
<b>DEMOGRAPHIC DATA</b>									
URBAN POPULATION (10 <sup>6</sup> )	20.6	6.3	18.8	41.8	27.7	37.1			152.2
URBAN AREA (10 <sup>3</sup> km <sup>2</sup> )	14.1	7.0	23.6	39.2	37.7	25.7			147.9
<b>TARGET DATA</b>									
<b>NUMBER OF TARGETS (EXCLUDING ICBMS)</b>									
TOTAL YIELD (MT) (EXCLUDING ICBMS)	312	268	513	680	712	545			3030
URBAN AREA (10 <sup>3</sup> km <sup>2</sup> )	156	134	256	340	356	273			1515
	7.9	3.2	12.3	18.0	16.6	15.6			73.7
<b>TARGETED BUILDINGS AND CONTENTS</b>									
FUEL LOAD PER URBAN AREA (g/cm <sup>2</sup> )	1.16	0.95	0.67	1.10	1.05	1.02			0.98
FUEL BURNED (Tg)	91.9	30.8	82.2	182.1	175.0	159.6			721.7
AVERAGE EMISSION FACTOR (g/g)	0.026	0.022	0.024	0.025	0.023	0.025			0.024
SMOKE PRODUCED (Tg)	2.4	0.7	2.0	4.6	4.0	4.0			17.6
<b>BURNABLE VEGETATION</b>									
FUEL LOAD PER URBAN AREA (g/cm <sup>2</sup> )	0.14	0.21	0.20	0.18	0.16	0.20			0.18
FUEL BURNED (Tg)	10.8	6.6	24.5	31.6	26.8	31.3			131.7
AVERAGE EMISSION FACTOR (g/g)	0.010	0.010	0.010	0.010	0.010	0.010			0.010
SMOKE PRODUCED (Tg)	0.1	0.1	0.2	0.3	0.3	0.3			1.3
<b>TARGETED HYDROCARBON STORAGE</b>									
FUEL BURNED (Tg)	30.6	17.7	59.7	65.0	69.5	35.6			278.1
AVERAGE EMISSION FACTOR (g/g)	0.061	0.066	0.065	0.060	0.062	0.048			0.060
SMOKE PRODUCED (Tg)	1.9	1.2	3.9	3.9	4.3	1.7			16.8
<b>TOTAL BURNABLES</b>									
FUEL LOAD PER URBAN AREA (g/cm <sup>2</sup> )	1.69	1.70	1.36	1.55	1.63	1.45			1.54
FUEL BURNED (Tg)	133.3	55.1	166.4	278.7	271.3	226.5			1131.5
AVERAGE EMISSION FACTOR (g/g)	0.033	0.036	0.037	0.032	0.032	0.026			0.032
SMOKE PRODUCED (Tg)	4.4	2.0	6.1	8.8	8.6	6.0			35.7

# SMOKE CLOUD SIMULATIONS

**VARIABLE FIRE RADIUS**  
(Heating rate =  $0.5 \text{ kW/m}^3$ )



**VARIABLE HEATING RATE**  
(Fire radius = 10 km)



## **CONCLUSION**

**FOR A 3000-MT ATTACK ON THE UNITED STATES,**

**JULY SMOKE PRODUCTION = 39 Tg**

**JANUARY SMOKE PRODUCTION = 36 Tg**

*STAN MARTIN & ASSOCIATES*

Consultants in Fire and Explosion Safety

CODE FOR EARLY-TIME FIRE PHENOMENOLOGY

ABSTRACT

A fire-start code to describe urban areas affected by nuclear explosions shall soon be available to implement efforts to evaluate the source term of global effects due to fire. Mechanistically based, insofar as the state of the technical art allows, the code combines a secondary-fire model of recent development with an established primary-fire-start model whose development matured in the company of a program of experimental and analytical advances--still ongoing--that originated in the early 1950s.

The presentation will stress revisions to the primary-fire model that derive from recent experimental insights, and will describe progress toward I/O utilization of existing map-format data bases and map-display software techniques.

# **CODE FOR EARLY-TIME FIRE PHENOMENOLOGY**

---

**Project Status Briefing**

**January 7, 1987**

**for the**

**DEFENSE NUCLEAR AGENCY**

**Contract No. DNA 001-85-C-0194**

**SRI Project PYU 8641**

DATE: 85MAY13

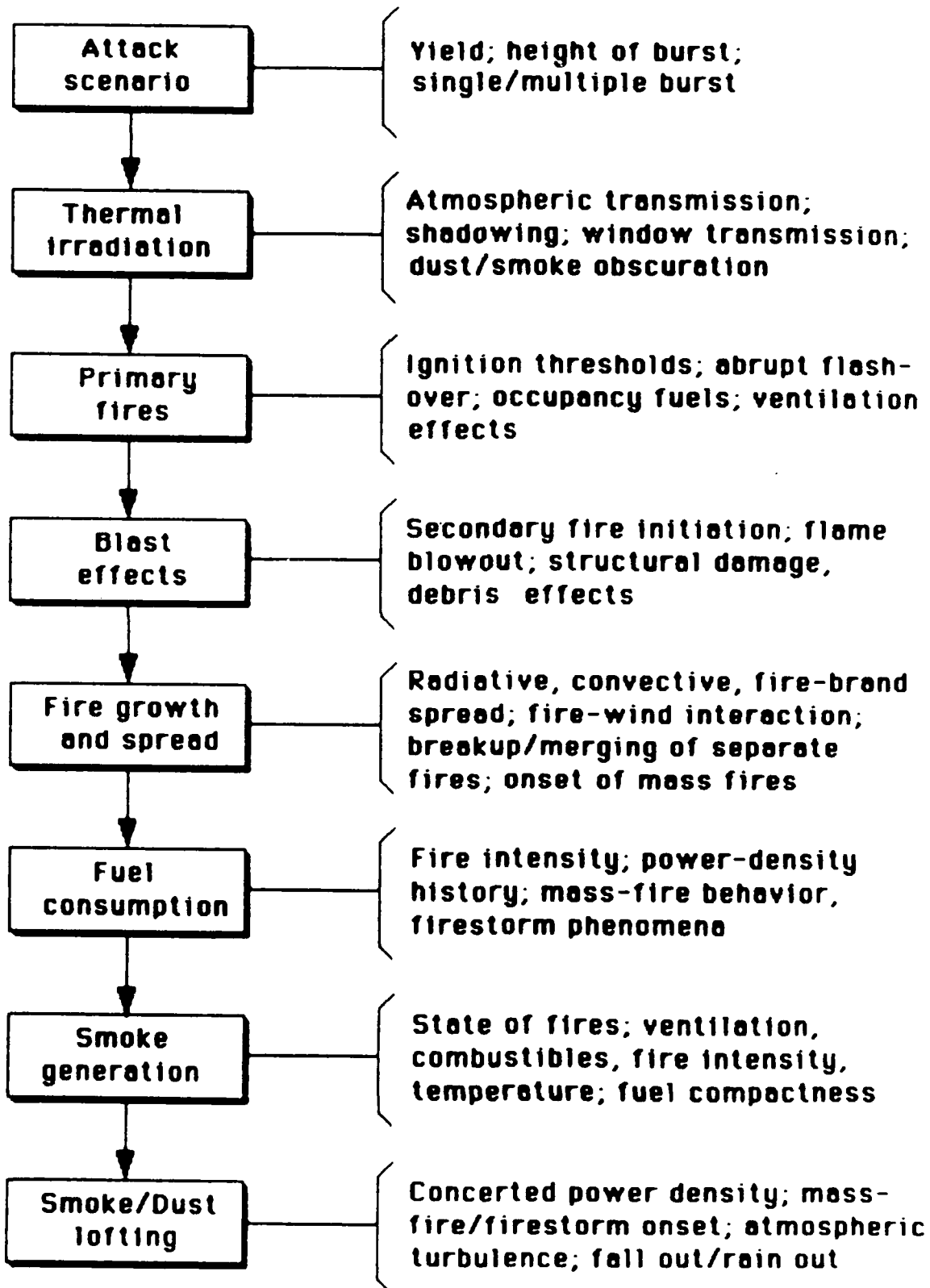
STATEMENT OF WORK

TASK 1: Develop computer codes for implementation of the SRI secondary fire model and for representation of an urban target area. Exercise code to predict secondary ignitions in a realistic urban area affected by one or more weapon detonations.

TASK 2: Update the primary fire model and code and interface it with secondary-fire ignitions code development under Task 1. Exercise the resulting code on selected urban areas, utilizing a weapon detonation scenario chosen in consultation with the DNA CTM.

TASK 3: Investigate modification of ignition distribution codes to account for multiburst effects.

# LARGE URBAN FIRES: A CHAIN OF EVENTS





STAN MARTIN & ASSOC.  
860 Vista Drive  
Redwood City, CA 94062

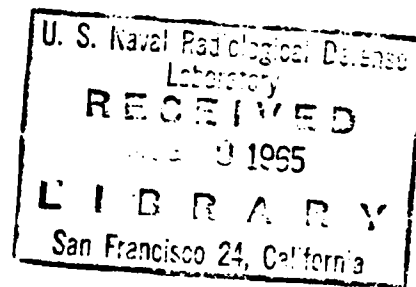
26659  
USNRDL-TR-866  
3 June 1965

c.5

# PRELIMINARY COMPUTER PROGRAM FOR ESTIMATING PRIMARY IGNITION RANGES FOR NUCLEAR WEAPONS

by

S. B. Martin  
S. Holton



**U.S. NAVAL RADIOLOGICAL  
DEFENSE LABORATORY**

**SAN FRANCISCO • CALIFORNIA • 94135**

26659

# EVALUATION OF NUCLEAR WEAPON THERMAL THREAT

August 1966

By:

Floyd I. John  
Thomas O. Passell

SRI Project 4949-360

STANFORD  
RESEARCH  
INSTITUTE



MENLO PARK  
CALIFORNIA

Prepared for:

OFFICE OF CIVIL DEFENSE  
DEPARTMENT OF THE ARMY - OSA  
UNDER WORK UNIT 4311C (1)

Through the:

CIVIL DEFENSE TECHNICAL OFFICE  
STANFORD RESEARCH INSTITUTE  
MENLO PARK, CALIFORNIA

Contract No. OCD-PS-64-201

This report has been reviewed by the Office of Civil Defense and approved for publication.  
This approval does not signify that the contents necessarily reflect the views and policies of  
the Office of Civil Defense.

Distribution of this document is unlimited

Summary  
URS 674-3



DEVELOPMENT AND APPLICATION OF  
AN INTERIM FIRE-BEHAVIOR MODEL

Final Report

April 1963

by

Stanley Martin  
Robert Ramstad  
Clifford Colvin

URS RESEARCH COMPANY  
1811 Trousdale Drive  
Burlingame, California

for

Office of Civil Defense  
Office of the Secretary of the Army  
Washington, D.C. 20310

through

U.S. Naval Radiological Defense Laboratory  
San Francisco, California 94135

Contract No. N00228-67-C-0710  
OCD Work Unit 2538C

OCD REVIEW NOTICE

This report has been reviewed in the Office of Civil Defense and approved for publication. Approval does not signify that the contents necessarily reflect the views and policies of the Office of Civil Defense.

This document has been approved for public release and sale;  
its distribution is unlimited.

IIT RESEARCH INSTITUTE  
Technology Center  
Chicago, Illinois 60616

DEVELOPMENT AND APPLICATION OF A  
COMPLETE FIRE-SPREAD MODEL:  
VOL. I (Development Phase)

Final Report  
June, 1968

by

Arthur N. Takata  
Frederick Salzberg

for  
Office of Civil Defense  
Office of the Secretary of the Army  
Washington, D. C. 20310  
through  
U. S. Naval Radiological Defense Laboratory  
San Francisco, California 94135

Contract No. N0022867C1498  
OCD Work Unit 2538B

OCD REVIEW NOTICE

"This report has been reviewed in the Office of Civil Defense and approved for publication. Approval does not signify that the contents necessarily reflect the views and policies of the Office of Civil Defense."

"This document has been approved for public release and sale. Its distribution is unlimited."

*Annual Report*

*September 1973*

## EVALUATION OF THE NUCLEAR FIRE THREAT TO URBAN AREAS

*By:* STEVE J WIERSMA and STANLEY B MARTIN

*Prepared for:*

DEFENSE CIVIL PREPAREDNESS AGENCY  
THE PENTAGON  
WASHINGTON, D.C. 20301

CONTRACT DAHC20-70-C-0219  
DCPA Work Unit 2561A

SRI Project PYU-8150

This report has been reviewed in the Defense Civil Preparedness Agency and approved for publication. Approval does not signify that the contents necessarily reflect the views and policies of Defense Civil Preparedness Agency.

*Approved by:*

NEVIN K. HIESTER, *Director*  
*Materials Laboratory*

CHARLES J. COOK, *Executive Director*  
*Physical Sciences Division*

DNA 4214T

# THE IMPACT OF FIRES PRODUCED BY TACTICAL NUCLEAR WEAPONS

Science Applications, Inc  
1200 Prospect Drive  
La Jolla, California 92037

December 1976

Topical Report for Period 11 August 1976—15 November 1976

CONTRACT No. DNA 001-76-C-0039

APPROVED FOR PUBLIC RELEASE;  
DISTRIBUTION UNLIMITED.

THIS WORK SPONSORED BY THE DEFENSE NUCLEAR AGENCY  
UNDER RDT&E RMSS CODE B364076464 V99QAXNL12203 H2590D.

Prepared for  
Director  
DEFENSE NUCLEAR AGENCY  
Washington, D. C. 20305

PSR Note 361

**METHODOLOGY FOR PREDICTING URBAN FIRE DAMAGE  
FROM NUCLEAR BURSTS**

R. D. Small  
H. L. Brode

December 1980

Contract No. DNA001-80-C-0065

Sponsored by  
Defense Nuclear Agency  
Washington, D.C. 20305



**PACIFIC-SIERRA RESEARCH CORP.**

1456 Cloverfield Blvd. • Santa Monica, California 90404



IMPACT OF STRUCTURAL DAMAGE ON MASS FIRES

by

Stanley B. Martin

given at a

Conference on

Large Scale Fire Phenomenology

held at:

National Bureau of Standards

Gaithersburg, Maryland

September 10-13, 1984

46

860 Vista Drive *San Diego, California 94062* (415) 365-4969





**EXPERIMENTAL EXTINGUISHMENT  
OF FIRES BY BLAST**

May 1982

Final Report

By: Jana Backovsky  
Stanley Martin  
Robert McKee

Prepared for:

**FEDERAL EMERGENCY MANAGEMENT AGENCY**  
Washington, D.C. 20472

Contract No. EMW-C-0559  
FEMA Work Unit 2564A

SRI Project PYU 3341

Approved for public release. distribution unlimited

FEMA REVIEW NOTICE. This report has been reviewed in the Federal Emergency Management Agency and approved for publication. Approval does not signify that the contents necessarily reflect the views and policies of the Federal Emergency Management Agency.

Approved by:

R. C. Phillips, Director  
Chemical Engineering Laboratory

G. R. Abrahamson  
Vice President  
Physical Sciences Division

DNA-TR-85-357

# MECHANISMS OF BLAST-FIRE INTERACTION

T. C. Goodale  
J. Backovsky  
SRI International  
333 Ravenswood Avenue  
Menlo Park, CA 94025-3434

31 May 1983

Technical Report

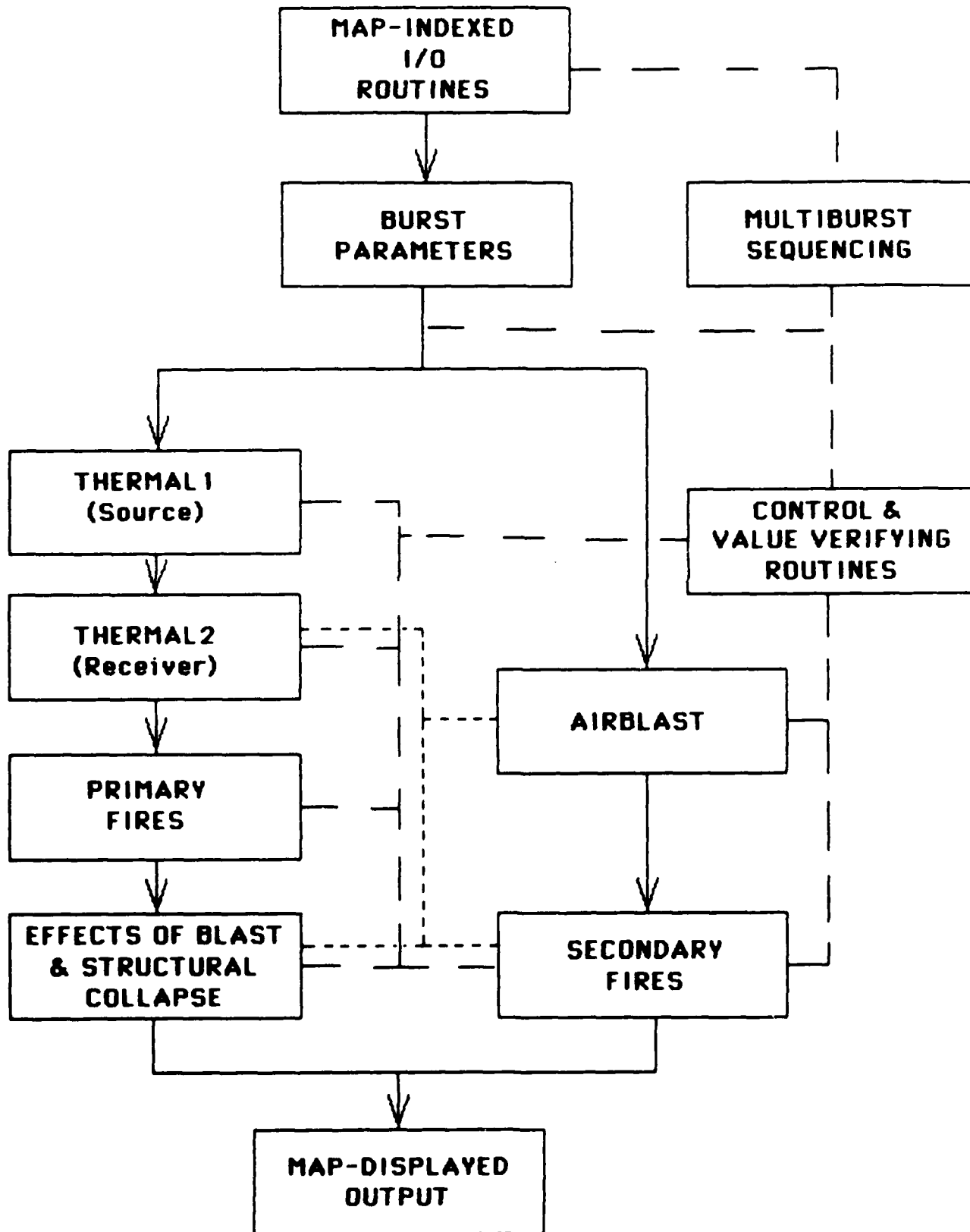
CONTRACT No. DNA 001-81-C-0118

Approved for public release;  
distribution is unlimited.

THIS WORK WAS SPONSORED BY THE DEFENSE NUCLEAR AGENCY  
UNDER RDT&E RMSS CODE B345082466 G54CAXYX00006 H2590D.

Prepared for  
Director  
DEFENSE NUCLEAR AGENCY  
Washington, DC 20305-1000

# ARCHITECTURE OF CODE



CURRENT STATUS

CODE COMPONENTS TO DATE  
(Dec. '86)

I/O Routines: Input map data (unfinished); Input sequence of bursts (map coord's, TOB, yield, HOB); Input <i>corresponding</i> "cloud variables" (visibility, cloud heights, cloud/haze classes, ground albedo)		
CONTROL Subroutines: Increment burst sequence Call THERMAL1 Increment map elements (unfinished) Compute distances & scaled distances Call AIRBLAST; Call THERMAL2 Call FIRES1; Call FIRES2		VALUE VERIFICATION Subroutines: VER1 VER1A VER2 VER3 (etc.)
AIRBLAST Suroutine: Peak OP Pos. -phase duration TOA Dust and its decay over time (unfinished)	THERMAL1 Subroutines: Evaluate fireball dimensions Compare to HOB Select FBGEOM Evaluate cloud "burnout" Select TRANS case Evaluate THPART, TMAX, HOBRAD, TAU	THERMAL2 Subroutines: Evaluate fraction of fireball "seen" Evaluate atm. trans. Evaluate out-of-doors fluence ( $2\pi$ -aureoled, both normal to line of sight and on horizontal plane) Estimate irradiance at airblast TOA
FIRES1 (primary-fire starts) Subroutines: Increment occupancies Evaluate ignition parameters Increment building stories Evaluate <i>local</i> shadowing Estimate window transmission Evaluate direct in-room $G, \mu(G)$ Estimate total thermal deposit'n Assess ENCORE Response Evaluate probs of exposure of room contents Evaluate probs of flashover Estimate freq of room fires/story Evaluate freq of building fires in each occupancy class Assess airblast perturbation		FIRES2 (secondary-fire starts) Subroutines: Increment structural types Evaluate damage levels Increment occupancies Evaluate $\alpha$ -fires Evaluate $\beta$ -fires Combine fire-start estimates
OUTPUT (listings and graphics) Routines: (unfinished)		

(Briefing -- last page)

Large Pool Fires in Nuclear Winter Studies  
N. R. Keltner  
Sandia National Laboratories

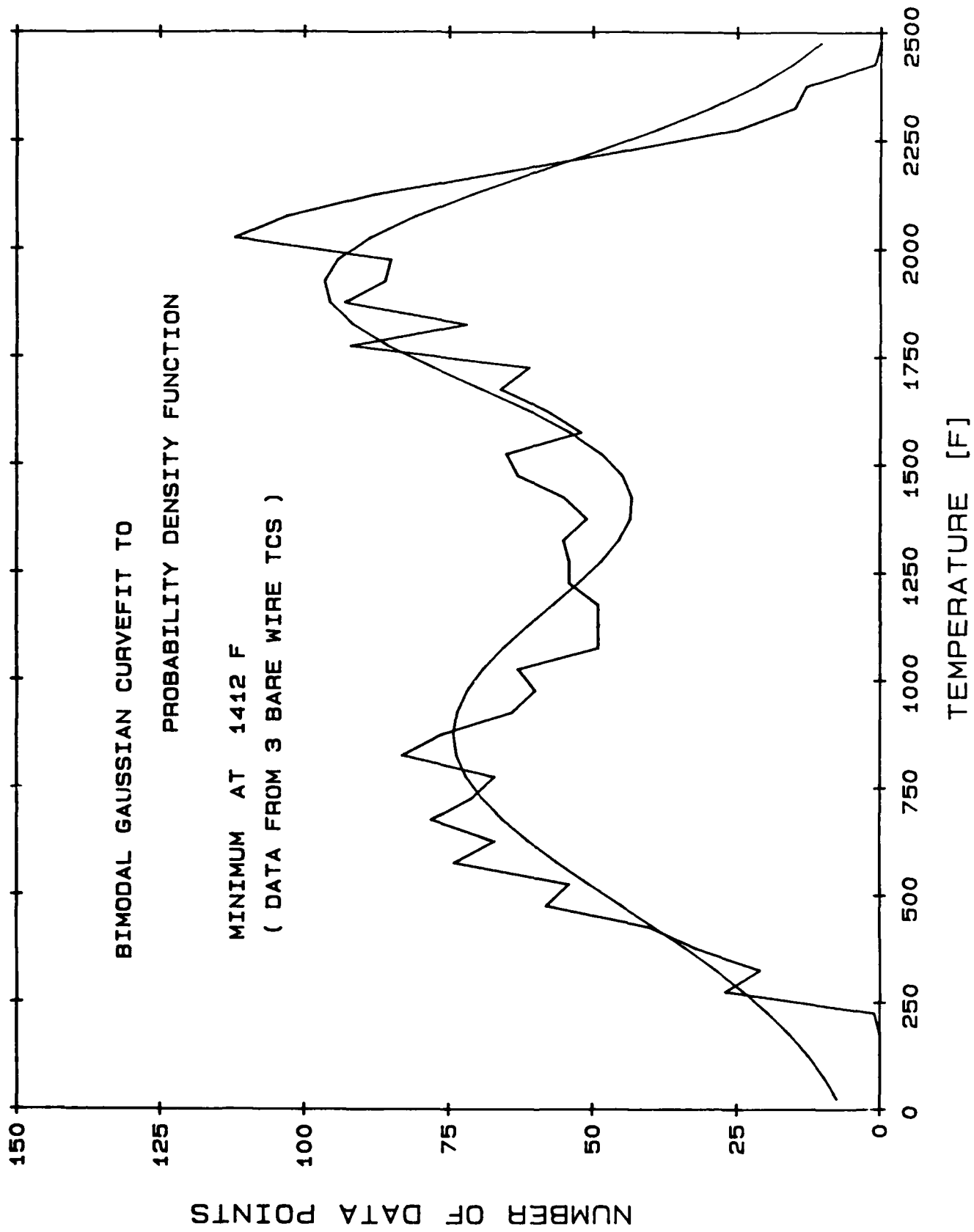
Sandia National Laboratories has conducted two large pool fires in support of our nuclear winter research on the smoke source term. The overall program involves small scale, intermediate scale, and a few large scale tests in an effort to address the questions related to scaling.

In February of 1986, a large fire was conducted as a transportation safety test of a nuclear materials shipping container. An extensive set of diagnostic measurements in the fire and the plume were included. The items of interest to the nuclear winter research community included: 1) temperatures, velocities, and heat fluxes in the lower flame region; 2) fuel consumption and heat flux to the fuel; 3) balloon and aircraft sampling in the plume 400 to 600m above the pool; 4) infrared measurements of the lower flame region; 5) video and movie coverage of the fire and the lower region of the plume; and 6) Lawrence Livermore National Laboratory's flow convergence measurements.

In March of 1987, a second large fire was conducted in support of the nuclear winter program and to provide additional diagnostic measurements. The measurements of interest to the nuclear winter research community included: 1) temperatures and velocities in the lower flame region up to 16m; 2) fuel consumption along with the total and radiative fluxes to the fuel surface; 3) aircraft sampling in the plume; 4) infrared measurements of the lower flame region; 5) video and movie coverage of the fire and the lower region of the plume; and 6) more detailed meteorological data.

The tests involved a JP-4 fire in a 9m x 18m pool. The facility is located in a mountain canyon east of Albuquerque. The fire duration was approximately one half hour.

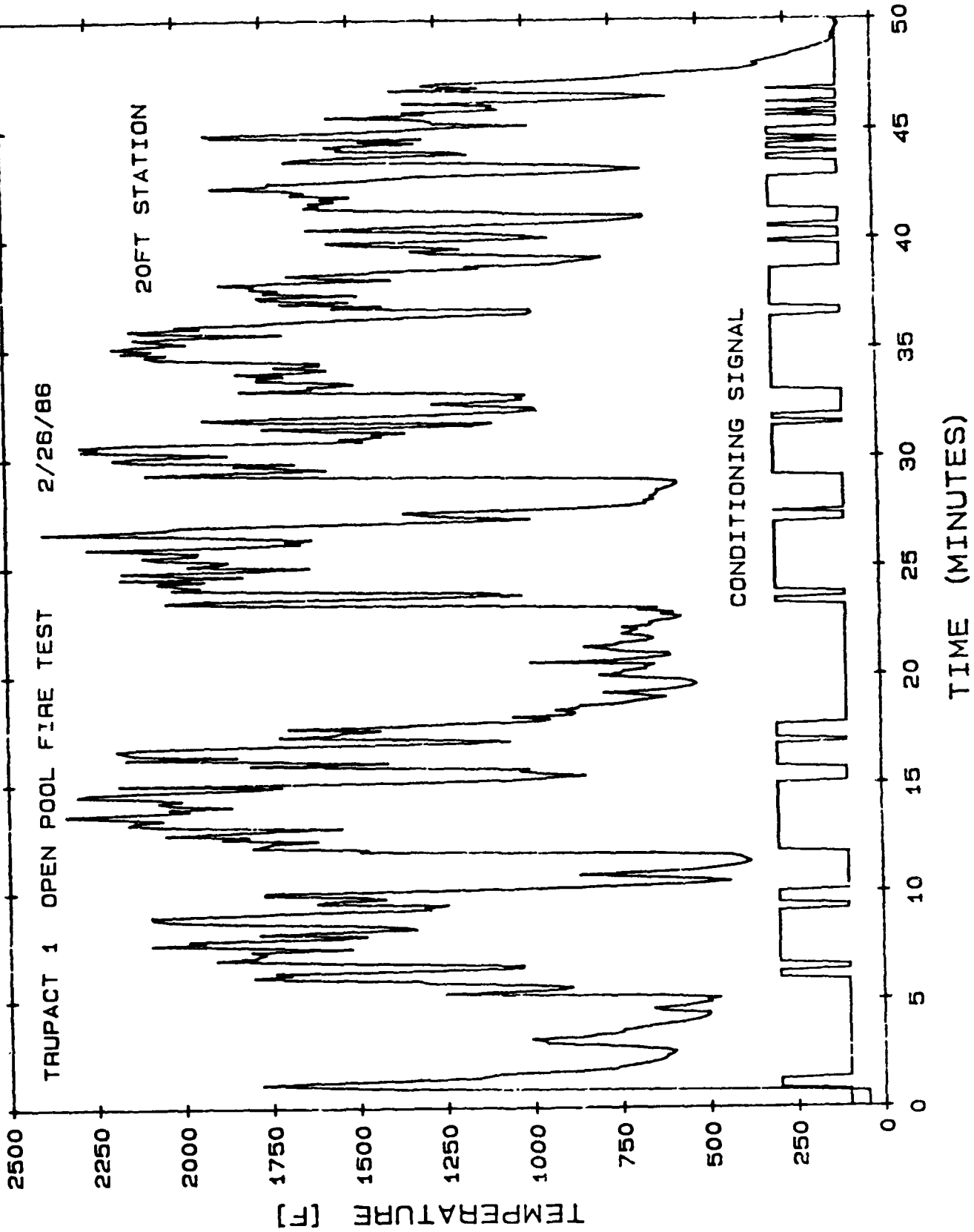
The analysis of the data from these large fires is beginning. We will attempt to integrate the data with that from the smaller fires.

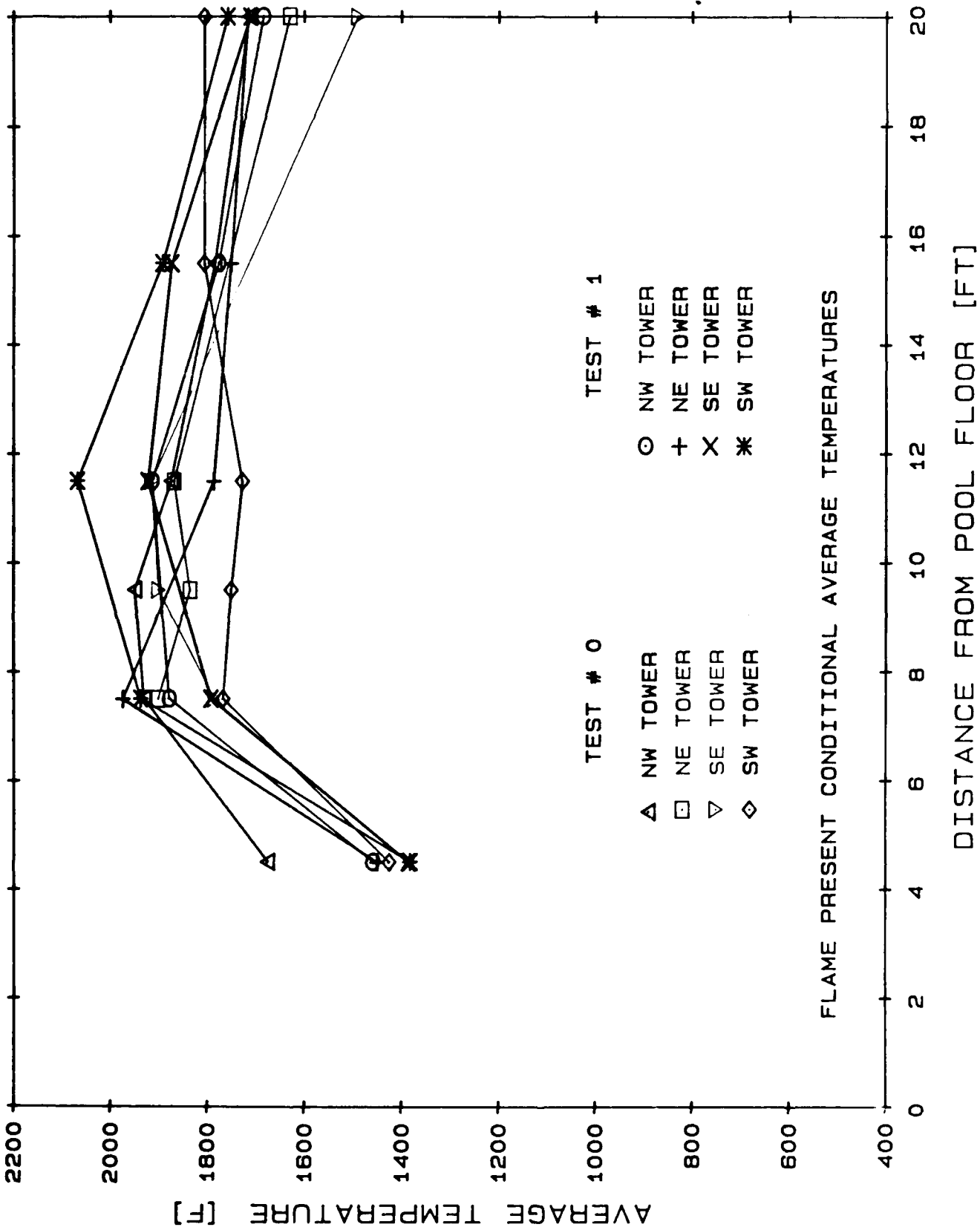


TRUPACT 1 OPEN POOL FIRE TEST

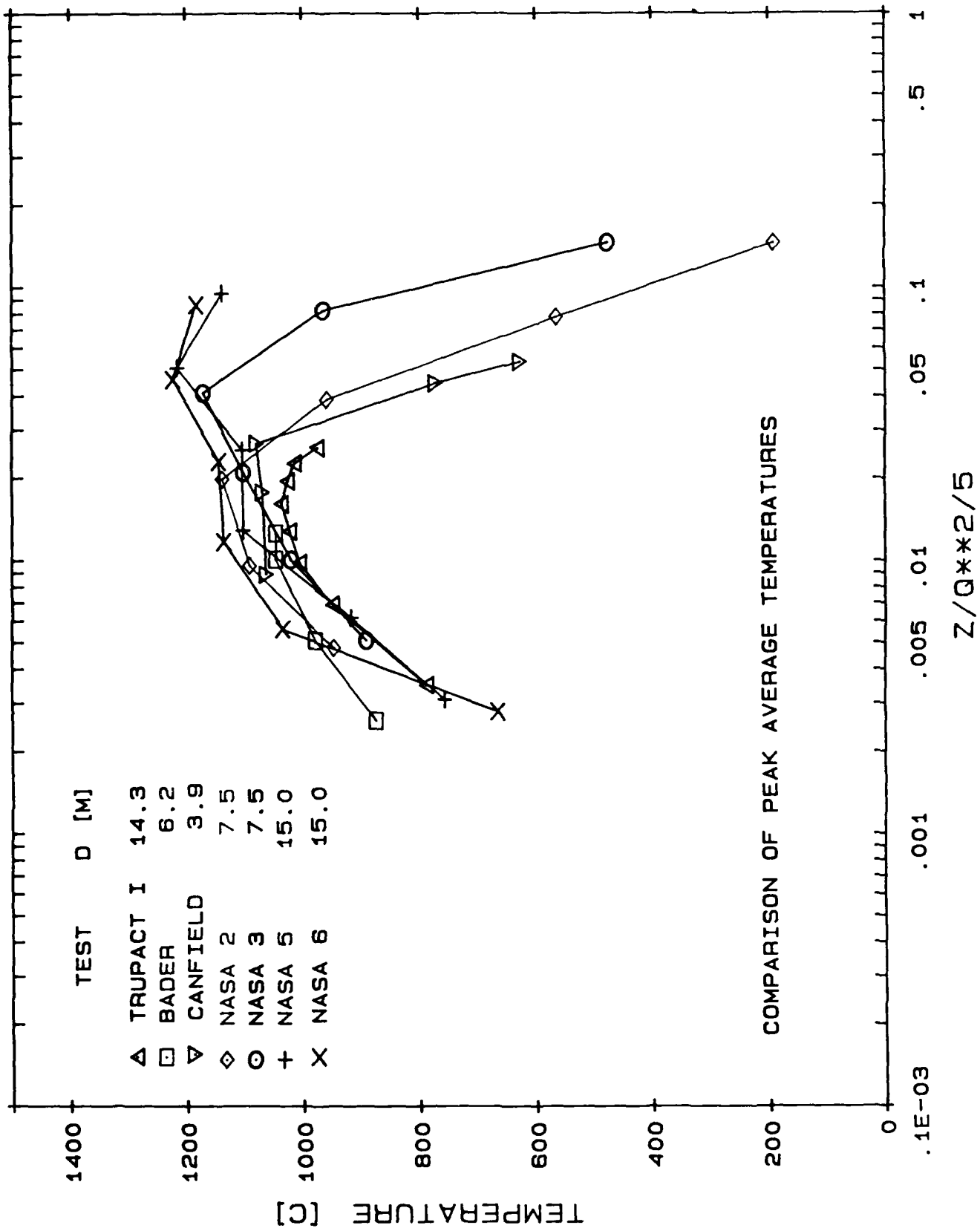
2/26/86

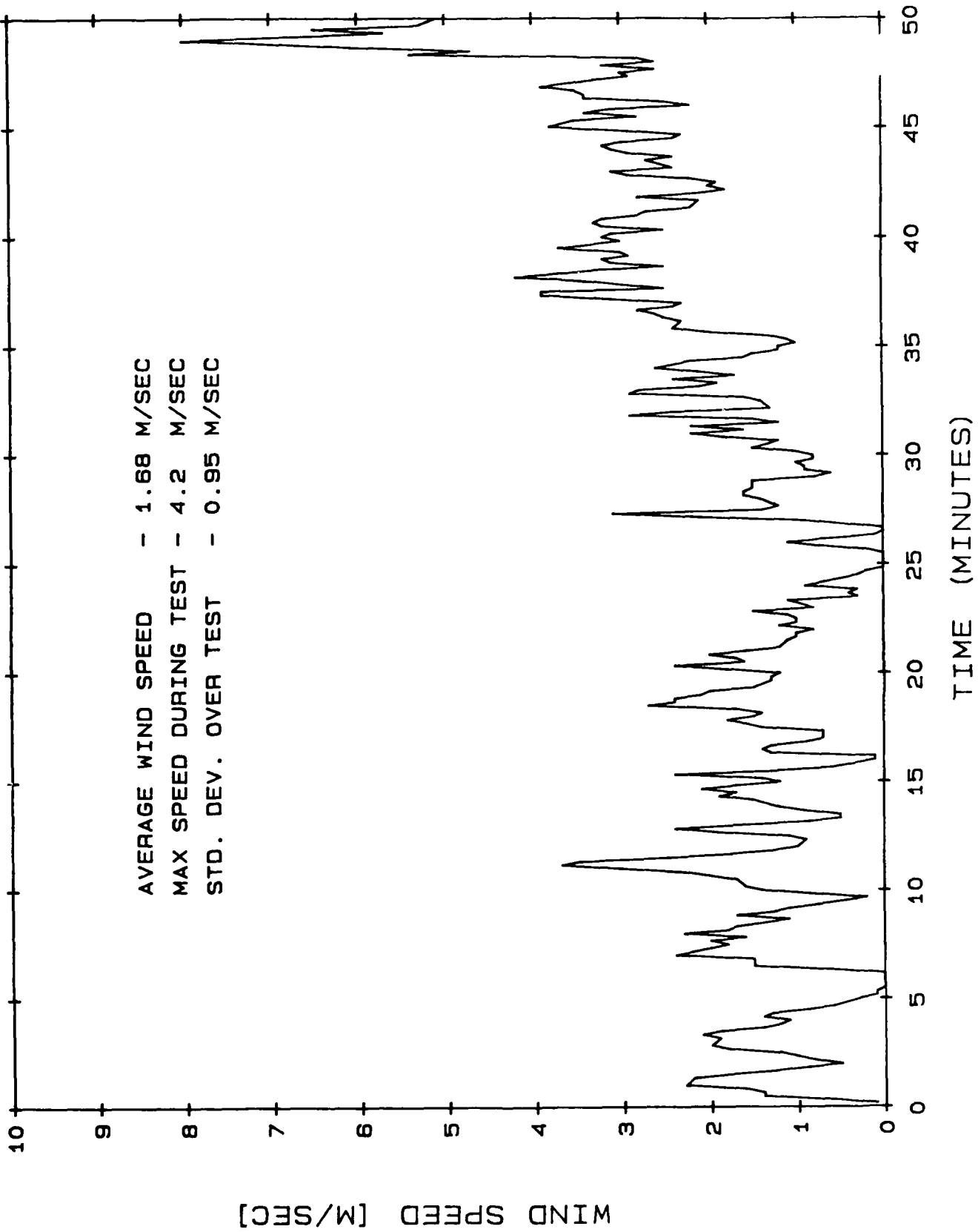
20FT STATION

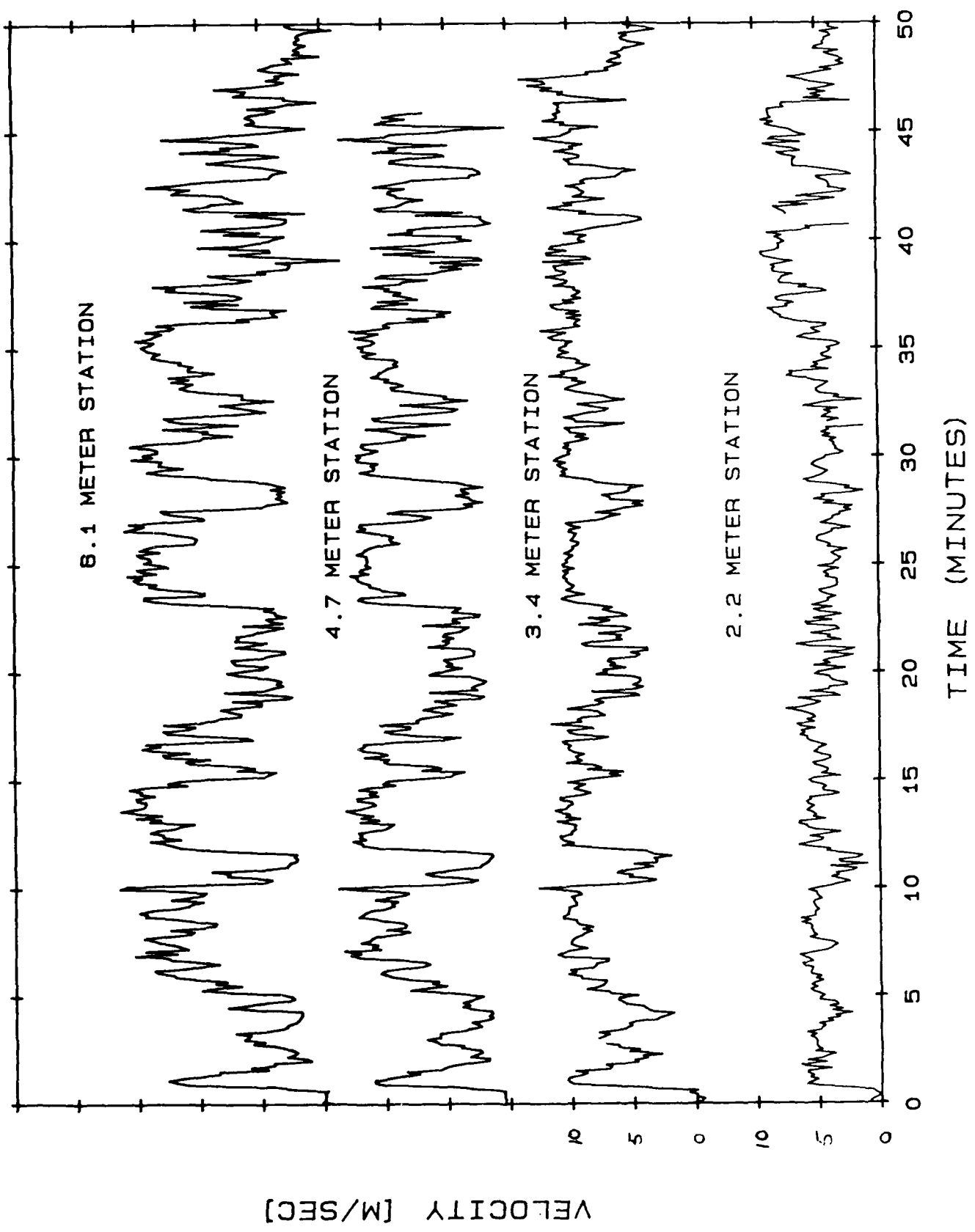




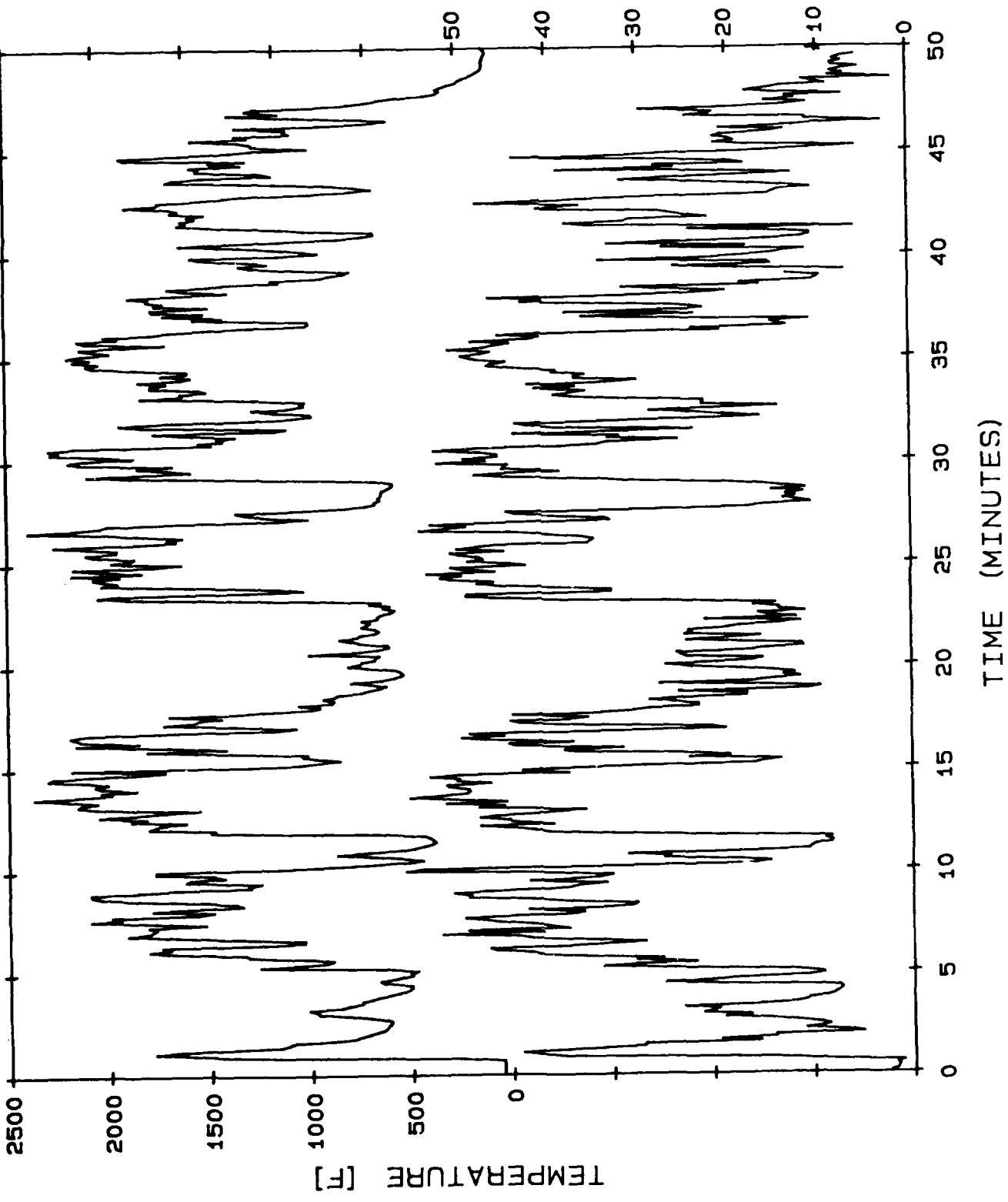


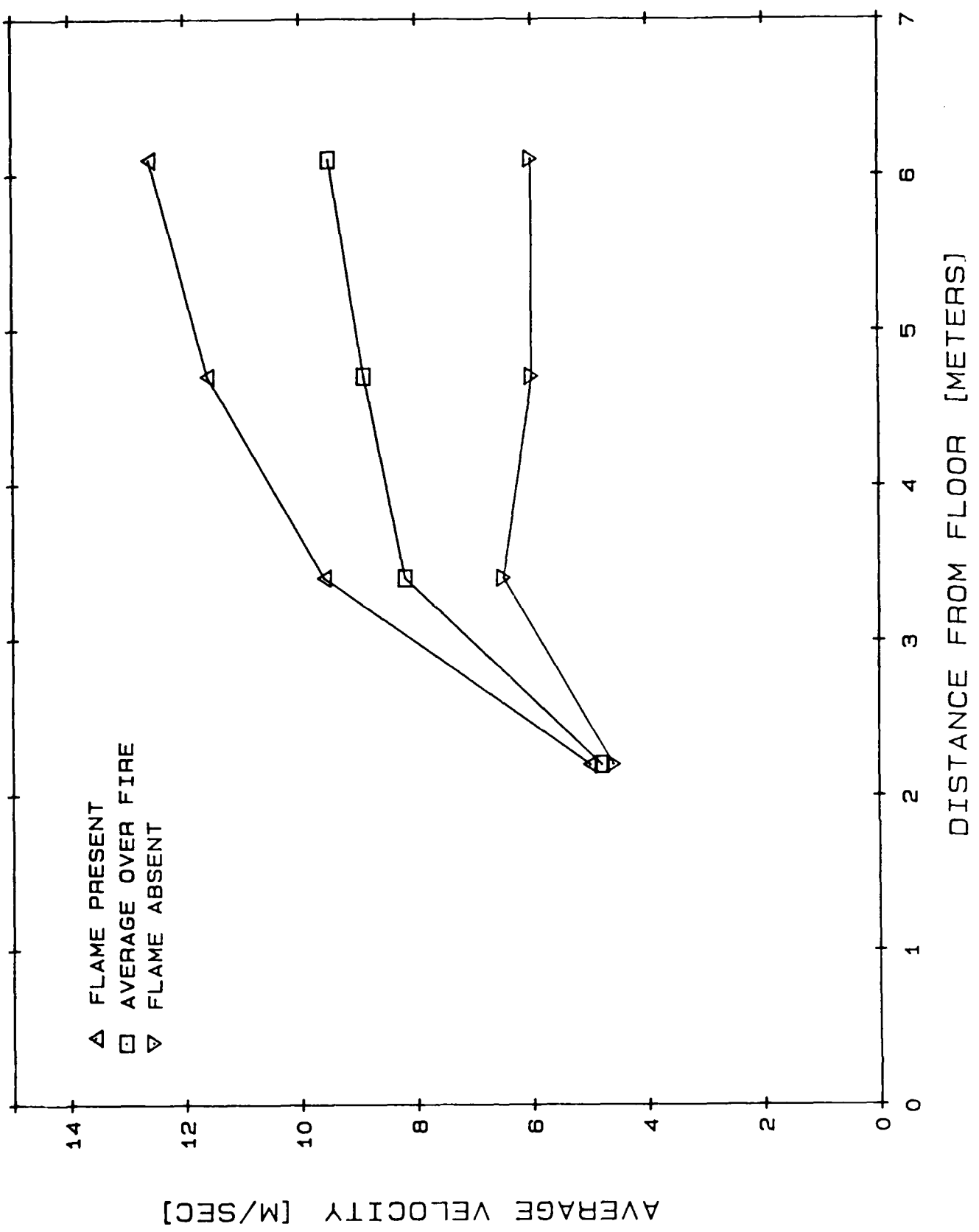






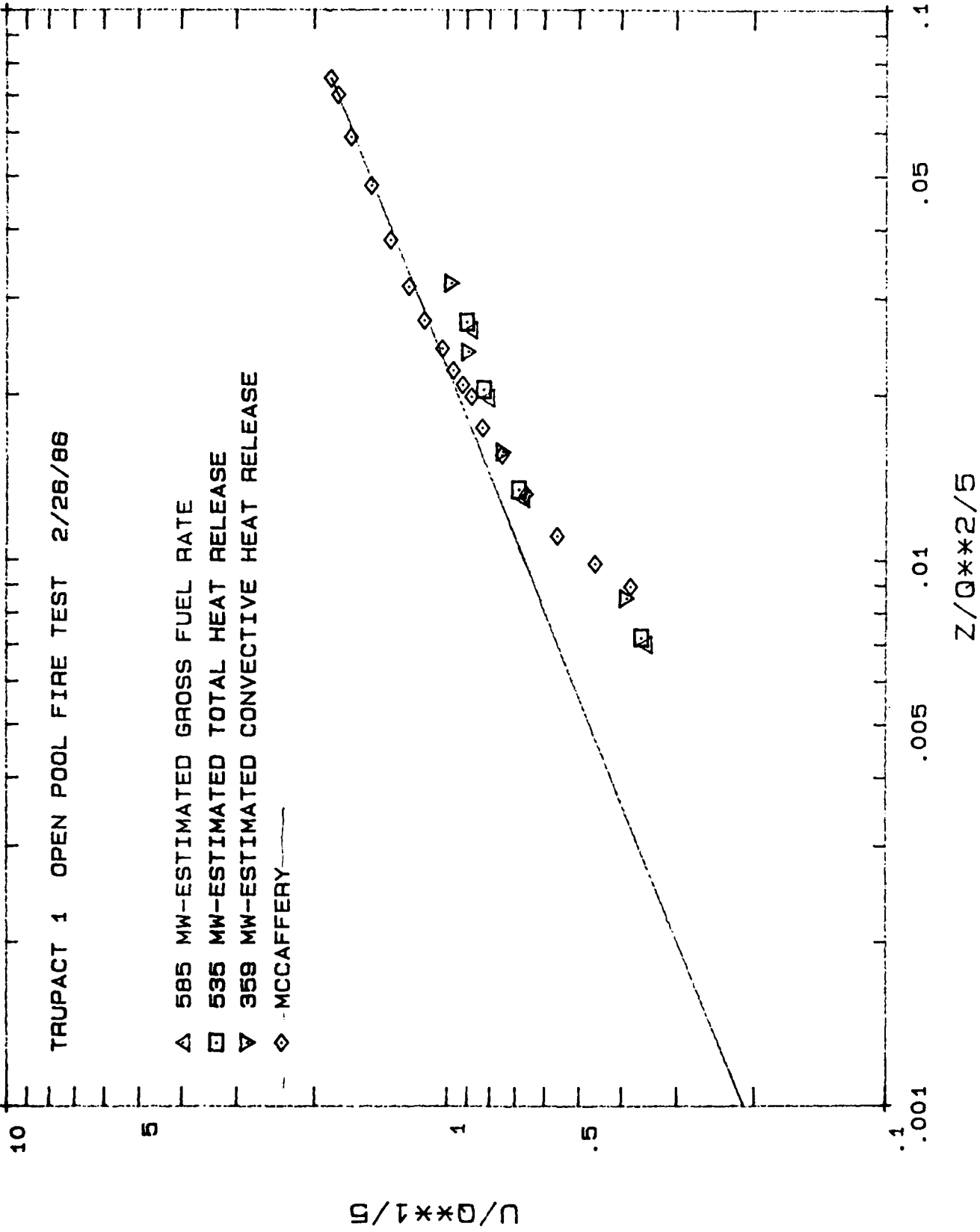
VELOCITY (FT/SEC)

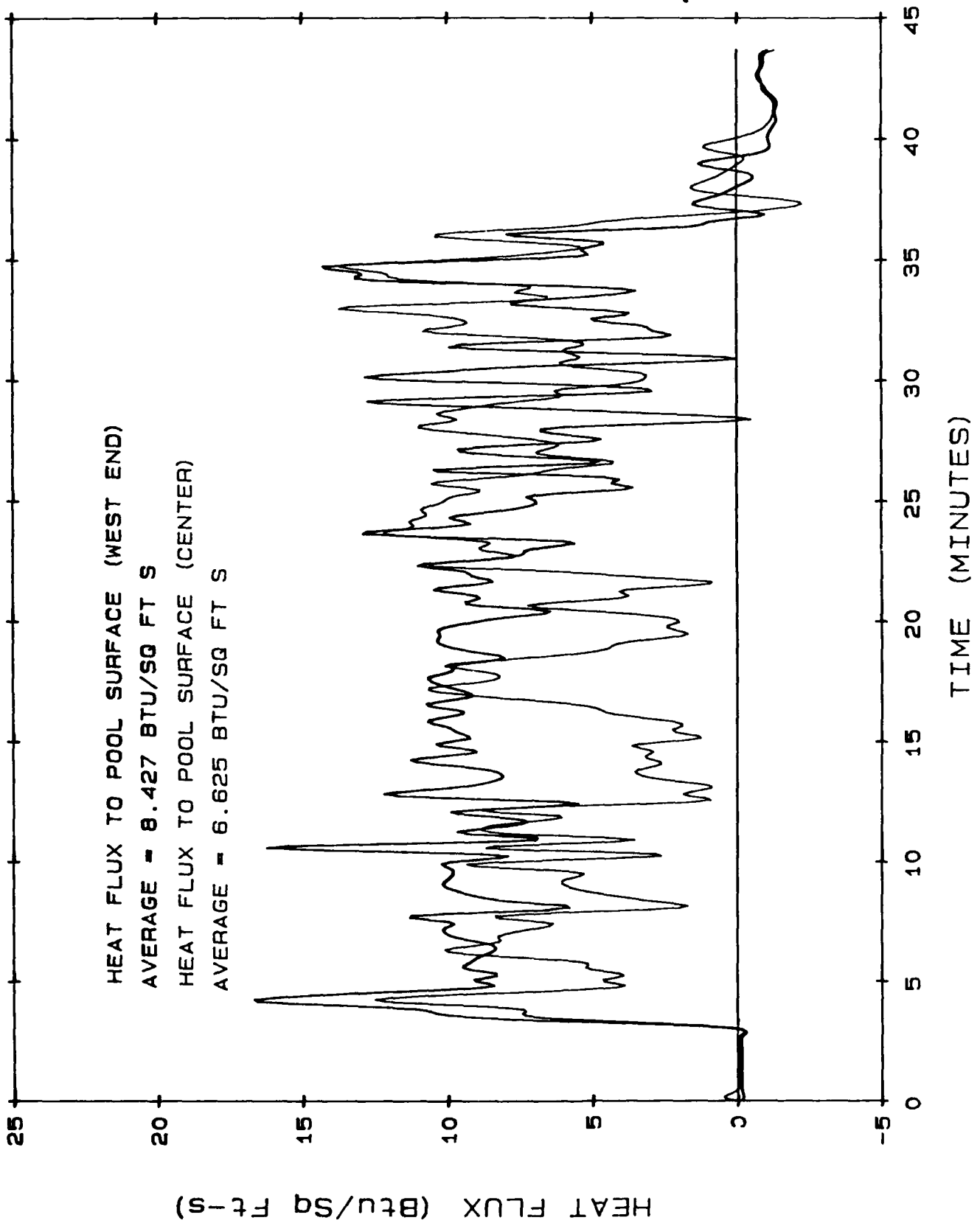




TRUPACT 1 OPEN POOL FIRE TEST 2/26/86

- △ 585 MW-ESTIMATED GROSS FUEL RATE
- 535 MW-ESTIMATED TOTAL HEAT RELEASE
- ▽ 359 MW-ESTIMATED CONVECTIVE HEAT RELEASE
- ◇ MCCAFFERY



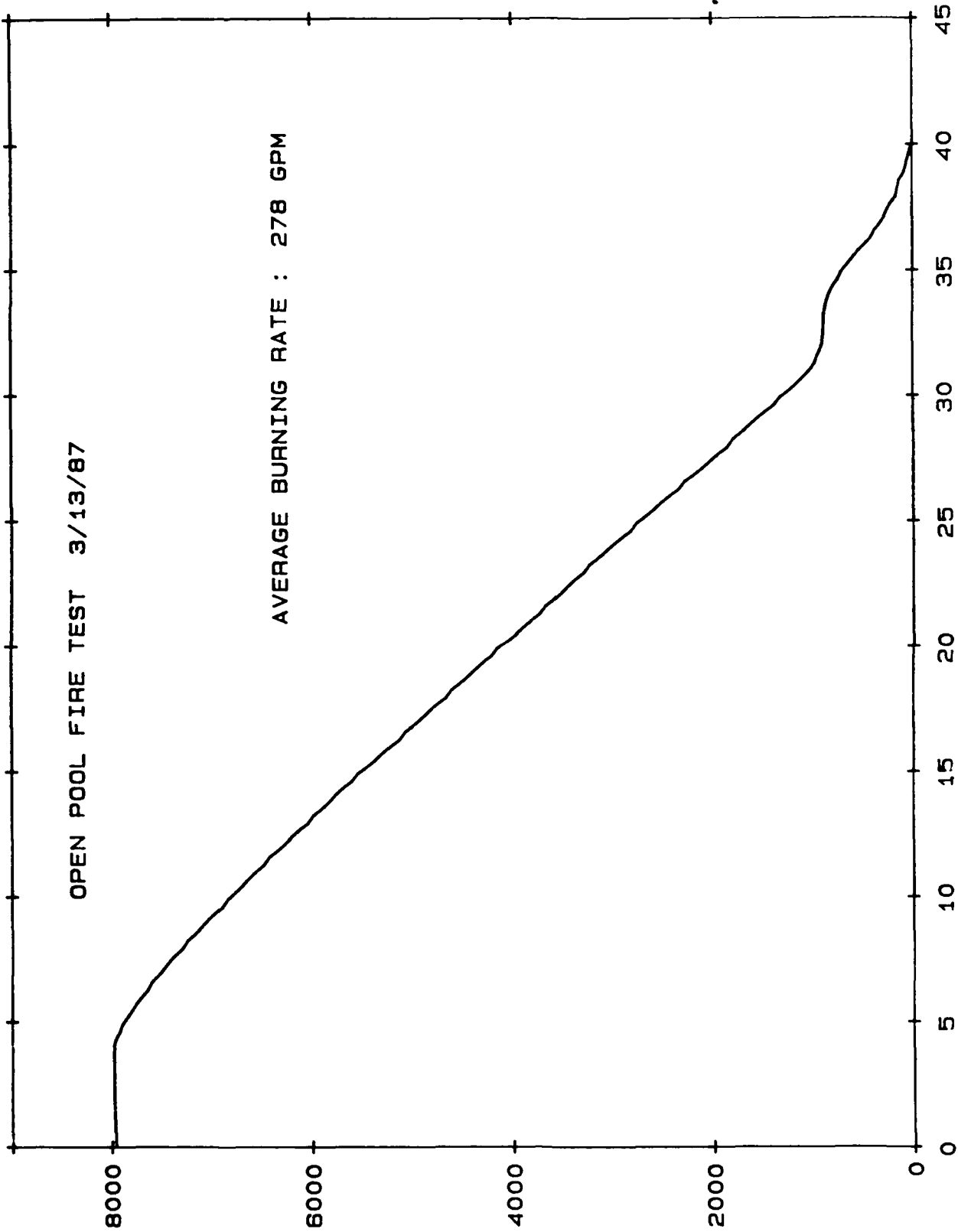


OPEN POOL FIRE TEST 3/13/87

AVERAGE BURNING RATE : 278 GPM

FUEL REMAINING (GALLONS)

TIME (MINUTES)





## LARGE FIRES AND AUSTRALIA

Stephen J. Pyne  
ASU West Campus  
2636 W. Montebello  
Phoenix, AZ 85017  
(602) 246-2802

### Fire Regimes

Australia exhibits an interesting array of fire regimes. The dominating interior is an enormous desert; fires are episodic, keyed to unusually heavy rains that liberate blankets of annual grasses; winter rainfall, not summer drought, dictates fire frequency and scale. An American counterpart would be the low sagebrush desert of the Great Basin. The southern perimeter has a Mediterranean climate, with grasslands, woodlands, forests, and urban centers subjected to annual fires and episodic but frequent conflagrations--probably the worst in the developed world. In an average eucalypt forest, 5 years is adequate for fuels to recover from one hot fire and sustain another. The southeastern quadrant is especially cursed because advancing cold fronts can draft warm, dessicated air out of the interior deserts; and nearly all historic holocausts have occurred under these conditions. Overall the fire scene most resembles Southern California. The northern perimeter belongs in the wet-dry tropics; most of the landscape is burned by lightning and anthropogenic fires each year during "the Dry." The closest American analogue is south Florida. Tasmania features a cool, maritime climate, heavy fuels, and severe fires during drought periods--a pattern similar to that typical of the Pacific Northwest.

Fire seasons advance annually from north to south. In the northern perimeter, fires burn during the winter "Dry." Along the southern perimeter they burn at the end of long Mediterranean-like summers. In Tasmania they are most common at the conclusion of summer and the onset of autumn. In general, January and February are the hottest fire months.

Grass is the primary fuel. Even where it does not dominate, it acts as an interstitial medium to communicate fire to otherwise disparate fuels. True forests (wet and dry sclerophyll, rainforest) comprise only 5-7% of Australian land surface. Woodlands and savannahs contribute an additional 7-8%. Collectively, wooded lands total about 15% of Australia. Nearly all of this is found in mountains or plateaus around the continental perimeter. The wooded lands are overwhelmingly composed of *Eucalyptus*, one of the Earth's great pyrophytes. By North American standards fuel loads are light, though nearly all fuel is available for combustion.

Australia remains a heavily urbanized nation--a collection of city-states. What is marvelous is that eucalypts, humans, and fires all crowd together, most intensely in Australia's "fertile crescent" from Brisbane to Adelaide. In one sense, they are competitive, and give Australia a fire scene without parallel in most of the developed world. In another sense, they have evolved a peculiar symbiosis in which natural and human colonizers have become, to varying extents, pyrophytes.

### Fires and Fire Practices

Fires are ubiquitous. Lightning is important locally. But the controlling source of ignition is human. Aborigines have burned since at least 40,000 yrs BP, and they continue to burn on reserves. Rural fire practices persist in many areas--with "burning off" still typical of many grazing lands, stubble ("straw") burning still characteristic of wheat farming, and sugar cane fired prior to harvesting. The legacy and continued

persistence of this casual, rural burning on a continental scale is a striking feature of the Australian scene--one of the critical features that distinguishes Australian fire history and geography from American.

Foresters adapted rural fire habits, rationalized them, and used the revised practices to underwrite fire protection. Hazard reduction burning is conducted on a prodigious scale, often sustained by aerial ignition. The Australian System of fire protection, unlike the American System, is thus based on fire use, not fire control. At its conceptual core, however, is a truism: that every fire can have its intensity abated and its damages lessened if its fuels have been reduced. The equivalent American truism is that every fire can be controlled if it is attacked soon enough. Both propositions are intrinsically, logically correct, but their real truth lies in the extent to which they can be realized operationally. The American emphasis has accordingly been on rapid detection and initial attack; the Australian, on fuel reduction burning. The rural origins of the Australian System are further accented by its strategy of extensive land management and by its reliance on volunteer fire brigades and private insurance.

Controlled burning is also at the heart of bushfire research. As many as 800 fires were burned in the field to concoct a grassland fire meter. In addition, large landclearing fires have been subjected from time to time to scientific scrutiny, and Australians participated in the mass fire research of the 1960s (Project Euroka). The variety of agricultural fuelbeds (including conifer plantations) provides interesting fuel arrays intermediate between those of wildlands and the laboratory. Australians have also pioneered in investigations about how people and houses interact with a fire--and how they survive.

### Large Fires

Wildfires are endemic. Potentially bad fire seasons occur about every 3 years; bad fires, about every 6-7 years; very bad fires, about every 13 years. Among those that have been studied in detail are the 1939 Victoria fires, the 1961 Western Australian fires, the 1967 Tasmanian fires (which burned into Hobart), the 1977 fires in Victoria, the 1974-75 fires in the interior (perhaps 30% of the Australian landsurface was involved), and the notorious Ash Wednesday fires of 1983, which devastated large portions of South Australia and Victoria, took 77 lives, burned over 2500 houses and over 2 million hectares of forest (5% of all Australian forests). Smaller fires have also been subjected to case study analysis.

In qualitative terms, the fuels, meteorology, and fire dynamics of these conflagrations are well understood and remarkably regular in their behavior. All occur in association with cold fronts. Dry, hot air is drafted out of the interior deserts ahead of the front, which drives fires south and east. After passage "southern buster" winds propel the fires north and east.

Australians prefer to describe the relevant fire behavior dynamics in terms of "acceleration" curves. At the first level, fires "accelerate" through the surface litter and grass. If shrubs or understory are present, then the fire may "accelerate" into another curve. A third "acceleration" involves tree canopies, though crown fires--on the North American model--are rare; rather it appears that large numbers of trees are individually or collectively torched by an intense, rapidly spreading surface fire. The use of an acceleration concept, however, has the added appeal that it relates rate of fire spread to fuel load--which of course is the fundamental argument underscoring the Australian System of fire protection through hazard reduction burning.

From a global effects perspective it should be noted that large fires are

wind-driven, that they involve light fuels (and demand them to achieve large areas), and that Australia is a large island surrounded by even larger oceans.

### Bushfire Research

The modern agenda for bushfire research is largely the creation of the late Alan McArthur, a CSIRO forester, who occupied a pivotal role from the mid-1950s to the mid-1970s. Essentially, the research program was designed to support and rationalize the Australian System of fire protection. It conducted case studies of large, damaging fires to identify typical patterns of behavior. It emphasized the benign nature of controlled burning through research into fire history, ecology, and bushfire smoke. Empirical, experimental, and field-based, it encoded its results into fire-danger rating meters and tables to guide hazard reduction burning. Its culmination came in the mid-1960s with the invention of aerial ignition methods--a deliberate "antipode" to "North American" waterbombing. Overall, Australian research styles more resemble Canadian than American models. (Or to restate the observation, Canadian fire research--in institutional structure and style--resembles Australia except for the distortions due to proximity to the United States.) For a few years, McArthur headed the CSIRO Division of Forest Research until his retirement in 1976.

In recent years, the agenda has confronted two sets of challenges. One is institutional. After McArthur's retirement, the bushfire research program disintegrated. The division mounted Project Aquarius (1982-84) to investigate, at the Prime Minister's insistence, the use of air tankers, a charge that was broadened into traditional subjects as well. This was a targeted project, not a permanent program, however. After Parliamentary hearings subsequent to the Ash Wednesday debacle, a National Bushfire Research Unit was created within CSIRO (1986). Commonwealth-sponsored research is now conducted through NBRU. In addition, the State forestry and rural fire services support some research; the Duntroon Bushfire Research Unit--the mathematics department at the Royal Military College--studies mathematical models of fire; and the Australian Counter-Disaster College includes some bushfire research, primarily from a civil defense perspective. Presently, NBRU is conducting elaborate field experiments to modernize fire danger rating meters and investigate the interaction of ambient and fire-induced winds on line fires. The institutional durability of the NBRU is difficult to determine.

The second set of challenges involve the conceptual foundations of the Australian System and the methodology that has evolved to sustain its research agenda. Broadacre hazard reduction burning is suitable for extensive land management. But Australia is rapidly reconstituting its rural landscape into specialized, intensively managed land units, and it is creating new categories of land use such as faunal conservation areas and the urban bush. A pluralism of fire practices is demanded: the Australian System will have to diversify: it will have to adopt better high-tech methods of suppression in selected areas, and it will have to refine prescriptions for burning to accommodate new, exotic fuels and a fuller spectrum of fire intensities. It cannot expand its empirical field tests to cover the full range of needs. While the Australian fire community has accepted some computerization, it uses the machines to process existing data, not to generate new scenarios or to project fire effects and behaviors into additional (perhaps untestable) environments. They need a robust fire behavior model.

Between Australia, Canada, and America there is a clear complementarity

of needs and abilities. No single country seems capable of mounting a national program of adequate dimensions, but collectively they could pool their concepts and research styles and attack the shared problem of a more universal fire model. Australia would make a commendable partner. Apart from a consortium, they could serve as subcontractors. Research is cost-effective, and Australians have a good sense of proportion, are skilled technicians, and have a sardonic sense of practical consequences.

#### Selected References

Bureau of Meteorology, *Proceedings of Fire Weather Services Conference* (1985)

N.P. Cheney, 1976, "Bushfire Disasters in Australia, 1945-1975," *Australian Forestry* 39(4): 245-268

J.C. Foley, *A Study of Meteorological Conditions Associated with Bush and Grass Fires and Fire Protection Strategy in Australia*. Bureau of Meteorology, Bulletin No. 38 (1947)

A. Malcolm Gill (ed), *Fire and the Australian Biota* (Australian Academy of Science, 1981)

A. Malcolm Gill and I.R. Noble (eds), *Bibliography of Fire Ecology in Australia* (1986)

R.H. Luke and A.G. McArthur, *Bushfires in Australia* (Australian Government Printing Service, 1978)

Stephen J. Pyne, "Large Fires and Australia: An Assessment of Global Effects Research Opportunities" (Report to Defense Nuclear Agency, 1987)

\_\_\_\_\_, "The Burning Bush: A Historical Geography of Australian Fire" (in preparation)

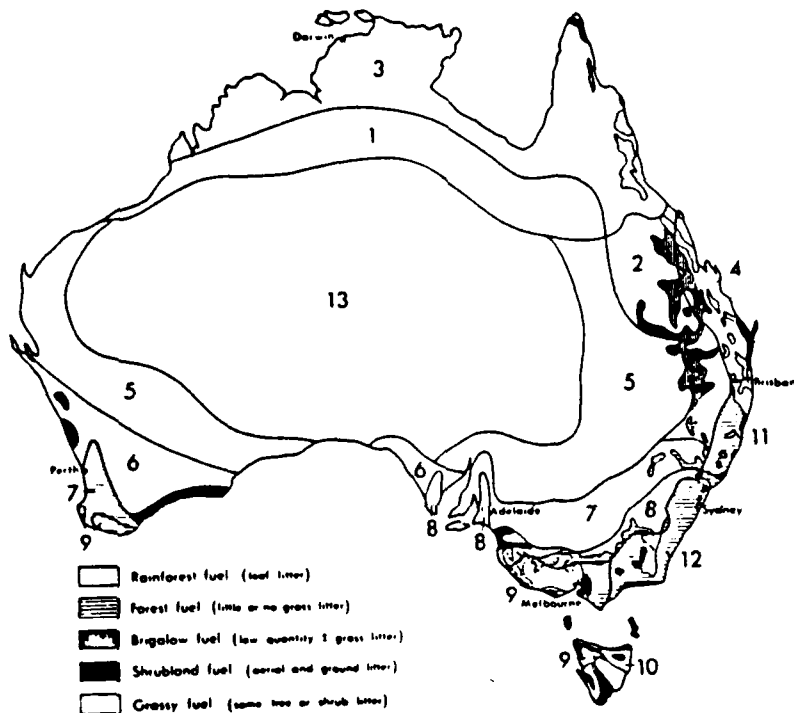


Figure 3.

Fuel types within fire season regions as used to define fuel dynamics regions.

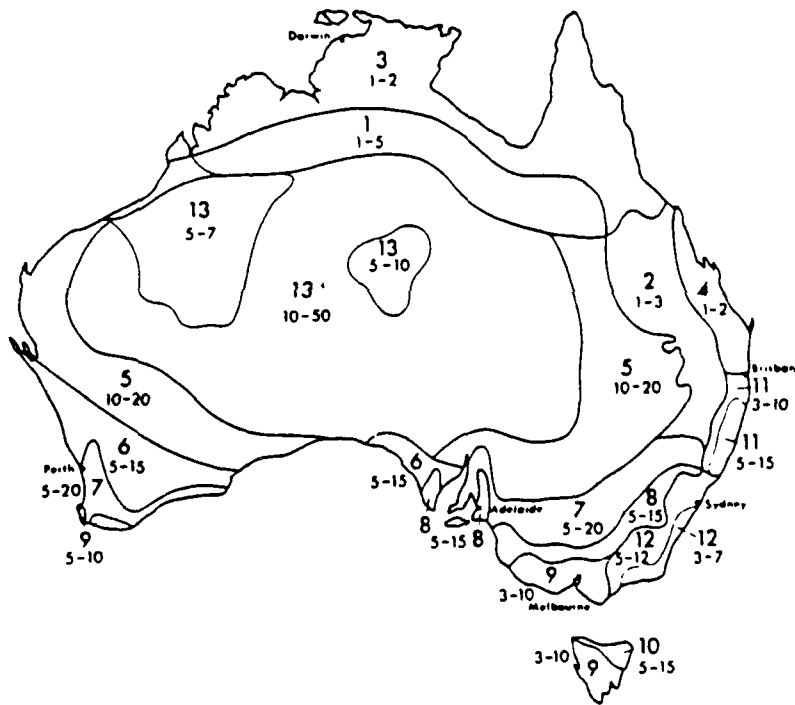


Figure 4.

Fire intervals for fire-season regions expressed as a range in years

## Atmospheric Chemistry Following a Nuclear War

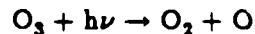
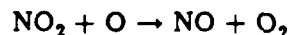
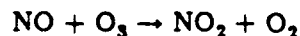
John W. Birks and Sherry L. Stephens

Department of Chemistry and Biochemistry and Cooperative  
Institute for Research in Environmental Sciences (CIRES)  
University of Colorado, Boulder, Colorado 80309

### ABSTRACT

Of the numerous environmental consequences of a major nuclear war, several potential problems of a chemical nature may be identified. These include 1) release of toxic chemicals from explosions and fires in cities and industry, 2) acidic precipitation, 3) accumulation of biogenic emissions in the darkened atmosphere, 4) oxidant formation following the return of sunlight, and 5) ozone depletion in the stratosphere. Stratospheric ozone depletion is expected to be the most serious effect, as it would result in a large increase in the flux of biologically damaging UV-B radiation to the earth's surface and would persist for several years.

There are several mechanisms by which the stratospheric ozone layer is expected to be disturbed. It has been known since 1972 that oxides of nitrogen produced in the nuclear fireballs and lofted into the stratosphere would cause ozone depletion via the catalytic cycle:



Estimates based on this mechanism alone suggest ozone depletion in the northern hemisphere of ~15-50% depending on the scenario. In recent years these estimates have declined as a result of reductions in the yields of the nuclear warheads deployed. Larger warheads deposit  $\text{NO}_2$  at higher altitudes where the catalytic destruction is more rapid and the residence time is longer.

Climate model calculations which are made interactive with nuclear war smoke show, in general, that smoke-laden air will be raised in temperature by as much as 90-100 K and will be lofted into the stratosphere. This could have several large and deleterious effects on the ozone column. These include 1) increasing the temperature of the stratosphere speeds up the rate limiting steps of ozone destruction cycles, 2) at elevated temperatures ozone reacts directly with soot particles, and 3) displacement of ozone at low altitudes to higher altitudes where ozone may come into photochemical equilibrium will result in ozone destruction. No model calculations that allow substantial interaction between dynamical and chemical perturbations have yet been carried out. Qualitatively, one can say that the potential exists for much larger than 50% ozone depletion developing within the first few months following a nuclear war. Depletions greater than 90% cannot be ruled out. Destruction of most of the earth's ozone layer could well be the most damaging effect of a nuclear war on the earth's ecosystems -- possibly much more damaging than the climatic effects ("nuclear winter") currently being addressed.

## INTRODUCTION

A number of possible perturbations in atmospheric chemistry following a nuclear war have been identified. Among these are:

- Toxic Chemical Releases
- Stratospheric Ozone Depletion
- Acidic Precipitation
- Suppression of Atmospheric Oxidants and  
Accumulation of Biogenic Emissions
- Oxidant Formation Following Soot Removal

Of these, stratospheric ozone depletion is expected to have the greatest impact on the biosphere in the aftermath of a major nuclear war. Release of toxic chemicals to the environment would be a major threat to life on a local basis. This report will briefly summarize the presentation made at the April 7-9, 1987 DNA Global Effects Meeting in Santa Barbara, California. More details may be found in two recent articles by the authors (Stephens and Birks, 1985; Birks and Stephens, 1986).

## TOXIC CHEMICALS

A multitude of toxic pollutants would be produced by the pyrolysis and partial combustion of chemicals, petroleum products, and synthetic materials stored in strategic, industrial, and urban areas. Military installations, chemical plants, gas and oil refineries, and urban centers contain vast stores of chemical and petroleum products, as well as the waste products of defense, industry, and everyday life. The tragedy of Bhopal, India, where a ruptured storage tank released methyl isocyanate, killing 5,000 people (*Chemical and Engineering News*, 1985), is a small indication of what might happen following a

nuclear war as the result of explosions near chemical plants. Clearly, in heavily industrialized regions, the kill area for nuclear explosions could be greatly increased by the release of poisonous chemicals into the atmosphere.

The U.S. production of organic chemicals is approximately  $200 \text{ Tg yr}^{-1}$ . The end use of the majority of these compounds is polymeric materials such as synthetic rubber, plastics, foam insulation and fabrics. The U.S. production in 1981 of several major organic and inorganic compounds are summarized in Tables I-III.

The first question that one might logically ask is whether chemical releases would make the atmosphere lethally toxic on a global or semiglobal basis. The answer is no. Even if an entire year's production of organic chemicals were released and uniformly mixed over half of the Northern Hemisphere, the total concentration of all chemical compounds would still be a factor of 5,000 times less than the 50 percent lethal dose ( $LD_{50}$ ) of hydrogen cyanide gas. Of course, most compounds are not nearly so toxic, and probably only 5-10 percent of a year's chemical production is in storage at any one time. Similarly, it is also true that toxic compounds such as carbon monoxide, acrolein, hydrogen chloride, hydrogen cyanide, sulfur dioxide, phosgene, and the oxides of nitrogen produced in urban fires could be significant causes of death only on a local basis. Thus, for the long-term survivors of a nuclear war, the concern with chemical releases would be similar to concern with delayed radioactive fallout, namely, mutations leading to cancers and birth defects. In this sense, we might, by analogy, refer to these effects as arising from the "chemical fallout."

Many of the most important mutagens would be nonvolatile compounds and would be associated with particulate matter. Once deposited in the soil and water, many of these compounds would be very stable against chemical and biological degradation and would be subject to bioaccumulation in a manner similar to that of radioactive isotopes. For example, a community of people becomes very concerned when a transformer fire, such as that



which occurred in Binghamton, New York, in 1981, contaminates an office building with soot rich in polychlorinated biphenyls (PCBs) (Schechter, 1983). However, as the result of a nuclear war, of the order of 1,000 cities of the Earth would become the equivalent of toxic waste dumps. Also, the lofting of toxic smoke to high altitudes by the fire storms and by the buoyancy of solar heating would ensure that these pyrotoxins would be distributed on a global basis as well.

Any realistic estimates of the levels of chemical contamination is virtually impossible, as thousands of different toxic chemicals would be produced, and the amounts of each would be highly dependent on the types and mixtures of fuels burned (e.g., wood, petroleum, asphalt, rubber, plastics) and the fire conditions, especially temperature and oxygen concentration. Estimates of biological effects are further complicated by the wide range of toxicities exhibited by the various isomers of a given parent compound. Dioxin, for example, is expected to be an important carcinogen introduced into the environment by the pyrolysis of PCBs and possibly other chlorine-containing compounds. However, the highly toxic compound 2,3,7,8-tetracholorodibenzodioxin (TCDD) is only one of 75 dioxin isomers. As seen in Table IV, the relative toxicities of these various isomers span more than six orders of magnitude.

While cognizant of the enormity of the uncertainty, it is still useful to make some calculations, however crude, of the increased cancer incidence that might be expected on a semiglobal basis for a few carcinogens, so that the seriousness of chemical contamination can be compared with that of radioactive contamination. To do this for PCBs and TCDD, we have used the average emission factors found in the Binghamton fire (Schechter, 1983). Assume that approximately 30% of the current world supply of PCBs (0.3 Tg) are affected by nuclear fires, that the soot emission factor is 10% (by weight), and that 15% of the soot is composed of unburned PCBs. If the soot is uniformly deposited over one-half the

Northern Hemisphere and mixed to a depth of 10 cm of soil, the level of contamination is calculated to be 0.1 ppb. If the soot fell on one-fourth of the world's freshwater lakes and if it were evenly mixed throughout the water, it would result in a calculated concentration of 0.09 parts per trillion. In Binghamton, the TCDD isomer of dioxin averaged only about 3.5 ppm of the soot, so that the calculated TCDD concentrations in soil and water would still be lower by more than four orders of magnitude. Using the same assumptions, the average concentrations of TCDD over half of the Northern Hemisphere are calculated to be 0.008 parts per trillion in soil and 0.01 parts per quadrillion in freshwater.

Using present recommendations for estimating cancer risk for those persons drinking water and eating fish from freshwater lakes (U.S. Environmental Protection Agency, 1984), the added risk of contracting cancer is calculated to be  $10^{-8}$  (one chance in  $10^8$ ) for PCBs and  $10^{-5}$  (one chance in  $10^5$ ) for the dioxin isomer TCDD.

Considering that the present risk of contracting cancer in one's lifetime is about 1 in 5, these numbers are not all that frightening. Of course, many other chemical carcinogens, about which we know even less, would be produced in the nuclear war fires. Nevertheless, these calculations strongly suggest that on a global or semiglobal basis, chemical carcinogenesis may not be a serious impact of nuclear war. We must realize, however, that the deposition of chemical toxins would be highly irregular. It is possible that a large fraction of the smoke aerosol would be removed within the first few hours by precipitation. For example, an estimated 5 to 10 cm of rain fell in Hiroshima 1 to 3 hours after the blast. Dust, rubble, and large amounts of radioactive matter were concentrated in the "black rain" that spread over a wide area, creating many secondary victims (The Committee for the Compilation of Materials on Damage Caused by the Atomic Bombs in Hiroshima and Nagasaki, 1981). It has been suggested that under certain meteorological conditions, convective clouds would form over burning cities and effectively scrub out much of the smoke.

This remains one of the hotly debated criticisms of the nuclear winter theory. For the lack of any better evidence, it has been common to assume that about half of the smoke produced by nuclear fires would be promptly removed (e.g., NRC, 1985).

The 1985 NRC study assumed that a total urban area of 250,000 km<sup>2</sup> would burn. Assuming that half of the toxic smoke was promptly deposited in an area of 1,000,000 km<sup>2</sup>, then the average concentrations of chemical toxins in soil and water within these urban areas would be higher than the concentrations calculated above by a factor of about 60. Of course, these areas would contain a large fraction of the surviving population. Cancer risks from chemical carcinogens would likewise be increased. The average cancer risk because of TCDD, for example, would be increased to  $7 \times 10^{-4}$  for those persons remaining in the urban areas. This is approximately equivalent to the cancer risk associated with receiving 7 rads of ionizing radiation. Considering that this calculation is based on one specific isomer of one class of compounds and that many other carcinogens would be produced by the nuclear fires, it is not unreasonable to suspect that long-term human and biological effects of the chemical fallout would be as important, if not more important, than that of radioactive fallout.

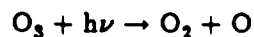
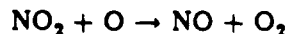
We have also identified asbestos as an important atmospheric contaminant following a nuclear war, and similar calculations show that the breathing of asbestos fibers during the first month following a nuclear war could result in about 10% as many cancers as are caused by exposure to ionizing radiation. It is important to note that it is possible that synergisms between chemical exposure and radiation exposure could also increase the cancer incidence following a nuclear war, but insufficient data exist to evaluate such effects.

An important difference between chemical toxins and radionuclides is that radioactive contamination is readily detected by relatively inexpensive Geiger counters, while the

TCDD isomer of dioxin, like many other toxic compounds, can only be determined by use of a gas chromatograph coupled to a mass spectrometer; the cost of the latter instruments are in the range \$100,000 to \$500,000. Thus, an important characteristic of chemical fallout is that living environments, food, and water could not be readily surveyed in order to determine their safety.

### STRATOSPHERIC OZONE DEPLETION

It was first recognized in 1972 that oxides of nitrogen produced in nuclear fireballs and lofted to the stratosphere could result in severe ozone depletion (Foley and Ruderman, 1973; Johnston, Whitten and Birks, 1973). Ozone in the stratosphere serves as a protective shield against ultraviolet radiation. Particularly significant to the biosphere is radiation in the ultraviolet-B (UV-B) region (280-320 nm). This finding that nuclear explosions could affect stratospheric ozone came as a result of the earlier recognition by Crutzen (1971) and Johnston (1971) that oxides of nitrogen serve as catalysts for ozone destruction according to the now well-known cycle of reactions:



Note that nitric oxide (NO) initiates the ozone destruction process, but is regenerated, so that no net consumption of nitrogen oxides occurs. In fact, each NO molecule introduced into the stratosphere can destroy about  $10^{12}$  to  $10^{13}$  ozone molecules during its residence time in the stratosphere (Brasseur and Solomon, 1984).

In 1975 the National Academy of Sciences evaluated the effect of a 10,000-Mt nuclear war on the stratospheric ozone shield (NRC, 1975). That study estimated a 30 to 70

percent reduction in the ozone column over the Northern Hemisphere and a 20 to 40 percent depletion for the Southern Hemisphere. Since that time, there has been a modernization of the nuclear arsenals; large multimegaton warheads have been replaced by more numerous warheads (due to MIRVing - Multiple, Independently Targetable, Reentry Vehicles), typically having individual yields of 100 to 500 kt. The degree of ozone depletion is highly dependent on the height of injection of oxides of nitrogen, and these smaller warheads produce bomb clouds that stabilize at much lower altitudes. The altitude distributions of the nitric oxide injections for the two scenarios evaluated in the recent 1985 study of the National Academy of Sciences (NRC, 1985) are superimposed on the ozone concentration profile in Figure 1. The NRC baseline scenario utilizes exactly half of the strategic warheads of every type in both the U.S. and Soviet arsenals, except for any weapons with yields greater than 1.5 Mt. For this scenario oxides of nitrogen would only be carried to altitudes as high as 18 km, and the maximal ozone depletion in the Northern Hemisphere, as shown in Figure 2, would be 17%. An excursion scenario considers that an additional 100 bombs with yields of 20 Mt each would be detonated. (At the time of the NAS report there were thought to be 300 such warheads in the Soviet arsenal.) For this scenario, oxides of nitrogen would reach an altitude of 37 km, and the maximal ozone depletion would be 43%. Note that the maximum in ozone depletion would occur after a period of 8 to 12 months, and it would take on the order of 10 years for ozone concentrations to return to normal. Thus, once most of the smoke and dust was removed from the atmosphere and sunlight began to break through, the biosphere would not receive normal sunlight but, rather, sunlight highly enriched in ultraviolet radiation.

No estimates of ozone depletion have yet taken into account the large perturbations in atmospheric physics and chemistry resulting from the dust and smoke emissions. The recent findings by climate modelers that the solar-heated smoke clouds would rise into the

stratosphere is extremely important in this regard. Figure 3 compares the distributions of smoke aerosol at day 20 following the start of a nuclear war in July for a passive tracer and interactive smoke (Malone, 1986). The introduction of smoke aerosol to the stratosphere would be expected to add to ozone destruction in at least three ways: 1) The absorption of solar radiation by the smoke particles would heat the stratosphere and increase the rates of reactions that catalyze ozone destruction (e.g., the  $\text{NO} + \text{O}_3$  reaction given in the cycle above). The effects of the stratospheric heating on the ozone column recently was investigated (Vupputuri, 1986). The results using the TTAPS soot injection scenario (Turco *et al.*, 1983) are shown in Figure 4. The model is a 1-D radiative convective model coupled to a 1-D chemical model of the stratosphere. Note that temperatures in the stratosphere increase by as much as 110 K. The effect of the temperature increase (Smoke Injection Only case) is an ozone depletion of  $\sim 28\%$ . When the catalytic effect of the bomb-produced oxides of nitrogen are included, the maximum ozone column depletion increases to about 50%. 2) The lofting of air to higher altitudes would transport ozone to regions where its lifetime is very short. This effect is not treated in the Vupputuri calculations of Figure 4. As seen in Figure 1, the maximum ozone concentration occurs at about 22 km. At higher altitudes ozone concentrations are in a photochemical steady state at much lower concentrations. As seen in Figure 5 (Brasseur and Solomon, 1984), the lifetime of "odd oxygen" is of the order of one year at 20 km, but only one hour at 50 km. Displacement of ozone from low altitudes where it is photochemically "safe" to high altitudes where it quickly comes into photochemical equilibrium would result in a large depletion in stratospheric ozone. 3) Reaction of ozone at particle surfaces would directly destroy ozone (Stephens, Rossi and Golden, 1986). One can calculate that 10 Tg of soot would titrate only about 8% of the mid-latitude ozone column. Thus the  $\text{O}_3 + \text{soot}$  reaction is probably more important as a potential means of removing soot from the stratosphere where its

effects on surface climate is otherwise prolonged by the long residence time characteristic of the stratosphere.

It is of utmost importance that future calculations of stratospheric ozone depletion be made interactive with 3-D climate calculations of the changes in the atmospheric physics and dynamics resulting from the large injections of dust and smoke. In the absence of such calculations, one can only say that the ozone depletions are likely to be much greater than 50% and that a depletion of the ozone column at mid-latitudes by as much as 90% or more cannot be ruled out at present. The ecological impacts of such a large depletion of the ozone column could be much greater than surface temperature changes.

#### CHANGES IN TROPOSPHERIC CHEMISTRY

Other effects of a major nuclear war on the chemistry of the atmosphere include the formation of acidic rain, the accumulation of reduced organic compounds such as sulfur compounds during the period of darkness, and the formation of photochemical smog once the smoke and dust particles have been removed from the atmosphere. Crutzen and Birks (1982) estimated that the average pH of the rain during the first month following a major nuclear war would be approximately 3. This is, of course, dependent on the assumptions made concerning the quantities of strong acids produced in the fires and subsequent atmospheric photochemistry. The amount of acid would need to be increased by an order of magnitude in order to lower the estimate to pH 2, however. Acid rain having pH values in this range frequently occurs in the industrial parts of the world without acute damage to the environment. Certainly, the acid rain would be one more insult to ecosystems already stressed by ionizing radiation, darkness, cold temperatures, and enhanced levels of ultraviolet radiation. Still, it may be considered one of the more minor effects of a nuclear war.

Decreased light levels in the troposphere and high particulate loadings would result in much reduced levels of oxidants such as  $O_3$ , OH,  $HO_2$  and  $H_2O_2$ . These oxidants, besides being a health hazard at high concentrations, serve the function of reacting with reduced compounds emitted by the biosphere to form compounds readily removed by rain. Depending on the degree of patchiness of the smoke and dust clouds, reduced compounds such as hydrogen sulfide, dimethyl sulfide, and methyl mercaptan could accumulate to much higher than normal concentrations. These compounds are not likely to pose a serious health hazard, but would contribute to a general "stench" of the air. Following the return of sunlight they would be oxidized to sulfuric acid and removed by rain. A period of intense photochemical smog with high oxidant levels could accompany the return of sunlight, but this is highly dependent on the lifetime of the oxides of nitrogen in the darkened atmosphere. Our box model calculations indicate that  $NO_x$  would be primarily partitioned as nitric oxide, which is not effectively removed by rain, and would be available for catalyzing photochemical smog formation once the sunlight returned.



REFERENCES

- Birks, J.W. and Stephens, S.L. (1986) "Possible Toxic Environments Following a Nuclear War," in *The Medical Implications of Nuclear War*, Institute of Medicine, National Academy of Sciences, National Academy Press: Washington, D.C.
- Brasseur, G. and Solomon, S. (1984) p. 208 in *Aeronomy of the Middle Atmosphere*, Reidel: Dordrecht, Netherlands.
- Chemical and Engineering News* (1985) February 11, p. 14.
- Crutzen, P.J. (1971) "Ozone Production Rate in an Oxygen-Hydrogen Oxide Atmosphere," *J. Geophys. Res.* **76**, 7311.
- Crutzen, P.J. and Birks, J.W. (1982) "The Atmosphere After a Nuclear War: Twilight at Noon," *Ambio* **11**, 115-125.
- The Committee for the Compilation of Materials on Damage Caused by the Atomic Bombs in Hiroshima and Nagasaki (1981) pp. 87-101 in E. Ishikawa and D.L. Swain (trans.), *Hiroshima and Nagasaki: The Physical, Medical, and Social Effects of the Atomic Bombings*, Basic Books: New York.
- Foley, H.M. and Ruderman, M.A. (1973) "Stratospheric NO Production from Past Nuclear Explosions," *J. Geophys. Res.* **78**, 4441.
- Johnston, H.S. (1971) "Reduction of Stratospheric Ozone by Nitrogen Oxide Catalysts from Supersonic Transport Exhaust," *Science* **173**, 517.
- Johnston, H.S., Whitten, G.Z., and Birks, J.W. (1973) "Effects of Nuclear Explosions on Stratospheric Nitric Oxide and Ozone," *J. Geophys. Res.* **78**, 6107-35.
- Malone, R.C. (1986) "Atmospheric Perturbations of Large-Scale Nuclear War," in *The Medical Implications of Nuclear War*, Institute of Medicine, National Academy of Sciences, National Academy Press, Washington, D.C.
- National Research Council (1975) *Long-Term Worldwide Effects of Multiple Nuclear Weapon Detonations*, National Academy Press: Washington, D.C.
- National Research Council (1985) *The Effects on the Atmosphere of a Major Nuclear Exchange*, National Academy Press: Washington, D.C.
- Schechter, A. (1983) "Contamination of an Office Building in Binghamton, New York by PCBs, Dioxins, Furans and Biphenyls after an Electrical Panel and Electrical

Transformer Incident," *Chemosphere* 12 669-80.

Stephens, S.L. and Birks, J.W. (1985) "After Nuclear War: Perturbations in Atmospheric Chemistry," *BioScience* 35, 558-62.

Stephens, S.L., Rossi, M.J. and Golden, D.M. (1986) *Int. J. Chem. Kin.* 18, 1133-49.

Turco, R.P., Toon, O.B., Ackerman, T.P., Pollack, J.B. and Sagan, C. (1983) "Nuclear Winter: Global Consequences of Multiple Nuclear Explosions," *Science* 222, 1283-92.

U.S. Environmental Protection Agency (1984) *Intermedia Priority Pollutant Guidance Documents. PCBs*, March.

Vupputuri, R.K.R. (1985) "The Effect of Ozone Photochemistry on Atmospheric and Surface Temperature Changes Due to Large Atmospheric Injections of Smoke and  $\text{NO}_x$  by a Large-Scale Nuclear War," *Atmos. Env.* 20, 665-79.

Table I

U.S. Production of Selected Polymer Starting Materials in 1981

Compound	Quantity, Tg
Ethylene	13.1
Propylene	6.4
Butadiene	1.4
Vinyl chloride	3.1
Ethylene dichloride	4.1
Formaldehyde	2.7
Ethylene oxide	2.3
Total of these compounds	33.1

Table II

U.S. Production of Selected Aromatic Compounds in 1981

Compound	Quantity, Tg
Benzene	4.5
Toluene	4.7
Ethylbenzene	3.6
Cumene	1.5
Styrene	3.0
Xylenes	4.6
Phenol	1.2
Total of these compounds	23.1

Table III

U.S. Production of Inorganic Chemicals in 1981

Compound	Quantity, Tg
H <sub>2</sub> SO <sub>4</sub>	36.9
H <sub>3</sub> PO <sub>4</sub>	9.0
HNO <sub>3</sub>	8.2
HCl	2.2
NH <sub>3</sub>	17.3
Cl <sub>2</sub>	9.6
Total of these compounds	83.2

Table IV  
Acute Lethality of Dioxin Isomers

Isomeric Cl position	LD <sub>50</sub> (μg/kg) in Guinea Pigs
2,8	300,000
2,3,7	29,000
2,3,7,8	1
1,2,3,7,8	3
1,2,4,7,8	1,125
1,2,3,4,7,8	73
1,2,3,6,7,8	100
1,2,3,7,8,9	100
1,2,3,4,6,7,8	7,200
1,2,3,4,6,7,8,9	4,000,000 <sup>a</sup>

<sup>a</sup>In mice.

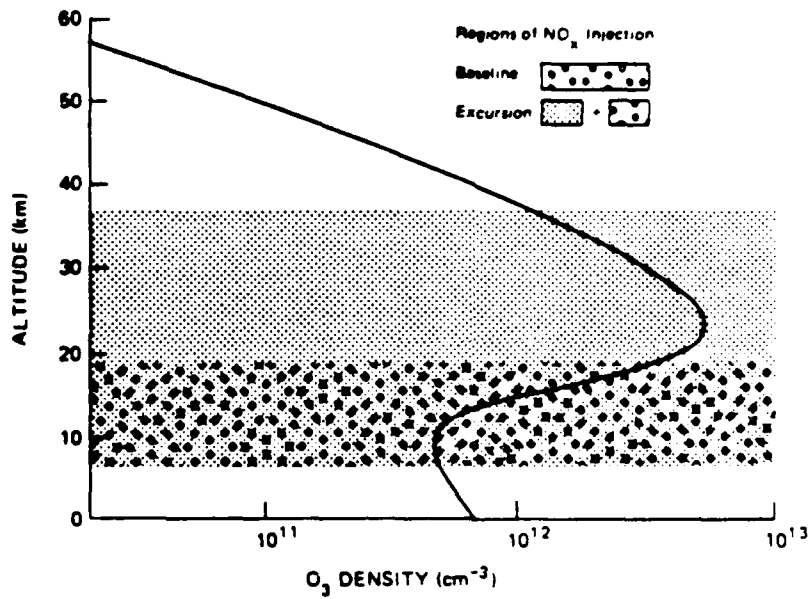


Fig. 1. Altitudes of injection of oxides of nitrogen for the NRC baseline and excursion nuclear war scenarios. The normal ozone concentration profile is also shown by the solid line (NRC, 1985).

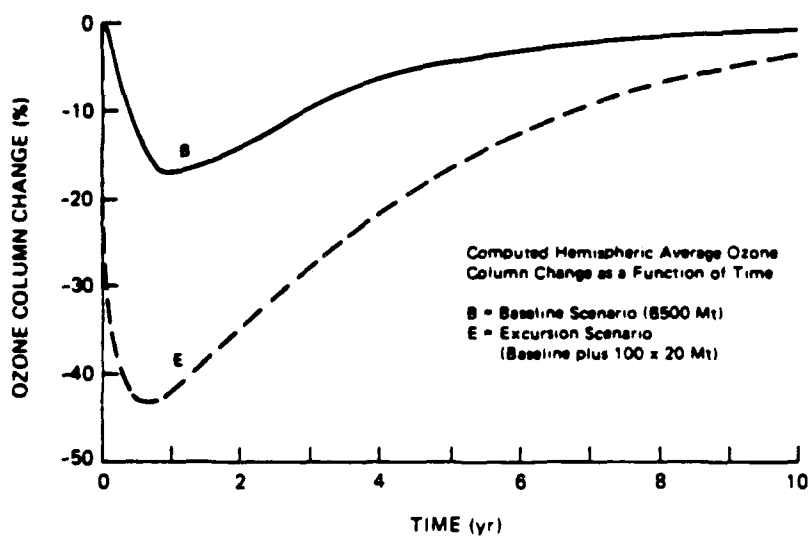


Fig. 2. Ozone depletion as a function of time following a nuclear war for the NRC baseline and excursion scenarios (NRC, 1985).

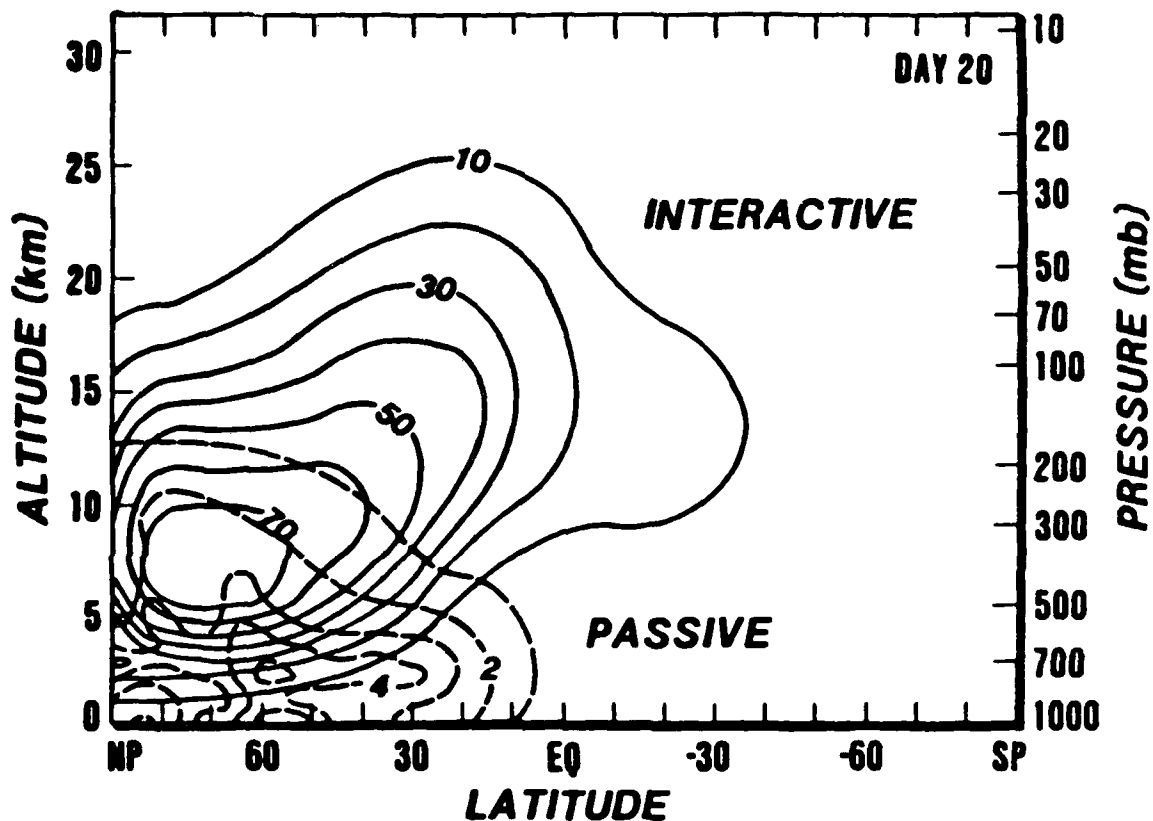


Fig. 3. Longitudinally averaged mass mixing ratios for July conditions at day 20. The dashed contours apply to a passive tracer, while the solid contours apply to interactive smoke. In each case 170 Tg of material was injected over the Northern Hemisphere continents with a low injection profile. The contours of mixing ratio are labeled in units of  $10^{-9}$  g material/g air (Malone, 1986).

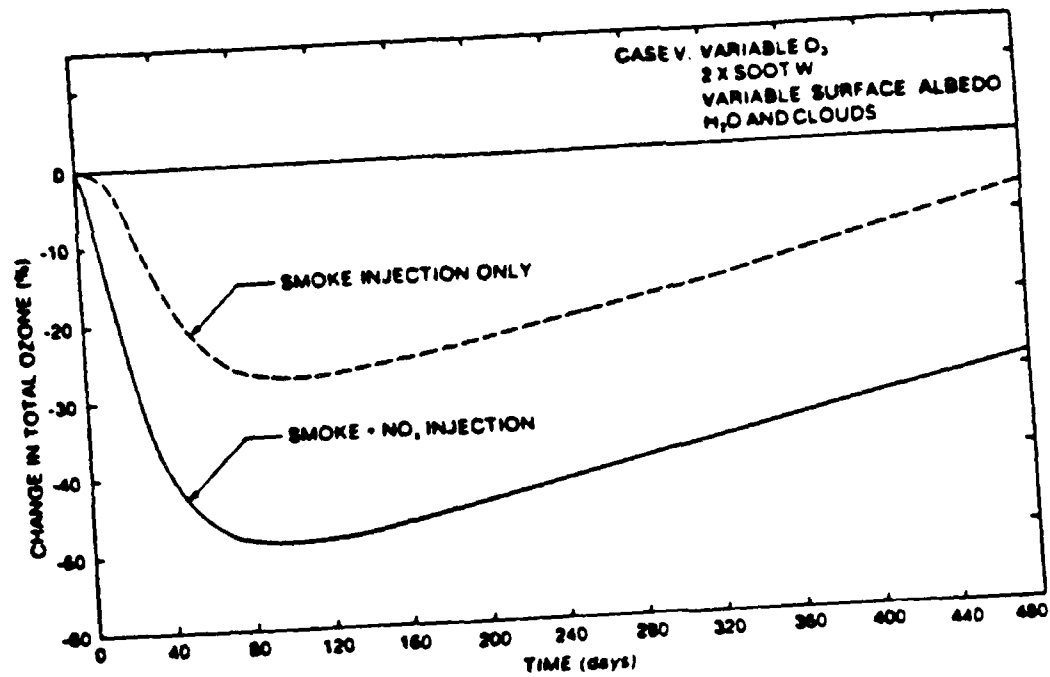
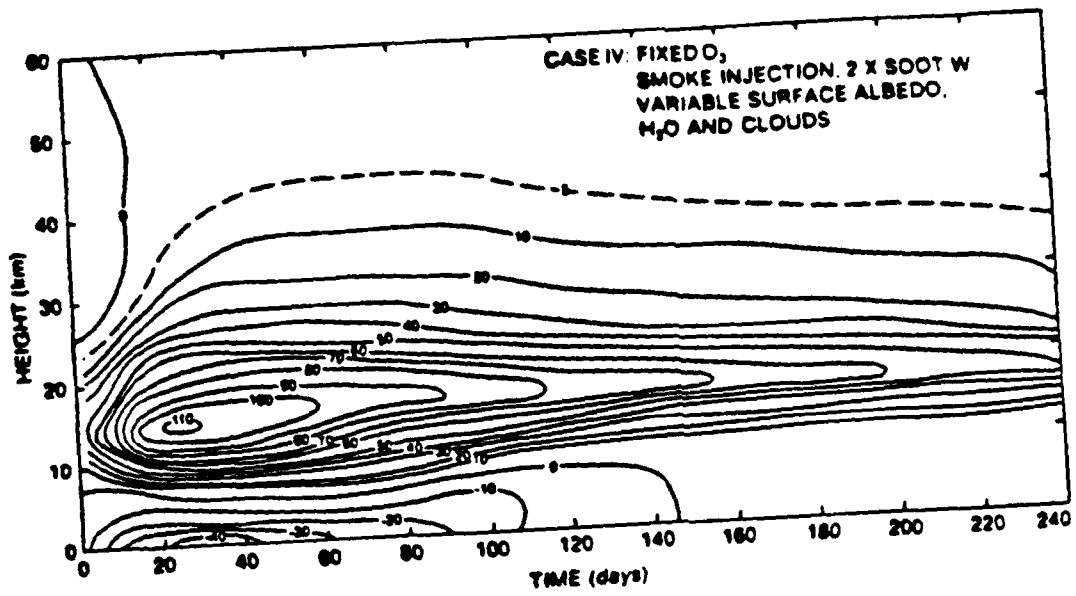


Fig. 4. Upper: Altitude-time cross-section of the calculated temperature changes (K) for the nuclear smoke injection scenario. Lower: Time evolution of the calculated changes in the total ozone column (in %) for nuclear smoke with and without NO<sub>x</sub> injections (Vupputuri, 1985).



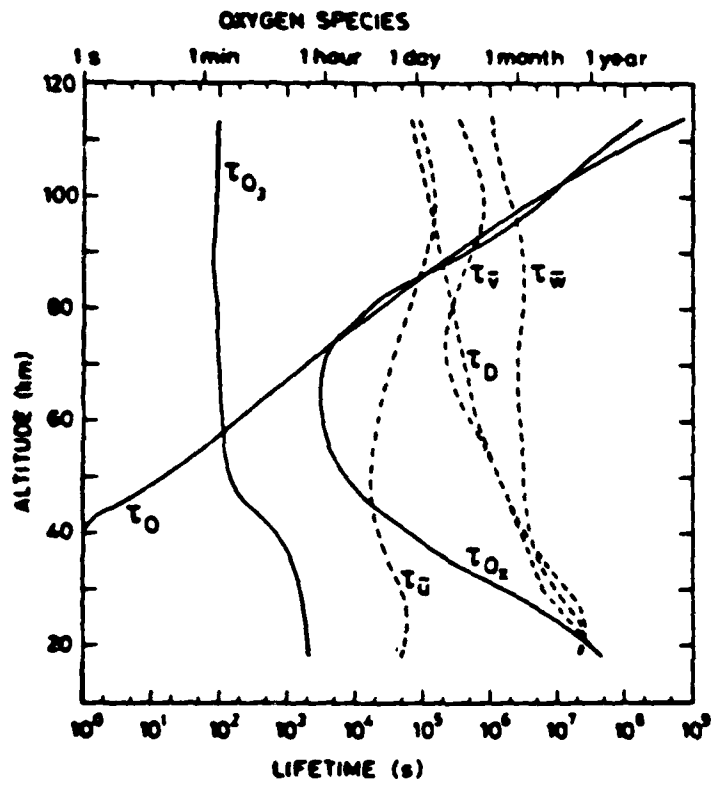


Fig. 5. Photochemical lifetimes of  $O_x$ ,  $O_3$ , and  $O$ , and characteristic transport lifetimes (Brasseur and Solomon, 1984).

SECTION 2  
SMOKE EMISSIONS

## Effect of Radiant Flux on Smoke Emission

G. W. Mulholland, V. Henzel<sup>1</sup>, V. Babrauskas  
National Bureau of Standards  
Gaithersburg, Maryland 20899, USA

### ABSTRACT

Smoke emission and the light extinction coefficient are measured for propane, heptane, PMMA, wood, Prudhoe Bay crude oil, and rigid polyurethane in the Cone Calorimeter for radiant fluxes up to 100 kW/m<sup>2</sup>. By increasing the specific burning rate in the Cone Calorimeter to match the burning rate in a large scale test, a good correlation is obtained between the smoke properties obtained with the Cone and the same properties obtained in large scale tests. Time-resolved data are obtained for both smoke concentration and the optical extinction coefficient. For wood, it was found that soot emission increases during the later part of the burn while the optical properties remain constant.

### 1. INTRODUCTION

An important element in assessing the hazard of a fire is the smoke emission. Smoke from a developing fire will affect the visibility of escape routes. At the present time there is a limited amount of information regarding emission and optical properties of smoke as a function of material burning and fire scale. While there have been some small scale studies on smoke emission (Bankston *et al.* [1], Tewarson [2]) for construction materials and materials found in buildings and houses, there is no general correlation allowing one to predict the smoke emission for a large scale fire based on small scale results.

The study reported here was motivated by the observation [1,2] that the burning rate of a fuel can have a pronounced effect on the smoke emission. The hypothesis to be tested is that, for a given fuel, the smoke emission is primarily controlled by the burning rate per unit area for the case of overventilated burning. The dependence of smoke emission upon the burning rate, however, may vary from fuel to fuel. In our study the smoke emission is measured as a function of burning rate for a number of fuels and the results compared with large scale free burn results. The burning rate is varied by changing the radiant flux to the sample.

### 2. SMOKE MEASUREMENTS

The most rudimentary smoke quantity is the smoke yield,  $\epsilon$ , which is defined as the mass of smoke aerosol generated per mass of fuel consumed. This quantity is determined by a mass flux method and by a carbon balance method. The key measurements in the flux method are the measurement of the mass of smoke

---

<sup>1</sup>Nuclear Research Center Negev. Beer-Sheva 84 190, Israel.

collected on a filter, the mass loss of the fuel, the air flow rate to the filter, and the total flow rate in the stack. The carbon balance method is based on the measurement of the carbon-containing combustion products including  $\text{CO}_2$ ,  $\text{CO}$ , and smoke aerosol. A standard 47 mm filter holder with glass fiber filters and a tapered element oscillating microbalance (TEOM) were used for filter collection. The TEOM contains a removable filter element at the end of an oscillating hollow rod, and the mass deposited on the filter is determined from the change in the frequency of the rod. A nominal flow rate of 2 l/min is maintained through the filter. The TEOM is virtually the only commercial instrument capable of providing time-resolved information on smoke emission for high concentrations of sooty smoke.

One of the principal optical properties of interest is the specific extinction coefficient of the fuel,  $K_f$ . For a flow system such as the Cone Calorimeter,  $K_f$  is obtained from the measurement of the extinction coefficient,  $K$ , for a He-Ne laser beam (633 nm) transmitted through the flowing smoke.

$$K_f = K / (\dot{m}_f / \dot{V}) , \quad (1)$$

where  $\dot{m}_f$  is the fuel mass loss rate and  $\dot{V}$  is the volumetric flow rate through the duct. As a heuristic example, a value of  $1 \text{ m}^2/\text{g}$  for  $K_f$  means that if the smoke produced by one gram of fuel were collected over a  $1 \text{ m}^2$  area, the light incident on this area would be blocked (intensity reduced by a factor  $e$ ). Another optical property of interest is the extinction coefficient per mass concentration of smoke  $K_s$ , defined by

$$K_s = K / m_s , \quad (2)$$

where  $m_s$  is the mass concentration of smoke. The quantity  $K_s$  is an intrinsic property of the smoke depending on the wavelength of light, the optical properties of the smoke, and on the size distribution of the smoke. The quantities  $K_f$  and  $K_s$  are related through the equation

$$K_f = \epsilon K_s . \quad (3)$$

### 3. EXPERIMENTAL PROCEDURE

The smoke emission measurements were performed in the Cone Calorimeter developed by Babrauskas [3]. The conical radiant source shown in Fig. 1 provides a uniform radiant flux over the  $100 \text{ cm}^2$  sample for radiant fluxes up to  $100 \text{ kW/m}^2$ . After a warmup period for the radiant source to reach steady state, the sample is inserted and ignited via a spark. The smoke aerosol and combustion gases rise through the conical heater into the exhaust hood and are sampled from a horizontal section of pipe as indicated in Fig. 1. The fuel burning rate is monitored with a load cell and, from monitoring the  $\text{O}_2$  consumption in the exhaust gases, the heat release rate of the fuel is determined [4]. Both the incident and transmitted laser beam are monitored with photodiodes to achieve the high level of precision in the determination of the percent transmission necessitated by the 10 cm path length. The gases sampled include  $\text{CO}$ ,  $\text{CO}_2$ ,  $\text{O}_2$ , and  $\text{H}_2\text{O}$ .

A square cross section diffusion burner (2.35 cm edge length) was used for burning propane. Both the heptane and Prudhoe Bay crude oil were burned in a 8.5 cm diameter cylindrical vessel made of glass. The wood, PMMA, and rigid polyurethane were in the form of square samples measuring 10 cm on an edge with a thickness of about 2.5 cm.

Large scale fires up to 350 kW were also studied with a large scale version of the Cone Calorimeter but without an external radiant flux. The apparatus has a maximum flow of about 2 m<sup>3</sup>/s through a 2.4 m by 2.4 m collection hood located 2.4 m above the floor. As indicated in Fig. 2, the smoke from the fire is mixed by a tripper plate and then sampled 5 duct diameters downstream by an isokinetic probe. The filter collection system allows sequential collection of three filter samples over the course of a burn and is designed to minimize particle loss by heating the sampling lines and filters to the stack temperature. As in the Cone, gas analysis and light extinction measurements were performed.

#### 4. RESULTS

The effect of the external radiant flux on the specific light extinction coefficient,  $K_f$ , is shown in Fig. 3 for propane, PMMA, and wood. Propane is unique, because the burning rate is not effected by the radiant flux. It is set by the fuel flow rate, which has a value of about 3 l/min for all four tests. The value of  $K_f$  for propane combustion increases by about a factor of three as the radiant flux is increased from 30 to 100 kW/m<sup>2</sup>. With increasing radiant flux, the smoke emission doubles as indicated in Table 1. The value obtained for  $\epsilon$  by the flux and carbon balance method agree to about 10 - 20 % for all materials. Only the values obtained by the flux method are reported in Table 1. Most entries in Table 1 correspond to an average of more than one test. Propane is the simplest case, since the external radiant flux affects the flame processes but not the generation rate of the fuel vapor. For all the other fuels, the external radiant flux affects both the generation rate of fuel vapor and the flame processes.

The mass burning rate of PMMA is approximately tripled by increasing radiant flux from 25 to 100 kW/m<sup>2</sup>; however, in this case both the smoke yield and  $K_f$  are relatively insensitive to the radiant flux. The results are also insensitive to the sample orientation.

For the case of red oak, the smoke measurements are difficult at low fluxes because of the low smoke production. The uncertainty in  $K_f$  is approximately  $\pm 0.005$ , which is comparable in magnitude to the observed value at the lowest radiant flux (see Fig. 3). Both the smoke yield and the specific extinction coefficient increase by almost a decade with increasing radiant flux. The major peaks in the specific extinction coefficient mirror the same peaks seen in the burning rate. The time dependence of  $\epsilon$  shown in Fig. 4 also has a similar shape, though in this case there is a high level of noise. The enhanced burning at the later stage apparently results from reduced conductive heat loss when the thermal "wave" propagates through the entire sample. As has been reported by Bankston *et al.* [1], the smoke generation is greater if the sample is burning in a horizontal rather than vertical orientation.

Heptane was the only fuel that exhibited a decrease in smoke emission with an increase in the radiant flux. The mass burning rate of heptane increases more rapidly with increasing radiant flux than the other fuels because of the higher vapor pressure of heptane. It was noted that for the heptane fires there was more pronounced boiling at the higher fluxes and also that the heat release rate was several times larger than for the other fuels. It is not known whether the decrease in smoke emission is a result of more efficient combustion in the flame at the higher radiant fluxes or a result of the high temperature in the exhaust system. For the other liquid fuel, Prudhoe Bay crude oil, the smoke emission was found to be relatively insensitive to the burning rate.

As discussed above, the specific extinction coefficient,  $K_s$ , is an intensive property of the smoke. The average value for each fuel is in the range 8 to 12 for the Cone data. The range in the average value of  $K_s$  for the same fuels in the large scale experiments, 7.8 - 9.1, is much less. The collection conditions are more variable in the Cone experiments, with stack temperatures ranging from 100°C to 400°C compared to 50°C to 175°C for the large scale experiments. Also, the sampling system is isokinetic with the gas and wall temperature matched for the large scale apparatus; whereas, for the Cone the temperature of the smoke decreases by as much as several hundred degrees before reaching the filter element. The large difference between the gas temperature and the temperature of sampling duct is expected to lead to significant particle deposition resulting from thermophoresis.

The quantity  $K_s$  is relatively constant as a function of time for burning wood as indicated in Fig. 5, even though both  $\epsilon$  and  $K_f$  increase significantly in the later stage of the burn. This result suggests that the optical properties of the soot remain relatively constant during the burn even though the soot emission is increasing.

The results for the large scale burns are compared with the Cone results for comparable burning rates in Table 2. The comparison for propane is somewhat artificial, because the burning rate is controlled by the gas flow rate and not by the external radiant flux. The lowest fuel flow rate for the large scale burner corresponds to the flame just barely covering the entire burner surface. It is an interesting coincidence that there is an abrupt increase in smoke emission with increasing fuel flow rate in the large scale experiments and a similar size increase in smoke emission with increasing radiant flux in the Cone.

The most reliably measured quantity for comparing large and small scale results is  $K_f$ , since smoke deposition in the filter sampling line does not effect this measurement. The large and small scale results in units of  $m^2/g$  respectively are: heptane 0.086 vs 0.078, Prudhoe Bay crude oil 0.956 vs 1.009, rigid polyurethane 0.788 vs 0.888, and wood 0.034 vs 0.028. The average percent difference is about 12%, which is similar to the expected experimental uncertainty. The largest difference is for wood. In this case, the large scale measurements were made with sugar pine and the small scale with red oak. In the other cases, identical materials were used at both scales. It is also found that there is good agreement in the smoke emission values for the large and small scale experiments for the same burning rates.

One limitation of this method for intercomparing small and large scale tests is the determination of the burning rate per area for complex structures such as cribs. We roughly estimated the effective burning area of the crib to be half of the total surface area of all the individual pieces. The factor of two reduction takes into account the limited burning of undersurfaces, the physical overlap of the individual pieces, and radiation shielding of lower pieces by upper pieces. Also, for the wood, we have taken an average of the vertical and horizontal results for the cone measurements.

## 5. DISCUSSION

Experimental results support a good correlation between small and large scale smoke emission results for the same specific burning rate. A demonstration of the general validity/utility of this approach must await measurements on a wider range of materials including composites and a more reliable way to estimate the burning area for complex structures.

Qualitatively, there are three ways in which large scale fires differ from small fires: the burning rate, the flame radiation, and the fluid flow. Applying an external radiant flux to a small sample enables one to match the burning rates for small and large scale and to mimic to some extent the larger fraction of radiant energy in the large fire, but not to reproduce the vigorous turbulent mixing of a large scale fire. Data are needed at fire scales up to at least 5 MW to determine the significance of the fluid flow in the plume and radiant feedback in regard to the small scale correlation.

Data from studies by Tewarson [2] and by Bankston *et al.* [1] are included in Table 2. It is seen that there is good agreement in the values of  $\epsilon$  for PMMA, but that Tewarson's value of  $\epsilon$  for heptane is a factor of two greater than our largest value. Also, the combustion efficiency reported by Tewarson, 0.93, is less than observed in this study.

Bankston *et al.* [1] report more than a two-fold decrease in smoke emission for wood as the radiant flux is increased from 25 kW/m<sup>2</sup> to 50 kW/m<sup>2</sup>, while we observe about a factor of two increase. The difference may result from our collecting smoke only after flaming combustion begins, while Bankston *et al.* [1] may have also collected "pyrolysis smoke" produced before ignition occurred. It is known that the smoke yield from wood during pyrolysis is much greater than during flaming combustion.

Bard and Pagni [5] have proposed a method for estimating the maximum conversion of fuel carbon to soot based on the measurement of the maximum volume fraction of soot within the flame. As a comparison, the maximum yields obtained with the cone are 0.016 for PMMA and 0.013 for wood compared to Bard and Pagni's prediction of 0.024 for PMMA and about 0.018 for wood [5].

The values of  $K_s$  obtained with the Cone ranged from 8 - 12 m<sup>2</sup>/g and from 7.8 - 9.1 m<sup>2</sup>/g for the large scale. Seader and Einhorn [6] obtained a mean value of 7.6 m<sup>2</sup>/g based on measurements on several plastics and wood in a chamber using a polychromatic light source. Neuman and Steciak [7] obtain values of 10.3, 10.3, and 10.5 m<sup>2</sup>/g for  $K_s$  based on flaming combustion of

heptane, douglas fir, and PMMA, respectively. The measurements were made at  $\lambda=633$  nm, which is essentially identical to the wavelength used in our study. These results are consistent with the statement that  $K_s$  for soot is independent of the fuel, though systematic differences among laboratories remain to be resolved.

#### 5. ACKNOWLEDGEMENTS

The authors gratefully acknowledge Nelson Bryner and William Twilley for assisting in obtaining and reducing the smoke data.

#### 6. REFERENCES

- [1] Bankston, C. P., Zinn, B. T., Browner, R. F., and Powell, E. A., Aspects of the Mechanisms of Smoke Generation by Burning Materials, Combustion and Flame, 41, 273-292 (1981).
- [2] Tewarson, A., Prediction of Fire Properties of Fuels, Twenty-First Symp. (Intl.) on Combustion, The Combustion Institute, Pittsburg, 563-570(1986).
- [3] Babrauskas, V., Development of the Cone Calorimeter - A Bench-scale Heat Release Apparatus Based on Oxygen Consumption (NBSIR 82-2611), [U.S.] Nat. Bur. Stand. (1982).
- [4] Huggett, C., Estimation of Rate of Heat Release by Means of Oxygen Consumption Measurements, Fire and Materials, 4, 61-65 (1980).
- [5] Bard, S., and Pagni, P. J., Spatial Variation of Soot Volume Fractions in Pool Fire Diffusion Flames, First Symp. (Intl.) on Fire Safety Science, C. E. Grant and P. J. Pagni, ed. New York, Hemisphere Pub., 361-369 (1986).
- [6] Seader, J. D., and Einhorn, I. N., Some Physical, Chemical, Toxicological, and Physiological Aspects of Fire Smokes, Sixteenth Symp. (Intl.) on Combustion, The Combustion Institute, Pittsburg, 1423 -1444 (1977).
- [7] Newman, J. S., and Steciak, J., Characterization of Particulates from Diffusion Flames, Combustion and Flame, 67, 55 - 64 (1987).



Table 1. Smoke Emission measured with the Cone Calorimeter

Fuel	Radiant Flux, kW/m <sup>2</sup>	Burning Rate, g/sm <sup>2</sup>	Comb. Eff.	Smoke Yield	K <sub>F</sub> , m <sup>2</sup> /g	K <sub>S</sub> , m <sup>2</sup> /g
Propane	0	176	0.98	0.0057	0.019	-
	30	176	-	0.0064	0.038	6.4
	50	176	0.98	0.0087	0.057	7.3
	100	176	-	0.0137	0.127	9.5
n-Heptane	0	10.0	0.99	0.0125	0.089	7.7
	10	24.0	0.94	0.0131	0.083	6.6
	20	31.9	0.97	0.0096	0.072	7.9
	30	58.4	0.99	0.0062	0.050	8.3
	a		0.93	0.027		
Prudhoe Bay crude oil	0	4.5	40.9 <sup>b</sup>	0.0982	1.060	11.7
	25	10.7	38.1	0.0955	1.012	10.8
	40	18.1	36.9	0.0830	1.006	12.5
	50	23.9	35.5	0.0835	0.978	11.7
PMMA	25	16.4	0.96	0.0152	0.159	10.9
	50	25.0	0.96	0.0137	0.169	12.5
	75	37.8	0.95	0.0121	0.167	11.3
	100	47.0	0.96	0.0160	0.164	10.8
	a		0.95	0.016		
Red Oak	25,V	8.9	11.8 <sup>b</sup>	0.0010	0.011	-
	25,H	8.3	10.6	0.0020	0.022	11.2
	50,V	11.7	11.3	0.0018	0.025	13.4
	50,H	11.8	10.9	0.0055	0.050	9.0
	75,V	14.7	11.4	0.0033	0.035	11.0
	75,H	14.6	10.8	0.0080	0.094	14.6
	100,V	18.9	11.3	0.0089	0.060	9.3
	100,H	18.7	11.5	0.0129	0.120	9.8
Douglas fir <sup>c</sup>	25			0.025		
	50			<0.01		
Rigid Polyurethane foam	50	5.3	0.85	0.0797	0.888	9.4

V and H refer to the vertical and horizontal orientation of the sample, respectively.

<sup>a</sup>Results by Tewarson.

<sup>b</sup>Average heat of combustion, MJ/kg.

<sup>c</sup>Results by Bankston *et al.* for sample 7.5 by 7.5 cm.

Table 2. Comparison of Small and Large Scale Smoke Emission Results

Fuel/Conditions	$\dot{Q}$ , kW	Burning Rate, g/sm <sup>2</sup>	Comb. Eff.	Smoke Yield	$K_f$ , m <sup>2</sup> /g	$K_s$ , m <sup>2</sup> /g
<u>Propane</u> , 1 m	110	2.8	1.03 <sup>a</sup>	0.0077	0.049	-
diff. burner	175	4.2	1.11 <sup>a</sup>	0.0168	0.154	8.1
	350	8.6	1.09 <sup>a</sup>	0.0199	0.161	7.8
2.35 cm burner						
0 kW/m <sup>2</sup>	4.2	176	0.98	0.0057	0.019	9.9
50 kW/m <sup>2</sup>	4.2	176	0.98	0.0087	0.051	7.3
100 kW/m <sup>2</sup>	4.2	176	-	0.0137	0.127	9.5
<u>n-Heptane</u> ,						
31 cm pool	70	24.9	0.89	0.0093	0.074	7.3
50 cm pool	240	28.3	0.94	0.0121	0.098	8.2
8.5 cm pool						
10 kW/m <sup>2</sup>	7.1	24.0	0.94	0.0131	0.083	6.6
20 kW/m <sup>2</sup>	10.0	31.9	0.97	0.0096	0.072	7.9
<u>Prudhoe Bay crude oil</u> ,						
40 cm pool	65	14.3	34.5 <sup>b</sup>	0.090	0.956	9.5
60 cm pool	185	(18.1)		0.085		8.7
8.5 cm pool						
25 kW/m <sup>2</sup>	2.3	10.7	38.1 <sup>b</sup>	0.0955	1.012	10.8
40 kW/m <sup>2</sup>	3.8	18.1	36.9	0.0830	1.006	12.5
<u>Wood</u>						
Sugar pine						
1 crib	56	8.7 <sup>c</sup>	12.9 <sup>b</sup>	0.0036	0.029	8.5
3 cribs	254	12.6	13.4	0.0042	0.040	9.4
Red oak, 10 cm						
25 kW/m <sup>2</sup>	1.0	8.6	11.2 <sup>b</sup>	0.0015	0.017	11.2
50 kW/m <sup>2</sup>	1.3	11.8	11.1	0.0037	0.038	11.2
<u>Polyurethane</u> ,						
rigid 1 crib	125	12.0 <sup>c</sup>	0.68	0.085	0.740	9.1
2 cribs	310	14.6	0.68	0.101	0.815	8.5
10 cm 50 kW/m <sup>2</sup>	2.5	15.6	0.85	0.0797	0.888	9.4

<sup>a</sup> The erroneously large combustion efficiency results from an uncertainty in the propane flow calibration.

<sup>b</sup> The heat of combustion in MJ/kg.

<sup>c</sup> The effective surface area for combustion is taken as half the total surface area of all the individual sticks.

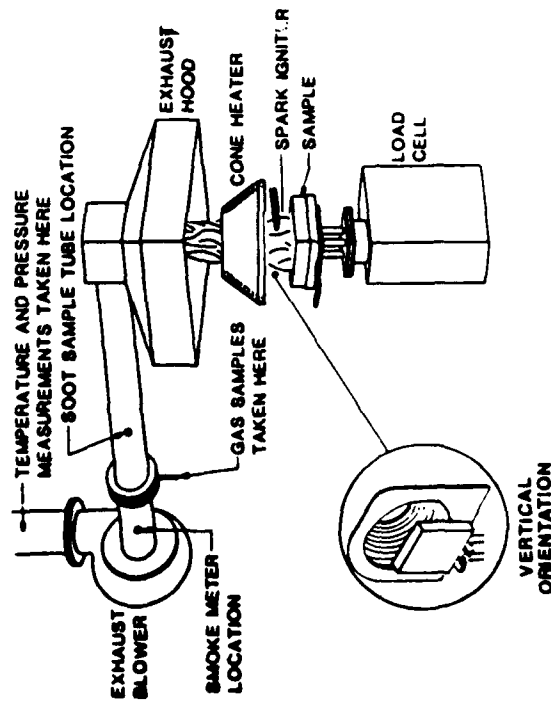


Fig. 1. Conceptual view of small scale test facility

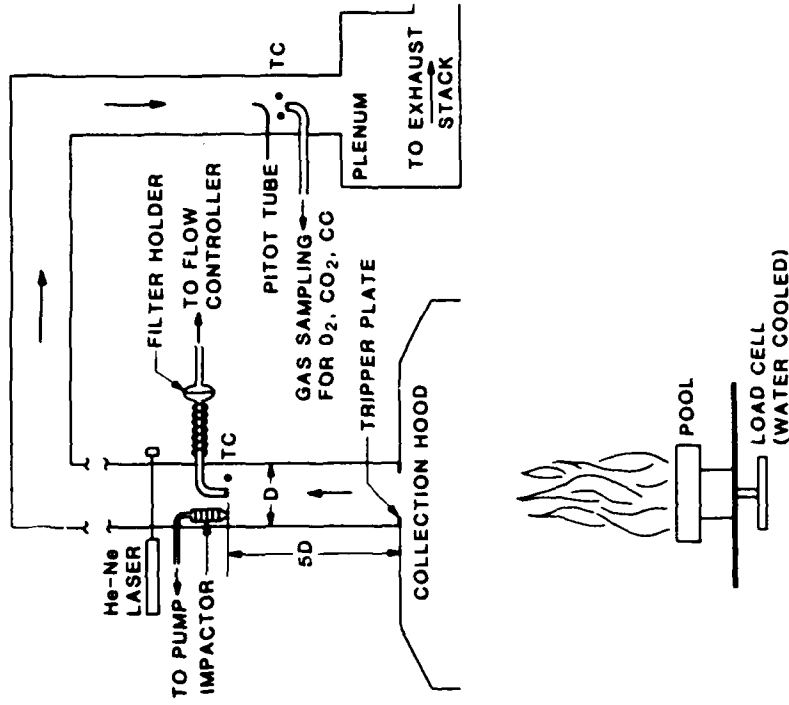


Fig. 2. Large scale facility for monitoring smoke emission/properties.

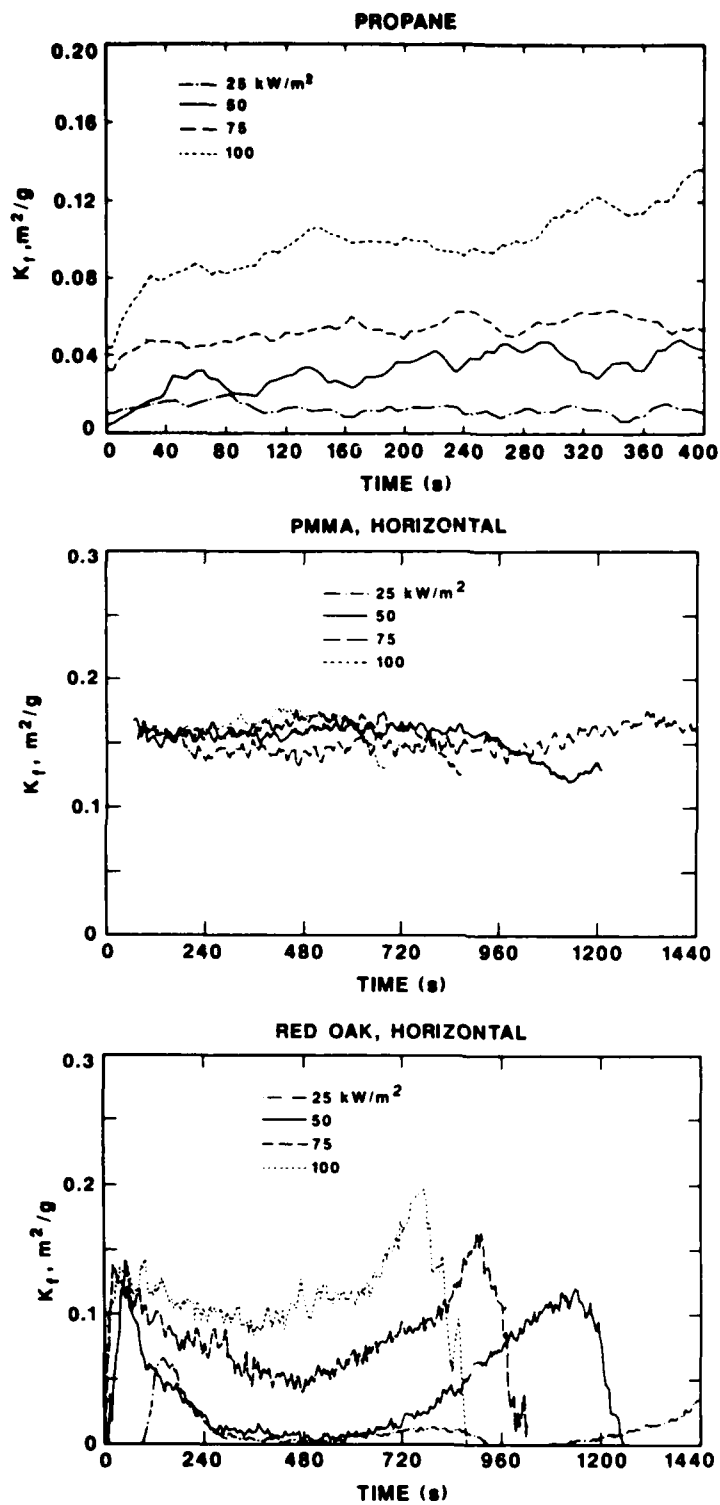


Fig. 3. Specific extinction area,  $K_f$ , versus time for radiant fluxes in range 25-100  $\text{kW}/\text{m}^2$

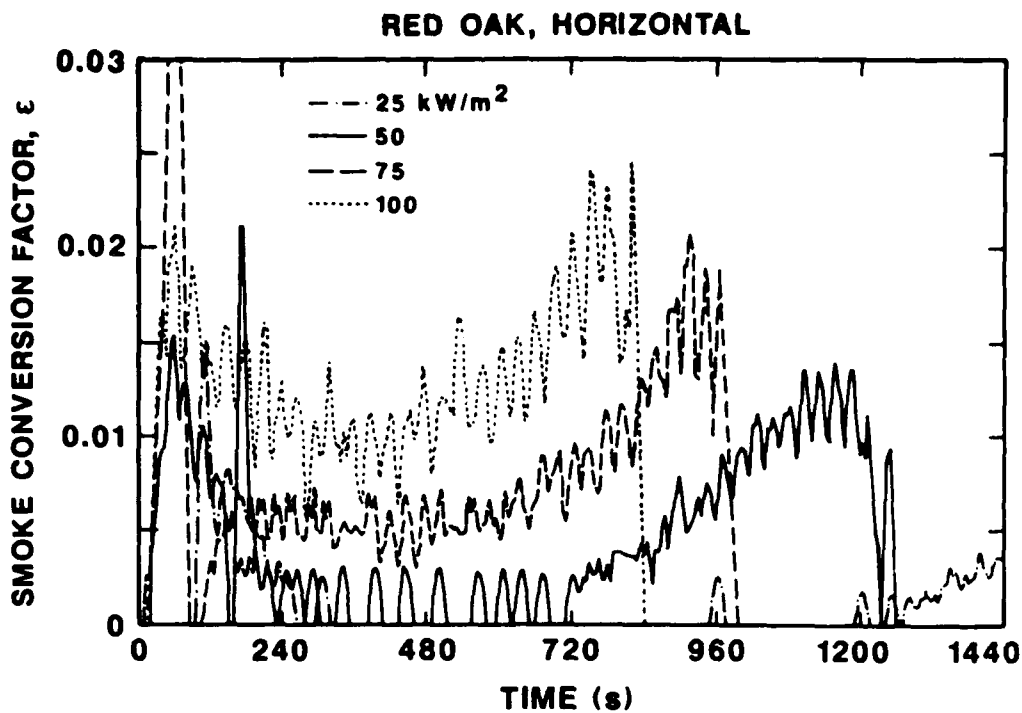


Fig. 4. Smoke conversion factor  $\epsilon$  versus time

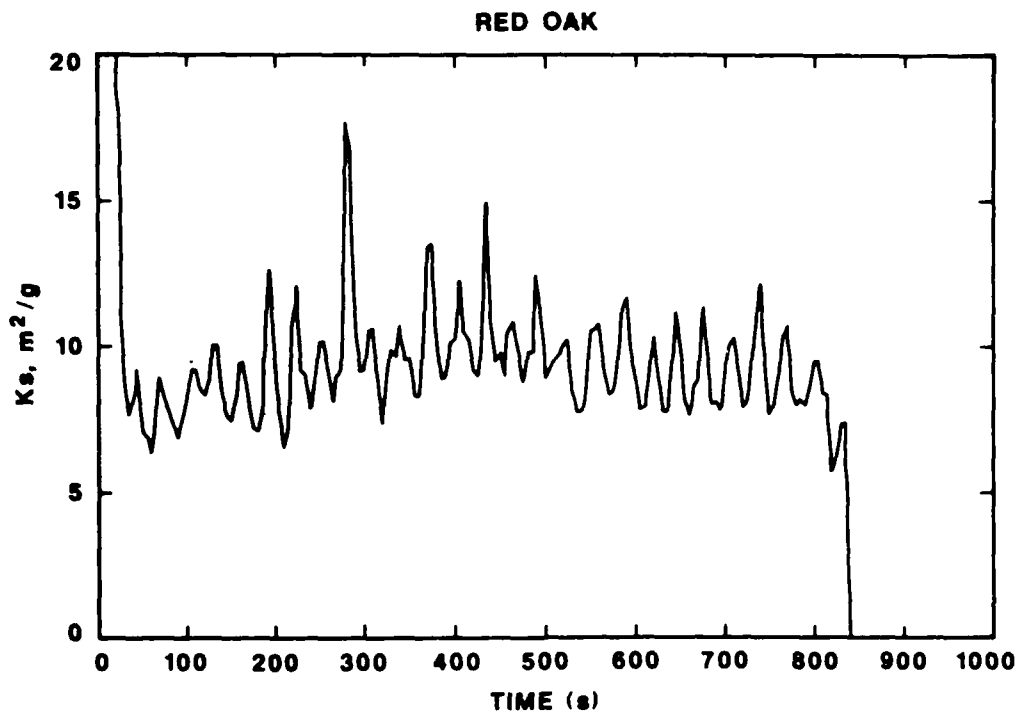


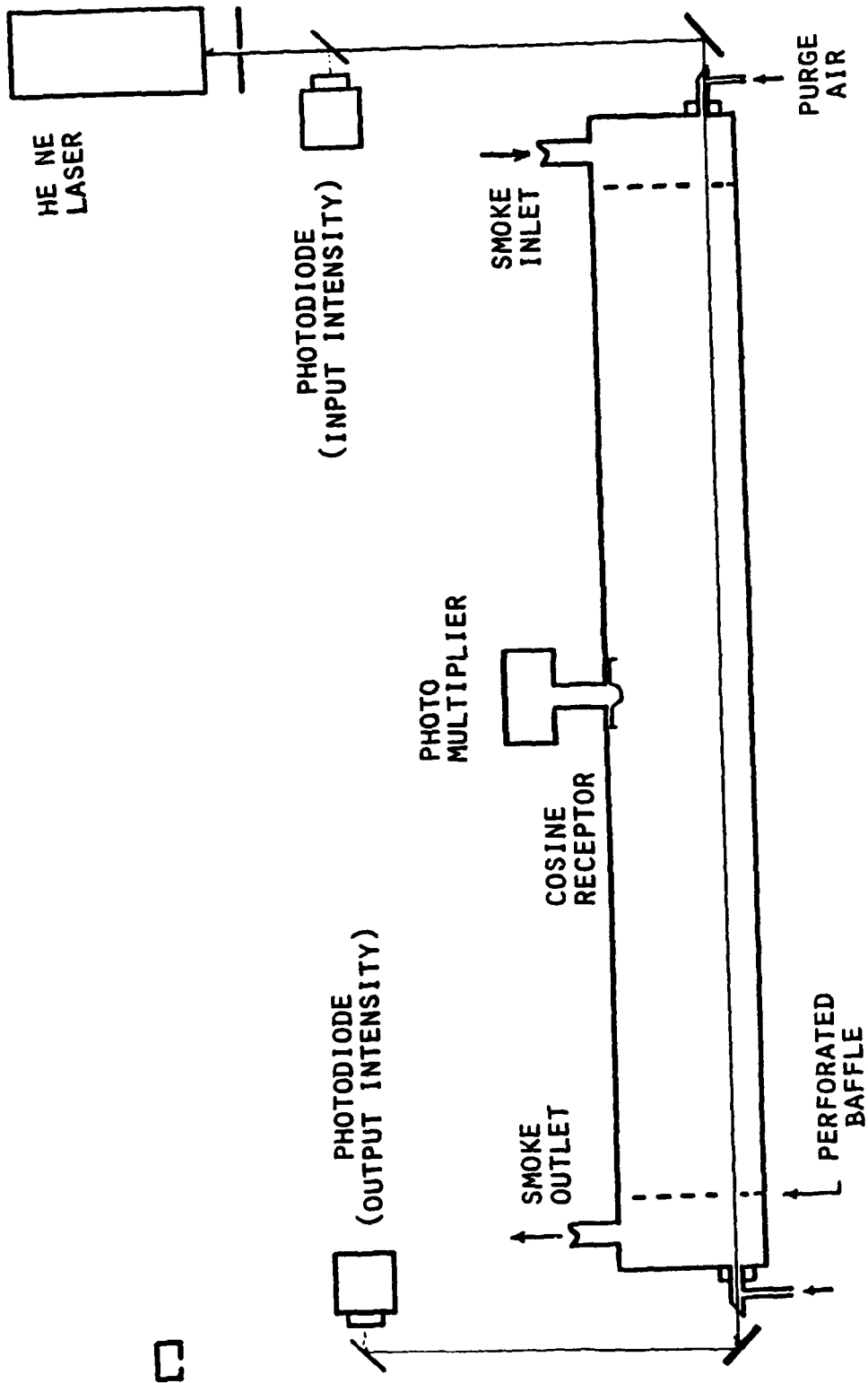
Fig. 5. Specific extinction coefficient  $K_s$  versus time for radiant flux of  $100 \text{ kW/m}^2$

George Mulholland  
Center For Fire Research  
National Bureau of Standards

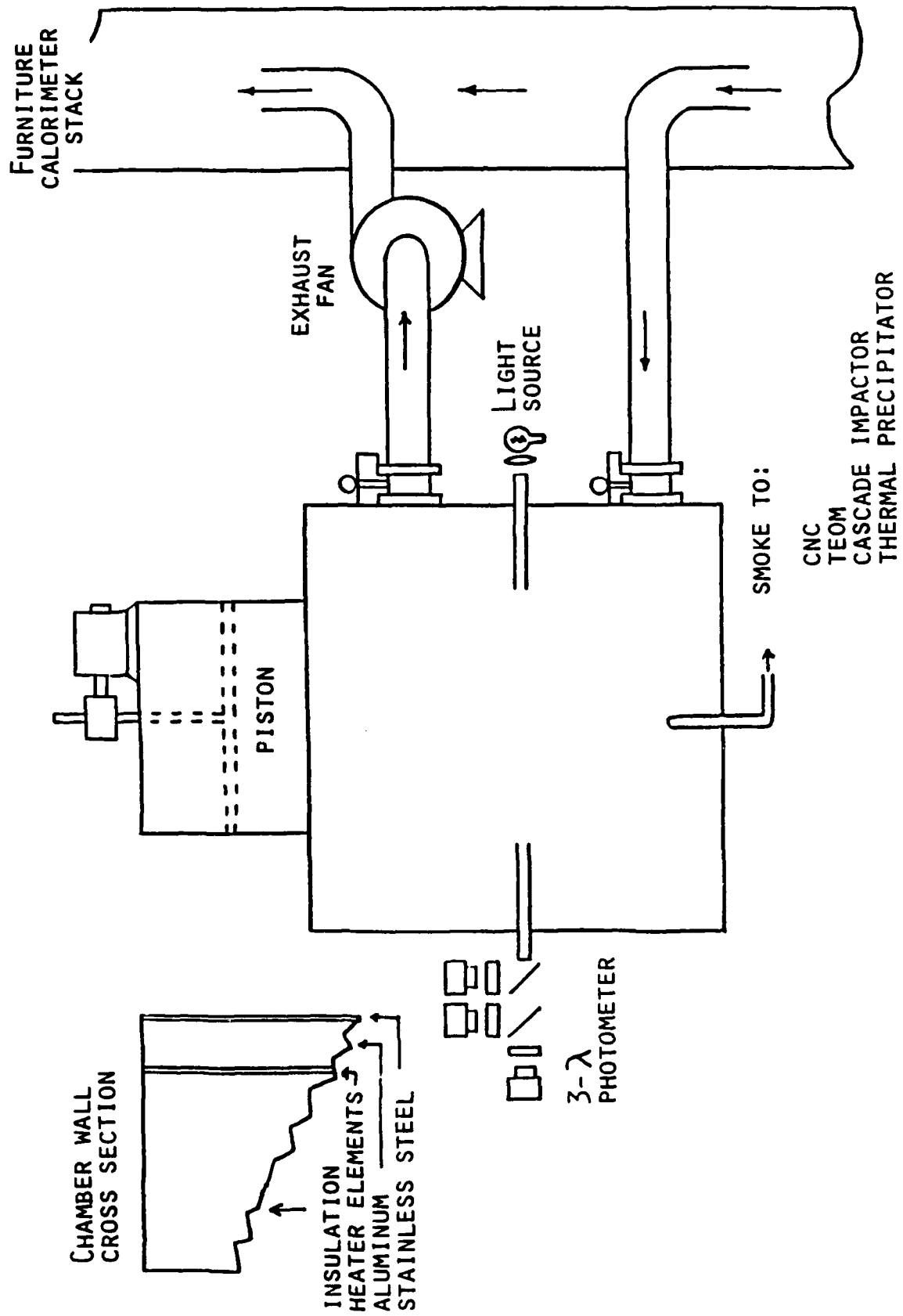
## PROGRESS REPORT

1. Light Scattering/Extinction Apparatus (Bryner)
2. Smoke Aging/Dilution Facility (Bryner)
3. Effect of Combustion Conditions on Smoke Generation
4. Mass Fire Flow (Baum)
5. The Drag and Torque on an Individual Soot Agglomerate (Baum)

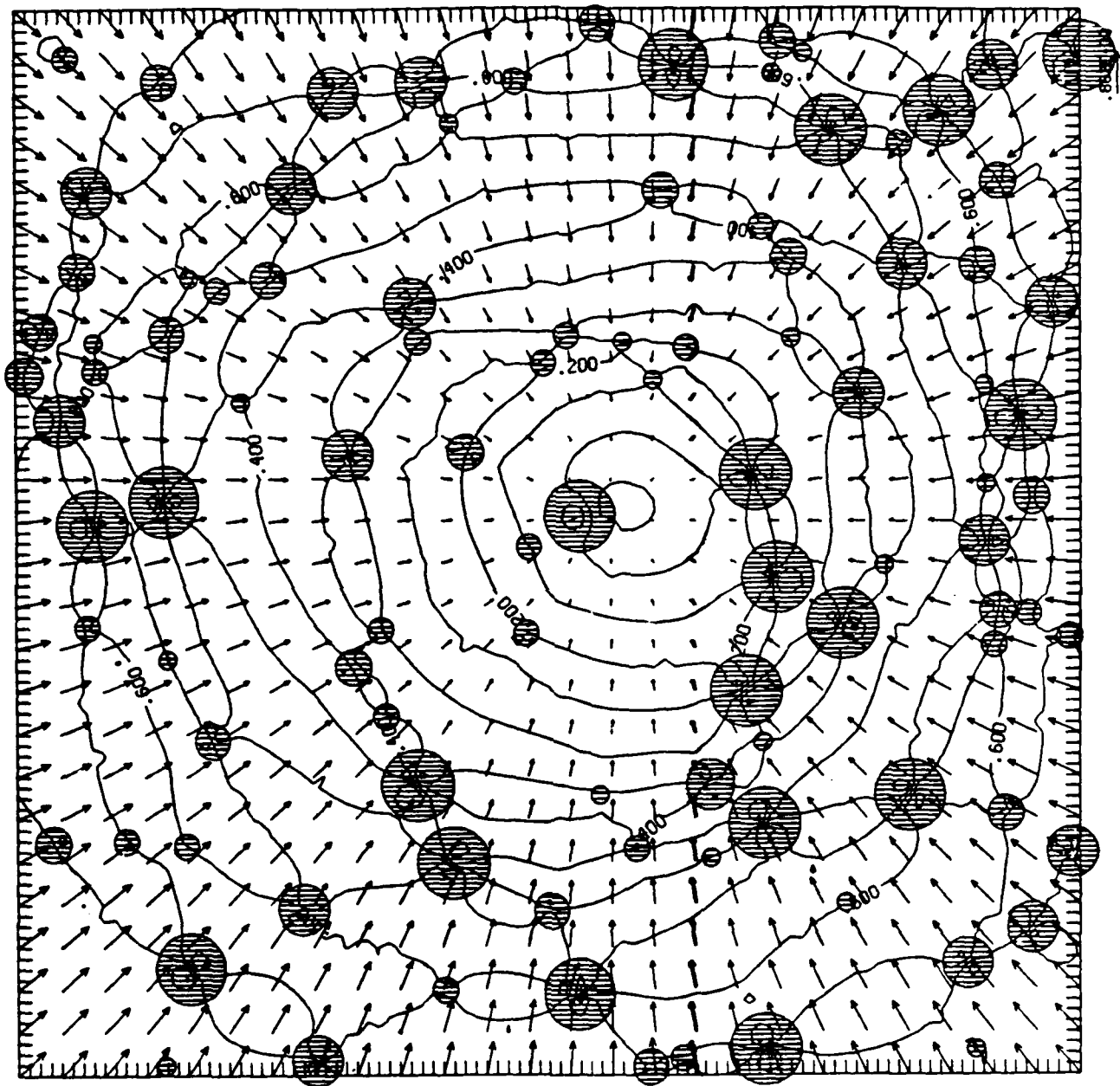
# SCATTERING AND EXTINCTION CELL



# SMOKE AGING AND DILUTION CHAMBER









GLOBAL EFFECTS PROGRAM TECHNICAL MEETING

DEFENSE NUCLEAR AGENCY

APRIL 7-9, 1987

SMOKE EMISSION FACTORS FROM BURNING WOOD AND ASPHALT

AS MEASURED IN MEDIUM SCALE EXPERIMENTS

by

Robert Brady Williamson, Nancy J. Brown, and Tihomir Novakov

Lawrence Berkeley Laboratory

773 Davis Hall

University of California

Berkeley, California 94720

ABSTRACT

The concept of "Nuclear Winter" is introduced and the smoke production of post-nuclear exchange fires is briefly discussed. A series of medium scale experiments to characterize smoke production from assemblies of exemplar urban materials is described. Smoke emission factors, (i.e., the mass of smoke per mass of fuel burned), were measured in ten different experiments. In addition, size fractionation studies were made with a cascade impactor. The percentages of "black" graphitic carbon and organic carbon have been determined for all the experiments as a function of particle aerodynamic diameter. Values in the range of .1 to .2% are reported for the smoke emission factors for Douglas fir whole wood and plywood burning under well ventilated conditions and over half of these emissions are black carbon particles with aerodynamic diameters less than 1  $\mu\text{m}$ . Douglas fir whole wood gave smoke emission factors in the range of 2 to 3.5% when burned under poorly ventilated conditions representing a building fire with combustion being controlled by air entering a window. The black carbon content in the limited ventilation was 50 to 75% of the total mass of the smoke particles, but the size distribution was much broader, with substantial quantities of particles up to 5  $\mu\text{m}$  in diameter. The smoke emission factor for burning asphalt roofing shingles is reported as 13.9% with over 90% being black carbon particles and over half of those are less than 1  $\mu\text{m}$ . The significance of these direct measurements of smoke emission factors is briefly discussed in the context of Nuclear Winter.

## LIST OF FIGURE CAPTIONS

- Fig. 1. A schematic diagram of the vertical parallel plate apparatus used to burn plywood is shown. During the experiment two faces of the plywood are exposed to an igniting flame from a gas burner which is shut off after the plywood is burning in a self sustaining manner.
- Fig. 2. This shows a schematic diagram of angled parallel plate apparatus used to burn asphalt roofing shingles. As in the plywood experiments the igniting flame of the gas burner is shut off after the shingles are burning in a self sustaining manner.
- Fig. 3. A plan view is shown of the experimental facility used in this work. Note that two cross-sections are marked for Fig. 4.
- Fig. 4. The cross-sections of the experimental facility marked in Fig. 3 are shown here. Note that the ventilation system is situated so that all of the effluent from the experiment can be monitored in the specimen collection system.
- Fig. 5. This histogram shows the overall smoke emission factors measured for burning wood under various conditions. The "Run Numbers" along the horizontal axis correspond to the experiments conducted with wood products. Note that experiments 12 and 13 were under limited ventilation conditions, while the others were conducted with adequate ventilation to allow for more complete combustion of the products.
- Fig. 6. This histogram shows the smoke emission factors for asphalt shingles along with the data for wood, which had been shown in Fig. 5. It is apparent that the asphalt shingles produce almost ten times more smoke than the wood cribs burned under limited ventilation conditions, and on the order of one hundred times the smoke produced by wood products under adequate ventilation conditions.
- Fig. 7. The variation of the smoke emission factors for the experiments with wood products burning under well ventilated conditions.
- Fig. 8. This shows a typical histogram of emission factors for different aerodynamic diameters. This histogram was obtained during experiment 5 with plywood by measuring the mass of smoke particles deposited on each stage of a cascade impactor.
- Fig. 9. This shows the emission factors as a function of aerodynamic diameters for one wood crib burning in the open.
- Fig. 10. The emission factors for asphalt roofing shingles are shown as a function of aerodynamic diameter.

LIST OF FIGURE CAPTIONS  
(Continued)

- Fig. 11. This shows the emission factors as a function of aerodynamic diameters for three wood cribs burning in the burn room.
- Fig. 12. This is a comparison of the mass of carbon obtained on the various stages and the final filter of the impactor and compare it to the mass of carbon obtained on the total filter. This figure shows the six well ventilated wood fires and a "blank" run with just the ventilation system operating and no fire.
- Fig. 13. This is a comparison of the mass of carbon obtained on the various stages and the final filter of the impactor and compare it to the mass of carbon obtained on the total filter for experiment 9 with asphalt shingles.

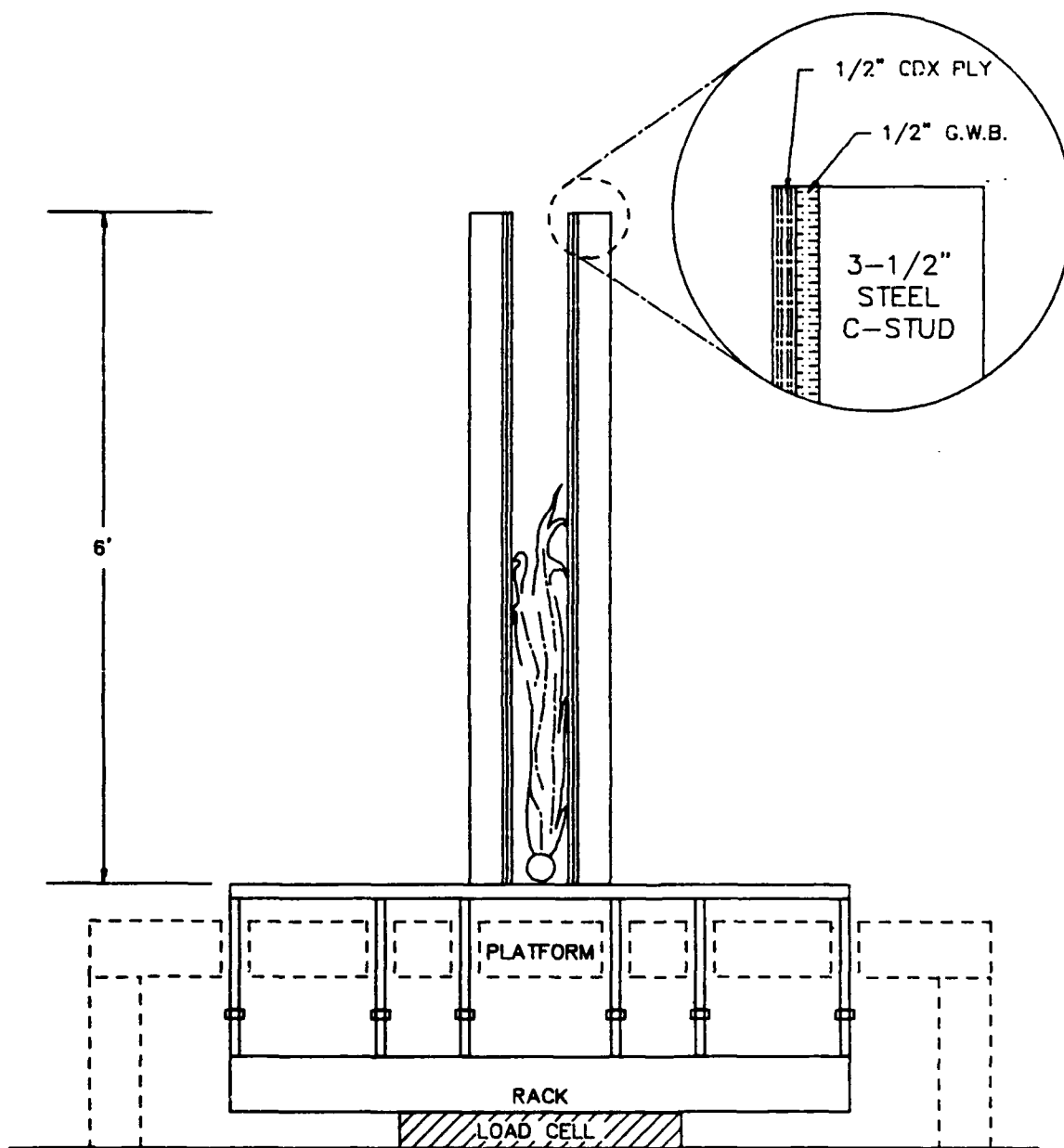


FIG. 1

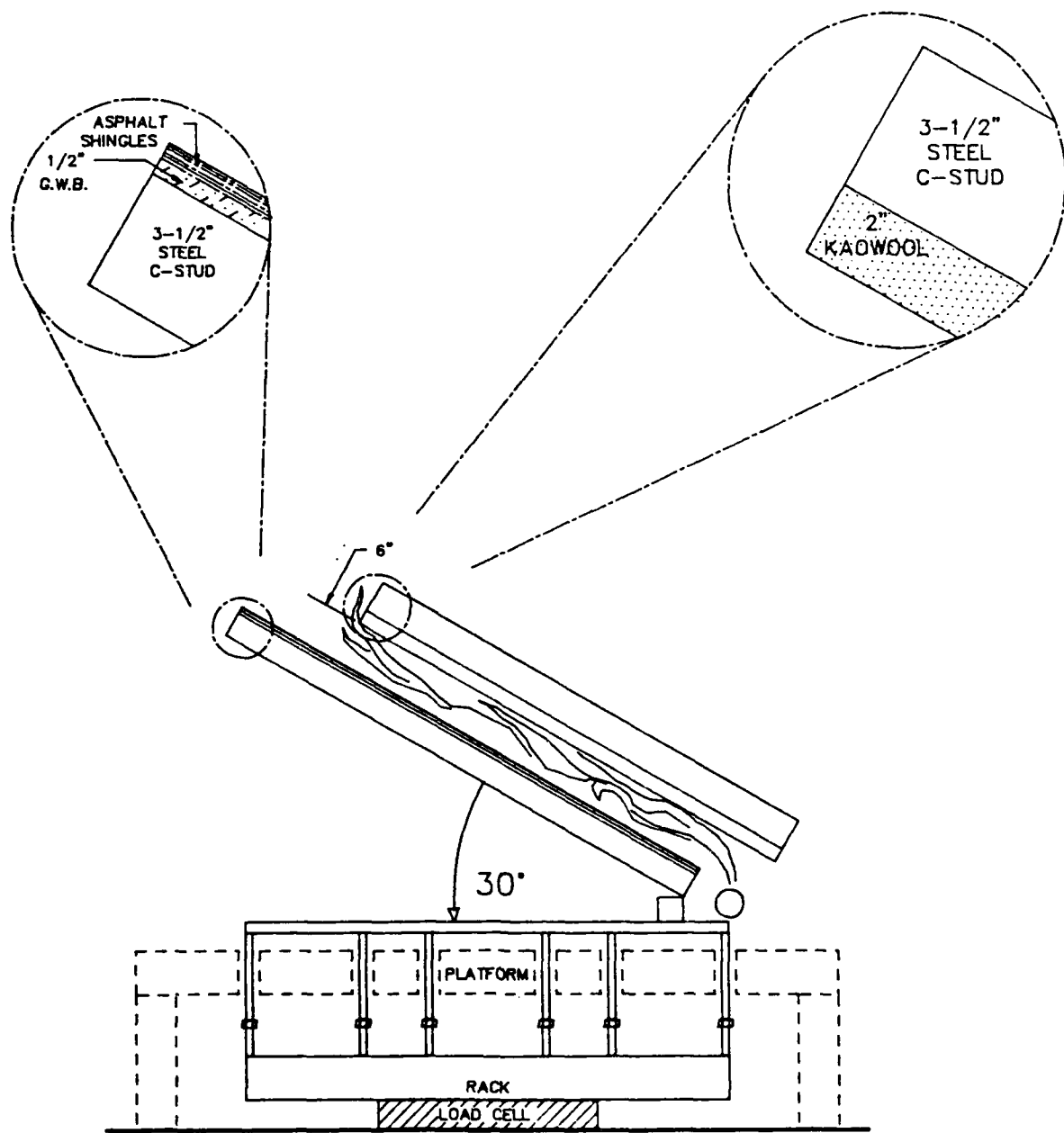


FIG. 2

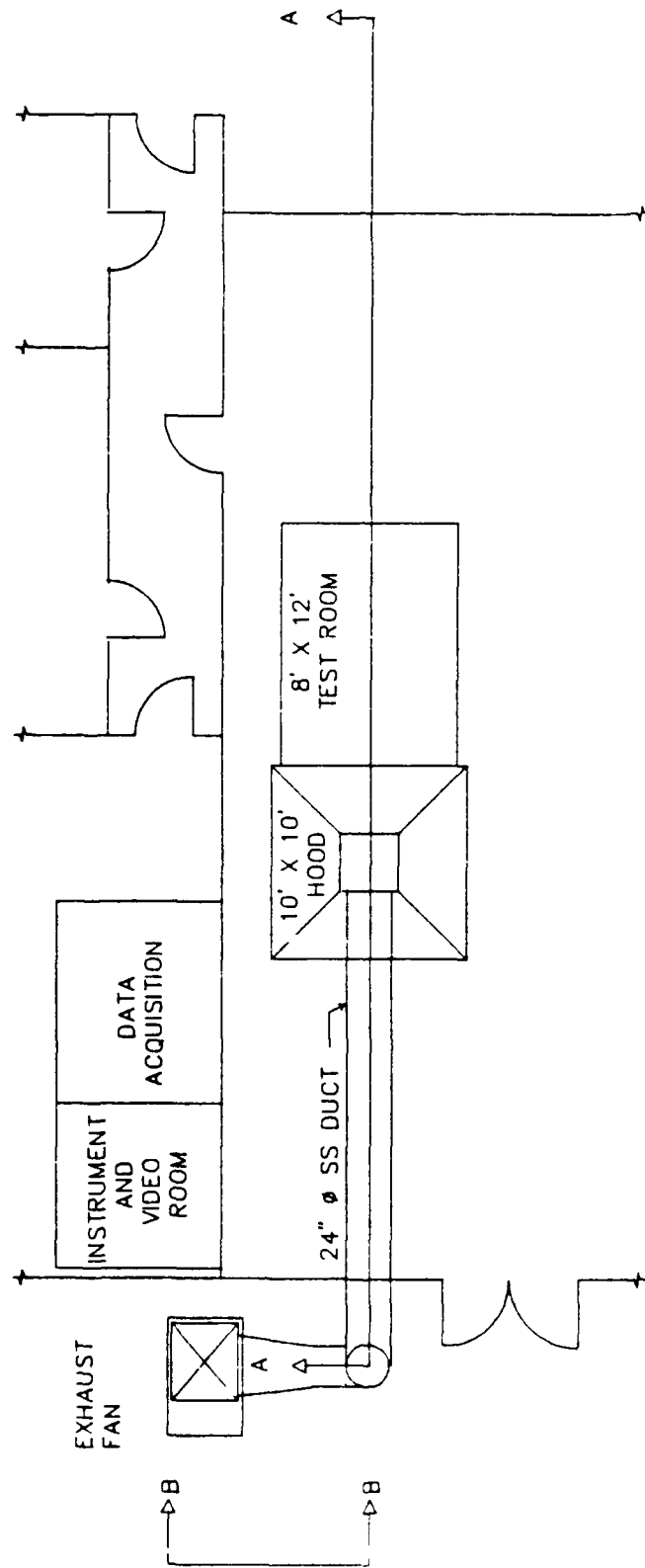


FIG. 3



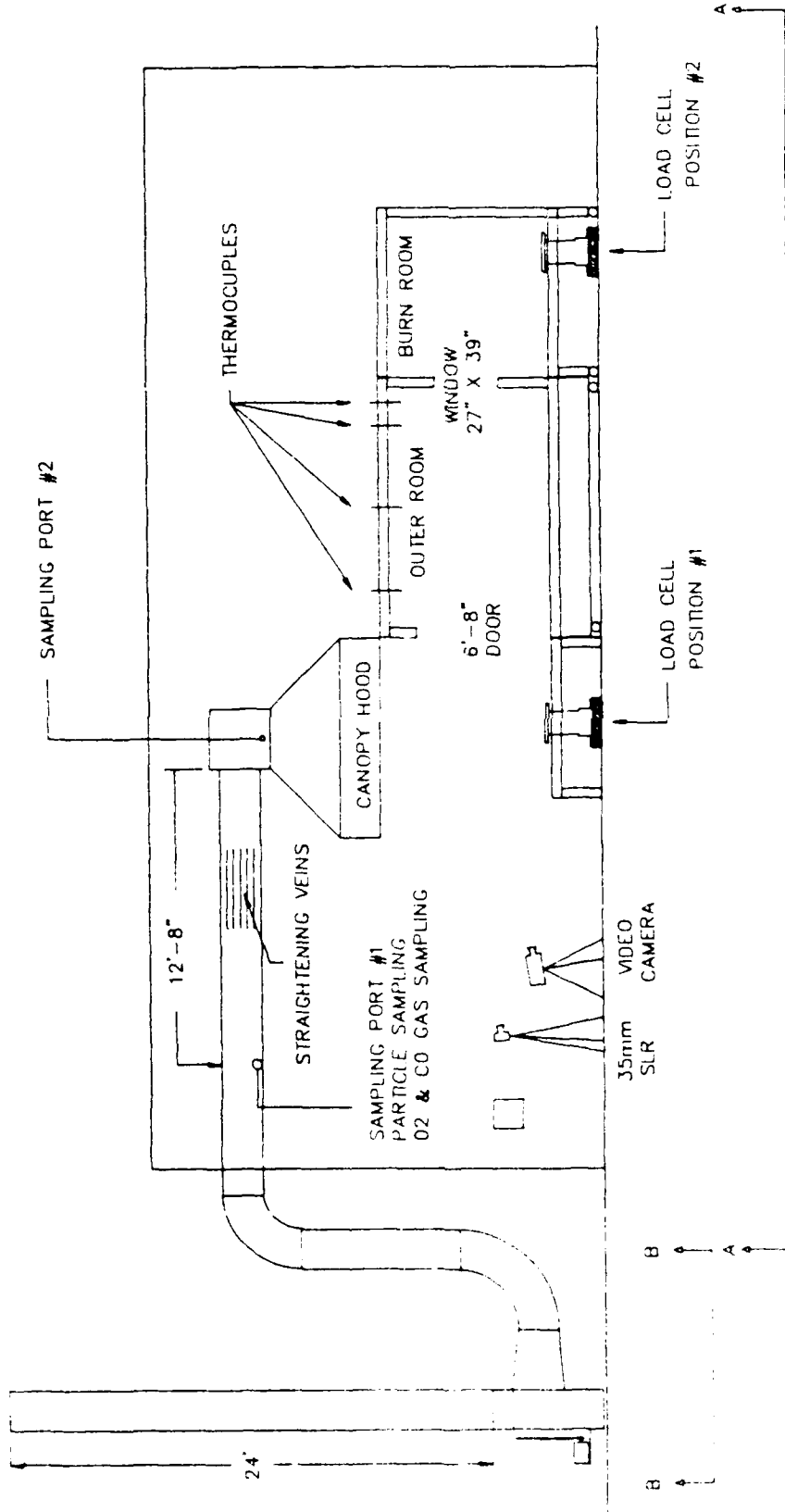


FIG. 4

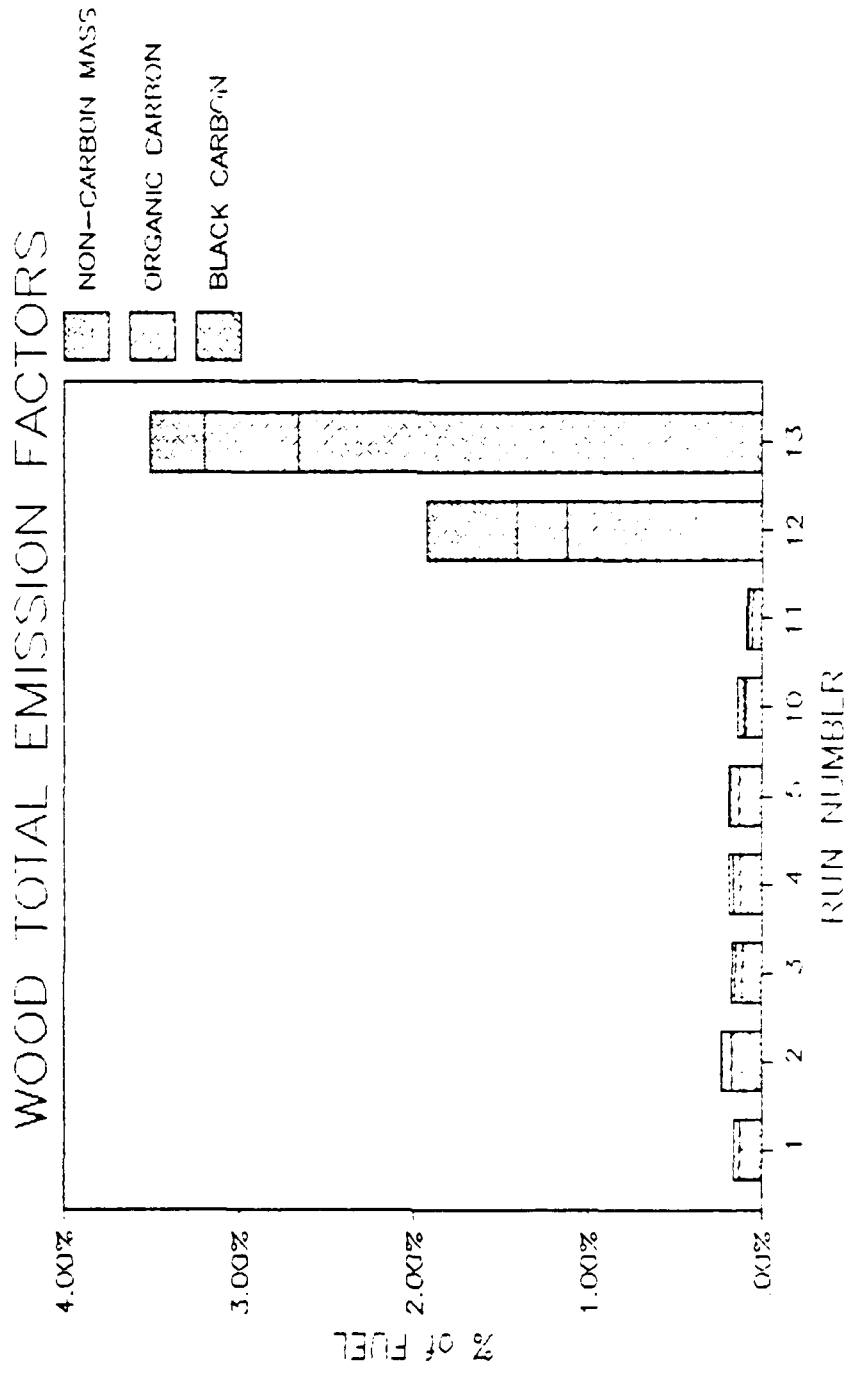


Fig. 5

# PARTICLE EMISSIONS

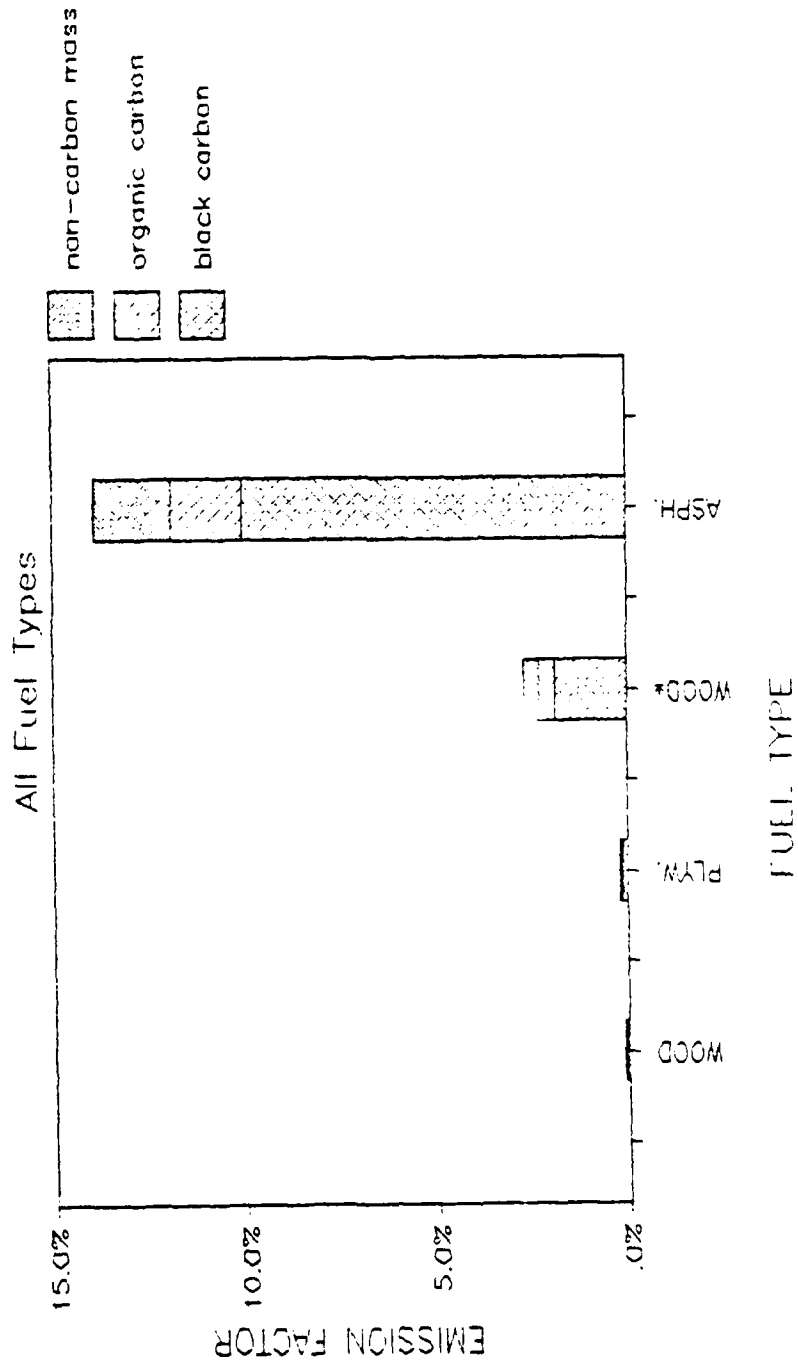
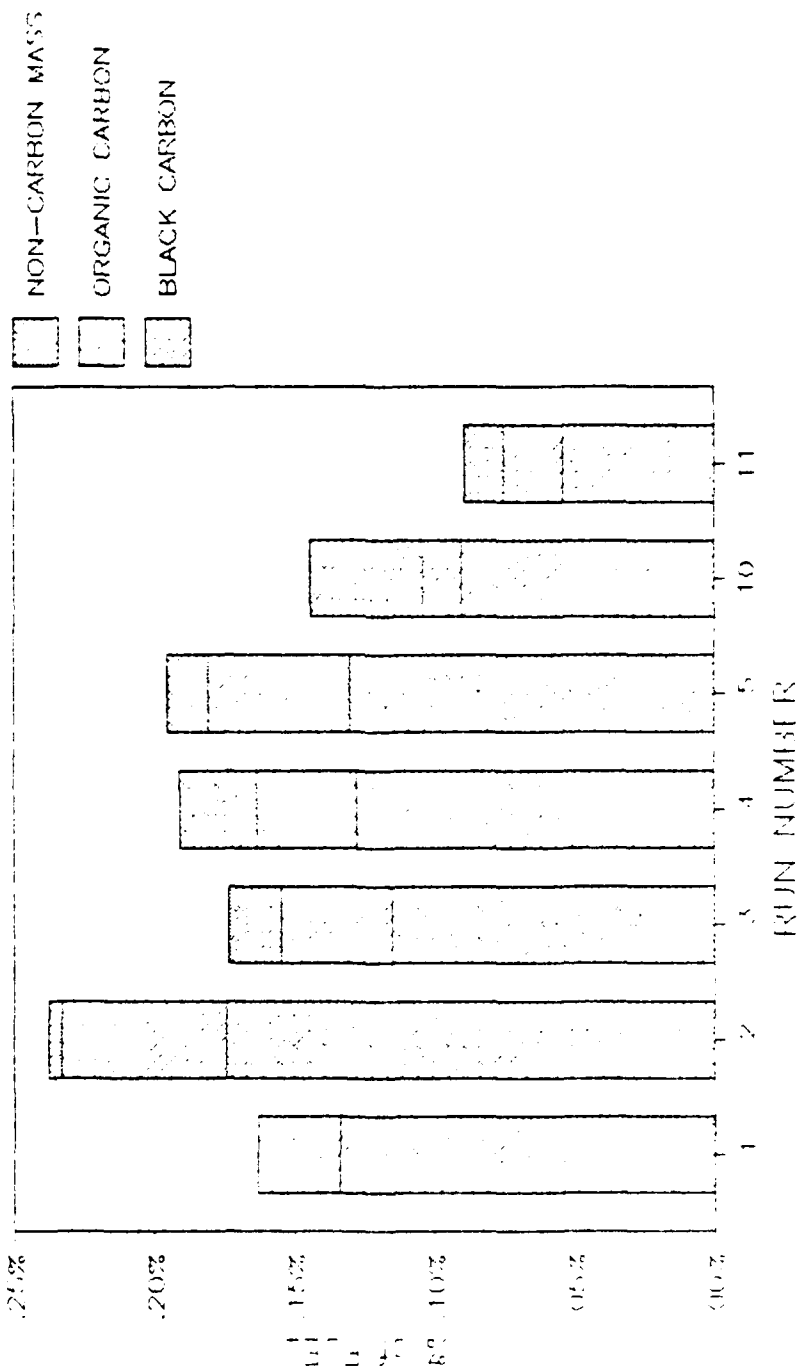


Fig. 6

# WOOD TOTAL EMISSION FACTORS



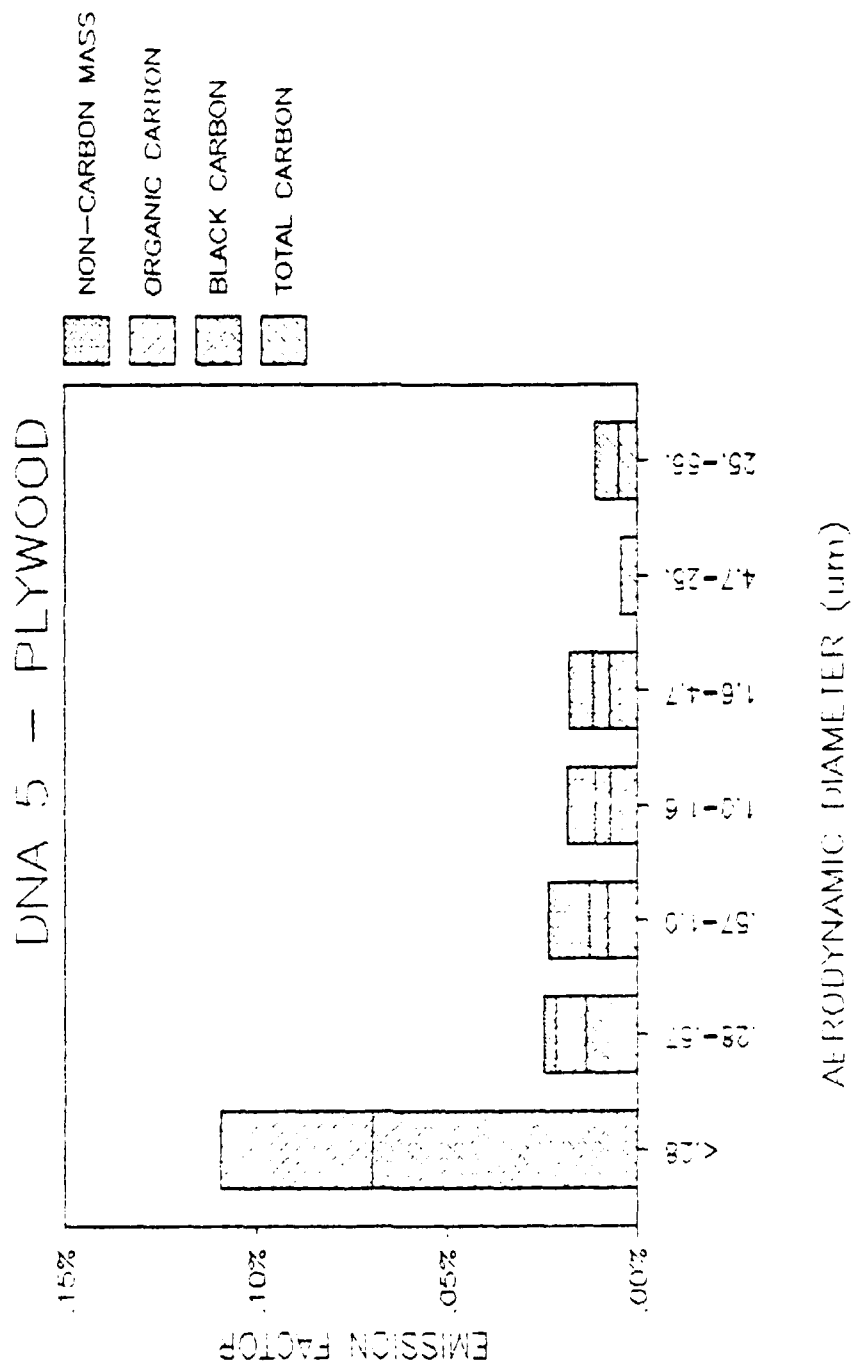


Fig. 6

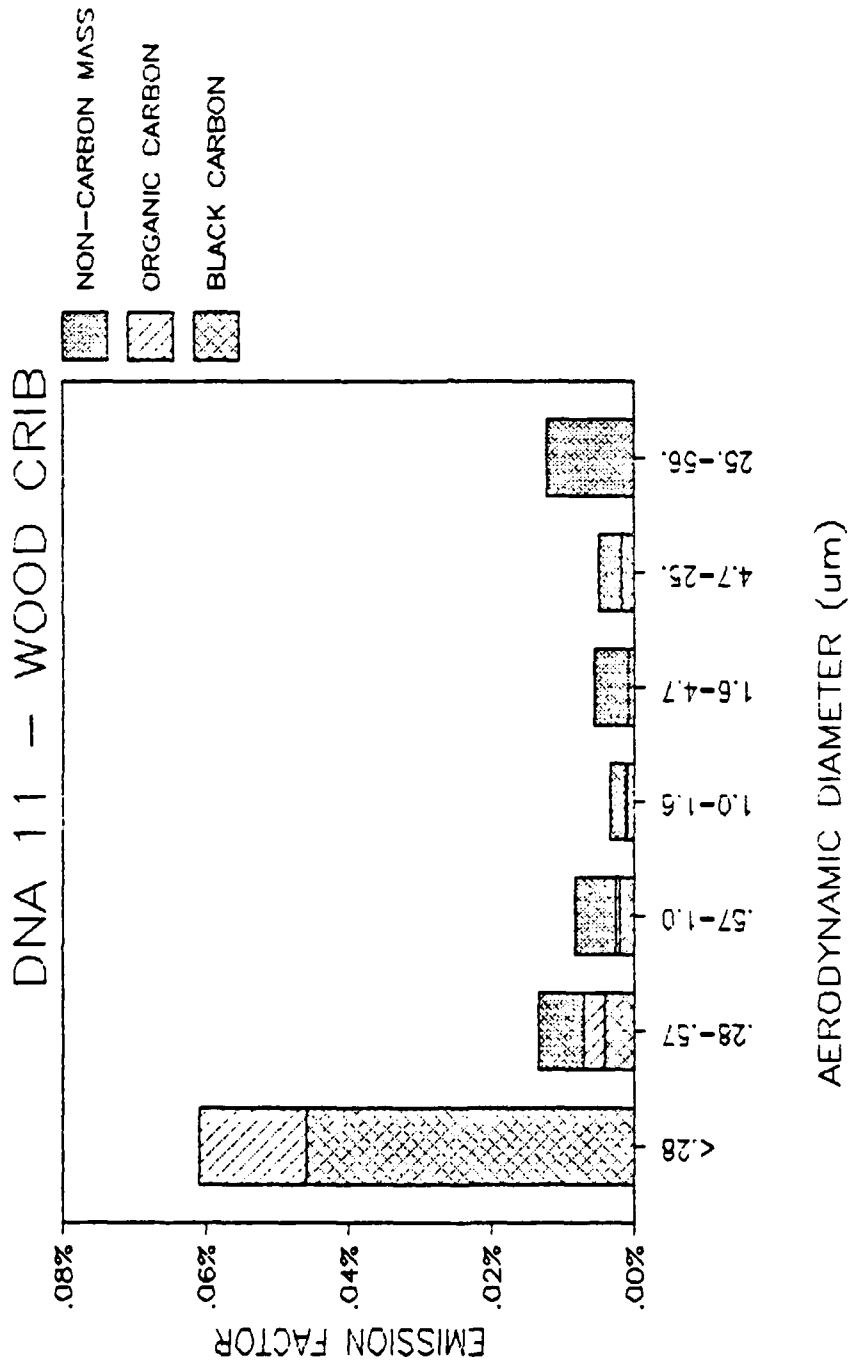


Fig. 9

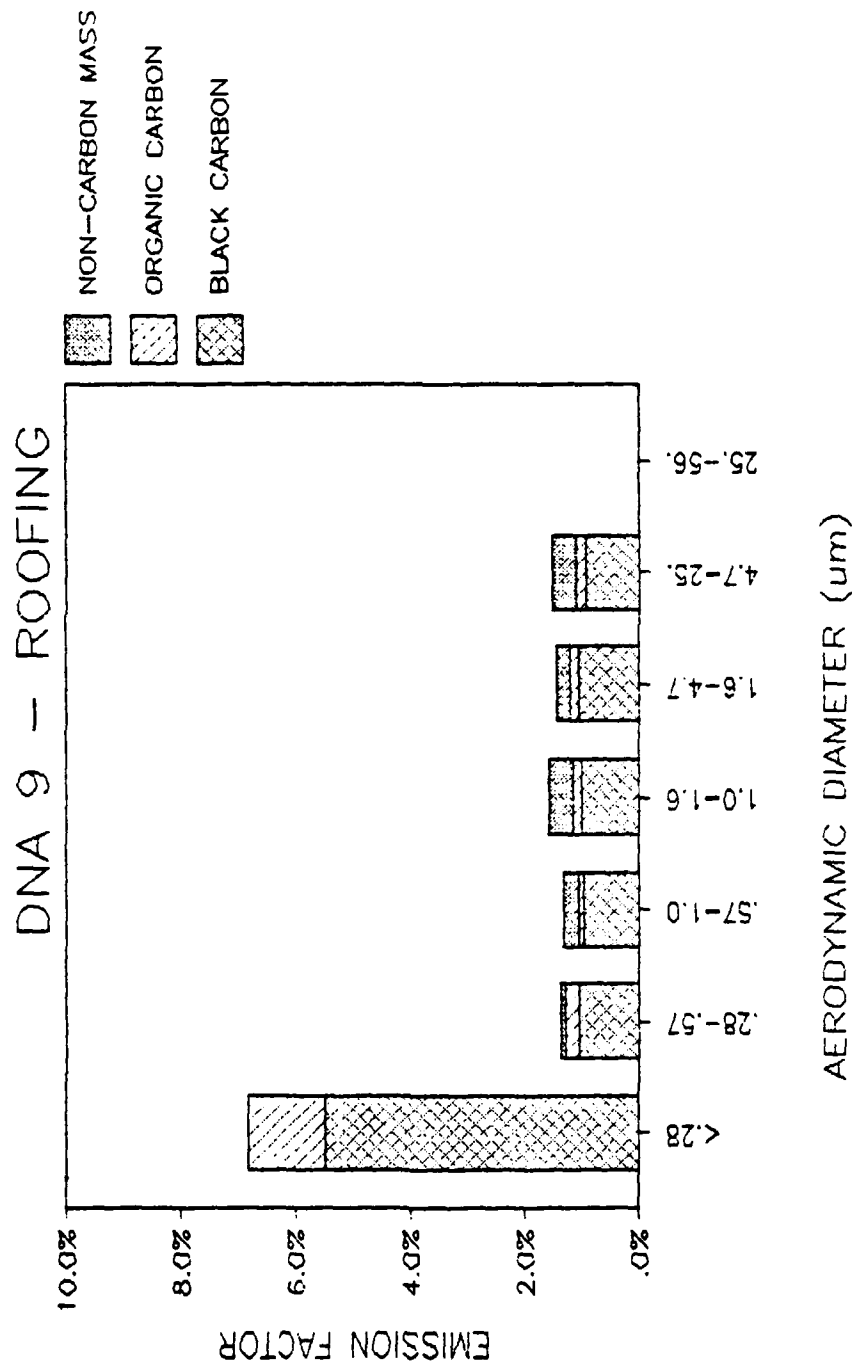


Fig. 10

# DNA 13 - 3 WOOD CRIBS IN ROOM

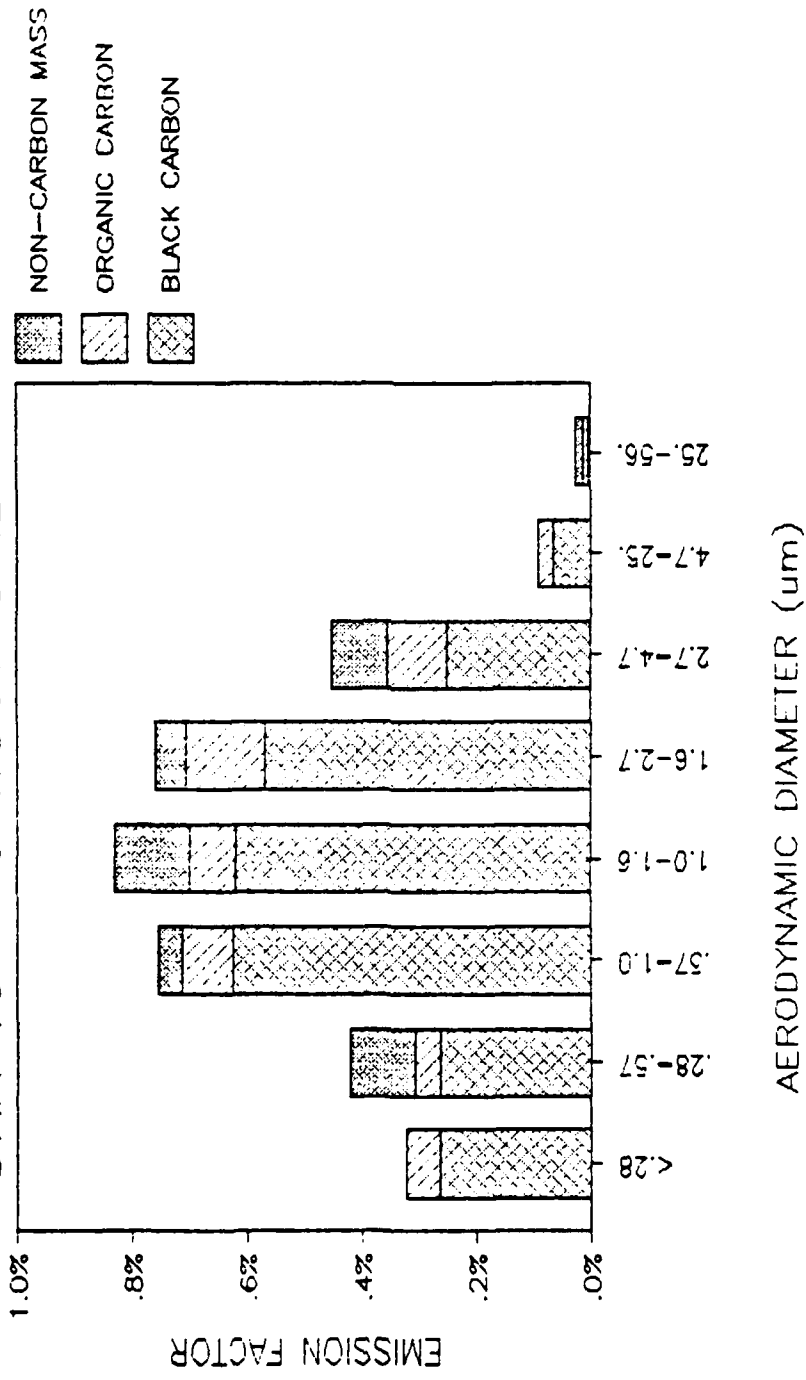


Fig. 11



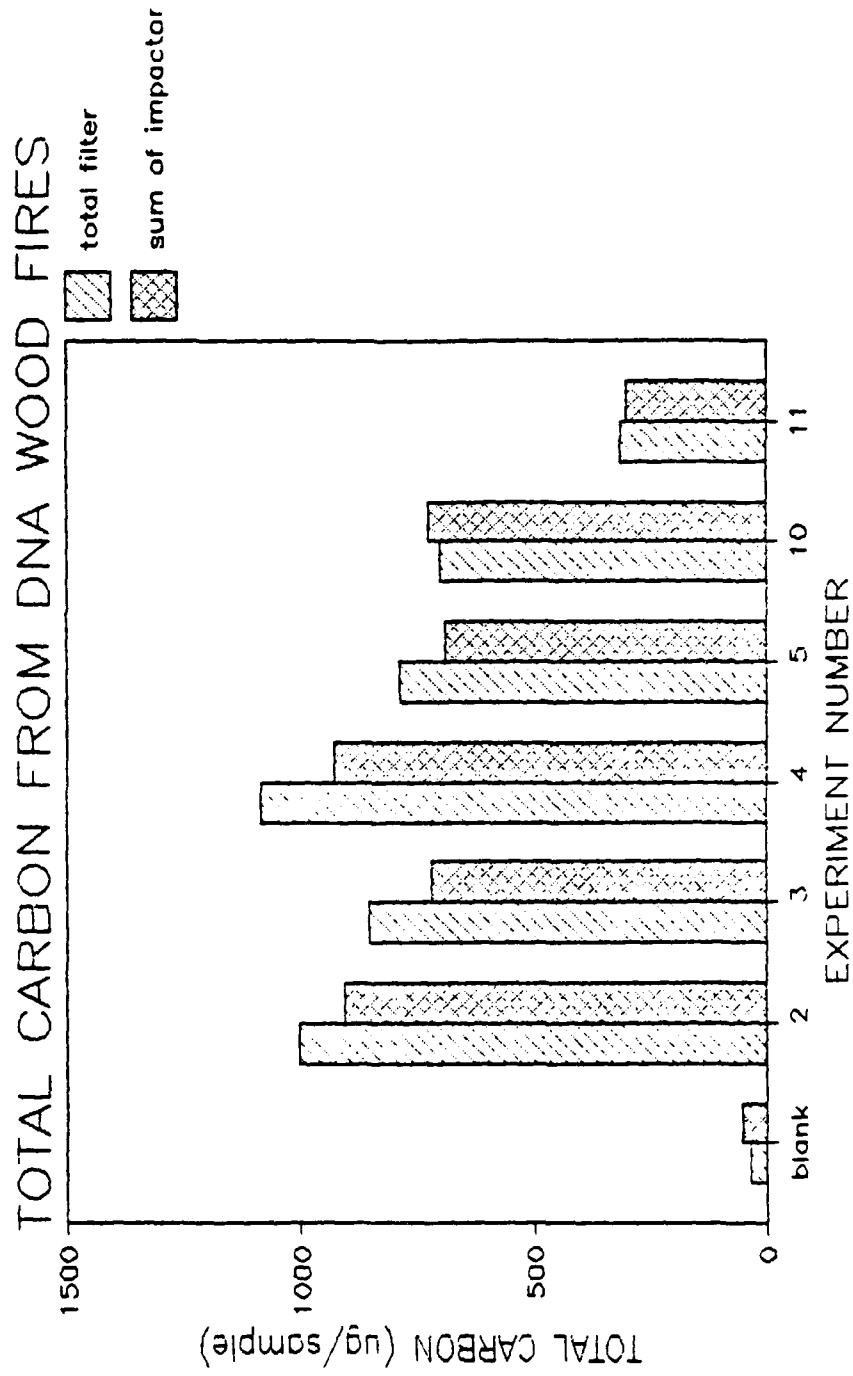


Fig. 12

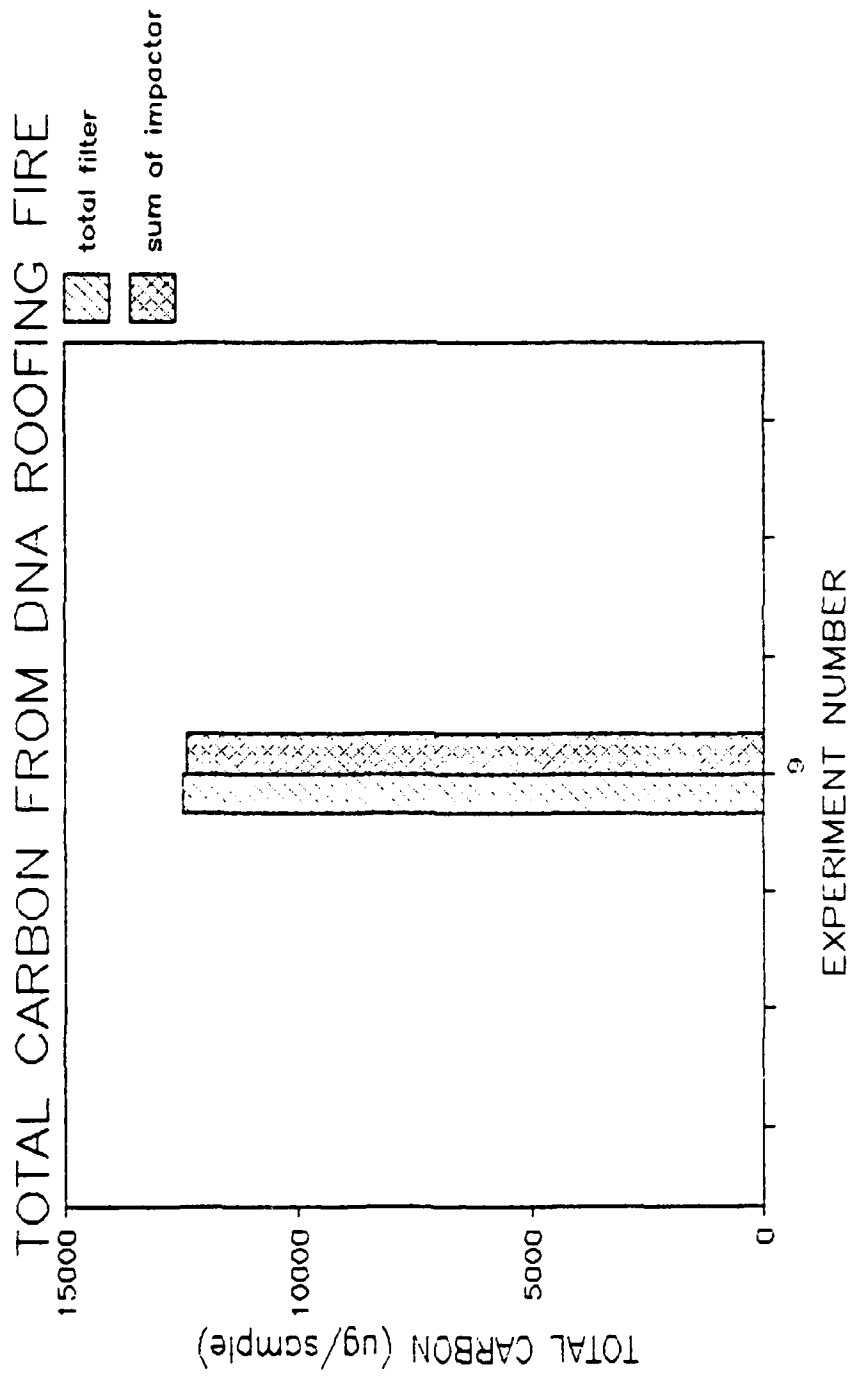


Fig. 13

Preliminary Measurements of the Absorption Properties  
of the Smoke from Burning Plastic Materials

E. M. Patterson

Georgia Institute of Technology  
Atlanta, Georgia 30332

As part of a study of the emissions of burning plastic materials, we have made a series of small scale burns with three different types of plastic materials: polystyrene, polyvinyl chloride, and polypropylene. We have also made some preliminary burns with admixtures of plastic in an inorganic material.

The flaming combustion of these materials has produced a highly absorbing smoke. We will present this preliminary data and discuss it in relation to earlier estimates of the absorption properties of similar smokes.

Room-Scale Smoke Characterization Testing at  
Sandia National Laboratories\*

by:  
Steven P. Nowlen  
David C. Williams  
Wayne Einfeld

Sandia National Laboratories  
Albuquerque, NM, 87185

A major emphasis of the Sandia National Laboratories (SNL) global effects research effort is to provide cross scale data on the characteristics of smoke particulate from liquid fuel fires. Fire scales investigated range from very small lab-scale experiments to very large experiments involving a 167 square meter pool fire. This presentation will focus primarily on the efforts associated with testing at an intermediate "room-scale" which involves testing of liquid fuel pools fires from 0.02 to 1.0 square meters in size. The efforts to be discussed are funded primarily through an internal SNL research and development fund and in part through Defense Nuclear Agency (DNA) funding.

For the room-scale testing, instrumentation currently being utilized for the characterization of the particulate includes cascade impactors, a differential mobility particle sizing system, laser based light scattering particle sizers, an integrating nephelometer, three wavelength optical extinction probes, and various filter sampling techniques. In addition, fuel consumption rate, plume temperatures, and effluent oxygen, carbon dioxide, and carbon monoxide concentrations are also monitored.

Experimentation at the room-scale has taken two forms. Several tests involving sampling of effluent from the facility stack have been performed. In addition a special chamber has been constructed at the facility for the investigation of the effects of aging on particulate characteristics. This aging chamber is constructed of electrically conductive plastic material and provides an aging volume of approximately 4.5 cubic meters (160 cubic feet). The chamber is housed within the test facility structure so that the ambient environment can be controlled and monitored. A relatively high density smoke sample is introduced into the chamber and then sampled periodically over a period of up to 48 hours. Two such aging experiments have been conducted to date.

Experimental work associated with the aging of smoke particulate is being conducted in conjunction with efforts to model the aerosol aging behavior analytically using the CONTAIN code and its aerosol module, MAEROS. These models were originally developed under the auspices of the U. S. Nuclear Regulatory Commission's program for the analysis of severe accidents in nuclear power plants. The goal of the current effort is to develop improved capabilities to model the aging behavior of smoke particulate analytically and to apply this capability to field-scale experiments. Ultimately it is expected that this effort will contribute to an understanding of the implications of aerosol aging with respect to the global effects issues.

\* This work performed at Sandia National Laboratories and supported by the US Department of Energy under Contract Number DE-AC04-76DP00789.

### A Brief Summary of Each of the Presentation Viewgraphs

#### A. Introduction

##### Slide A-1:

Research into nuclear winter or global effects smoke characterization issues at Sandia National Laboratories was initiated in 1985. Associated efforts have drawn on the expertise of several groups at Sandia involved in various aspects of experimental fire research, experimental aerosol measurements, and analytical modeling of aerosol behavior.

##### Slide A-2:

The Sandia efforts have focussed on investigation of local fire conditions, aerosol generation rates and properties, and the long term aging behavior of smoke aerosol. The investigation of these phenomena is required in order to provide source term input for the global circulation models use to predict the global effects of smoke lofted during a nuclear exchange. The Sandia effort includes a variety of projects including the conduct of fire experiments from lab-scale to near field-scale, the upgrading of an instrumented aircraft for use in nuclear winter smoke characterization studies, and analytical modeling of aerosol behavior.

##### Slides A-3,4

A major goal of the Sandia effort is to provide cross-scale correlations of the smoke generation properties. Liquid fuel fires (primarily JP-4 jet fuel) from as small as a few square centimeters (such as that shown in Slide A-3) to as large as 167 square meters (such as that shown in Slide A-4) have been conducted as a part of this effort. The range of fire scales spans 5-6 orders of magnitude. By investigating the behavior of a fairly simple, yet quite credible and prominent, fuel source over a wide range of fire scales we expect to show whether or not significant scaling effects exist with respect to both yield rates of smoke for the fuel and the properties of the smoke aerosol generated. These studies could have a significant effect on how smaller scale aerosol generation experiments are conducted by answering the question "how small is too small". As it will never be possible to test most materials in anything approaching the real scale answering this question is vital to obtaining accurate predictions of smoke generation parameters from experiments conducted at less than the actual scale.

##### Slide A-5

The focus of this discussion is on tests conducted in a "room-scale" facility. This facility, shown in both external and internal views in Slide B-1, is comprised of an underground bunker measuring 50x24x18 feet. This bunker has been divided into two enclosures, one for the housing of test instrumentation and a second for the actual conduct of test fires. The fire test enclosure measures 25x24x18 feet. Enclosure ventilation is controlled and variable, and is provided through a distributed per meter duct system. Fire products exit the enclosure through a stack at the top-center of the enclosure. Above the enclosure the stack is partially enclosed to provide a sheltered area for housing stack sampling instrumentation. This facility was originally developed for the U.S. Nuclear Regulatory Commission Fire Safety Research Program and has been used since 1975 in a variety of fire characterization related efforts.

Slide A-6

This slide shows a typical room-scale fire. This particular fire involved JP-4 fuel in a round pool with a diameter of 0.5 m (an area of 0.2 sq.m.). The fuel consumption rate in this case was 5-6 g/s. Note that this fire, and indeed all of the fires conducted to date at the room-scale, display turbulent plume behavior such as one would expect in the real scale. It should also be noted that the test fires are relatively small in comparison to the enclosure size and that direct interaction of the fire with the enclosure surfaces does not occur.

Slide A-7

There are three aspects to the focus of the room-scale efforts; (1) sampling from the facility stack, (2) long term aerosol aging experiments, and (3) analytical modeling of aerosol aging behavior. The stack sampling efforts are primarily in support of the effort to provide cross-scale correlation of the smoke generation parameters. The aerosol aging efforts represent a coordinated experimental and analytical effort to characterize the behavior of smoke aerosol over the long term. Each of these three aspects is to be discussed in the remainder of the presentation.

## B. Stack Sampling

### Slide B-1

Room-scale stack sampling efforts have focused on the fuel JP-4. Pool sizes tested to date range from 0.02 to 0.2 sq m. The facility is capable of using pools as large as 1.0 sq.m though pools of this size present some problems for the instrumentation due to the density of the smoke generated. The facility ventilation rate is variable though in general the ventilation rate utilized is such that the fires remain highly over ventilated. While the effects of oxygen deprivation, ambient humidity, and smoke recirculation could be investigated in this facility such investigations have not yet been undertaken.

### Slide B-2

Instrumentation applied to the room-scale stack sampling efforts includes cascade impactors, filters for measurement of total mass, on line analysis of carbon monoxide, carbon dioxide, oxygen, and total unburned hydrocarbon concentrations, and three wavelength optical extinction probes. Also utilized are several instruments used on the Sandia instrumented aircraft including a Differential Mobility Particle Sizer (DMPS), an integrating nephelometer, grab sample capabilities, and ASASP and FSSP laser scattering particle size counters. Use of the instrumented aircraft instrumentation is providing the cross-scale data we desire while simultaneous use of the more conventional cascade impactors is providing the opportunity to directly correlate results from the more exotic instruments to that obtained with the impactors often used in other efforts.

### Slide B-3,4

Slide B-3 shows typical smoke mass/size distributions obtained using the cascade impactors. The ordinate represents a normal probability distribution of percent of smoke mass while the abscissa represents a logarithmic distribution of aerodynamic diameter. The fact that the experimental data is very well represented by a straight line on this projection implies that for the range of particle sizes to which the impactors are sensitive the particle mass distributions of raw smoke are well represented by a log-normal distribution. These slides actually shows the data gathered for three sizes of JP-4 pool fire. While some differences in the size distributions are apparent it is not certain whether or not these plots are sufficient to imply a statistically significant factor. Further experimentation is expected to either verify or refute the effects illustrated in these plots. At least on a gross basis the smoke mass/size distributions over the order of magnitude represented here are quite similar. As the pool size decreases the mass median diameter appears to shift upward and the width of the distribution appears to narrow (as shown by the decreasing standard deviation).

### Slide B-5

This slide shows the particle number distributions as measured by the two laser scattering particle sizers for each of two experiments. These two plots are typical of the results obtained. Note that the peak of the distribution seems to have shifted downwards slightly in the smaller pool as opposed to the larger pool. Again, further experimentation will be required to verify the validity of this effect.

Slide B-6

This slide shows plots of the particulate number versus size distribution as measured by the DMPS system for each of two JP-4 pool fire sizes. These plots are typical of several samples taken during testing. Note that each of the two plots shows a peak in number concentration near 0.6 microns diameter. Note however that the peak for the smaller pool seems "softer" (i.e. less pronounced) than that for the larger pool. This again may be a legitimate effect of fire scale though further testing will be required to verify the effect. Also note that very little particulate is observed in the range from 0.017 to 0.2 microns diameter. These results appear to be consistent with the results obtained using the cascade impactors (shown in Slide B-6) and with the results obtained using the laser scattering probes (shown in Slide B-7). In particular the somewhat "softer" peak indicated here for the smaller pool is also reflected in the laser probe data.



### C. Experimental Aging Investigations

#### Slide C-1,2

Experimental efforts associated with characterization of the aging behavior of smoke aerosol are utilizing an electrically conductive aging chamber to hold a large sample of smoke for sampling. The chamber volume is 160 cubic feet (4.5 cubic meters). The chamber is housed within the instrument enclosure at the room-scale facility and is hence isolated from both the external environment and from direct effect of the fire (e.g. thermal radiation, high temperatures, etc.). A sample of smoke aerosol is introduced into the aging chamber through a short run of duct directly from the burn enclosure. The chamber is then sealed and the smoke is sampled periodically for, typically, 24 hours.

#### Slide C-3

Most of the instrumentation used for stack sampling is also used in the aging experiments. This instrumentation includes cascade impactors, total filter samples, optical extinction probes (3), the differential mobility particle sizer, and the laser scattering particle size counters. The primary data of interest is the total airborne mass versus time, the particle size characteristics versus time, and the specific optical extinction coefficient versus time.

#### D. Analytical Aging Studies

Vugraph D1. Results of the smoke aging experiments were compared with simulations using the CONTAIN code for the analysis of nuclear power plant containments during core melt accidents. This code was developed for the Nuclear Regulatory Commission (NRC) in support of the NRC's severe accident research program. The code includes coupled models for a wide variety of accident phenomena and plant equipment [Be85], many of which are not relevant here. CONTAIN includes a coupled treatment of thermal-hydraulic phenomena and aerosol phenomena. The code uses a control volume approach, in which the system of interest is represented by one or more control volumes, called cells, which may be interconnected in any desired fashion. Each cell is assumed to be well-mixed. All calculations to be presented for the smoke aging experiments used a single-cell representation of the aging chamber.

The CONTAIN aerosol model, called MAEROS, has been documented separately [Ge80, Ge82], but the CONTAIN implementation of MAEROS is modified somewhat from the stand-alone versions. The code models processes that remove aerosols at cell boundaries, including deposition by diffusion, thermophoresis, diffusiophoresis, and gravitational settling. The treatment of aerosol agglomeration processes includes contributions to the agglomeration kernels from Brownian diffusion, differential gravitational settling, turbulent shear effects, and turbulent inertial effects. Only the agglomeration models are of direct interest to global effects analysis, but processes removing aerosol at the chamber boundaries are also important in the aging experiments.

Vugraph D2. In CONTAIN (or MAEROS), the aerosol size distribution is divided into a number (typically 20) of subranges, called sections, and the rate of interaction between particles in the various sections is calculated. This rate is proportional to the numbers of particles in each of the two interacting size sections multiplied by the agglomeration kernel,  $K(d_1, d_2)$ , for interaction between particles of size  $d_1$  with particles of size  $d_2$ . (The present discussion is somewhat oversimplified; the code actually treats a continuous distribution of particle sizes within each section and does not make the approximation of representing each section with a discrete particle size.) The kernel is a function of several parameters describing the aerosol properties and atmospheric conditions. These parameters include the diameters of the interacting particles,  $d_1$  and  $d_2$ ; the effective density,  $\rho_p$ , of the particle; the dynamic shape factor,  $\chi$ , which is a multiplier to the drag calculated for a spherical particle; and the agglomeration shape factor,  $\gamma$ , which is a multiplier to the collision diameter calculated for a spherical particle. In addition, the kernels for turbulent shear and turbulent inertial agglomeration depend upon the turbulent energy dissipation density,  $\epsilon$ .

The dependence of the agglomeration kernels used in CONTAIN upon these parameters is sketched in the vugraph. There are also dependencies upon atmosphere properties (pressure, temperature, composition) which are not shown. It is apparent that the dependencies upon the governing parameters are strongly coupled, non-linear, and quite different for the different agglomeration processes.

The CONTAIN aerosol module also treats steam condensation on (and water evaporation from) solid aerosols. The smoke aging experiments were conducted at fairly low relative humidities, however, and these condensation/evaporation processes did not affect the present analysis.

Vugraph B3. Calculations using the CONTAIN code were performed and compared with the experimental results. At present, the experimental results which are available and which are suitable for code comparisons are limited to the data on total airborne mass concentration and aerodynamic size distribution as a function of time. Initial conditions in the calculation were taken from the mass loading derived from the first filter sample, with a size distribution (aerodynamic mass median diameter (AMMD) and geometric standard deviation ( $\sigma_g$ )) derived from the first impactor measurement. The initial size distribution was assumed to be log-normal, although the code does not impose any requirement that the size distribution must remain log-normal as the calculation proceeds.

The impactor measurements give the size distribution as a function of  $d_a$ , the aerodynamic diameter. In terms of the parameters of the CONTAIN aerosol model,  $d_a$  is given by

$$d_a = d_p (\rho_p / \rho_{oo})^{1/2} / \chi^{1/2}, \quad (D.1)$$

where  $\rho_{oo}$  is the reference density (1000 kg/m<sup>3</sup>) used in the definition of the aerodynamic diameter. Any combination of  $d_p$ ,  $\rho_p$ , and  $\chi$  input to the code for the initial aerosol description may be regarded as being equally consistent with the experimental values, provided only that the code input values are chosen subject to the constraint that the initial value of  $d_a$  as given by Eq. D.1 still be equal to the initial experimental value of  $d_a$ .

Sensitivity studies were performed for the aerosol input parameters, subject to the constraint given by Eq. D.1 and the measured values of the AMMD and  $\sigma_g$  at the start of the experiment. Note that no constraint at all thereby results for the agglomeration shape factor,  $\gamma$ . Though  $\chi$  and  $\gamma$  can in principle be interpreted theoretically in terms of actual particle shapes, it is common to estimate these parameters empirically by back-fitting code calculations to the results of aerosol experiments. Often values substantially different from unity are thereby obtained [Li85]. These values are sometimes difficult to justify theoretically, i.e., in terms of actual particle shapes.

Vugraph D4. Fully-dense graphite has a bulk density  $\rho_o$  of about 2000 kg/m<sup>3</sup>, but it is expected that dry soot aerosols (such as those involved here) will form loose agglomerates having  $\rho_p \ll \rho_o$ . Using a simple fractal model for aerosol structure, with the fractional dimensionality,  $D$ , equal to 2.3, a value of  $\rho_p$  equal to 63 kg/m<sup>3</sup> was estimated as providing a reasonable starting point for the analysis of the first aging experiment. It must be emphasized that there was little experimental support for the specific values of the parameters assumed as input to the fractal model and this density must be

viewed as very uncertain. Qualitatively, the low density is consistent with the experimental observation of light, fluffy aerosol deposits, with little evidence of an oily component that could significantly increase effective densities.

In the vugraph, CONTAIN calculations for aerosol concentrations as a function time are compared with the experimental results assuming  $\chi = 1$ ,  $\rho_p = 63$ , and  $\gamma$  values of 1.0, 2.5, and 4.0. Though there is some scatter in the experimental data, it is clear that the calculations with  $\gamma = 1$  give a concentration decay rate that is considerably too slow, while the calculations with  $\gamma = 2.5$  and 4 provide reasonable envelopes to the experimental data.

Vugraph D5. In this vugraph, the experimental AMMD values are compared with the code calculations for the same cases as those for which the concentrations were presented in vugraph D4. There were significant differences between the experimental size distributions derived from the high-flow and the low-flow impactors. The reasons for these differences have not yet been determined. The best fit to the high-flow impactor data is provided by the  $\gamma = 2.5$  curve; however, neither of the other two curves can be considered to be in gross disagreement with the data, in view of the scatter in the data. Neither these calculations nor any others that were performed yielded a reasonable fit to the low-flow impactor data for AMMD. It is believed likely that the model used here could not be forced into agreement with the low-flow AMMD data, no matter what aerosol parameters were chosen as input.

Vugraphs D6 and D7. In the experiment, the effective particle density  $\rho_p$  is very uncertain and, furthermore, the level of turbulence is not known. Although turbulent intensities were likely extremely low during most of the time (for one thing, stable temperature profiles existed throughout), a mixing fan was occasionally operated for short periods, which could have raised turbulence to significant levels during its operation, even though it was operated only briefly and at a minimal power level. (The fan was used in order to overcome vertical stratification due to gravitational settling; turbulence levels during operation are not known.) These vugraphs illustrate the potential significance of  $\rho_p$  and the turbulent intensity,  $\epsilon$ , for the aging analysis. Solid and dashed curves give results calculated for  $\rho_p = 1000 \text{ kg/m}^3$  and  $10 \text{ kg/m}^3$ , respectively; heavy and light curves give results calculated, respectively, for  $\epsilon = 0.001$  and  $0.0$  SI units ( $\text{SI} = \text{m}^2/\text{s}^2 = \text{J}/\text{kg}\cdot\text{s}$ ). Several points may be noted:

- o Turbulence at the level considered here has a negligible effect upon the high-density particles but a large effect upon the low density particles. This difference may be readily understood in terms of the agglomeration kernels in vugraph D2: the shear term, in particular, varies as  $d_p^2$ , and  $d_p$ , in turn, varies as  $\rho_p^{-1/2}$ , for a given value of  $d_a$ . (Similar considerations show there is a strong interaction between turbulence and  $\gamma$ .)

- For the same initial value of  $d_a$ , the high-density particles give more rapid depletion and agglomeration than the low-density particles in the absence of turbulence, while the reverse is true for  $\epsilon = 0.001$ .
- For the high-density particles, the curves calculated for  $\gamma = 1$  do not deviate greatly from the experimental results, even though the results obtained assuming  $\gamma = 1$  and lower particle densities gave poor agreement with the data, assuming  $\epsilon = 0$ .
- On the other hand, the curve calculated with  $\gamma = 1$ ,  $\rho_p = 10$  and  $\epsilon = 0.001$  gave as good an agreement with the data as any of the calculations in vugraphs D4 and D5.
- It is clear that fits to aerosol experiments can be nonunique, especially if there is not a good characterization of the particle density and the level of turbulence. Without a better control of these parameters, aerosol parameters derived from experiments such as these can be used only with caution in calculations involving conditions that are very different from those of the experiment.

It should be noted that models for turbulent agglomeration, even given the value of  $\epsilon$ , have received only limited experimental testing. Qualitatively, there is little doubt that the effect does exist.

Vugraphs D8 and D9. Only agglomeration effects are of importance to aerosol aging in global effects analysis, but boundary effects are also important to the experiment, since the aging chamber was relatively small. It is therefore important to consider whether the experiment is, in fact, sensitive to the agglomeration effects of interest. In order to determine the impact of boundary effects alone upon the analysis, calculations were run for the parameter sets ( $\rho_p = 1000$ ,  $\gamma = 1$ ,  $\epsilon = 0$ ) and ( $\rho_p = 63$ ,  $\gamma = 2.5$ ,  $\epsilon = 0$ ) with the initial aerosol concentration reduced by a factor of  $10^5$ , which effectively eliminates agglomeration. Results are compared with the calculations at the actual experimental concentrations in these vugraphs. The results suggest that, for the high density particle representation, the calculation of airborne mass may not be very sensitive to agglomeration parameters; i.e., the boundary effects appear to be dominant. For the  $\rho_p = 63$ ,  $\gamma = 2.5$  calculation, both agglomeration and boundary effects are important in controlling the airborne concentration as a function of time. For both particle representations, it is evident from vugraph D9 that the AMMD as a function of time is largely determined by the agglomeration processes, not the boundary effects.

Vugraphs D10 and D11. These vugraphs show results of simulations of the second aging experiment using three sets of aerosol parameters shown previously to give reasonable fits to the first experiment under the assumption of negligible turbulence:  $\rho_p = 1000 \text{ kg/m}^3$ ,  $\gamma = 1$ ;  $\rho_p = 63 \text{ kg/m}^3$ ,  $\gamma = 2.5$ ; and  $\rho_p = 63$ ,  $\gamma = 4.0$ . It is seen that the parameters giving an acceptable fit to the first experiment also yield a reasonable fit to the second, without any additional "tuning". It is also worth noting that there is no reason to believe that turbulence levels in the two experiments were the same (there is some reason to believe turbulence was less in the second). This

suggests that turbulent effects may not have been important during these experiments, since parameters derived assuming zero turbulence when turbulence was actually important would not be likely to give good agreement for a second experiment having different levels of turbulence.

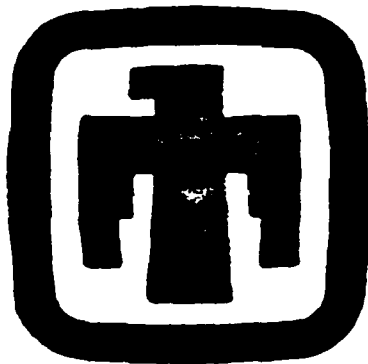
The present experiments and analyses have been discussed in terms of the particle aerodynamic diameters, since this is the experimentally-determined parameter. Optical properties of the smoke will show only an indirect relation to the aerodynamic diameter, and factors not considered here (precipitation scavenging, cloud processing, etc) may ultimately prove more important than dry agglomeration in governing the optical properties of global dispersions of smoke. Nonetheless, it does appear that smoke aging through agglomeration may have a nonnegligible impact upon global effects analysis [Pe86], and smoke aging experiments such as those discussed here can contribute toward the evaluation of this impact.

#### References.

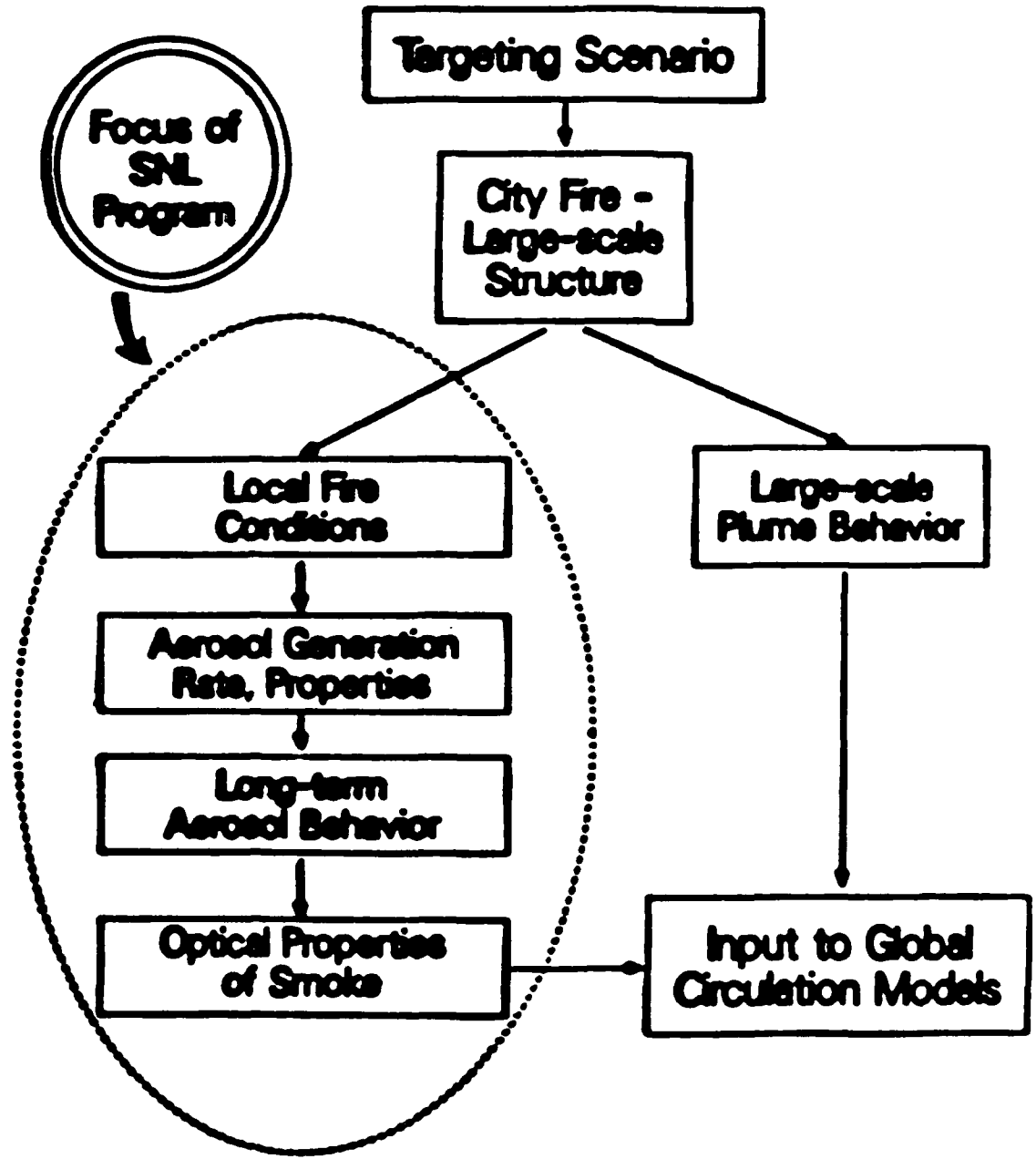
- Be85 K. D. Bergeron et al., "User's Manual for CONTAIN 1.0, A Computer Code for Severe Nuclear Reactor Accident Containment Analysis", Sandia National Laboratories, NUREG/CR-4085 (SAND84-1204), May 1985.
- Ge80 F. Gelbard and J. H. Seinfeld, J. Colloid. Interface Sci., 78, 485 (1980).
- Ge82 F. Gelbard, "MAEROS User Manual", Sandia National Laboratories, NUREG/CR-1391 (SAND80-0822), 1982.
- Li85 R. J. Lipinski et al., "Uncertainty in Radionuclide Release Under Specific LWR Accident Conditions", Sandia National Laboratories, SAND84-0410, February 1985.
- Pe86 J. E. Penner, "Progress in Developing the Smoke Source Term for "Nuclear Winter" Studies: Major Uncertainties", UCRL-94226 (Preprint), Lawrence Livermore National Laboratory (March 1986).

A-1

**Status of  
Nuclear Winter Research at  
Sandia National Laboratories**

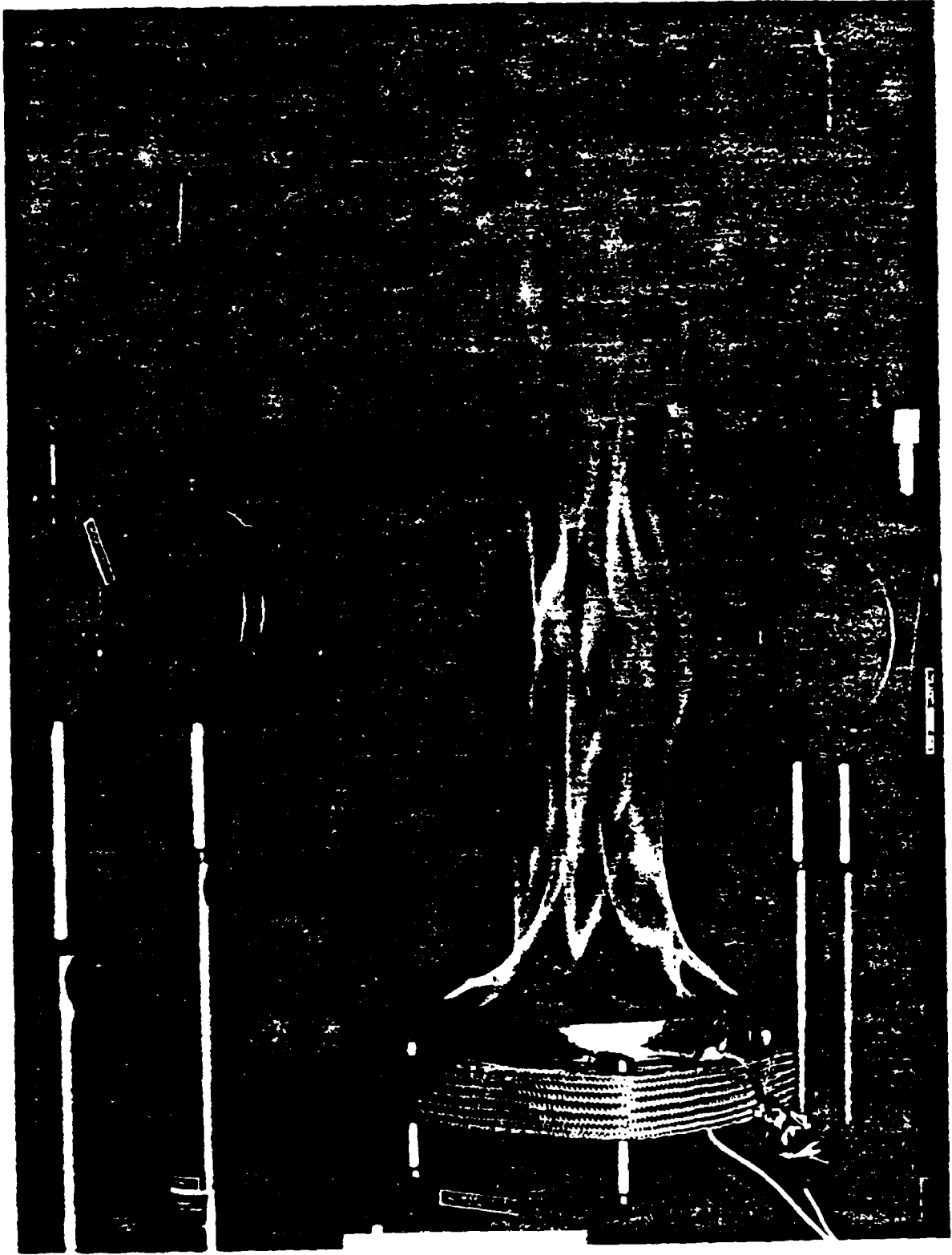


# PHENOMENA IMPACTING NUCLEAR WINTER SOURCE TERM

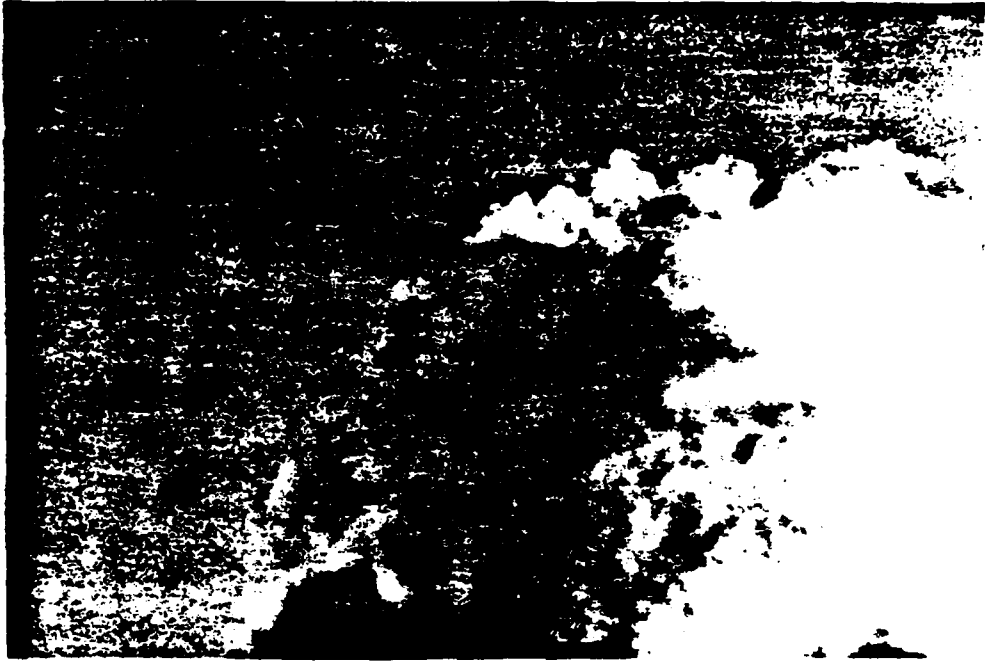




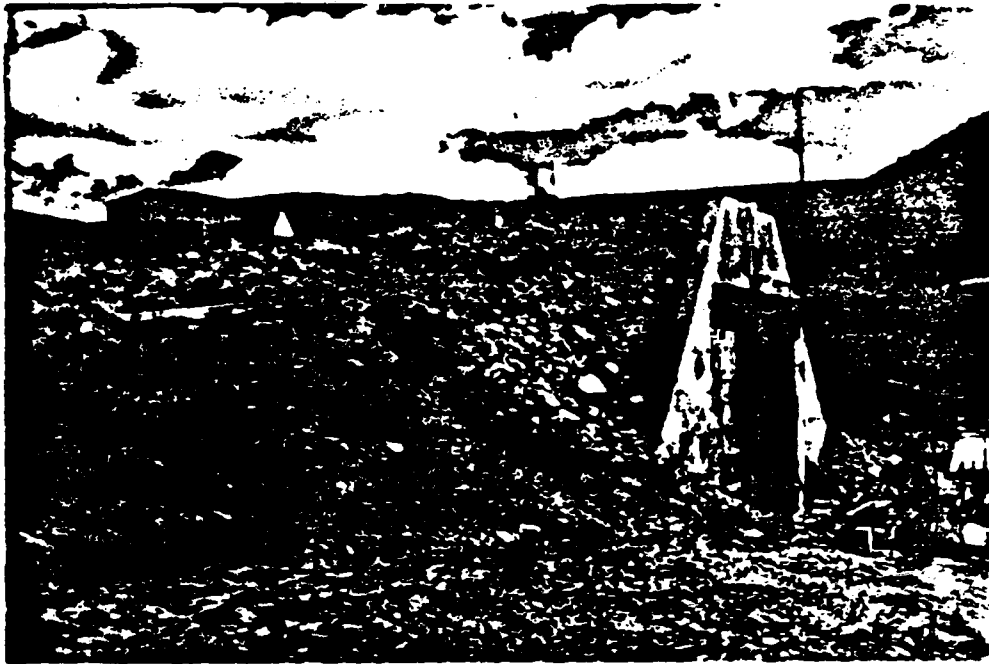
A-3



A-4



A-5



A-6



## **Room-Scale Smoke Characterization Efforts**

### **Three Areas of Focus:**

- Stack Sampling
- Aerosol Aging Experiments
- Analytical Modeling of Aerosol Aging

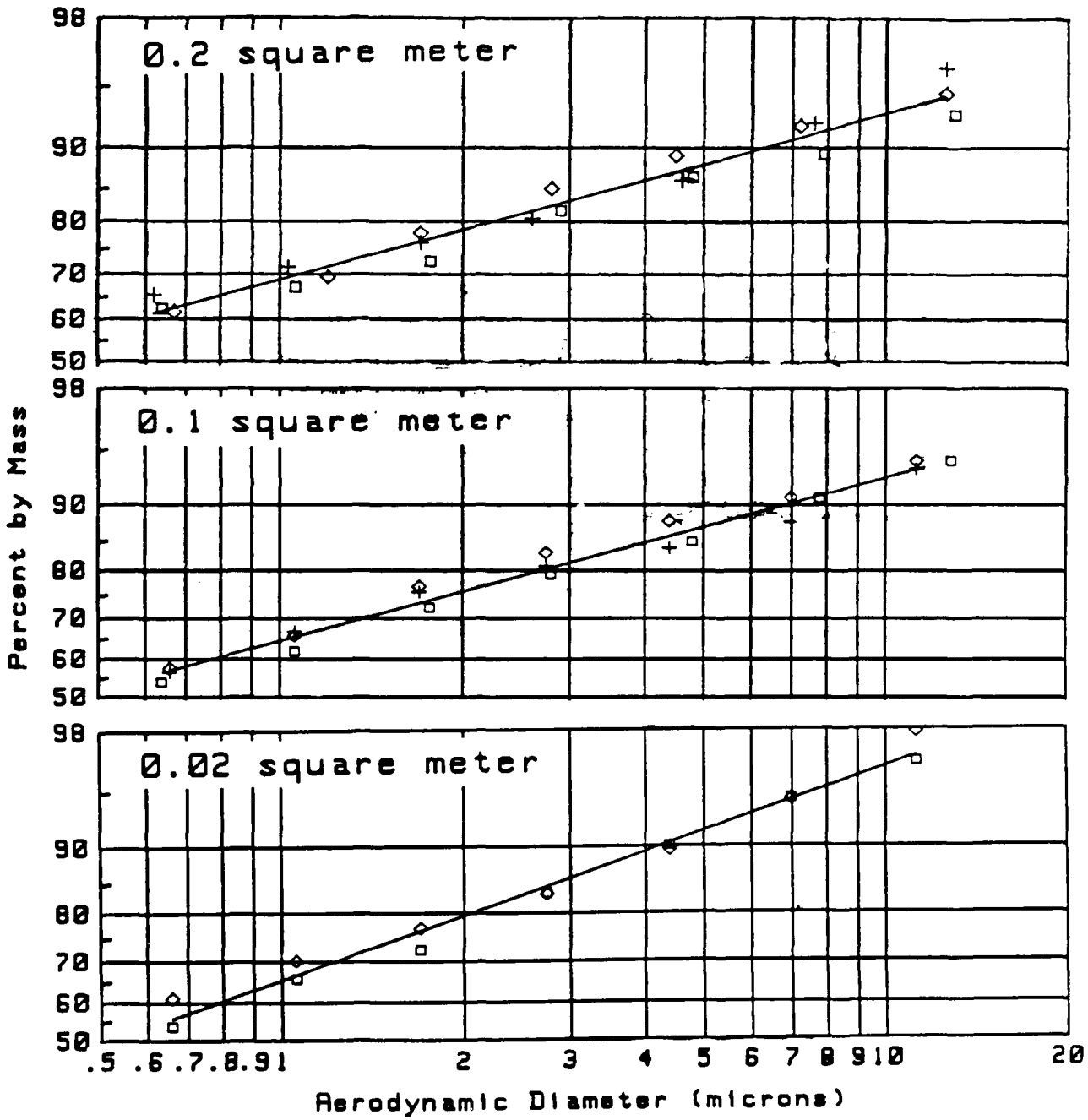
## Stack Sampling Test Parameters

- JP-4 Fueled Pool Fires
- Pool Sizes from 0.02 to 0.2 m<sup>2</sup>  
(pools up to 1 m<sup>2</sup> possible)
- Ventilation is Variable

# Stack Sampling Instrumentation

- Cascade Impactors
- Total Mass Filter Samples
- On-Line Gas Analysis  
(CO<sub>2</sub> CO THC)
- Optical Extinction Probes
  - OMPS
  - AGRSP
  - FGSP
- Integrating Nephelometer
  - Grab Samples

B-3

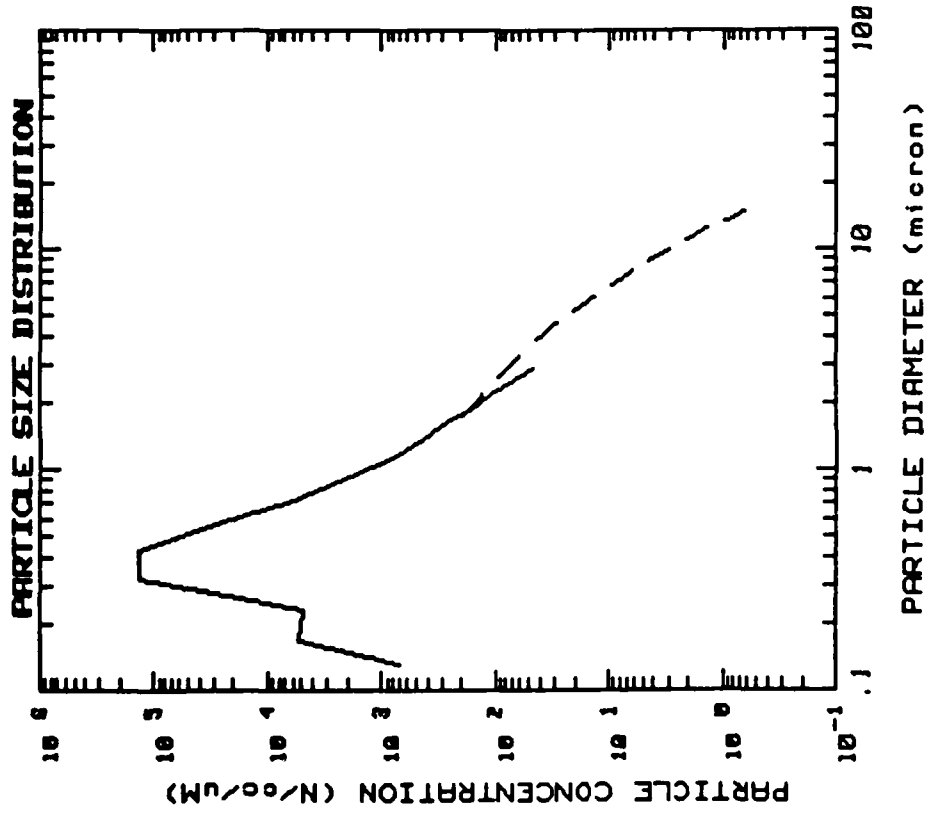


Percent of smoke mass accounted for by particulate smaller than the indicated size

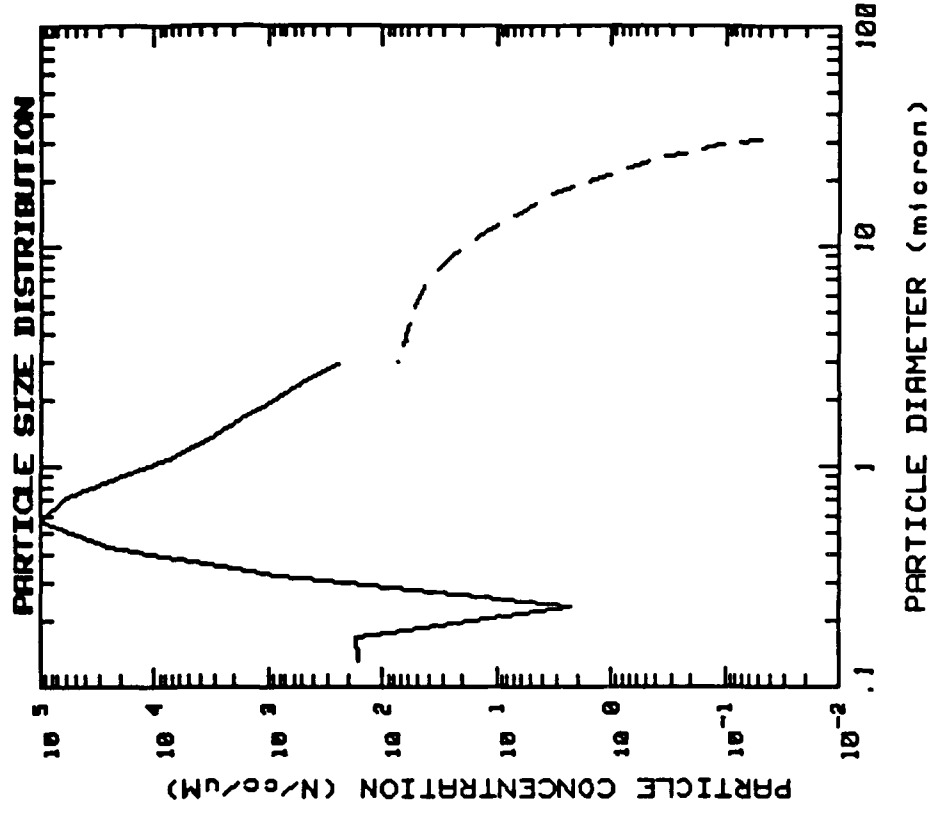


Summary of Impactor Data for  
Raw Smoke Sampled at the Stack  
of the Room-Scale Facility

Pool Size	Mass Median Diameter	Log-Normal Stnd. Dev.
0.02 m <sup>2</sup>	0.52 microns	5.13
0.10 m <sup>2</sup>	0.45 microns	8.28
0.20 m <sup>2</sup>	0.32 microns	10.2



Pool Size = 0.02 m<sup>2</sup>

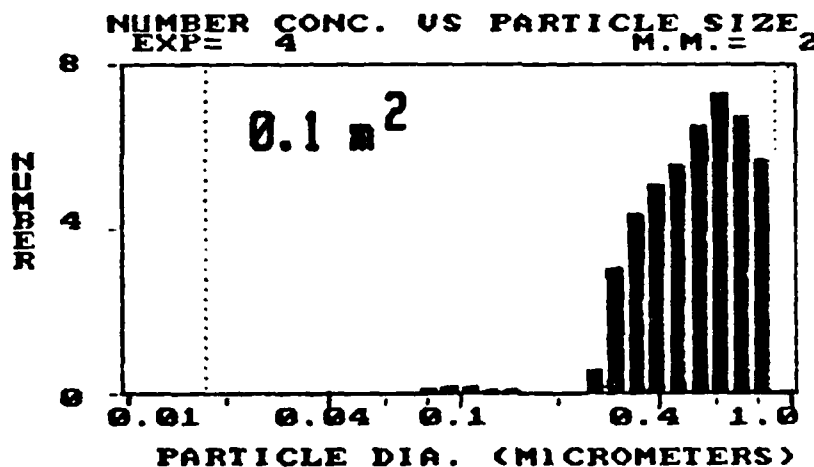
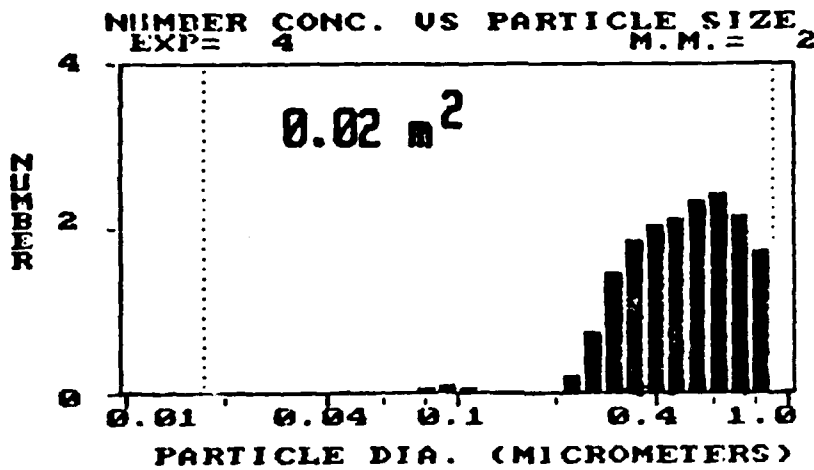


Pool Size = 0.1 m<sup>2</sup>

Typical particle number/size distributions as measured by the ASASP and FSSP probes for two JP-4 pool fire sizes.

B-5

B-6

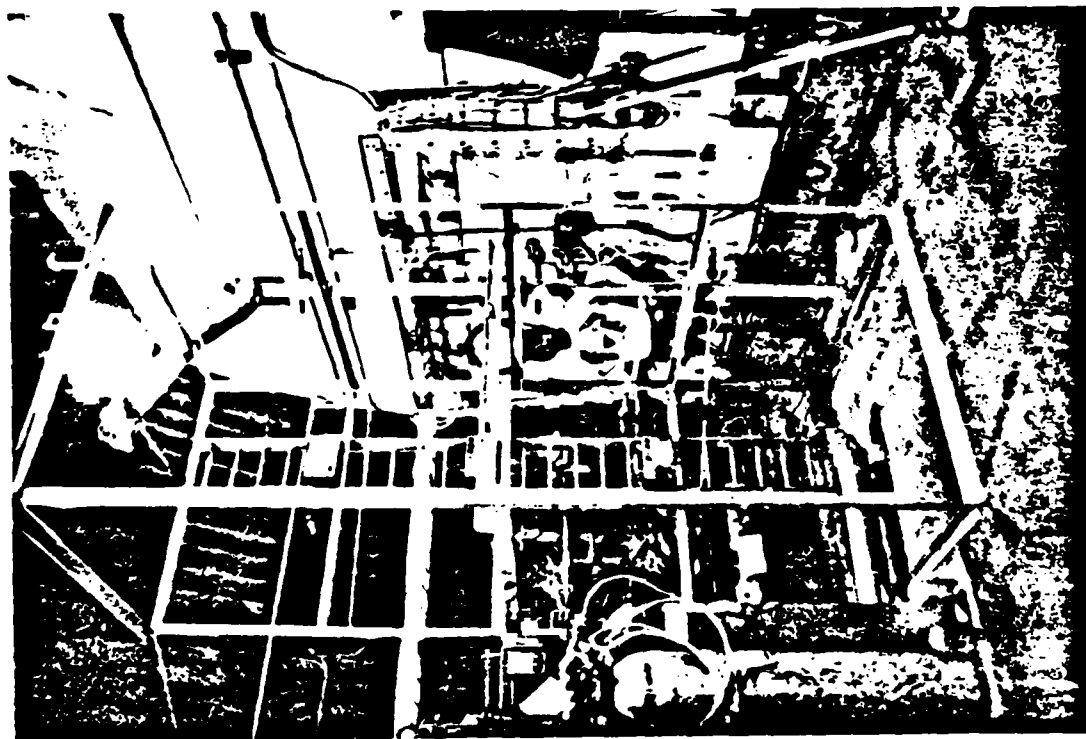


Typical smoke particulate number versus size distributions for JP-4 pool fires as measured by the Differential Mobility Particle Sizer

## **Aerosol Aging Test Parameters**

- Aging Chamber Constructed of Electrically  
Conductive Plastic
  - Chamber Volume 4.5 m<sup>3</sup> (160 ft<sup>3</sup>)
- Chamber Isolated in Stable Environment
- Aerosol Introduced Into Aging Chamber  
Directly From Burn Enclosure
  - Typical Test Lasts 24 Hours

C-2



# Aerosol Aging Experiment Instrumentation

- Cascade Impactors
- Total Mass Filter Samples
- Optical Extinction Probes
  - OMPS
  - PARSP

## CONTAIN Code for Severe Accident Analysis

- \* Developed for Nuclear Power Plant Containment Analysis During Severe Accidents -- NRC Sponsored.
- \* Integrated Treatment of Thermal-Hydraulic, Aerosol and Radionuclide Phenomena
- \* Includes MAEROS Aerosol Module
  - Treats aerosol deposition by diffusion, thermophoresis, diffusiophoresis, and gravitational settling
  - Treats agglomeration by Brownian, gravitational, turbulent shear, and turbulent inertial mechanisms



Fig. D1

## Agglomeration Kernels in CONTAIN

**Brownian:**  $\propto (\gamma/\chi)f(d_1, d_2)$   
(function  $f$  has complex dependence upon  $d_1, d_2$ ; favors agglom. of small particles)

**Grav.:**  $\propto (\gamma^2/\chi)\rho_p d_2^2(d_1^2 - d_2^2)$

**Turb. Shear:**  $\propto \gamma^3(d_1 + d_2)^3 \varepsilon^{1/2}$

**Turb. Inertial:**  $\propto (\gamma^2/\chi)\rho_p \varepsilon^{3/4} d_2^2(d_1^2 - d_2^2)$

**Where**

$\gamma$  = agglomeration shape factor

$\chi$  = dynamic shape factor

$d_1, d_2$  = particle diameters ( $d_p$ );  $d_1 \geq d_2$

$\rho_p$  = particle density

$\varepsilon$  = turbulent energy dissipation density



Fig. D2



## CONTAIN Simulations of Aging Experiments

- \* Use Experimental Initial Values of Concentration ( $C_0$ ), AMMD, Geom. Std. Deviation ( $\sigma_g$ )

	<u><math>C_0</math>, kg/m<sup>3</sup></u>	<u>AMMD, <math>\mu\text{m}</math></u>	<u><math>\sigma_g</math></u>
AGE-1	$5.0 \times 10^{-4}$	0.70	4.6
AGE-2	$2.0 \times 10^{-4}$	0.42	7.7

- \* Input  $C_0$ ,  $\sigma_g$  values directly from experiment
- \* Input Initial Mass Median Diameter and  $\rho_p$  Consistent with Experimental AMMD
- \* Use  $\gamma$  as Fitting Parameter ( $\chi=1$ , all)
- \* Sensitivity Studies on Turbulence

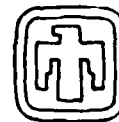


Fig. D3

AGE-1: CONCENTRATION; EFFECT OF  $\gamma$  (WITH  $\rho_p=63, \epsilon=0$ )

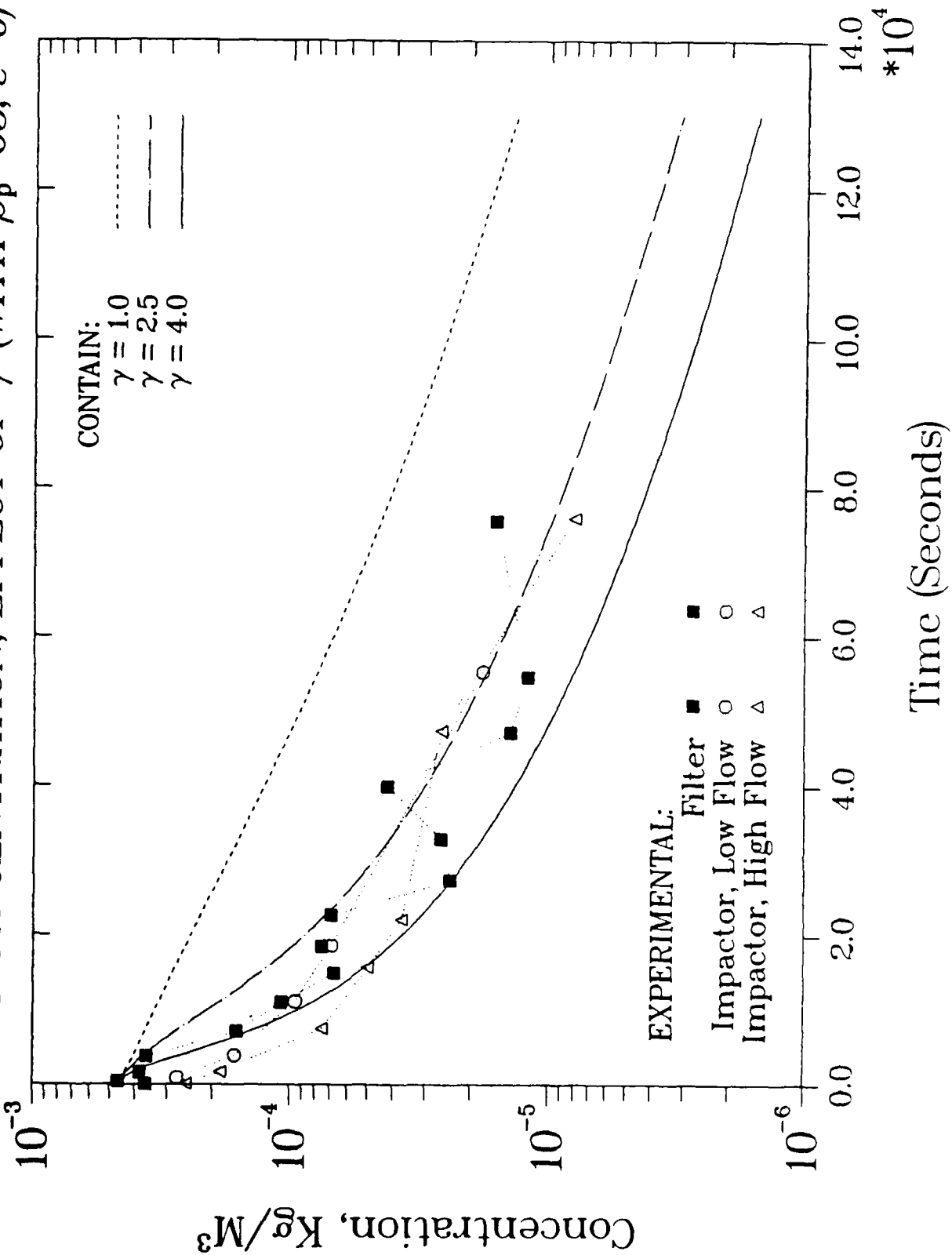


Fig. D4

AGE-1: AMMD; EFFECT OF  $\gamma$  (WITH  $\rho_p=63, \epsilon=0$ )

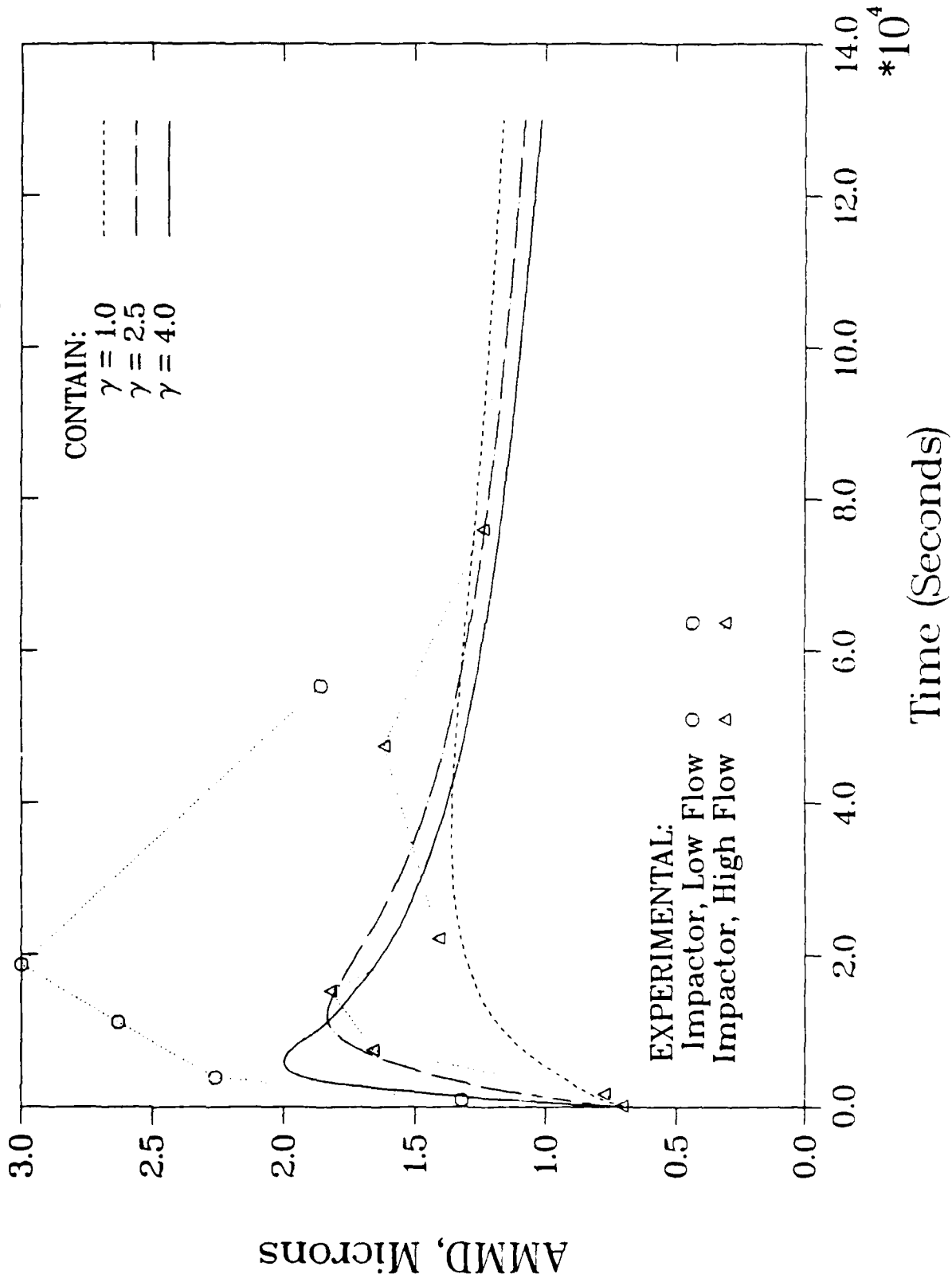


Fig. D5

# AGE-1: CONCENTRATION; EFFECT OF $\epsilon$ AND $\rho_p$

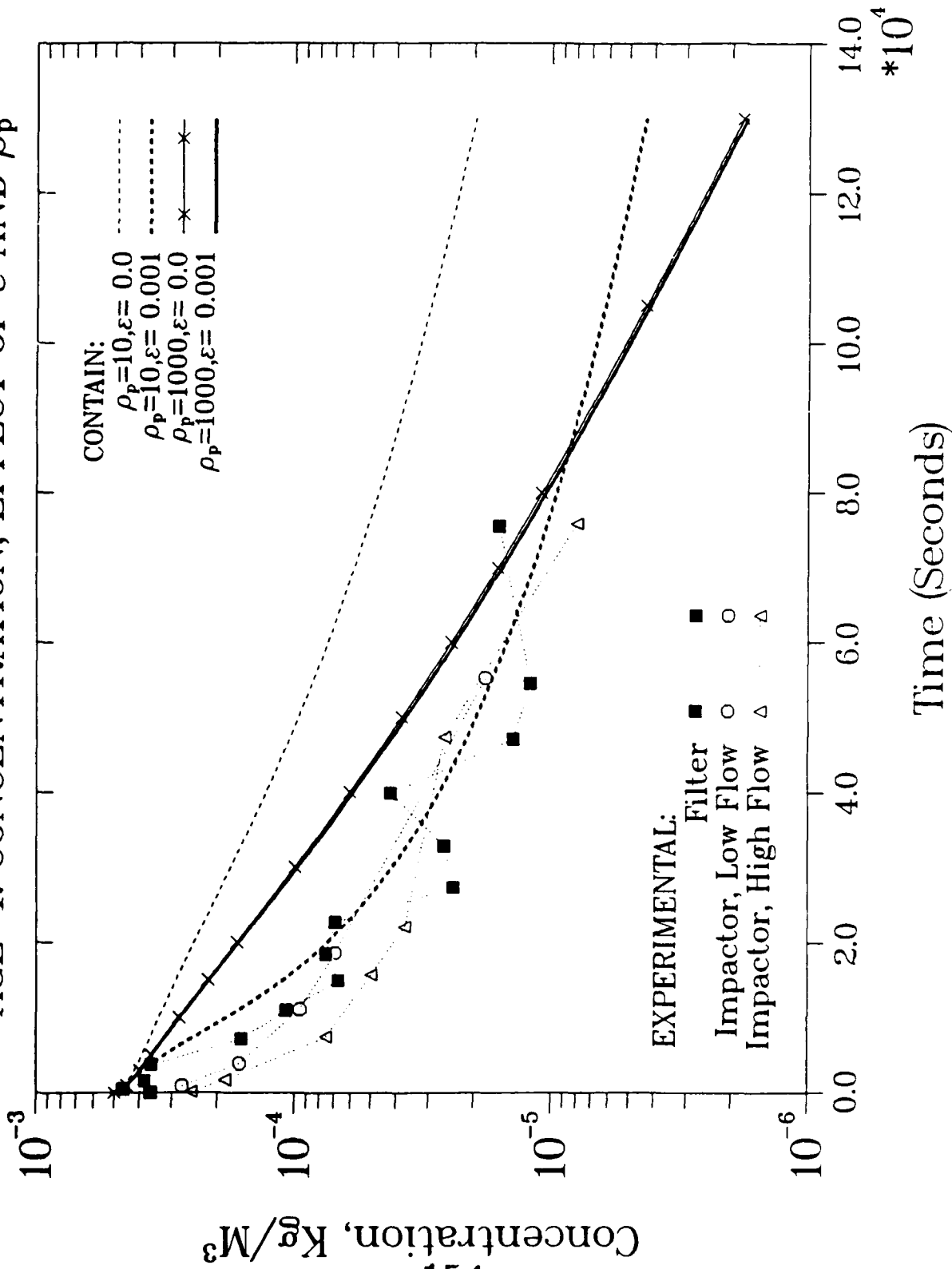


Fig. D6

# AGE-1: AMMD; EFFECT OF $\rho_p, \epsilon$

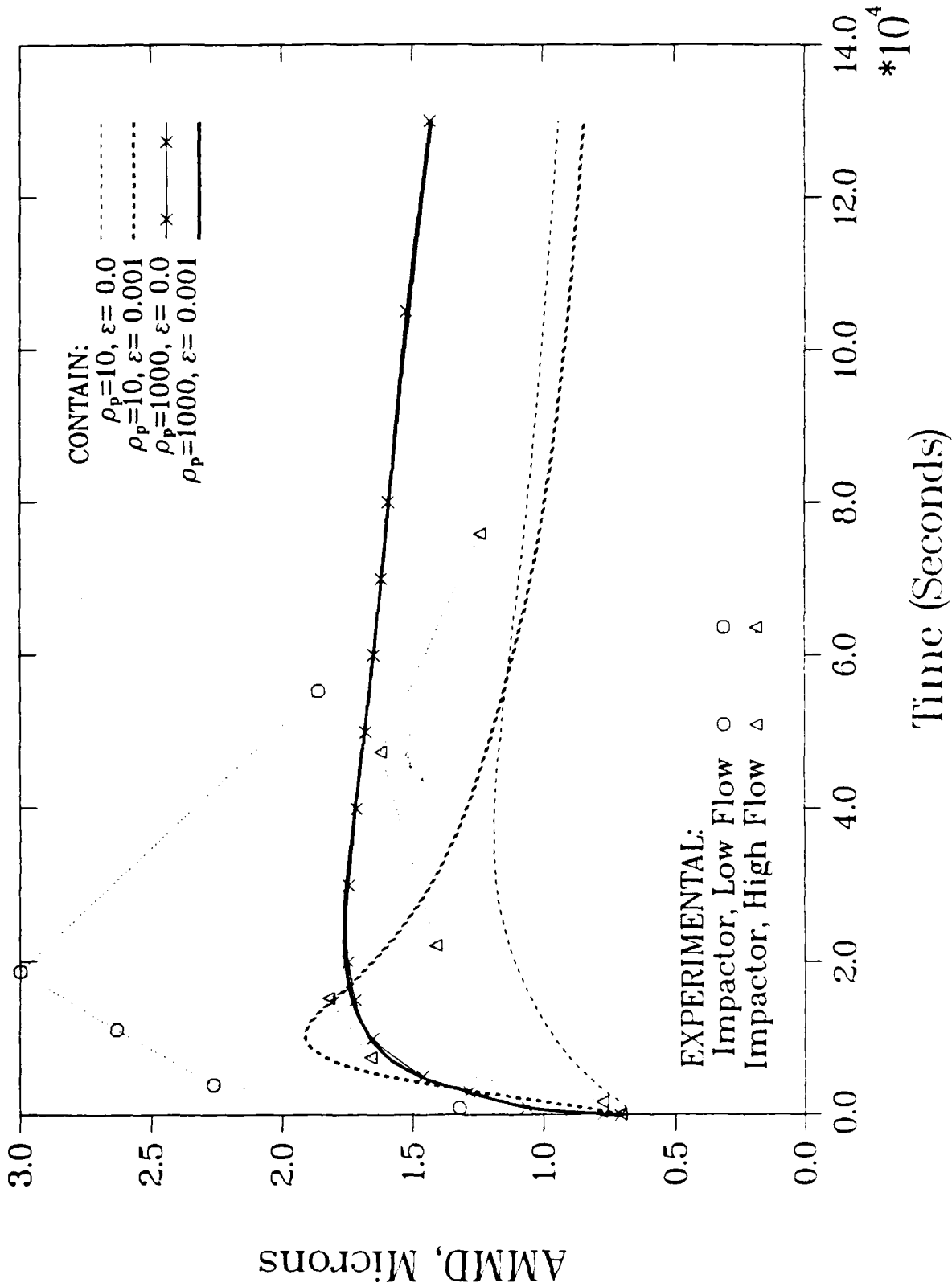


Fig. D7

# AGE-1: CONCENTRATION; EFFECT OF AGGLOMERATION

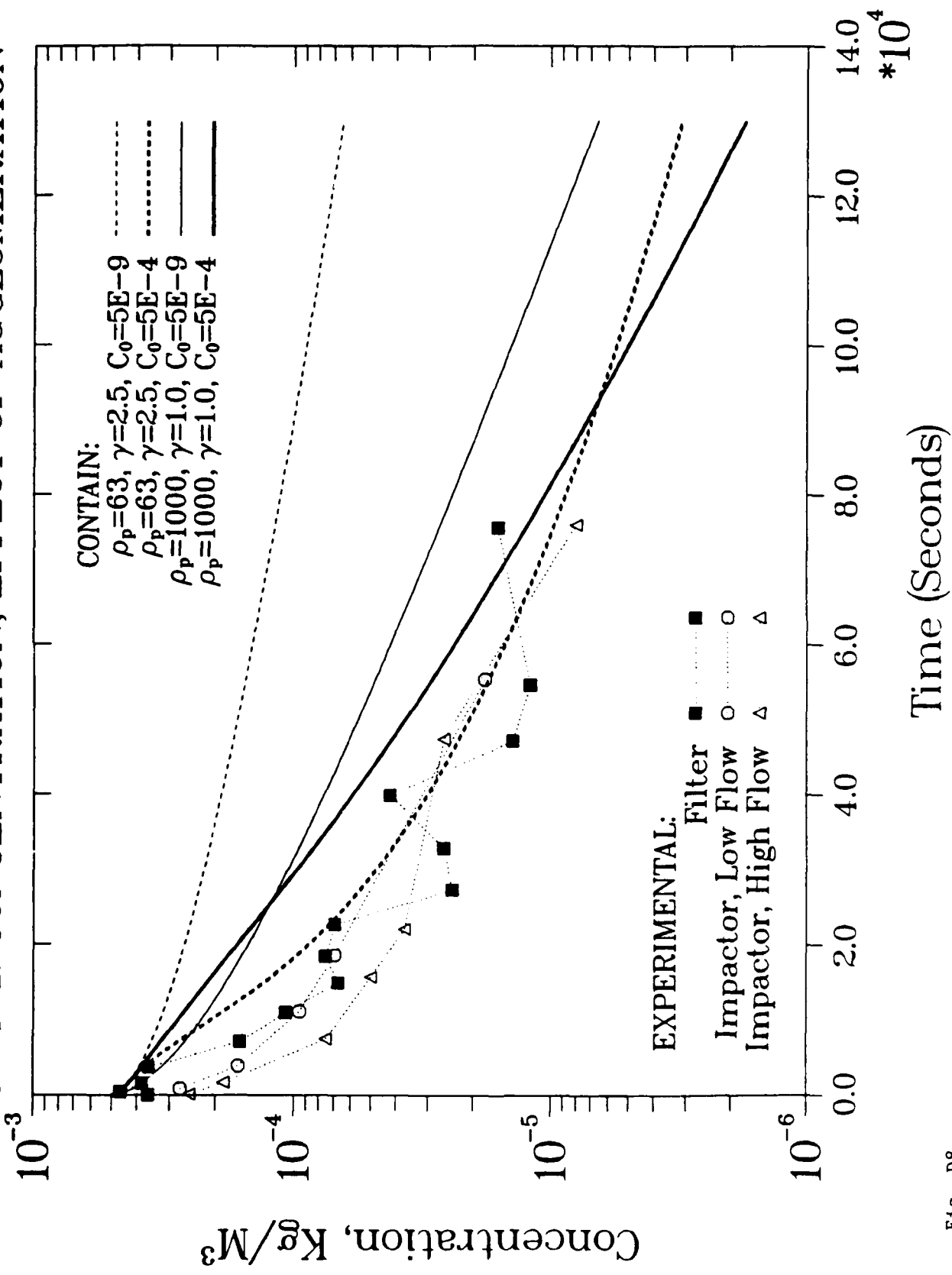


Fig. D8

# AGE-1: AMMD; EFFECT OF AGGLOMERATION

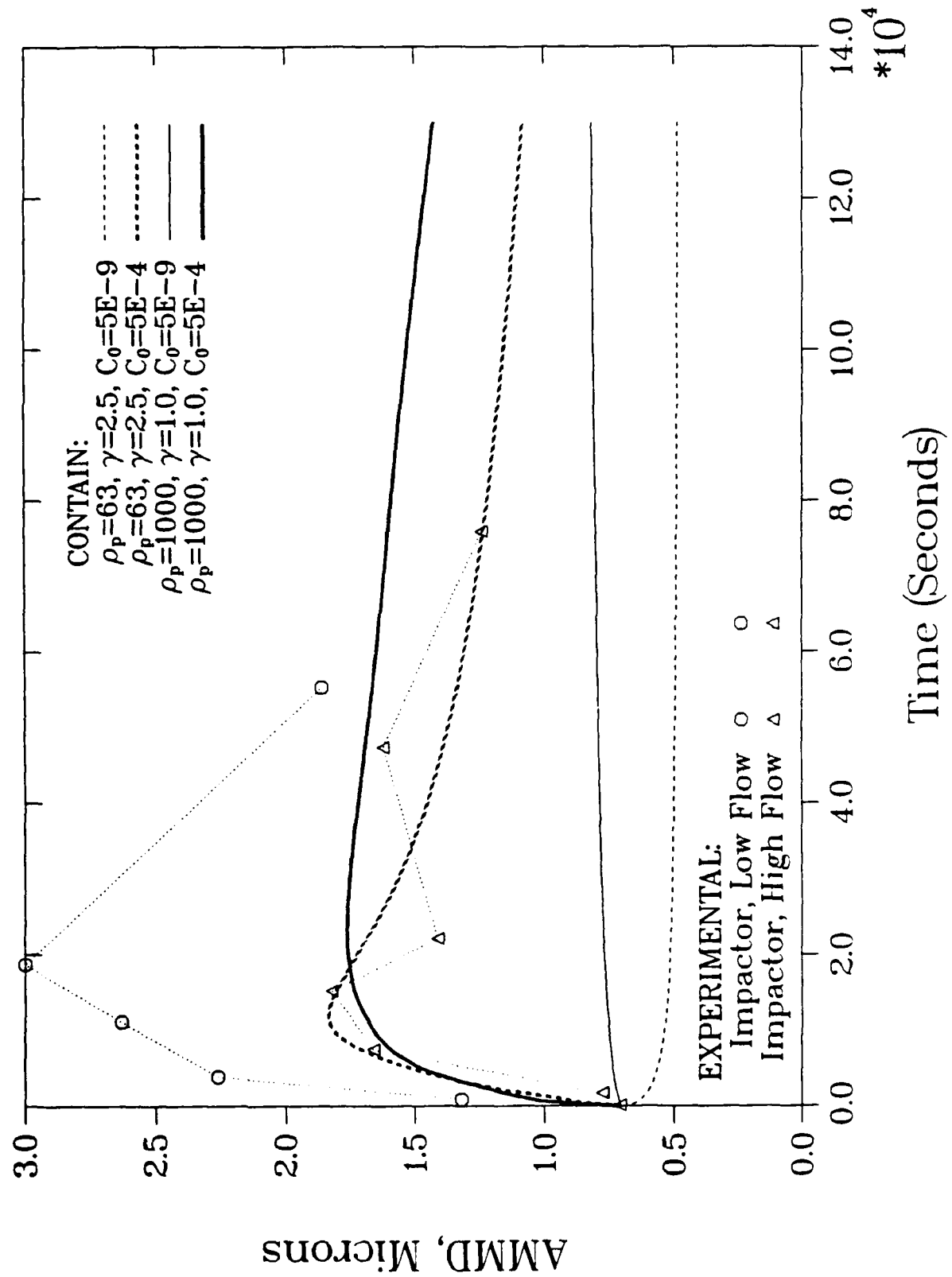


Fig. D9

# AGE-2: CONCENTRATION; EFFECT OF $\rho_p$ , $\gamma$ ( $\epsilon = 0$ )

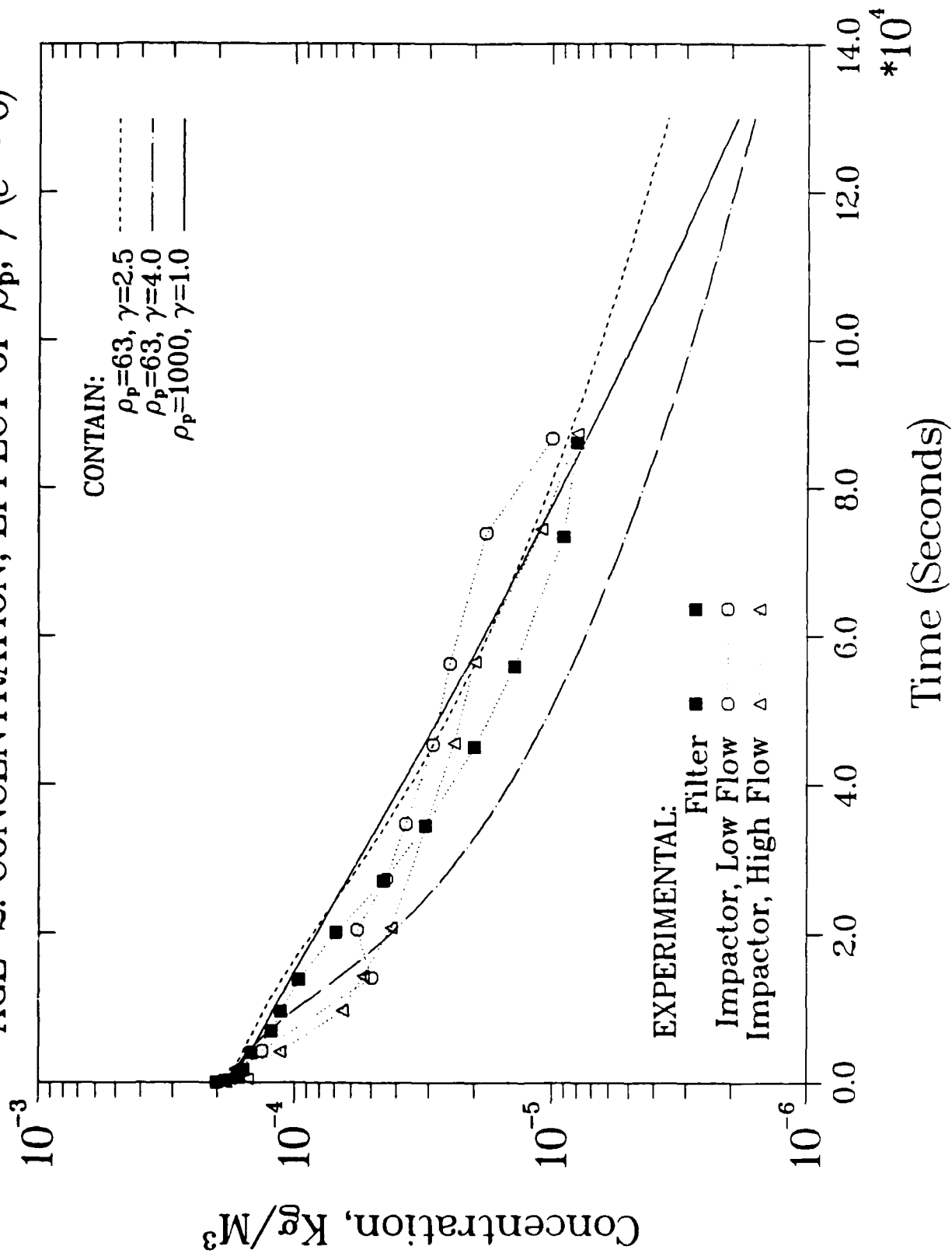


Fig. D10



# AGE-2: AMMD; EFFECT OF $\rho_p, \gamma$ ( $\epsilon = 0$ )

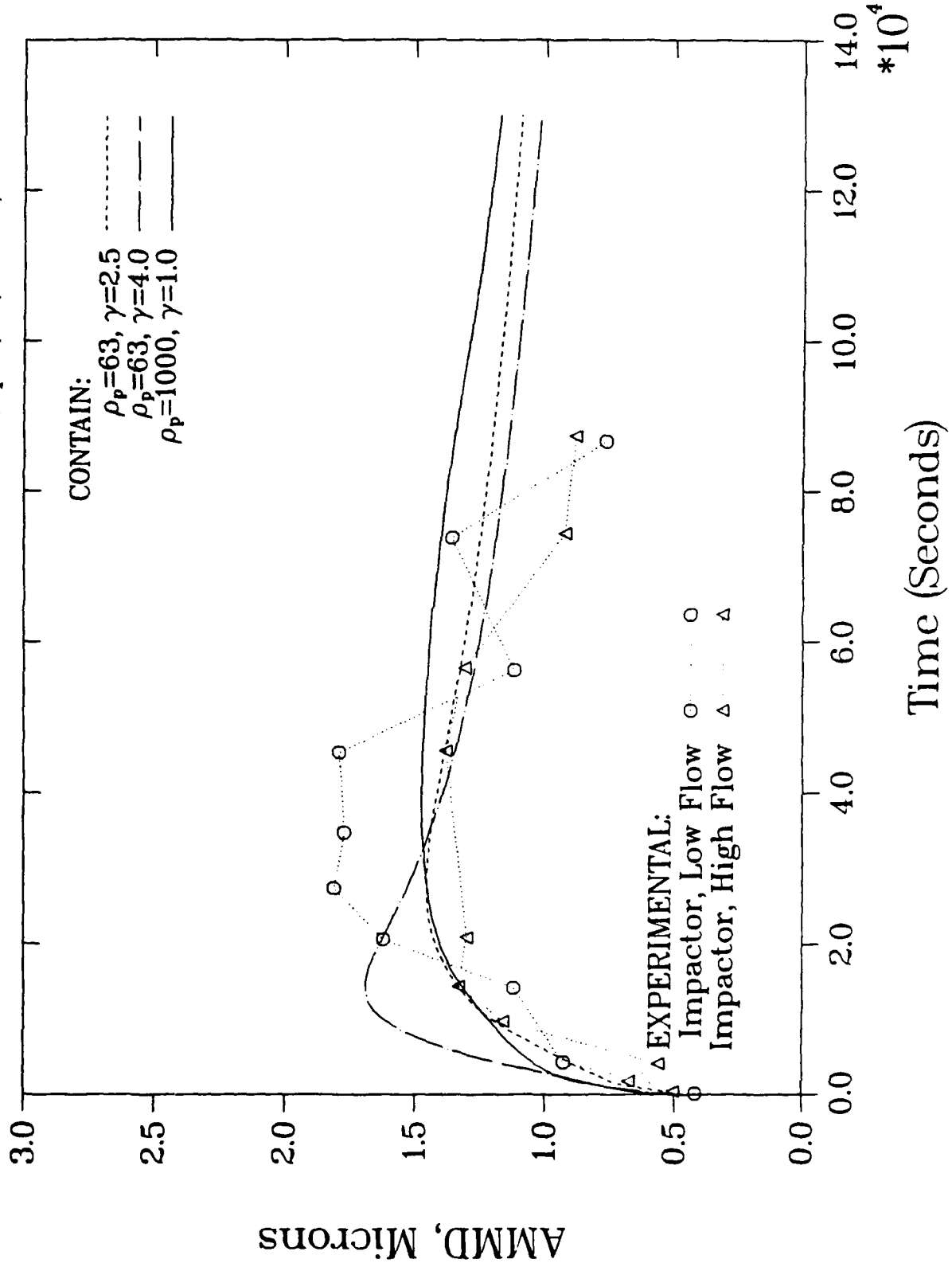


Fig. D11

JP-4 POOL FIRES: PRELIMINARY DATA ON SCALING - W. Einfeld, B. Mokler, D. Morrison, S. Nowlen, and B. D. Zak, Sandia National Laboratories, PO Box 5800, Albuquerque, New Mexico, 87185

As part of the Defense Nuclear Agency's Nuclear Winter Program, Sandia National Laboratories is engaged in a study of the impact of fire scale on smoke emission factors and smoke properties from JP-4 jet fuel pool fires. At the smaller scales, stack sampling techniques have been used. At the larger scales, the same instrumentation on the Sandia twin Otter research aircraft also used to sample and characterize the smoke from prescribed forest burns has been employed. Cross comparison of the data from the small and large scale techniques was done on the small scale fires. To date, data have been obtained on fires ranging from .02 to 167 square meters in area. These early data suggest that the emission factor goes through a minimum perhaps between 1 and 10 square meters, and then rises very significantly. The transition from near laminar to fully turbulent burning is believed responsible for the initial decline in emission factor with increasing size at the small scale end. The rise in emission factor for larger fires is believed to be due to burning rate and related oxygen depletion effects. Elemental carbon content also appears to climb somewhat as the scale of the fire increases. While these data still must be confirmed and extended by further experiment, they do suggest that emission factor and specific absorption data from laboratory scale fires must be approached with care in application to event scale.

**JP-4 POOL FIRES: PRELIMINARY DATA ON SCALING**

**W. Einfeld, B. Mokler, D. Morrison, S. Nowlen, and  
B. D. Zak**

**April, 1987**

**Sandia National Laboratories  
Albuquerque, New Mexico**

**SCALING PROBLEM:**

**Emission factors and smoke optical characteristics are usually measured for laboratory scale fires of  $<0.1$  sq m cross sectional area. How do the laboratory scale results relate to smoke from 100,000,000 sq m event scale fires?**

**JP-4 POOL FIRES: WHY?**

**-Applicability**

**-Reproducibility**

**-Experience**

**-Cost Savings**

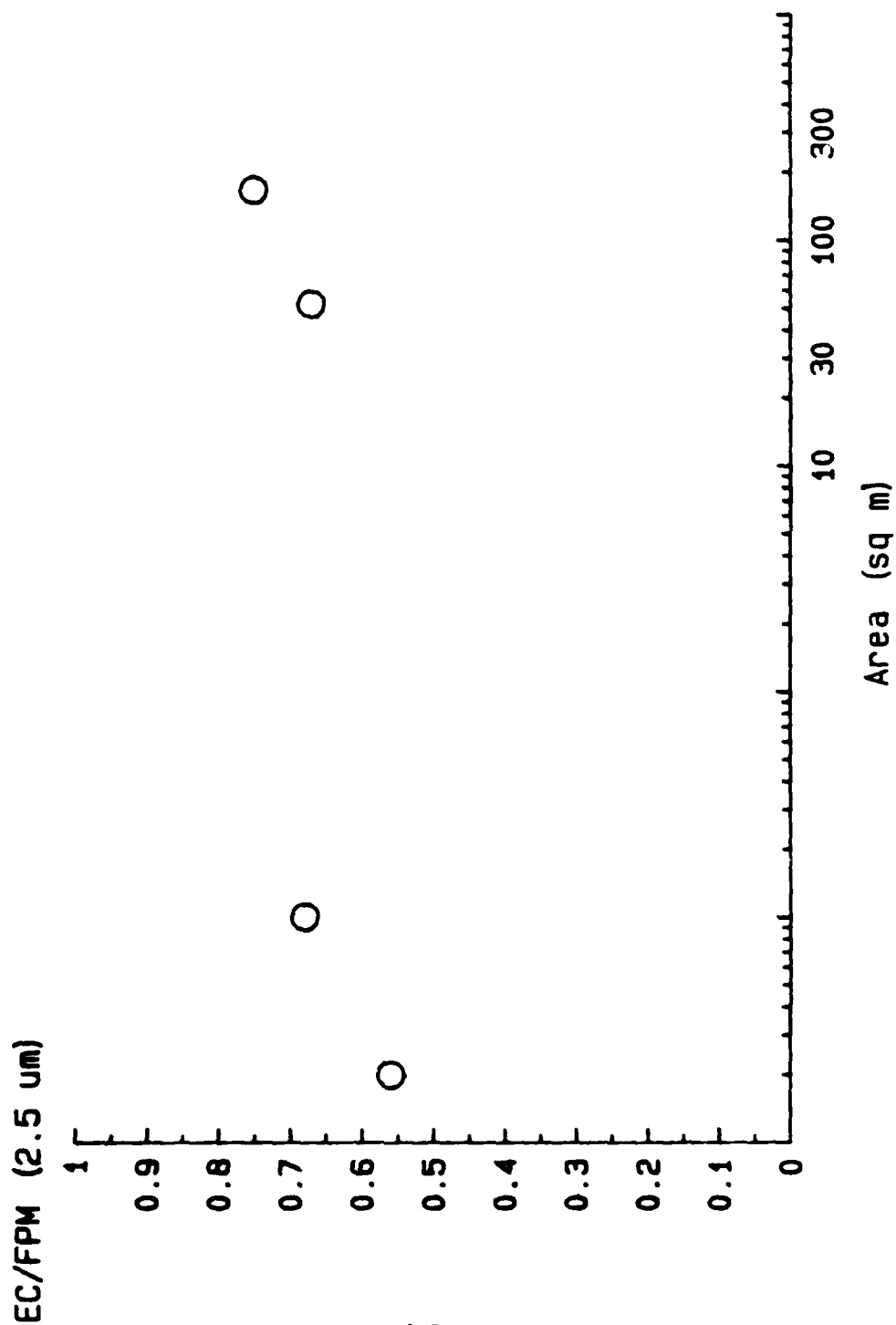
**METHODS**

**-Small Scale Fires - Stack Techniques**

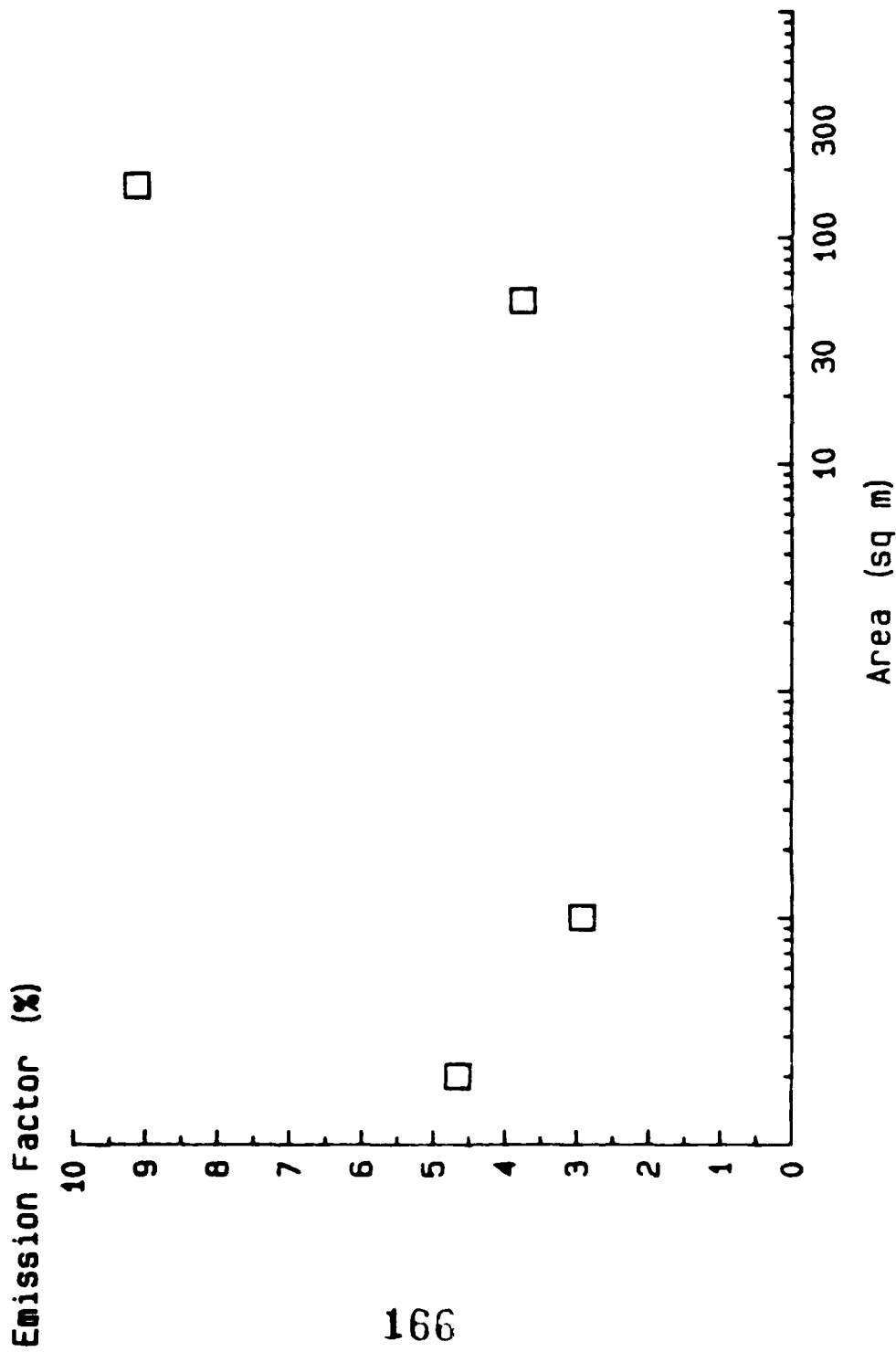
**-Large Fires - Aircraft Sampling Techniques**

**-Intercomparison on Small Scale**

# ELEMENTAL CARBON SCALING JP-4 POOL FIRES



EMISSION FACTOR SCALING (<2.5  $\mu\text{m}$ )  
JP-4 POOL FIRES





**SCALE INTERCOMPARISON**

<b>Size (sq m)</b>	<b>EF (&lt;2.5 um)</b>	<b>EC/FPM (&lt;2.5 um)</b>
<b>.02</b>	<b>4.66(.17)%</b>	<b>0.56(.03)</b>
<b>0.1</b>	<b>2.93(.06)%</b>	<b>0.68(.02)</b>
<b>52</b>	<b>3.76(.90)%</b>	<b>0.67(.05)</b>
<b>167</b>	<b>9.14(1.03)%</b>	<b>0.75(.06)</b>

**QUESTIONS:**

**Is the scaling effect real?**

**What is the shape of the curve for other fuels and fuel types?**

**How do we determine the asymptotic values for very large fires?**

**How do we make use of all the small scale data?**

**How do we extrapolate to event scale?**

**Where do we go from here?**

Paper Submitted for Presentation at The "Global Effects Program"  
Technical Meeting, Santa Barbara, 7 - 9 April 1987

Smoke Particle Emission Factors and Optical Characteristics of the Smoke  
from the Lodi Canyon Burn

L. F. Rodke, and J. Lyons  
Department of Atmospheric Sciences, University of Washington  
Seattle, Washington 98195  
and  
R. Weiss  
Radiance Research

ABSTRACT

Measurements were made of the smoke particle emission factor for the Lodi burn near Los Angeles on 12 December 1987. The carbon balance method yields comparable results using different data bases. The emission factor was  $\sim 1\%$  ( $10\text{g kg}^{-1}$  of fuel).

Measurements of particle optical absorption, via direct determination of extinction and scattering at visible wavelengths (550nm center-weighted wavelength) gave a single-scattering albedo in the range 0.83-0.92 in the smoke from the fire. These comparatively direct, in situ, measurements show promise in not only providing plume average characteristics but in revealing the optical structure of the plume on scales of a few hundred meters or less.

## Characteristics of Particles Generated by an Urban Fire Storm

D. E. Fields, M. G. Yalcintas, and J. M. Crenshaw

Health and Safety Research Division  
Oak Ridge National Laboratory\*  
Oak Ridge, TN 37831

### ABSTRACT

We have considered aerosol generation in the Hiroshima urban fire storm by studying aerosols deposited on a plaster wall immediately following the firestorm. These aerosols were rained out during an intense storm that was characterized by a "black rain". An apparently high graphite concentration suggested by electron photomicrographs and confirmed using Raman spectroscopy, SIMS (surface ionization mass spectroscopy), and ESCA (electron scattering for chemical analysis) supports a hypothesis that combustion temperatures exceeded 1000°C, while the distribution of particle sizes (30% less than 1 micron diameter) suggests that the residence time of particles in the atmosphere would be long, if they were not removed by rainout. This study suggests that particle properties used in nuclear winter scenarios should be based on optical and sedimentation properties of graphite plates, rather than those of low-temperature soots.

---

\*Operated by Martin Marietta Energy Systems, Inc., for the U.S. Department of Energy under contract DE-AC05-84OR21400.

28 APR 1967

## Chemical Reactivity of Smoke Particles with Ozone

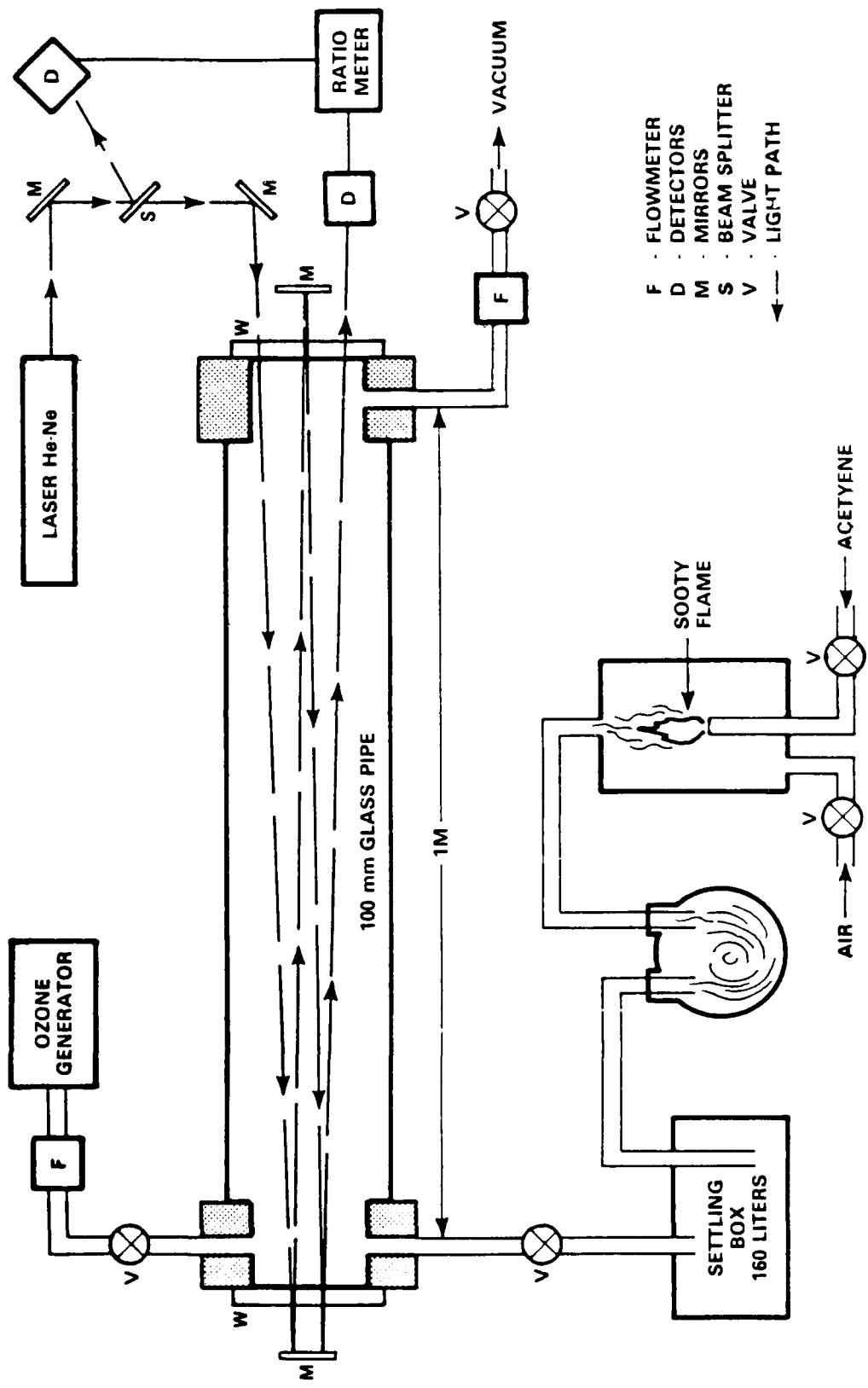
D. M. Silver, N. deHaas, R. M. Fristrom, and M. J. Linevsky

Applied Physics Laboratory, The Johns Hopkins University  
Laurel, MD 20707-6099

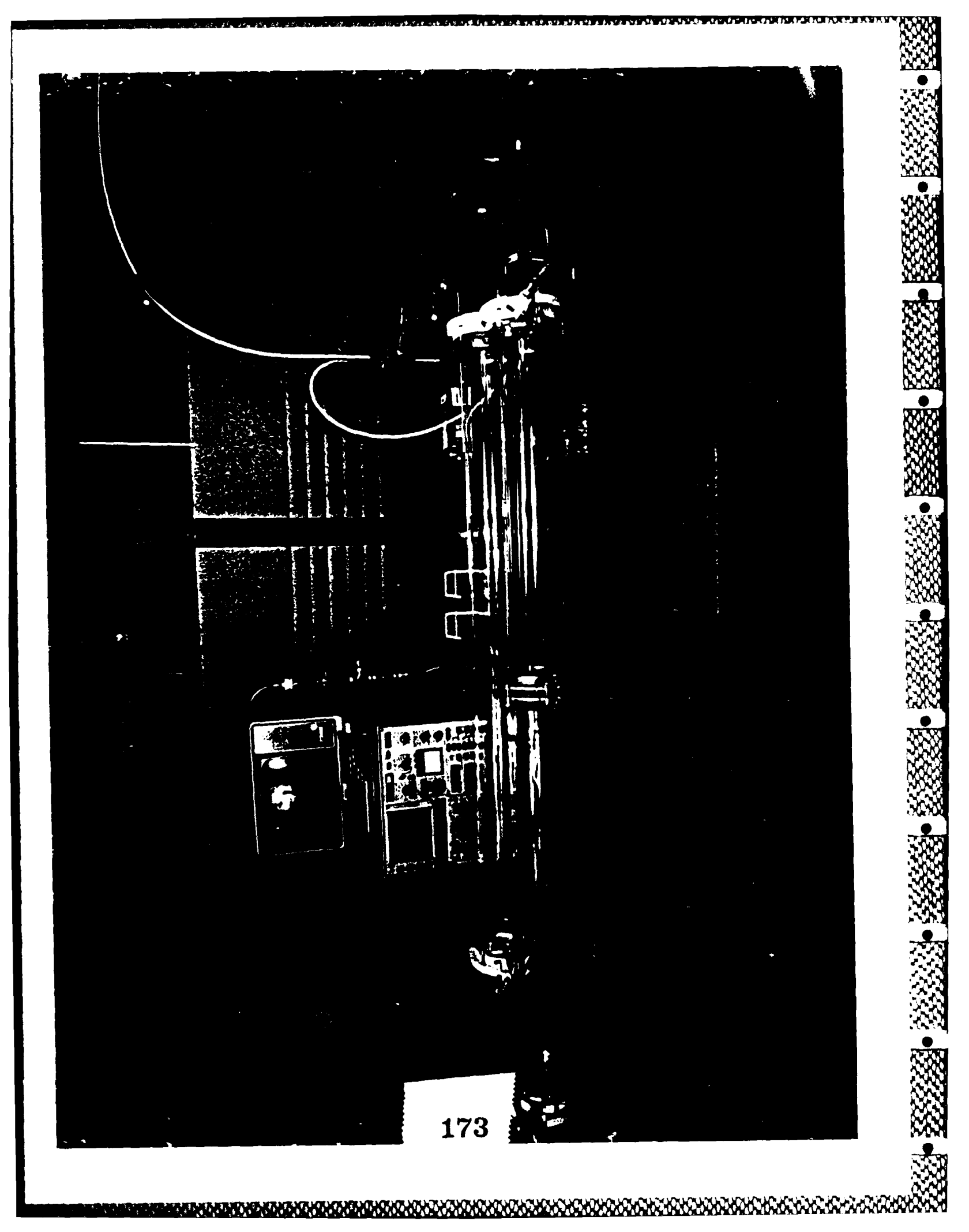
### ABSTRACT

A laboratory apparatus has been constructed to examine the reaction of smoke particles with ozone. Smoke can be generated in a burner or obtained otherwise and allowed to settle and age in a container of large volume. After a designated time, the residual buoyant smoke particles that remain suspended are passed into two parallel reactor tubes. These reactors differ by the presence or absence of ozone in the flow. The time course of the transmission of light through these two smoke columns provides a measure of the stability and reactivity of the smoke with and without ozone. Measurements were attempted on smoke collected in situ from the Lodi Canyon fire and transported to the laboratory. No results were obtained due to the low concentration of suspended smoke particles and the weak absorption of light through the smoke column. However, results will be reported on smoke particles from a partially pre-mixed acetylene-air flame.

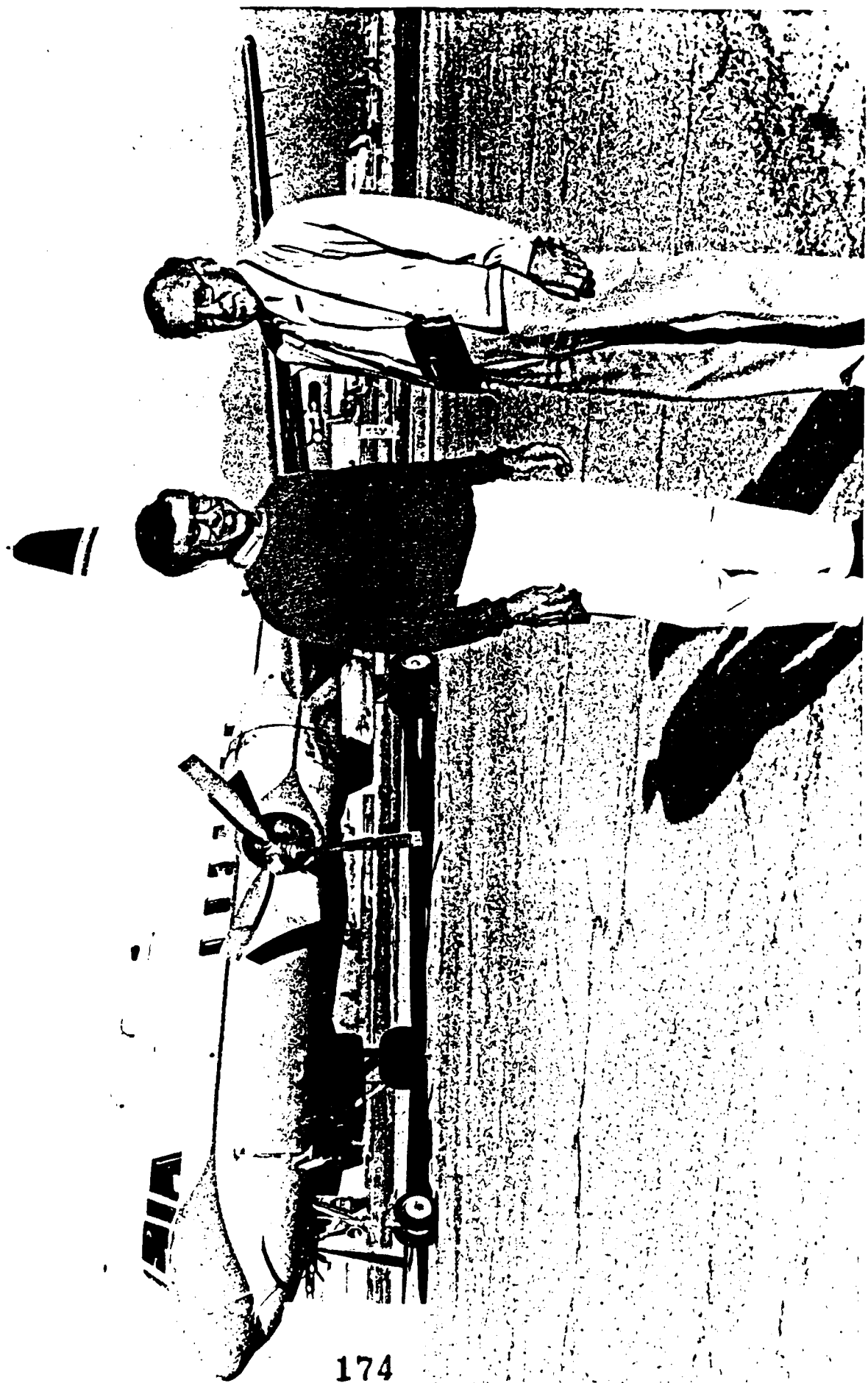
DNA Global Effects Meeting, Santa Barbara, California, 7-9 April 1987



- F · FLOWMETER
- D · DETECTORS
- M · MIRRORS
- S · BEAM SPLITTER
- V · VALVE
- · · LIGHT PATH

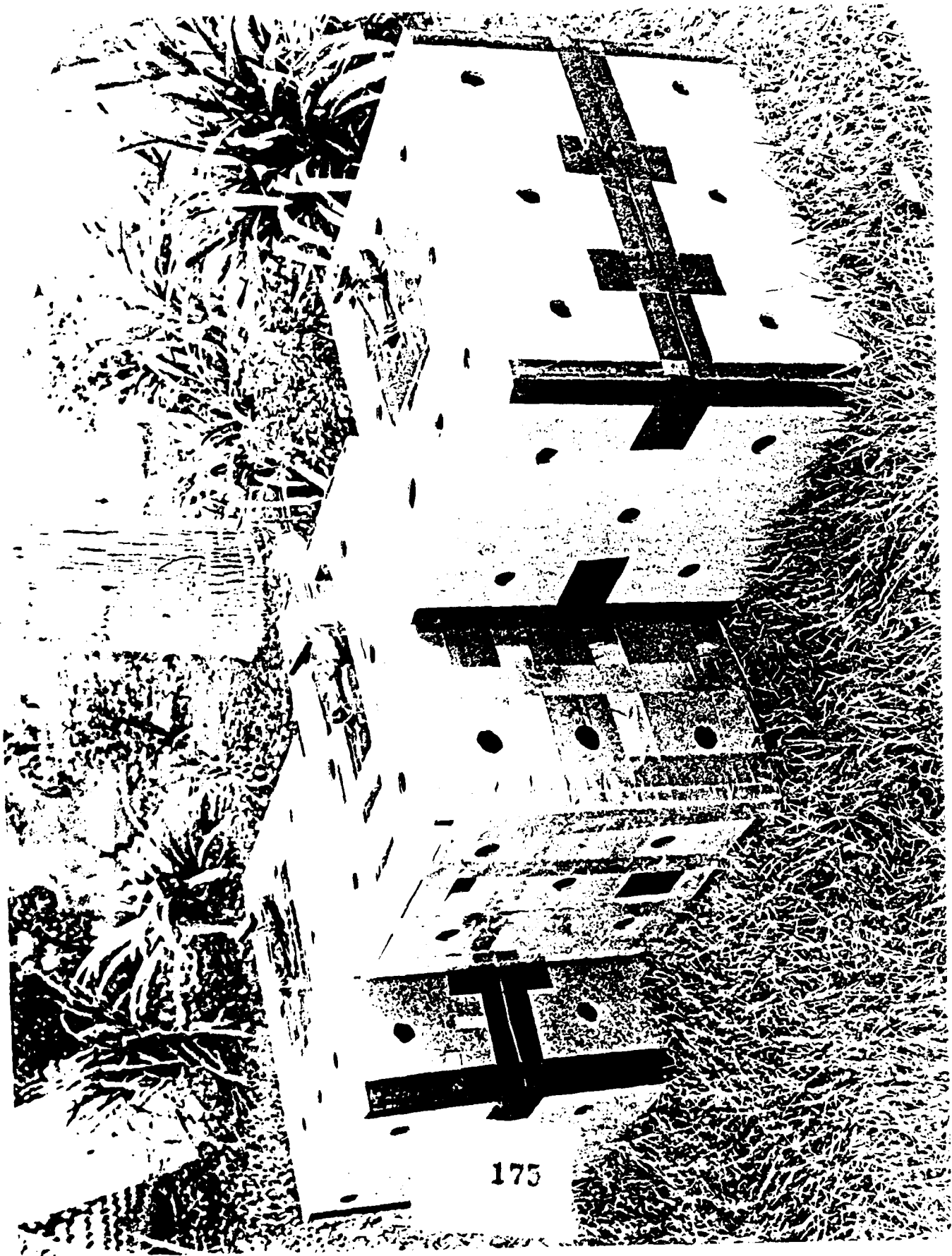


173



174





175



176

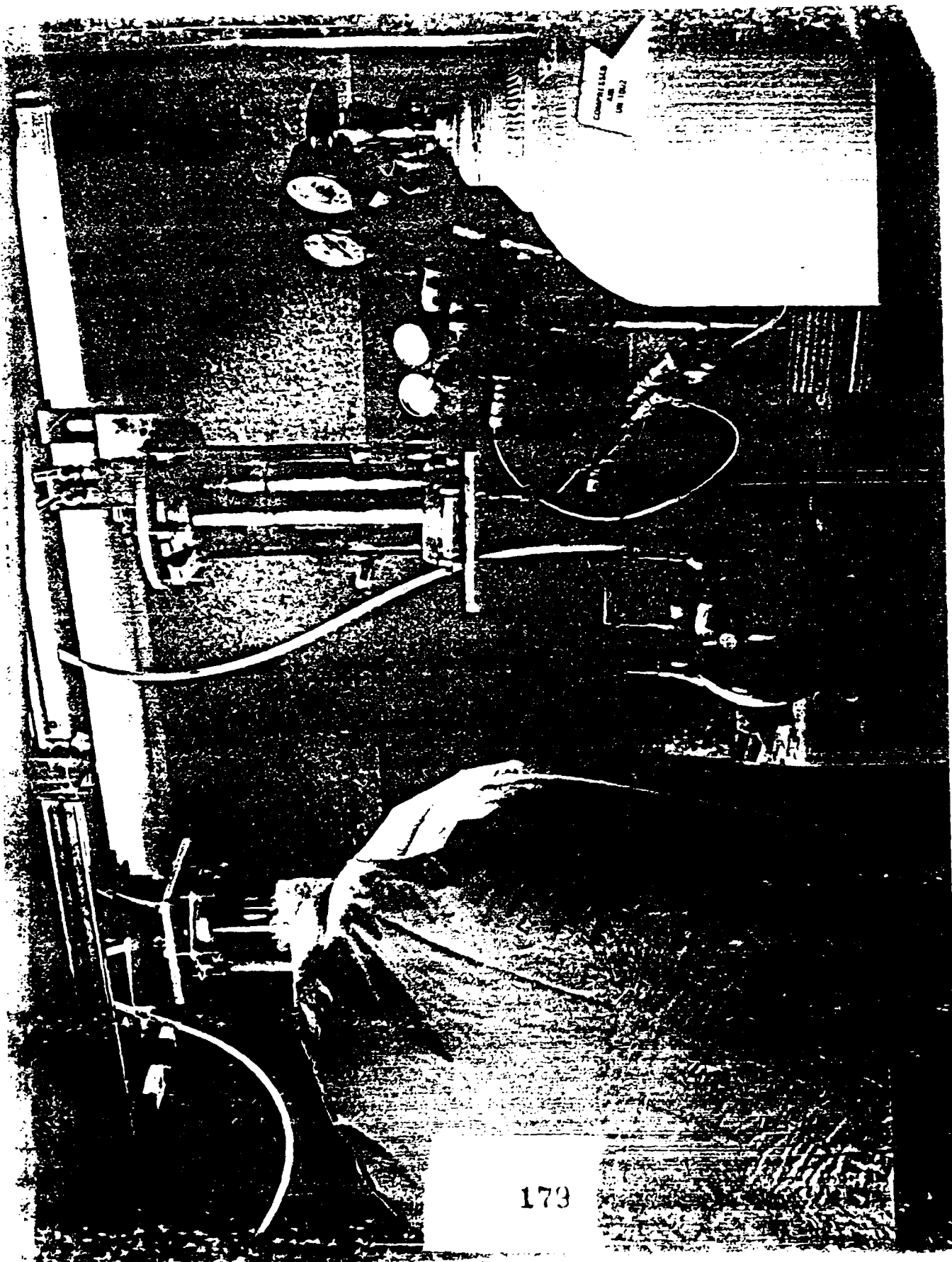


177



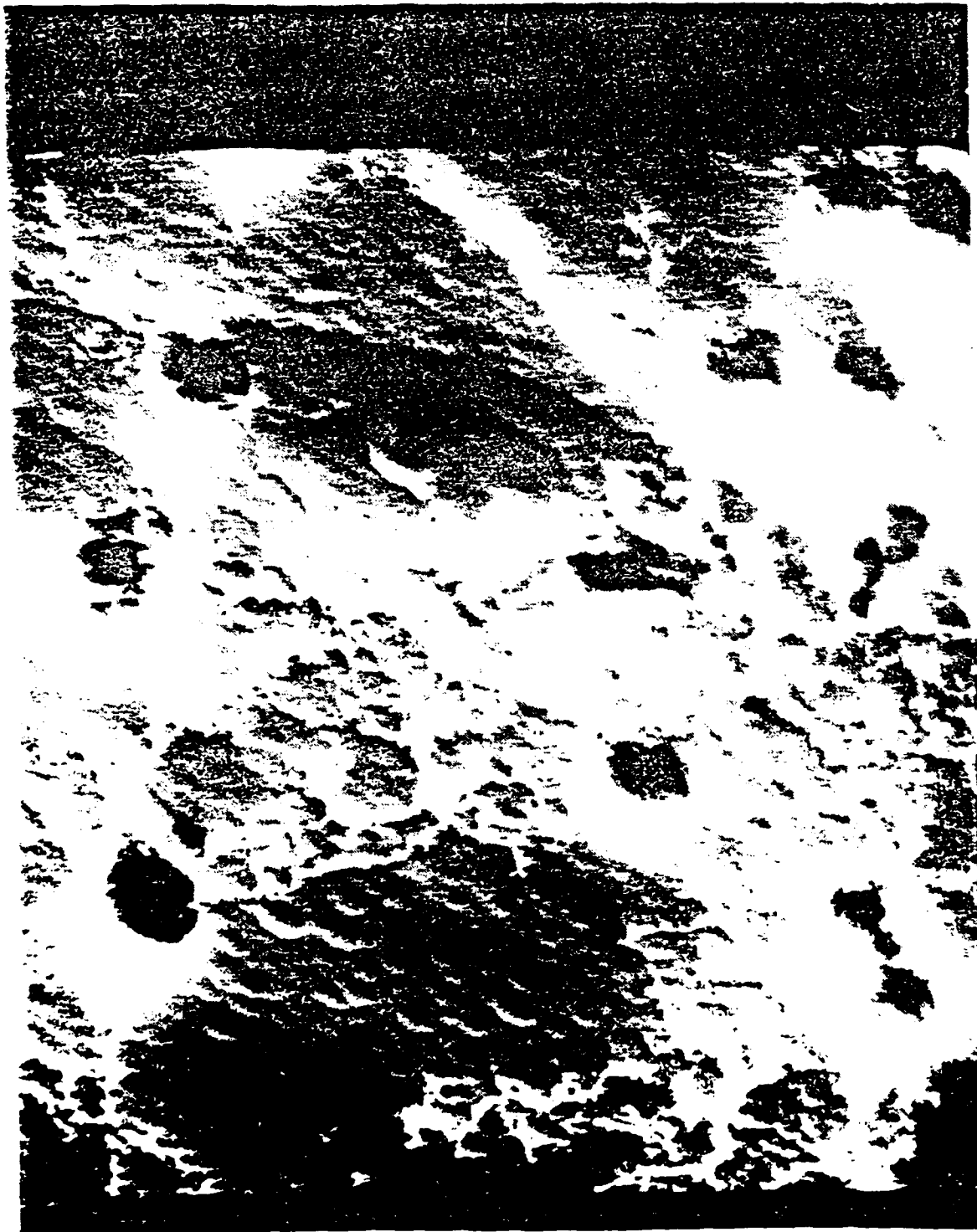


178



COMPLETED  
DATE  
BY

173



Acetylenic Smoke (SEM 2000 x)



Xylenic Smoke (SEM 3600 x)



Cellulosic Smoke (SEM 3600x)





Cellulosic Smoke (SEM 6000x)

## Transmission of light through smoke column

$$I = I_0 \exp(-a b c_s)$$

$a$  = extinction coefficient

$b$  = length of smoke column

$c_s$  = concentration of smoke

$\ln(I_0/I)$  is linearly proportional to  
smoke concentration

$$\ln(I_0/I) = a b c_s$$

Rate of disappearance of smoke

$$-\frac{dC_s}{dt} = k C_o C_s$$

$k$  is second-order rate constant

$C_o$  is concentration of ozone

$C_s$  is concentration of smoke

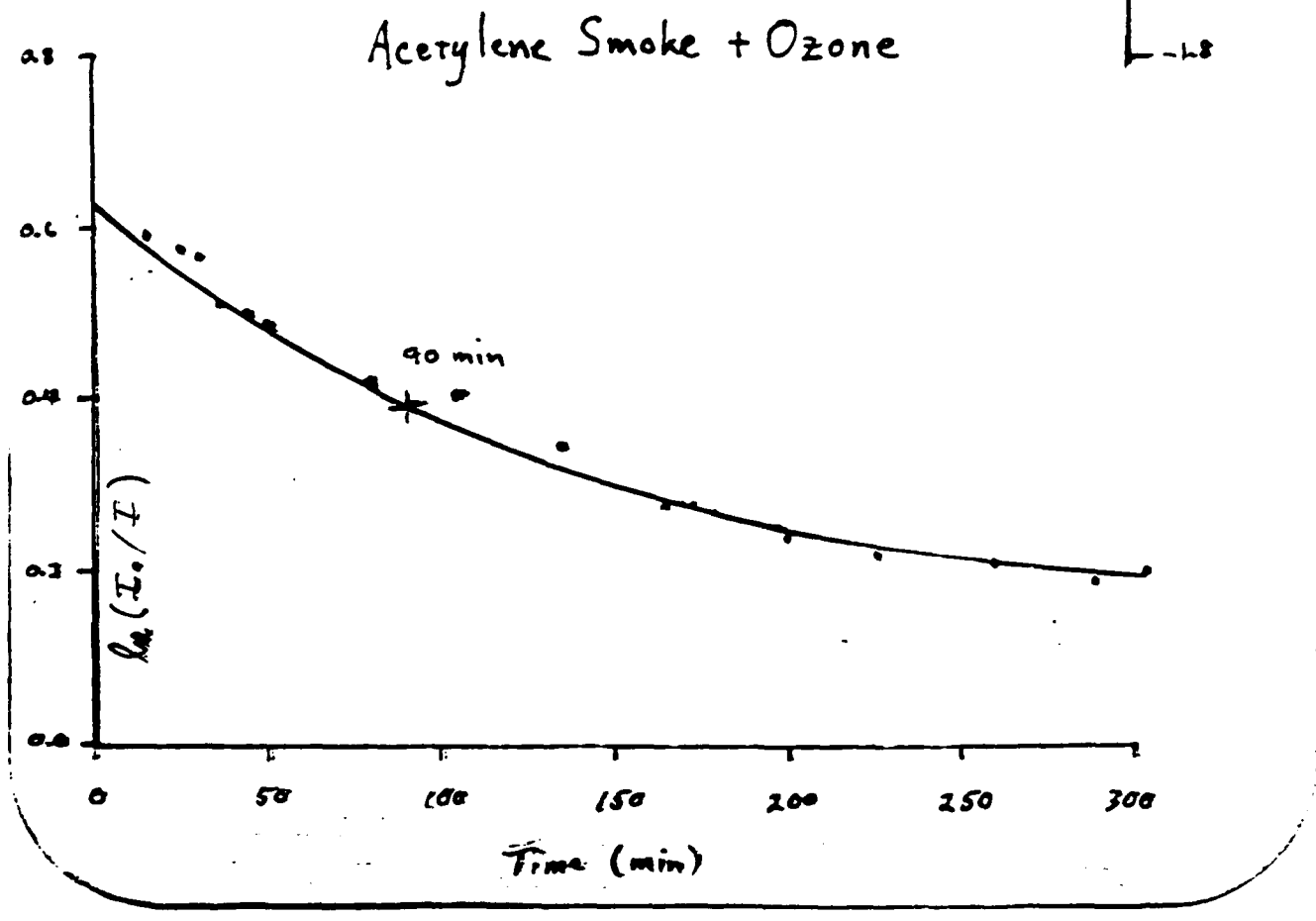
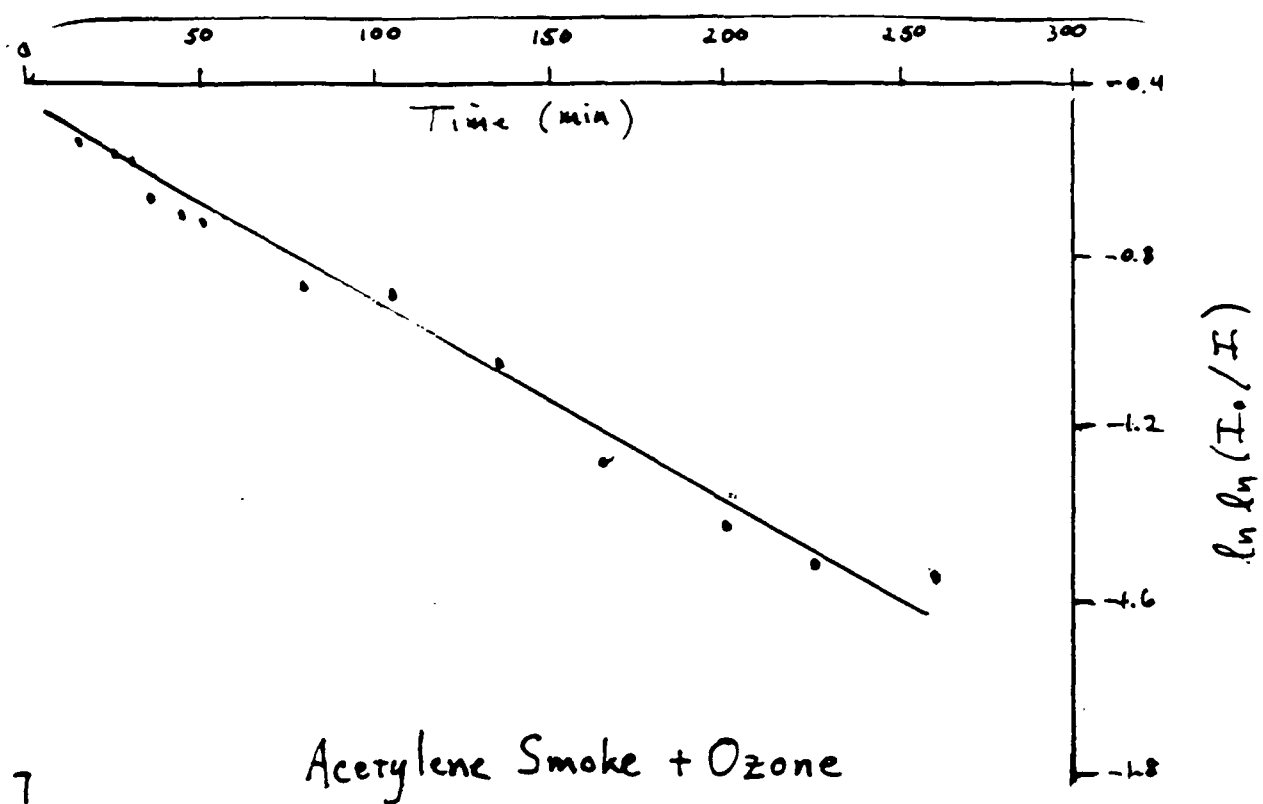
With excess ozone, rate is pseudo first-order in smoke concentration: ( $C_o$  assumed constant)

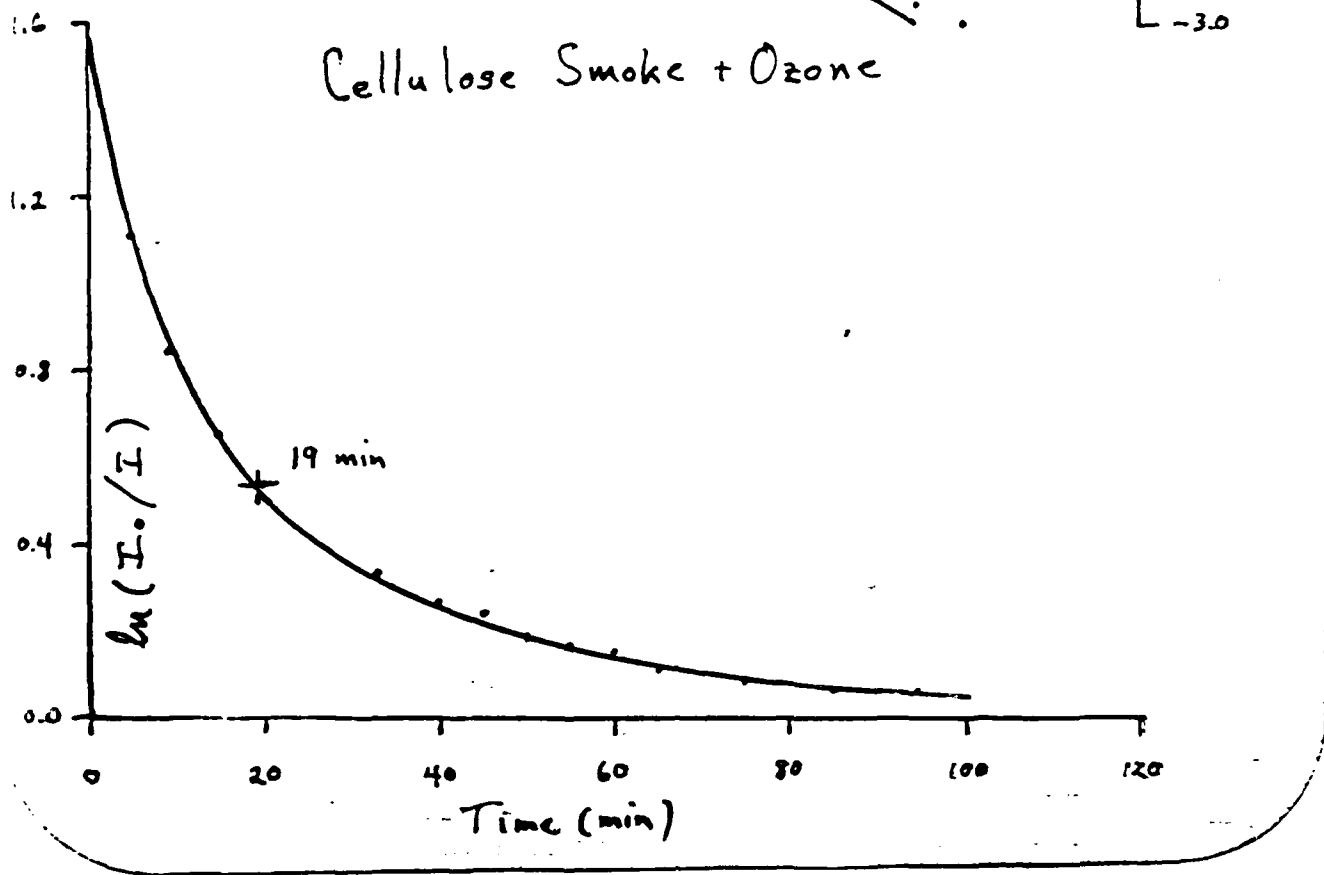
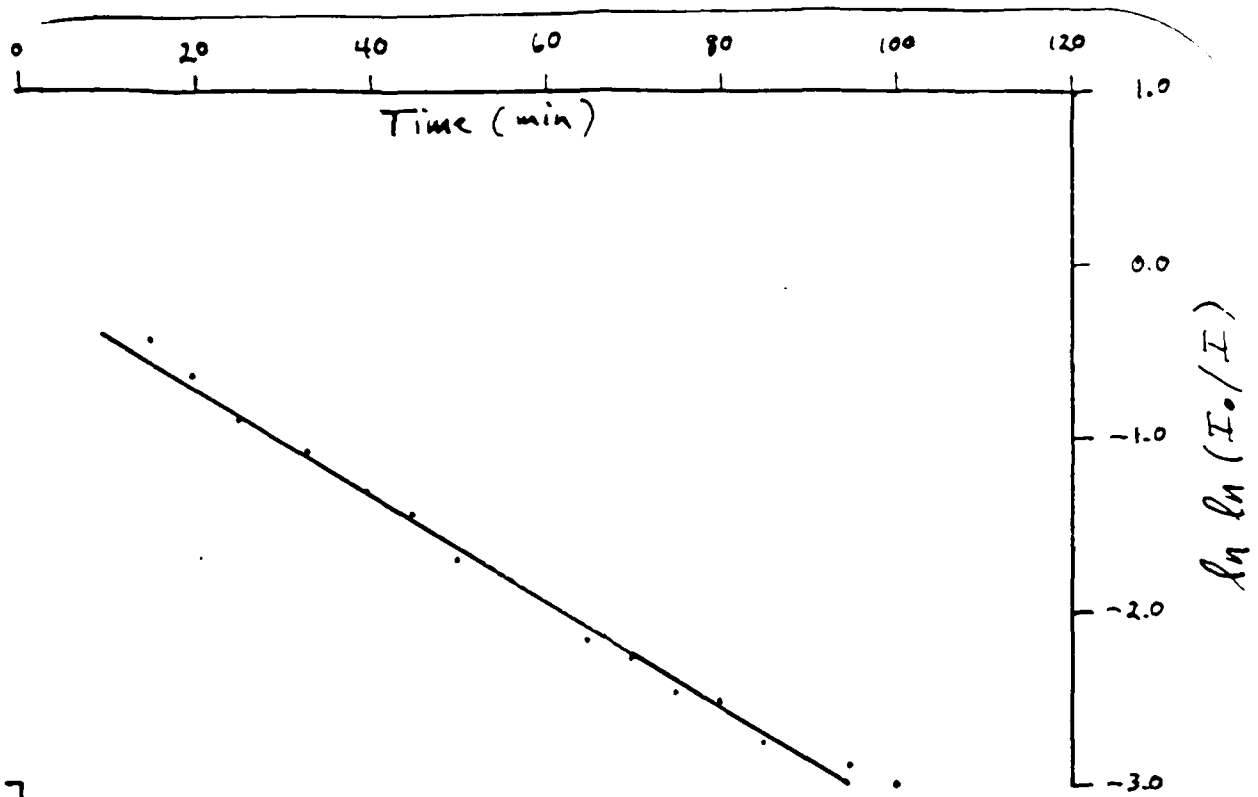
$$\therefore C_s = A \exp(-k C_o t)$$

But  $\ln(I_o/I)$  is proportional to  $C_s$

$$\therefore \ln \ln(I_o/I) = A' - k C_o t$$

is., linearly proportional to time  
if the reaction is pseudo  
first-order in smoke concentration





Smoke-Ozone mixtures exhibit a time dependent change in optical transmission at  $6328 \text{ \AA}$ .

- Half-life depends on source of smoke
- Kinetics appear to have first-order dependence on smoke concentration

Translated to "nuclear winter" atmospheric conditions, the optical transmission is doubled from its initial value in a time range of a month.

THE HETEROGENEOUS REACTION OF OZONE ON

CARBONACEOUS SURFACES

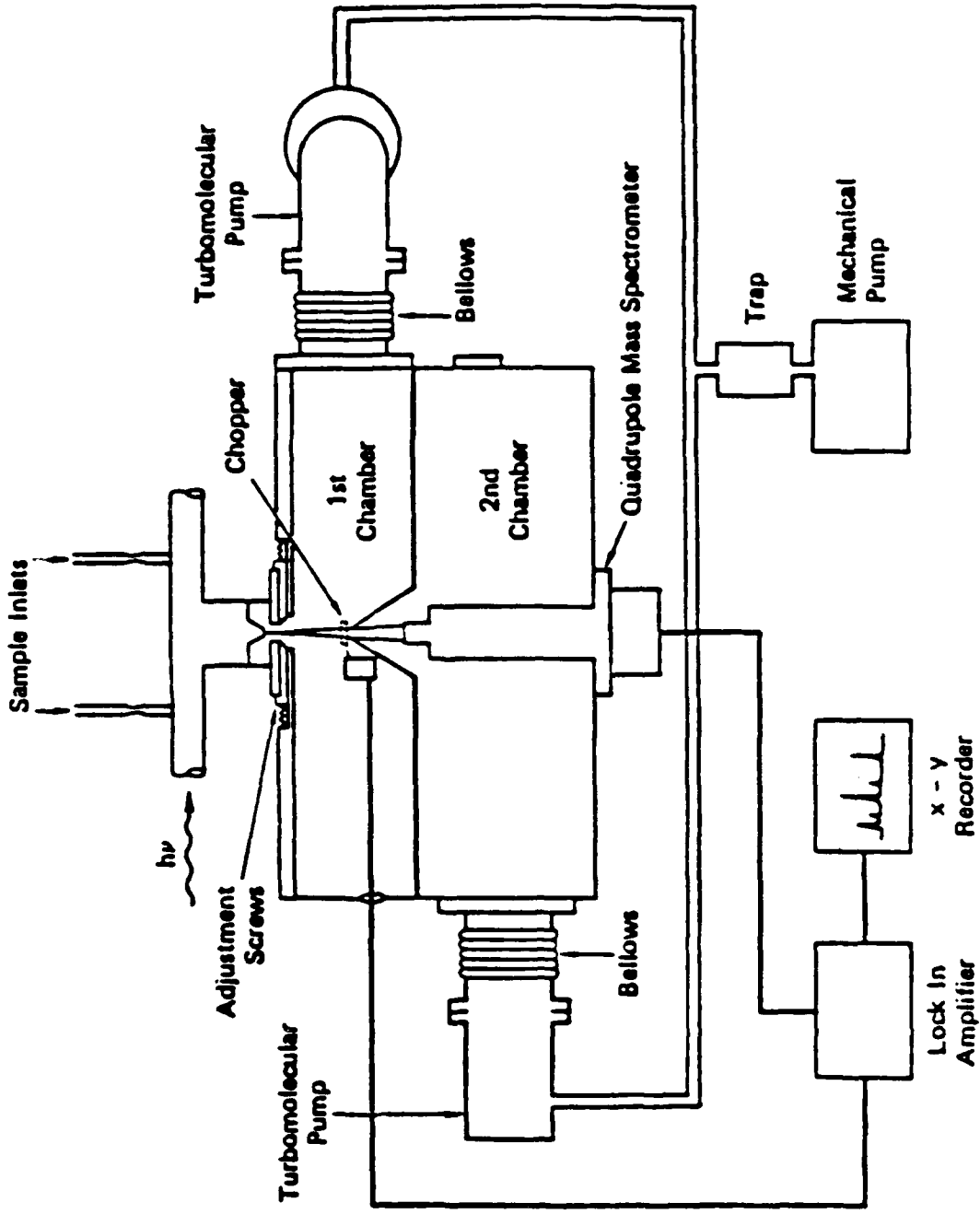
SHERRY STEPHENS, MICHEL J. ROSSI

AND DAVID M. GOLDEN

DEPARTMENT OF CHEMICAL KINETICS

CHEMICAL PHYSICS LABORATORY

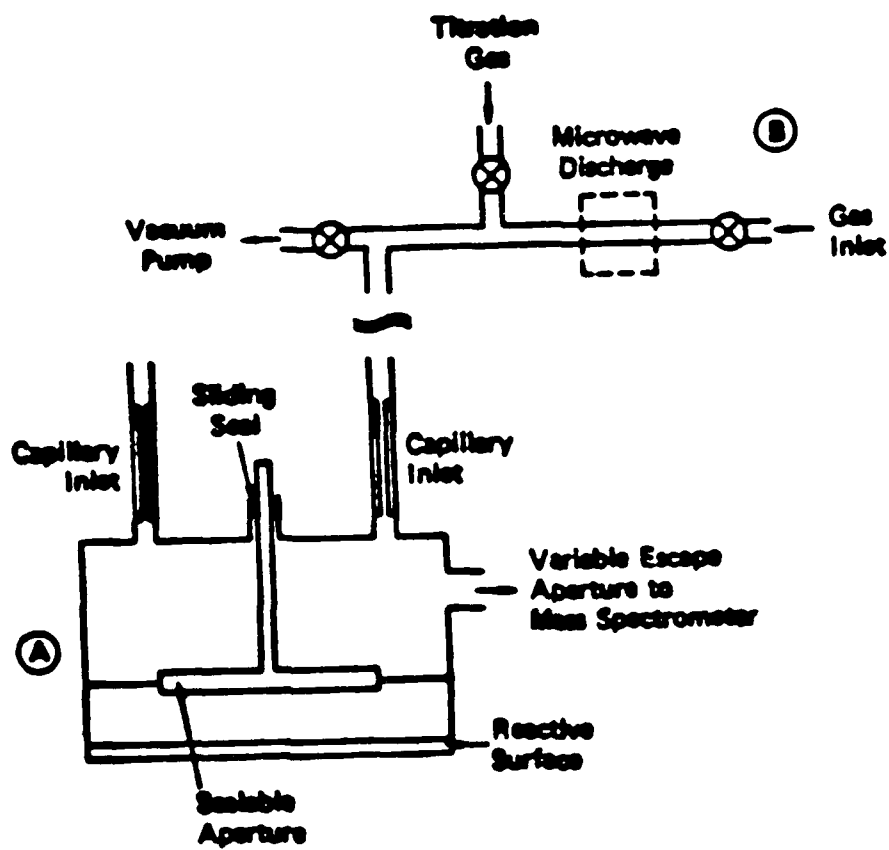
SRI INTERNATIONAL, MENLO PARK, CA 94025



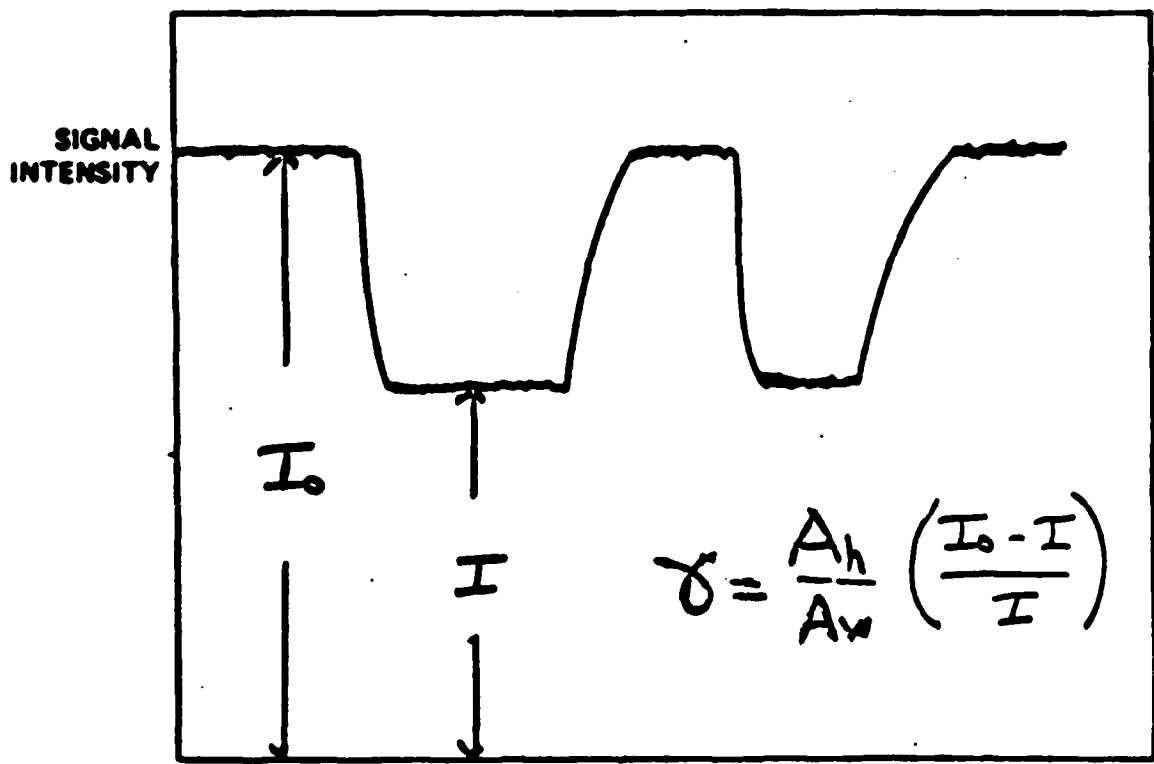
JA-372683-25A

SCHEMATIC OF VERY LOW-PRESSURE PHOTOLYSIS APPARATUS





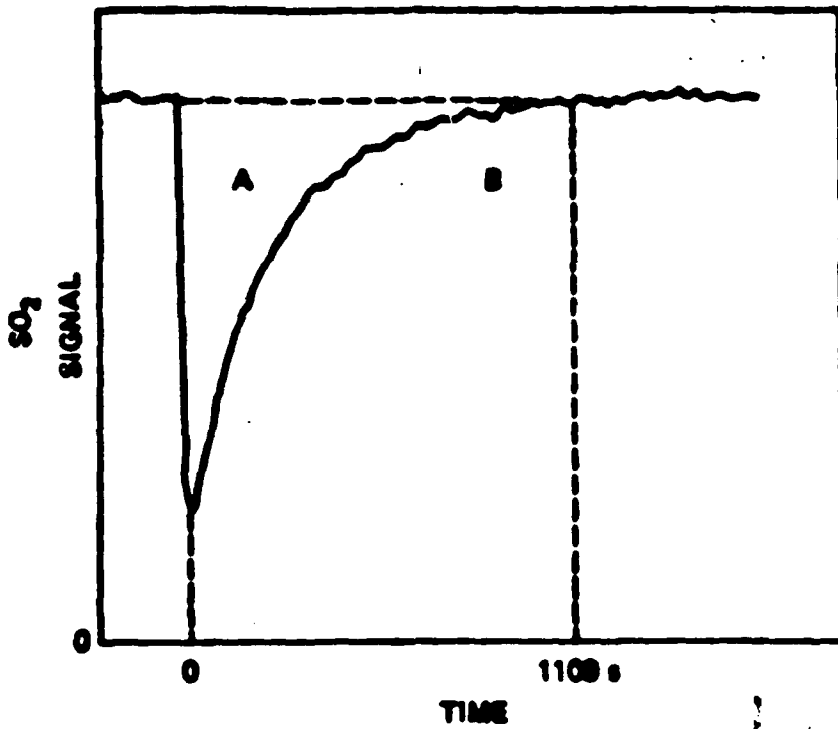
GA-7873-14



SA-7873-2

FIGURE TYPICAL EXPERIMENTAL DATA

Saturation



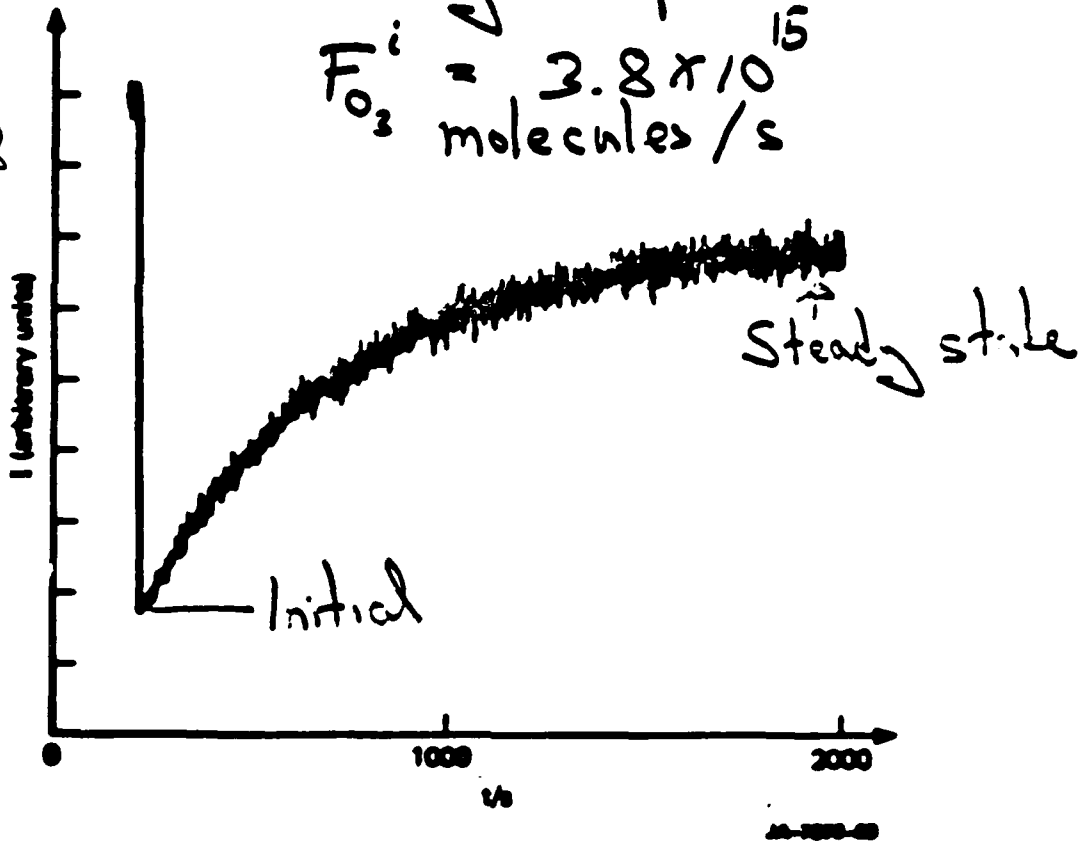
Soot

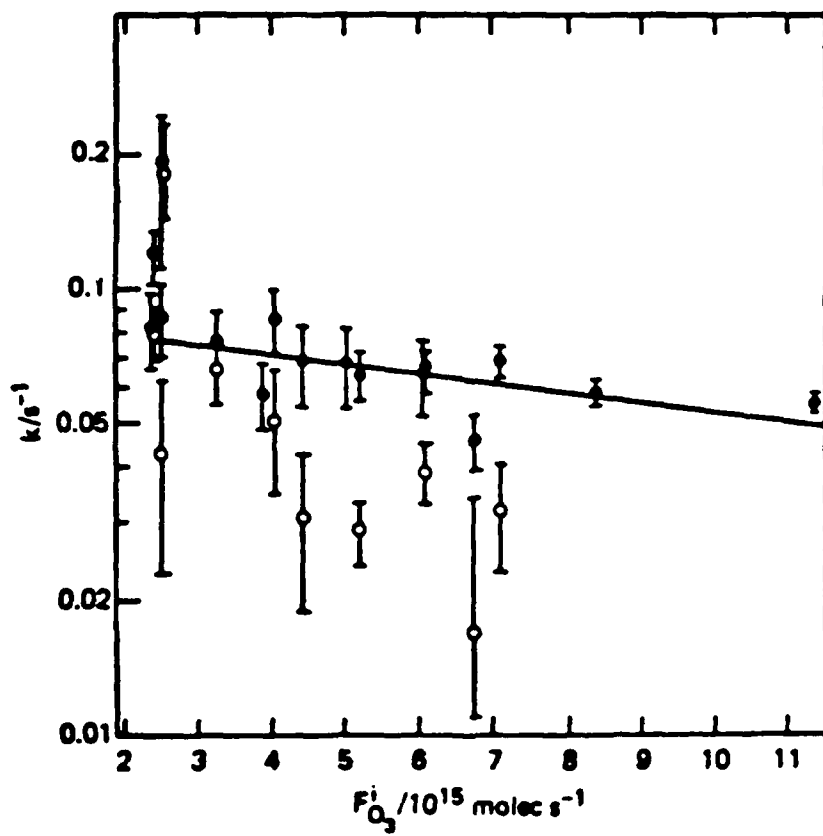
O<sub>3</sub> / "Soot"

30 mg sample

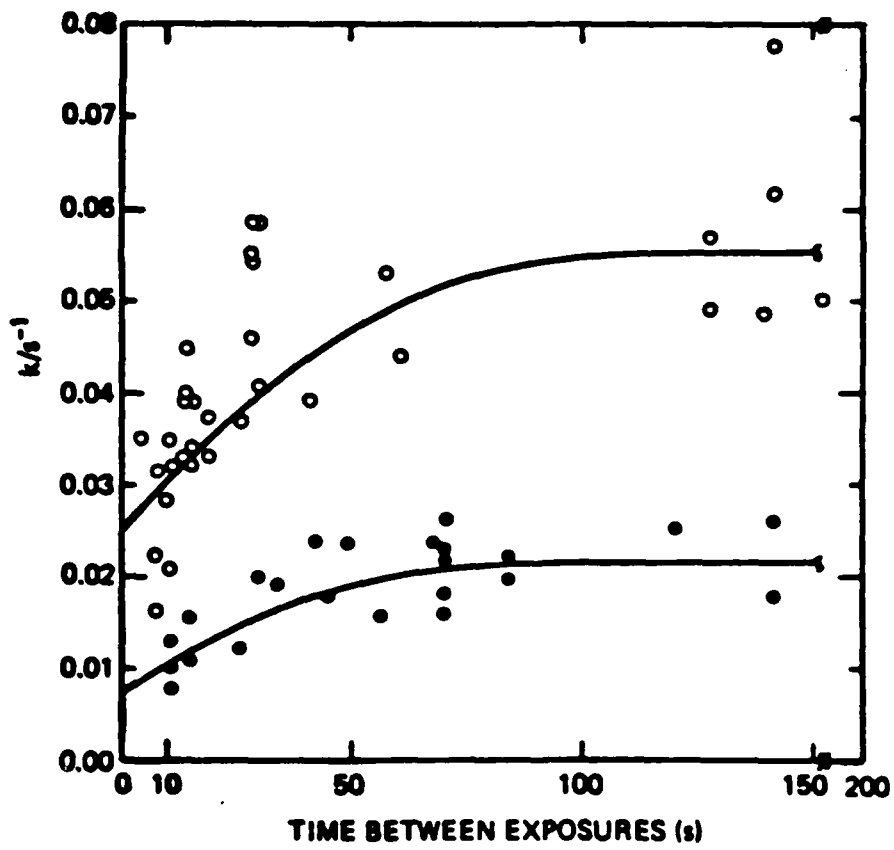
$$F_{O_3}^i = 3.8 \times 10^{15} \text{ molecules/s}$$

m/e = 48

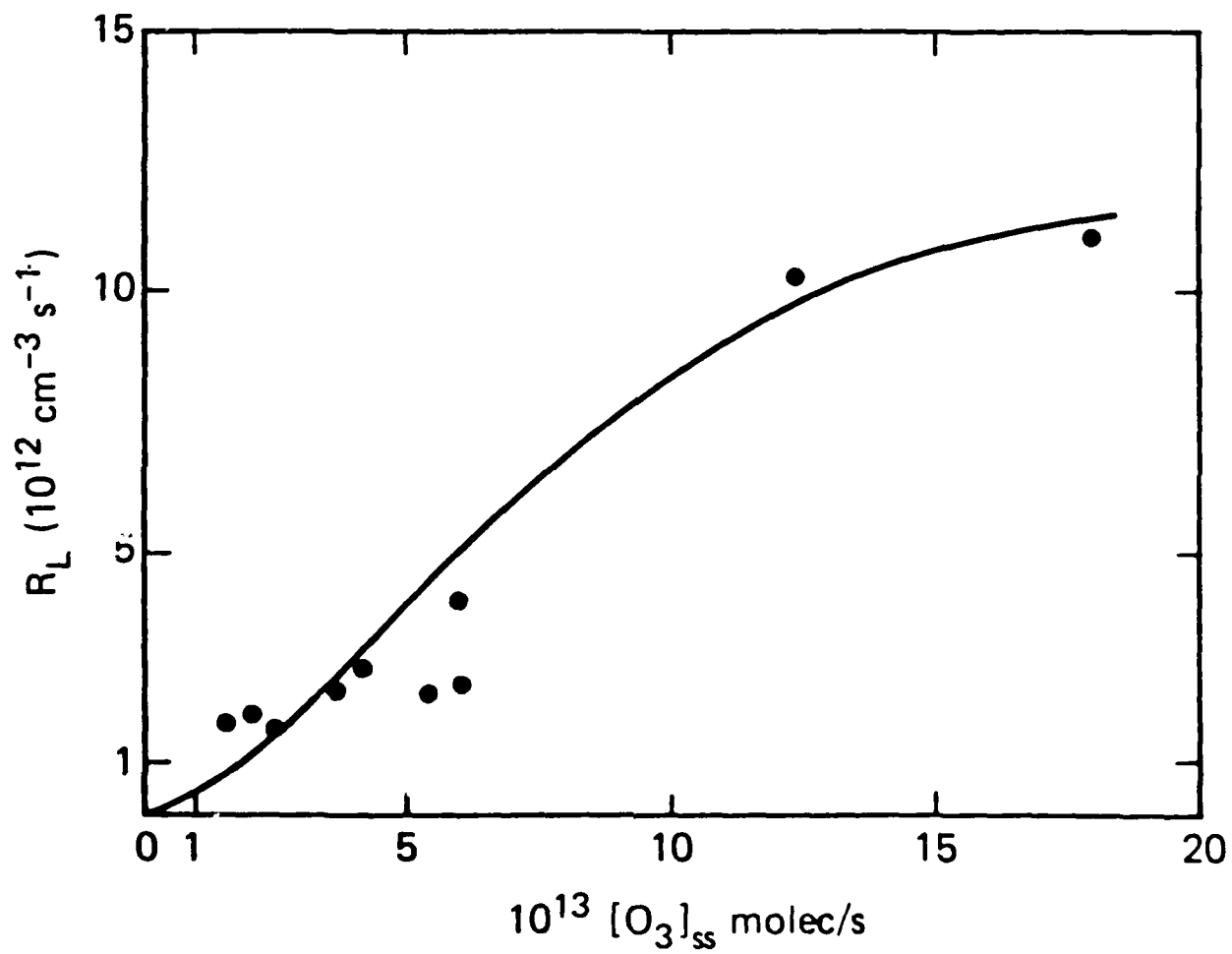




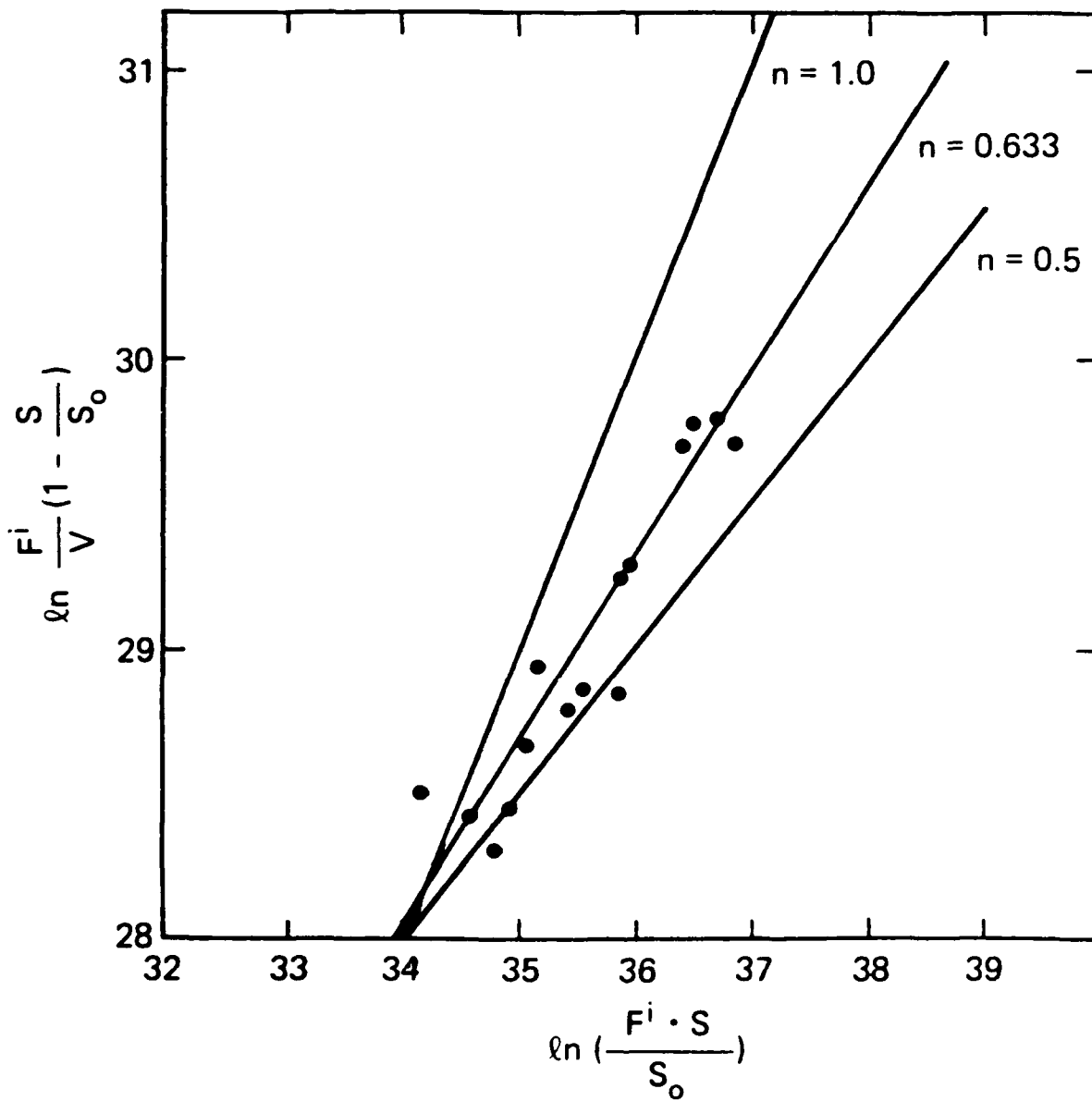
JA-7873-84



JA-7873-88



JA-7873-69



JA-7873-63



Table 1  
 INITIAL STICKING COEFFICIENTS  $\gamma$  FOR CARBON SAMPLE III  
 AT DIFFERENT FLOW RATES OF  $O_3$  ( $F_{O_3}^1$ )

$F_{O_3}^1 / 10^{15} \text{ molec s}^{-1}$	${}^1\gamma_o / 10^{-5}$	${}^2\gamma_o / 10^{-5}$
4.9	61.3	4.1
9.9	—	3.5
2.2	—	4.9
4.4	254.2	3.8
11.4	—	3.3
2.8	—	3.5
1.4	292.9	11.3
1.7	413.1	7.1
5.7	—	4.0
8.9	30.7	4.1
11.5	22.4	2.7
3.0	137.5	4.6
2.6	80.9	5.1
3.8	45.2	3.9
3.4	20.7	4.1
1.9	107.1	5.2

${}^1\gamma_o$  = sticking coefficient for clean surface.

${}^2\gamma_o$  = sticking coefficient for previously exposed surface.

Table 2

MASS BALANCE DATA FOR CARBON SAMPLE III IN TERMS OF FLOW  
RATES OF A GIVEN SPECIES (units of  $10^{15}$  molec  $s^{-1}$ )

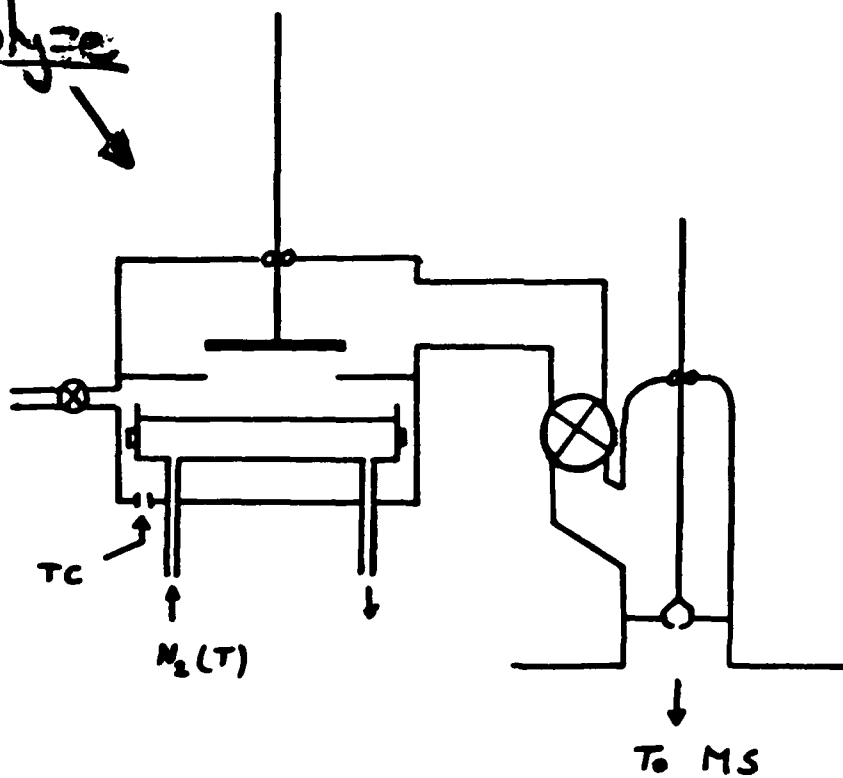
$F_{O_3}^1$	$F_{O_3}^0$	$2 F_{CO_2}^0$	$F_{CO}^0$	$F_{O_2}^0$	$\Delta F_{O_3}^a$	$\Sigma F_C^b$
1.41	.82	.17	.05	—	.59	.22
8.9	7.9	.26	.10	—	1.0	.36
9.1	7.5	—	—	2.0	1.6	—
8.2	7.5	—	—	.7	.7	—
12.8	9.5	.38	.15	2.15	3.3	.53
12.8	12.3	.076	.028	.5	.5	.1
12.8	12.1	.10	.035	—	.7	.13 <sub>5</sub>
3.05	1.9	.23	.08 <sub>5</sub>	1.2	1.15	.31
2.94	2.3	.10	.02	.6	.6	.12
2.7	1.8	.3	.07	—	.9	.37
2.6	2.0	.16	.02	—	.6	.18
2.5	2.05	.14	.01	—	.5	.15
3.9	3.2	.21	.05	—	.7	.26
3.9	3.3	.15	.04	—	.6	.19
3.9	3.4	.13	.01	—	.5	.14
3.6	2.8	.20	.04	—	.8	.24 <sup>1</sup>
3.5	2.8 <sub>5</sub>	.18	.02	—	.65	.2
3.3	2.9	.08	.02	—	.4	.1
1.85	1.3	.18	.05	.55	.55	.23
1.85	1.3	.13	.05	.55	.55	.18
1.95	1.5	.14	.04	.45	.45	.18
1.80	1.4	.12	.03	.35	.40	.15

$$a) \Delta F_{O_3} = F_{O_3}^1 - F_{O_3}^0$$

$$b) \Sigma F_C = 2F_{CO_2}^0 + F_{CO}^0$$

# Variable Surface Temperature Reactor

Photolyze



## 1-D VS. 3-D MODEL RESULTS

---

*Compare land, annual, hemispheric, surface temperature decrease over the 10 coldest contiguous model days.*

---

### I. NCAR 3-D Model (ca. 1986-87)

#### A. July, Northern Hemispheric land ( $^{\circ}\text{C}$ )

0-10 km CD,  $\Delta T = -11.7$

0-7 km CMR,  $\Delta T = -8.4$

#### B. Convert to Annual Mean ( $\times 0.67$ )<sup>†</sup>

Thus,  $\Delta T_{3D} = -5.6$  to  $-7.8$

### II. TTAPS 1-D Model (1983)

#### A. Annual, Hemispheric, All-Land Planet ( $^{\circ}\text{C}$ )

Baseline,  $\Delta T = -36$ .

#### B. Convert to Land/Ocean Planet ( $\times 0.5$ )<sup>‡</sup>

Thus,  $\Delta T_{1D} = -18$ .

### III. Compare,

$\Delta T_{1D} = -18$ .

$\Delta T_{3D} = -5.6$  to  $-7.8$

---

**1-D to 3-D Ratio: 2.3 to 3.2**

---

<sup>†</sup> Based on earlier NCAR Jan., Apr., July simulations and on Annual/July insolation ratio.

<sup>‡</sup> Mean of TTAPS correction factors: 0.3 (coastal) and 0.7 (interior).

## Nuclear Winter: Global Consequences of Multiple Nuclear Explosions

R. P. Turco, O. B. Toon, T. P. Ackerman  
J. B. Pollack, Carl Sagan

The model predictions discussed here generally represent effects averaged over the Northern Hemisphere (NH).

Figure 2 shows the surface temperature perturbation over continental land areas in the NH calculated from the dust and smoke optical depths for several scenarios.

Actual temperature decreases in continental interiors might be roughly 30 percent smaller than predicted here, and along coastlines 70 percent smaller (10).

# Nuclear Winter: Global Consequences of Multiple Nuclear Explosions

R. P. Turco, O. B. Toon, T. P. Ackerman  
J. B. Pollack, Carl Sagan

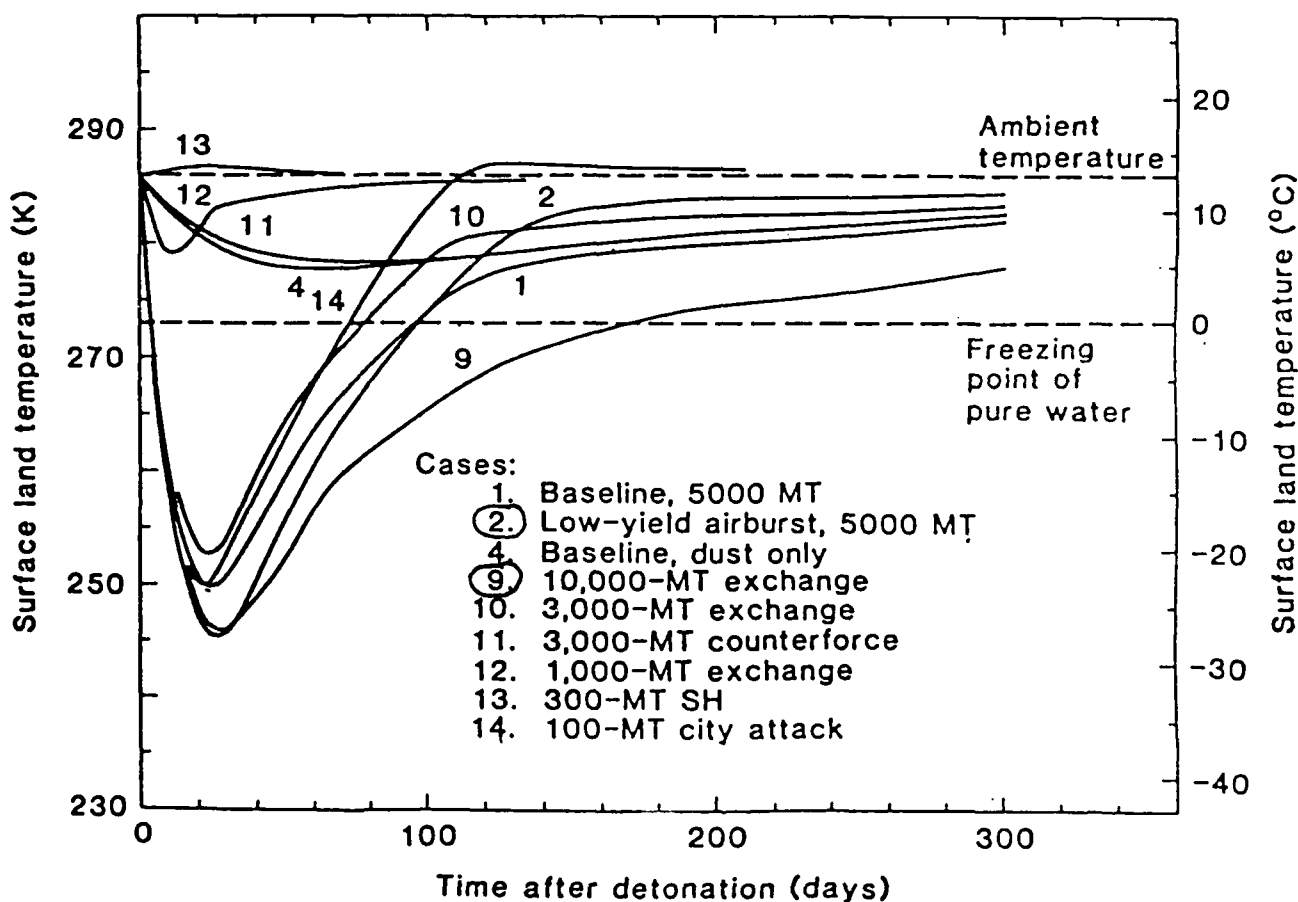


Fig. 2 Hemispherically averaged surface temperature variations after a nuclear exchange. Results are shown for several of the cases in Table 1. (Note the linear time scale, unlike that in Fig. 1). Temperatures generally apply to the interior of continental land masses.

## Nuclear Winter: Global Consequences of Multiple Nuclear Explosions

R. P. Turco, O. B. Toon, T. P. Ackerman  
J. B. Pollack, Carl Sagan

Among the cases shown, even the smallest temperature decreases on land are  $\approx 5^\circ$  to  $10^\circ\text{C}$  (cases 4, 11, and 12), enough to turn summer into winter.

### Observed Summer - Winter Ranges

<u>Latitude (<math>^\circ\text{N}</math>)</u>	<u>Range (<math>^\circ\text{C}</math>)</u>
20	10.
30	19.
40	27.
50	34.
60	36.

# NUCLEAR WINTER AND ITS IMPLICATIONS

---

---

## HEARINGS BEFORE THE COMMITTEE ON ARMED SERVICES UNITED STATES SENATE NINETY-NINTH CONGRESS FIRST SESSION

OCTOBER 2 AND 3, 1985

*Printed for the use of the Committee on Armed Services*

Chairman GOLDWATER. Senator Cohen?

Senator COHEN. Dr. Sagan, one of the criticisms we have heard is that the original TTAPS study greatly exaggerated the potential consequences.

Do you agree that the conclusions you have reached in that study were greatly exaggerated?

And the second question would be what have you learned since 1983 with continued research in this field?

Dr. SAGAN. That claim has been made, but if you look at all the recent studies, the work at the National Center for Atmospheric Research, for example, the work at Los Alamos National Laboratory, even the work at Livermore National Laboratory, you will find that temperature declines of 10 to 40 degrees occur in all of those models under certain circumstances, even short of a full exchange.

That is exactly the temperature range that we predicted in the original TTAPS study. I think it is absolutely straightforward that there is no significant disagreement and that fact is widely recognized.



# NUCLEAR WINTER AND ITS IMPLICATIONS

---

---

## HEARINGS

BEFORE THE

COMMITTEE ON ARMED SERVICES

UNITED STATES SENATE

NINETY-NINTH CONGRESS

FIRST SESSION

OCTOBER 2 AND 3, 1985

Printed for the use of the Committee on Armed Services

Dr. SAGAN.

It is sometimes said in criticism of the nuclear winter that the nuclear winter effects occur only in the worst case. As I tried to indicate, that simply is not true. It now looks that much less than the full strategic arsenals, perhaps 1 percent of the arsenals, would be sufficient to bring about nuclear winter. But this raises an important question.

It seems to me that the only truly safe circumstances is to make sure that there are so few strategic nuclear weapons that nuclear winter could not be triggered, no matter what—even if everyone went crazy. Nobody knows just what number that is, but it does appear to be sufficient to represent a very powerful retaliatory capability and, therefore, there is at least the prospect that massive reductions in nuclear arsenals carried out bilaterally and verifiably could bring the arsenals below the threshold for triggering nuclear winter and still preserve, if we so wish, an invulnerable retaliatory capability.

# NUCLEAR WINTER AND ITS IMPLICATIONS

---

---

HEARINGS  
BEFORE THE  
COMMITTEE ON ARMED SERVICES  
UNITED STATES SENATE  
NINETY-NINTH CONGRESS  
FIRST SESSION

—————  
OCTOBER 2 AND 3, 1985  
—————

Printed for the use of the Committee on Armed Services

whether the cure is not being confused with the disease.

*R. Perle:* I believe that the danger of a nuclear winter should cause us to redouble our efforts to bring about significant reductions in the number and destructive capacity of nuclear weapons. It should support the refinement of our strategic plans in the direction of weapons with reduced yield and greater accuracy aimed, not at civilians but at military forces. It should encourage a reexamination of the doctrine of mutual assured destruction and a greatly enhanced interest in strategic defense.

These are the policies of this administration. They are pol based on an appreciation of the catastrophic consequences of a nuclear war.

# NUCLEAR WINTER AND ITS IMPLICATIONS

---

---

HEARINGS  
BEFORE THE  
COMMITTEE ON ARMED SERVICES  
UNITED STATES SENATE  
NINETY-NINTH CONGRESS  
FIRST SESSION

OCTOBER 2 AND 3, 1985

Printed for the use of the Committee on Armed Services

Chairman GOLDWATER. Senator Cohen?

Senator COHEN. Mr. Chairman, Senator Nunn asked how many cities must dance on the head of a nuclear warhead exchange. What strikes me about this discussion is that these concepts are all cast as polar extremes.

If anyone supports the theory or concept of nuclear winter, therefore, they ought to support the freeze, be it unilateral or mutual, they want to abandon research on SDI and they want to remove immoral targeting of cities.

I find that an extreme position to take. Most of the people, including myself, on this committee do support the theory, I think, of nuclear winter but do not support the freeze and have not supported the freeze, do support research on SDI and also see the wisdom of a dramatic reduction in offensive weapons, possibly coupled with some transition to defensive systems. but much lower levels of both offensive and defensive.

WASHINGTON, D.C. 20005

Front Page	Edit Page	Other Page
---------------	--------------	---------------

WALL STREET JOURNAL  
-EASTERN EDITION-

M - 757, 135

85

NOV 25 1986

## *Nuclear Autu*

While it is true that the magnitude of land surface cooling in the Northern Hemisphere projected by climatic modeling studies has been reduced for the most part since TTAPS calculations in 1983, I would certainly not characterize the state of the art in "nuclear-winter" research as "a shaky scientific conjecture." Nor would I describe my presentation to a scientific audience at NASA Ames laboratory in February 1986, as Mr. Seitz did, to the effect that " 'nuclear winter' had succumbed to scientific progress." Since I am cited as that "progress," let me summarize briefly what I believe current research on "nuclear winter" to be.

It is not simply "July temperature

EOS Vol 67 No. 32 August 12, 1986  
pages 617-621

# Nuclear Winter, Or Nuclear Fall?

A. Berger

Université Catholique de Louvain,  
Institut d'Astronomie et de Géophysique  
Georges Lemaitre,  
Louvain-la-Neuve, Belgium

## Introduction

Climate is universal. If a major modern nuclear war (i.e., with a large number of small-yield weapons) were to happen, it is not even necessary to have a specific part of the world directly involved for there to be cause to worry about the consequences for its inhabitants and their future. Indeed, smoke from fires ignited by the nuclear explosions would be transported by winds all over the world, causing dark and cold. According to the first study, by Turco *et al.* [1983], air surface temperature over continental areas of the northern mid-latitudes (assumed to be the nuclear war theatre) would fall to winter levels even in summer (hence the term "nuclear winter") and induce drastic climatic conditions for several months at least. The devastating effects of a nuclear war would thus last much longer than was assumed initially. Discussing to what extent these estimations of long-term impacts on climate are reliable is the purpose of this article.

Because avoiding nuclear war, with its overall consequences, is one of the major challenges that our modern society has to face as we near the end of the 20th century, reviews of the most recent and reliable results obtained since the pioneer papers [Crutzen and Birks 1982; Turco *et al.*, 1983; Ehhlich *et al.*, 1984] have begun to be published widely. They discuss mostly the perturbations in atmospheric chemistry, the climatic effects, the biological impacts on man and on the biosphere, and the long-term global effects on society and on the earth [Levi and Rotham, 1985; National Research Council (NRC), 1985; British Medical Association, 1986; Golitsyn and Phillips, 1986; Kumratiiev and Nikol'sky, 1986; MacCracken, 1986; Peterson, 1986; Special Committee on Problems of the Environment (SCOPE), 1986; Thompson and Schneider, 1986] (see also the series of eight papers on the climatic and biological consequences of nuclear war in *BioScience*, vol. 35, p. 536). The dangers of a nuclear war were also compared to the hazards of large natural geophysical events, similar to

those associated with the major extinctions found in the fossil record of the past 250 million years [Knox and Smith, 1984]. These scientific papers conscientiously give the state-of-the-art in such research, with all the working hypotheses and uncertainties. However, to quote Sagan (1985) (as cited by Teller [1985] and Morrison [1986]),

in parallel with an inclination in the popular literature to exaggerate the consequences of nuclear war, there has also been a tendency in many professional announcements to minimize or ignore the consequences of nuclear war... (mainly because) of the considerable uncertainty that dominates the calculations of atmospheric response to nuclear war.

Faced with these two extreme attitudes, this article is intended to present objectively some of the findings obtained by reliable groups of scientists who have demonstrated their scientific integrity previously in a logical progression [Schneider *et al.*, 1986].

## Long-Term Climatic Effects of Nuclear War

Research on nuclear winter is proceeding rapidly [Berger, 1985a; Pittock, 1986]. Computer modeling of nuclear winter has indeed already gone through three generations, from the one-dimensional radiative convective models used by Turco *et al.* [1983] (referred to as TTAPS, for the authors' initials), through three-dimensional general circulation models in which smoke could affect the atmospheric circulation but was not itself moved by the winds, to more realistic models that allow smoke to move interactively with the atmosphere.

Major uncertainties still exist, however, especially in quantifying the initial distribution of smoke and dust and in modeling the complex interactions that happen in the climate system. Some of the processes involved would contribute to

• A lesser cooling of the earth's surface. These processes include the wash-out of the smoke by convective rainfall induced in intense fire plumes or its coagulation into particles larger than 1  $\mu\text{m}$ , although recent in situ and satellite observations by Y. T. Kaufman and R. Turco of large forest fires (which are still much smaller than fires caused by nuclear war) do not show the effectiveness of these processes [Pittock, 1986].

• A considerable lengthening of the quantities of smoke stratosphere, and to smoke in the troposphere increased vertical speed, and a much slower, and a much slower, the surface would be

A set of global interactive smoke climate winter. They indicate of smoke general Treaty Organization Pact territories in J upward and across weeks, but the dip is less pronounced; hemisphere land as large in July but however, recent simulations of fuel loads more relevant climate temperature change fall" more closely after.

## First- and Second-Generation Climate Model

Let us now try to discuss through these experiments. During TTAPS scenario of the atmosphere we quantities of pollutant urban and industrial 240,000 km<sup>2</sup>, and grasslands (also km<sup>2</sup>). First analysis involved in the war theater (in NATO and Warsaw that more than 100 be produced by the smoke mass of 225 and the U.S. National (NAS) study used 1 1985). It should be that this NAS estimate closer to the plausible smoke amount than Mt could be a lower considered to be a mitigation for a medium of dust injected, in (in TTAPS, 65 Mt) total residential time relatively small millioptical depths of 2 such injections into small fraction of the penetrate to the surface

# Press Intelligence, Inc.

WASHINGTON, D.C. 20005

---

Front	Edit	Other
Page	Page	Page

---

WALL STREET JOURNAL

-EASTERN EDITION-

757,135

85

NOV 25 1986

## Nuclear Autu

It is not simply "July temperatures upward of +50 degrees F. in mid-America" that Mr. Seitz reported I said to the Ames meeting, for the figure he cites is for average temperatures in one particular case. We have run many cases over a range of plausible assumptions for smoke generated by fires in the aftermath of a large nuclear war, and average temperature drops in mid-America could be substantially different from that +50 F. value he cites—perhaps 10 or more degrees different in either direction, depending on what assumptions are made. Moreover, the average temperature drop is of little importance, for, as every farmer knows, it isn't the average temperatures they worry about in the late spring or early fall, but the extreme cold nights. One frost can end a growing season. If this happened in the middle of a normal growing season it

# Press Intelligence, Inc.

WASHINGTON, D.C. 20005

Front Page	Edit Page	Other Page
------------	-----------	------------

WALL STREET JOURNAL  
-EASTERN EDITION-

85

M - 757, 135

NOV 25 1986

## Nuclear Autumn

On the Nov. 5 editorial page, Russell Seitz attempts to debunk the theory of "nuclear winter," especially the version first offered in 1983 by Richard Turco, Carl Sagan and colleagues—collectively referred to by the acronym TTAPS. Inasmuch as he reports on work by me and Starley Thompson here at the National Center for Atmospheric Research to bolster his case, I feel it is appropriate to provide our interpretations, some of which differ substantially from the impression given by Mr. Seitz.

While it is true that the magnitude of

substantially reduced to that of the earliest appropriate to classify our "The depths of Nuclear winter be distinguished days of summer." Those

In Foreign Affairs wrote: "... even a milder winter—what we called could be followed by major It is probable that a winter direct effects makes the a.

# The Melting of 'Nuclear Winte

By RUSSELL SEITZ

*"Apocalyptic predictions require to be taken seriously, higher standards of evidence than do assertions on other matters where the stakes are not as great."*

- Carl Sagan

Foreign Affairs: Winter 1983-84

The end of the world isn't what it used to

---

*Even a Soviet scientist at the critical mee  
guys are fools. You can't use mathematical m  
...You're playing with toys."*

---

idic advisory board that drew heavily from  
such organizations as the Union of Con-

said it was closed  
sensationalism and

will remain hostages to zeal.

Historians of science may one day view this entire episode as a bizarre comedy of manners; having known Sin at Hiroshima, physics was bound to run into Advertising sooner or later. But what about the politics of this issue? Does all this matter? Sagan evidently thinks it does. Characteristically, he has taken the trouble of responding to the new generation of critical scientific studies by hiring a cartoonist. An animated version of his obsolete apocalypse has been appended to his updated television documentary "Cosmos—A Special Edition." Throughout this fall, prime time audiences worldwide will watch in horror as the edge of darkness overspreads planet Earth. They will hear Sagan prophesy that the Reagan administration's SDI program will provoke so overwhelming an increase in Soviet missile throw weight as virtually to



# The Melting of 'Nuclear Win

By RUSSELL SETZ

*"Apocalyptic predictions require, to be taken seriously, higher standards of evidence than do assertions on other matters where the stakes are not as great."*

- Carl Sagan

Foreign Affairs: Winter 1983-84

The end of the world isn't what it used to

*Even a Soviet scientist at the critical 1  
guys are fools. You can't use mathematical  
...You're playing with toys."*

scientific advisory board that drew heavily from such organizations as the Union of Communist said it was charged with curbing sensationalism

What is being advertised is not science but a pernicious fantasy that strikes at the very foundations of crisis management, one that attempts to transform the Alliance doctrine of flexible response into a dangerous vision. For "Nuclear Winter" does exist—it is the name of a specter, a specter that is haunting Europe. Having failed in their campaign to block deployment of Nato's theater weapons, the propagandists of the Warsaw Pact have seized upon "Nuclear Winter" in their efforts to debilitate the political will of the citizens of the Alliance. What more destabilizing fantasy than the equation of theater deterrence with a global *götterdämmerung* could they dream of? What could be more dangerous than to invite the Soviet Union to conclude that the Alliance is self-deterred—and thus at the mercy of those who possess so ominous an advantage in conventional forces?

Dr. Sagan and the Physicians for Social Responsibility may deny that their good intentions could lead anywhere but to massive

# NATIONAL INTEREST

"NUCLEAR WINTER" MELTS DO  
*by Russell Seitz*

FORECASTING CHINA'S FUTUR  
*by Michel Oksenberg & Kenneth Lieberthal*

A Conversation *Zbigniew Brzezinski with Owen Harries*

Reflections on America's Role *by Robert W. Tucker*

Suez: The Unwashed Slate *by Diana Schaub*

Australia Next? *by Peter Samuel & Colin Rubenstein*

The Idea of Human Rights *by Roger Pilon*

Essays & Comments:

Michael Novak, George Weigel, Morton Kondracke,  
Charles Wolf, Jr., Ralph Cwerman & Richard Starr

NUMBER 5 / FALL 1986 / \$4.50

THE WALL STREET JOURNAL

## The Melting of 'Nuclear

By RUSSELL SEITZ

"Apocalyptic predictions require, to be taken seriously, higher standards of evidence than do assertions on other matters where the stakes are not as great."

- Carl Sagan

Foreign Affairs, Winter 1982

*Even a Soviet scientist at the  
guys are fools. You can't use mat.  
..You're playing with toys."*

*Man and the Biosphere: A Test of Systems*

by

*Analysis and Experiments with Computers*, by

Hugh W. Ellsaesser

N. N. Moicyeyev, V. V. Aleksandrov and

Lawrence Livermore National Laboratory

A. M. Tarko, "Nayka," Moscow, 1985.

P. O. Box 808

Livermore, CA 94550

May 1986

stress. Therefore, a nuclear war will mean either disappearance of the human race or its degeneration to a level below the pre-industrial. In such conditions the possibility of the complete disappearance of the human race cannot be excluded.

These results depend little on the nuclear war scenarios examined if as a consequence



THE SECRETARY OF DEFENSE

WASHINGTON THE DISTRICT OF COLUMBIA

Honorable Barry Goldwater  
Chairman  
Committee on Armed Services  
United States Senate  
Washington, D.C. 20510

2100

Dear Mr. Chairman:

I am pleased to submit the Report requested by Sectic of the FY1986 Department of Defense Appropriations Act, or potential climatic effects of nuclear war. Despite signif

experienced, could be potentially serious (particularly with regard to agri- culture), they are substantially less threatening than the earlier apocalyptic predictions. It must, however, be reemphasized that these new observations are themselves tentative and are subject to revision as the research continues and better input data become available for use in the models. Thus, the current results and observations should not be used for planning purposes.

## Nuclear Winter: Global Consequences of Multiple Nuclear Explosions

R. P. Turco, O. B. Toon, T. P. Ackerman  
J. B. Pollack, Carl Sagan

The model predictions discussed here generally represent effects averaged over the Northern Hemisphere (NH).

Figure 2 shows the surface temperature perturbation over continental land areas in the NH calculated from the dust and smoke optical depths for several scenarios.

Actual temperature decreases in continental interiors might be roughly 30 percent smaller than predicted here, and along coastlines 70 percent smaller (10).

# Nuclear Winter: Global Consequences of Multiple Nuclear Explosions

R. P. Turco, O. B. Toon, T. P. Ackerman  
J. B. Pollack, Carl Sagan

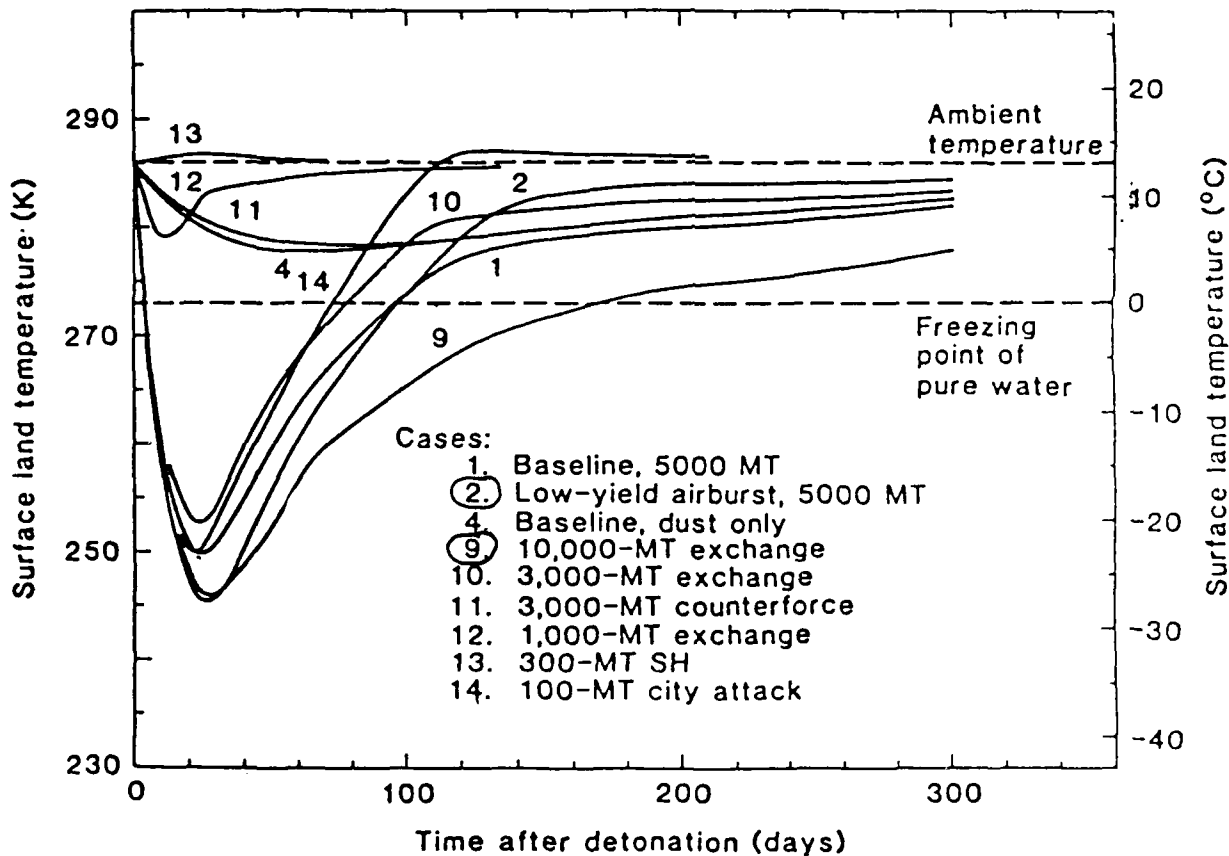


Fig. 2 Hemispherically averaged surface temperature variations after a nuclear exchange. Results are shown for several of the cases in Table 1. (Note the linear time scale, unlike that in Fig. 1). Temperatures generally apply to the interior of continental land masses.

## Nuclear Winter: Global Consequences of Multiple Nuclear Explosions

R. P. Turco, O. B. Toon, T. P. Ackerman  
J. B. Pollack, Carl Sagan

Among the cases shown, even the smallest temperature decreases on land are  $\approx 5^\circ$  to  $10^\circ\text{C}$  (cases 4, 11, and 12), enough to turn summer into winter.

### Observed Summer - Winter Ranges

<u>Latitude (<math>^\circ\text{N}</math>)</u>	<u>Range (<math>^\circ\text{C}</math>)</u>
20	10.
30	19.
40	27.
50	34.
60	36.

## 1-D VS. 3-D MODEL RESULTS

---

*Compare land, annual, hemispheric, surface temperature decrease over the 10 coldest contiguous model days.*

---

### I. NCAR 3-D Model (ca. 1986-87)

#### A. July, Northern Hemispheric land ( $^{\circ}\text{C}$ )

0-10 km CD,  $\Delta T = -11.7$

0-7 km CMR,  $\Delta T = -8.4$

#### B. Convert to Annual Mean ( $\times 0.67$ )<sup>†</sup>

Thus,  $\Delta T_{3D} = -5.6$  to  $-7.8$

### II. TTAPS 1-D Model (1983)

#### A. Annual, Hemispheric, All-Land Planet ( $^{\circ}\text{C}$ )

Baseline,  $\Delta T = -36$ .

#### B. Convert to Land/Ocean Planet ( $\times 0.5$ )<sup>‡</sup>

Thus,  $\Delta T_{1D} = -18$ .

### III. Compare,

$\Delta T_{1D} = -18$ .

$\Delta T_{3D} = -5.6$  to  $-7.8$

---

**1-D to 3-D Ratio: 2.3 to 3.2**

---

<sup>†</sup> Based on earlier NCAR Jan., Apr., July simulations and on Annual/July insolation ratio.

<sup>‡</sup> Mean of TTAPS correction factors: 0.3 (coastal) and 0.7 (interior).



# Nuclear winter may not be so bad

By TODD MALMSBURY  
Camera Staff Writer

The frozen, dark landscape produced by devastating climate effects of "nuclear winter" have been dramatically overstated, according to two Boulder researchers.

Though effects could still be severe in some areas, global freezing would not take place. And the actual effects might better be described as "nuclear fall."

"Despite the continued potential for serious nuclear winter effects, there

does not seem to be a real potential for human extinction; nor is there a plausible threshold for severe environmental effects," write Stephen Schneider and Starley Thompson in the summer issue of Foreign Affairs, a national journal, which will be out in early June. "Thus, the two unique conclusions of the original nuclear winter idea with the most important implications for policy have been removed."

Schneider is deputy director of the Advanced Study Program at the National Center for Research in Boulder,

Thompson is an atmospheric scientist at NCAR.

Working with former NCAR scientist Curt Covey, Thompson and Schneider have used a super computer to conduct "atmospheric modeling" of what would occur following a nuclear war.

Their findings, developed over three years of work, still show localized freezing and potential temperature drops that could damage key food crops in some regions, according to an advance copy of their article. And the indirect effects of nuclear war, espe-

cially famine in the Third World, could still kill more people than blasts, fire and radiation in targeted countries.

"The end of humanity was never a credible scenario," said Schneider. "Outsiders (to the research) thought there could be an end of the world, but none of the insiders did."

"The reality is still quite scary, but it is not doomsday," Schneider said. Astronomer Carl Sagan organized a conference in Washington, D.C., in October 1983 to announce the nuclear winter theory to the world. At that confer-

ence, Sagan set the tone for nuclear winter by stating: "We have achieved the capability for the certain destruction of our civilization and perhaps of our species as well."

The theory, developed by Paul Crutzen, then an NCAR scientist, and John Birks of the University of Colorado, hypothesized that huge fires in cities and forests, caused by nuclear blasts, would send millions of tons of smoke billowing upward.

The smoke would blot out nearly all

Boulder, CO

\* Friday, May 23, 1986

DAILY CAMERA 3A

FROM PAGE 1A

# FOREIGN AFFAIRS



SUMMER 1986

*Starley L. Thompson*  
*Stephen H. Schneider*

## NUCLEAR WINTER REAPPRAISED

The difficult issue of chronic climatic effects (months to years) has not received nearly as much attention as the acute nuclear winter effects (one to 30 days), but will undoubtedly assume greater research importance in the future. A substantial fraction (perhaps ten to 30 percent) of smoke injection from any massive nuclear war would likely reside in the stratosphere for months before finally being removed from the atmosphere. Although the obscuration of sunlight caused by such a shroud would not be sufficient to cause severe surface cooling, it could create other serious climatic effects, e.g., anomalous late spring and early autumn frosts, or a disruption of normal monsoon and summer rainfall over continental areas. Such effects could greatly hamper agricultural recovery in those areas still having sufficient social stability and economic resources to carry out viable agricultural practices.

# FOREIGN AFFAIRS



SUMMER 1986

*Starley L. Thompson*  
*Stephen H. Schneider*

## NUCLEAR WINTER REAPPRAISED

war. But considering all the chronic, indirect effects of a large nuclear war separately may be a misleading exercise; all the chronic effects would, to some degree, act synergistically with each other, and with the direct weapons effects, to produce unprecedented worldwide human misery.

The interaction between a failure of the Asian summer monsoon and the disruption of international trade in food, for example, would be a potent prescription for mass starvation on the Indian subcontinent. Many other interactions can be speculated upon, such as those of radiation-induced depression of the human immune system, disruption of medical services and epidemics of contagious diseases; such synergisms deserve the serious study that might allow us to draw less speculative conclusions. Therefore it is still quite plausible that climatic disturbances, radioactive fallout, ozone depletions and the interruption of basic societal services, when taken together, could threaten more people *globally* than would the direct effects of explosions in a large nuclear war

Bangkok Post, p. 3

ATURDAY FEBRUARY 14, 1987

HOME NEWS

กรุงเทพฯโพสต์ วัน

## Nuclear war will wipe out humanity — scientist

ABOUT 100,000 people might survive a nuclear war between the superpowers, and they eventually would be ravaged by psychological and genetic pressures, a Soviet scientist said in Bangkok yesterday.

"The survivors would not be homo sapiens but would be homo schizophrenics," said Anatoly Dorodnitsin, chairman of the Soviet National Committee of the International Scientific Committee on Problems of the Environment (SCOPE).

Dorodnitsin said as many as five billion people — virtually the world's entire population — would die from nuclear blasts, radioactive contamination and starvation in a nuclear conflict.

Freezing temperatures brought by

tary consequences. Studies showed the southern hemisphere will not (be able to) avoid tragic consequences," he said.

Members of SCOPE, an international nuclear war study group, met here in a closed-door session this week to assess global environmental problems. Discussions ended yesterday. The organisation has members from 34 nations.

Dorodnitsin quoted UN World Health Organisation estimates 100 million to one billion people would be killed by a nuclear war.

It was possible for some life to continue, he said, but: "The lucky survivors, maybe 100,000, won't be able to carry on. Psychological studies showed humans wouldn't be able to withstand the genetic and biological conse-

quences." He did not say where the survivors most likely would be found or elaborate on the genetic and biological factors.

He criticised the US "star wars" plan to build a space-based defence shield against nuclear attack, saying preemptive first strikes were "self-defeatist and a waste of money".

The US, he said, would have to spend about \$10 trillion to cover "star wars" costs.

"The Soviet Union now has no such means (to counter star wars) but in time, we will have to answer that," Dorodnitsin said. He denied the Soviet Union was developing its own space-based weapons.

SCOPE will hold its next meeting in the Soviet Union. No date was given.

Consequences of Large-Scale Nuclear War  
for Ecological Systems, and Proposed Research Needs

Herbert D. Hoover  
Technology Application Center  
University of New Mexico  
Albuquerque, NM 87131

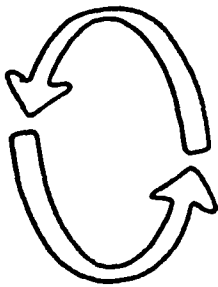
In order to fully understand the global effects of a large-scale nuclear war, we must consider the interactive environmental consequences in terms of the physical and biological components of the biosphere. A great deal of research emphasis has been placed on the effects of nuclear war on the physical environment (e.g., changes in atmospheric composition and related changes in climate), but little work has been done to clearly establish the vulnerability of natural ecosystems and agro-ecosystems. The recently completed SCOPE-ENUWAR study concluded that the indirect effects of nuclear war on the biosphere would be greater than the direct effects. Furthermore, this study concluded that the overall effects of reduced temperature, reduced light, and associated physical effects of nuclear war would differ greatly for different ecosystems as a function of ecosystem location and species composition. Among the most vulnerable are modern agro-ecosystems, which depend upon human subsidies. The vulnerability of agricultural crops to changes in climate and societal disruptions, coupled with inadequate food stores for most of the global human population, suggests that starvation in the first year following a large-scale nuclear war could double the total number of human fatalities now projected, and that most of these additional deaths would occur in non-combatant nations.

There are a number of uncertainties in the climate projections that directly affect the ability of biologists to assess the consequences of nuclear war. First, biologists need to know the rate of onset of climate changes, spatial and temporal variation in temperature excursions, the duration of these changes, how extremes in temperature would be changed, and how precipitation patterns might be altered. From the biological perspective, greater attention must be given to identifying the components of ecosystem resistance and resilience that would determine response to changes in climate. Also, we need to examine more closely the potential synergistic effects of climatic change on natural and agro-ecosystems. Finally, better and more appropriate ecosystem models must be applied to this problem. It is likely that collaborative research between physical and biological scientists will lead to a better understanding of feedback mechanisms pertinent to this problem, and also important to the current growing emphasis in the atmospheric and biospheric sciences on studying the Earth as an integrated system.

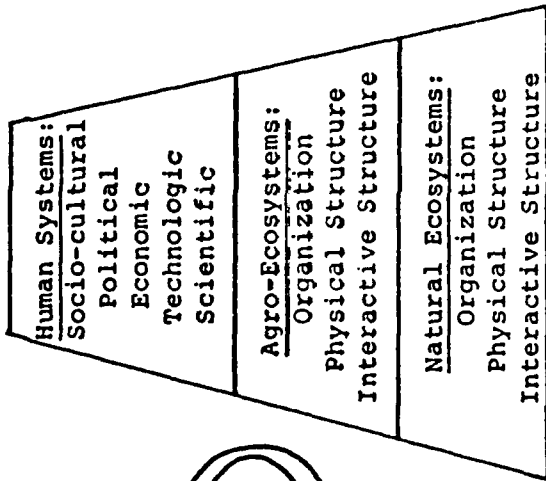
**Physico-Chemical Factors  
of the Environment**

**Radiation Inputs**

- Atmosphere
- Hydrosphere
- Lithosphere



**Components of the  
Biosphere**



**Integrative  
Variables**

**Human Systems:  
Distribution & Exchange  
of**

- Resources
- Commodities
- Currency

**Agro-Ecosystems:**

- Crop Yield
- & Quality
- Per Unit Effort

**Natural Ecosystems:  
Distribution & Cycling  
of**

- Energy &
- Chemical Elements

Figure 1. Depiction of certain critical components of the ecosphere relevant to the analysis of the full consequences of nuclear war.

## Key Conclusions from SCOPE-ENUWAR Study

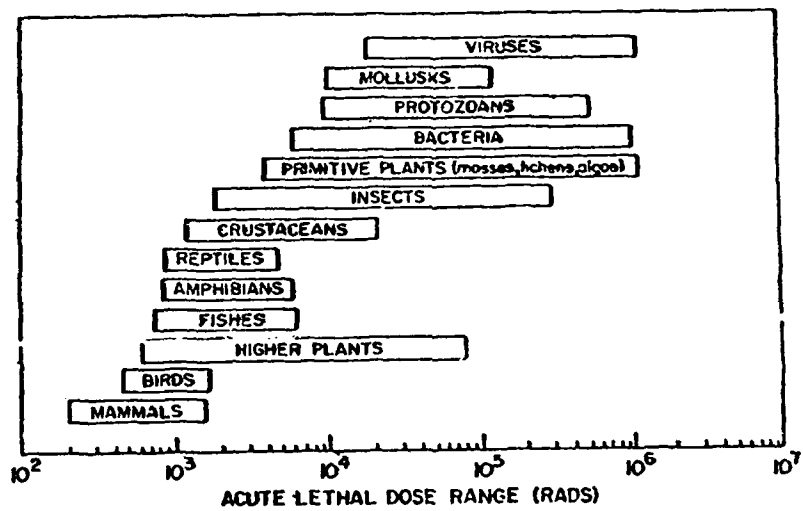
- \* Indirect Effects > Direct Effects
- \* Ecological Effects
  - Unprecedented in Extent and Intensity
  - Different Ecosystems with Different Vulnerabilities
  - Long-Term Recovery Prospects
- \* Natural Ecosystems - Human Carrying Capacity < 1% Global Population
- \* Agroecosystems Most Vulnerable to Disturbance
- \* Agricultural Effects
  - Temperature Most Important
    - Few degrees vice tens of degrees
    - Many mechanisms for temperature effects
  - Other Climatic Effects Also Important
  - If No Climatic Effects, Still Problem Human Subsidies
- \* Possibility of Elimination or Severe Disruption in Grain Production
  - for at least N.Hemisphere
  - for at least one growing season
- \* Food Limitations Critical
  - Stores Depleted Prior Next Growing Season
  - Stores Could Support Only Small Fraction of Global Population for 1 Yr
- \* Other Effects
  - Radiation
    - global fallout - little effect
    - local fallout - large effect
  - UV-B - potentially large effect
  - Air Pollutants - potential local effects
  - Synergisms
- \* Societal Effects - little studied, potentially large effects

---

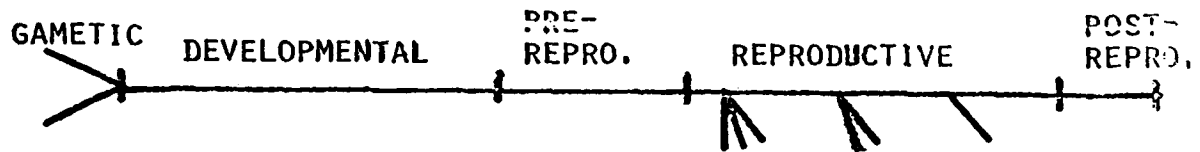
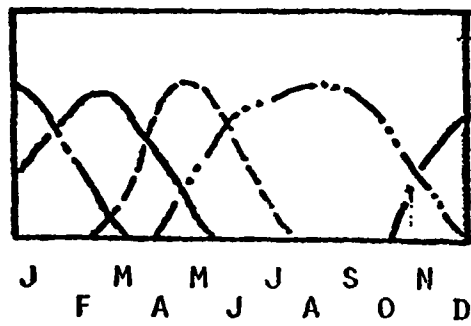
SOURCES OF INSIGHT FOR BIOLOGICAL/ECOLOGICAL EFFECTS:

- \* EXTINCTION EVENTS
- \* ATMOSPHERIC TEST SERIES
- \* EXPERIMENTS WITH RADIATION POINT SOURCES AND SIMULATED FALLOUT
- \* SIMULATION MODELS
- \* LITERATURE REVIEW / SYNTHESIS





% OF  
POP.



EFFECTS MAY BE:

LETHAL

SUB-LETHAL

NON-LETHAL

Table 2. Summary of ionizing radiation effects on various plant community types (from Whicker and Schultz 1982).

**ESTIMATED SHORT-TERM RADIATION EXPOSURES  
REQUIRED TO DAMAGE VARIOUS PLANT  
COMMUNITIES<sup>17,200,214,215</sup>**

Community type	Exposures in kR to produce		
	Minor effects	Intermediate effects	Severe effects
Coniferous forest	0.1-1	1-2	>2
Deciduous forest	1-10	5-35	>10
Shrub	1-5	5-20	>20
Tropical rain forest	4-10	10-40	>40
Rock outcrop (herbaceous)	8-10	10-40	>40
Old-fields (herbaceous)	3-10	10-100	>100
Herbaceous forest understorey	20-40	40-60	>60
Grassland	8-10	10-100	>100
Herbaceous invaders	40-60	60-160	>160
Moss-lichen	10-100	50-500	>200

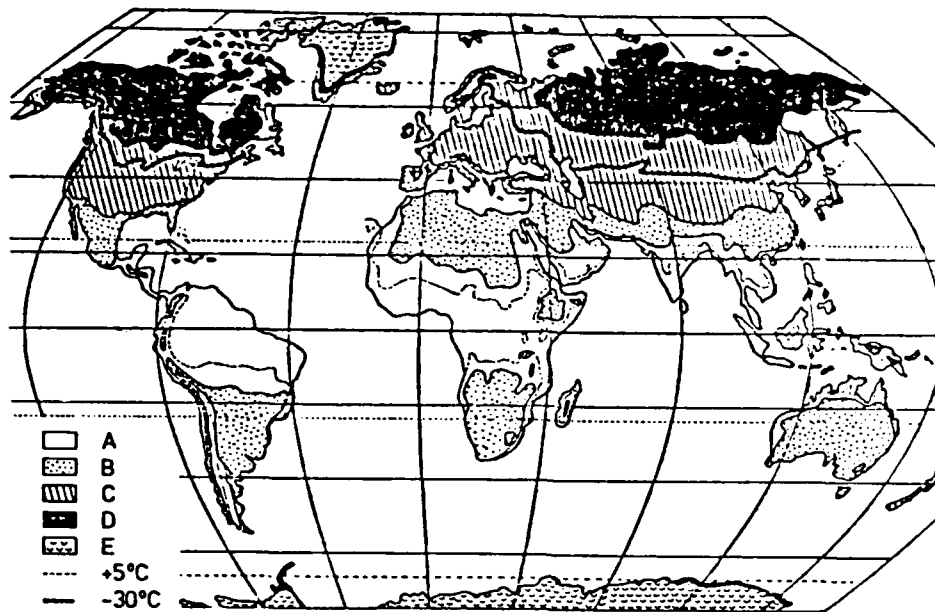
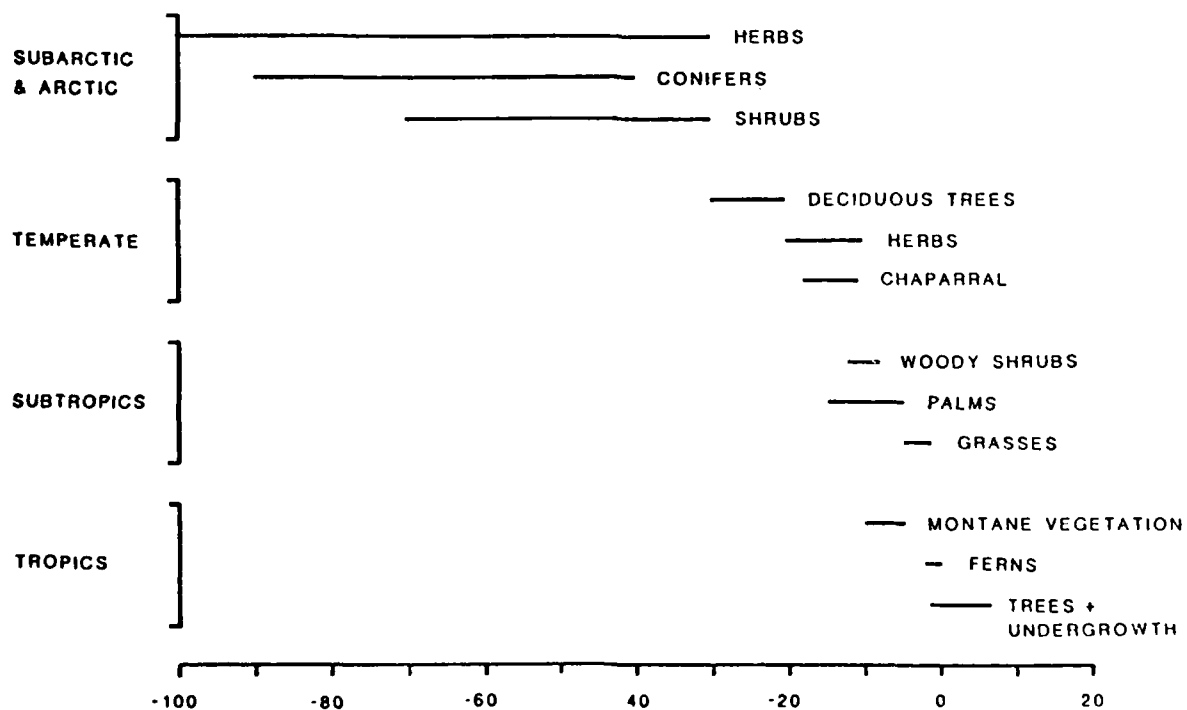
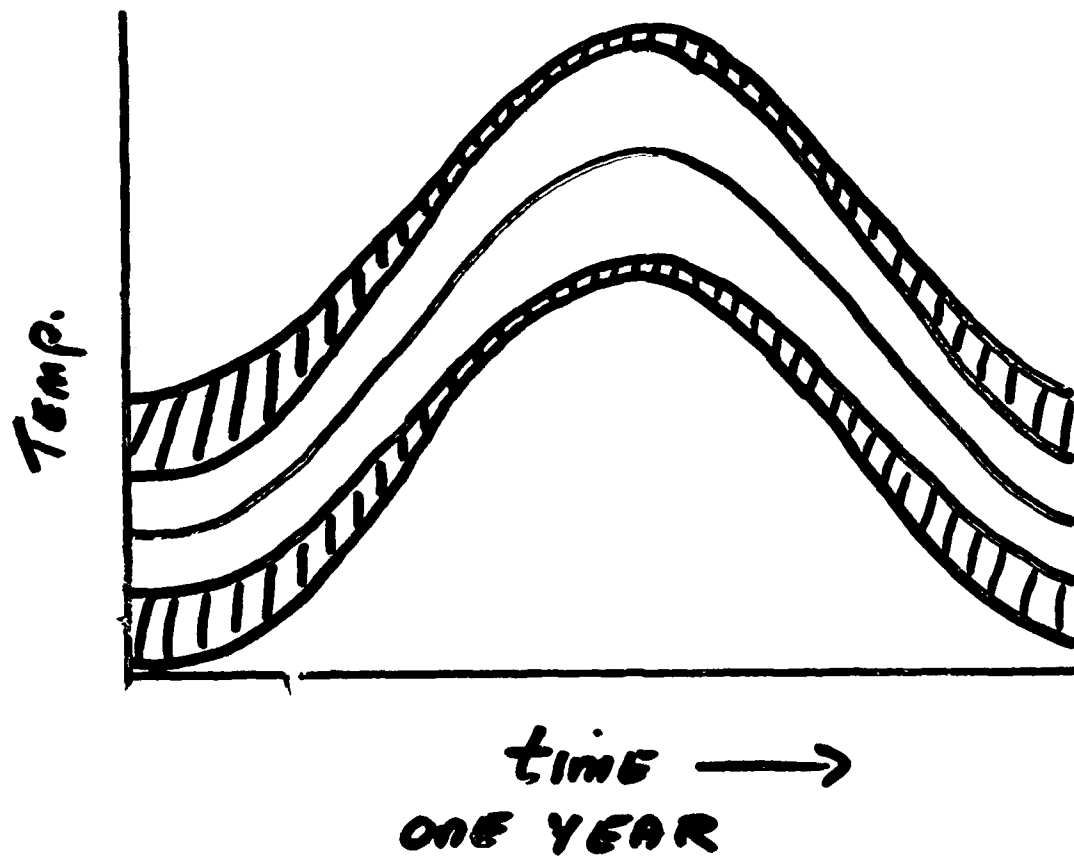


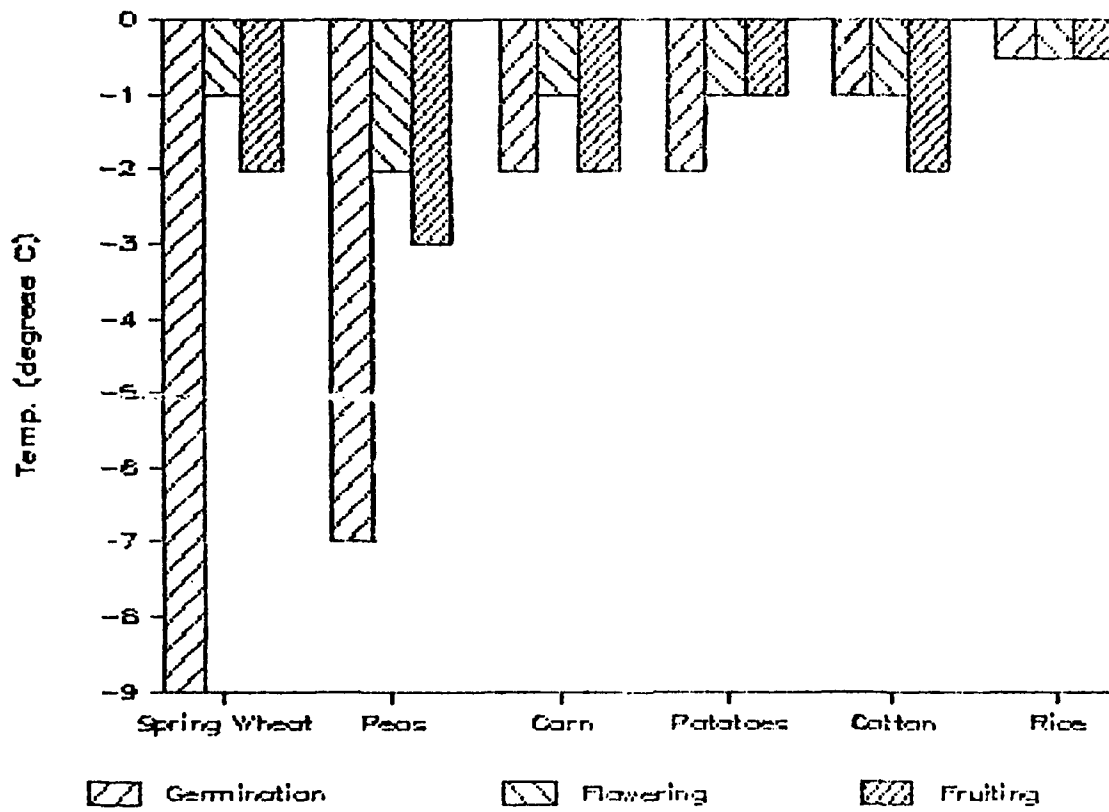
Figure 7. Approximate map illustrating temperature conditions limiting plant distribution. "A" = frost-free zone; "B" = zone of episodic frosts to  $-10^{\circ}\text{C}$ ; "C" = zone of average annual minimum of  $-10^{\circ}\text{C}$  to  $-40^{\circ}\text{C}$ ; "D" = zone of average annual minimum less than  $-40^{\circ}\text{C}$ ; and "E" = polar ice. "----" =  $+5^{\circ}\text{C}$  isotherm; "...." =  $-30^{\circ}\text{C}$  average annual minimum isotherm. (from Larcher and Bauer 1981)



# SEASONAL VARIATION in vulnerability



## Frost Resistance



ULTRAVIOLET LIGHT EFFECTS

REDUCED PHOTOSYNTHESIS

REDUCED LEAF EXPANSION

ALTERED ROOT/SHOOT RATIOS

DEPRESSED FLOWER DEVELOPMENT

LOSS OF APICAL-BUD DOMINANCE

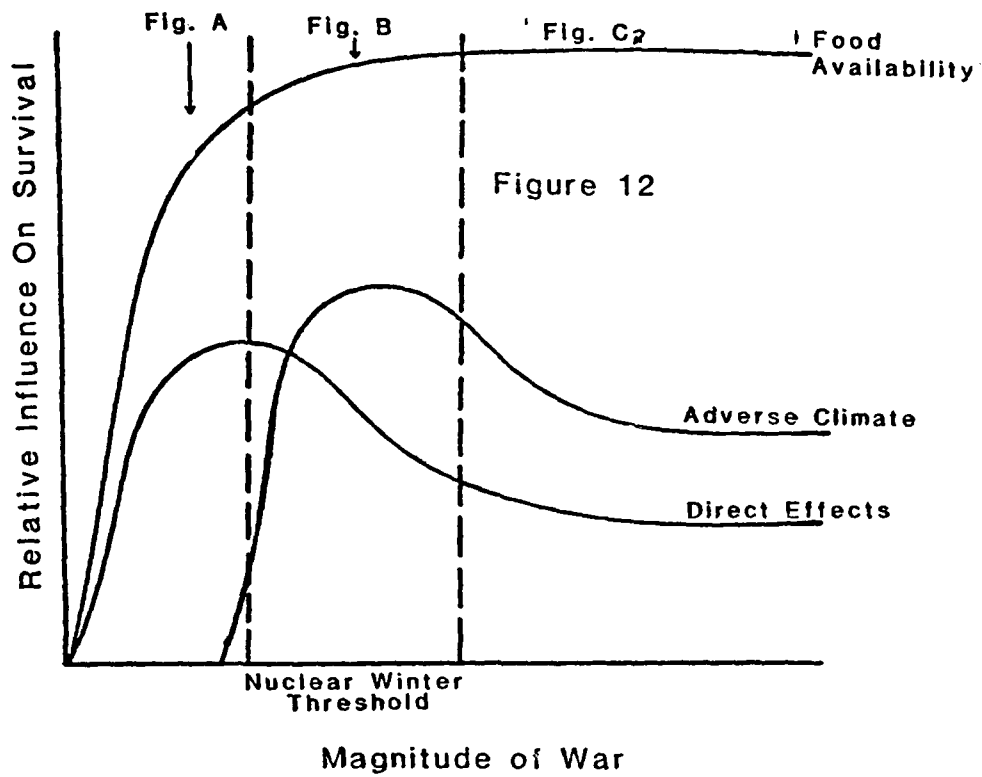
LEAF ABSCISSION

ALTERED MINERAL NUTRIENT UPTAKE

**Table 2.** Consequences of various physical stresses on biological systems resulting from nuclear war. This generalized representation includes both acute and chronic stresses and global, not local, effects. Stresses: Temp = air temperature reductions, Light = incident sunlight reductions, PPT = precipitation reductions, Radiation = fallout radiation, UV-B = increased UV-B from ozone depletion. Symbols reflect both the extent of a stress on a system and the vulnerability of that system to that stress: O = essentially no effect, ● = little effect, ●● = medium effect, ●●● = large effect.

System	Temp	Light	PPT	Radiation	UV-B
Tundra/alpine	O	●	●	●	●●
Temperate forests	●●	●	●	●●	●●
Grasslands	●	●	●●	●	●●
Tropical forests	●●●	●	●●	●	●●
Lakes and streams	●●●	●	●●	●	●●
Estuaries	●●	●●	●	●	●●
Marine	O	●●●	O	O	●●





Mechanism of Effect	Post-Nuclear war (time)										
	0	1 hr	1 day	1 wk	1 mo	3 mo	6 mo	1 yr	2 yr	5 yr	10 yr..
Blast	█										
Thermal Radiation	█										
1 <sup>st</sup> Ionizing Radiation	█										
Fires		█	█	█	█	█	█	█	█	█	█
Air Pollution			█	█	█	█	█	█	█	█	█
Stratospheric O <sub>2</sub> Reduction			█	█	█	█	█	█	█	█	█
Light Reductions			█	█	█	█	█	█	█	█	█
Temperature Reductions			█	█	█	█	█	█	█	█	█
Frozen Water Supplies			█	█	█	█	█	█	█	█	█
Food Shortages			█	█	█	█	█	█	█	█	█
Medical System Collapse			█	█	█	█	█	█	█	█	█
Diseases: Contagious (shelter period)			█	█	█	█	█	█	█	█	█
Epidemics (post vectors)			█	█	█	█	█	█	█	█	█
Psychological Stress			█	█	█	█	█	█	█	█	█
Radiation	█	█	█	█	█	█	█	█	█	█	█

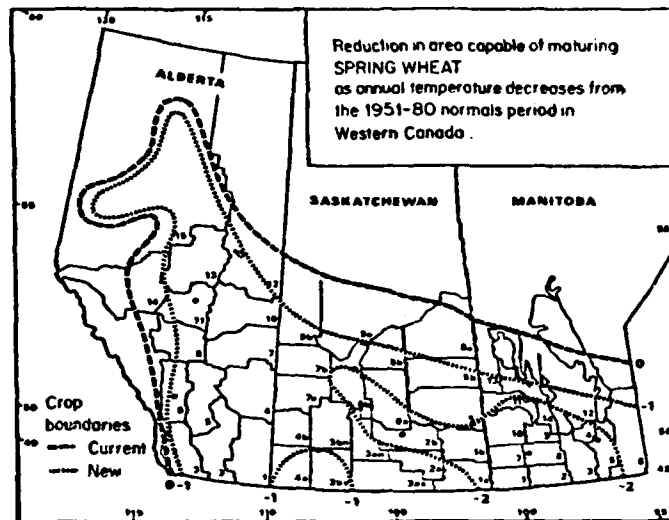


Figure 4.8a Reduction in area capable of maturing spring wheat as average temperatures are reduced by 1°C and 2°C from normals of 1951-1980. Based on Agriculture Canada model simulations by Stewart (1985)

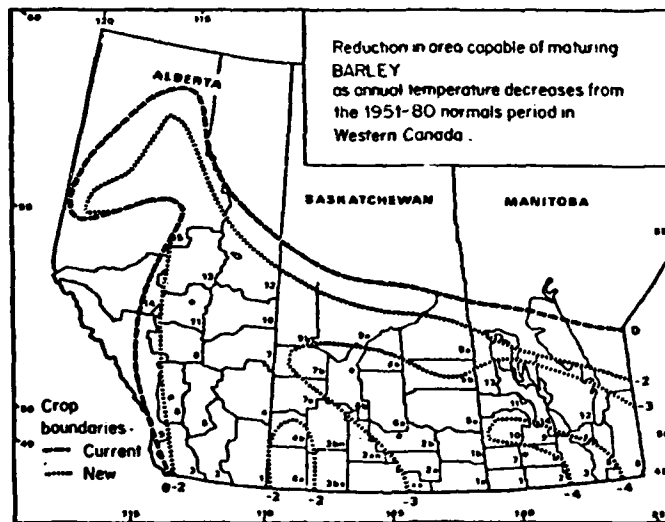
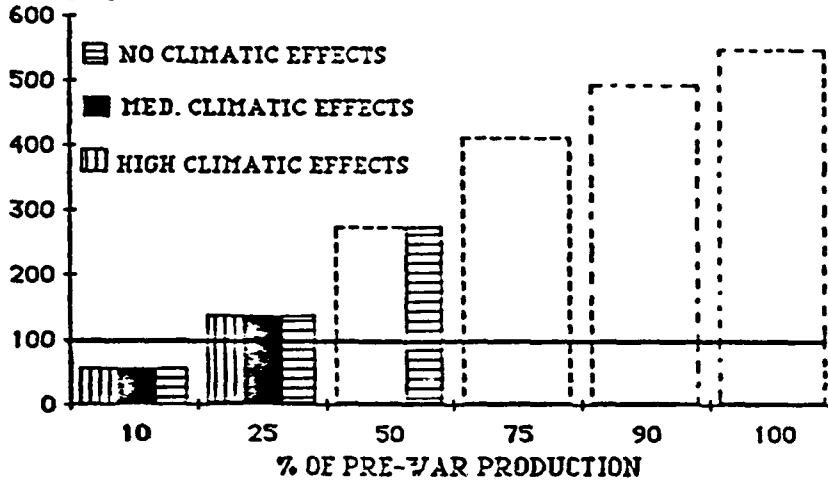


Figure 4.8b Reduction in area capable of maturing barley as average temperatures are reduced by 1°C and 2°C from normals of 1951-1980. Based on Agriculture Canada model simulations by Stewart (1985)

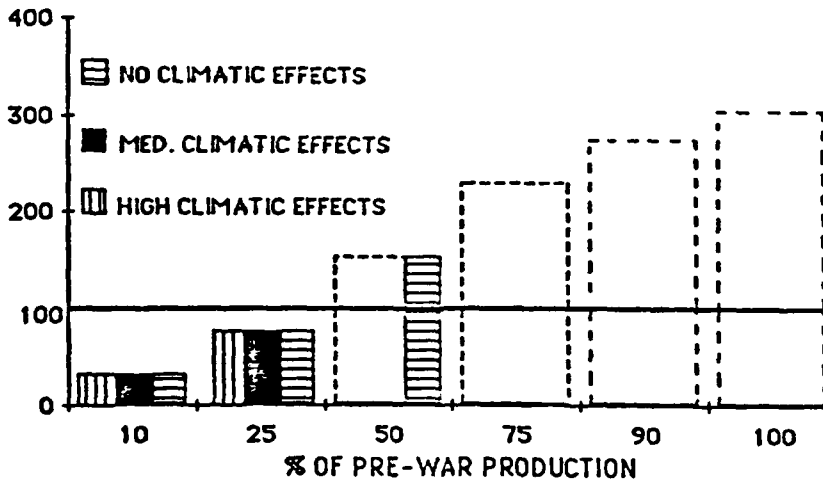
% OF PRE-WAR  
POPULATION

U.S.A.



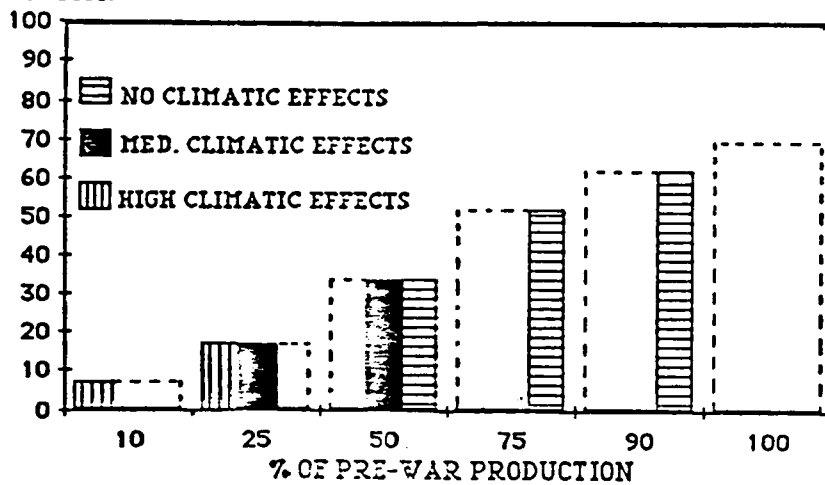
% OF PRE-WAR  
POPULATION

U.S.S.R.



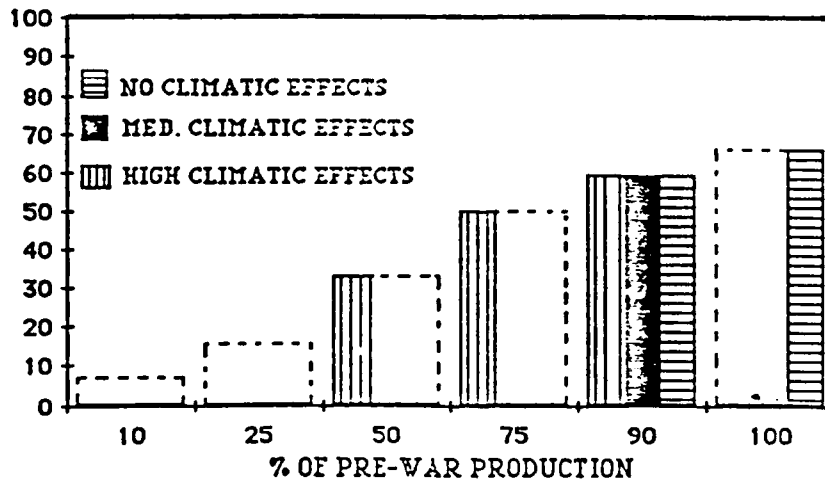
% OF PRE-WAR  
POPULATION

### KENYA



% OF PRE-WAR  
POPULATION

### NIGERIA



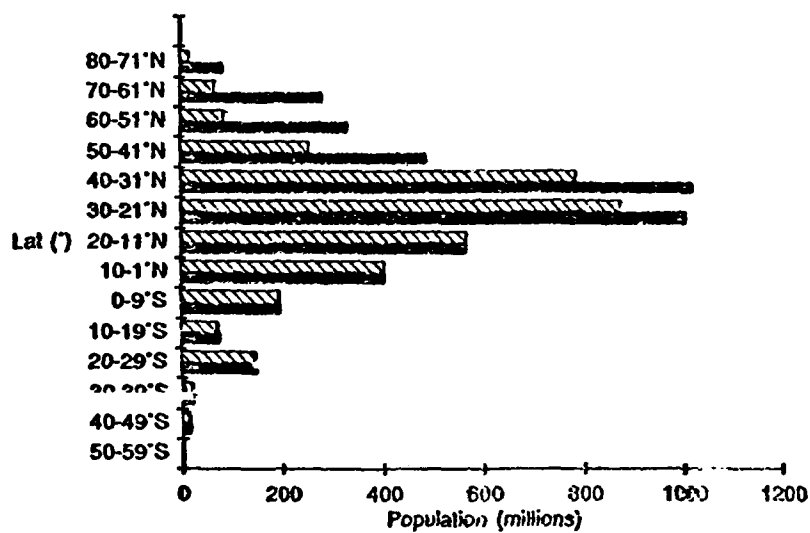


Figure 7.1 Human population distributed across latitudinal bands at current levels (solid bars) and after the direct effects of a large-scale nuclear war (striped bars) (based on calculations derived from Harwell, 1984; Ambio, 1982; and Bergstrom et al., 1983)

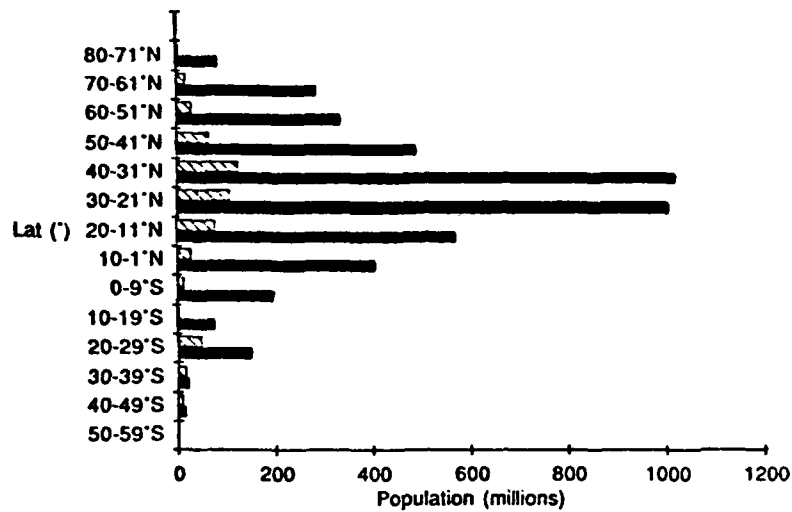


Figure 7.3 Vulnerability of human population to loss of food production if occurring when food stores are at a minimum. Current population (solid bars) and optimal number of survivors after one year (striped bars) (see discussion of assumptions in text) are shown across latitudinal bands

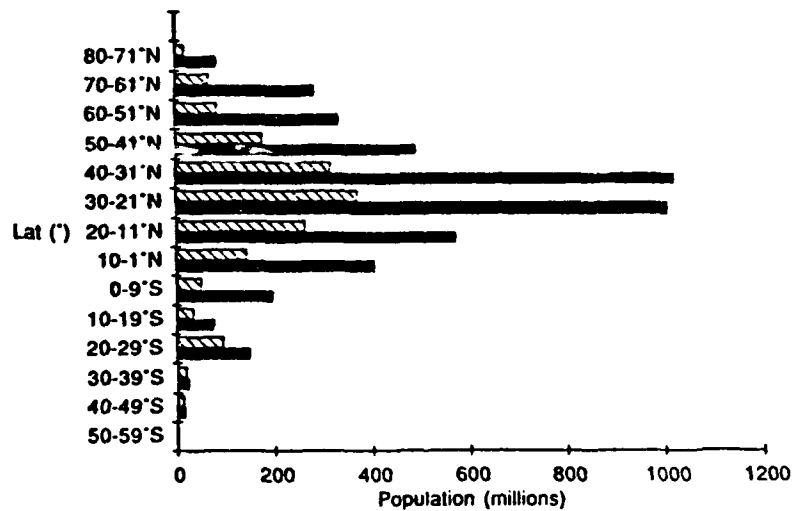


Figure 7.4 Vulnerability of human population to loss of food production if occurring when food stores are at the median level. Current population (solid bars) and optimal number of survivors after one year (striped bars) (see discussion of assumptions in text) are shown across latitudinal bands

## RESEARCH NEEDS

### \* REFINE CLIMATIC PROJECTIONS

- RATE OF ONSET
- SPATIAL AND TEMPORAL VARIATION
- DURATION
- EXTREMES VS. AVERAGES
- PRECIPITATION CHANGES

### \* REFINE BIOLOGICAL UNDERSTANDING

- IDENTIFY COMPONENTS OF RESISTANCE  
VS. RESILIENCE
- EXAMINE SYNERGISTIC EFFECTS
- DEVELOP APPROPRIATE ECOSYSTEM MODELS

### \* INTERDISCIPLINARY RESEARCH NEEDS

- BIOCLIMATIC FEEDBACKS

SECTION 3

MICROPHYSICS



CATEGORY 3

HOW MOTIONS INFLUENCE AEROSOL SCAVENGING IN CLOUDS.

John Hallett  
Desert Research Institute  
Reno, Nevada 89506

Removal of aerosol in clouds occurs through direct condensation to give cloud droplets, or by Brownian capture on pre-existing particles. The efficiency with which this process removes droplets and thus cleansing the atmosphere is linked to the precipitation efficiency of the cloud systems, which can vary from zero (small cumulus) to 70% in a steady state, near adiabatic, precipitating system. The efficiency of aerosol removal is therefore critically linked with the scale of the convective system and the rate at which it mixes (or does not mix) with its environment. These considerations critically influence the results and credibility of any numerical simulations of aerosol removal.

This work is supported by Lawrence Livermore National Laboratory.

**POTENTIAL NUCLEATION SCAVENGING OF SMOKE PARTICLES OVER LARGE FIRES, A PARAMETRIC STUDY\*****ABSTRACT**

Leslie L. Edwards and Joyce E. Penner, Lawrence Livermore National Laboratory, P.O. Box 808, L-262, Livermore, CA 94550, USA

Several numerical climate models have analyzed the potential attenuation of solar radiation (and resulting surface temperature decrease) caused by large amounts of smoke injected into the atmosphere by massive fires predicted to be ignited during hypothesized nuclear exchanges. Through improved models and measurements the range of uncertainty of the magnitude of the attenuation has been somewhat narrowed. However, much uncertainty remains as to the nature (chemical properties, solubility, shape, optical properties, etc.) of the smoke particles.

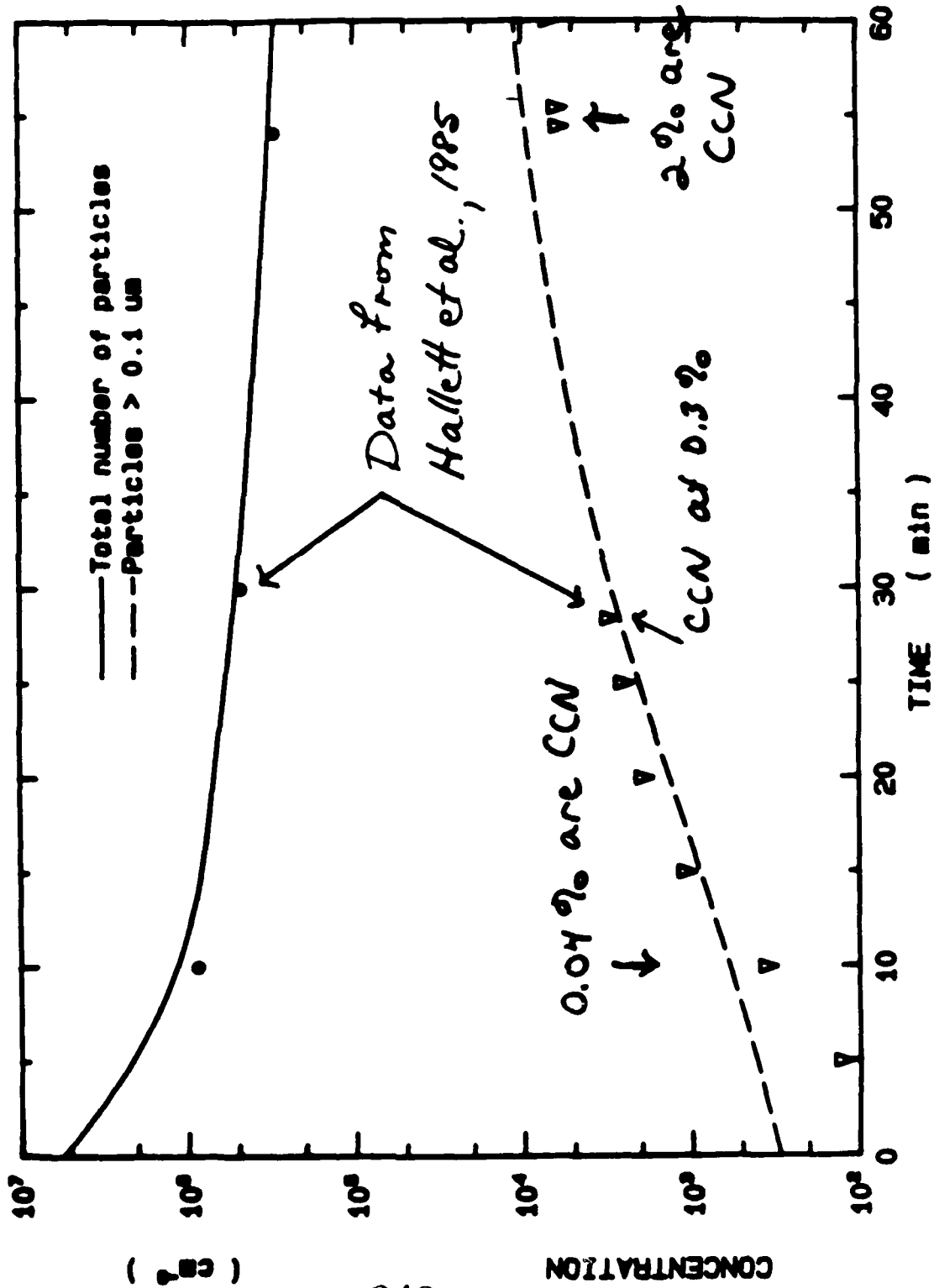
Considerable evidence has been accumulated to suggest that nucleation scavenging where smoke particles serve as cloud condensation nuclei may be an important mechanism for incorporating these submicron particles into cloud water. The fraction of smoke nucleated depends on the cloud environment as well as the affinity to water of the smoke particles.

A numerical model of detailed microphysics of condensation growth on aerosol and drop distributions is employed to produce a parametric study of the dependence of nucleation to a range of conditions. We consider number concentrations of  $10^3/\text{cm}^3$  to  $10^6/\text{cm}^3$ , updraft speeds from 1 to 50 m/s and aerosol (smoke) particles from fully water soluble to insoluble but wettable. The study provides insight into how well we must characterize smoke particles for use in model calculations.

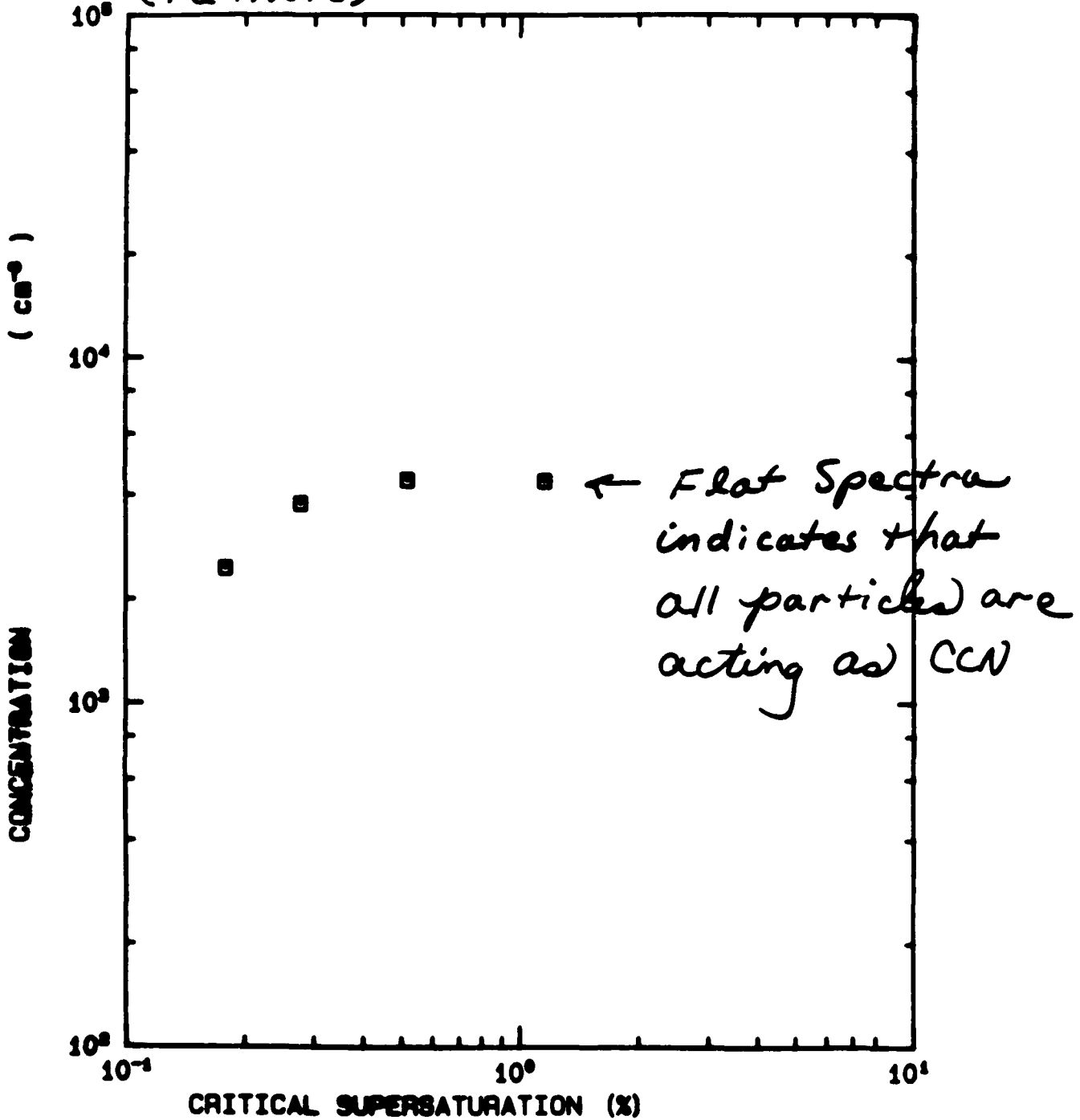
---

\*This work was performed under the auspices of the U.S. Department of Energy by the Lawrence Livermore National Laboratory under contract No. W-7405-Eng-48.

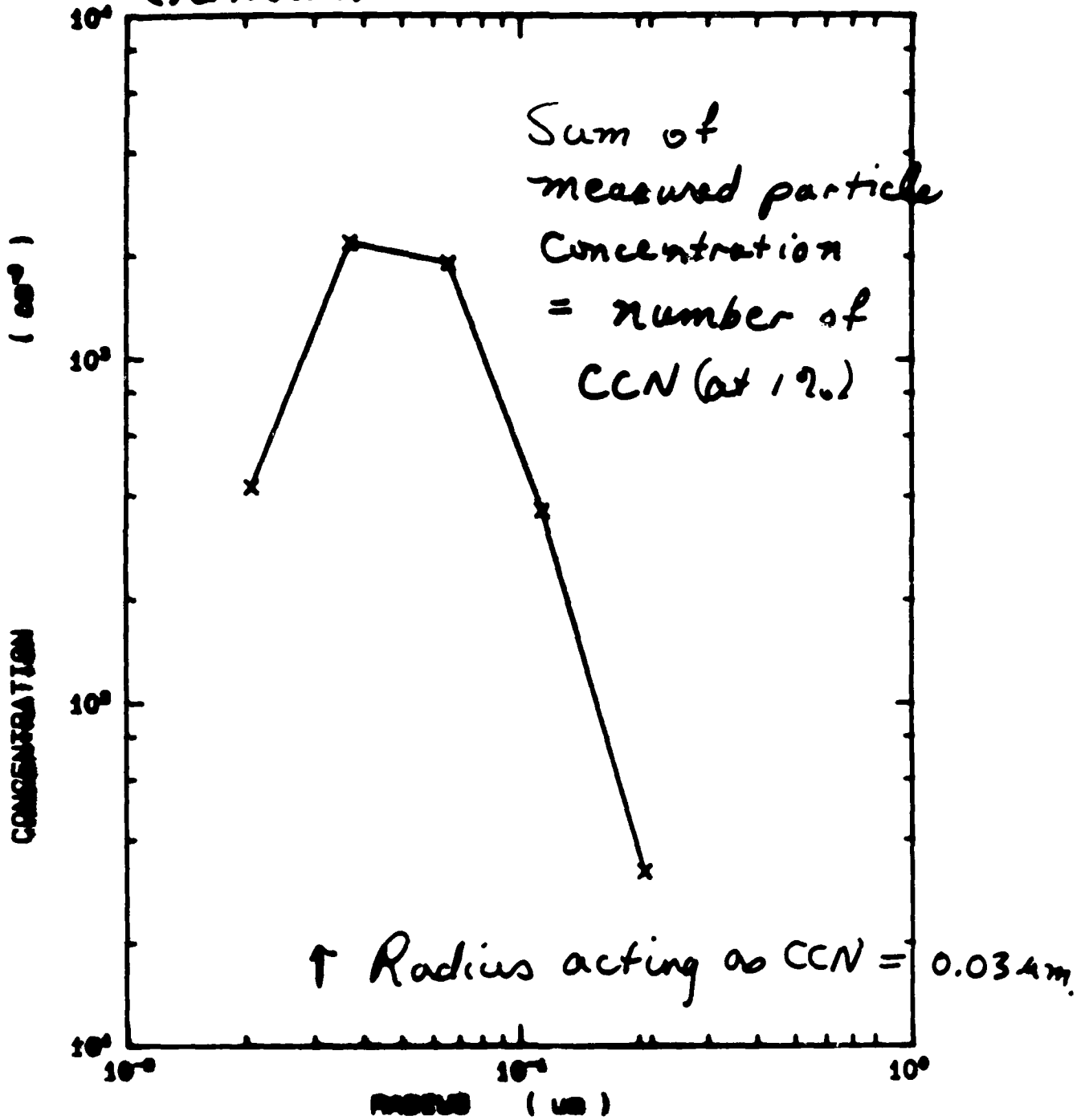
Fraction of CCN increases as smoke  
ages.



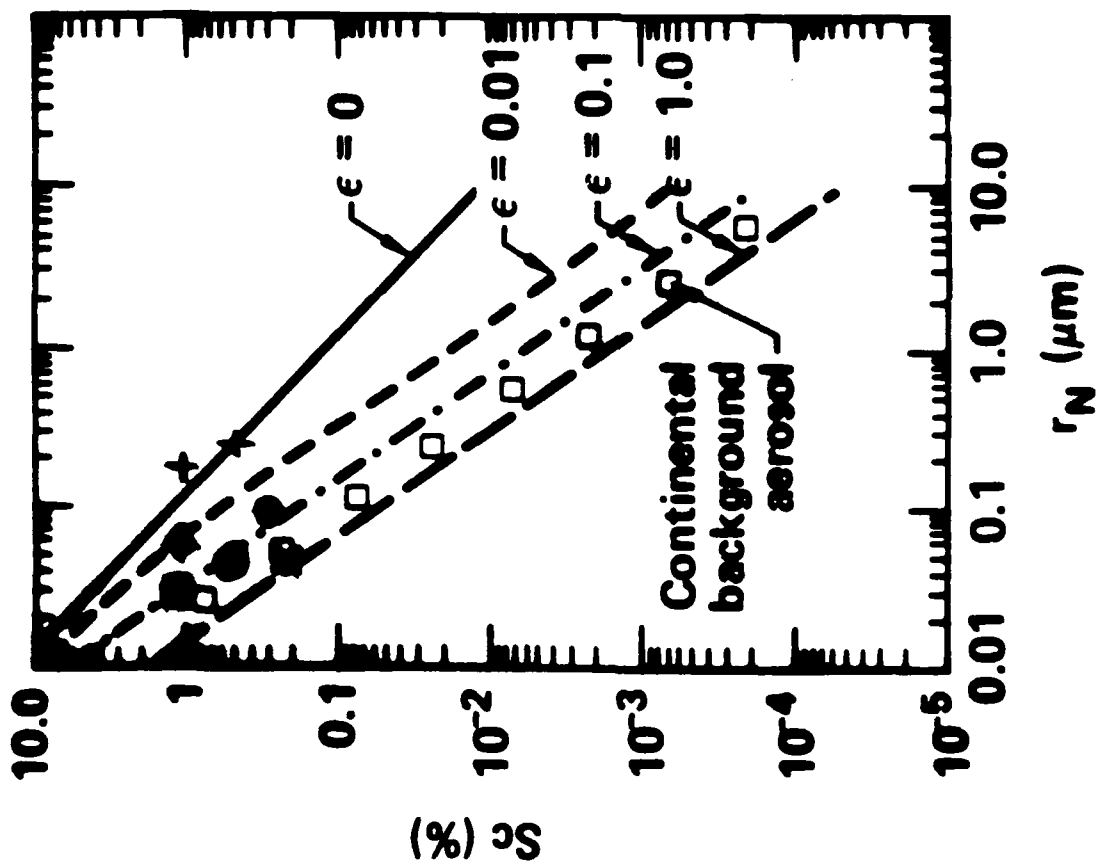
CCN SPECTRA OF AGED ACETYLENE SMOKE  
(16 hours)



EAA SIZE SPECTRA OF AGED ACETYLENE SMOKE  
(16 hours)



# Critical supersaturation:



- + Inferred from Metcrom (Radke)
- ⊙ Eagon et al. 1974  
Radke et al. 1978
- ⊕ Hallett et al. 1975  
1-hour acetylene
- ⊕ Hallett et al. 1975  
16-hour acetylene
- ⊕ Hallett et al. 1976  
diesel/gasoline
- x Radke et al. 1978  
forest slash

Conclusion.

Very small particles can act as CCN.

if  $S_c \sim 1\%$ :

$r \sim 0.03 \mu\text{m}$  for acetylene smoke

$r \sim 0.08 \mu\text{m}$  for gasoline/diesel

$r \sim 0.2 \mu\text{m}$  for Metectron smoke

Question: What is  $S_c$  above fire?

## **Detailed Microphysics Model (warm rain)**

---

Drop number distribution:  $f_d(r)$

Aerosol Mass in drops:  $g_{AP,d}(r)$

Processes modeled:

Activation

Condensation/Evaporation

Collection of aerosol particles by drops

Coalescence of drops

Breakup of drops

Advection, diffusion, sedimentation

Aerosol number distribution:  $f_{AP}(r)$

(Dry) Aerosol mass in aerosols:  $g_{AP,a}(r)$

Processes Modeled:

Activation

Condensation/Evaporation

Collection of aerosol particles by drops

Coagulation of aerosol particles

Advection, diffusion

Applications in nuclear war studies.

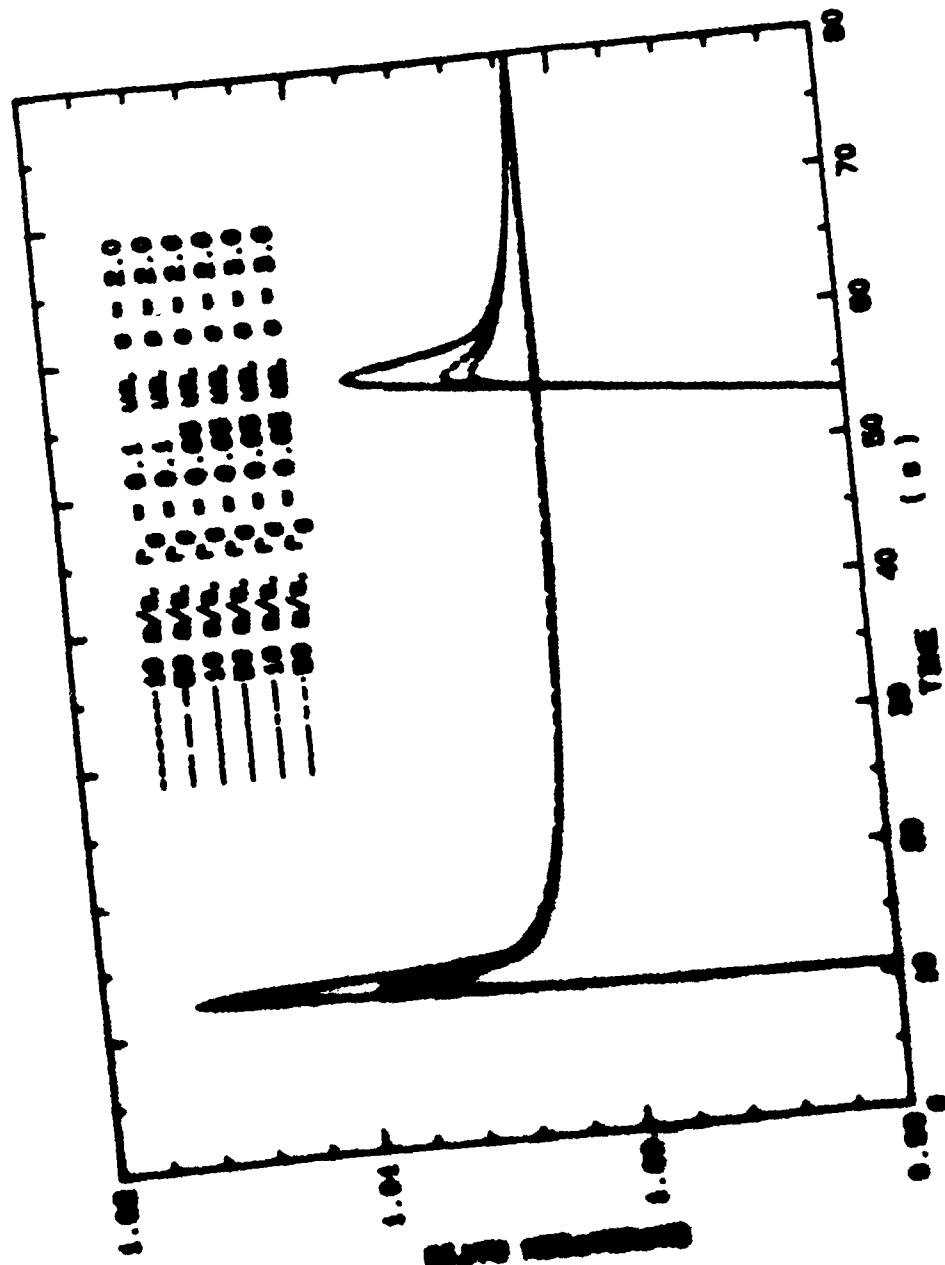
Changes in  $k_a$ ,  $k_p$  via coagulation, "cloud processing".

Rainout of particles:

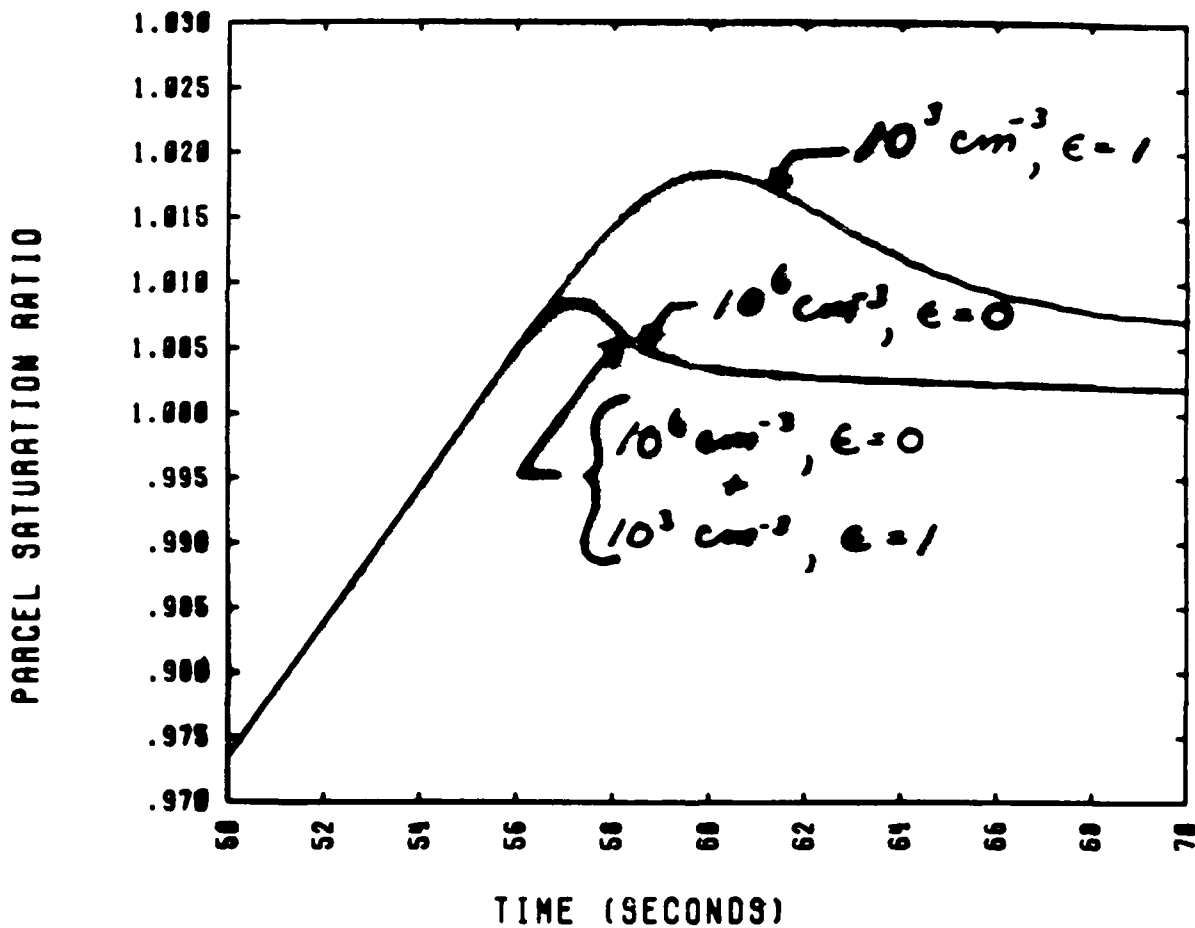
mechanism: nucleation scavenging



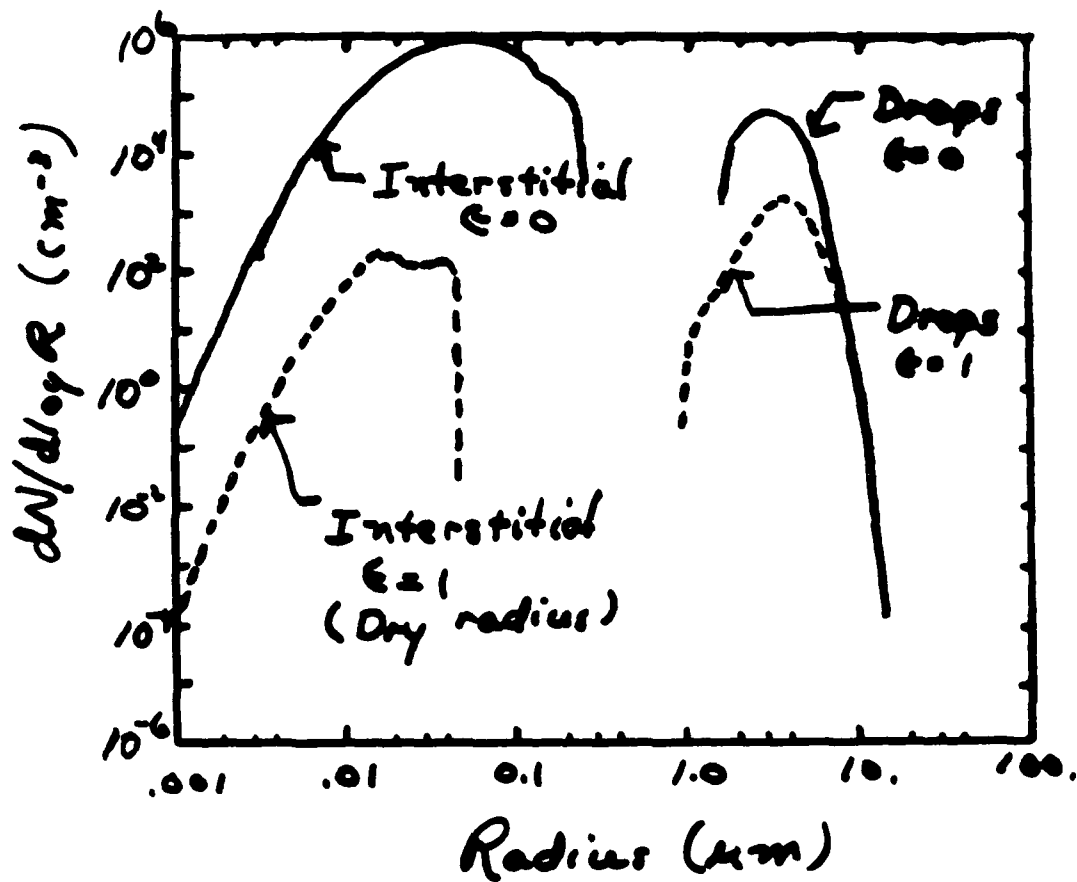
The highest saturation ratio is determined by the balance between the rate of condensation onto aerosol particles and the rate of decrease in saturation vapor pressure (which is determined primarily by the updraft velocity).



Effect of background soluble aerosol  
on nucleation scavenging of  
insoluble aerosol.



The scavenging of smoke aerosol ( $\epsilon=0$ ) is unaffected by the presence of soluble, background aerosol.



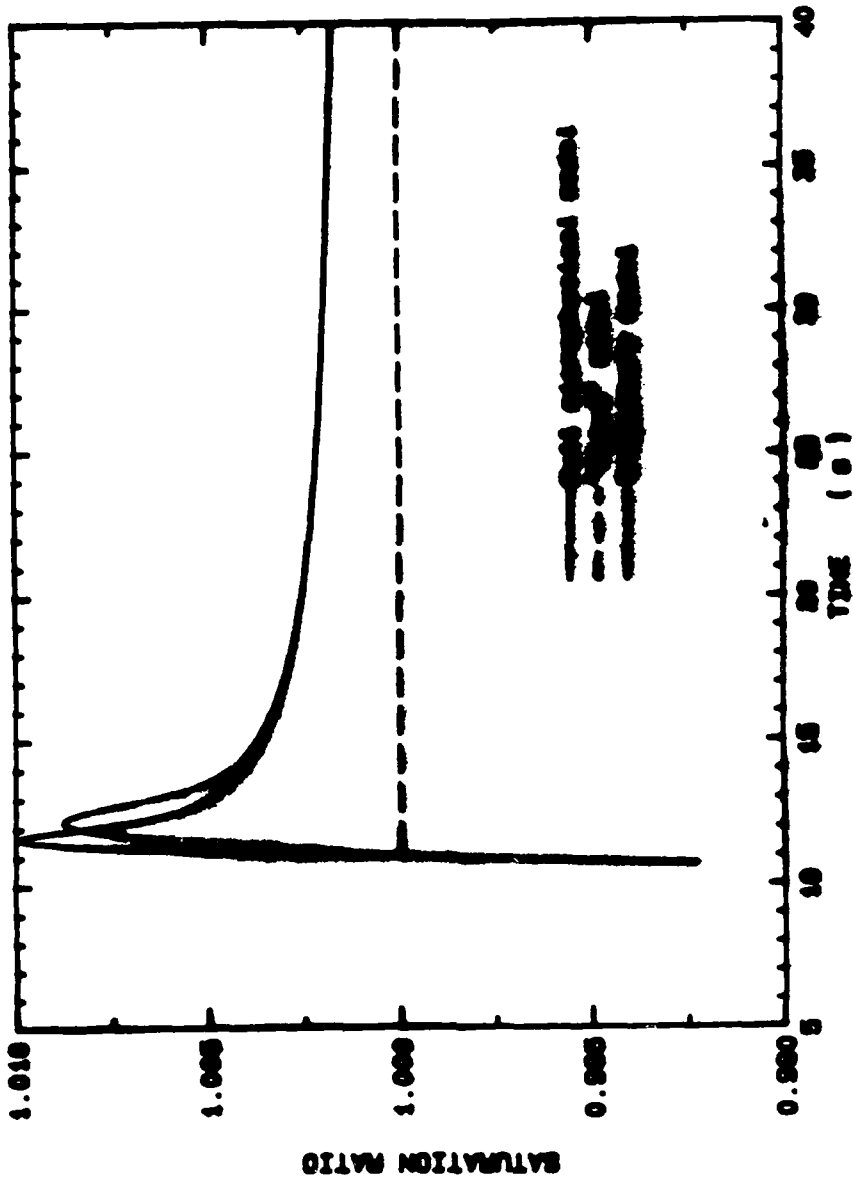
## Current Parameterizations in Cloud Models

If  $w_v < w_{v,sat}(T)$  then  $w_v$  is predicted from the advection equation.

If  $w_v > w_{v,sat}(T)$  then  $S_g \equiv 1$  and  $w_v = w_{v,sat}(T)$ . The remaining water vapor is instantaneously assumed to form drops.

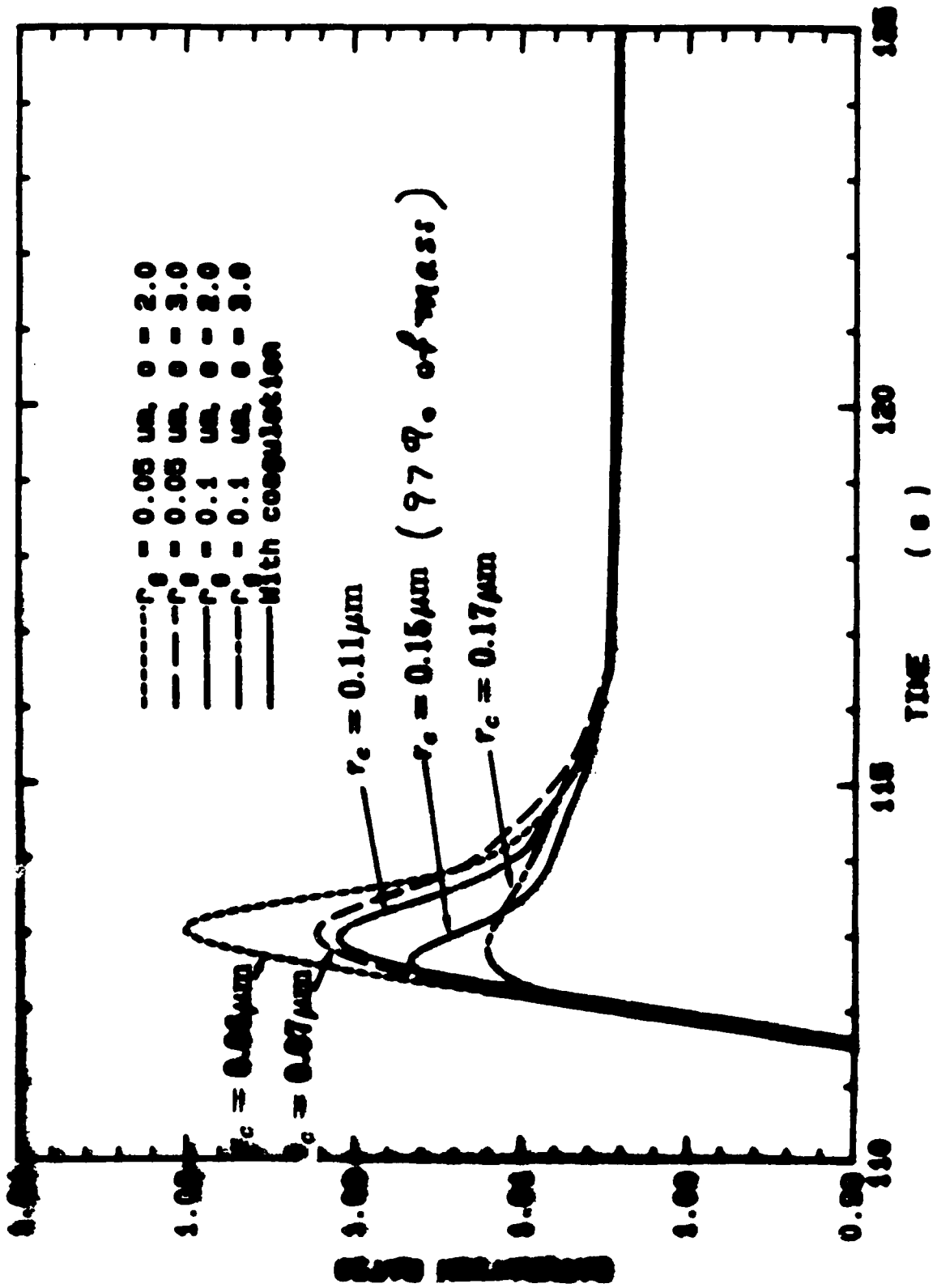
To study "condensation nucleation" in a cloud model, we have used the cloud model to predict  $\overline{N}(t)$  and  $(w_v + w_L)(t)$ . The detailed microphysical model is used to predict  $S_g$  and  $w_L(t)$  and to account for the size and number of aerosol particles nucleated.

**Test Case:  $10^6$  particles/cm<sup>3</sup>**

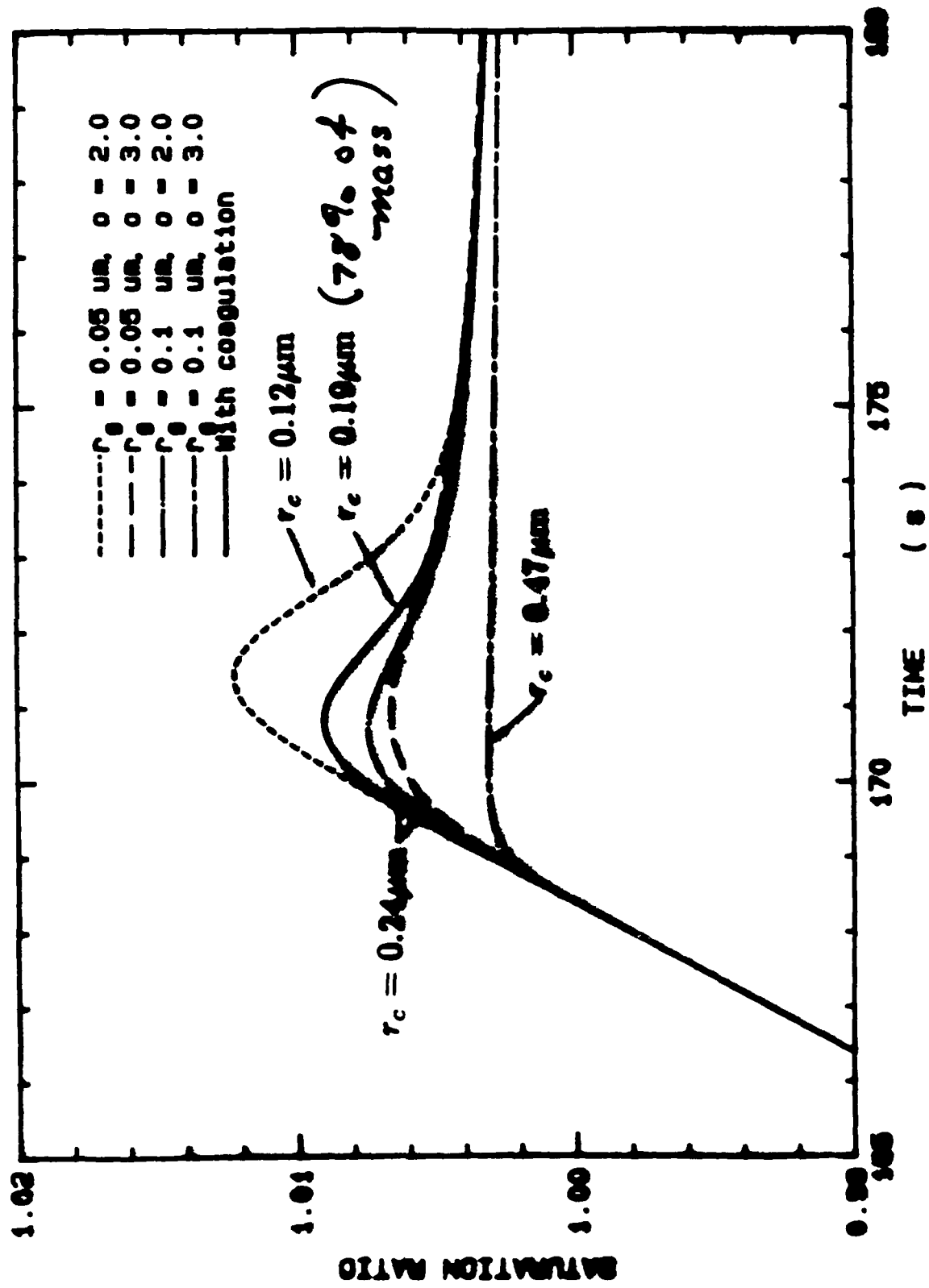


**For saturation values below about 2%, the expected underestimate of  $S_a$  is small.**

# Minimum Extinction Rate in Refractory Model for High Intensity Fire

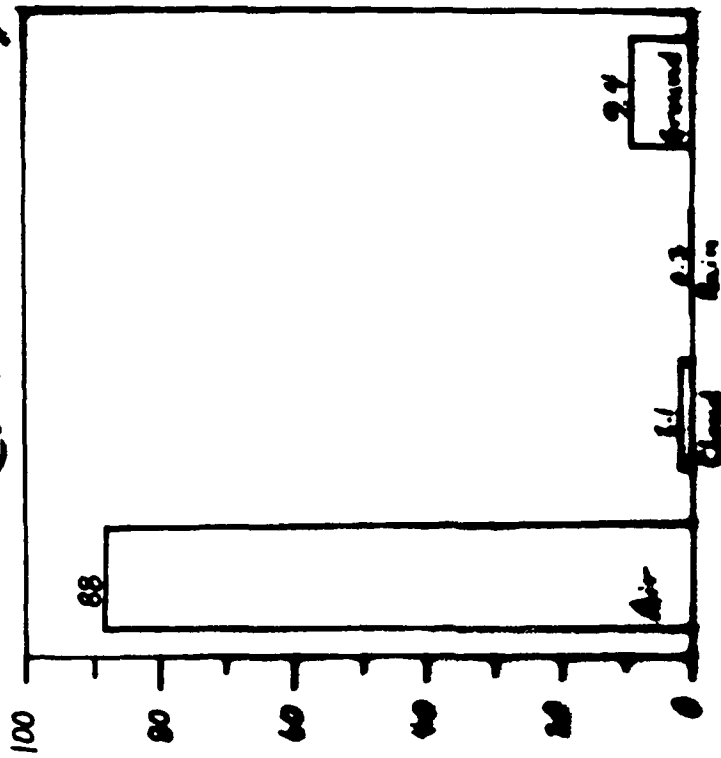


**Maximum Saturation Ratio in Trajectory Model for Medium Intensity Fire.**

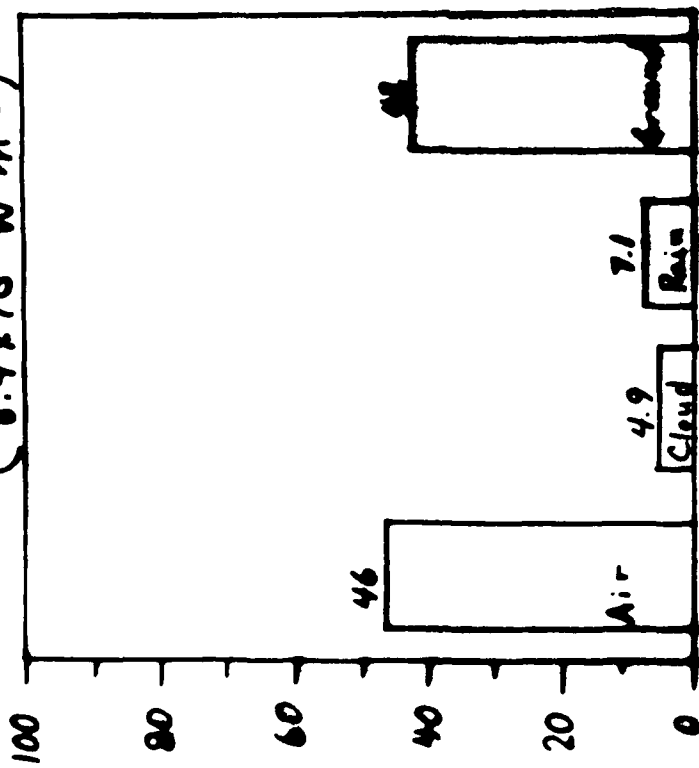


# Precipitation Scavenging - Initial Results (Bredt)

Medium intensity fire  
( $1.4 \times 10^4 \text{ W m}^{-2}$ )



High intensity fire  
( $8.9 \times 10^4 \text{ W m}^{-2}$ )





## **Conclusions**

- For idealised spherical particles with  $\epsilon_v = 0$  all particles with radii  $> 0.15\mu\text{m}$  will be incorporated into cloud drops by nucleation scavenging above high intensity fires.
- All particles with radii  $> 0.19\mu\text{m}$  would be captured by this mechanism above medium intensity fires.
- More work is needed to characterise the scavenging of realistic representations of smoke particles.

"Scavenging of Aerosol Particles by Ice Crystals"

Norman L. Miller and Pao K. Wang  
Department of Meteorology  
University of Wisconsin  
Madison, WI 53706

Abstract

Substantial amount of ice crystals exist in the upper part of the troposphere all the time in the form of cumulonimbus anvils or detached cirrus sheets. They may interact with atmospheric aerosol particles and become contaminated. These ice crystals may be involved later in precipitation processes and therefore play the role of removing particles from the atmosphere. In order to quantitatively assess this removal process we have developed a theoretical model for the determination of the collection efficiency of aerosol particles by ice crystals. The effects of Brownian diffusion, phoretic and electric effects, and the inertial impaction will be discussed.

"Characterization of Combustion Aerosol for Haze and Cloud Formation"

J. Hallett, J.G. Hudson, and F. Rogers  
Desert Research Institute  
University of Nevada System  
Reno, Nevada 89506

I. LABORATORY COMBUSTION PROCEDURES

A. Objectives

1. To capture a representative sample of the combustion aerosol without biases, losses of portions of the particle size spectra, or exposure to substances or conditions which would alter the nucleation properties of the particles;
2. Wherever possible, to specify the scaling factors which would relate the laboratory-scale combustion setup to a combustion situation of relevance to climate change, and to attempt to state and quantify any necessary compromises.

B. Generic Setup

Figure 1 shows the general arrangement applied to all combustion aerosols.

C. Premixed Acetylene Fuel

Figure 2 illustrates the apparatus used for the study of premixed acetylene flame aerosols. The included table summarizes the range of oxygen/fuel ratios used.

D. Tentative Version, JP-4 Aviation Fuel Burner

Figure 3 shows a simple burner used to produce JP-4 diffusion flames. The fuel temperature is first raised to about 95°C, and milliliter quantities are ignited; the fuel consumption rate is about 1 ml in 100 seconds.

### E. Wood (Construction Lumber) Fuel

Perforated cubes are manufactured from standard 2-inch by 2-inch dry white pine construction grade lumber. These typically weigh about 30 grams; approximately 10 grams are consumed in 100 s of combustion. The aerosol is collected by an extraction tube similar to that in Figure 3.

## II. MEASUREMENTS

### A. Results for Acetylene Soot Aerosols

#### 1. Low Oxygen Settings

Figure 4 shows the typical chain aggregates resulting from low-oxygen acetylene combustion. Fig. 5 illustrates the condensation nuclei (CN), and cloud condensation nuclei (CCN) data as a function of aerosol aging time, for the low oxygen/fuel ratio case. The CN count decreases with time, due to coagulation and diffusion losses. The CCN counts are much more constant in time, even showing slight increases. The maximum CCN/CN ratio is about 0.5 for CCN active at 0.7% supersaturation.

#### 2. High Oxygen Settings

Fig. 6 shows the typical "clumped", as opposed to chained, aggregates resulting from the higher oxygen/fuel ratios (approx. 1.6). Fig. 7 shows the CN and CCN data, with the result that the CN concentrations and the concentrations of CCN (active at 0.7% supersaturation) are nearly equal after about 4 hours aging; the CCN/CN ratio approaches 1.0. Figure 8 is similar to Figure 7, and represents another high-oxygen acetylene fuel case. Figure 9 is a CCN activity spectrum (differential distribution) taken midway through the sequence displayed in Figure 8.

### B. Results for JP-4 Aviation Fuel

1. Figure 10 is similar to Figures 5, 7, and 8 showing the CN and CCN data for this fuel, as a function of aging time. The CCN/CN ratios are very low with respect to other fuels thus far studied, and reach a maximum of only about 0.01.
2. Figure 11 shows a CCN activity spectrum (differential distribution) from the start of the sequence shown in Figure 10.

### C. Results for Wood (White Pine Construction Lumber) Fuel

1. Figure 12 is similar to Figures 5, 7, 8, and 10 showing the CN and CCN data for this fuel, as a function of aging time. CCN/CN ratios are high, approaching unity near the end of the sequence.
2. Figure 13 shows a CCN activity spectrum (differential distribution) taken at the start of the sequence shown in Figure 12.

## III. CCN Spectrometer Calibrations

The DRI 8-stage instantaneous spectrometer was compared to an older, single-stage continuous-flow diffusion chamber (CFD) in order to evaluate the spectrometer calibration procedure which is based on water-soluble calibration aerosols. The CFD device provides CCN spectra which are independent of any assumptions of water solubility, but which require a lengthy, labor-intensive process. Figures 14, 15, 16 and 17 show CCN activity spectra (in cumulative distributions) taken by these two devices, for acetylene, JP-4, and wood fuels. The degree of agreement is considered good enough to tentatively validate the instantaneous spectrometer calibration procedure; the discrepancies which are sometimes shown, usually indicating higher counts by the spectrometer, are thought to be within the uncertainty of the measurement.

#### IV. Conclusions

Combustion aerosols (soot) from three fuels have been studied, with respect to nucleation behavior. Morphology studies have also begun. Cloud condensation nuclei (CCN) constitute a larger percentage of the total particle population (as estimated by the condensation nuclei (CN) count) for wood and high-oxygen acetylene, than is the case for low-oxygen acetylene and JP-4 aviation fuel soots.

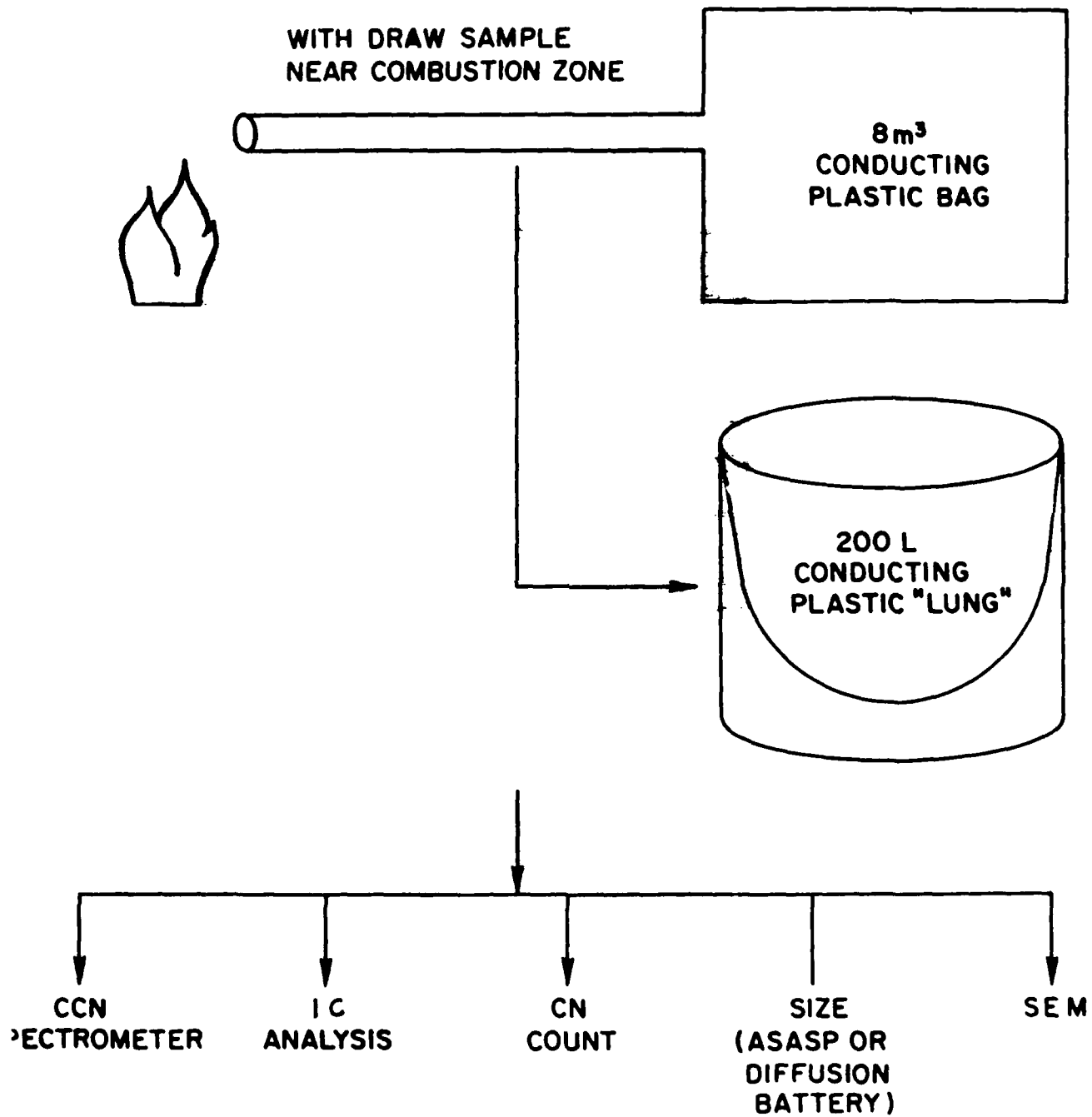


FIG. 1 Generic combustion aerosol generation and sampling arrangement.

# PREMIXED ACETYLENE FLAME

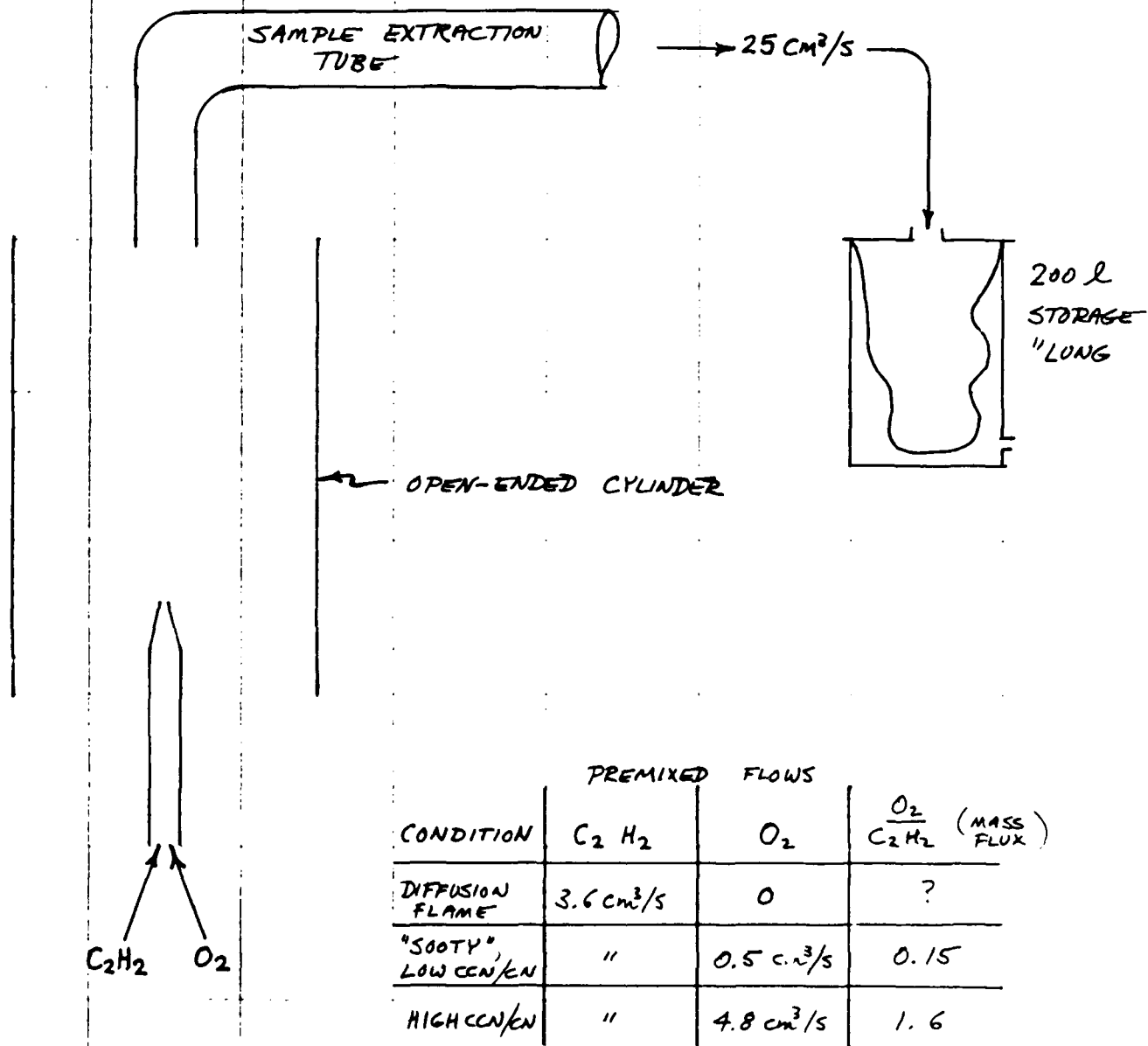
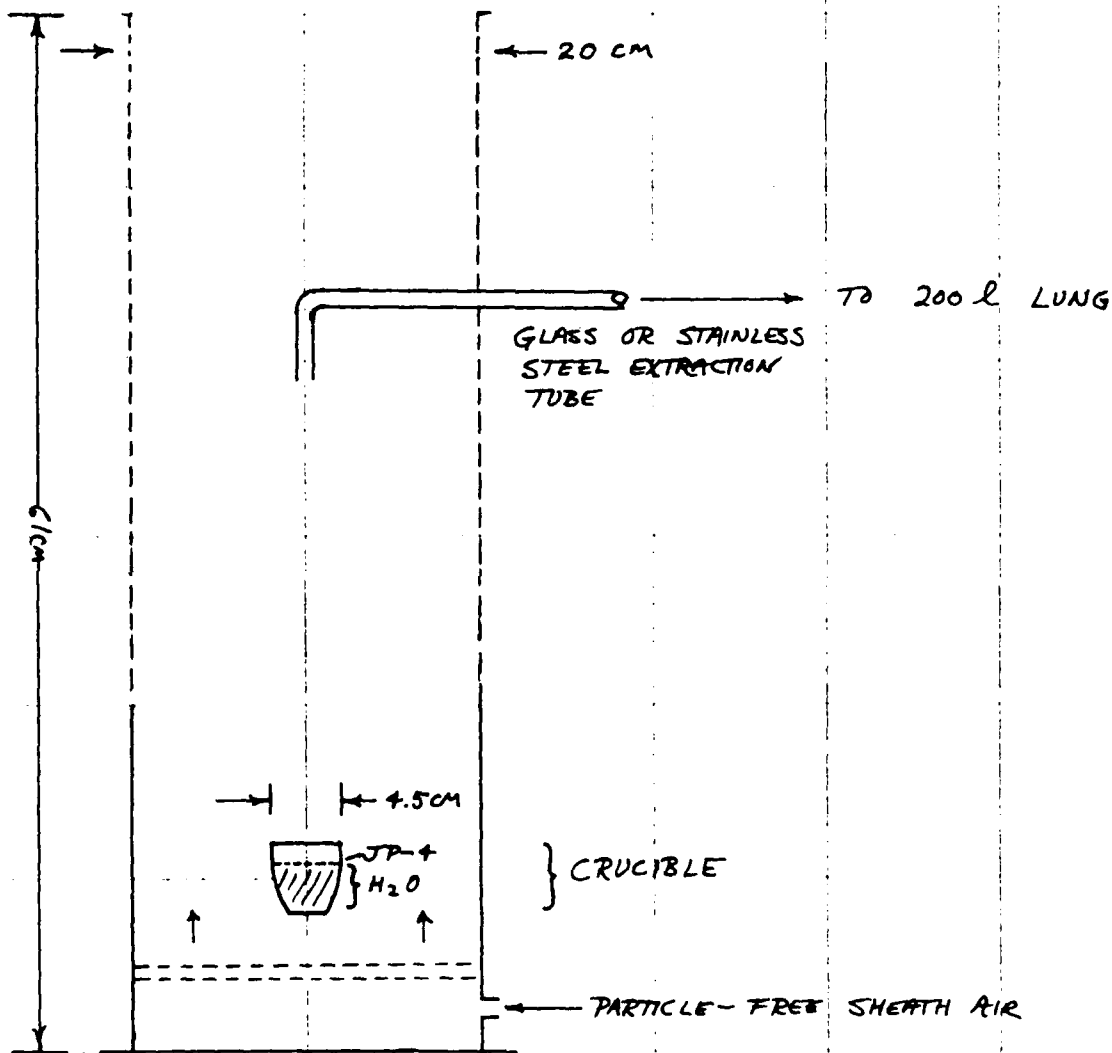


FIG. 2 Arrangement for premixed acetylene flame.

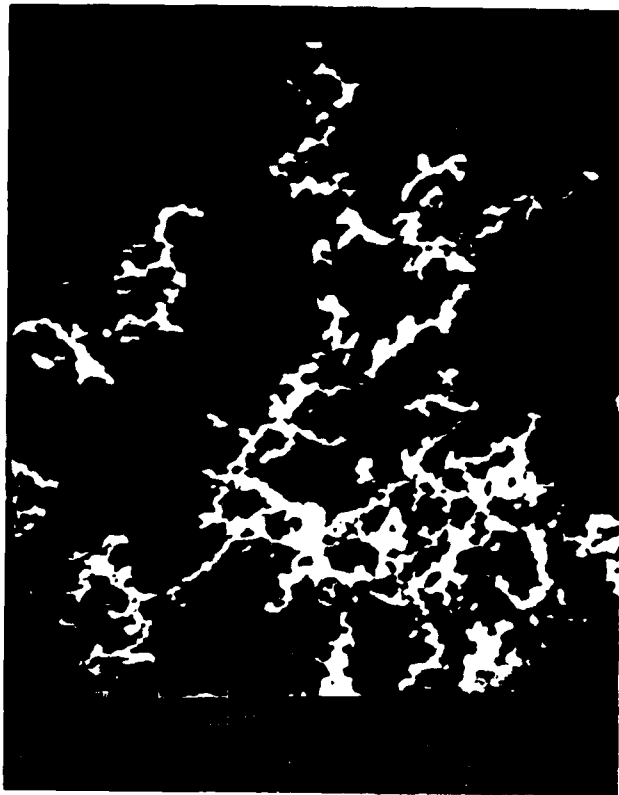


# JP-4 BURNER, FIRST VERSION (3/87)



- TENTATIVE PROCEDURE :
- (1) 1 ML JP-4 FLOATS ON WATER IN CRUCIBLE
  - (2) WATER PREHEATED TO  $\sim 95^{\circ}\text{C}$
  - (3) JP-4 BURNS  $\approx 1\text{ ML} / 100\text{ S}$
  - (4) SAMPLE 10-30 S, DILUTE 1:400

FIG. 3 Tentative arrangement for burning JP-4 aviation fuel.

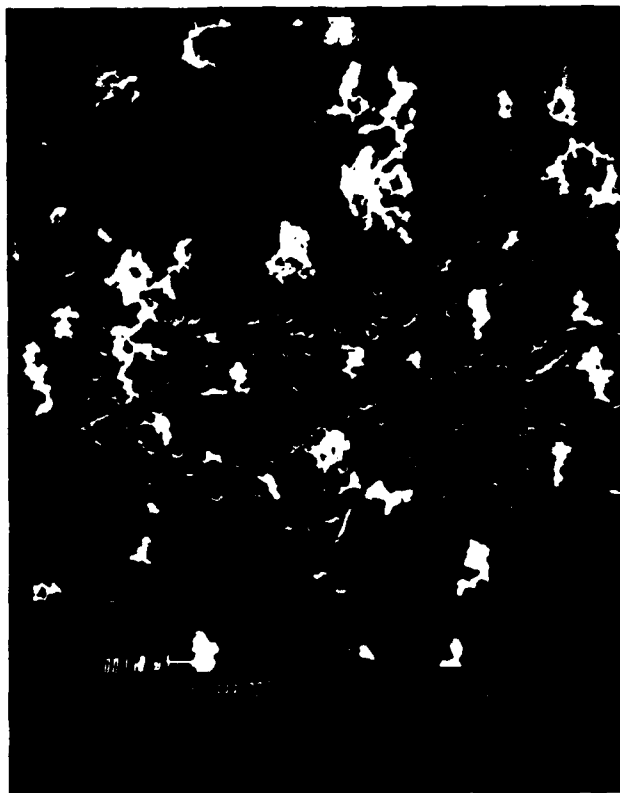


FILTERS # 53, 54  
LOW O<sub>2</sub> FLOW,  
ACETYLENE

(SAMPLES FOR SANDIA  
ASASP / FSSP)

86/09/04-05

~ 10,000 X



~ 5000 X

FIG. 4 Scanning electron microscope photos, acetylene soot produced with low oxygen settings.

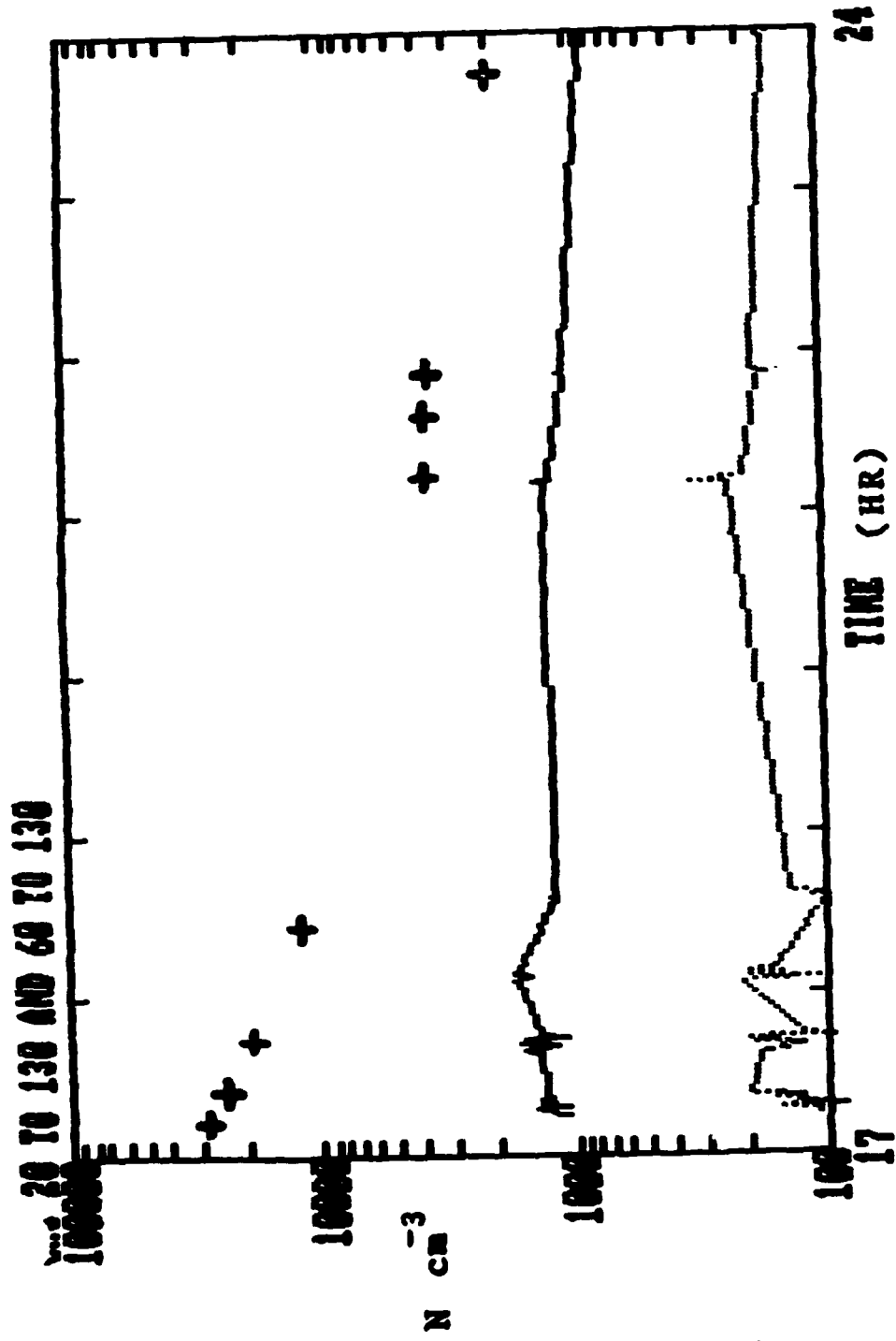


FIG. 5 Condensation nuclei (CN) and cloud condensation nuclei (CCN) data, low-oxygen acetylene soot.

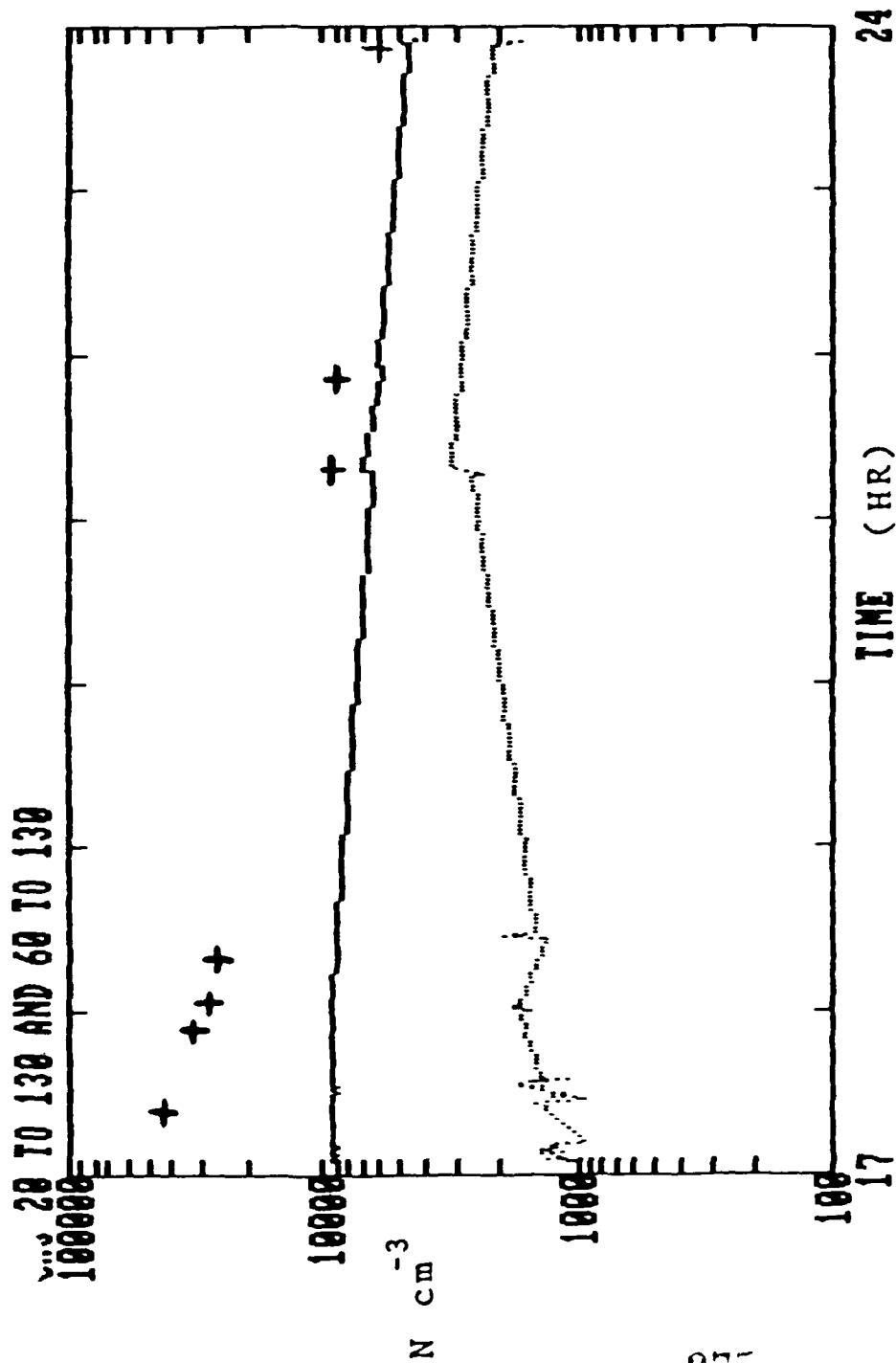


FILTER # 59 5000X



FILTER # 58 5000X

FIG. 6 Scanning electron microscope photos, acetylene soot produced with high oxygen settings.



MORE OXYGEN

- + CN
- CCN at 0.7% Sc
- ... CCN at 0.4% Sc

FIG. 7 Condensation nuclei (CN) and cloud condensation nuclei (CCN) data high-oxygen acetylene soot.

CHS 20 TO 130 AND 50 TO 130

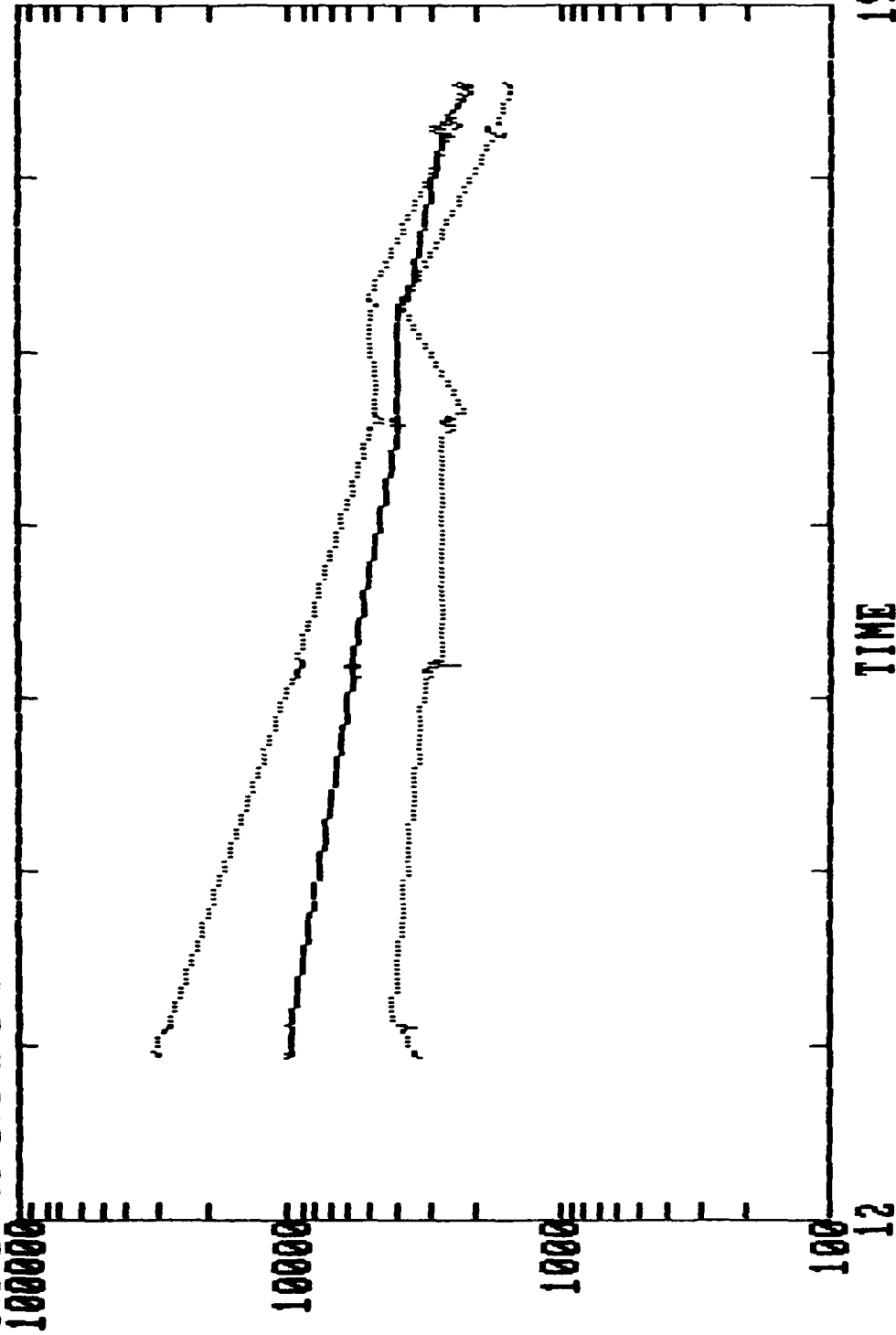


FIG. 8 Condensation nuclei concentration (top data trace) and cloud condensation nuclei concentrations active at 1% supersaturation (middle trace) and 0.6% supersaturation (bottom trace). Fuel is high-oxygen acetylene, similar to Figure 7.

619 632:12.0 836 06.79 28.5 298-0.11 1.68 3.70 4.78 5.00 7.97 8.07 8.23 57  
 56 15 66 0 24 110 55 116 80 26 4 2 0 1  
 10000  
 REND

TIME = 03 31 16 32 12.0

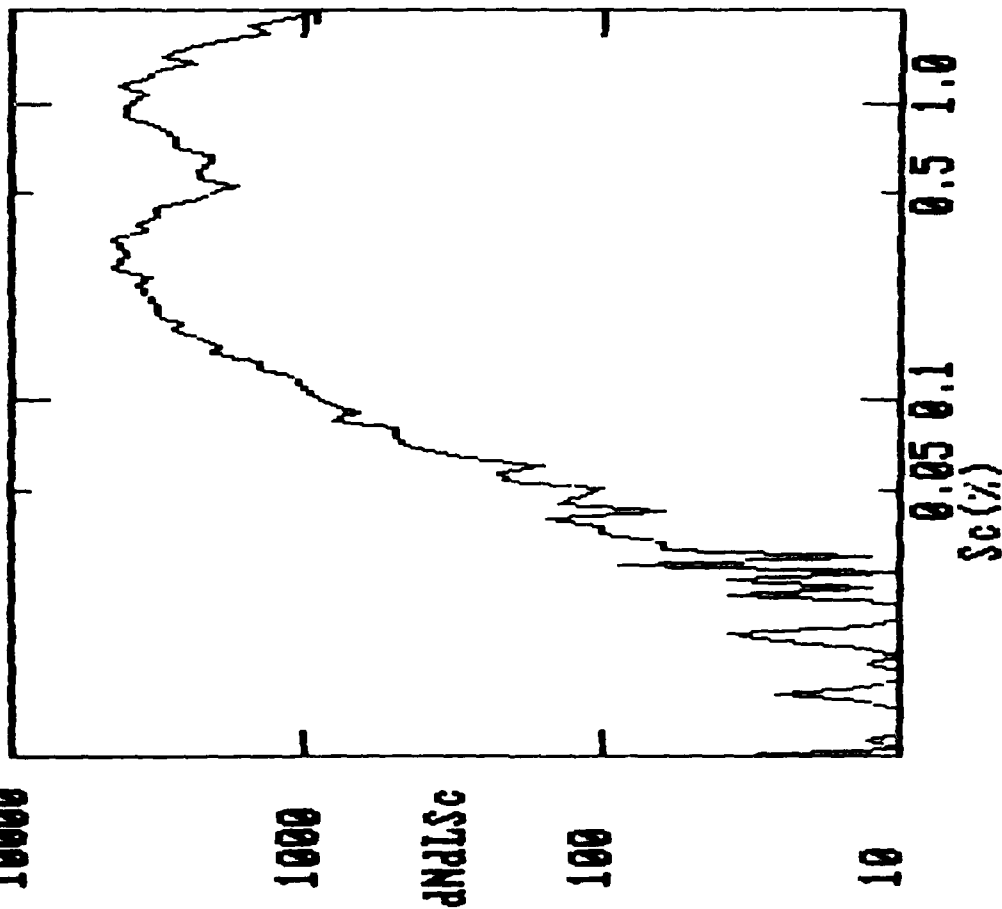


FIG. 9 Cloud condensation nuclei concentrations as a function of applied supersaturation, high-oxygen acetylene fuel. Data taken midway through sequence shown in Figure 8.

CHS 20 TO 130 AND 50 TO 130

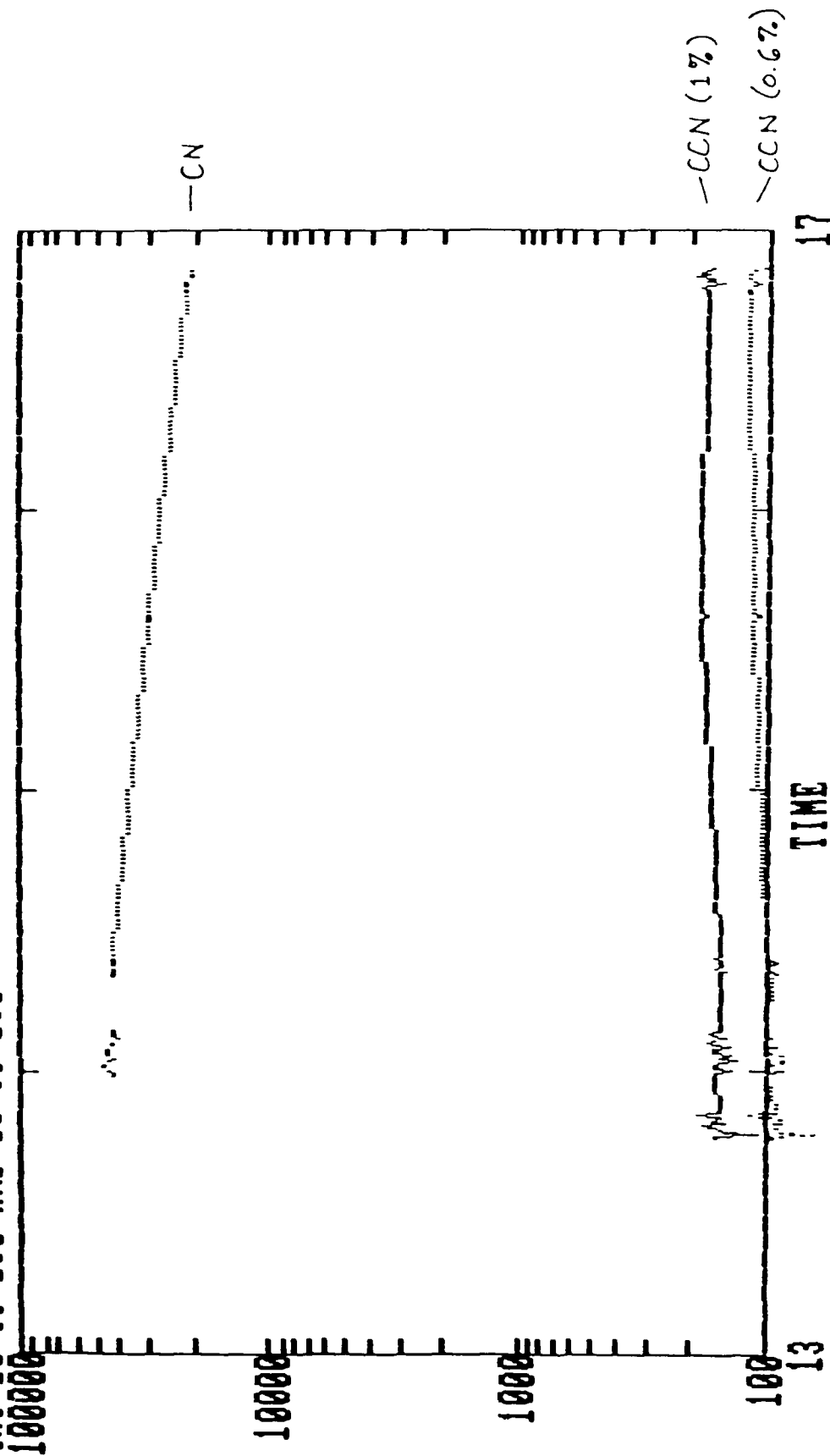


FIG. 10 Condensation nuclei concentration (top data trace), and cloud condensation nuclei concentrations, active at 1% supersaturation (middle trace) and 0.6% supersaturation (bottom trace). Soot from JP-4 aviation fuel.



230 348:46.0 837 13.84 28.5 307-0.08 1.84 3.74 4.97 4.96 8.15 8.22 7.91 58  
 56 19 68 0 1 2 1 3 1 0 0 0 0 0  
 1000 RENO

TIME = 04 01 13 48 46.0

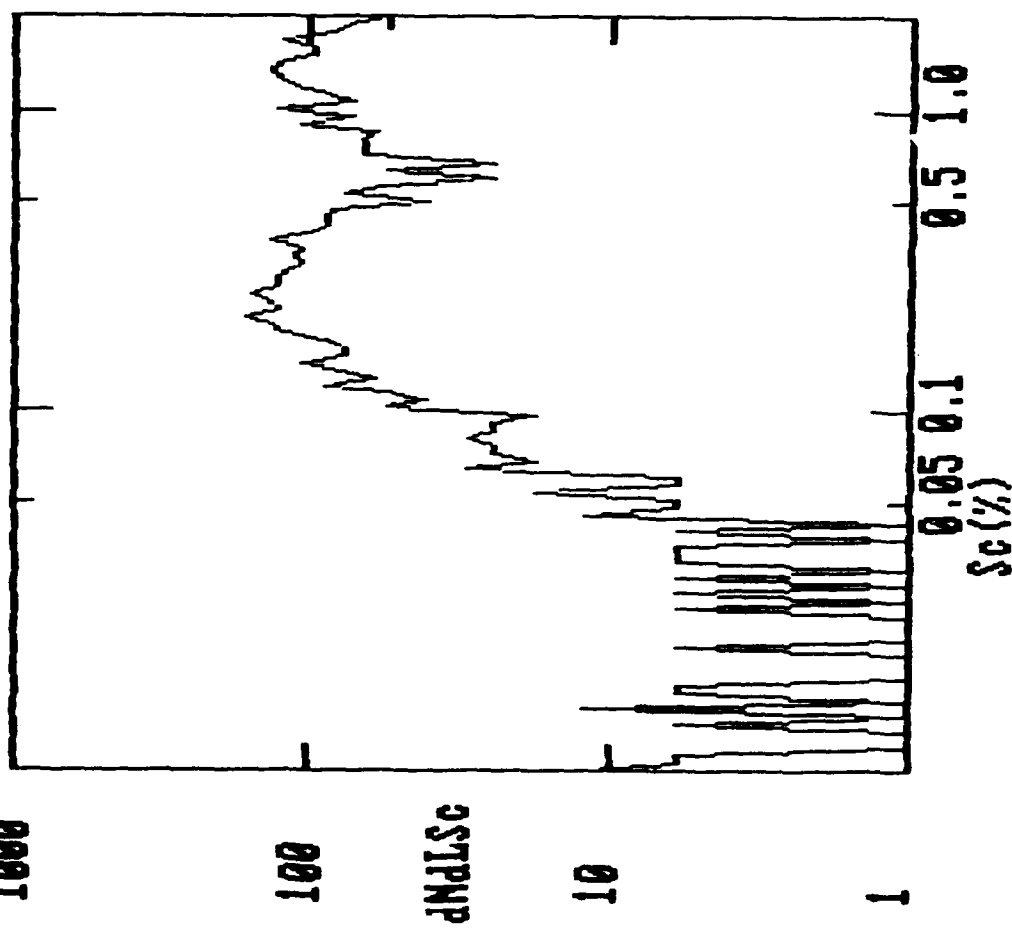


FIG. 11 Cloud condensation nuclei concentrations as a function of applied supersaturation, JP-4 aviation fuel soot. Data taken at the start of sequence shown in Figure 10.

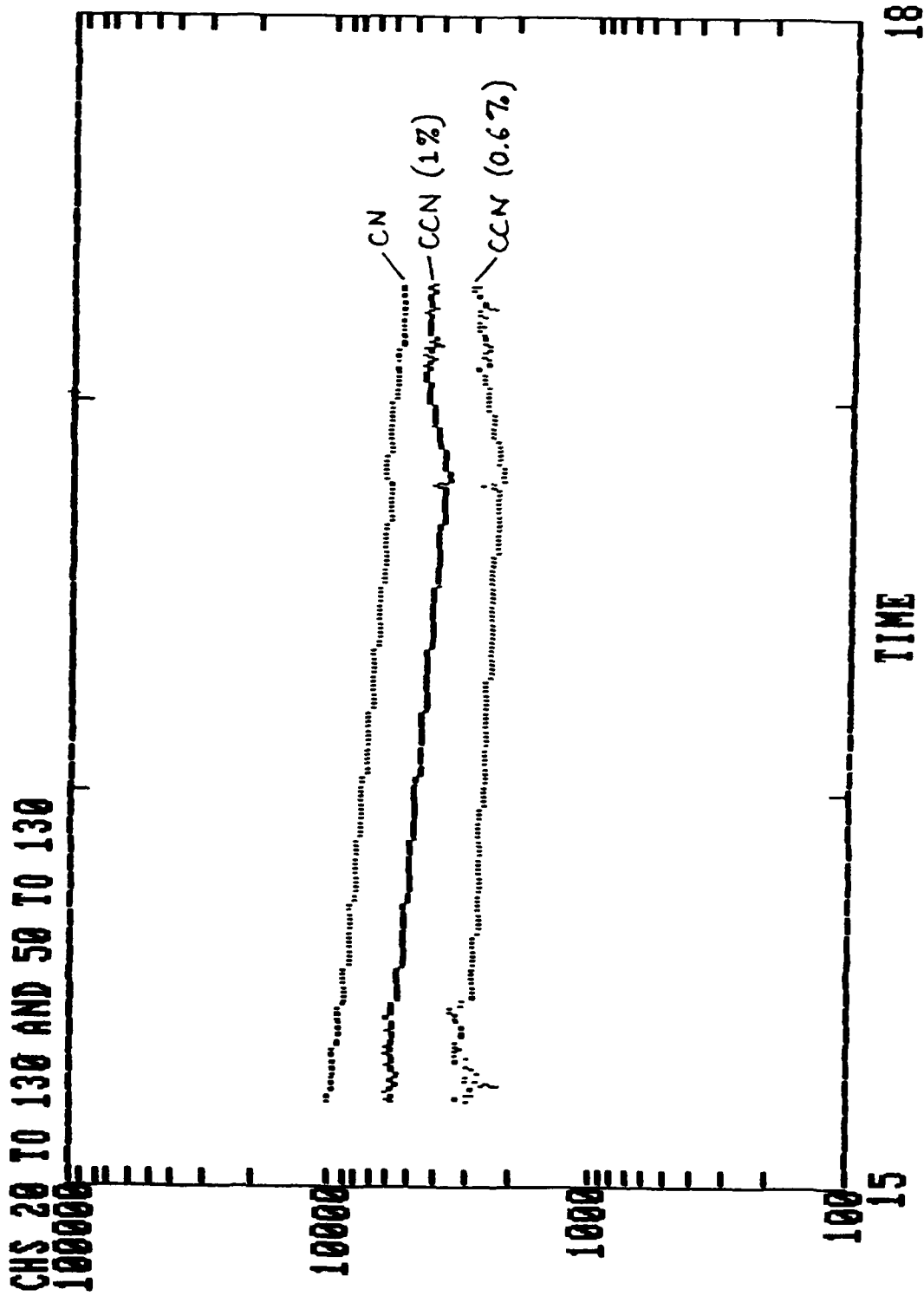


FIG. 12 Condensation nuclei concentrations (top data trace), and cloud condensation nuclei concentrations, (active at 1% supersaturation (middle trace) and 0.6% supersaturation (bottom trace). Soot from wood fuel.

93:512:48.5 827 09.89 28.5 303 0.11 1.83 3.65 4.77 4.96 7.81 8.25 8.08 49  
 46 14 62 13 194 84 64 222 24 1 1 1 0 0  
 10000 REND

TIME = 04 03 15 12 48.5

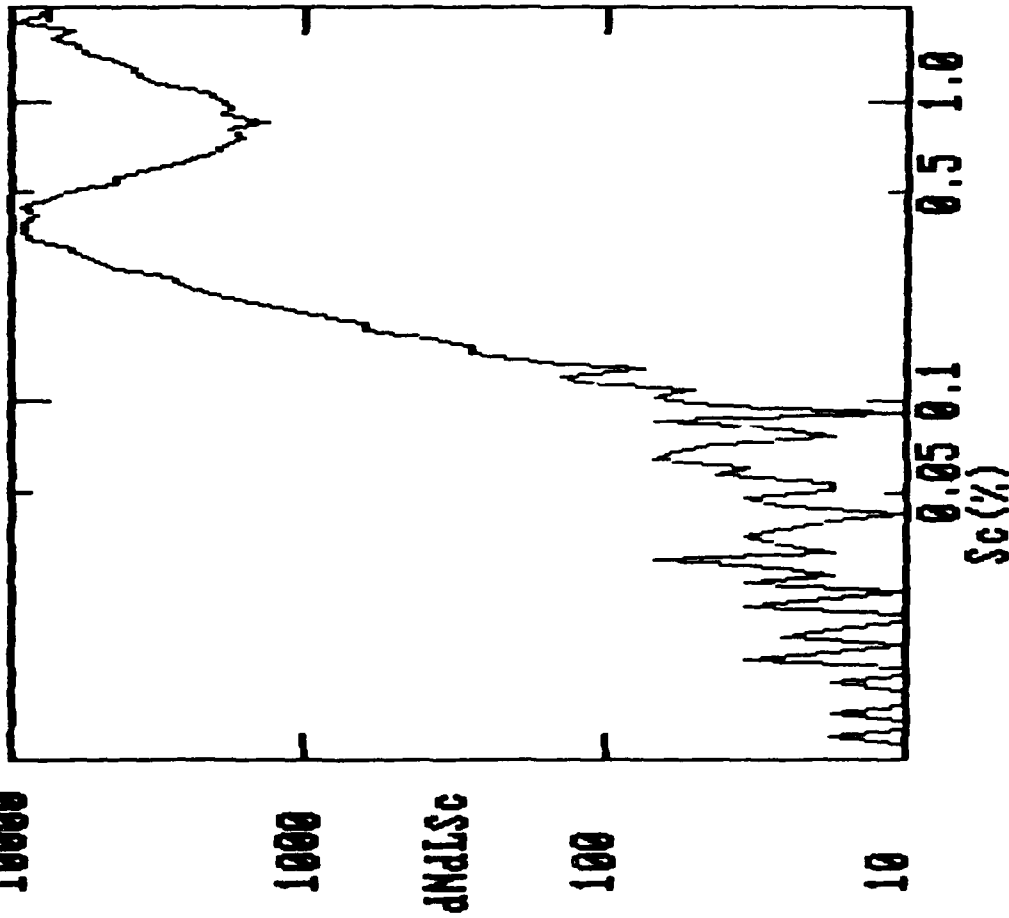


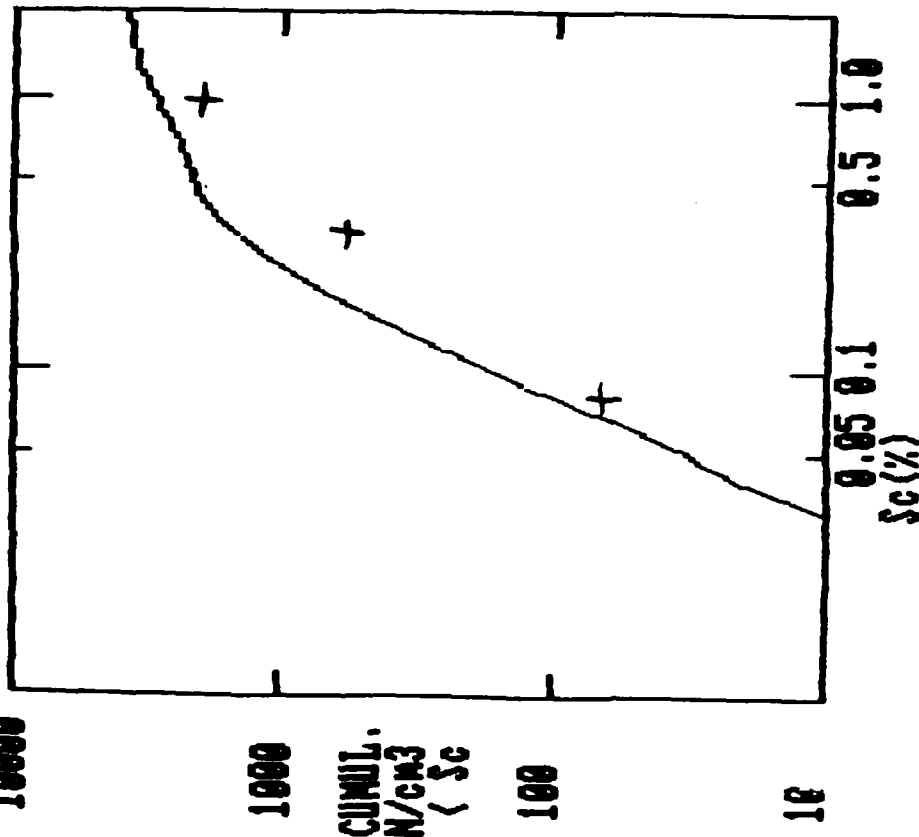
FIG. 13 Cloud condensation nuclei concentrations as a function of applied supersaturation, wood soot. Data taken at start of sequence shown in Figure 12.

619:632:12.0 836 06.79 28.5 298-0.11 1.68 3.70 4.78 5.00 7.97 8.07 8.23 57  
 56 15 66 3929 3831 3278 2413 1728 731 216 49 13 5 2  
 10000 BEND

TIME = 03 31 16 32 12.0

SLOPE 1% + .4%, K= .4258555

SLOPE .1% + .04%, K= 2.31217



ACETYLENE, + = CFD

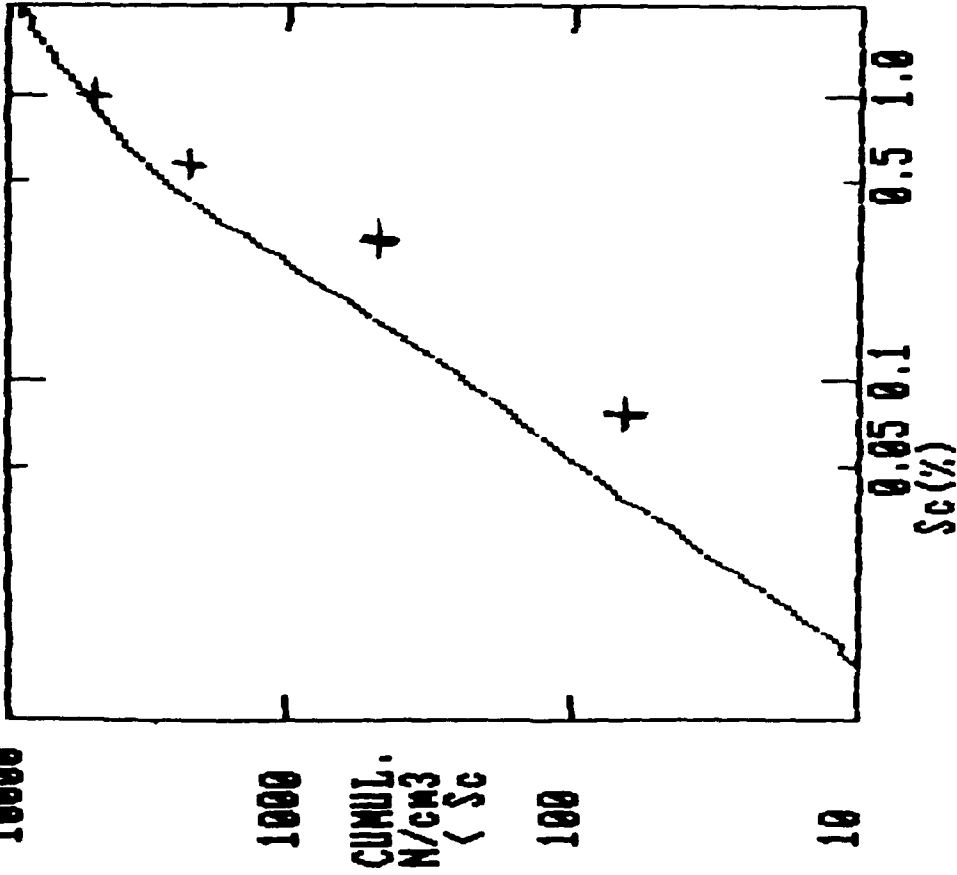
FIG. 14 Low-oxygen acetylene soot: cloud condensation nuclei concentrations as a function of applied supersaturation. Comparison of 8-stage spectrometer (continuous trace) and single stage diffusion chamber (+).

419\*257:09.5 838 12.16 28.5 306 0.06 1.86 3.68 4.79 5.05 8.06 8.15 8.11 43  
 46 15 72 8907 6051 3640 1699 657 274 125 52 22 11  
 10000 RENO

TIME = 03 31 12 57 09.5

SLOPE 1% + .4%, K= .8736307

SLOPE .1% + .04%, K= 1.359835



ACETYLENE, + = CFD

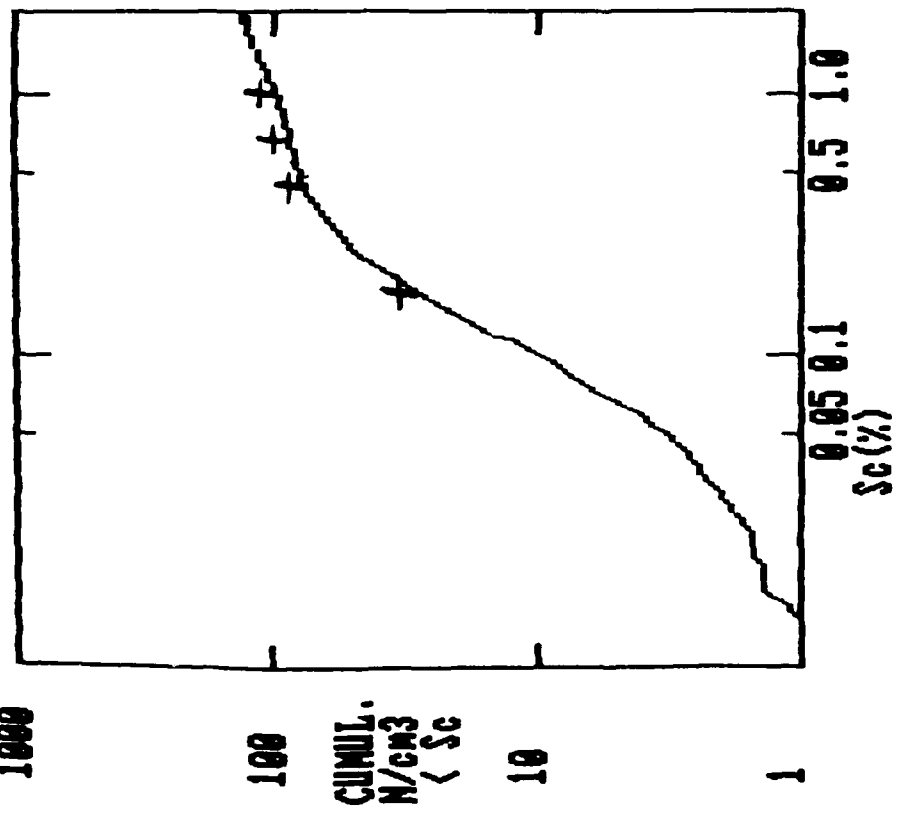
FIG. 15 High-oxygen acetylene soot: cloud condensation nuclei concentrations as a function of applied supersaturation. Comparison of 8-stage spectrometer (continuous trace) and single-stage diffusion chamber (+).

000 348:46.0 837 13.84 28.5 307-0.00 .84 3.74 4.97 4.96 8.15 8.22 7.91  
 19 68 145 134 107 88 00 35 12 4 2 2 1  
 1000 REMO

TIME = 04 01 13 48 46.0

SLOPE 1% + .4%, K= .290958

SLOPE .1% + .04%, K= 1.490738



JP-4, + = CFD

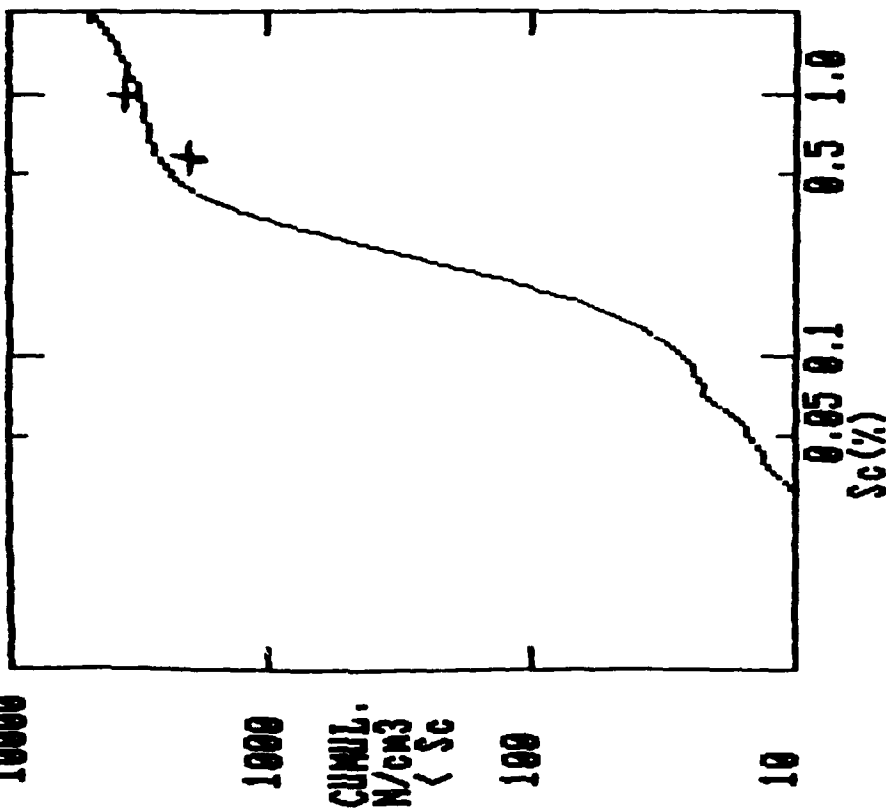
FIG. 16 JP-4 aviation fuel soot: cloud condensation nuclei concentrations as a function of applied supersaturation. Comparison of 8-stage spectrometer (continuous trace) and single-stage diffusion chamber (+).

03 512:48.5 827 09.89 28.5 303 0.11 1.83 3.65 4.77 4.96 7.81 8.25 8.08 AD  
 14 62 5787 4941 3359 2847 11.7 125 29 18 11 5 1  
 10000 BEND

TIME = 04 03 15 12 48.5

SLOPE 1% + .4%, K= .4579835

SLOPE .1% + .04%, K= .8247221



WOOD, + = CFD

FIG. 17 Wood fuel soot: cloud condensation nuclei concentrations as a function of applied supersaturation. Comparison of 8-stage spectrometer (continuous trace) and single-stage diffusion chamber (+).

## UMR COMBUSTION AEROSOL FACILITY

D.E. Hagen, M.T. Trueblood, and D.R. White

University of Missouri-Rolla

Rolla, MO 65401

Introduction. There has been considerable recent interest in the hydration properties of combustion aerosols, eg. at the 1985 Amer. Assoc. Aerosol Research conference in Albuquerque, the 1986 Global Effects Program Technical meeting at NASA Ames, and the 1986 Amer. Meteor. Soc. Cloud Physics conference in Snowmass. Both the warm cloud condensation behavior and ice nucleating ability of combustion aerosols have important atmospheric implications. Our interest focuses on the microphysical and microchemical interaction of water with these aerosols.

UMR Cloud Simulation Facility. The heart of the facility consists of two cooled wall expansion cloud chambers. They are supported by a number of peripheral subsystems, eg. air preparation, aerosol generation, cloud observation systems. The chambers are designed to subject a sample of moist aerosol laden air to a predetermined profile of temperature and pressure, approximating those occurring naturally during various processes which take place in the atmosphere. Hence the facility provides an opportunity to observe and study various atmospheric processes under prolonged, controlled, measurable and repeatable conditions. Possible experiments include condensational droplet growth, ice nucleation, ice growth, scavenging, coalescence, optical properties of cloud particles, etc.



Combustion Aerosol Facility. A combustion aerosol facility has recently been added to the list of subsystems for the cloud simulation chambers. The goal is to generate a variety of combustion aerosols, using a variety of fuels, under controlled, reproducible, and observed conditions. These aerosols can then be characterized and shaped (modify their size distribution) in the existing aerosol laboratory. Then their hydration behavior can be examined in the static environment provided by the continuous flow thermal diffusion cloud chambers and haze chambers or in the dynamic environment provided by the expansion cloud chambers.

Our present burners are designed to burn a wide variety of liquid fuels. Our simplest burner is an unmodified camping lantern. It has the disadvantage of having the fuel tank attached to the burner; this posing a possible fire hazard. Our primary burner consists of the head of an old liquid fuel blow torch. It is now fitted with an air flow control sheath, an external fuel tank, and a temperature controlled fuel delivery system. A new burner is being built to improve the aerosol stability.

The combustion chamber consists of a cylindrical (44 cm diameter, 61 cm height) metal bell jar, which was once a part of a vacuum system. It features an observation window to view the flame, provisions to externally control the torch's needle fuel valve, and provisions for electrical and gas feed-throughs. The combustion exhaust gasses are mostly vented outdoors with some small fraction being passed into the aerosol laboratory apparatus.

Aerosol Laboratory. The aerosol laboratory consists of apparatus designed to generate, characterize, and shape aerosols. We have a number of condensation and ice nuclei aerosol generators, but these are not of interest here. More relevant are an electrical (mobility) aerosol classifier system consisting of 5 units of in-house design and one commercial unit (TSI). These can be computer controlled and can be used to produce a monodispersed (in size) aerosol, or a modified polydispersed aerosol. Several optical particle counters are available to size drops and measure concentrations. Continuous flow thermal diffusion cloud chambers, haze chambers, and alternating gradient thermal diffusion cloud chambers are available to activate aerosols and measure their critical supersaturation spectra. A new cold continuous flow thermal diffusion chamber is available for ice nucleation studies. It is supported by a numerical model that accounts for the probabilistic nature of the ice nucleation processes underway within the chamber.

Expansion Chamber. The expansion chamber is the primary facility for examination of the aerosol's dynamic hydration behavior. The chamber's cooled wall feature removes wall effects to allow hydration effects to be studied in their natural time frame. Details of the chamber are given in the literature and so will not be repeated here.

Since combustion aerosol results from the expansion chamber are not yet available, we will now briefly describe some results for NaCl aerosols. Analogous results for combustion aerosols will soon be available. These are warm cloud droplet growth

the fuel generator region is greatly reduced. Furthermore we can make adjustments to the character of the combustion air flow to the flame.

A simple analysis was performed on the critical supersaturation data to extract the amount of soluble material, assumed to be sulfuric acid, associated with the carbon aerosol. In a manner similar to that used in a previous analysis on fluorescent laser dye aerosols. Kohler theory was applied twice, first assuming that the soluble material formed a distinct droplet attached to the carbon particle, and second assuming that the carbon particle was totally immersed within the liquid droplet. The results are shown in Table I.  $D_p$  denotes the total particle diameter in microns,  $S$  the measured critical supersaturation in percent, and  $R$  the ratio of soluble mass to total particle mass. The first analysis method was found to yield a larger value for the soluble mass fraction ( $R$ ).

experiments. A sample of moist aerosol laden air is subjected to an expansion and supersaturation, the aerosol activates, and the resulting droplet growth rates are measured optically. The data is compared with condensational droplet growth theory, assuming an unknown sticking coefficient, and the measured results are thereby translated into a measurement of sticking coefficient. Values for sticking coefficient are continually determined as the experiment proceeds, and so the evolution of sticking coefficient with time is observed. Figure 1 gives an example of the observed behavior of sticking coefficient ( $\beta$ ) as time and therefore drop size ( $a$ ) proceeds.

Carbon Aerosol Experiments. Preliminary experiments have been performed using our torch burner with white gas as the fuel. The combustion aerosol was examined with the continuous flow thermal diffusion chamber to determine the aerosol's critical supersaturation spectrum. This is shown in Fig 2. The solid line shows a linear least squares fit to the data. The critical supersaturation spectrum for NaCl aerosol is also shown for comparison. The data shows more scatter than expected. This problem may be resolved by our new burner. The best fit is approximately parallel to the NaCl data, but with a somewhat smaller downward slope and a much higher critical supersaturation. Curves of this type should be higher for fuels with small sulfur contents and lower for those with higher contents.

A new burner is being built to improve the flame and combustion aerosol stability. The feedback between the flame and

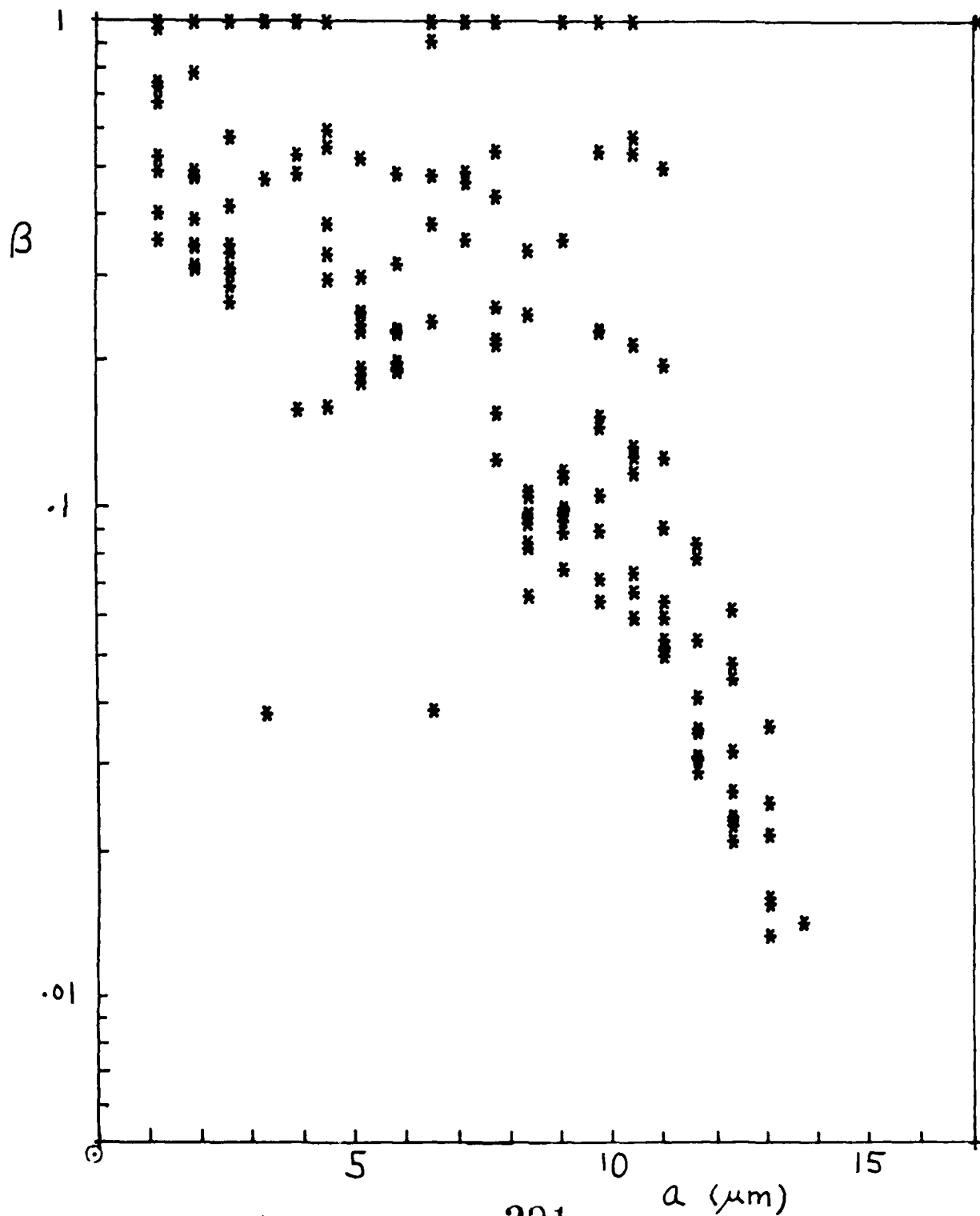


Fig 1

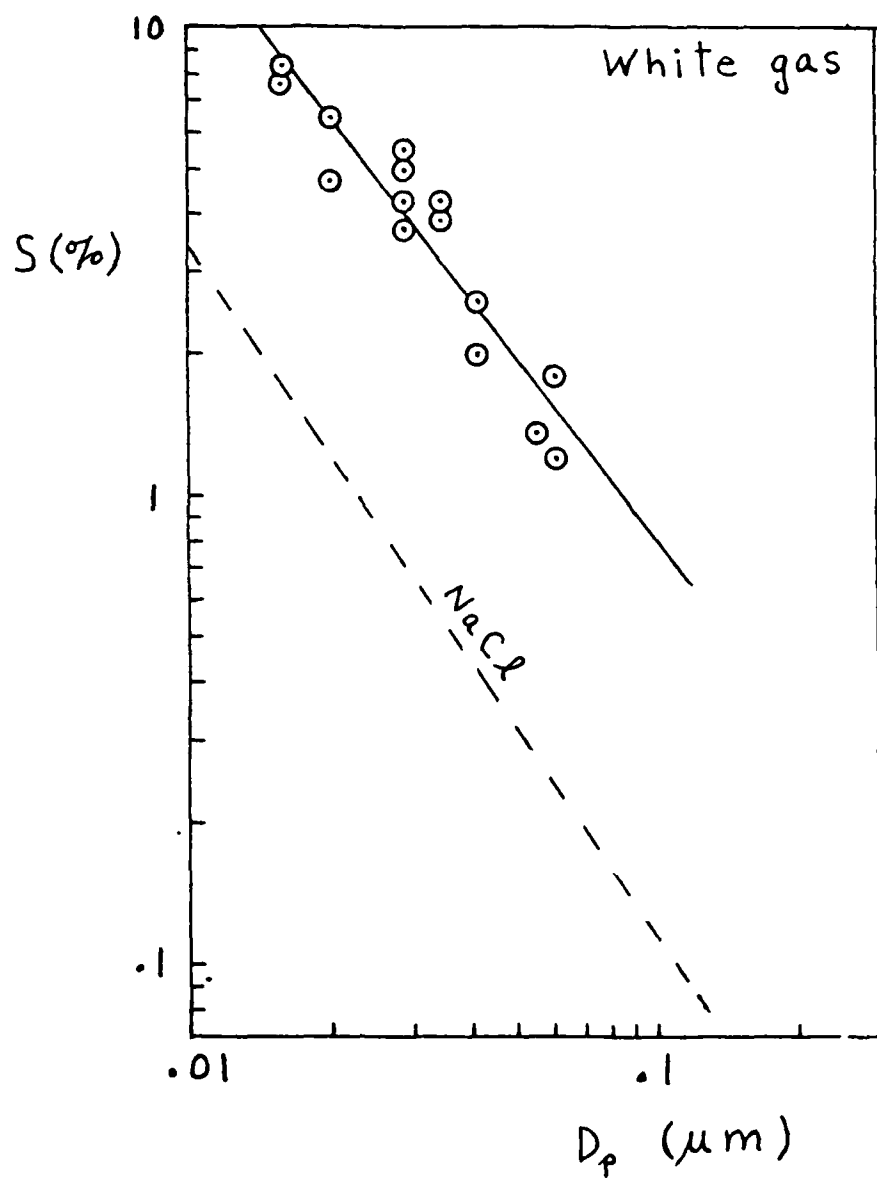


Fig 2

TABLE I

Dp (micron)	.013	.02	.03	.06	.10
S (%)	11.43	6.55	3.87	1.58	.816
R (method 1)	.069	.065	.056	.042	.033
R (method 2)	.034	.037	.037	.033	.027

## ABSTRACT

## UMR Combustion Aerosol Facility

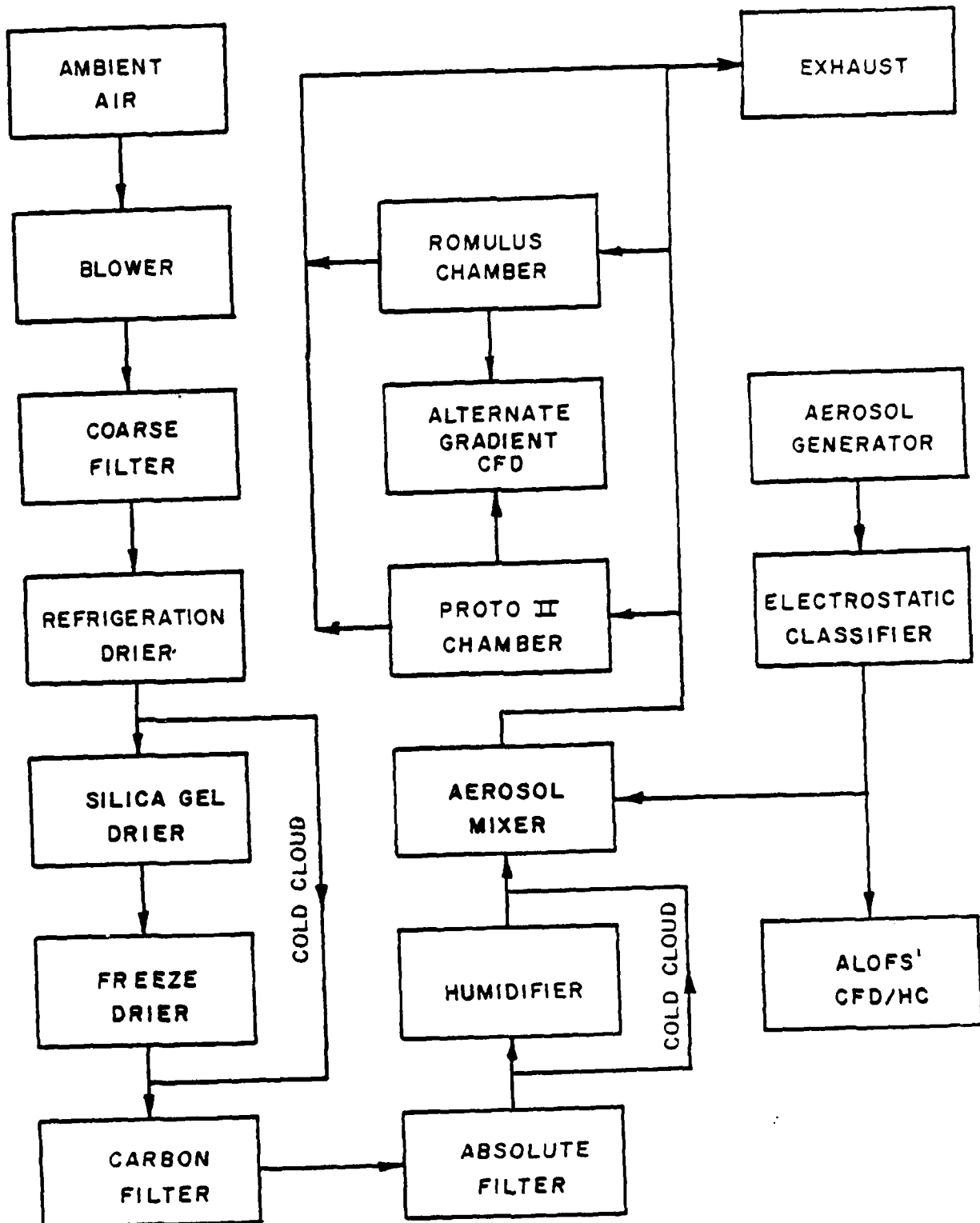
D.E. Hagen, M.T. Trueblood, and D.R. White  
University of Missouri-Rolla

There has been considerable recent interest in the hydration properties of combustion aerosols, eg. at the 1985 Amer. Assoc. Aerosol Research conference in Albuquerque and the 1986 Amer. Meteor. Soc. Cloud Physics conference in Snowmass. Both their warm cloud condensation behavior and ice nucleating ability have important atmospheric implications. At UMR we have a substantial cloud simulation facility (White, et. al., 1987) designed for the laboratory study of atmospheric processes (eg. nucleation, growth, scavenging, coagulation,...) under realistic conditions (ie. temperature, pressure, and supersaturation) and time scales. A combustion aerosol capability has recently been added to this facility. We can generate a variety of combustion aerosols, under controlled and observed conditions, characterize and shape (modify their size distribution) these aerosols, and then examine their hydration behavior under either warm or cold conditions. In this paper we describe our combustion system (burner and containment vessel), and relevant parts of the cloud simulation facility (aerosol system, warm and cold diffusion cloud chambers, and expansion cloud chamber). Results are shown for the critical supersaturation profiles for aerosols from burning alcohol and white gas in a blowtorch. Kohler theory analysis of the data is performed using methods presented earlier (Hagen and Trueblood, 1985) for fluorescent dye aerosols.

White, D.R., J.L. Kassner, J.C. Carstens, D.E. Hagen, J.L. Schmitt, D.J. Alofs, (1987); "University of Missouri-Rolla Cloud Simulation Facility: I. Proto II Chamber", Rev. Sci. Instrum., accepted.

Hagen, D.E., and M.T. Trueblood, (1985); "Aerosols Suitable for Fluorescent Water Drop Tagging Experiments", Proc. of Amer. Assoc. Aerosol Research Conf., Albuquerque, p. 235.





**SIMULATION FACILITY**

Fig. 1. Simulation Facility

## EXPERIMENTS

---

Droplet growth

Scavenging

Aerosol

Gas

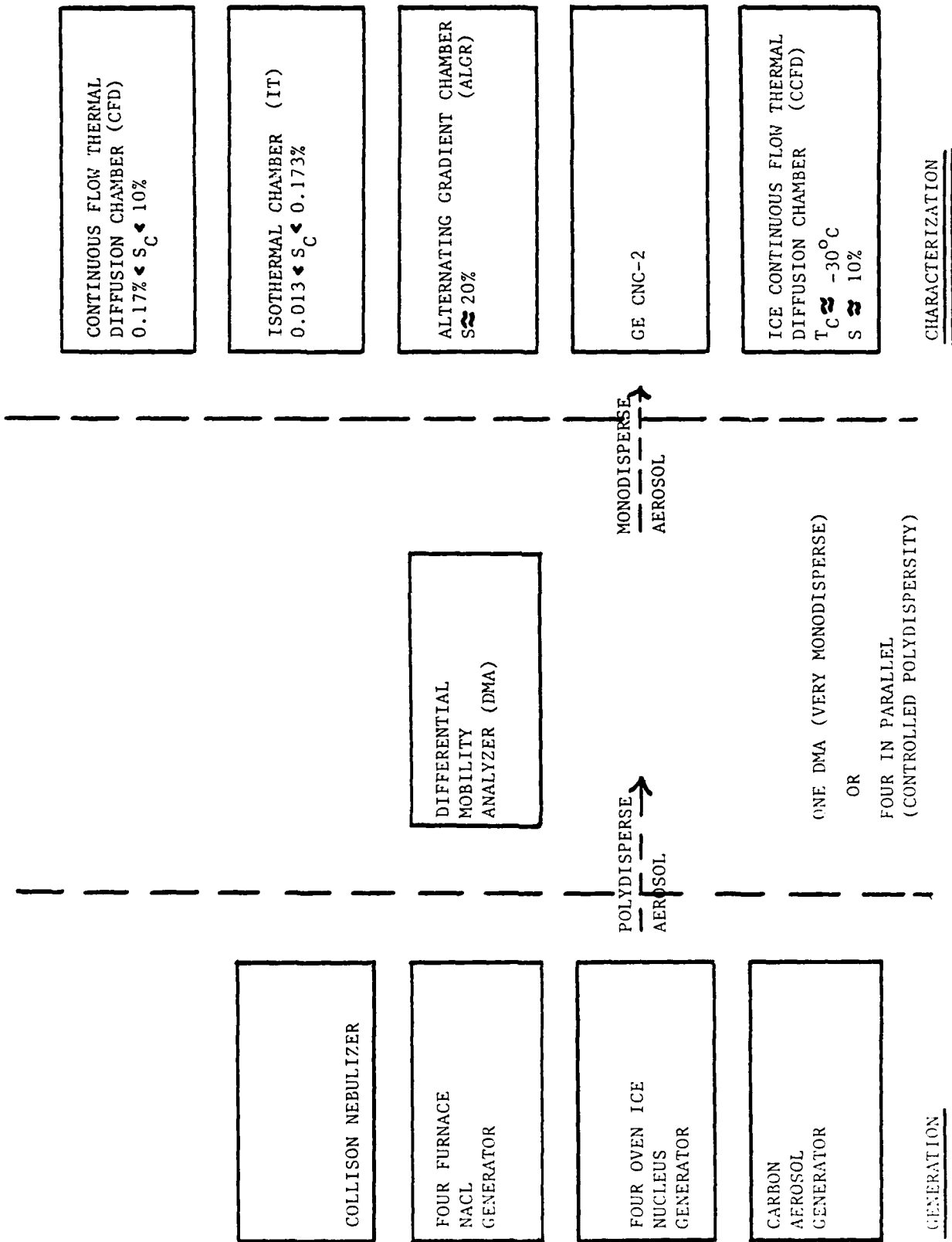
Ice nucleation

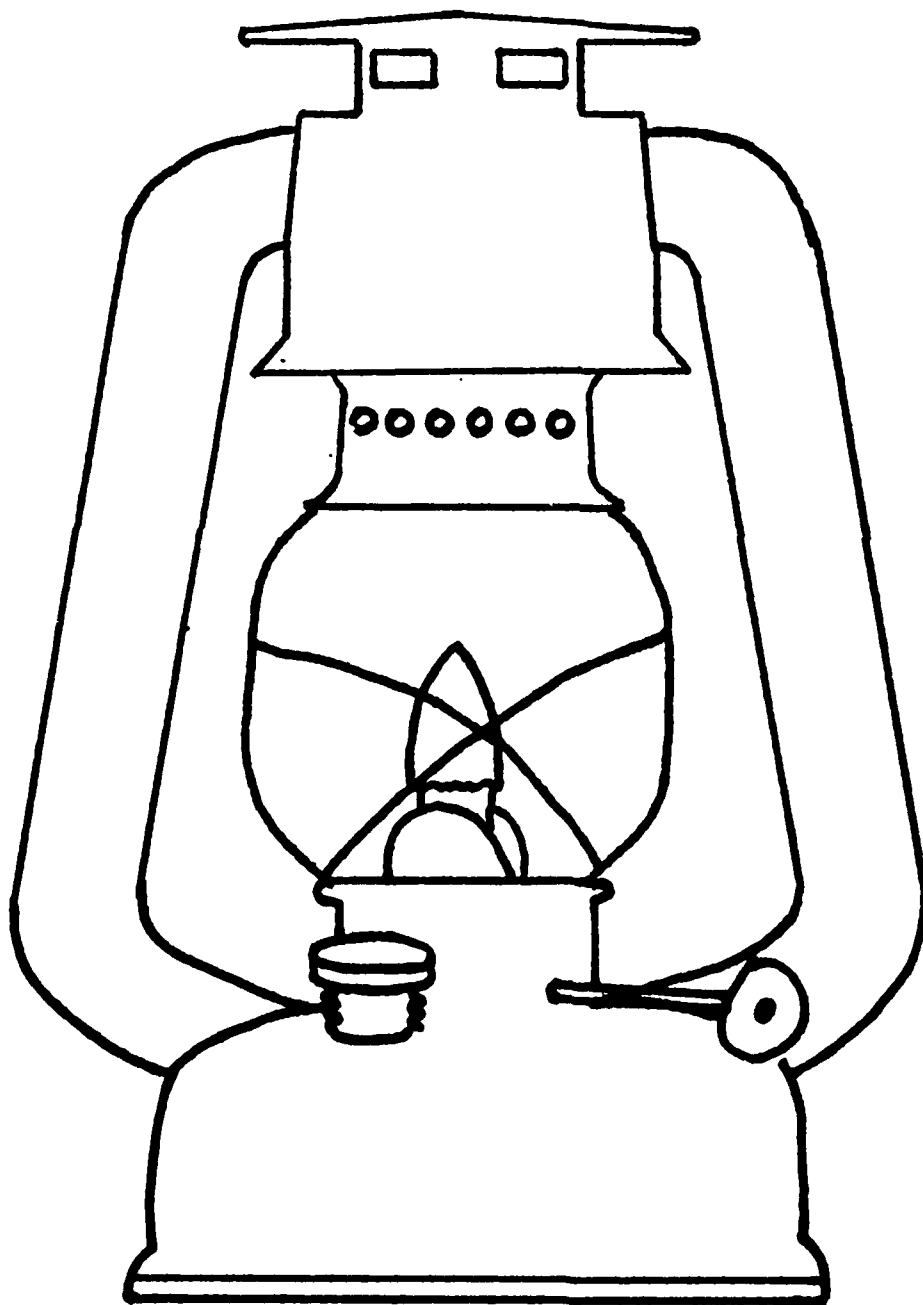
Ice growth habit

Collision coalescence

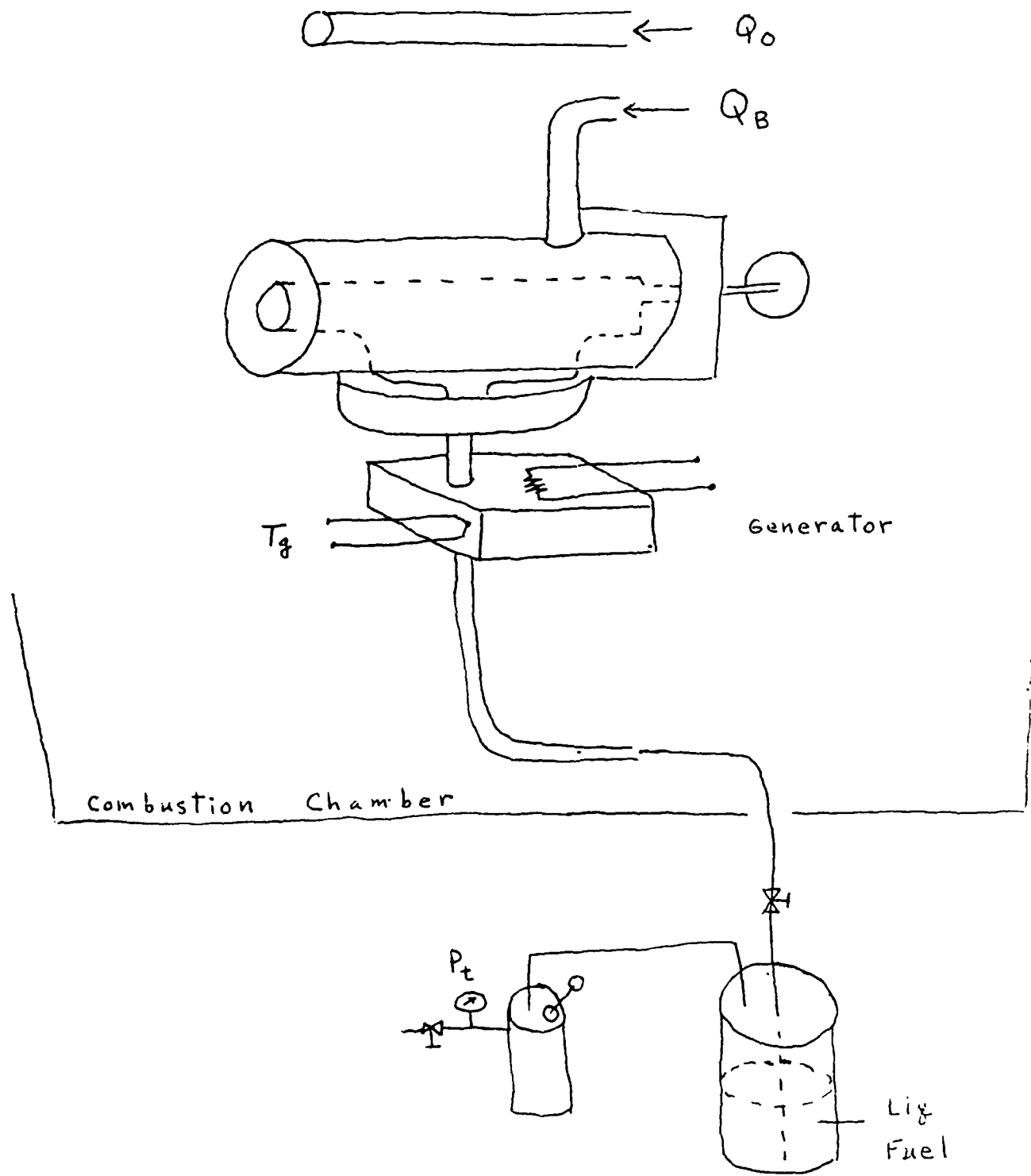
Optical properties of cloud

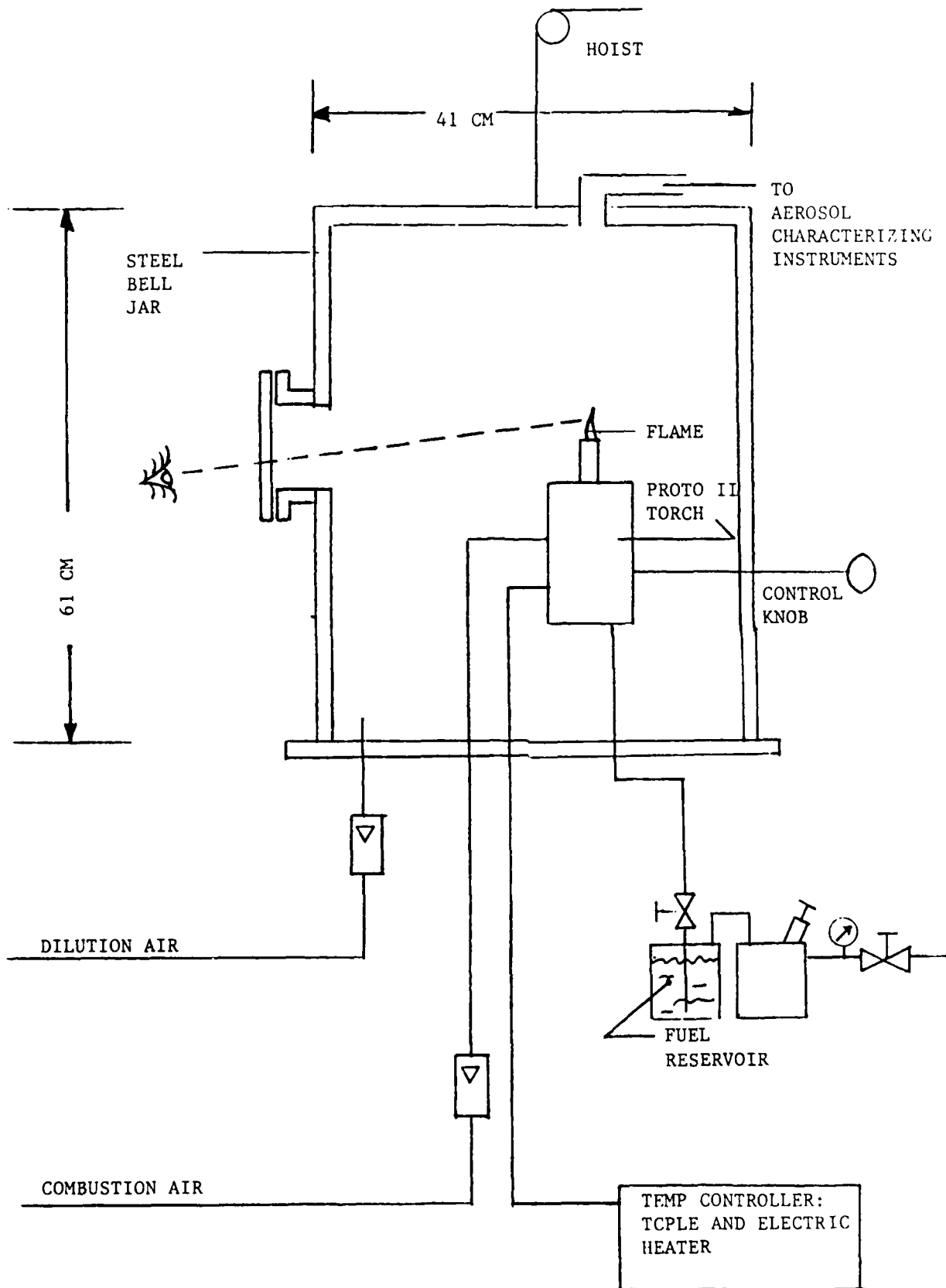
Fluid dynamics

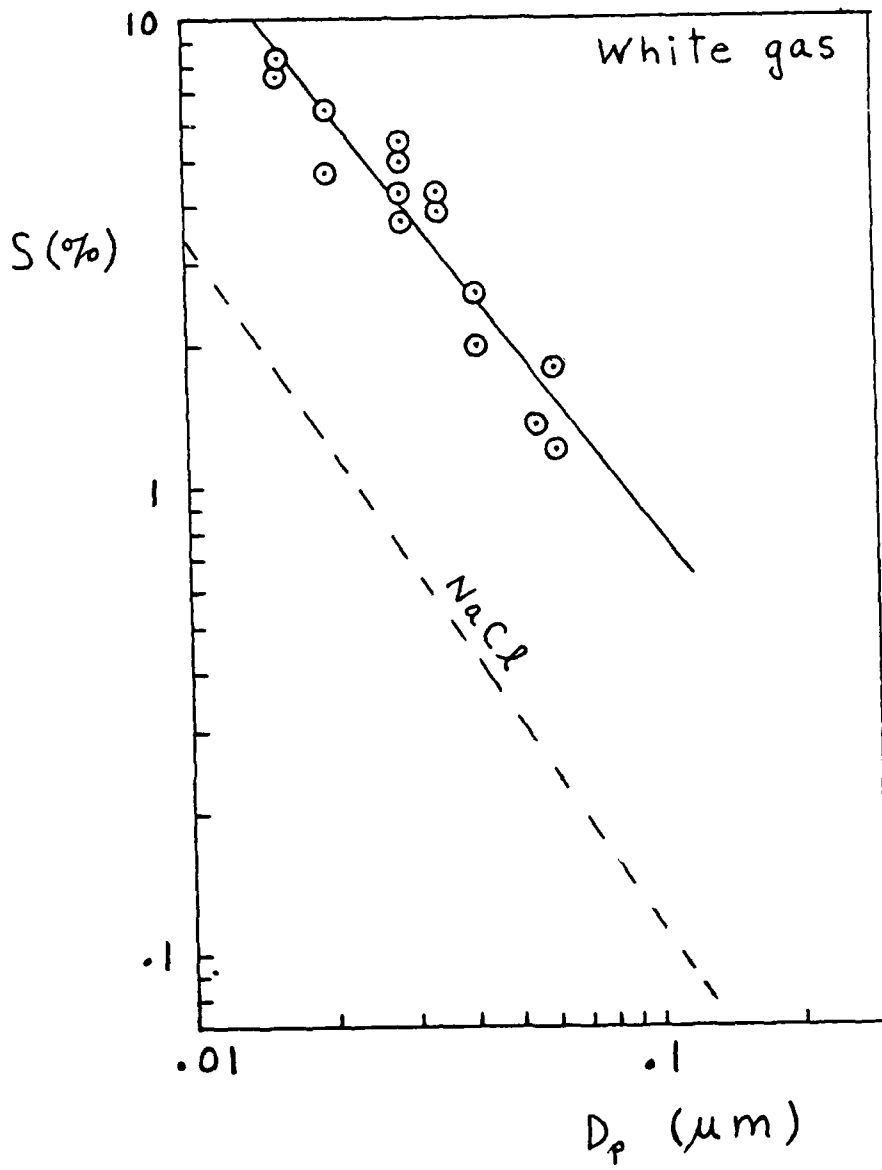




KEROSENE LANTERN CARBON AEROSOL GENERATOR







# COMBUSTION (WHITE GAS) AEROSOL

## SOLUBLE MASS FRACTION

$D_p$ (micron)	.013	.02	.03	.06	.10
S (%)	11.43	6.55	3.87	1.58	.816
$\phi_1$	.81	.71	.68	.67	.68
$m_{s1}$ ( $10^{-18}$ g)	.159	.537	1.58	9.44	34.6
$R_1$	.069	.065	.056	.042	.033
$\phi_2$	.69	.68	.67	.67	.71
$m_{s2}$ ( $10^{-18}$ g)	.0784	.311	1.05	7.41	28.1
$R_2$	.034	.037	.037	.033	.027

$$\langle R_1 \rangle = .053$$

$$\langle R_2 \rangle = .034$$

$$\sigma = .015$$

$$\sigma = .004$$



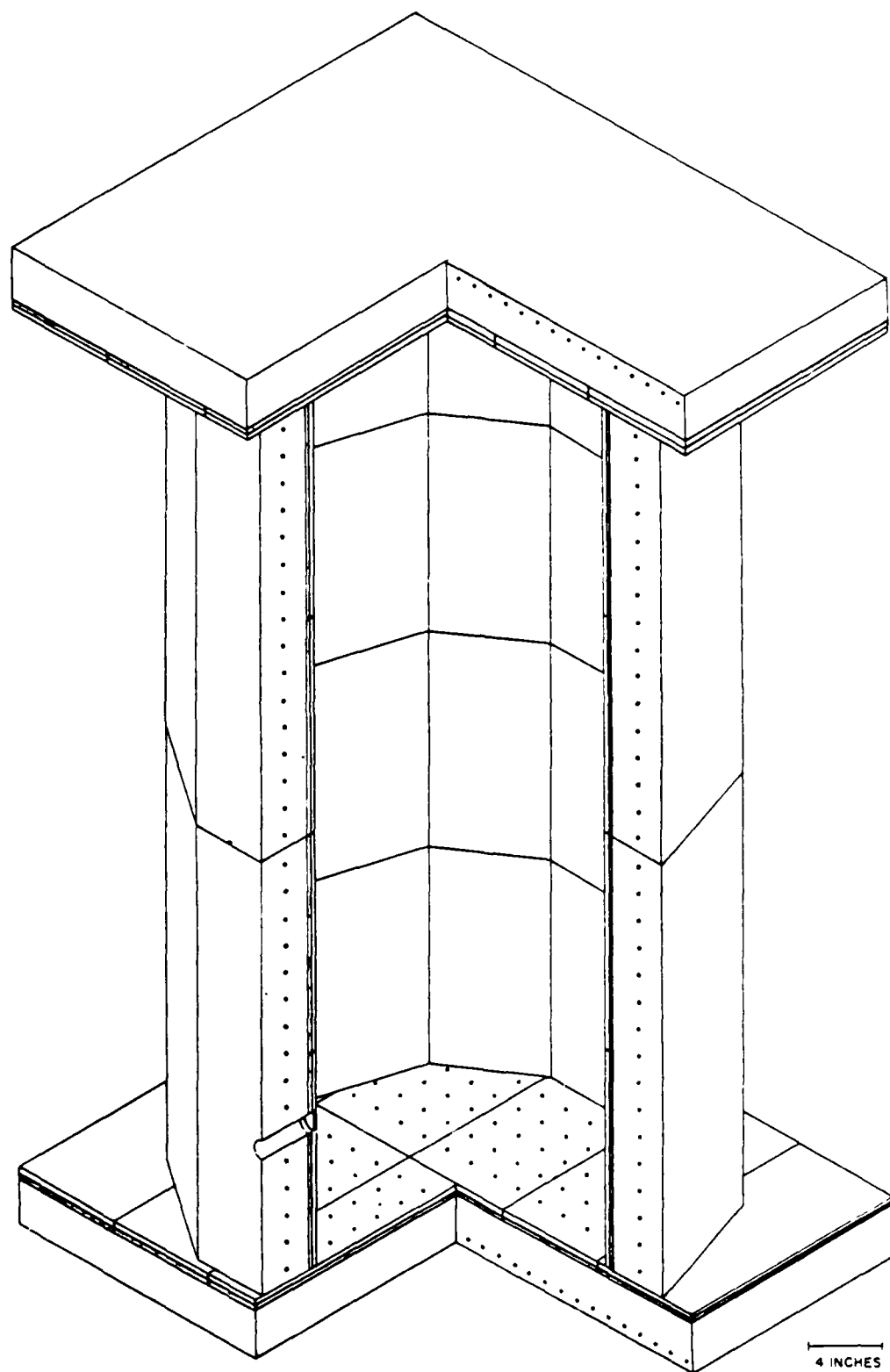


Fig. 2. Proto II Chamber

TABLE I.  
PROTO II CHAMBER OPERATING PARAMETERS

Temperature	
Range:	40° to -40°C
Control:	
Holding:	At fixed temperature RMS deviation from spacial average, 40 sensors
Cooling:	Maximum rate
	Wall temperature lag from control point
	RMS deviation from spatial average
Temperature Measurement Resolution	0.030°C
Temperature Measurement Accuracy	10°C/min
	0.01°C/(°C/min)*
	0.080°C at 6°C/min
	0.040°C at 3°C/min
	0.001°C
	+0.005°C
Pressure	
Reference pressure absolute accuracy:	+0.01%, dead weight pressure gauge
Dynamic sensor range:	0 to 15 kPa differential
Resolution:	+0.006 kPa
Control:	
Holding:	Standard deviation with time about average
Expansion:	Maximum rate
	0.065 kPa
	0.5 kPa/s (12°C/min wet adiabatic)
Offset from command	0.065 kPa
Standard deviation with time	0.05 kPa
Wall Cooling Method	Thermoelectric modules plus fluid thermostating of heat sinks
Sensitive Volume Dimensions	
Diameter:	46 cm
Height:	
One section:	61 cm
Two sections:	122 cm

\*             
Cooling Rate

PROFILE.67 RAMP, 10 DEG/MIN, 100/CM\*\*3

DATE CREATED: 9/ 3/86 TIME CREATED: 12: 0:36

X:TIME Y:TEMPERATURE

LEFT TICK MARK X-AXIS: 0.000

XUNIT: 10.000

LOW TICK MARK Y-AXIS: 0.000

YUNIT: 1.100

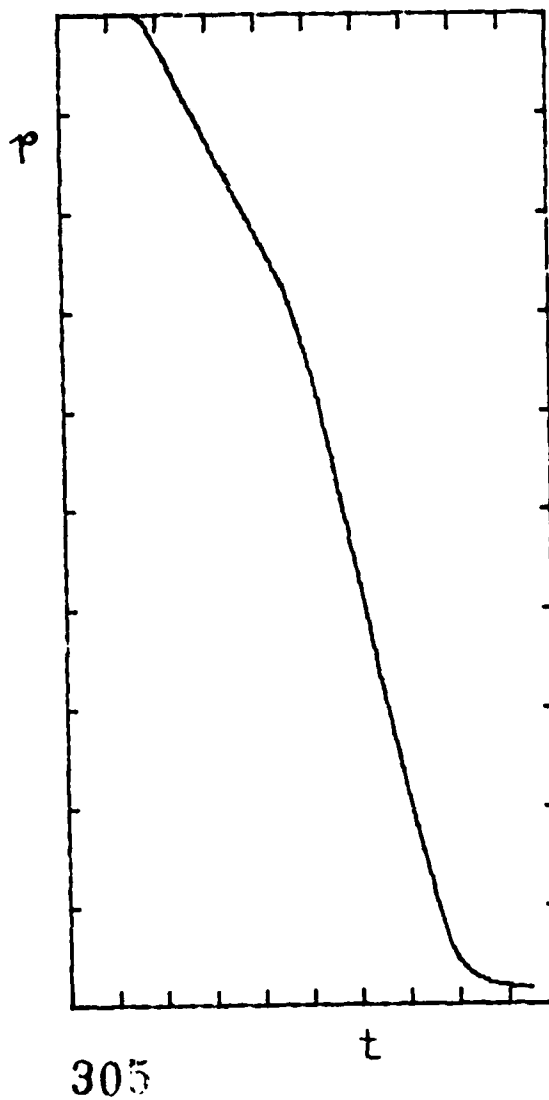
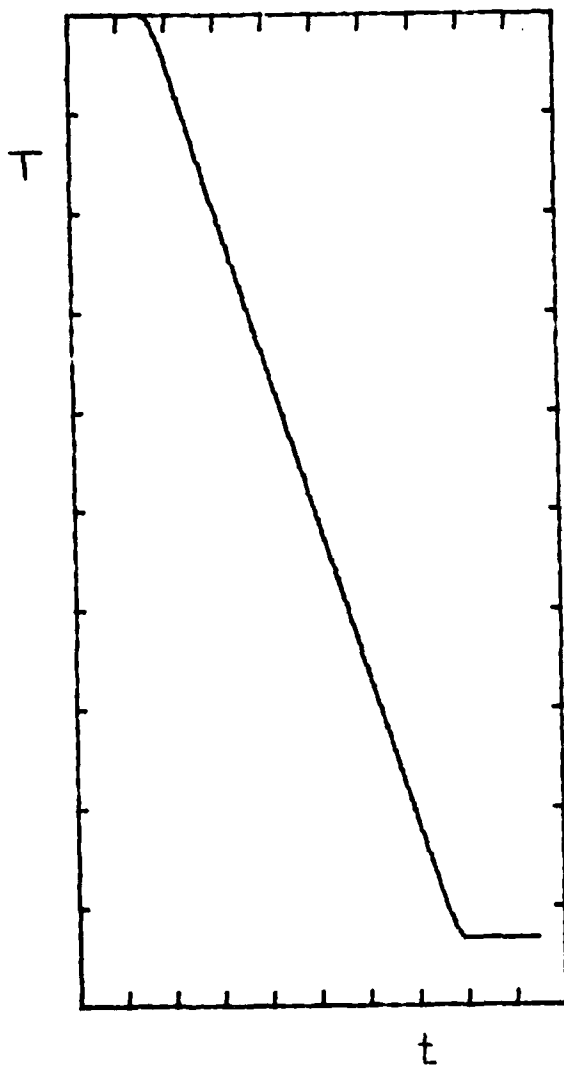
X:TIME Y:PRESSURE

LEFT TICK MARK X-AXIS: 0.000

XUNIT: 10.000

LOW TICK MARK Y-AXIS: 11.2000

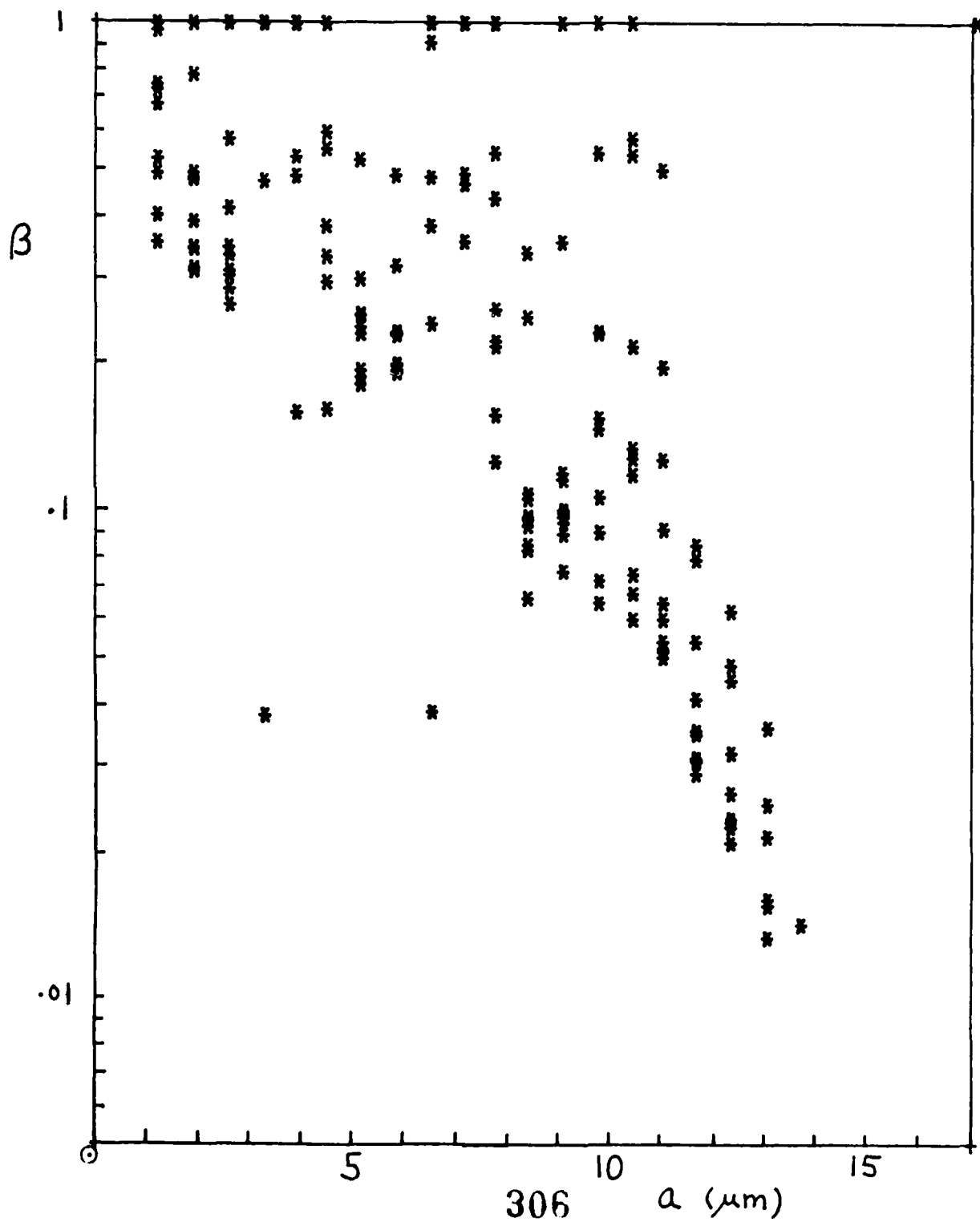
YUNIT: 0.2900



SERIES NACL121786

1/28

LOG10(BETA) VS A(MICRON)



PROFILE.79, OSC, 100/CM\*\*3

DATE CREATED: 9/18/86 TIME CREATED: 11: 0:35

X:TIME Y:TEMPERATURE

X:TIME Y:PRESSURE

LEFT TICK MARK X-AXIS: 0.000

LEFT TICK MARK X-AXIS: 0.000

XUNIT: 15.000

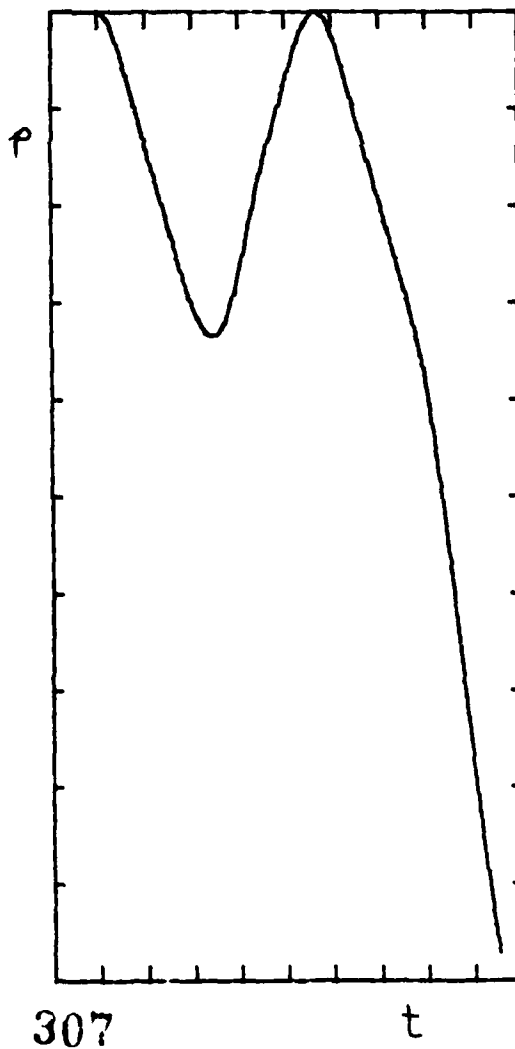
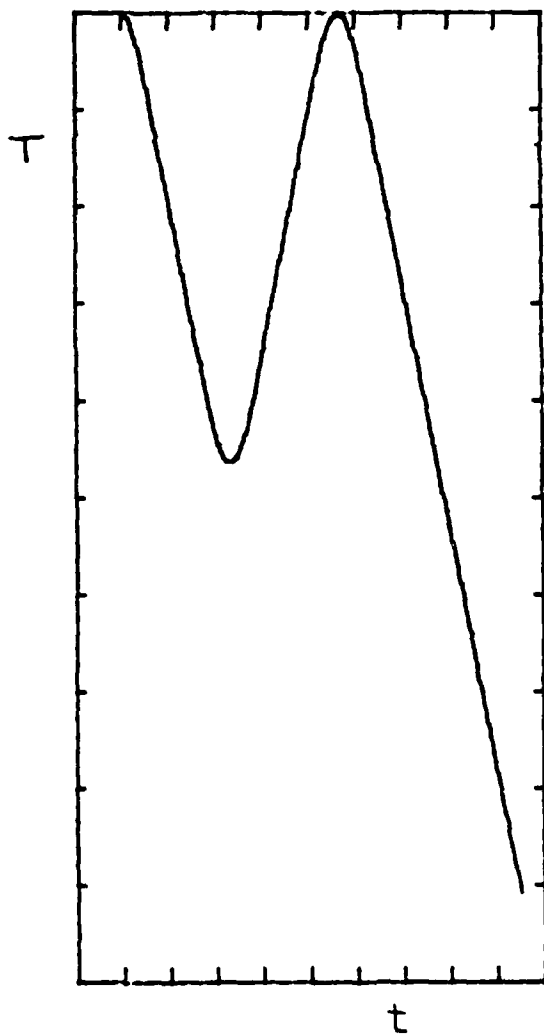
XUNIT: 15.000

LOW TICK MARK Y-AXIS: 10.000

LOW TICK MARK Y-AXIS: 11.7000

YUNIT: 1.000

YUNIT: 0.2400



## COLD CFD

Vertical plates.

Vertical flow.

115 cm (l), 12 cm (w), 0.7 cm (t)

Minimum cold plate temp  $-30^{\circ}\text{C}$ .

$S_{\text{max}} \sim 10\%$ .

OPC - thermostated Climet MN 208.

$(T_c + T_h)/2$ .

Pulse height analysis available.

Windows.

A LABORATORY CLOUD CHAMBER FOR  
TESTING SOME NUCLEAR WINTER HYPOTHESES

APRIL 8, 1987

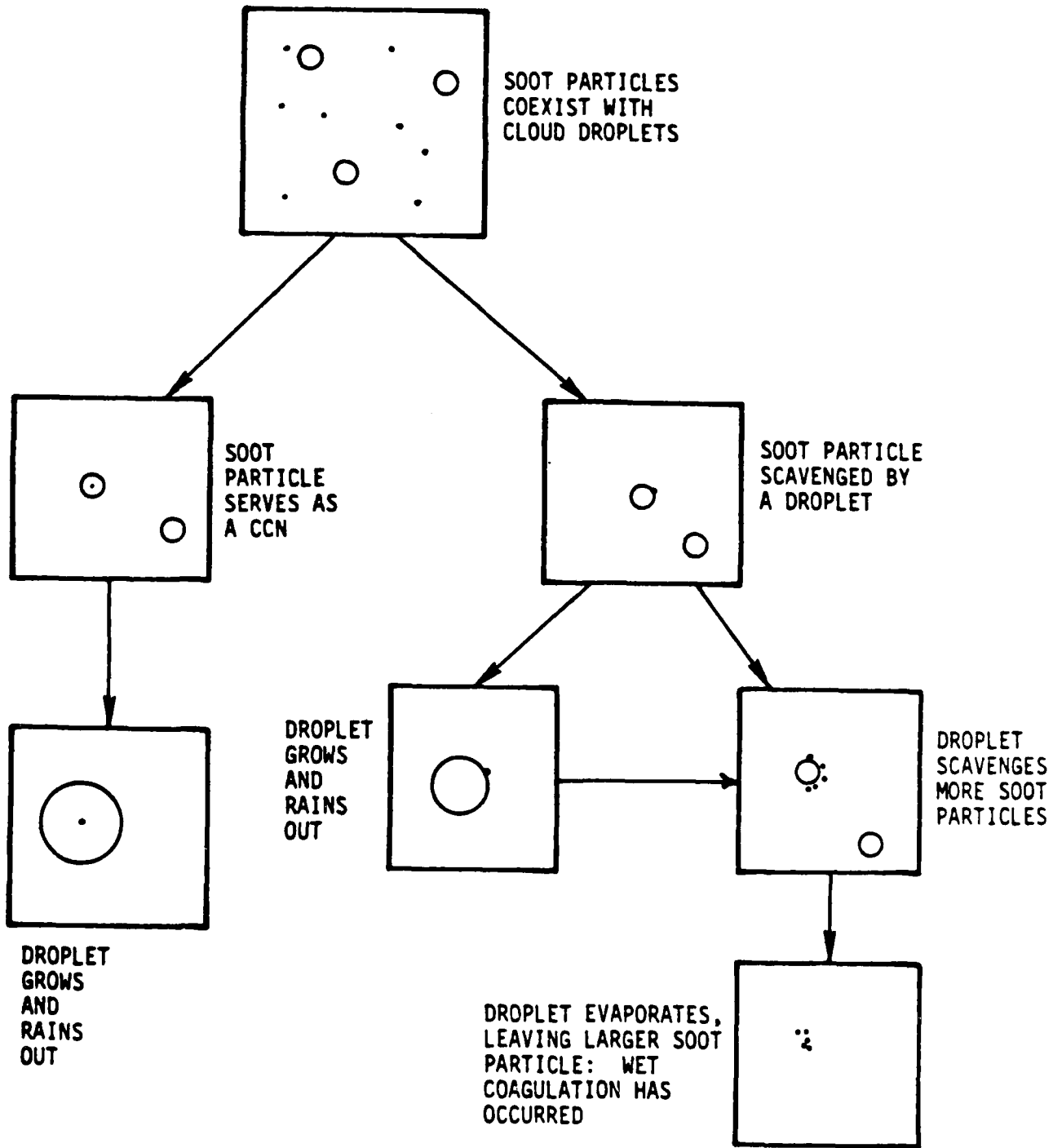
G. CARRIER\*  
F. FENDELL  
B. LAKE  
D. KWOH  
K. BEACH  
R. WAGNER

DNA GLOBAL EFFECTS PROGRAM  
TECHNICAL MEETING

\*HARVARD UNIVERSITY

TRW SPACE & TECHNOLOGY GROUP  
ONE SPACE PARK  
REDONDO BEACH, CALIFORNIA 90278

SOME POSSIBLE PATHS FOR THE INTERACTION OF  
SOOT PARTICLES WITH CLOUD DROPLETS





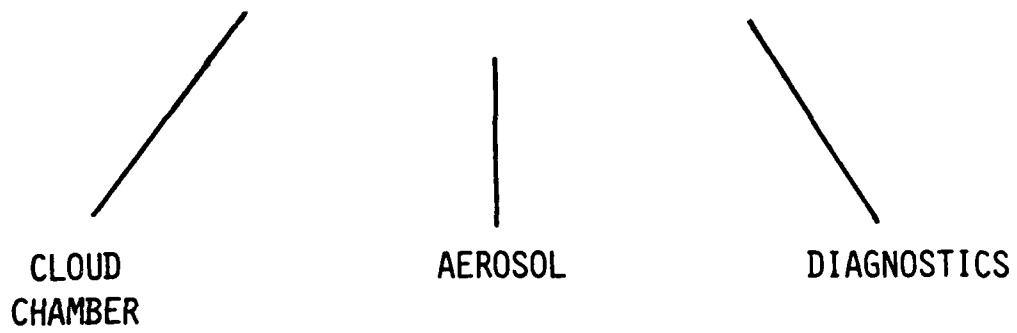
SOME SPECIFIC WET COAGULATION HYPOTHESES THAT CAN BE TESTED/EXAMINED:

- IS WET COAGULATION AN IMPORTANT PROCESS?
- IF IT IS, IS EXTINCTION AFFECTED?
- IS CHARGE EFFECT IMPORTANT IN WET COAGULATION?

## EXPERIMENT STRATEGY

- GENERATE SMOKE AND ENTRAIN IT IN A CLOUD CHAMBER WITH A LONG LASTING CLOUD FOR  $\geq 1/2$  HR.
- MEASURE SMOKE PARTICLE SIZE BEFORE AND AFTER ENTRAINMENT
- MEASURE EXTINCTION OF LASER BY SMOKE BEFORE AND AFTER ENTRAINMENT
- SLOWLY FINE-TUNE/CONTROL PARAMETERS: PARTICLE AND CLOUD DROPLET SIZE, DENSITY AND CHARGE

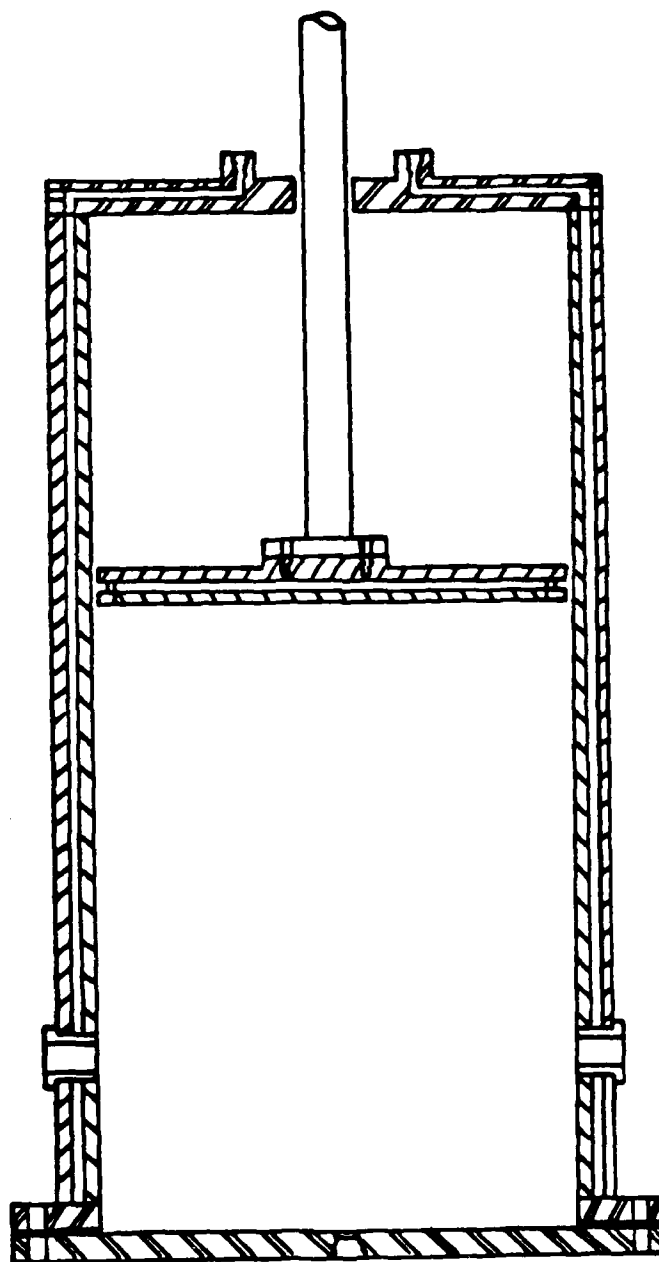
TECHNOLOGIES INVOLVED IN A LAB CLOUD CHAMBER EXPERIMENT



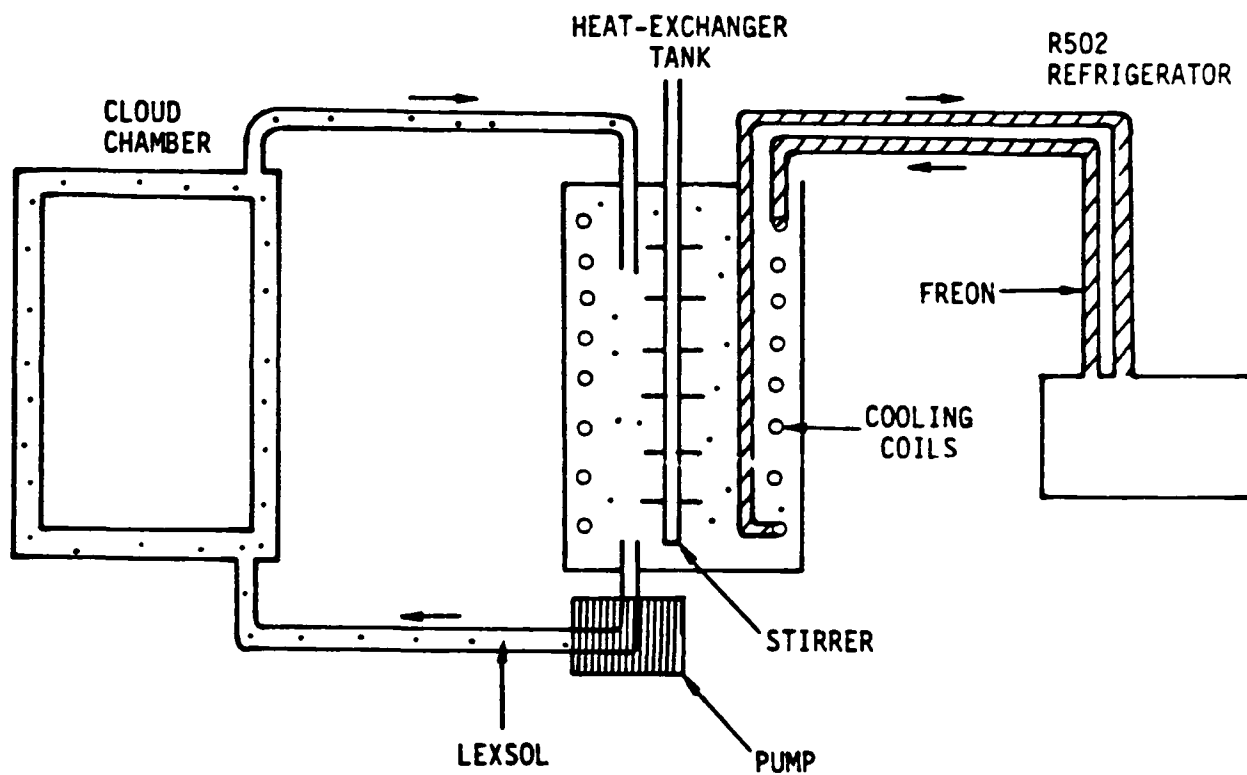
## CLOUD CHAMBER REQUIREMENT

- TEMPERATURE RANGE TO - 50°C
- TEMPERATURE TRACKING BETWEEN WALL AND GAS TO MINIMIZE WALL EFFECT AND CONVECTION
- MAKE A LONG LASTING CLOUD

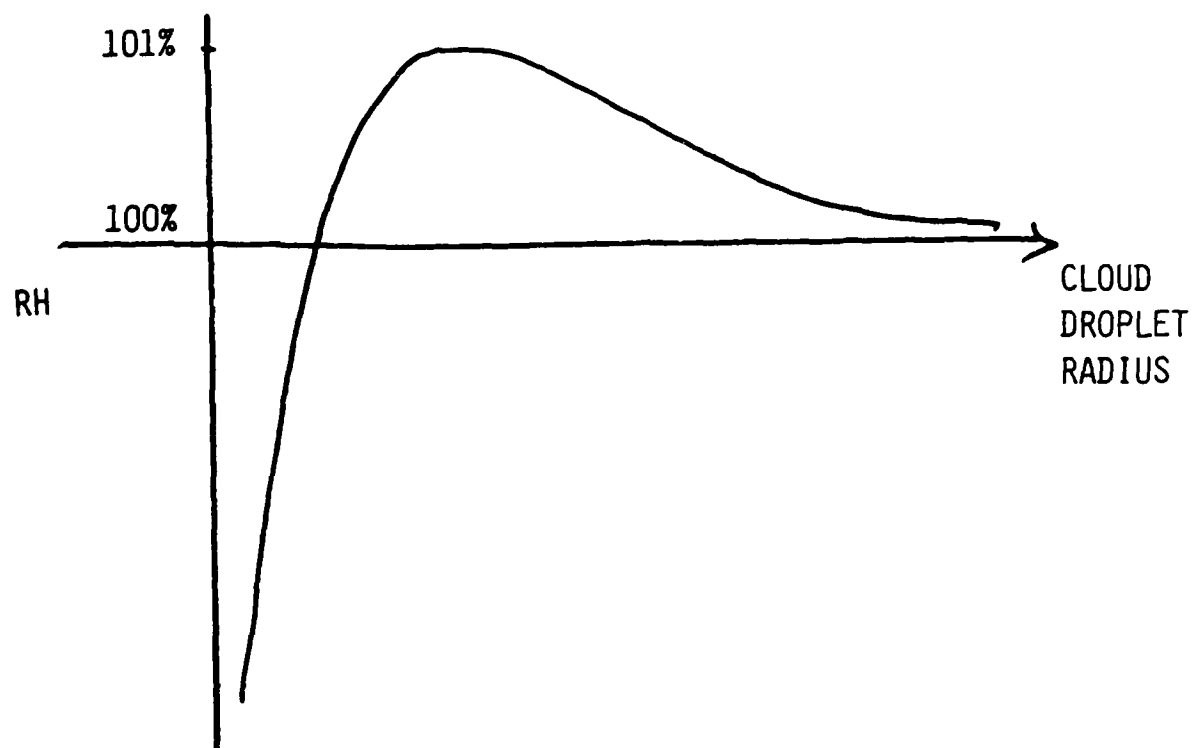
CROSS-SECTIONAL VIEW OF THE CLOUD CHAMBER. THE INTERIOR DIMENSIONS ARE DIAMETER OF 61 CM AND LENGTH OF 122 CM.



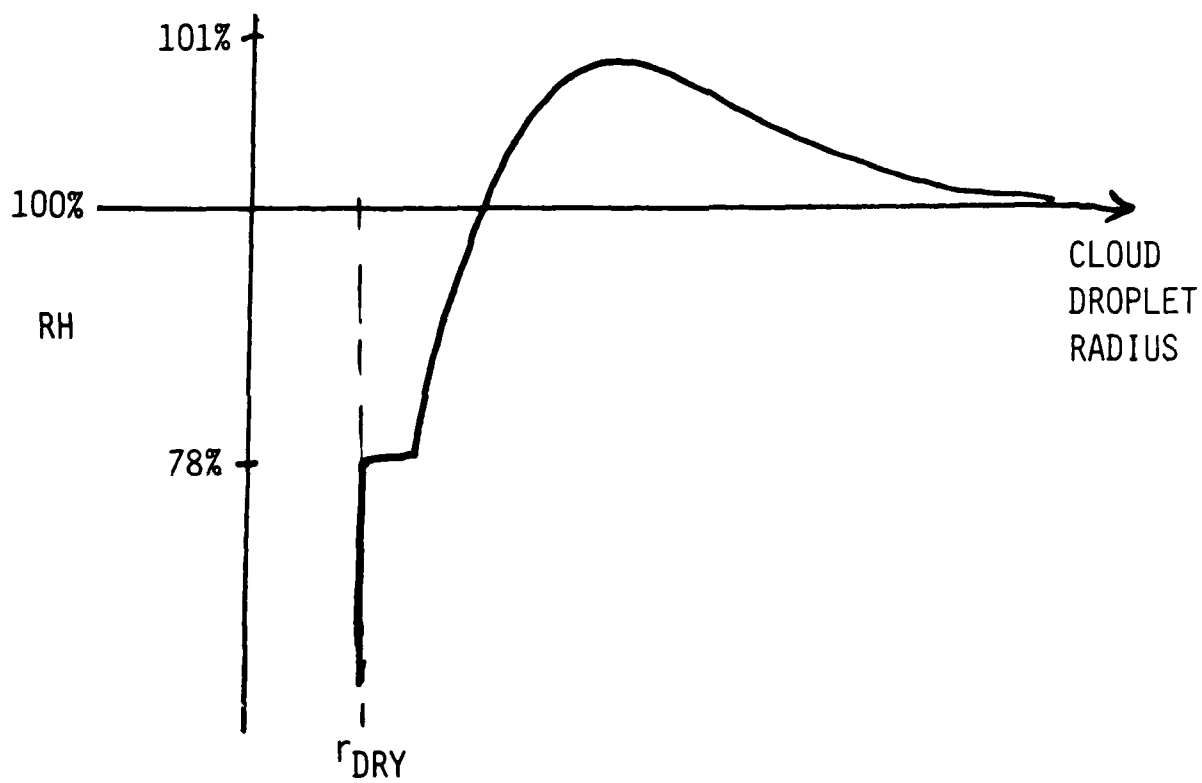
COOLING-SYSTEM SCHEMATIC FOR THE CLOUD CHAMBER



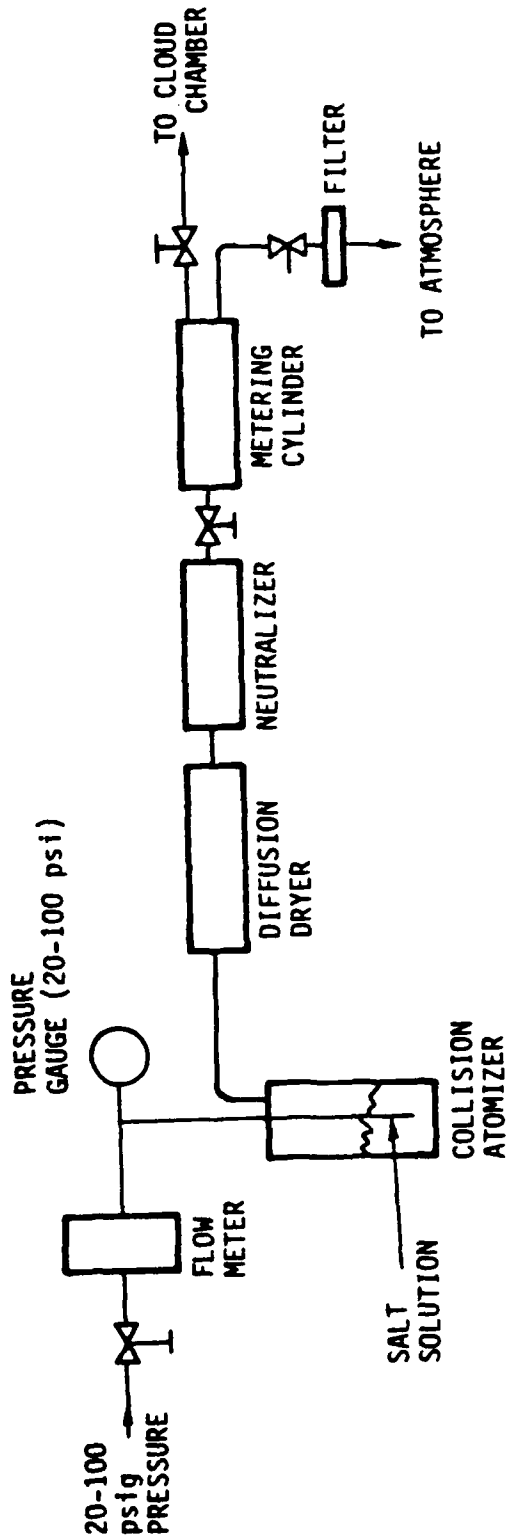
THE DIFFICULTY OF MAKING A LONG LASTING CLOUD



SOLUTION - MAKE A HAZE WITH SALT AEROSOL INJECTION

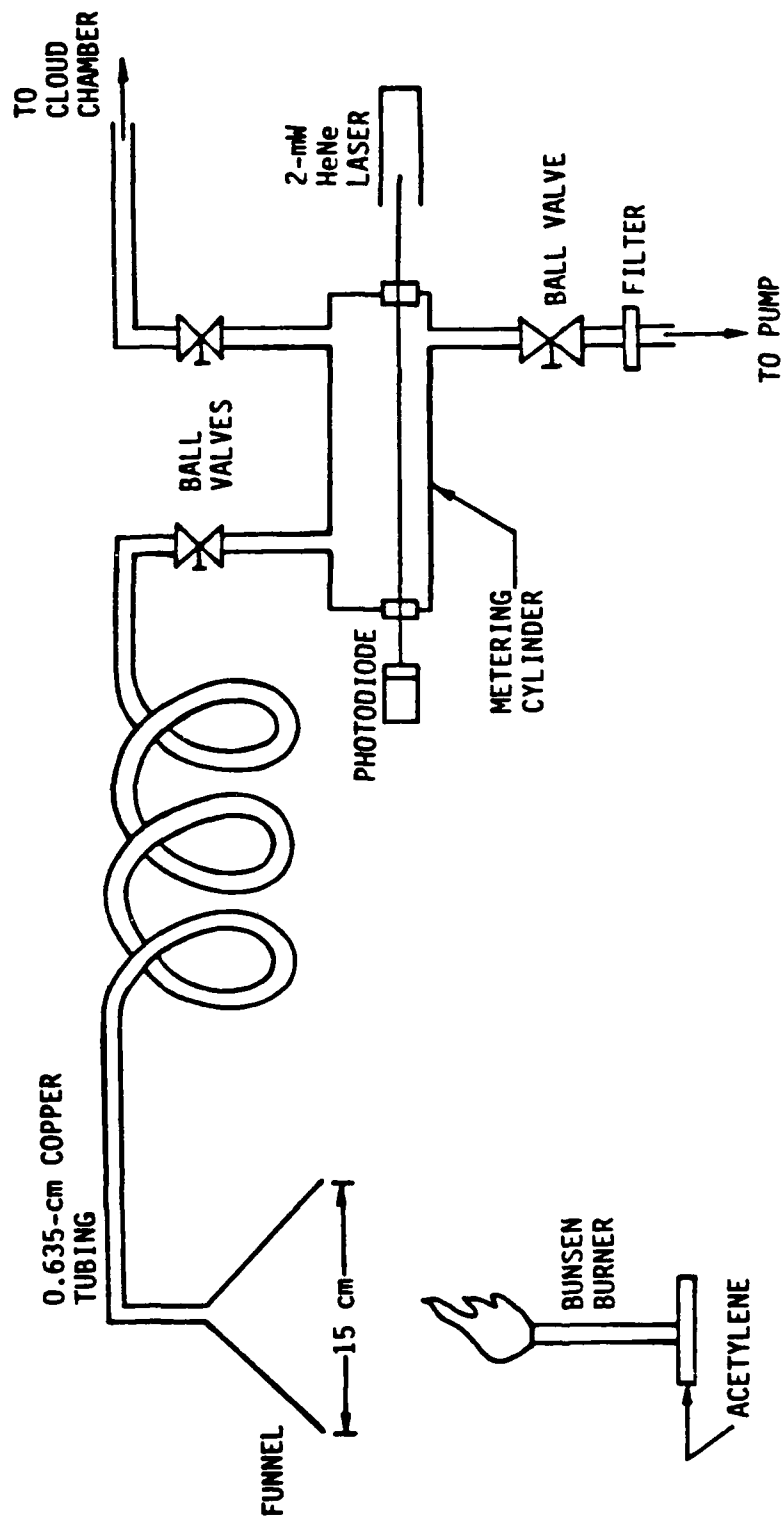






SALT-AEROSOL GENERATION AND INJECTION SYSTEM

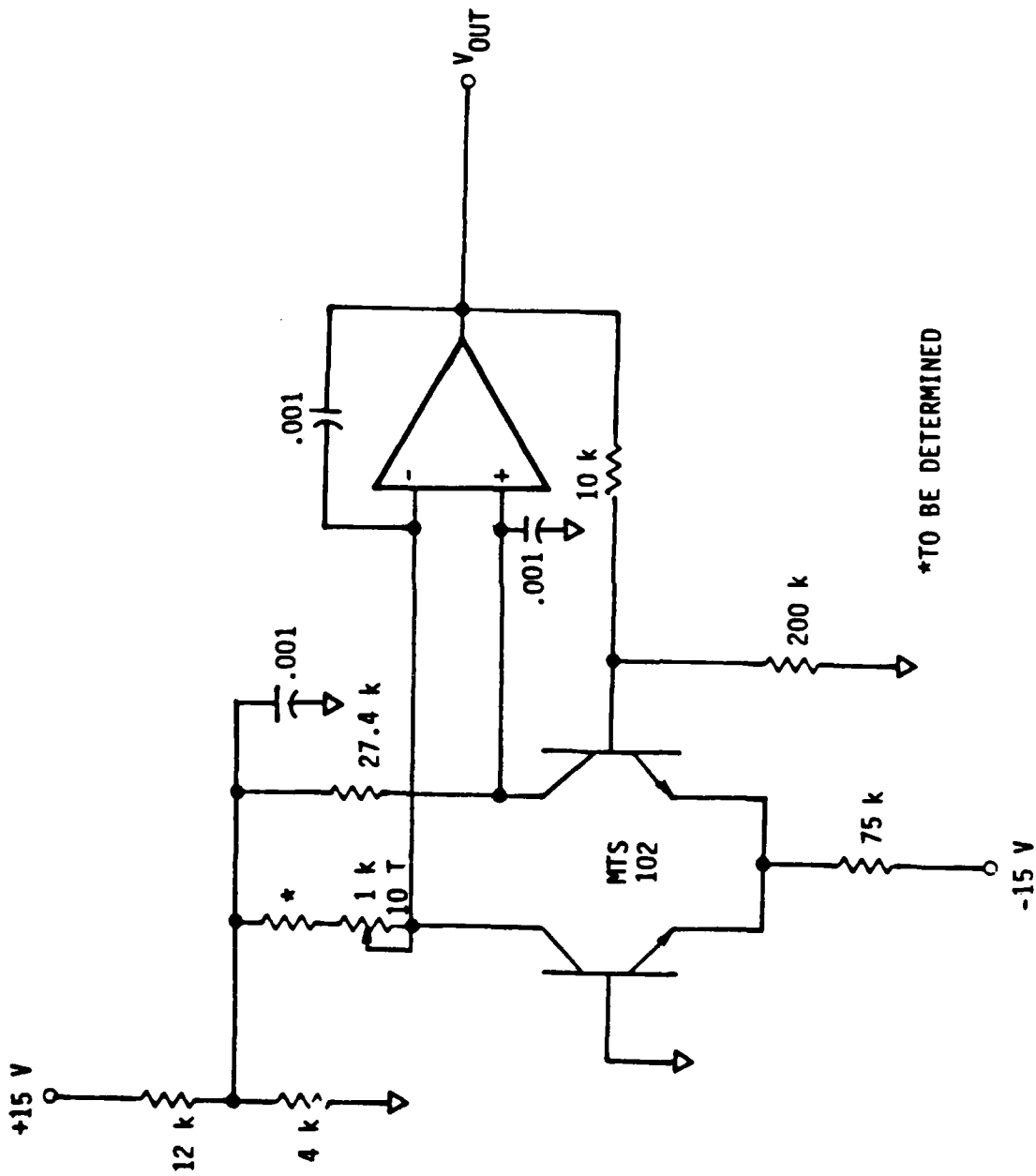
(1 psi =  $6.89 \times 10^3$  Pa.)



Smoke collection and injection system

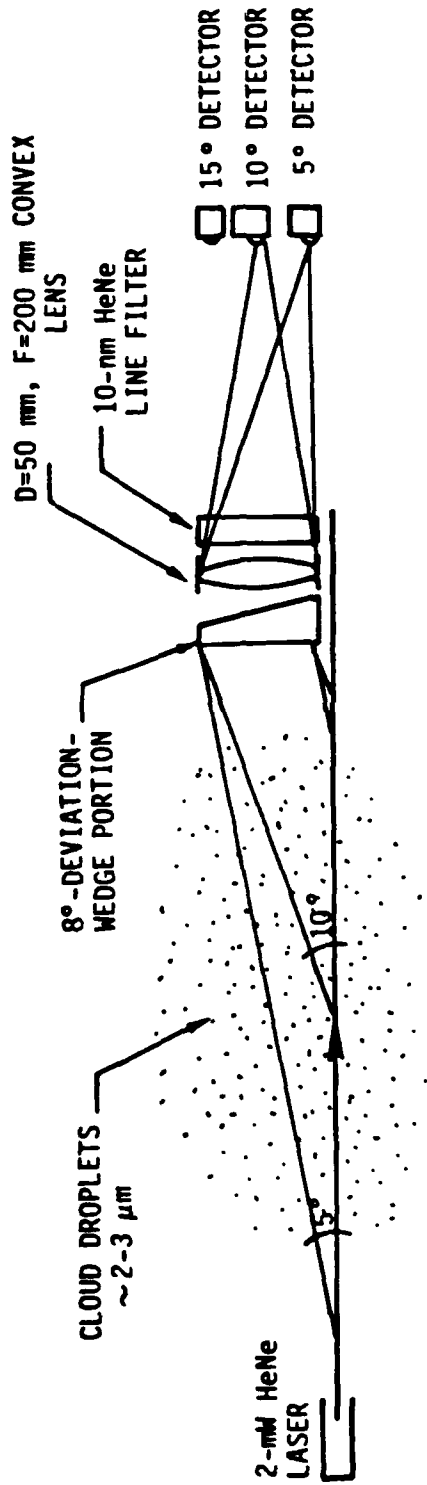
## DIAGNOSTICS

- TEMPERATURE
- CLOUD DROPLET SIZE
- EXTINCTION MEASUREMENT
- PARTICLE SIZE MEASUREMENT

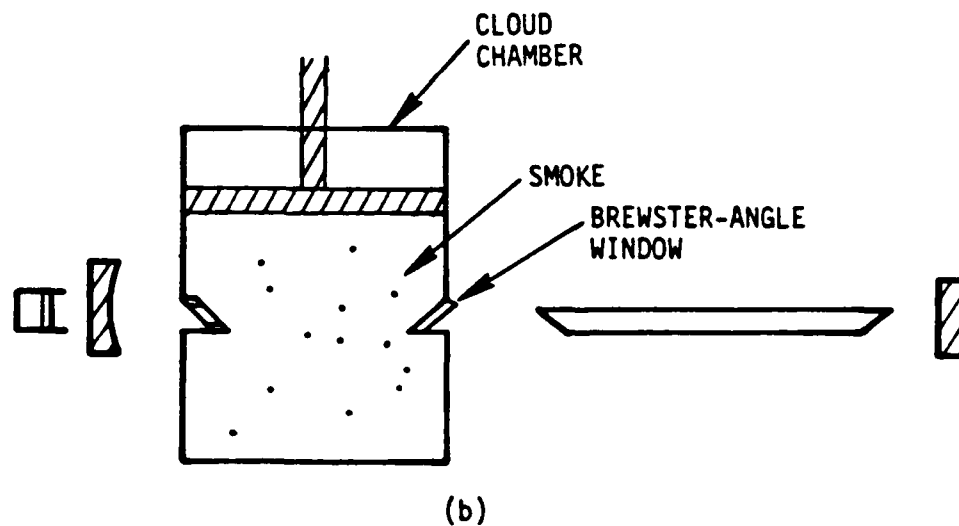
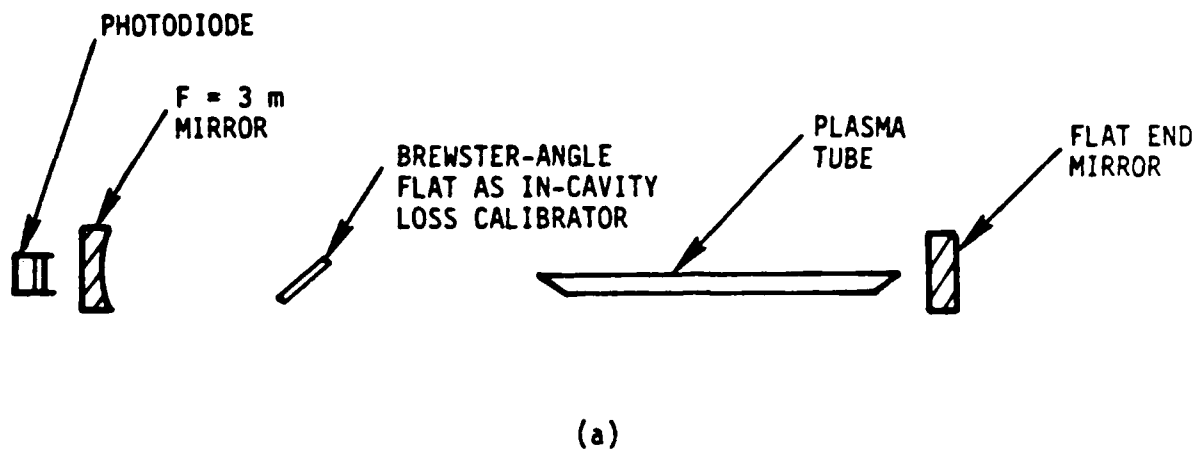


\*TO BE DETERMINED

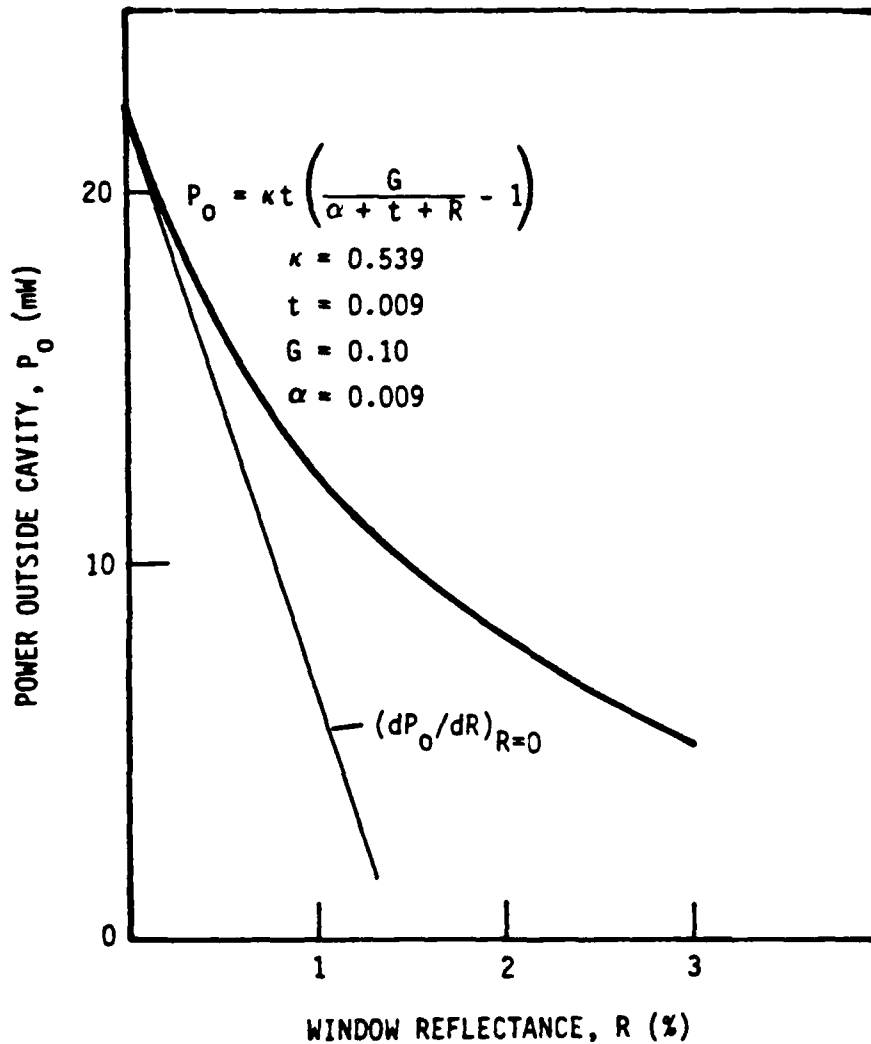
Schematic for transistor differential thermometry. (The notation k for resistors implies kΩ; the notation T for potentiometer implies turns; absence of notation near capacitors implies μf; and MTS 102 denotes a particular Motorola transistor to be used for this purpose.)



Cloud-droplet-size-measurement system, using 5°, 10°, 15° Fraunhofer diffraction in the forward direction.



Extinction-of-light-by-smoke measurement using the laser-cavity-extinction-photometer method: (a) laser output versus in-cavity-loss calibration by a Brewster-angle flat; (b) cloud chamber in place for an actual extinction measurement.



Laser-output power versus in-cavity loss owing to reflectance of the Brewster-angle flat of 2-mm-thick fused silica (as it deviates from the Brewster angle). The end mirror of the laser has radius 3 m and 0.9% transmittance. The empirical formula for the laser-output power versus loss is manufacturer-supplied and has been confirmed by trial. The slope of the curve as the in-cavity loss  $R \rightarrow 0$  yields the asymptotic loss-amplifying factor (or "efficiency") of the design as almost 70.

## PARTICLE SIZE MEASUREMENT

- SUCTION SAMPLE AIR INTO SMALL CYLINDER BY WITHDRAWING A PISTON
- COLLECT SOOT SAMPLES BY GRAVITATIONAL SETTLING ONTO TEM GRIDS
- DO 600 SAMPLES OF TEM AT 100,000 X



SECTION 4

PLUME DYNAMICS

## SURFACE VECTOR WIND FIELDS IN FIRES

Thomas Y. Palmer

PHYSICAL DYNAMICS, P0278  
Fallbrook, CA 92028

Experimental observations of medium to large scale fires show some of them to have a "firestorm" pair of vertically oriented, contra-rotating vortices involving much of the burning area. The firestorm fires need a shallow, strongly sheared wind layer in the boundary layer over the fire with slower winds above. This is similar to the low level jet which has been found to be associated with tornadoes. Strong fire winds are possible, since the net vorticity about the whole fire is zero. This obviates the search for mesoscale atmospheric swirls thought to be necessary for past firestorms.

The city firestorms of World War II had such shallow local flows such as a sea-land breeze or valley winds. Such flows can occur in wild fires over ridges, in sea breeze regimes and in some valley flow situations--areas notorious for strong firewhirls and firestorm conditions.

There is evidence that the vertical vortex pairs bend over to the horizontal, curl around and join to form a vertically rising vortex ring. This is a cyclical process which may cause the "puffing" observed in large fires, which can be described by the theories of intermittent turbulence and layer replacement as first described by Danckwerts (1951). A more recent description (although not necessarily more appropriate to a fire) has been given by Thomas (1980).

One of the predictions of layer replacement theory is that the dimensionless group:

$$(V^*)^2 / (\nu)f = k$$

where  $V^*$  is the friction velocity,  $(\nu)$  is the eddy viscosity,  $f$  is the characteristic frequency of the turbulent burst process and  $k$  is a universal constant is constant for similar processes. Laboratory measurements indicate that " $f$ " is about 133 (Thomas, 1981). Experiments in chaparral fires (Palmer, 1984, unpublished ms.), the Project Flambeau Fires (Palmer, 1983) and the data presented here gives " $k$ "'s of; 146, 141, and 138.

The time lapse VCR-TV presentation of the observed vector flow field around a large fires illustrates these effects. Although Figure 1 only shows samples taken every minute for ten

minutes the measurements were made every ten seconds over several hours and clearly show the "puffing" cycles.

Conclusions: It appears from this experimental data that large fire turbulent descriptors such as the coefficient of eddy viscosity can be experimentally determined by measurements outside the fire. This should make computer simulations more realistic.

#### REFERENCES

- Danckwerts, P.V., 1951: Significance of liquid-film coefficients in gas absorption. *Amer. Inst. Ch. Eng. Jour.*, 43:1460-1467.
- Palmer, T. Y., 1983: Project Flambeau Experimental Measurements. In *Proc. 17th Asilomar Conf. on Fire and Blast Effects of Nuclear Weapons*, May 30- June 3, 1980, LLNL, CONF 8305107, Livermore, CA pp66-70.
- Thomas, L.C., 1980: A surface rejuvenation model of wall turbulence: Inner laws for  $V^+$  and  $T^+$ . *Int. J. of Heat and Mass Trans.* 23:1099-1104
- Thomas, L.C., 1981: Model of the turbulent burst phenomena; Predictions for eddy viscosity. *AIAA Jour.* 19: 1600-1602.

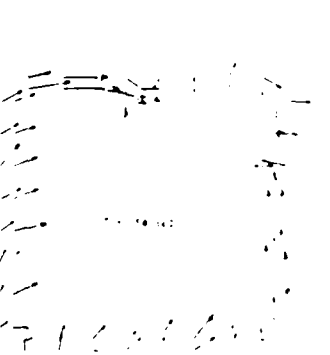
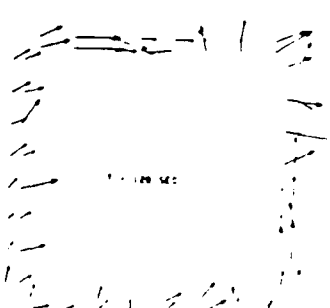
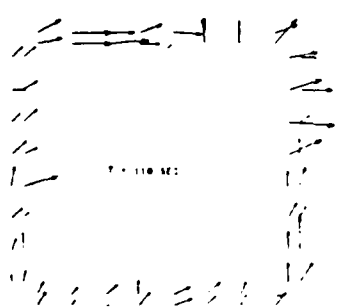
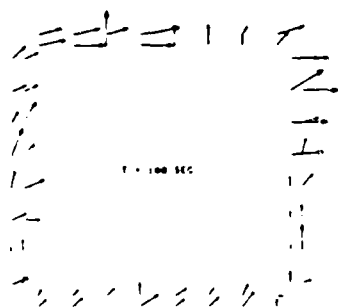
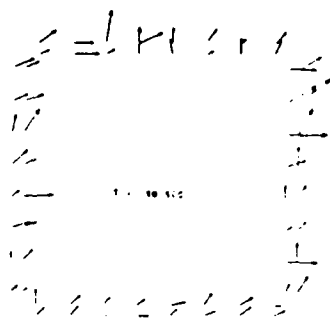
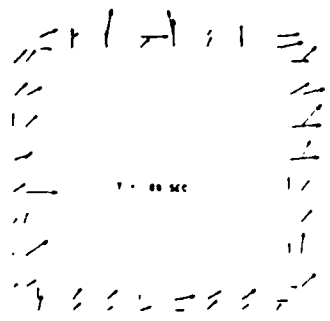
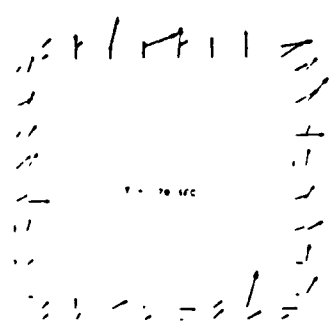


PLATE 2

## FIRE PLUME-SURFACE INTERACTIONS

W. M. Porch

Lawrence Livermore National Laboratory  
Livermore, CA 94550

## 1. INTRODUCTION

The relative concentration of submicron and supermicron size particles and high turbulence in large fire plumes can radically change the aerosol size evolution in the fire plume. These size changes affect the potential for visibility reduction and long range transport. We have developed a coupled hydrodynamic plume aerosol coagulation model including condensation in the first hour of the aerosol evolution in the fire.

We have extended aerosol plume evolution calculations beyond the first hour of the plume to several days transport times. This was done with a 10 level model with parameterized vertical and horizontal diffusion, sedimentation and coagulation. The optical effects of the evolving concentration and size distributions were modeled assuming Mie scattering and absorption. We have also tested the hydrodynamic part of the modeling with wind convergence measurements in a large jet fuel pool fire.

Large area grass, brush and forest fires are important seasonal contributors to western visibility reduction. On rare occasions these fires in the West can be large enough to affect atmospheric optical properties in the East (Elsley, 1951). In spite of this, very little is known about the size distribution and concentrations of large fire aerosols, especially within the active fire plume. The aerosol properties of large fires are beginning to be studied as part of our Laboratory's studies of global effects of nuclear war. Though experimental efforts are beginning, most of our work to date has involved numerical models of the hydrodynamics of large fires coupled with coagulation calculations (Porch et al., 1986). These studies have pointed to the potential importance of supermicron scavenging of submicron aerosol by turbulent processes in the active fire plume.

## 2. MODEL DESCRIPTION

The model used to simulate the optical effects of large fire aerosol consists of several elements. The first element computes the evolution of aerosol size distribution from the time varying concentration derived from a hydrodynamic fire plume model. After one hour the computed concentration and size distribution are input into a layer between 2 and 4 km and used to initialize a one-dimensional model which includes vertical diffusion and dilution derived from a scale dependent horizontal diffusion algorithm (Walton, 1973). The optical extinction as a function of wavelength for the layer is calculated based on an assumed aerosol complex index of refraction and the continued evolution of the concentration and size distributions.

In the early fire plume and smoke layer, aerosol coagulation is calculated based on equations described in Porch et al (1986) These equations include coagulation due to Brownian motion, differential-settling by sedimentation and turbulent

shear. Brownian processes dominate the coagulation of particles with radii smaller than  $0.1 \mu\text{m}$  throughout the period of calculation. Sedimentation only affects coagulation of the very large particles greater than  $10 \mu\text{m}$  radius. The turbulent coagulation is only important in the early fire plume and affects the intermediate size particles between  $0.1$  and  $10 \mu\text{m}$  radius.

## 3. MODEL INPUT ASSUMPTIONS

As with all model simulations, the results depend critically on assumed input values. Therefore, a range of values were tested for the most critical parameters. The critical parameters in this simulation include initial aerosol size distribution and concentration, humidity, and dispersion of the aerosol plume. Other parameters were chosen based on the few measurements and observations which have been made in large fires

Initial mass concentrations of smoke particles smaller than  $1 \mu\text{m}$  radius were assumed to range from  $5 \times 10^{-8}$  to  $5 \times 10^{-9}$   $\text{g}/\text{cm}^3$ . Three different size distributions were chosen which included a wide variety of aerosols larger than  $1 \mu\text{m}$  radius. The first size distribution is a single peak lognormal distribution with a geometric mean radius  $r_m$  of  $0.045 \mu\text{m}$  and geometric standard deviation ( $\sigma_g$ ) of 1.75. This distribution is based on laboratory fire aerosol size distributions measured by Patterson and McMahon (1984). The second is bimodal with a second lognormal peak at a supermicron geometric mean radius at  $5 \mu\text{m}$  with the same  $\sigma_g$  as the submicron particles. This size distribution was chosen to simulate the extreme case of a firestorm with surface winds high enough to suspend soil and burning material to an average mass concentration of  $5 \times 10^{-6}$   $\text{g}/\text{cm}^3$ . The third size distribution, shown in Fig. 1 (and probably the most applicable), is based on measurements in a prescribed forest slash burn fire (Radke et al., 1983). One can see from the volume distribution in Fig. 1 that the supermicron particles, though relatively few in number, dominate the aerosol volume

It was assumed that the density of the particles did not change with coagulation. This is probably valid for the generally oily particles usually associated with forest fire smoke. However, dry soot and flyash accumulate surface area faster than volume in the coagulation process (Mulholland et al., 1986). To partially account for this, a specific gravity of 1  $\text{g}/\text{cm}^3$  was assumed for both the lognormal and slash burn aerosol size distribution while a value of  $0.5 \text{g}/\text{cm}^3$  was assumed for the supermicron part of the two-peak lognormal size distribution.

After the plume stabilizes, the concentration will decrease due to vertical and horizontal diffusion. Horizontal diffusion was simulated using a scale dependent diffusion algorithm based on fire areas of 40 to 400  $\text{km}^2$  and an assumed energy dissipation rate of  $25 \text{cm}^2 \text{s}^{-3}$ . An energy dissipation rate of  $4000 \text{cm}^2 \text{s}^{-3}$  was assumed for the first hour of the fire plume

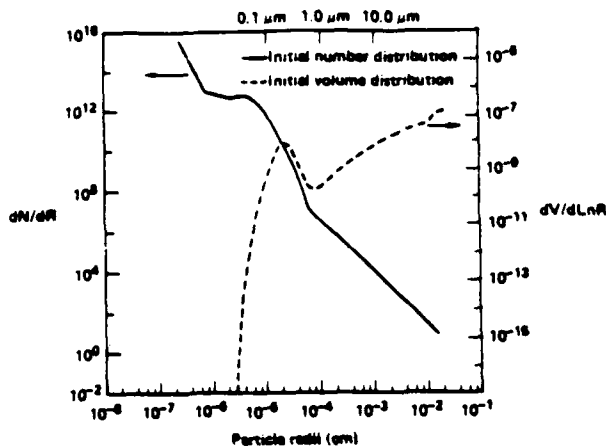


Fig. 1. Number and volume size distribution observed by Radke et al. (1983) in a prescribed forest slash burn.

Vertical diffusion was calculated using a hyperbolic tangent functional fit between 0 and 10 km to standard atmospheric vertical dispersion measurements.

An optical index-of-refraction of 1.5–0.05  $i$  was assumed, which is close to the values measured by Grams et al. (1972) over Boulder, Colorado for aerosols from forest fires in California (1.55–0.044  $i$ ). Porch et al. (1973) showed that a higher absorption coefficient would reduce the magnitude of anomalous extinction predicted from the model.

#### 4. RESULTS

The results of this study show the aerosol size distribution evolution for the three size distributions, the development of the vertical distribution of concentrations from the one dimensional model, and the resultant optical effects. These results are compared in context of the observations associated with the 1950 forest fire smoke from Canada.

Figure 2a shows the calculated evolution of the slash burn size distribution shown in Fig. 1. Figures 2b and 2c show the evolution of the single and double peak lognormal size distributions, respectively. These calculations assumed an initial submicron mass concentration of  $5 \times 10^{-8}$  g/cm<sup>3</sup>, a 160 km diameter fire area and no humidity effects or gas-to-particle conversion. These figures show that, although the initial shapes of the submicron part of the distribution are quite different, Brownian coagulation processes tend to collapse this part of the distribution to a similar shape in the concentrated fire plume in the first hour. There is a small difference in the small particle sizes between 0.1 and 1  $\mu$ m for the double peak lognormal size distribution. This is because of turbulent coagulation interaction between these sizes and the supermicron particles. Although these differences appear small in the size distribution, the optical extinction effect can be as high as a factor of two in the early plume optical depths (Porch et al., 1986). The supermicron distributions remain quite different with only a slight tendency for differential settling out of the 2 km aerosol layer to smooth out major differences at the largest sizes.

Figure 3 shows how the vertical distribution of aerosols of 0.1, 1 and 2.5  $\mu$ m radius evolve in the one dimensional model for the prescribed burn size distribution with an initial concentration of  $5 \times 10^{-8}$  g cm<sup>3</sup> and a fire diameter of 160 km. This

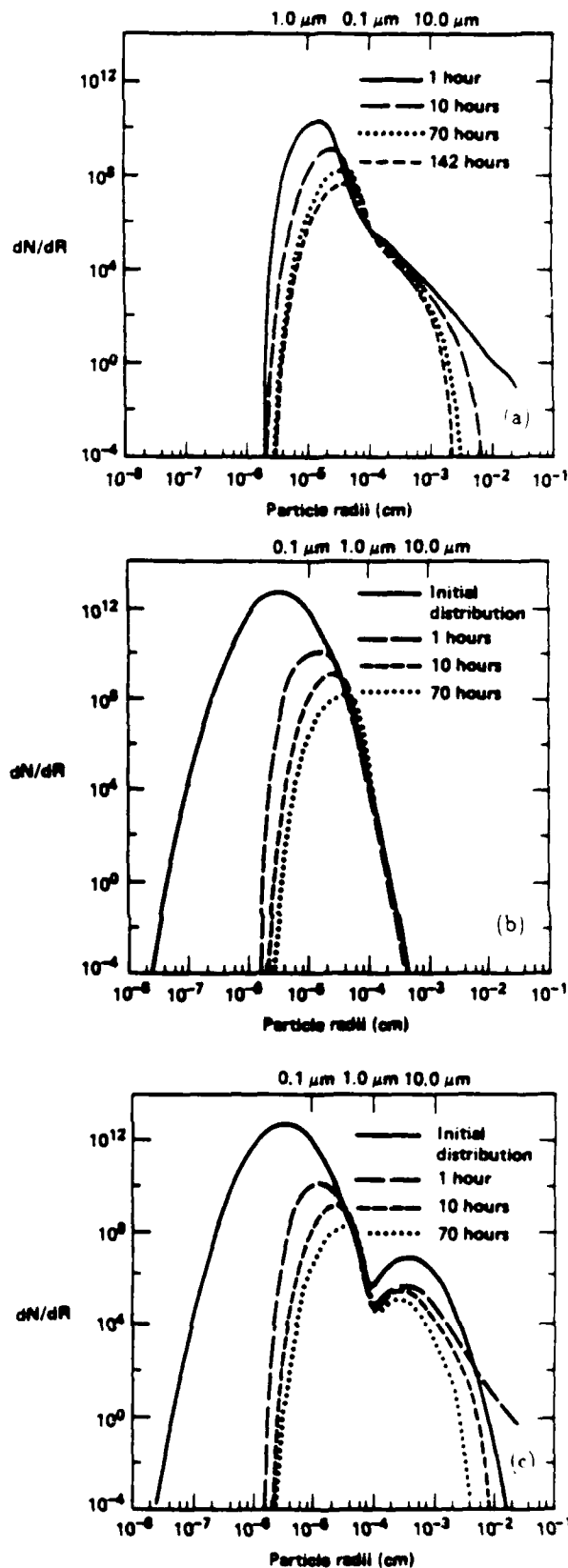


Fig. 2. Size distribution evolution using coagulation and dilution assumptions described in text (a) for the prescribed burn size distribution in Fig. 1. (b) for a single peak lognormal distribution, and (c) a two peak distribution including high concentrations of supermicron aerosols.

figure shows that while the largest particles diffuse and settle, the 1  $\mu\text{m}$  particles actually increase in number as the 0.1  $\mu\text{m}$  and larger particles coagulate.

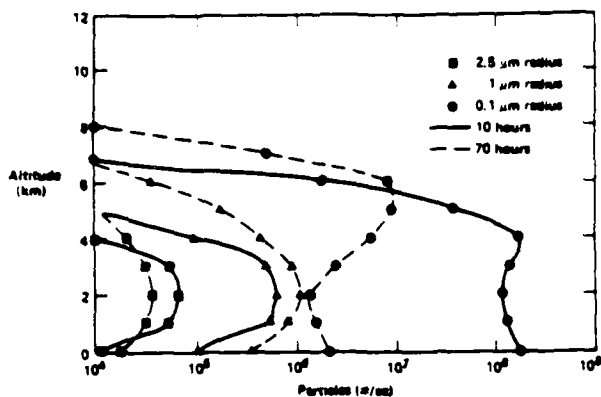


Fig. 3. The vertical concentration distribution for the prescribed burn aerosol size distribution (Fig. 2a) after 10 and 70 hours for three particle size distributions.

The optical depths for a 1 km layer between 3 and 4 km using the prescribed burn size distribution and initial concentrations of  $5 \times 10^{-9}$  and  $5 \times 10^{-8}$  g/cm<sup>3</sup> have been calculated. High humidity effects are not included in these calculations. Comparison of the optical effects using these calculations for the evolution of the two initial submicron concentrations show that, while anomalous extinction takes hours to days to develop, whether it develops at all depends critically on the initial submicron aerosol concentration in the fire. The length of time needed for anomalous extinction to appear is a function of the size of the fire as it affects the horizontal dispersion. Figure 4 shows the development of  $\alpha$  with time for the three different size distributions for a 160 km fire. This figure shows that the number of large particles in the distribution is not nearly as important as the submicron concentration. This is because supermicron particles scatter light with very little  $\lambda$  dependence (this is why clouds are white). This observation extends the interpretation given in an earlier paper Porch et al., 1973). The theoretical studies of aerosol characteristics in Porch et al. (1973) associated with anomalous extinction assumed a single peak lognormal distribution and showed that a nearly monodisperse aerosol size distribution closely peaked to 0.5  $\mu\text{m}$  radius is required. Here we show that only a sharp falloff of particle sizes smaller than 0.5  $\mu\text{m}$  is required, which is similar for all three distributions. The larger particle sizes have relatively little effect on  $\alpha$ , however, their neutral contribution to  $\tau_{\text{ext}}$  may actually help in overcoming the  $\lambda^{-4}$  dependence of Rayleigh scattering. These calculations have not included cloud or humidity effects. Capping cloud and cloud encounter effects have been tested with the model. We found that if humidity hysteresis is assumed (i.e., particles dry to a size larger than their original size before encountering saturated air) humidity effects can increase the possibility of anomalous extinction even for lower initial aerosol concentrations in the fire ( $5 \times 10^{-9}$  g/cm<sup>3</sup>).

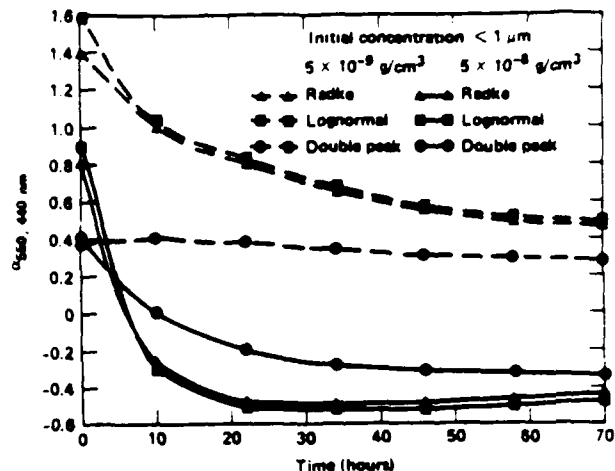


Fig. 4. The extinction efficiency factor assumed for the smoke particles.

## 5. EXPERIMENTAL PLUME DYNAMICS STUDY

It is difficult for a hydrodynamic microphysical model to treat all aspects of plume rise, humidity, turbulence and coagulation up to several kilometers and also contain grid sizes small enough to properly model the surface winds. The surface wind speeds and depth of the enhanced wind layer feeding the fire are important in determining the supermicron aerosol concentration generated by wind and to some extent the shape of the plume isoconcentration contours.

An experiment was conducted during the 45 minute jet fuel fire at Sandia National Laboratory (Fig. 5) in 1986 to provide data to test surface layer wind predictions in numerical models. This experiment measured the surface wind convergence using optical cross-wind sensors in a triangular array surrounding the fire (Fig. 6). The cross-wind sensors determine the component of the wind perpendicular to the optical path between the transmitter and receiver. The wind convergence is determined by summing the wind entering the triangle, multiplying by the length of the perimeter of the triangle and dividing by the enclosed area. This provides a spatially averaged number which is relatively independent of proximity to the fire (which is not the case with a single anemometer tower). This is more useful for model testing. Figure 7 shows the results of this measurement for the Sandia pool fire. The maximum convergence compares very closely with a jet fuel fire conducted at Dugway, Utah (convergence  $\sim 0.1$  1/s) and is about a factor of three smaller than estimates of the convergence in the Meteoron large area oil burner fires described by Bence et al. (1986). The development of the convergence with time differed between the Sandia and the Dugway fire. The Dugway fire showed convergence within minutes of the start of the fire, whereas the Sandia fire measurements took about 15 minutes to begin to show appreciable convergence. The difference is probably due to the fact that the region surrounding the Dugway fire was extremely flat while the terrain relief is greater at the Sandia fire (Fig. 6). This means the effective height of the optical paths in the Sandia case were higher than the 1.5 m in the Dugway case. It also shows that initially the convergence zone is quite shallow for a pool fire and grows deeper as the air and the ground radiatively heat from the fire.



Fig. 5. Photograph of Sandia jet fuel fire plume January 1986.

## 6. CONCLUSIONS

This simulation of the general conditions associated with fires like the 1950 Canadian forest fires shows the critical importance of initial submicron aerosol concentrations and the area covered by the fire to the evolution of the wavelength dependence of extinction. The actual optical depths calculated in this analysis turn out to be similar in magnitude to the highest values reported in 1950. This is perhaps fortuitous as there is no way to include shear and three dimensional plume breakup in a one dimensional model. The fact that the actual fire lasted several days over such a wide area helped establish this unusual one-dimensionality. The initial size distribution assumed was found to have only a small effect on the wavelength dependence of extinction after 3 days of plume transport. However, fire capping cloud and near saturation humidity effects were found to be important. Convergence measurements at the Sandia jet fuel pool fire indicate that, though convergence values eventually grew to those associated with similar fires, the convergence zone feeding the fire initially grows from a depth only a few meters deep to a greater depth as the air and ground radiatively heat.

## ACKNOWLEDGEMENT

The authors would like to thank D. Gillette for his help with the model development, L. Edwards for help with the numerical analysis, and R. Fritz for providing the experimental information for the convergence measurements at Dugway.

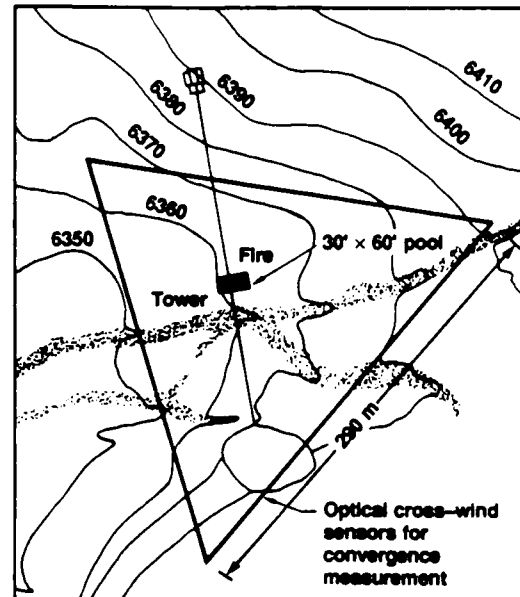


Fig. 6. Triangular array of cross-path wind sensors for convergence measurement of Sandia fire.

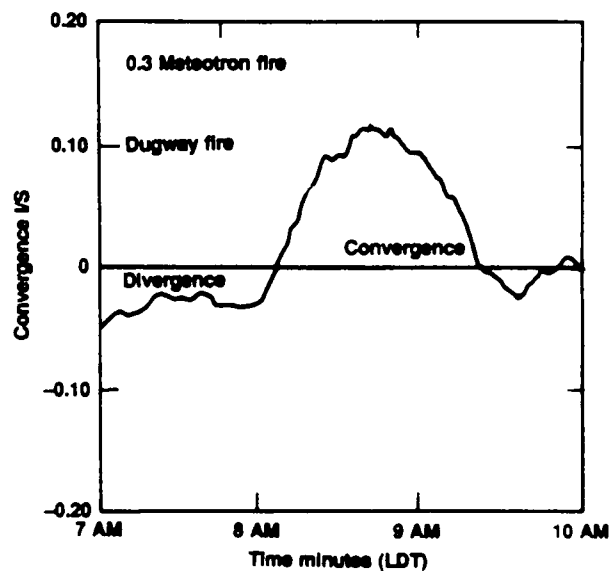


Fig. 7. Convergence as a function of time using a 20 minute smoothing triangular filter including comparisons with peak values of convergence from other fire tests.

This work was performed under the auspices of the U.S. Department of Energy by the Lawrence Livermore National Laboratory under contract No. W-7405-Eng-48.



## REFERENCES

- Bénech, B., Noilhan, J., Druilhet, A., Brustot, J. M. and C. Charpentier, (1986). Experimental study of an artificial thermal plume in the boundary layer. Part I. flow characteristics near the heat source. *J. Climate and Appl. Meteorol.*, 25, 418-437.
- E. M. Elsley, 1951. Alberta forest-fire smoke—24 Sept. 1950, *Weather*, January pp. 22-26.
- Grams, G. W., Blifford, I. H., Schuster, B. G. and J. J. Deluisi, 1972. Complex index of refraction of airborne fly ash determined by laser radar and collection of particles at 13 km. *J. Atmos. Sci.*, 29, pp.900-905.
- Mulholland, G. W., Mountain, R. D. and H. Baum, 1986. Simulation of aerosol agglomeration in the free molecular and continuum flow regimes, NBSIR86-3342, National Bureau of Standards, Gaithersburg, MD, 44p.
- Patterson, E. M. and L. C. McMahon, 1984. Absorption characteristics of forest fire particulate matter. *Atmos. Environ.*, 18, pp.2541-2552.
- Porch, W. M., Ensor, D. S., Charlson, R. J. and J. Heintzenberg, 1973. Blue Moon: is this a property of background aerosol? *Applied Optics* 12, pp.34-36.
- Porch, W. M., Penner, J. E., and D. A. Gillette, 1986. Parametric study of wind generated super- $\mu\text{m}$  particle effects in large fires, *Atmos. Environ.*, 20, pp.919-929.
- Radke, L., Lyons, J., Hegg, D., Hobbs, P., Sandberg, D. and D. Ward, 1983. Airborne monitoring and smoke characterization of prescribed fires on forest lands in Western Washington and Oregon, EPA 600/X-83-047, Environmental Protection Agency, Wash. D.C., 122p.
- Walton, J. J., 1973. Scale-dependent diffusion, *J. Appl. Meteorol.*, 12, pp.547-549.

## THE EFFECTS OF TURBULENCE AND SWIRL ON PLUME RISE FROM LARGE-AREA FIRES

Steve Marcus  
Russell Gaj  
Martin Rosenblatt

California Research and Technology, Inc.

Turbulence can retard plume rise by diluting the buoyancy and momentum of the rising fluid, and swirl can affect plume rise by influencing the large-scale dynamics and/or turbulence associated with the plume. In order to investigate these phenomena, a version of the axisymmetric DICE code incorporating both parameterized turbulence and a tangential velocity component has been developed.

The turbulence sub-model was validated by simulating the plume from an experimental fire conducted at the Metatron research facility in France on Oct. 23, 1973. Since the plume in that experiment penetrated a considerable distance into an overlying inversion layer, the success of that simulation indicates that the DICE code is capable of correctly simulating the penetration of a firestorm plume into the stable layers of the stratosphere.

Several simulations of a 10-km radius firestorm were carried out, in order to assess the effects of turbulence on plume rise from large-area fires. In the baseline case the plume penetrated well into the stratosphere, reaching a maximum altitude of 22 km. When the mixing lengths were decreased by a factor of 4 from the baseline case, the maximum plume height increased by 12 km; if the mixing lengths are held to their baseline values in the lowest kilometer of the grid; however, the enhancement in plume height is only 4 km. These results show that the entrainment of cooler air into the boundary layer is the primary mechanism by which turbulence retards plume rise from large-area fires.

One case incorporating the tangential velocity component has been run, assuming an initial swirl velocity field which reaches a maximum of 10 m/sec at the edge of the fire. Swirl velocities in excess of 200 m/sec were generated in the interior of the fire after the inflow layer fully developed, owing to the approximate conservation of angular momentum in the model boundary layer. While this run did not account for the effects of swirl on turbulence, the interaction of swirl with large-scale dynamics caused the plume stabilization height to decrease by 3 km from the baseline case. It is possible that swirl may act to suppress turbulence, as a stable density stratification does. The results of this study have shown that in order to dramatically enhance plume rise from large-area fires, the swirl velocity field must effectively suppress the buoyancy-generated turbulence responsible for the entrainment of ambient air into the boundary layer.

# **CLOUDS FORMED BY LARGE AREA FIRES**

**BY**

**K. E. HEIKES, L. M. RANSOHOFF,  
AND R. D. SMALL**

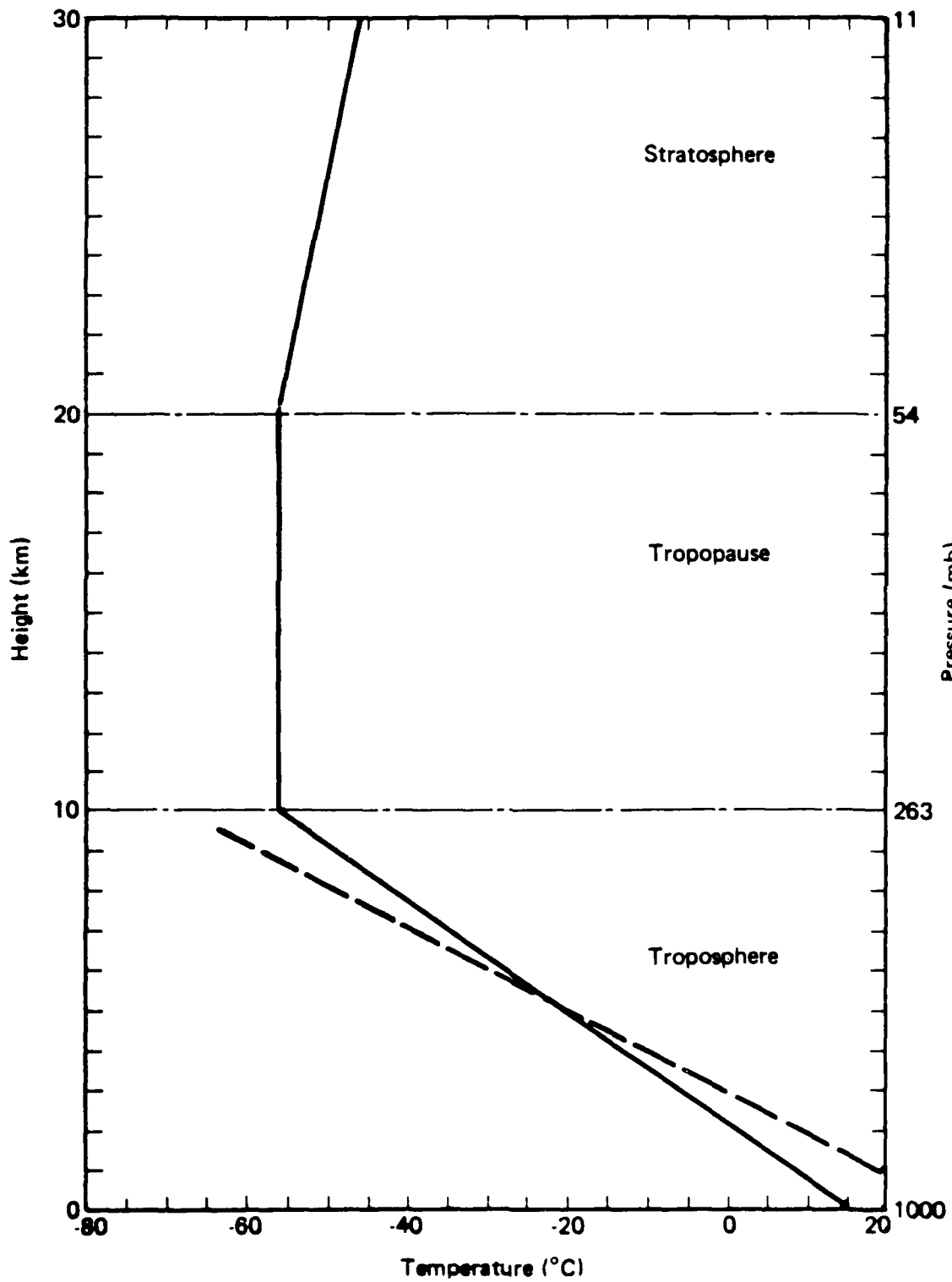
**PACIFIC-SIERRA RESEARCH CORPORATION**  
A SUBSIDIARY OF EATON CORPORATION

**12340 SANTA MONICA BOULEVARD  
LOS ANGELES, CALIFORNIA**

# INTRODUCTION

- **MOTIVATION: DETERMINE HEIGHT OF SMOKE INJECTION**
  
- **LARGE SMOKE CLOUD DIFFERS FROM CLASSICAL PLUME**
  - **LITTLE LOSS OF BUOYANCY DUE TO ENTRAINMENT**
  - **SMOKE SPREADING DUE TO STRATIFICATION**
  
- **INPUT PARAMETERS**
  - **FIRE SIZE: 0(100 km<sup>2</sup>)**
  - **HEATING RATE: DEPENDS ON FUEL LOADING AND LENGTH OF BURN**
  
- **ATMOSPHERIC STRATIFICATION AND MOISTURE**
  - **STABLE LAPSE RATE INHIBITS PLUME RISE**
  - **LATENT HEATING/COOLING AFFECTS BUOYANCY**
  - **FIREWINDS INDUCT LOW-LEVEL MOISTURE**

# U.S. STANDARD ATMOSPHERE, 1962



# PHOTOS

**CHAPLEAU, ONTARIO**

**(3 AUGUST 1985)**

**LODI CANYON, CALIFORNIA**

**(12 DECEMBER 1986)**

**ALASKA WILDFIRE**

**(8 JULY 1972)**

# MODEL DESCRIPTION

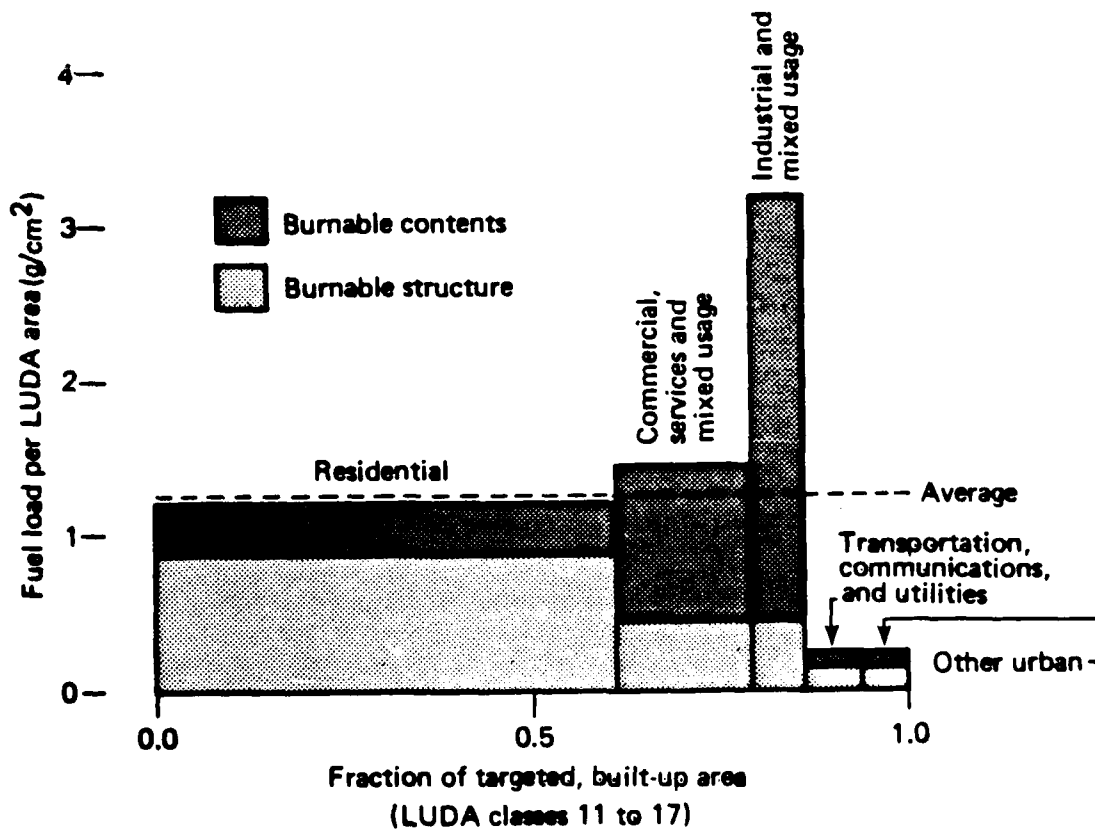
- **NUMERICAL TECHNIQUE**
  - LAGRANGIAN/EULERIAN SOLUTION
  - VARIABLE ZONING, 56 x 56 GRID
  - MODEL DOMAIN: 30 km (HEIGHT) x 70 km (RADIUS)
  
- **GOVERNING EQUATIONS**
  - COMPRESSIBLE, TIME DEPENDENT
  - TWO-DIMENSIONAL (AXISYMMETRIC, ZERO AZIMUTHAL VELOCITY)
  - EDDY VISCOSITY AND CONDUCTIVITY
  
- **INITIAL CONDITIONS**
  - QUIESCENT
  - PRESCRIBED TEMPERATURE
  
- **BOUNDARY CONDITIONS**
  - TOP: FREE-SLIP, ISOTHERMAL
  - BOTTOM: NO-SLIP, INSULATOR
  - CENTERLINE: FREE-SLIP, INSULATOR
  - OUTER RADIUS: FREE-SLIP, PRESCRIBED TEMPERATURE

# HEAT AND SMOKE SOURCE TERMS

- VOLUME HEATING NEAR GROUND
  - 5, 7, 10 km RADII
  - 1.00, 0.50, 0.25 kW/m<sup>3</sup>
  
- RADIATIVE COOLING
  
- SMOKE EMISSION PROPORTIONAL FIRE HEATING
  
- LATENT HEATING/COOLING DUE TO PHASE TRANSITIONS DEPENDING ON TEMPERATURE AND PRESSURE
  - CONDENSATION, EVAPORATION
  - MELTING, FREEZING
  - SUBLIMATION
  
- PRECIPITATION

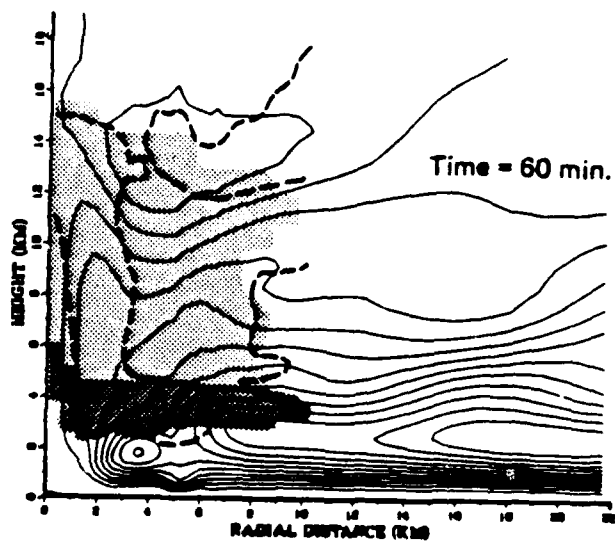
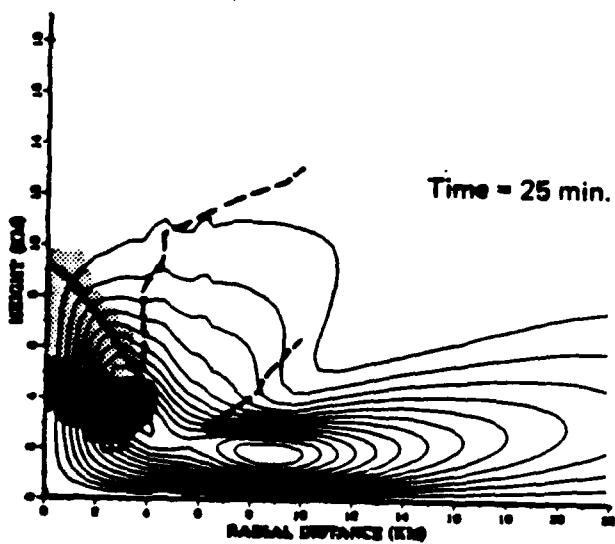
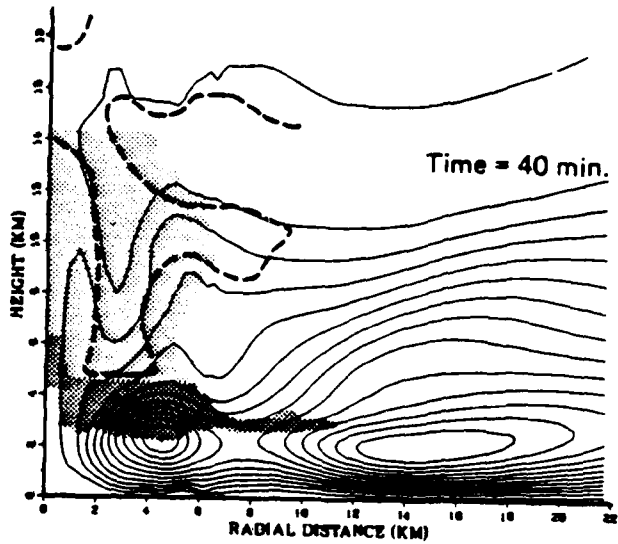
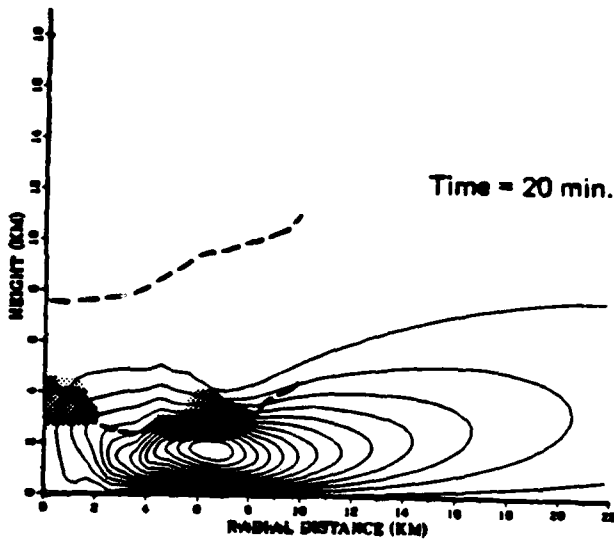
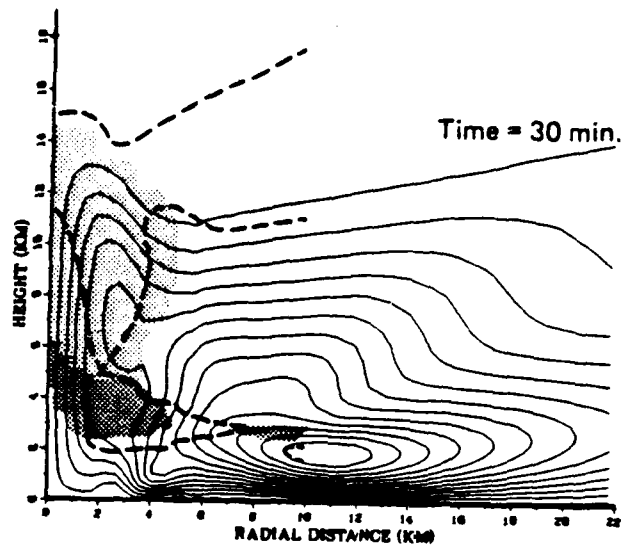
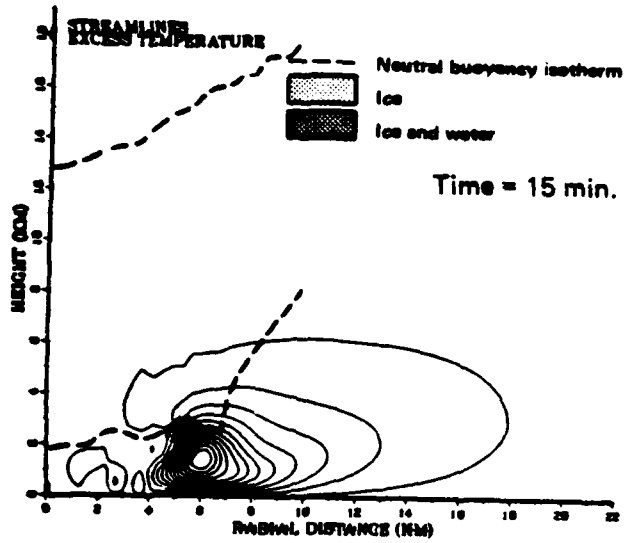


# TARGET AREA BUILDING CLASSES AND FUEL LOADINGS



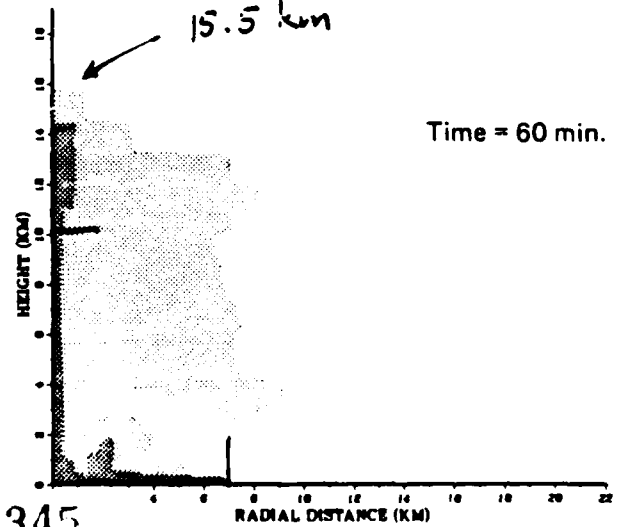
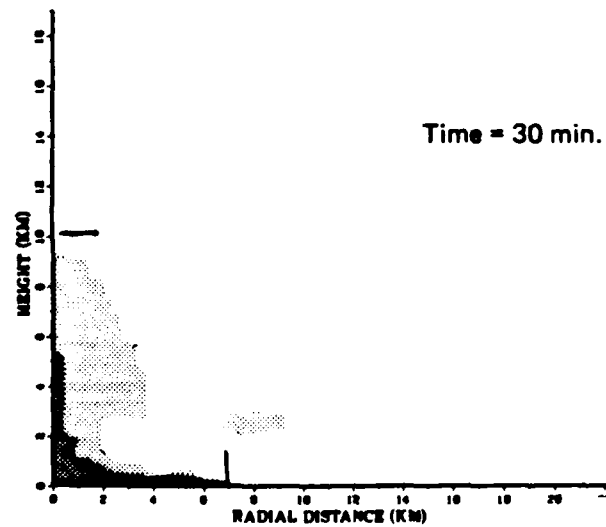
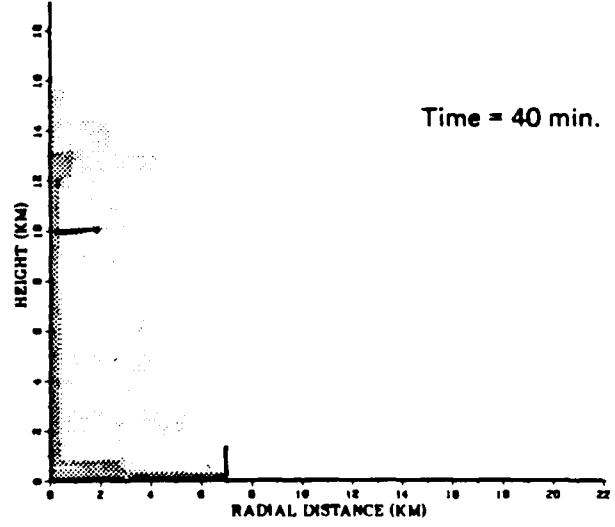
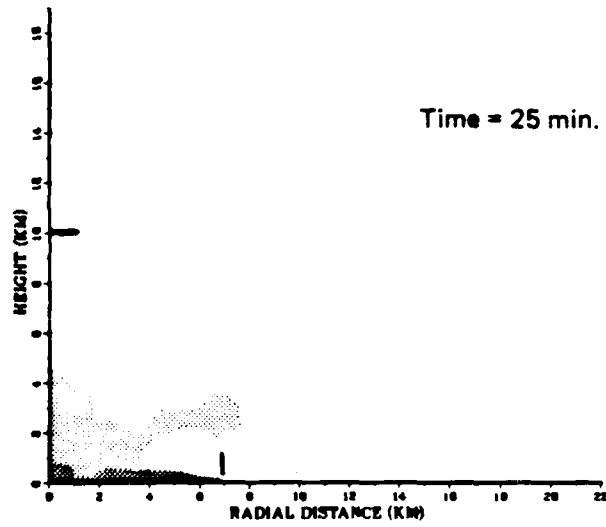
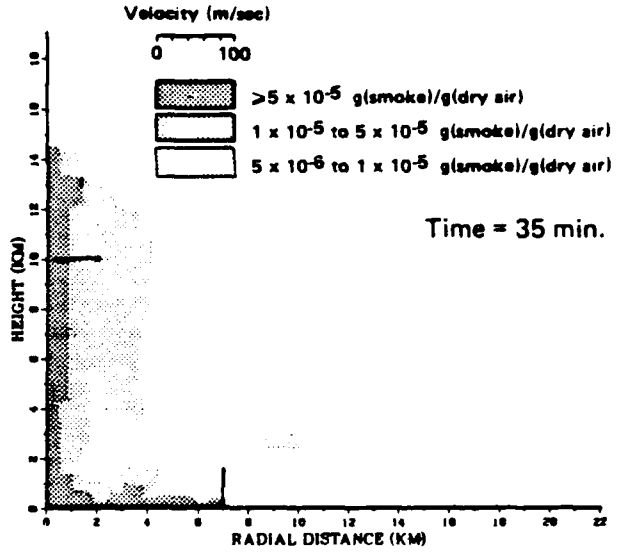
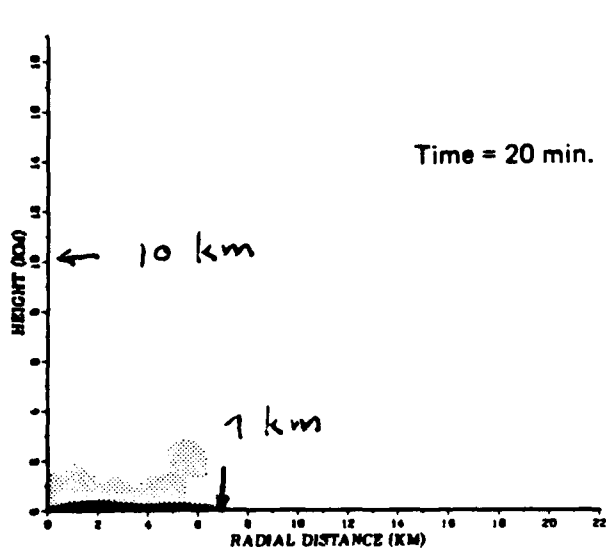
# MOISTURE CLOUD SIMULATION

(HEATING RATE =  $0.5 \text{ kW/m}^3$ , FIRE RADIUS = 7 m)



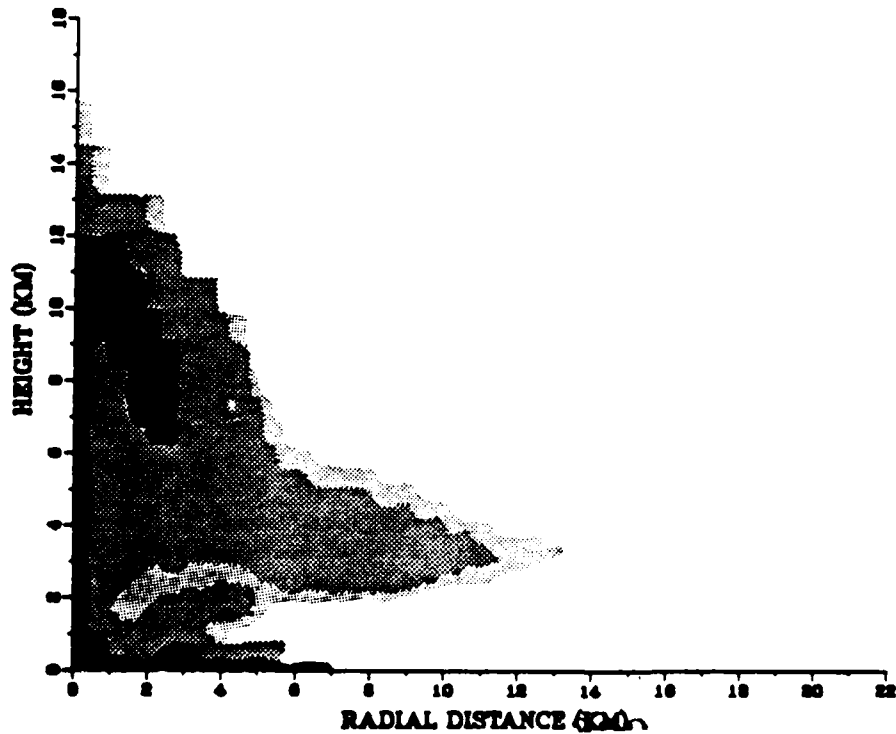
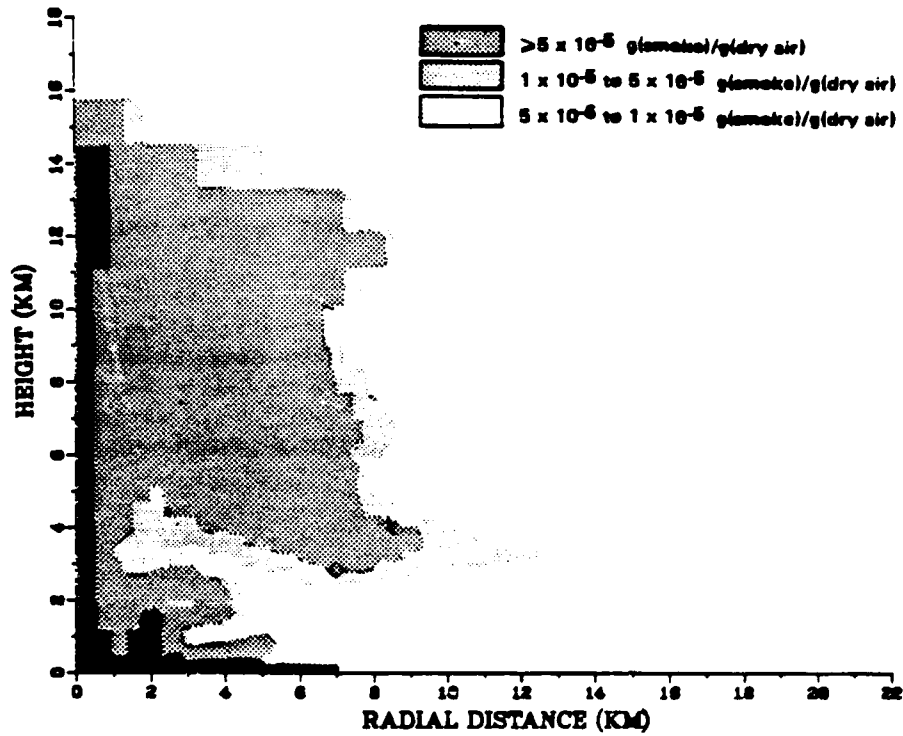
# SMOKE CLOUD SIMULATION

(HEATING RATE =  $0.5 \text{ kW/m}^3$ , FIRE RADIUS = 7 km)



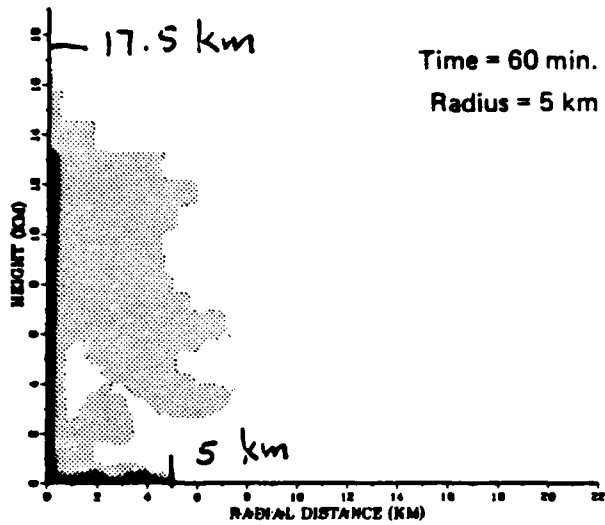
# MOIST/DRY COMPARISON

(HEATING RATE =  $0.5 \text{ kW/m}^3$ , FIRE RADIUS = 7 km)

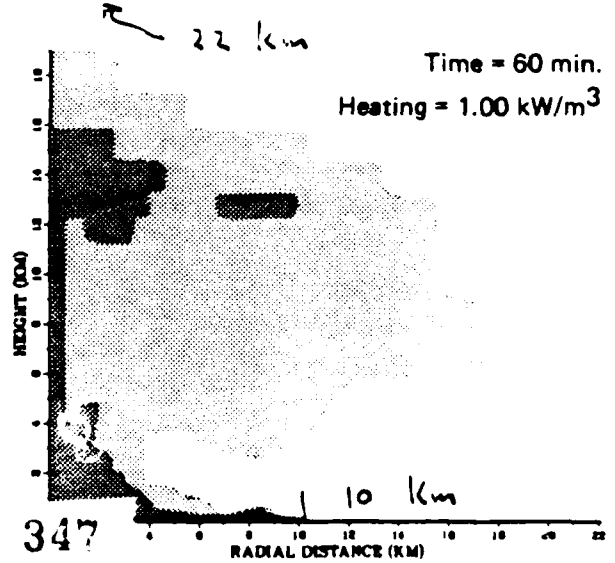
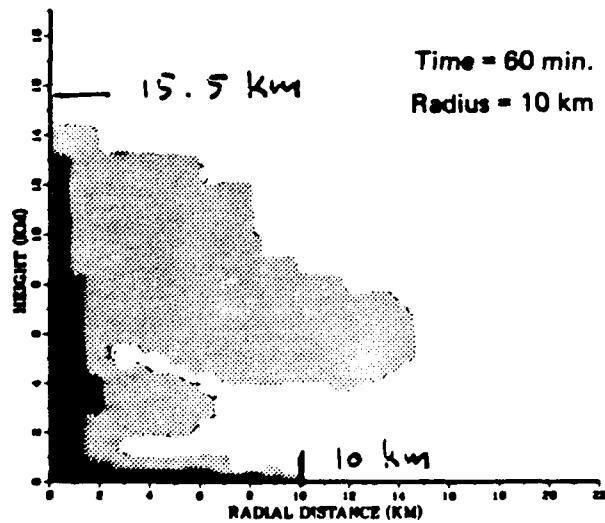
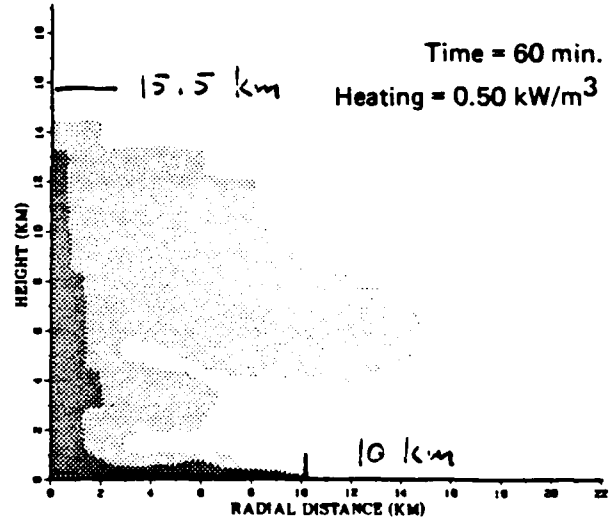
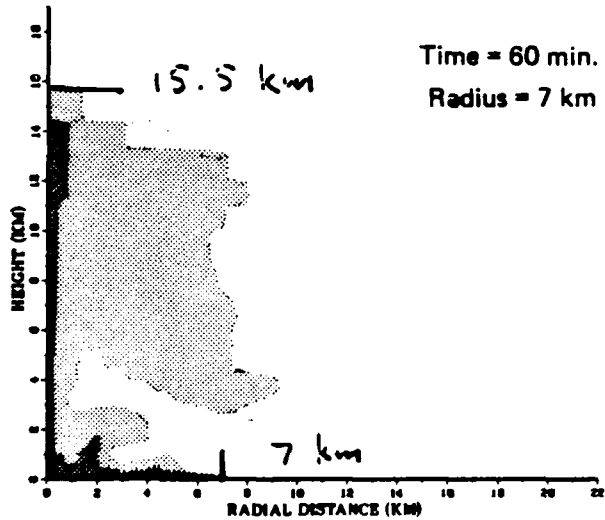
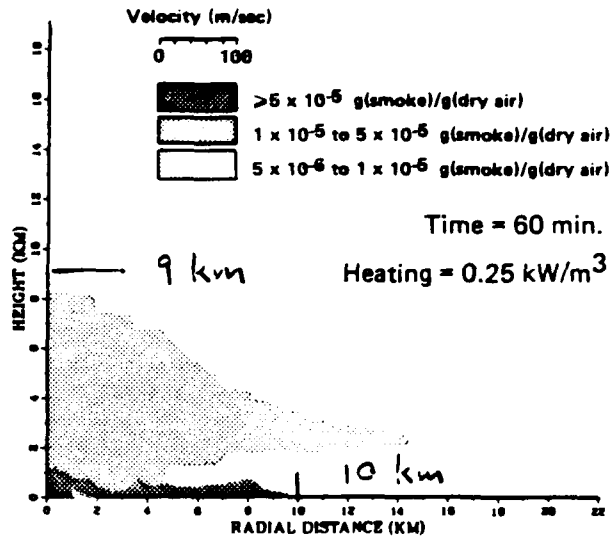


# SMOKE CLOUD SIMULATIONS

**VARIABLE FIRE RADIUS**  
(Heating rate =  $0.5 \text{ kW/m}^3$ )



**VARIABLE HEATING RATE**  
(Fire radius = 10 km)



# CONCLUSIONS

1. HEATING RATE, NOT TOTAL HEAT OUTPUT, DETERMINES PLUME HEIGHT
2. ATMOSPHERIC MOISTURE IMPORTANT TO PLUME GROWTH
3. SMOKE REMAINS NEAR FIRE IN THE ABSENCE OF MEAN WIND
4. SEASONAL AND LATITUDINAL ATMOSPHERIC VARIATIONS IMPORTANT
5. PRECIPITATION SCAVENGING LIKELY TO REDUCE SMOKE INJECTION

# SMOKE INJECTION INTO THE ATMOSPHERE FROM LARGE AREA FIRES

D. P. Bacon, R. A. Sarma

Science Applications International Corporation  
1710 Goodridge Dr., McLean, VA 22102

F. H. Proctor

MESO, Inc  
28 Research Dr.  
Hampton, Va 23666

SAIC-86/1922  
October, 1986

Updated March, 1987

## ABSTRACT

For the past four years, a considerable amount of research has been devoted to the concept of "nuclear winter". This paper is an attempt to put one aspect of this problem into context: the amount of smoke injected into the atmosphere and the variability of this amount with the initial conditions. The goal was to bound the problem of smoke injection in order to provide modellers of other parts of the nuclear winter scenario with guidance for future work. We have determined that the effect of spatial and temporal variations in the fire source have little effect on the final vertical distribution of the smoke produced by large area fires, but that the ambient atmospheric conditions have a great deal of impact on the final distribution. For cases in which the ambient atmosphere is highly stable, the smoke can only form a stratus layer; in cases in which the atmosphere is unstable, the release of latent heat of condensation and fusion lifts the smoke plume to the tropopause. In this latter case, however, the amount of water lofted is of the order of 100 times the amount of smoke. This water allows scavenging processes to remove or alter the properties of the smoke. Depending on assumptions regarding smoke properties and the meaning of "scavenged", up to 95 % of the smoke produced can be scavenged. Even without scavenging the smoke, the presence of this much water could lead to an increased albedo of the cloud which would partially cancel the atmospheric heating caused by the smoke. These latter effects are not part of the current study, but should be investigated using a global circulation model.

## 1. Introduction

Ever since the December, 1983 paper of Turco, et. al. [Turco, et. al., referred hereafter as TTAPS] there has been considerable speculation on the possibility of the occurrence of a "nuclear winter" following a large-scale nuclear exchange. Considering that the hypothesis is not amenable to experimental verification, the only possible route to the verification of the hypothesis is via comparison of various computer simulations. As our knowledge of nuclear weapon effects and atmospheric processes improves, the realism of the simulations should increase.

Analysing the nuclear winter scenario in order to build up a "decision tree" for the determination of the most sensible route to investigate its various assumptions and their influence on the final results, we readily identify the following necessary areas of uncertainty: (1) the nuclear war scenario which includes the number of weapons, the location and type of target including the

combustible inventory nearby, the yield and height of burst of each weapon, and the time of year of the attack (which has a considerable effect on the fire radius in some climates); (2) the fire initiation and spread process and the chemistry of large area fires (which impacts the amount of smoke production) [cf. Palmer, 1981]; (3) the fire plume dynamics which transports the smoke from the fire region into the upper troposphere and lower stratosphere and the prompt scavenging processes which transport the smoke back to lower altitudes or remove it entirely [cf. Small, et. al., 1984, Cotton, 1985, and Penner, et. al., 1986]; (4) and the long-term atmospheric chemistry and transport of the smoke in the meso-scale and global-scale atmosphere including the effects of solar irradiation absorbed by the smoke [cf. Malone, et. al., 1986 and Covey, et. al., 1984]. The TTAPS team made estimates of the factors in areas (1)-(3) and focussed its study on (4). In this paper, we would like to discuss only the third area given above; however, we hope that

by investigating the sensitivity of the plume dynamics to various initial conditions (which are the purview of area (2) above) we may bound the problem to be expected by those performing meso-scale and global-scale modeling.

In this paper we shall first focus on the role of the spatial distribution and temporal history of large area fires on the plume dynamics and show that for the conditions of interest for "nuclear winter" these parameters are not important to first-order. We shall then show the effect of the ambient meteorology on the plume dynamics and show that the vertical distribution of temperature and humidity is of prime importance in determining the plume dynamics: without moisture and its concomitant release of latent heat, the smoke plume cannot penetrate the tropopause and enter the stratosphere; with moisture present, scavenging processes take effect that reduce the impact of the smoke injection by both reducing the smoke injected into the stratosphere as well as by injecting water into the stratosphere along with the smoke, which may shorten the smoke residence time.

## 2. The Model

The simulations reported in this paper were performed with a modified version of the two-dimensional axisymmetric Terminal Area Simulation System (TASS). This was originally developed by one of the authors (FHP) as part of his doctoral research [Proctor, 1982] into tornado development and which has since been extensively modified for various other studies [Proctor, 1986, and 1987a]. The three-dimensional version of TASS has been validated against five case studies of cumulonimbus convection - ranging from short-lived single-cell convection to long-lasting super-cell convection [Proctor, 1987b]. For this study, TASS was modified to allow for a surface heat source to be specified as a function of radius and time. The amount of smoke produced was determined by assuming that the predominant fuel was hardwood with a thermal release upon combustion of approximately 20 MJ/kg and a 2 % smoke emission factor; this gives a smoke release of  $10^{-3}$  kg/MJ of heat released.

The basic model solves ten prognostic equations: two equations for momentum, one each for the pressure deviations and the potential temperature (from which the density and temperature are diagnosed), and six coupled equations for the various water components (vapor, non-precipitating cloud droplets and ice crystals, rain, snow, and hail). The model has been modified to allow for the transport of multiple classes of massless tracer particles (smoke) and massive aerosols (dust) and solves an additional equation for each class. For the simulations reported here, we kept track of 4 classes of smoke: (1) hydrophylic which is scavengable; (2) hydrophobic which is not; (3) smoke encased in cloud droplets; and

(4) smoke which was once in a drop or droplet that evaporated. We are currently adding the capability to track the smoke transport via precipitation processes.

The multiple classes of smoke are intended to allow us to consider the smoke as possessing different properties as time passes and the smoke is processed by its interaction with moisture. For example, the smoke is introduced in two classes hydrophylic and hydrophobic; these can be thought of as dry and oily smoke or nucleatable and non-nucleatable. The hydrophobic smoke is allowed to exponentially decay into nucleatable smoke with an e-folding time of  $\tau$ ; this process allows for secondary combustion or slow oxidation processes to be considered. Finally smoke which has gone through a condensation/evaporation cycle is segregated from raw smoke in order to allow for it to be considered differently. We make these simple models knowing their limitations in the hope of determining whether the final result is sensitive to the details of the models.

## 3. The Simulations

For these simulations, the TASS model was run with a grid resolution of 500 m and a computational domain of 30 km radius by 30 km vertically. The simulations reported in this paper can be divided into several series: (1) a study of the sensitivity of the smoke lofting to the details of the heat source spatial distribution or time history; (2) a study of the sensitivity of the smoke lofting to the ambient atmospheric conditions at the time of the fire; (3) a study of the effect of the total fire heat input (MJ) on the smoke lofting; and (4) a study of the role of scavenging on the amount and type of smoke which is still resident in the atmosphere after a few hours. We would like to discuss each of these series in that order.

It is important to note at this time that the simulations reported cannot be compared in *exact detail* from one to the other due to the interaction of the smoke plume with the ambient atmosphere; cases which lead to condensation earlier release the latent heat of the ambient moisture earlier and hence to a higher cloud at that time. This disagreement is one primarily of phase and so we will be comparing the simulations in terms of parameters which are not time-dependent such as the maximum altitude which the plume reached or the stabilization altitude of the cloud.

### 3.1 Fire Source Study

#### 3.1.1 Spatial Distribution

The first question we investigated was whether the fire plume would depend on the spatial and temporal details of the fire or whether the atmosphere would "integrate" over the fire with these details proving unimportant. To this end we studied several fires. The baseline fire had the spatial distribution shown in Fig. 1a - a



uniform  $50 \text{ kW/m}^2$  surface heat source out to 10 km radius. The second fire which we studied was an annular fire with a uniform  $78 \text{ kW/m}^2$  fire intensity between 6 and 10 km radius (see Fig. 1b). The third fire was a modification of the second which reduced the fire intensity in the annulus by 5 % and put a heat source of  $63 \text{ kW/m}^2$  over the center 2 km radius (Fig. 1c). All three fires had the same total power integrated over the surface - 16 TW. The time history of the fire for these cases consisted of a 45 min linear ramp, a 60 min plateau, and a 45 min linear decay back to 0 (See Fig. 2a). Thus, each of these fires yielded the same total energy input into the system: approximately  $10^{17} \text{ J}$ .

The ambient conditions for temperature and humidity used for this sequence of runs were those of an unstable atmosphere - the 0000Z sounding on April 10, 1979 at Lake Charles, LA (Fig. 3). This sounding has a moist surface layer which extends to 2 km above the ground and a tropopause of 14 km. Between 6 and 7.5 km AGL there is another moist region. The lifted index of the sounding is -8 degrees Celsius.

Figure 4 shows the baseline fire smoke plume at selected times. The smoke concentration contours are overlaid on a contour plot of the vertical velocity. The outer smoke contour represents the  $10^{-10} \text{ g/cm}^3$  smoke concentration contour, the middle contour is  $10^{-9} \text{ g/cm}^3$ , and the inner contour is  $10^{-8} \text{ g/cm}^3$  ( $1 \text{ g/cm}^3 = 10^3 \text{ kg/m}^3$ ). At early time a solenoidal circulation forms at the edge of the fire causing the smoke plume to rise more at the edge of the fire than at the center. Once a sufficient inflow of surface air is established, the center region can rise, and does so with great rapidity due to the heat energy accumulated during the early phase (See Fig. 4b). The low-level convergence of humid air caused by the fire leads to development of a towering cumulonimbus via the release of latent heat. Figure 4c shows the plume at 50 min and indicates the effect that the latent heat release has on the plume dynamics. Between 40 and 50 min, roughly  $4 \times 10^{16} \text{ J}$  is released through the latent heat of condensation and freezing; this is approximately 4 times the sensible heat release of the fire during this period. (See Fig. 5 which compares the latent heat release and the energy output of the fire. Latent heat release is more effective than surface heating as it occurs right in the cloud without suffering the dilution from mixing that an equivalent amount of sensible heat would encounter from the surface up to the altitude of the cloud.) The tower reaches an altitude of 23 km AGL and therefore carries both smoke and moisture to stratospheric altitudes. The amount of moisture at the top of the cloud is roughly 2-3 orders of magnitude greater than the amount of smoke; hence the tropospheric/stratospheric mixing which takes place at the top of the cloud entrains both smoke and moisture into

the stratosphere.

At 50 min the plume, which has overshoot the tropopause, has reached its maximum altitude; the system then relaxes to a quasi-steady state at 70 min, which is the situation shown in Fig. 4d. The system is now driven primarily by the convection *triggered* but *not directly driven* by the fire; As further convection takes place, the anvil spreads out radially. As long as the fire exists at all, the fire induced convergence will inhibit precipitation induced divergence at the surface. Figure 4e shows the plume just as the surface heat source ends at 150 min. Once the surface heat source is removed, the precipitation induced downdraft strengthens and upon reaching the ground creates a surface radial outflow which transports the low-level smoke with it. This is shown in the final frame of this series, Fig. 4f which shows the plume at 180 min (30 min after the fire ended).

Against this baseline case, we would now like to compare two other spatial distributions of the fire and two other time histories. Figure 6 shows the smoke concentration contours at the same times as Fig. 4 for the annular fire described above. The first difference to note is that the annular plume initially rises faster than the baseline case due to the higher heat release at the surface ( $50 \text{ v. } 78 \text{ kW/m}^2$ ) and since the solenoidal circulations developed both inside and outside the annulus tend to drive the annulus higher. After a very short while, however, the plume moves radially inward off the surface heat source due to the low level convergence leading to the formation of a second thermal over the fire region. The additional entrainment caused by the creation of two distinct thermal plumes reduces the maximum altitude which the smoke can attain. This is seen in Fig. 6d which shows the plume at 80 min in what we earlier referred to as a quasi-steady-state. This plume however, is neither as strong as the baseline case nor co-located with the heat source and therefore the precipitation comes out of the system much earlier commencing at about 30 min. By 130 min most of the precipitation has fallen out of the cloud; this should be compared with the baseline case in which the precipitation did not reach the surface until around 50 min and continued until approximately 3 hours. The earlier commencement of precipitation induced a low level divergence earlier than in the baseline case and caused more radial transport of the smoke.

The third case that was investigated is one in which the fire intensity over the annulus just described was reduced by 5 percent and a uniform heat source of  $63 \text{ kW/m}^2$  was added over a two kilometer radius at the center. Note that the overall heat output rate remains same as the previous two cases. In this case also, the plume rises rapidly in the beginning compared to the baseline case. Figure 7a shows the plume at 20 min. Once the low

level convergence is set up, the thermal above the annular fire starts moving towards the axis and the central thermal intensifies. This is shown in Fig. 7b, in which the base of the annular thermal is seen merging with the thermal on axis at 40 min. By 60 min the central thermal has become predominant and a new bubble is seen forming over the annulus (Fig. 7c). The plume has reached an altitude of 21 km. Comparing with Fig. 6c, it is evident that this plume is convectively more intense than the annular case which reached an altitude of only 15 km at this time. In fact this modified annular case and the baseline case exhibit the same cloud top heights at this time. Figure 7d shows the plume at 80 min. As in the previous two cases the plume can now be thought of as in a quasi-steady-state, and the convergence set up by the fire helps counteract the divergence caused by precipitation which otherwise would have weakened the convective circulation significantly. Figures 7e and 7f show the plume at 150 and 180 min respectively. At both these times the plumes are higher than the annulus case. The cloud top heights for the modified annulus case were only slightly less than the baseline case at all times after the plumes have reached their maximum altitudes, but the former showed more lateral spreading of the smoke at lower levels after about 90 min.

Our conclusion from the three cases discussed above is that the surface heat distribution is not as important as the total heat input as long as special cases (such as the perfect annulus) are avoided. Since these special cases are unlikely in nuclear winter scenarios, this is not an issue. The atmosphere will effectively integrate over the heat source and, once the thermal column is established, the latent heat released by the condensation and freezing of ambient moisture will be the principal driver of the plume dynamics. Figure 8 shows this integral effect by comparing the integrated mass above a given altitude for the different simulations. Note that in all cases, the smoke mass stabilised in the vicinity of the tropopause. (Note also that the addition of an axial heat source brought the annular case closer to the baseline case as expected.) The amount of smoke v. altitude is compared with the amount of water which is shown in the figure using a scale 100 times bigger; approximately 100 times more moisture is lofted than smoke.

### 3.1.2. Temporal Distribution

While the plume dynamics only depends weakly on the spatial distribution of the surface heat source, the dependence on the time history is another matter. Two additional time histories were used for simulations with the baseline spatial distribution discussed above. These histories are shown in Figs. 2b-c: a 1-hour fire source which multiplied the maximum surface heat intensity by 2.33 and had a 15 min ramp, a 30 min plateau, and a

15 min decay; and a 1-hour fire source which multiplied the maximum surface heat intensity by 7 and had a very fast burn followed by a smoldering period which lasted 40 min. Figure 9 shows the evolution of the plume for the second temporal distribution (Fig. 2b). The plots at 10, 20, and 30 min indicate that while the fire may heat up rapidly, the atmospheric response lags the fire. Whereas in the baseline case, the plume reached its peak altitude just after the fire reached peak intensity, now the peak altitude is not reached until 15 min after the peak of the fire is attained (See Fig. 9c.) This is explained by looking at Fig. 10 which shows the latent heat release for this case. Note that the fire reaches its peak intensity (See Fig. 2.) at 15 min while the peak latent heat release (which dominates the fire after 20 min) lasts until 30 min. Another feature to note in Fig. 9 is that the end of the fire now results in the release of the suspended precipitation and the cessation of the convective activity. The fire ceases at 60 min now as opposed to 150 min in the baseline case and therefore less total moisture is processed by the cloud.

Figure 11 shows the results of the simulation with the fast burn/smoldering fire discussed above. The results agree with the discussion of the previous paragraph during the early phase of the fire; however, the precipitation comes out of the cloud only when the fire is totally shut down (60 min), not when the intensity drops (20 min). This is because even the small perturbation from the smoldering fire is enough to trigger the unstable sounding with the resulting convective updraft suspending the precipitation. Note that even though the peak heating rate of this case was 7 times that of the baseline case, the smoke plume stabilised at approximately the same altitude as in the baseline case. This is seen more clearly in Fig. 12 which shows the integrated mass plots for the three cases used in the temporal variation study. As in the spatial variation cases, the amount of water present is typically two orders of magnitude higher than the amount of smoke.

This series of simulations reinforces our earlier conclusion regarding the effect of spatial variations: the atmosphere is basically a large mechanical heat engine with a thermal and mechanical inertia which causes it to integrate small-scale perturbations. This is not to say that these spatial or temporal variations do not produce real effects in the plumes, rather these effects are small compared to the overall system. This difference will be rather strongly demonstrated in our next discussion which relates to the role of the ambient meteorology in plume dynamics.

## 3.2. Sensitivity to Meteorological Conditions

To understand the importance of the ambient mete-

orology on the plume dynamics we began with a replication of the baseline simulation *sans moisture*. This simulation is shown in Fig. 13 in tandem with the baseline case and indicates the effect that the latent heat release has on the plume. Without the moisture and its concomitant heat release, the only source of buoyancy is the sensible heat from the and the plume stabilizes some 10 km lower than with the moisture. Contrast this marked difference with the few kilometer differences noted in the spatial and temporal variation study. Clearly the dominant physical process driving the plume dynamics is the latent heat release; the question is the variability of the ambient conditions at a given site. This was the subject of another series of runs.

In keeping with our goal of bounding the problem, we performed simulations using three 1200Z soundings obtained at Bismarck, ND in 1974: February 5, October 3, and December 3. These soundings had tropopause heights of 8.0, 11.5, and 12.5 km, and lifted indices of 12, 10, and 24 degrees C, respectively. Figure 14 shows the results of these simulations. The difference in the smoke plumes in the December and October simulations is due to the differing stability of the ambient atmosphere; the former had a very stable sounding which resulted in the formation of an apparent stratus deck while the latter was reminiscent of our baseline case. The similarity of the December and February simulations in spite of the large difference in the ambient tropopause is due to the fact that the high stability results in a plume which never makes it to the tropopause. This is shown more clearly in the integrated mass plot, Fig. 14d.

The conclusion from the sounding sensitivity study is that unlike the spatial and temporal variation in the fire source term, the ambient atmospheric conditions have a great deal of impact on the plume dynamics and consequently on the stabilization altitude of the smoke. The ambient stability of the air mass has a very strong effect in all cases while, as expected, the tropopause height above the ground does not seem to influence the plume in cases in which the stability of the air is such as to prevent the plume from reaching the tropopause in the first place.

### 3.3. Fire Energy Study

As a final check of the importance of the surface heat flux versus the importance of the ambient atmospheric conditions, we performed two additional simulations using the baseline fire scenario except that the fire intensity was reduced by a factor of 5 in one case and 25 in the other. These simulations indicate the lower limit on the sensible heat input effect on the plume dynamics. The case in which the surface heat intensity was reduced by a factor of 25 deposits over the 2.5 hour duration of the fire roughly the same amount of energy as the sun normally

deposits over the same region in 3.5 hours (and only one-third as much as the sun over the entire computational domain). Figure 15 compares the results of these simulations with the baseline case; for this unstable sounding, the plume will rise to the tropopause almost regardless of the amount of energy deposited into the atmosphere as sensible heat. Thus the net effect of the fire is to raise the smoke plume by a few kilometers, but in all cases, the smoke cloud stabilizes within a couple kilometers of the level of the ambient tropopause.

After reviewing these simulations, we concluded that the potential to loft smoke from large area fires such that it will stabilize at high altitude does not exist *unless the atmosphere is already conditionally unstable*. In any case, for all of the simulations we have run, the smoke has stabilized within a few kilometers of the ambient tropopause or lower; ambient wind shear, which cannot be modelled with our axisymmetric code, is expected to cause additional turbulent entrainment leading to a lower cloud stabilization altitude. Even without this, however, for cases leading to stabilization at and above the ambient tropopause, a significant amount of moisture will condense out and be co-located with the smoke. This implies that the modified atmosphere, and particularly the modified troposphere/stratosphere boundary can be expected to have very different properties from those considered up until now. These include, but are not limited to, albedo effects and long-term phoretic scavenging and water chemistry effects. The issue of scavenging is not restricted to late times however, the study of prompt scavenging effects forms the final section of this paper.

### 3.4. Scavenging Study

As a final piece to this puzzle, we considered the possibility of prompt scavenging of the smoke due to nucleation. The effects of aerosols on cloud formation and the effects of cloud processes on aerosol concentrations have been known to be quite extensive. A large firestorm such as the ones studied in this paper produces a very large quantity of smoke particles which may serve as cloud condensation nuclei (CCN). Stith, *et. al.* [1981] estimates that in a forest fire as much as  $10^{10}$  to  $10^{11}$  CCN may be produced for each gram of wood that is burned. As seen in the earlier discussion the ensuing convection also processes a large quantity of water vapor. The capability of an aerosol particle to serve as CCN depends on the physical and chemical properties of the particle such as the wettability of the particle surface and the presence of water-soluble matter on the particle [Pruppacher and Klett, 1978]. In a polluted atmosphere clouds and subsequent precipitation play a major role in the removal of aerosol from the atmosphere. This removal process is effected via many processes among which nucleation scavenging, dynamic capture by hydrometeors,

and phoretic processes are the most dominant. In cases where the source of aerosol is co-located with the source of heat which generates the convection, aerosols in considerable quantities will be present in the updraft and hence in the region where the bulk of the condensation is taking place. So in the study of aerosol removal by hydrometeors one has to consider the process of nucleation scavenging.

We have included a model for nucleation scavenging [Sarma, 1986] in a series of TASS simulations. At this time we do not track smoke particles once they are incorporated into cloud liquid and we do not consider smoke particles as good ice nuclei. The fraction of aerosol that is activated for nucleation is made dependent on the levels of supersaturations attained in the cloud. We have assumed that the smoke is monodisperse with a diameter of  $0.4 \mu\text{m}$  ( $10^{-6}$  m). Such particles will reach critical supersaturations at supersaturation values of less than about 0.1 % [Junge and McLaren, 1971]. As the physical properties of the smoke particles may be dependent on the type of fuel that is burned in the fire we classify smoke into two classes; (1) hydrophylic smoke comprising of the smoke particles that can serve as CCN and (2) hydrophobic smoke comprising of the smoke particles that are initially completely non-wettable. We also let the hydrophobic smoke transform to the hydrophylic class as these smoke particles age in the atmosphere. This transformation is characterized by an e-folding time of  $\tau$  for the conversion of hydrophobic smoke into hydrophylic smoke.

In an attempt to bound the effect of nucleation scavenging, three runs were made with the Lake Charles sounding shown in Fig. 3 as input and using the baseline fire distribution profile (Figs. 1 and 2). The partition of smoke into hydrophylic and hydrophobic categories and the e-folding time  $\tau$  determining the transformation of hydrophobic smoke to hydrophylic smoke were varied between these runs. For the first run, 10 % of total smoke produced was assumed to be hydrophylic, and the hydrophobic smoke e-folding time was assumed to be 5 hours. For the second run these numbers were 10 % and 0.5 hours, respectively, and for the third run they were 90 % and 0.5 hours, respectively.

Figure 16 shows the effect of including nucleation scavenging on smoke distribution. Figure 16a shows the smoke distribution for the baseline case (without scavenging) at 180 min and Figs. 16b and 16c show the distribution of hydrophylic and hydrophobic smokes respectively at 180 min for the first case discussed in the preceding paragraph. From Fig. 16b it is seen that the hydrophylic smoke distribution shows two distinct regions. The lower region is the result of the direct emission from the source. This region does not extend above 7.5 km in altitude as most of the hydrophylic smoke was

scavenged out through the nucleation process. The region of hydrophylic smoke above 10 km was caused by the slow transformation from hydrophobic smoke. Figure 16d shows the integrated smoke distribution in the vertical at 180 min. The total smoke at this time is  $8.0 \times 10^7$  kg (this includes smoke that was advected out of the domain through the right boundary) whereas  $9.6 \times 10^7$  kg of smoke were produced at the source. This implies that roughly 16 % of the smoke was removed via nucleation scavenging.

For the second case the partition between hydrophylic smoke and hydrophobic smoke was kept the same but the e-folding time  $\tau$  was reduced to 30 min. Figure 17 shows the integrated mass curves of total smoke, hydrophylic smoke and hydrophobic smoke for this case. Note that more than 50 % of the total smoke produced by the fire (indicated by the baseline curve) has been scavenged. This increase in scavenging rate is due to the fact that even though only 10 % of the smoke produced was scavengable, the hydrophobic smoke quickly aged to produce scavengable hydrophylic smoke. In the earlier case by the time the hydrophobic smoke aged to hydrophylic smoke most of it had been transported to the upper regions of the plume where condensation was not taking place.

For the last case the ratio of hydrophylic smoke to the total smoke was increased to 90 % (the e-folding time  $\tau$  was held at 30 min as in the previous case). This means that more smoke was available for nucleation earlier in the simulation. The effect on total smoke remaining after 180 min is seen from Fig. 18. Almost 95 % of the smoke that was produced has been scavenged.

These results show the effects of including just one scavenging mechanism - nucleation scavenging. The total remaining in the atmosphere for the three scavenging case discussed above is plotted as a function of time in Fig. 19. The total smoke produced by the fire is also plotted for reference. It is clear from this figure that the amount of smoke scavenged depends strongly on the amount of smoke that was hydrophylic and also on the aging time of the hydrophobic smoke. For the meteorological situation considered, the convection produces high enough supersaturations and condenses enough cloud water to effectively scavenge most of the CCN (hydrophylic smoke particles) that are introduced into the updraft of the plume. In general, the amount of smoke scavenged in this manner will to a large extent depend on the physical and chemical properties of the smoke produced during the fire and the amount of water processed in the convection triggered by the fire. Work is currently in progress to include scavenging via dynamic capture as well.

#### 4. Conclusions

In any paper covering material produced over a multi-year period, it is impossible to present all of the supporting material; we have tried, however, to present sufficient detail of our simulations so that a consistent chronology of smoke transport and scavenging could be established. Our goal in this effort was to try to bound the question of the amount of smoke which was injected into the atmosphere from large area fires in order to provide some guidance to those computational teams modelling the meso-scale and global-scale features of "nuclear winter".

To this end, we have the following four conclusions: (1) The details of the fire spatial or temporal distribution has little effect on the vertical distribution of the smoke after stabilization. (2) The ambient meteorology, however, plays a major role in determining the altitude of stabilization. A dry, stable atmosphere will force the plume to stabilize at low altitudes while a large area fire will trigger convective activity in a wet, unstable atmosphere. This latter case, though, possesses the possibility for considerable scavenging (up to 95 %) of the smoke depending on the chemical properties of the aerosol. (3) Ignoring scavenging, moist cases also result in the injection of a tremendous amount of moisture into the upper atmosphere along with the smoke. Approximately 100 times as much water as smoke is injected. The impact of this water injection on meso- and global-scale models of "nuclear winter" should be studied. (4) The determining factors in scavenging of the aerosol via nucleation scavenging (the only mechanism considered in these simulations) are the chemical properties of the smoke produced by the fire and the aging process of the smoke. These properties should be determined by experiments for use in future scavenging studies.

In future studies, we hope to include the effects of winds on the plume dynamics using the three-dimensional version of TASS. We also plan to include additional scavenging mechanisms (phoretic effects and inertial capture) in order to investigate their impact on the amount of smoke which is not scavenged by nucleation scavenging. Finally, we are presently including in the model the capability to follow the smoke through the precipitation phase (smoke - droplet - rain drop - graupel - transport to warmer temperature - droplet shed from graupel - free smoke after evaporation of droplet).

## Acknowledgements

This work was supported by the Defense Nuclear

Agency and the support of Drs. David Auton and George Ulrich and Mr. Peter Lunn is graciously acknowledged.

## REFERENCES

- Cotton, W. R., 1985: Atmospheric Convection and Nuclear Winter. *Amer. Sci.*, **73**, 275-280.
- Covey, C., S. H. Schneider, and S. L. Thomson, 1984: Global Atmospheric Effects of Massive Smoke Injections from a Nuclear War: Results from General Circulation Model Simulations. *Nature*, **308**, 21-25.
- Junge, C., and E. McLaren, 1971: Relationship of Cloud Nuclei Spectra to Aerosol Size Distribution and Composition. *J. Atmos. Sci.*, **28**, 382-390.
- Malone, R. C., L. H. Auer, G. A. Glatzmaier, M. C. Wood, and O. B. Toon, 1986: Nuclear winter: Three-dimensional Simulations including Interactive Transport, Scavenging and Solar Heating of Smoke. *J. Geophys. Res.*, **91**, 1039-1053.
- Palmer, T. Y., 1981: Large Fire Winds, Gases and Smoke. *Atmos. Environ.*, **15**, 2079-2090.
- Penner, J. E., L. C. Haselmen, Jr., and L. L. Edwards, 1986: Smoke-Plume Distribution above Large-Scale Fires: Implications for Simulation of "Nuclear Winter". *J. Climate Appl. Meteor.*, **25**, 1434-1444.
- Proctor, F. H., 1982: Numerical Study on the Evolution of Tornadoes. *Ph. D. Dissertation. Texas A & M University*. (University Microfilms International, Ann Arbor, MI, No 83-09-693).
- , 1986: Three-Dimensional Simulation of the 2 August CCOPE Hailstorm with the Terminal Area Simulation System. *World Meteorological Organization Technical Document No. 199*, p. 227-240.
- , 1987a: The Terminal Area Simulation System - Volume I: Theoretical Formulation. NASA Contractor Report NASA CR- 4046.
- , 1987b: The Terminal Area Simulation System - Volume II: Verification Cases. NASA Contractor Report NASA CR- 4047.
- Pruppacher, H. R., and J. D. Klett, 1980: Microphysics of Clouds and Precipitation. *D. Reidel Publishing Company*, p714.
- Sarma, R. A., 1986: Numerical Simulation of the Formation and Transport of Sulfate in Convective Clouds. *PhD Dissertation. Colorado State University*. (University Microfilms International, Ann Arbor, MI).
- Small, R. D., D. A. Larson, and H. L. Brode, 1984: Asymptotically Large Area Fires. *J. Heat Transfer*, **106**, 318-324.
- Stith, J. L., L. F. Radke, and P. V. Hobbs, 1981: Particle Emissions and the Production of Ozone and Nitrogen Oxides from the Burning of Forest Slash. *Atmos. Environ.*, **15**, 73-82.
- Turco, R. P., O. B. Toon, T. Ackerman, J. P. Pollack, and C. Sagan, 1983: Global Atmospheric Consequences of Nuclear War. *Science*, **222**, 1283-1292.

# FIRE SPATIAL DISTRIBUTION

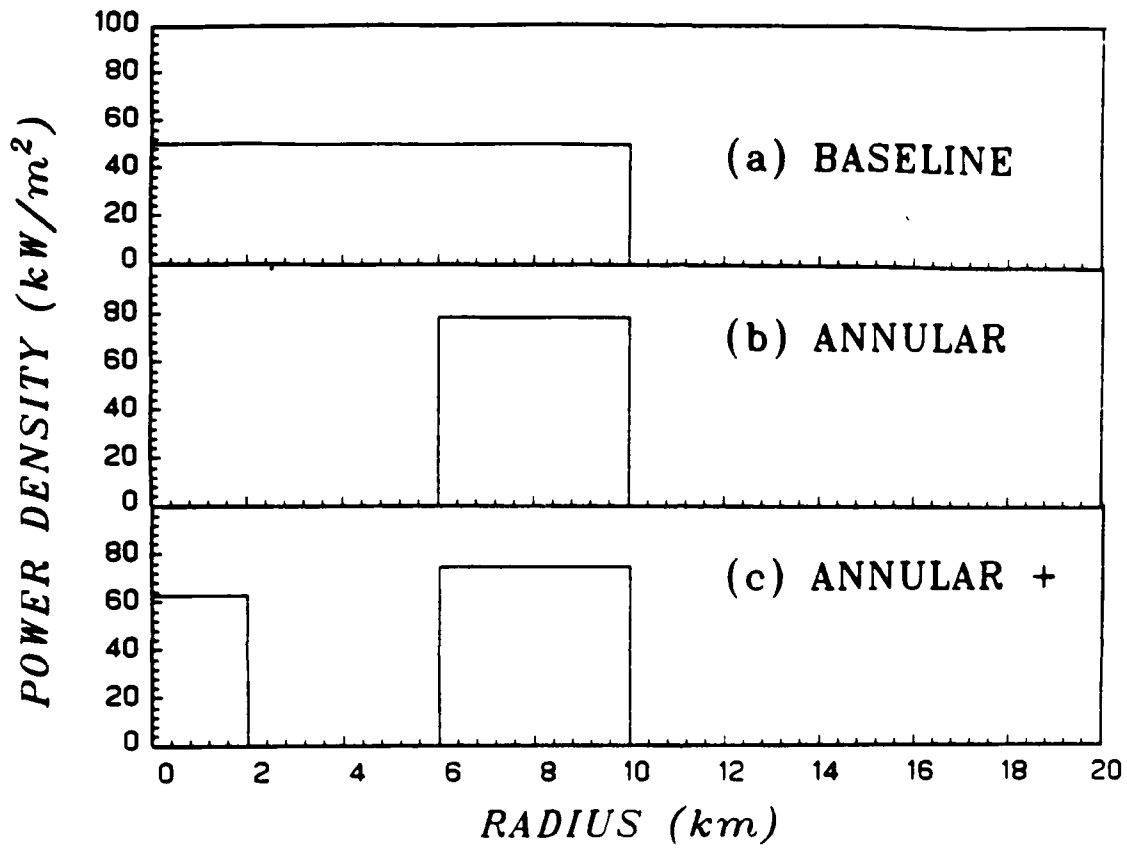


Figure 1: Spatial Distribution of the Fire for (a) the baseline, (b) the annular, and (c) the modified annular cases.

# FIRE TIME HISTORY

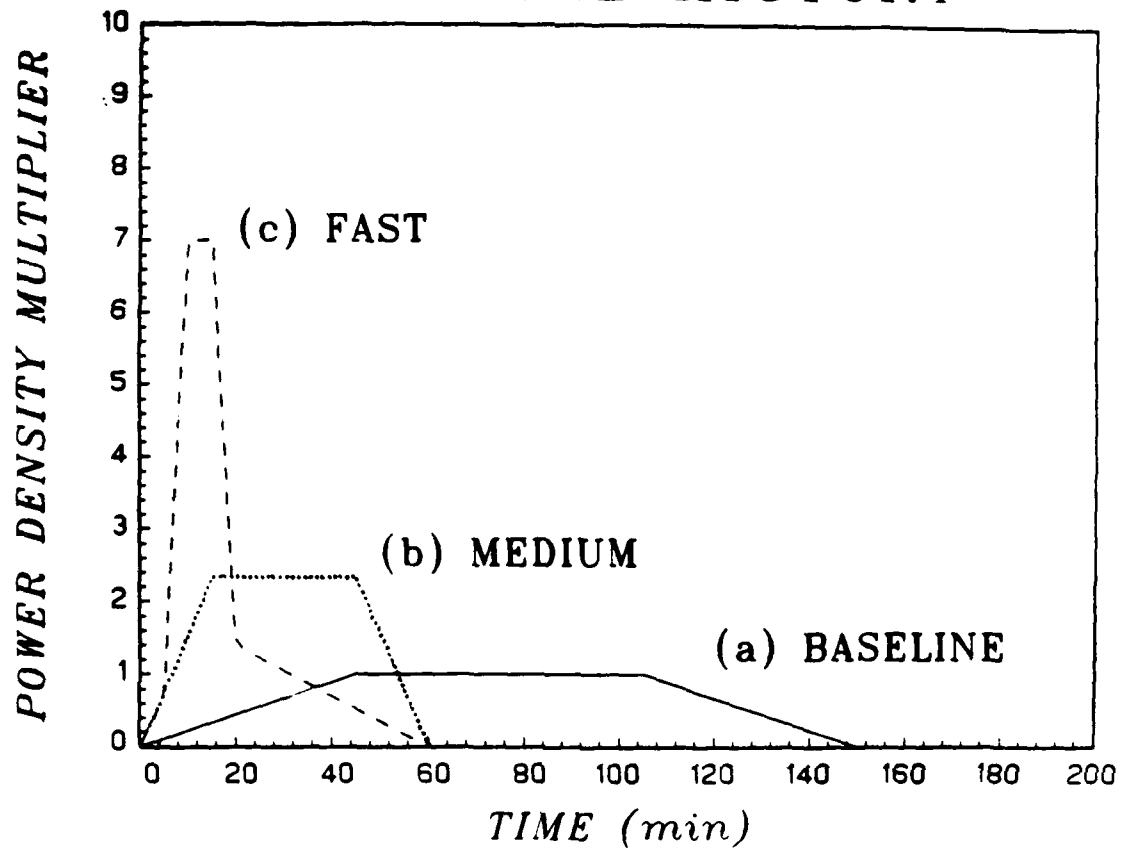


Figure 2: Time history of the fire for (a) the baseline, (b) the medium burn, and (c) the fast burn cases.

LCH ANL. © 00Z 4-10-79

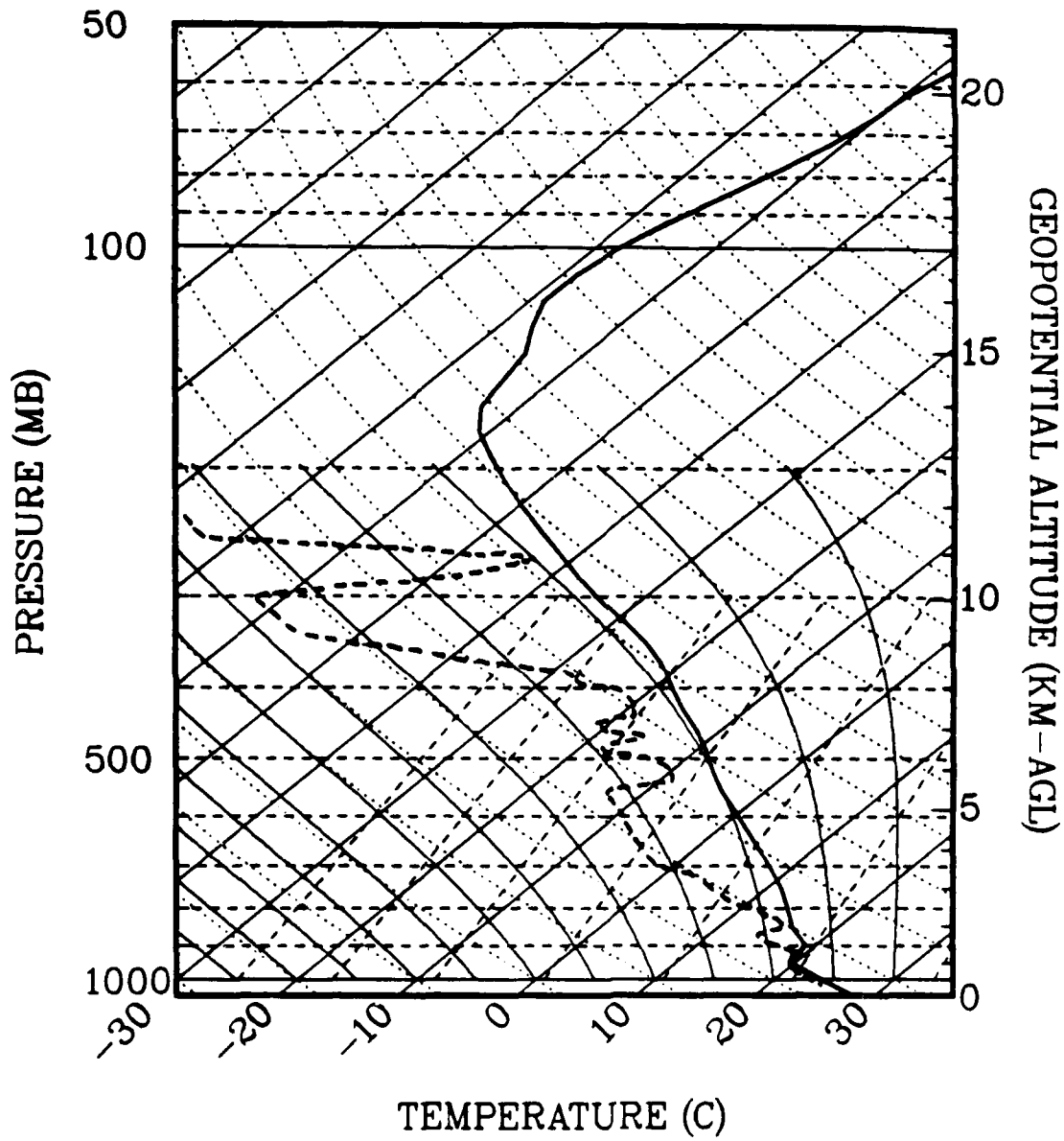


Figure 3: Atmospheric sounding for Lake Charles, LA at 0000Z on April 10, 1979 used in these simulations.



## Latent Heat Released - Baseline

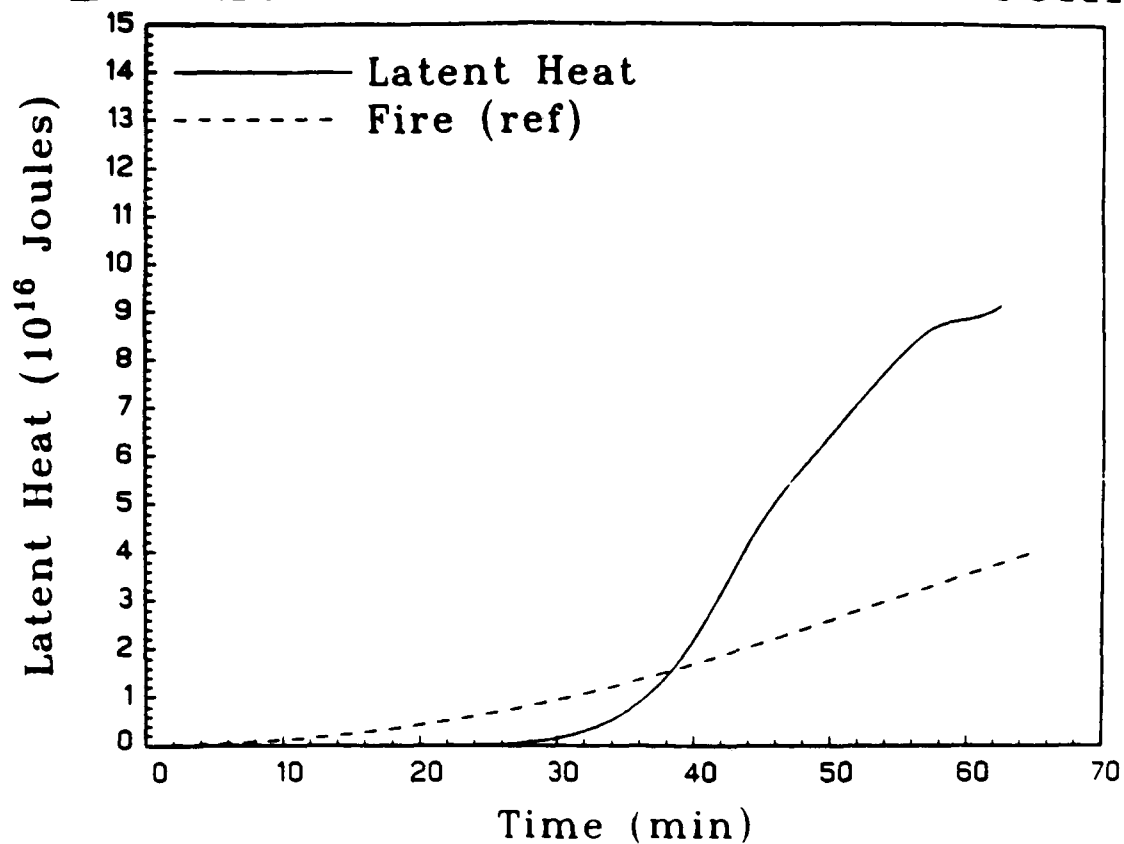


Figure 5. The cumulative latent heat released v. time for the baseline simulation. The cumulative fire sensible heat output is shown for reference.

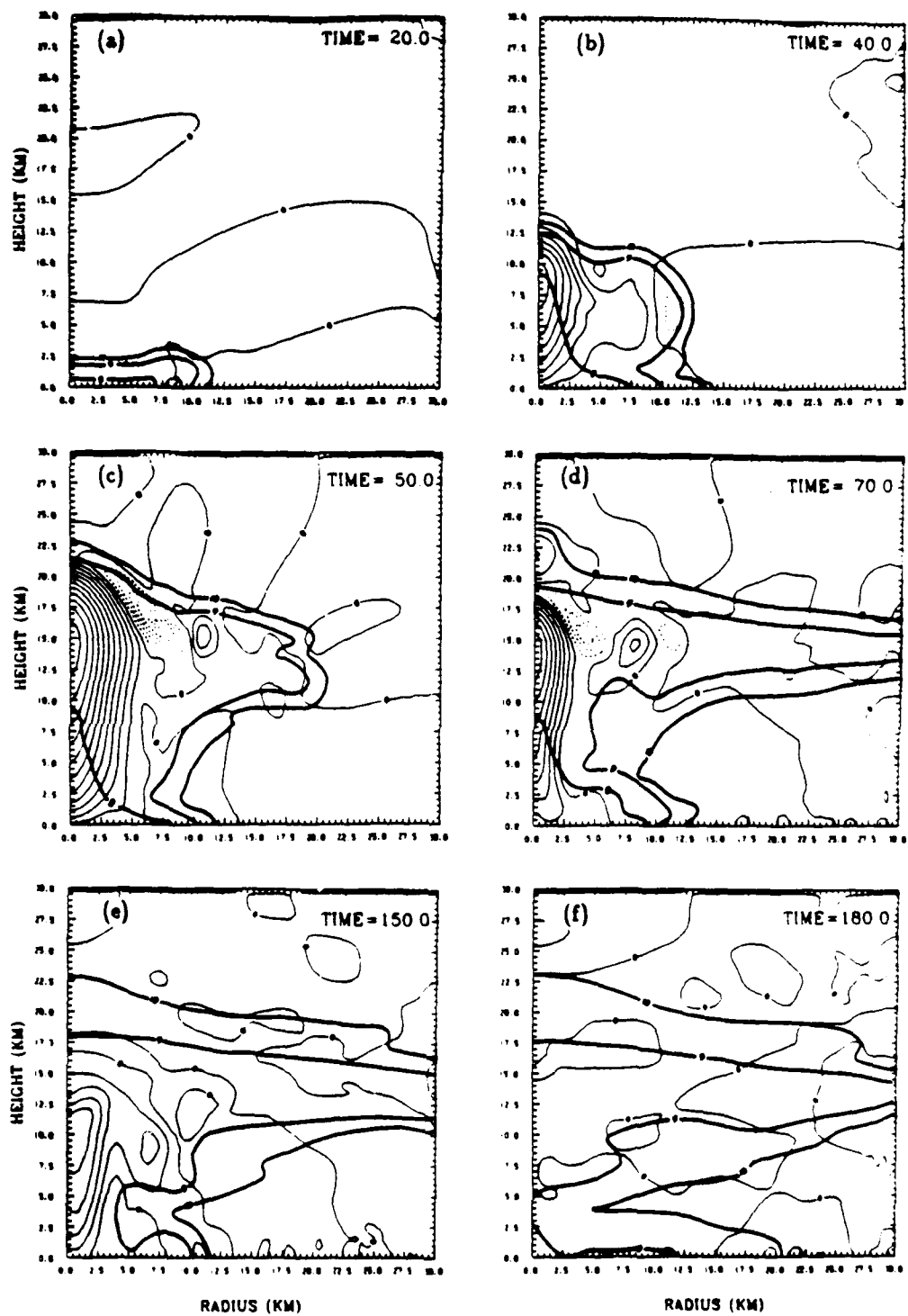


Figure 4: The smoke concentration contours overlaid on the vertical velocity contours for the baseline simulation at times: (a) 20, (b) 40, (c) 50, (d) 70, (e) 150, and (f) 180 min. The smoke concentration contours of  $10^{-10}$ ,  $10^{-9}$ , and  $10^{-8}$  g/cm<sup>3</sup> are shown; the vertical velocity contours are at intervals of 10 m/s.

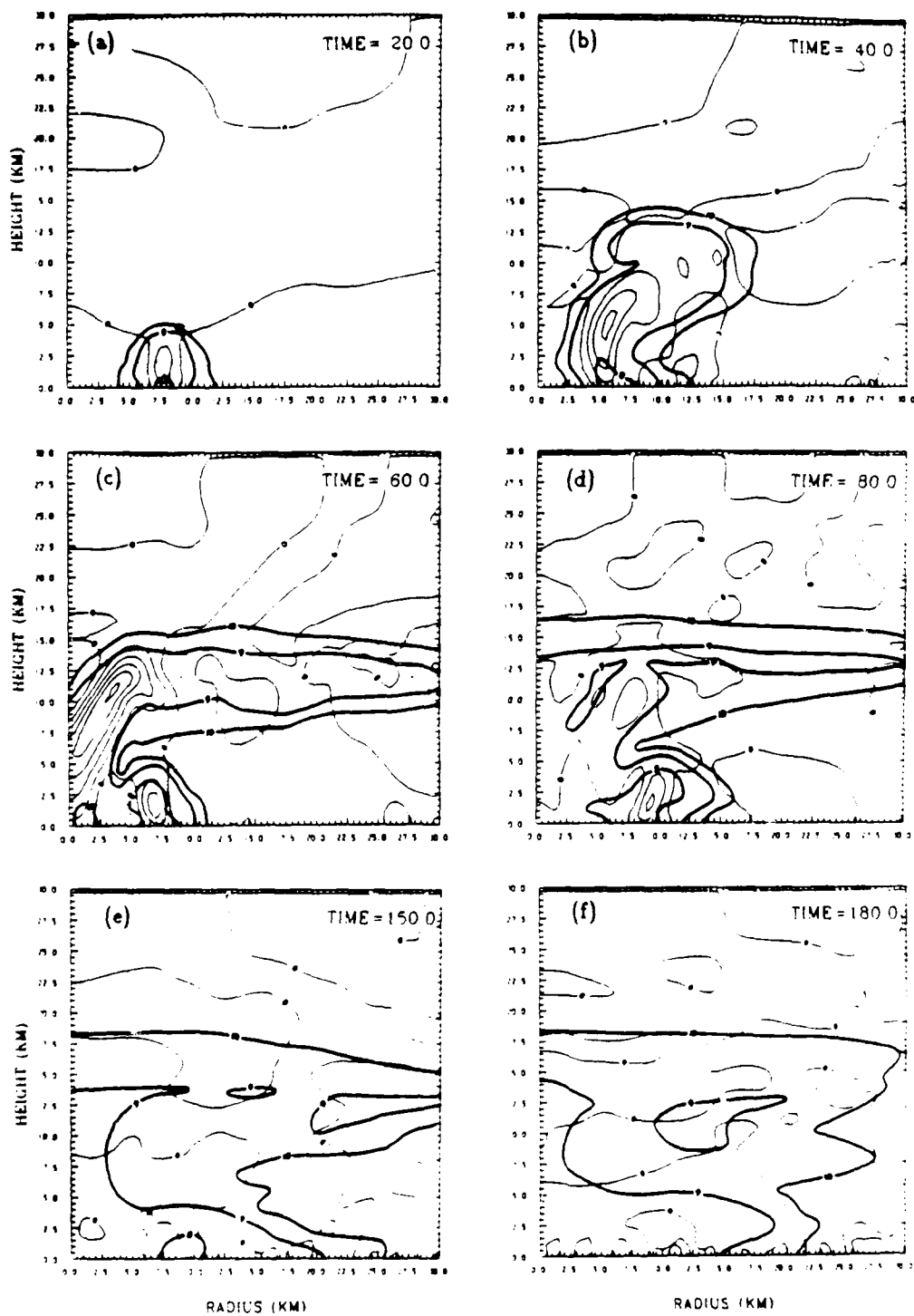


Figure 6. The smoke concentration/vertical velocity contours for the annular case at times: (a) 20, (b) 40, (c) 60, (d) 80, (e) 150, and (f) 180 min. The format is the same as Fig. 4.

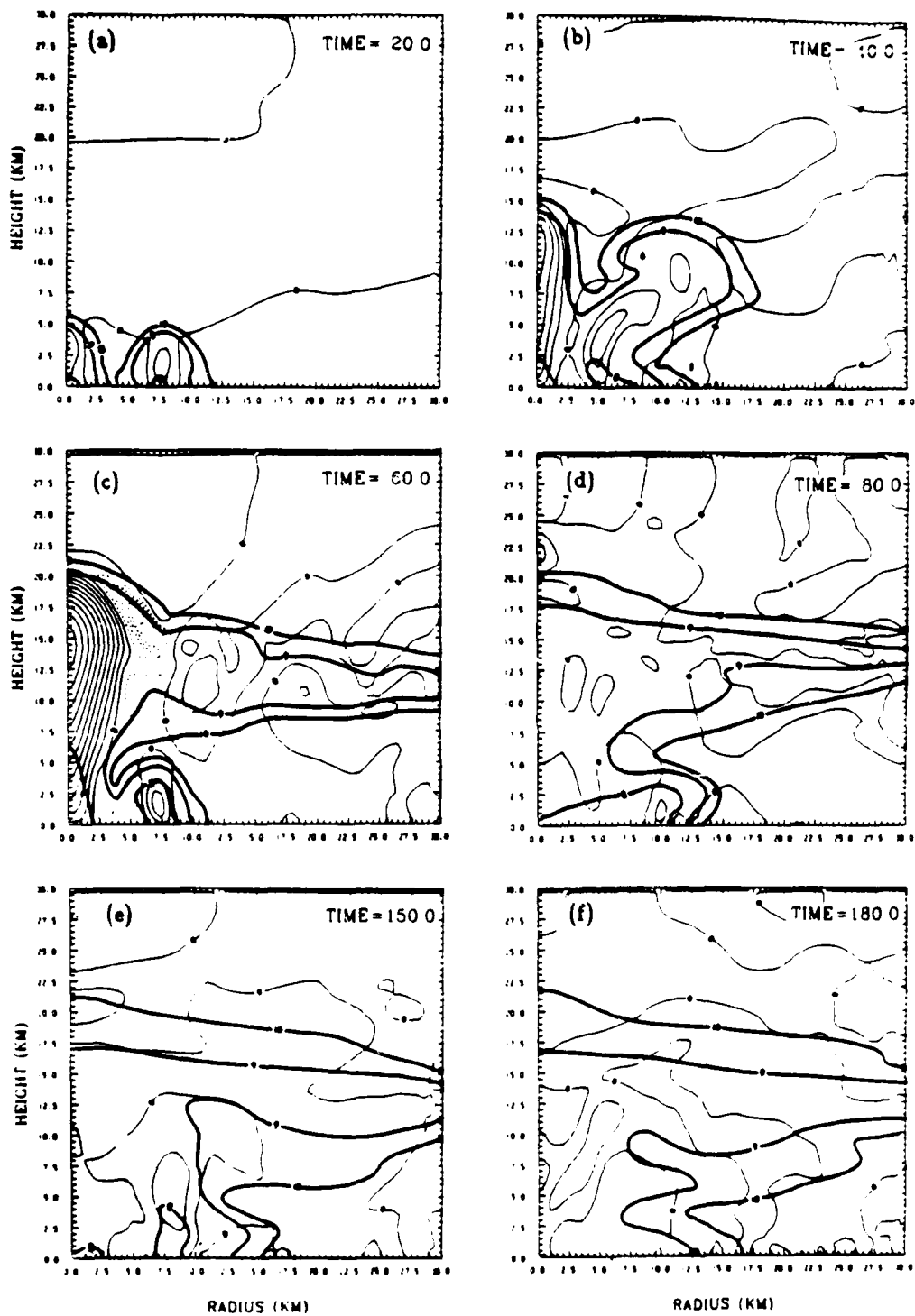


Figure 7. The smoke concentration/vertical velocity contours for the modified annular case. The times and format are the same as Fig. 6.

SMOKE

TIME=180.0

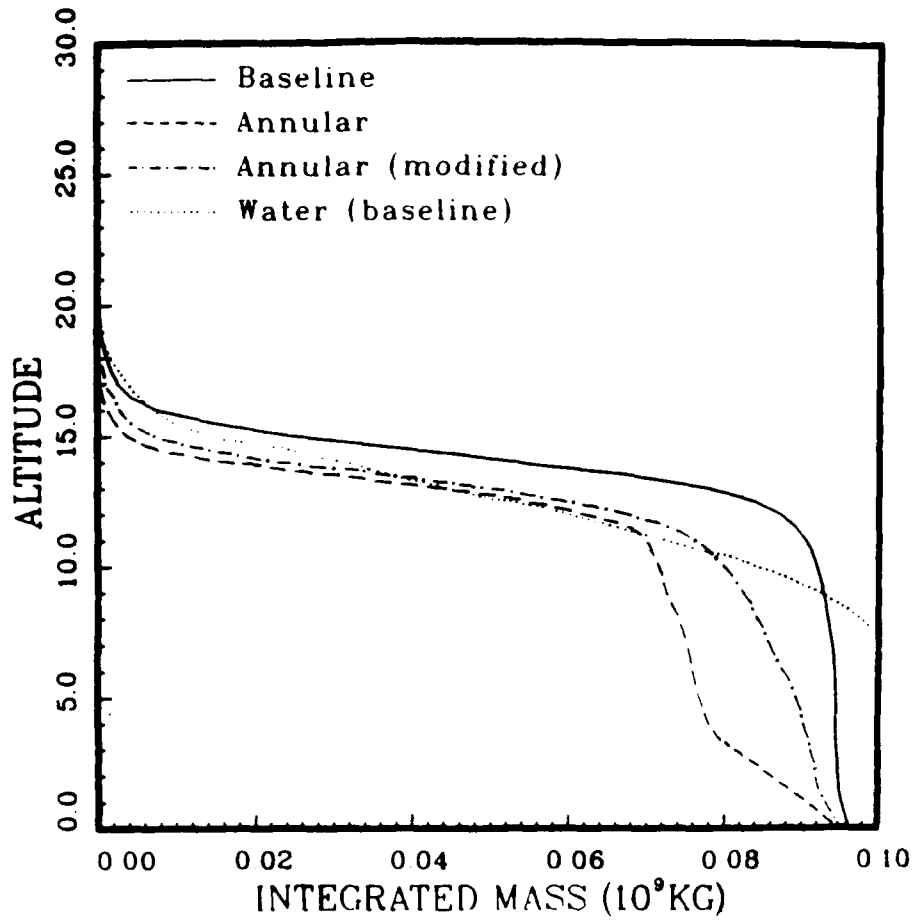


Figure 8. The cumulative smoke mass distribution v. height for the three spatial variation simulations. The cumulative mass is integrated downward so that the mass above a given level may be read directly. The cumulative water distribution is plotted as a reference using a scale 100 times that used for the smoke.

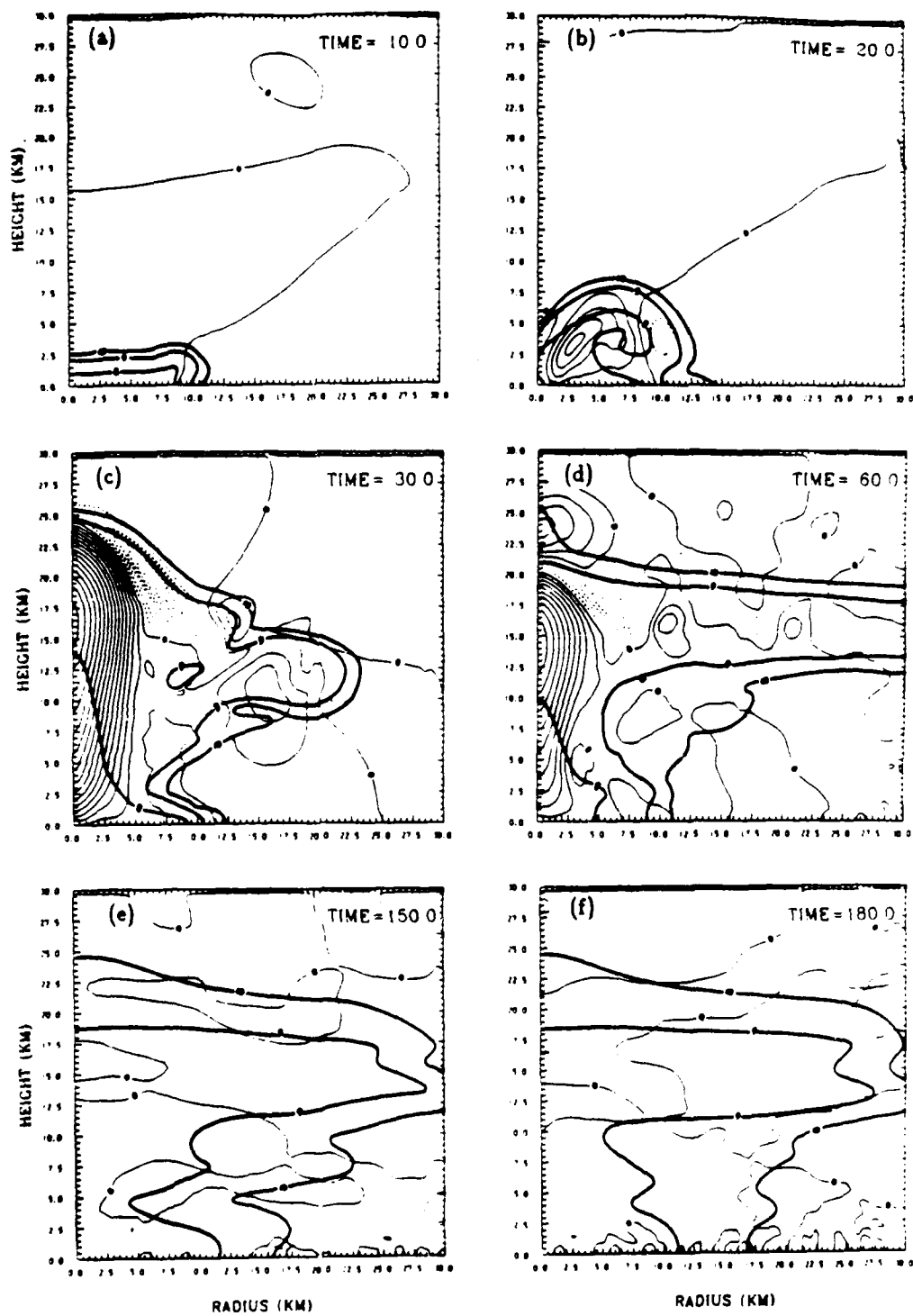


Figure 9. The smoke concentration/vertical velocity contours for the medium burn simulation at times: (a) 10, (b) 20, (c) 30, (d) 60, (e) 150, and (f) 180 min. The format is the same as Fig. 4.

# Latent Heat Released - LSOT1

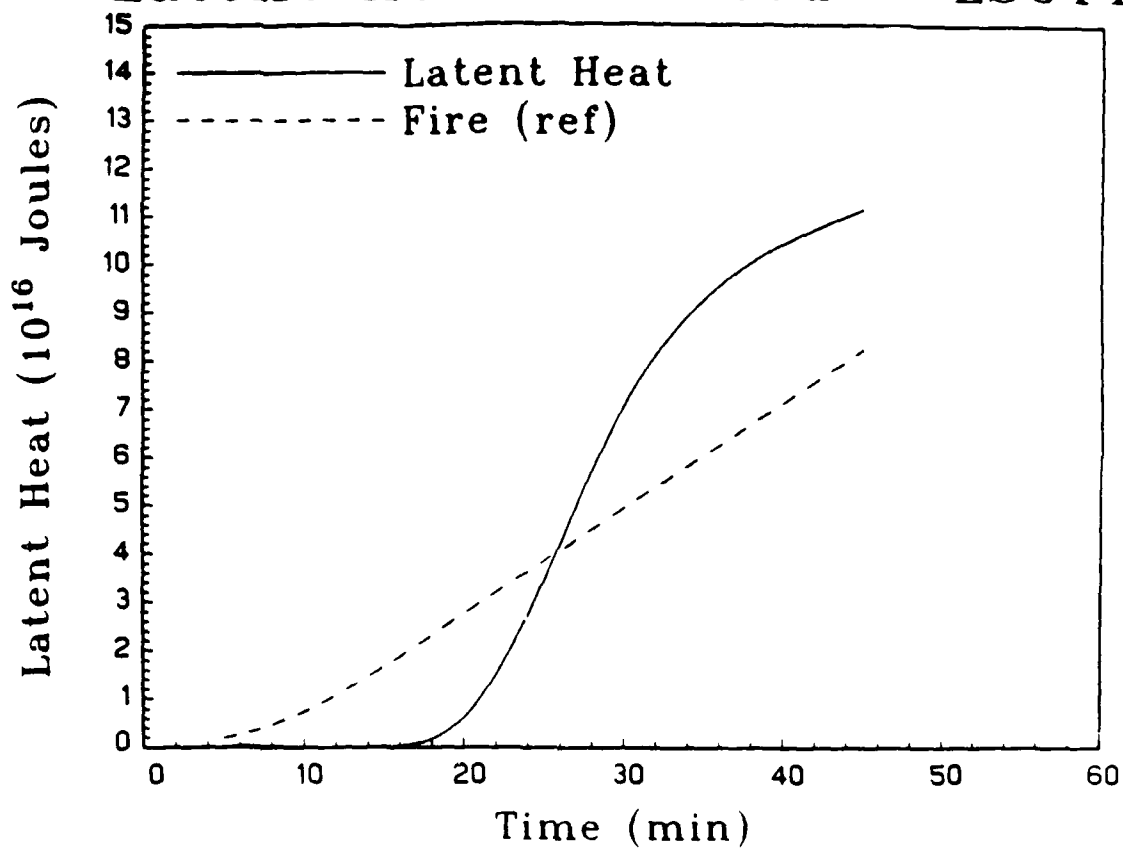


Figure 10. The cumulative latent heat released v. time for the medium burn simulation. The cumulative fire sensible heat output is shown for reference.

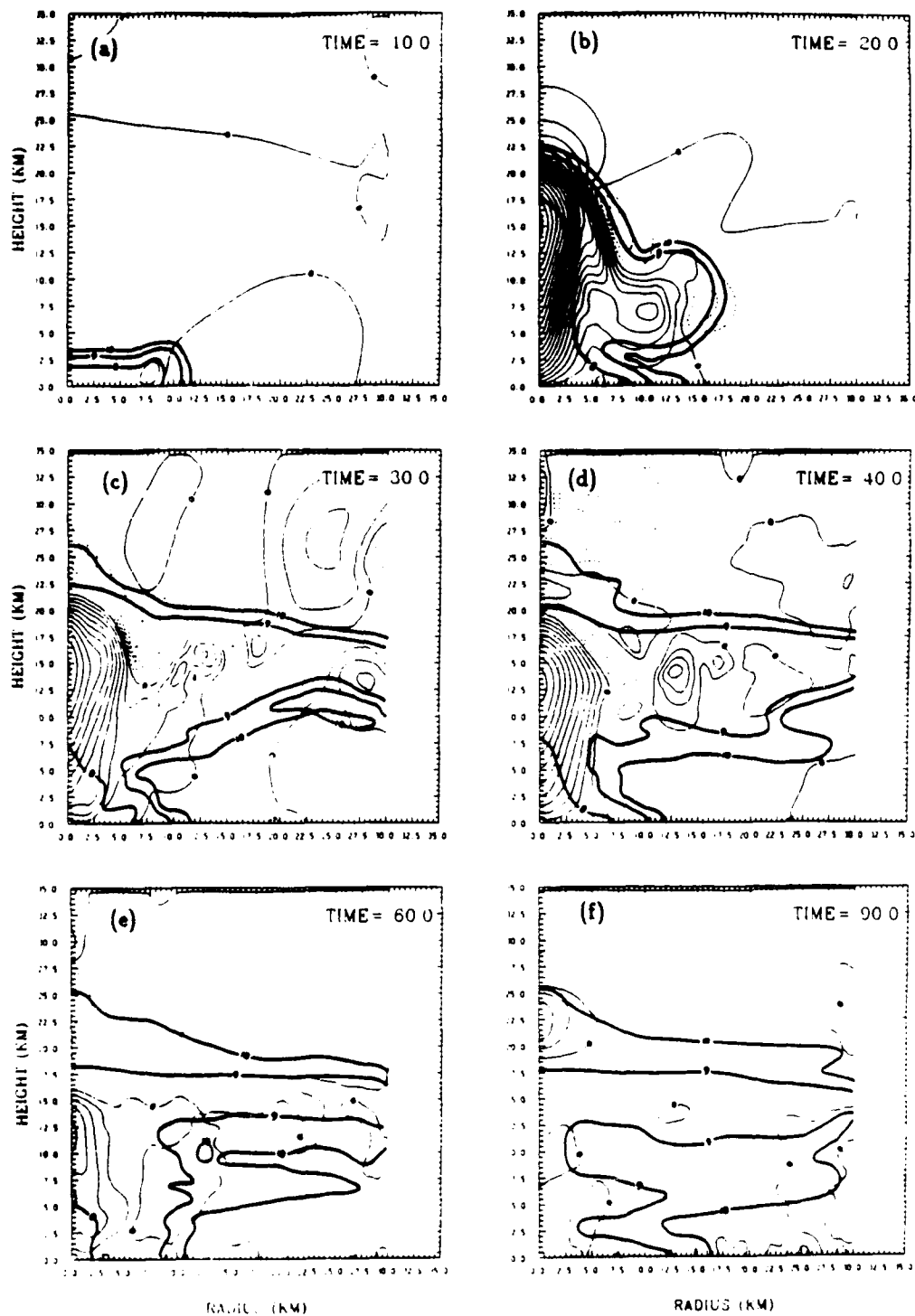


Figure 11. The smoke concentration/vertical velocity contours for the fast burn simulation at times: (a) 10, (b) 20, (c) 30, (d) 40, (e) 60, and (f) 90 min. The format is the same as Fig. 4.



SMOKE

TIME=180.0

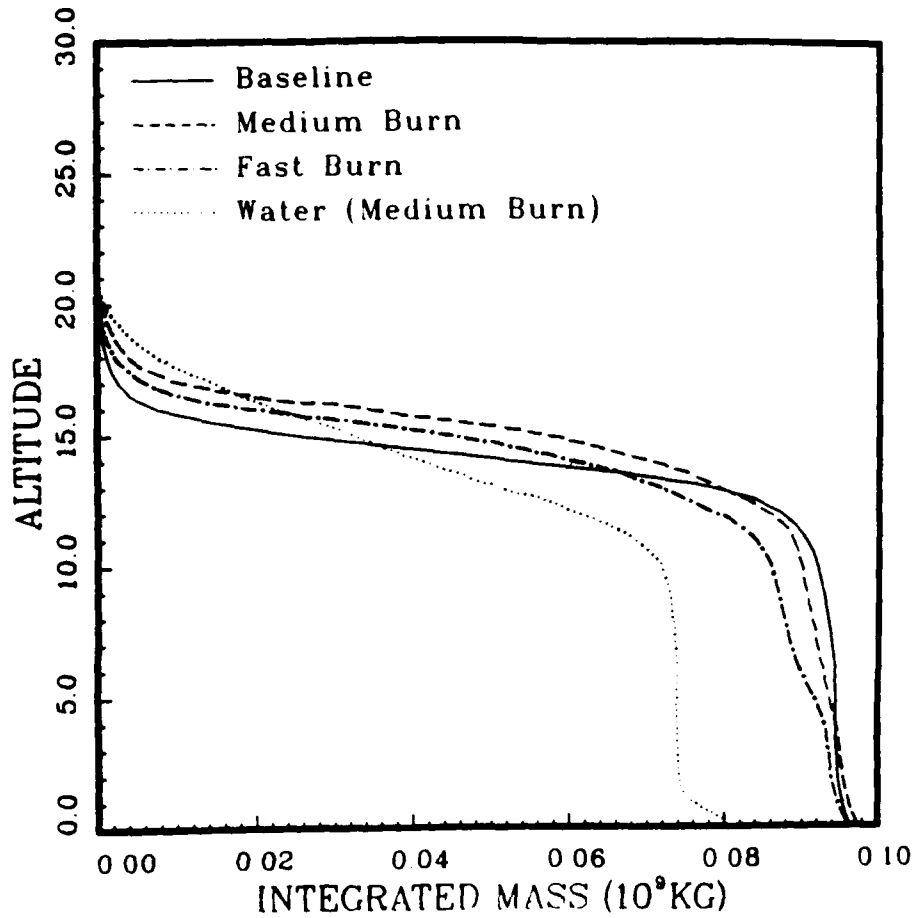


Figure 12. The cumulative smoke distribution v. height for the three temporal variation simulations (including the baseline case). The cumulative water distribution for the medium burn simulation is plotted as a reference using a scale 100 times that used for the smoke.

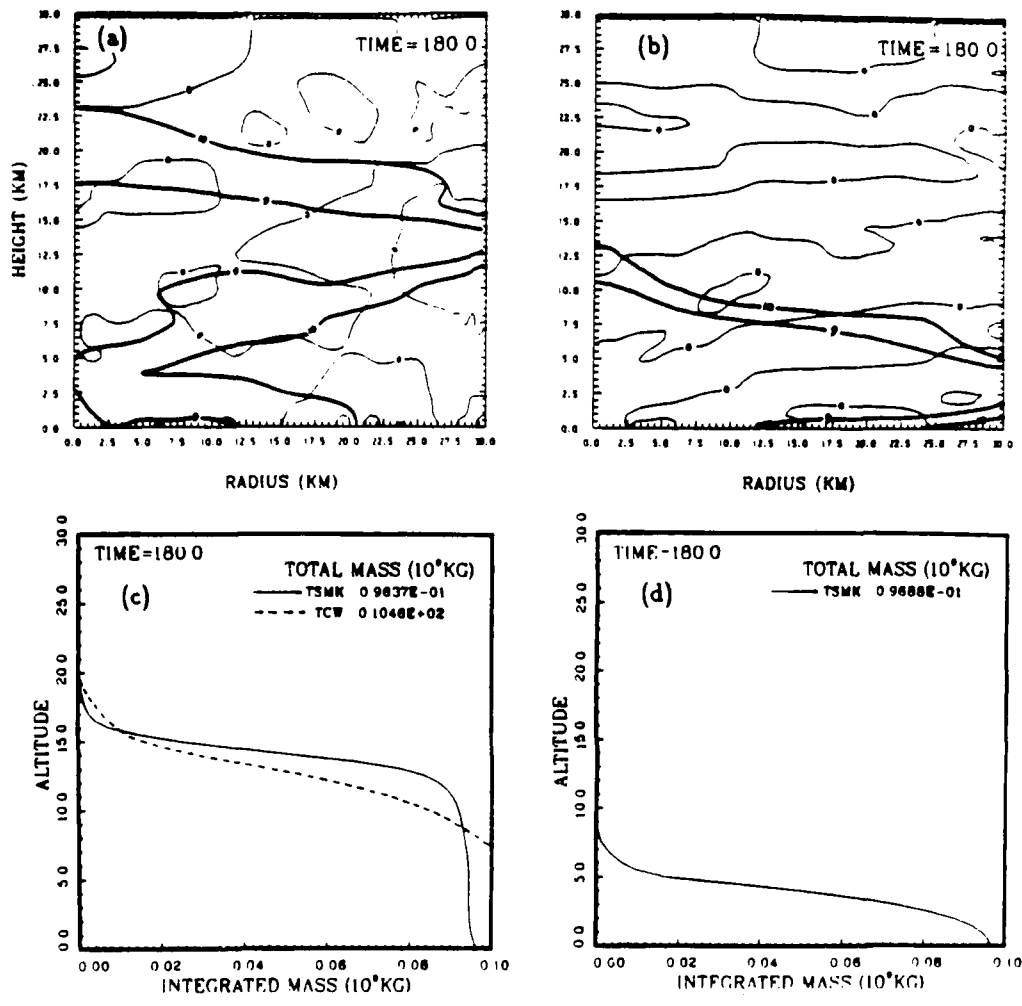


Figure 13. The smoke concentration/vertical velocity contours for the (a) baseline and (b) baseline dry simulations. The cumulative distribution curves are shown for these two cases in (c) and (d), respectively.

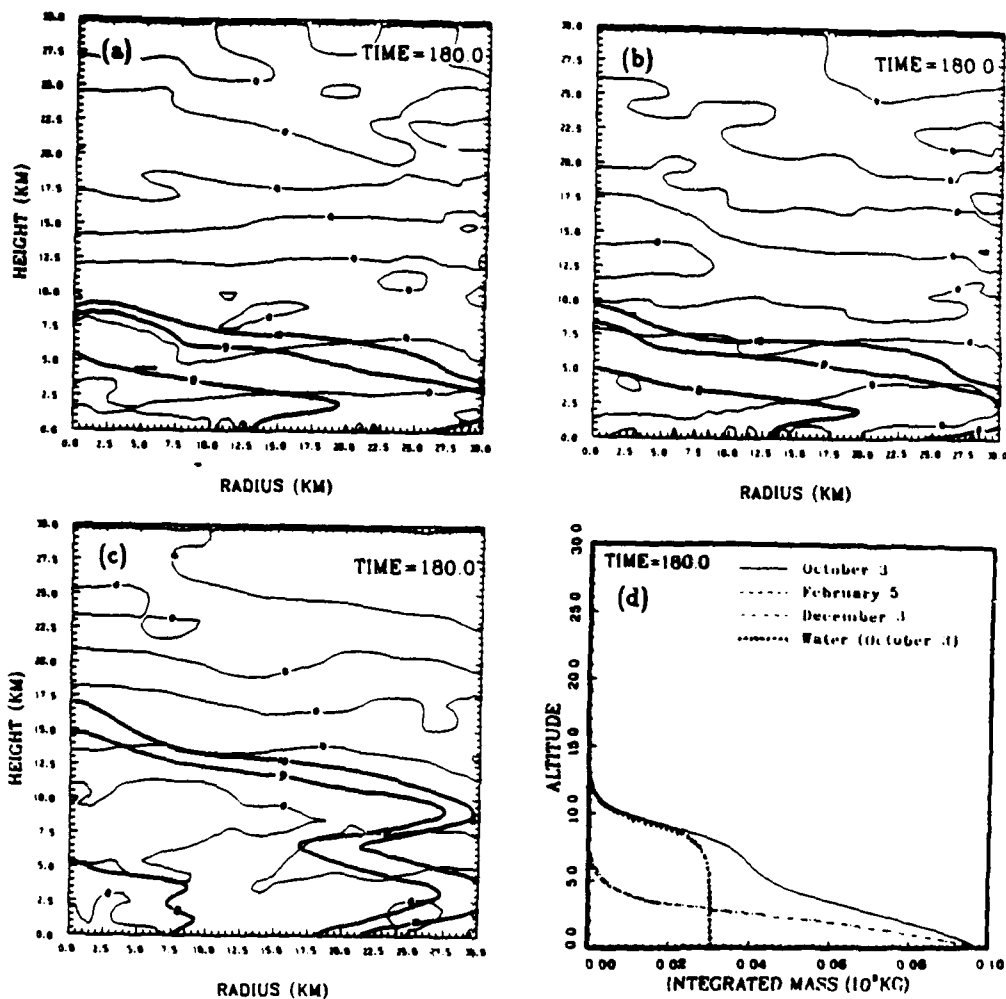


Figure 14. The smoke concentration/vertical velocity contours for the three simulations using soundings from Bismarck, ND: (a) December 3, 1974; (b) February 5, 1974; and (c) October 3, 1974. The cumulative smoke distributions for the three simulations are shown in (d) along with the water distribution for the October 3rd.

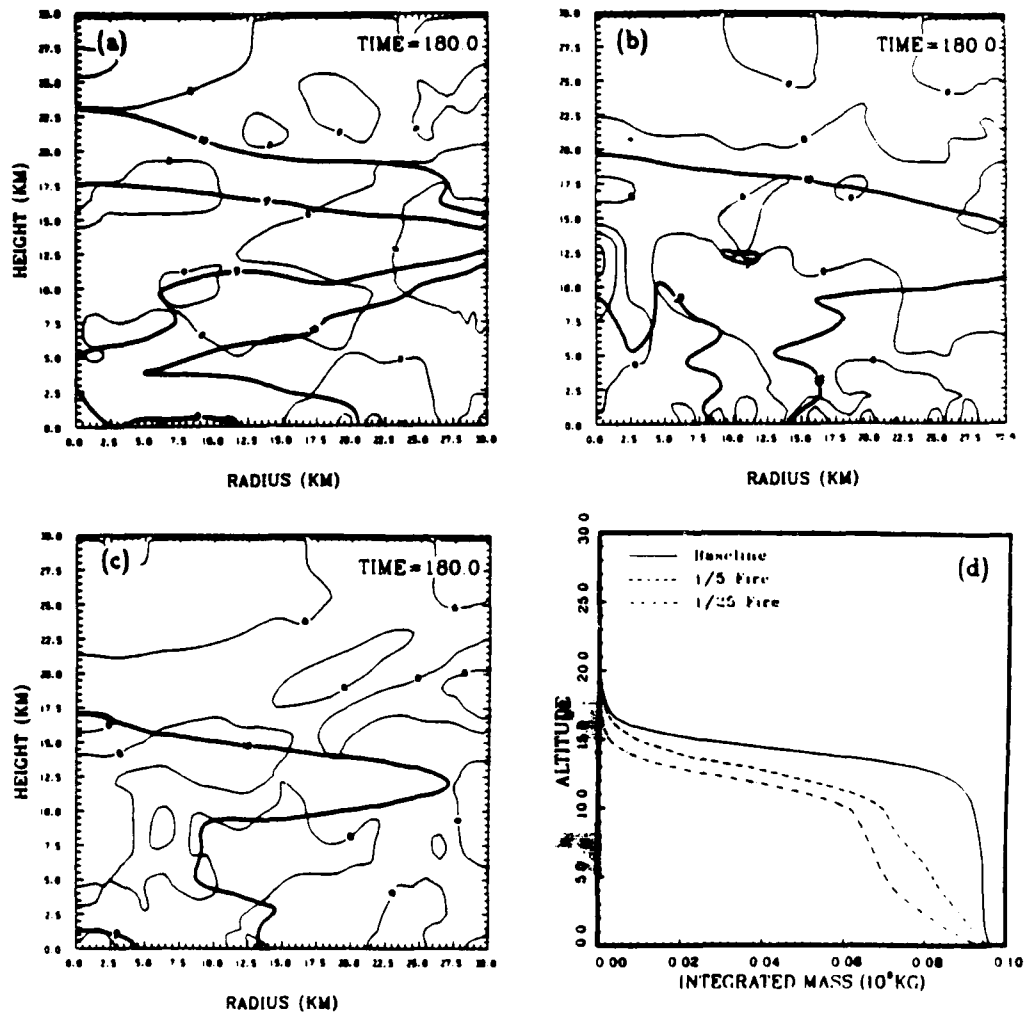


Figure 15. The smoke concentration/vertical velocity contours for the energy variation study: (a) baseline; (b) baseline reduced by a factor of 5; and (c) baseline reduced by a factor of 25. The cumulative smoke distribution for all three cases is shown in (d).

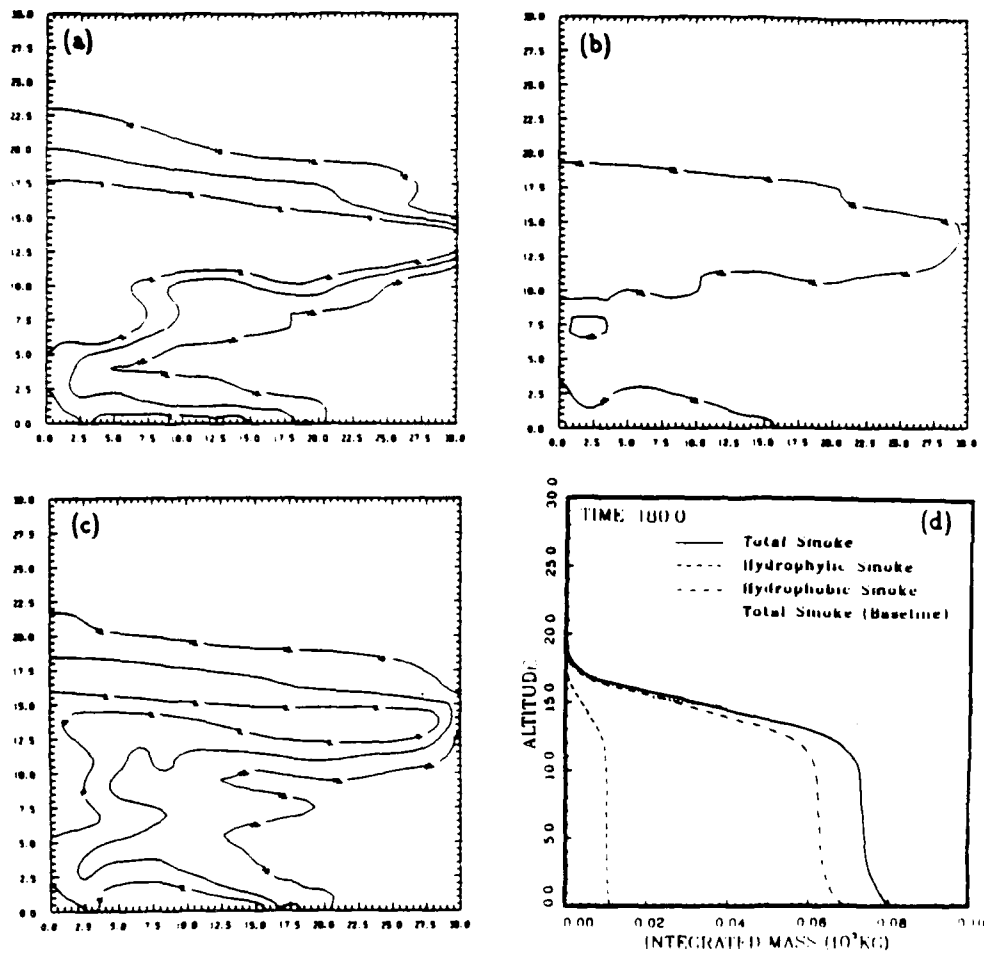


Figure 16. The effect of nucleation scavenging with 10 % of the emitted smoke being hydrophylic and the e-folding time  $\tau$  equal to 5 hours. Figure (a) is the baseline total smoke concentration contours, (b) is the hydrophylic smoke contours, and (c) is the hydrophobic contours, all at 180 min. The cumulative distribution curves are shown in (d).

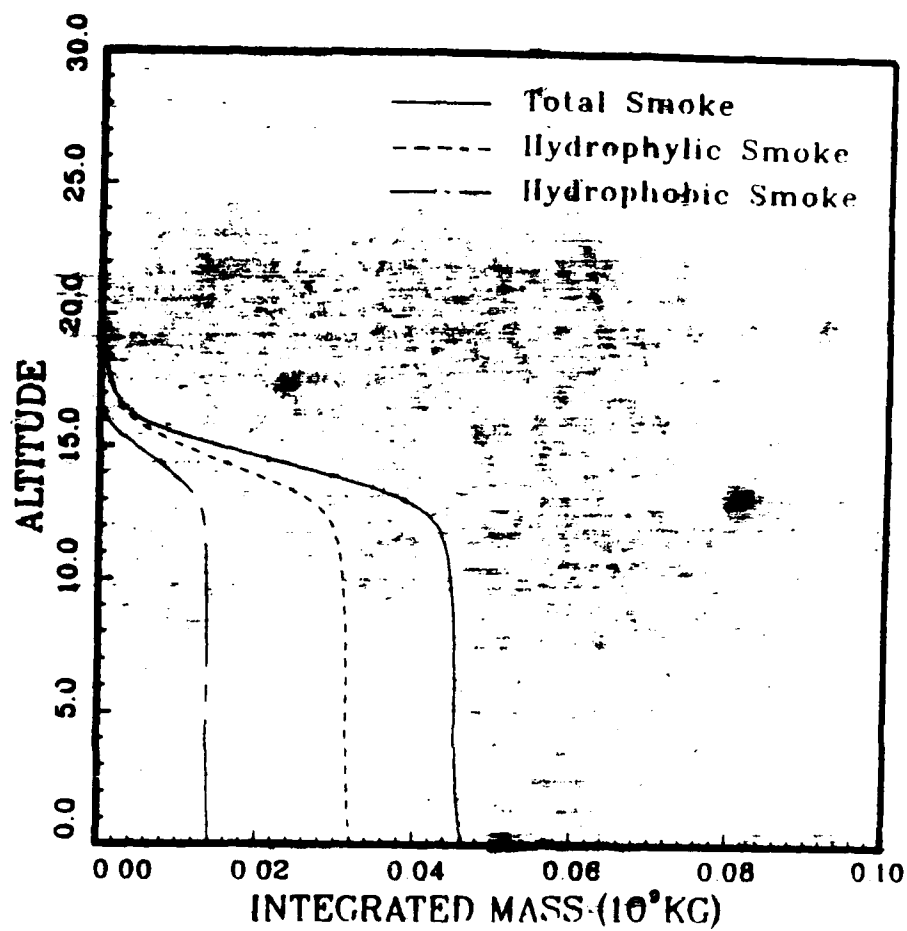


Figure 17. The cumulative smoke distribution curves at 180 min. into the simulation with 10 % hydrophylic smoke emission and  $\tau$  equal to 0.5 hours.

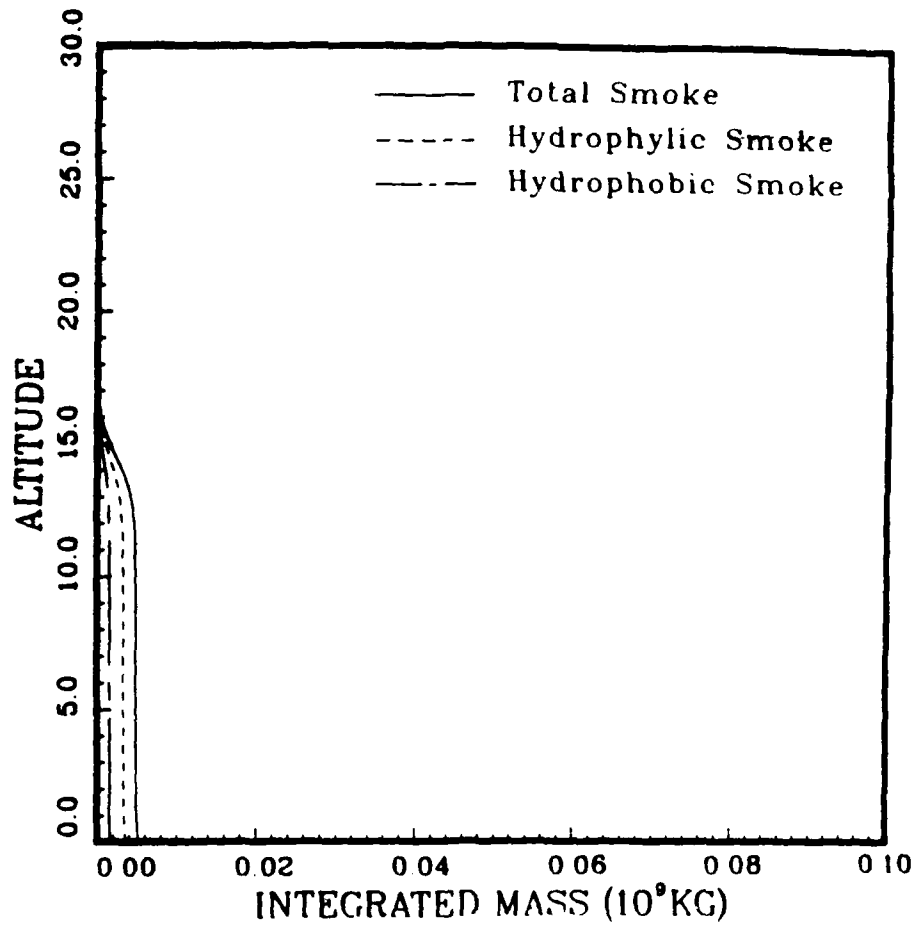


Figure 18. The cumulative smoke distribution curves at 180 min. for the case with 90 % hydrophylic smoke emission and  $\tau$  equal to 0.5 hours.

# Total Smoke - Lake Charles

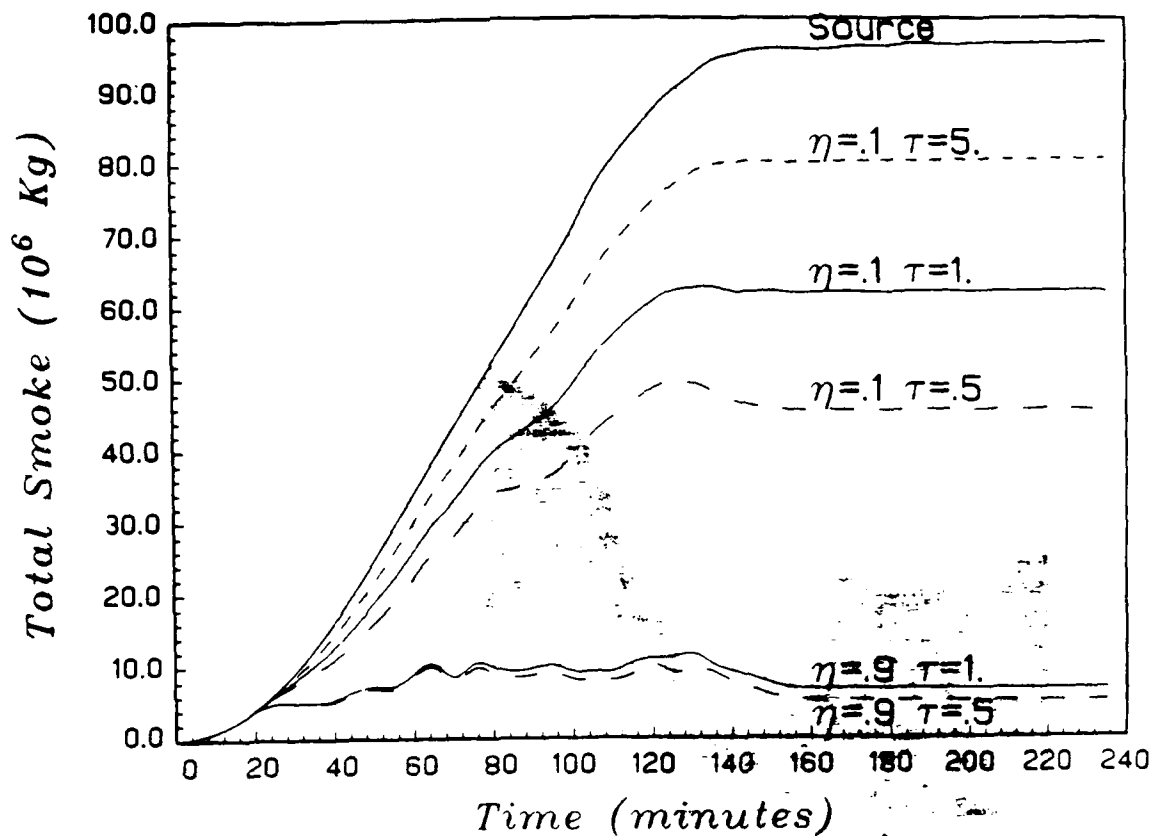


Figure 19. The total amount of smoke remaining in the atmosphere as a function of time for five simulations run with varying hydrophylic smoke fraction  $\eta$  and e-folding time  $\tau$ .



---

---

**Numerical Simulation of Nucleation  
Scavenging within Smoke Plumes above Large Fires**

---

---



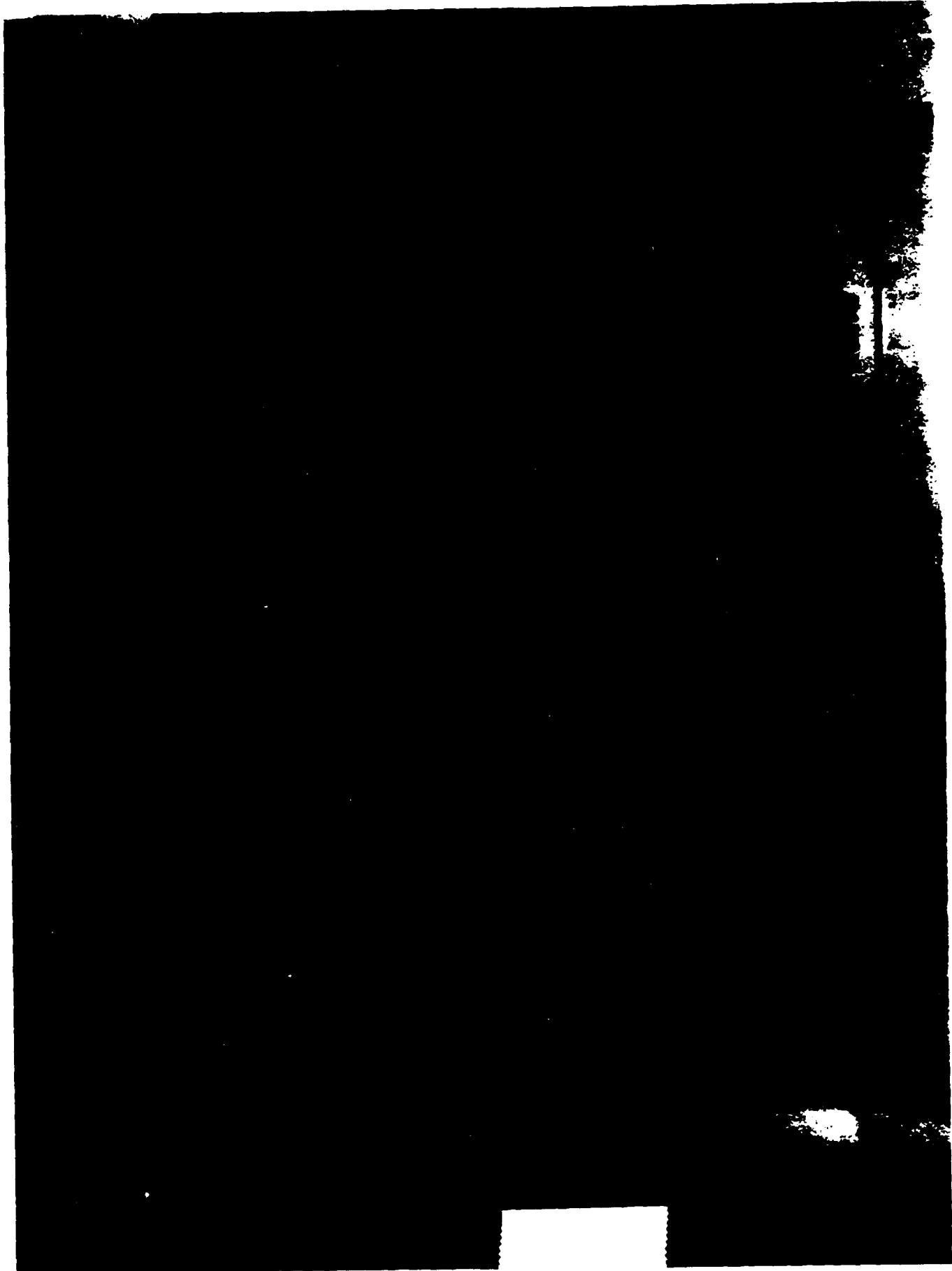
**Michael M. Bradley  
Lawrence Livermore National Laboratory**

## **The numerical model**

---



- **Two-dimensional**
- **Time-dependent**
- **Nonhydrostatic**
- **Compressible**
- **Eulerian**
- **Terrain-following coordinate system**
- **Cloud and rain parameterization**
- **Dynamic equations are fully nonlinear**
- **Flux form of substance transport equations  
(using fourth-order spatial differencing)**



377

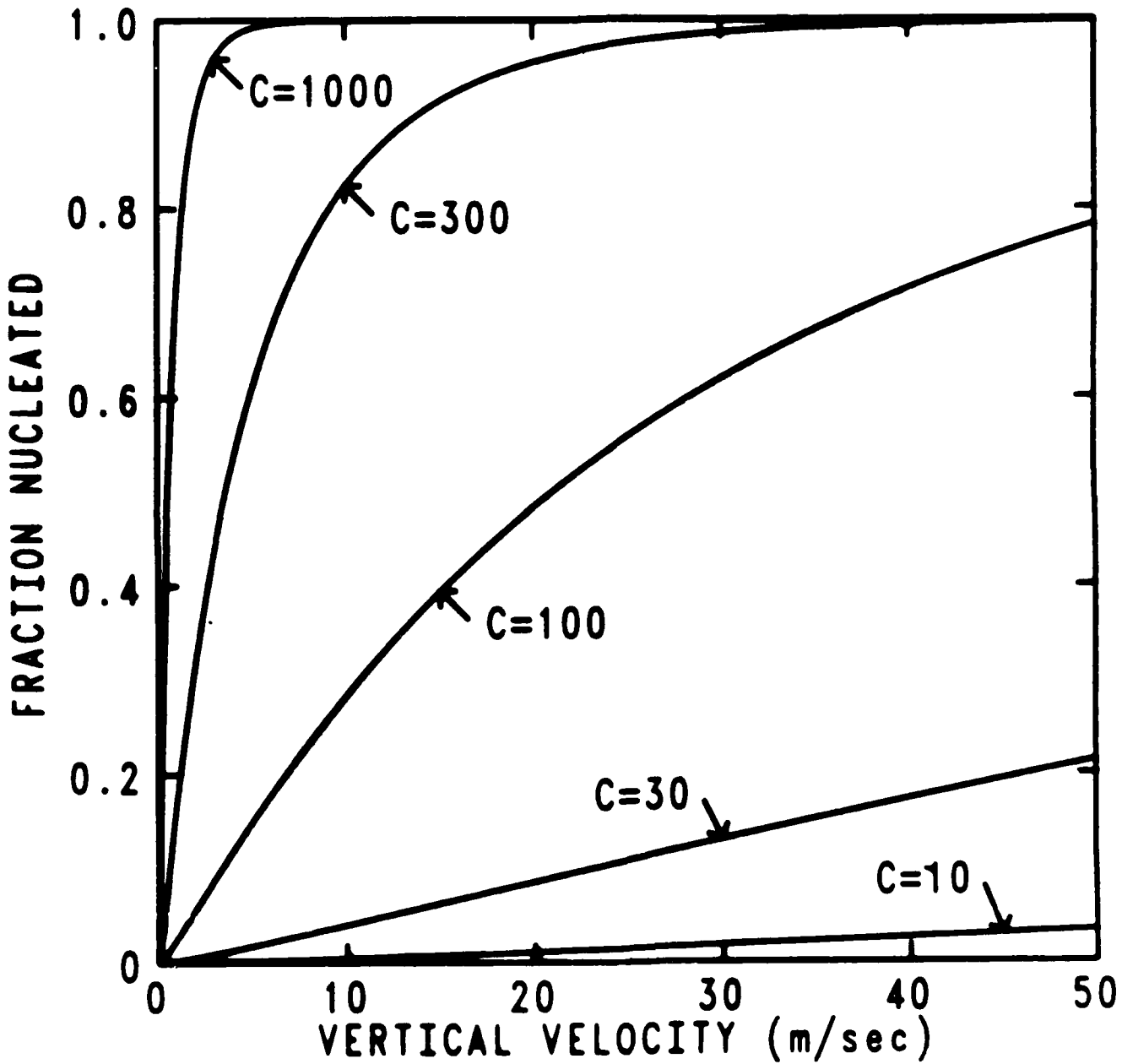


# Parameterization for Nucleation Scavenging

Fraction Nucleated:

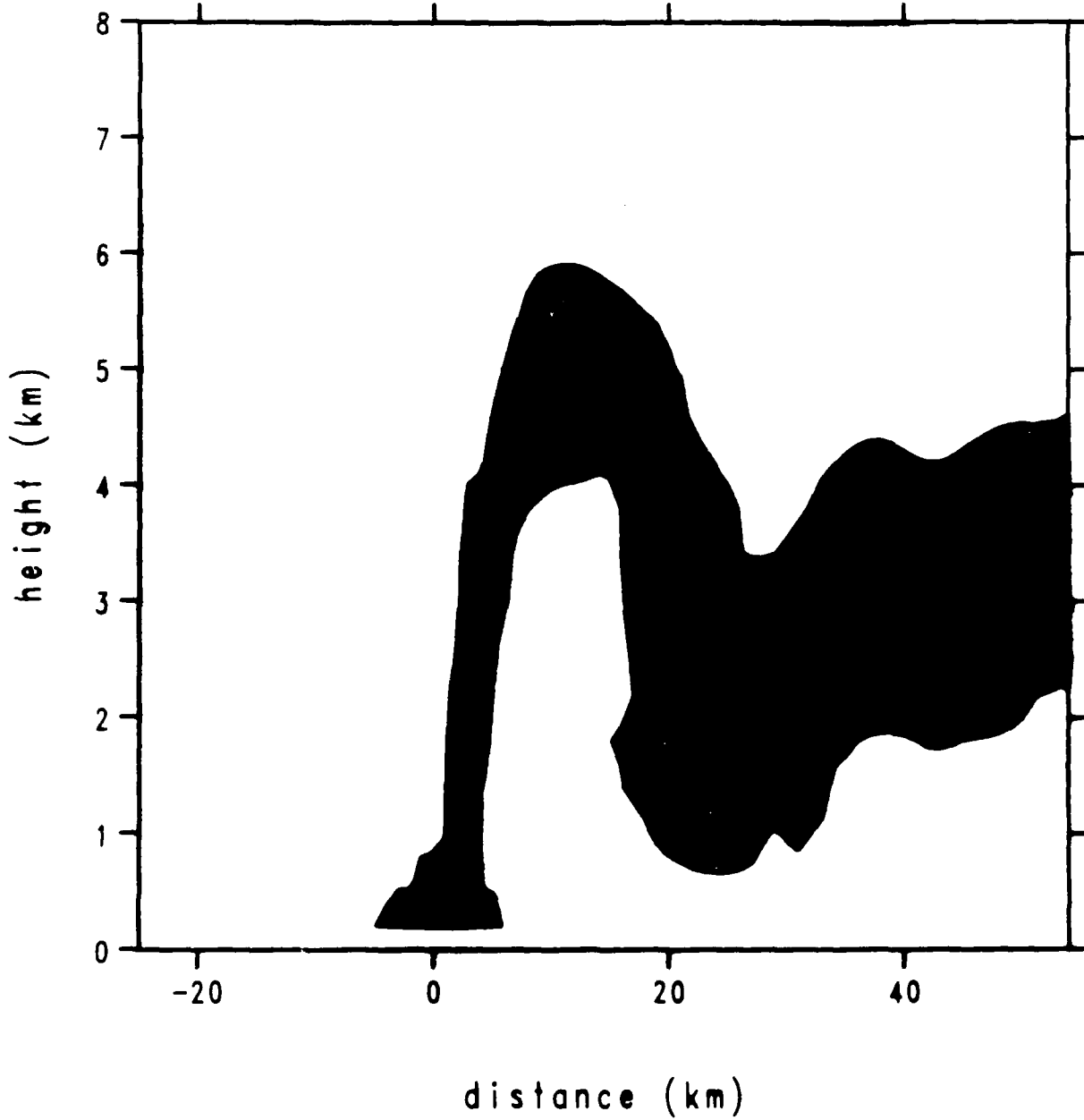
$$f_N = 1 - (1 + Cy)e^{-Cy}$$

$$y = .0025W^{5/8}$$



INTERSTITIAL SMOKE (g/cm\*\*3)

60 min

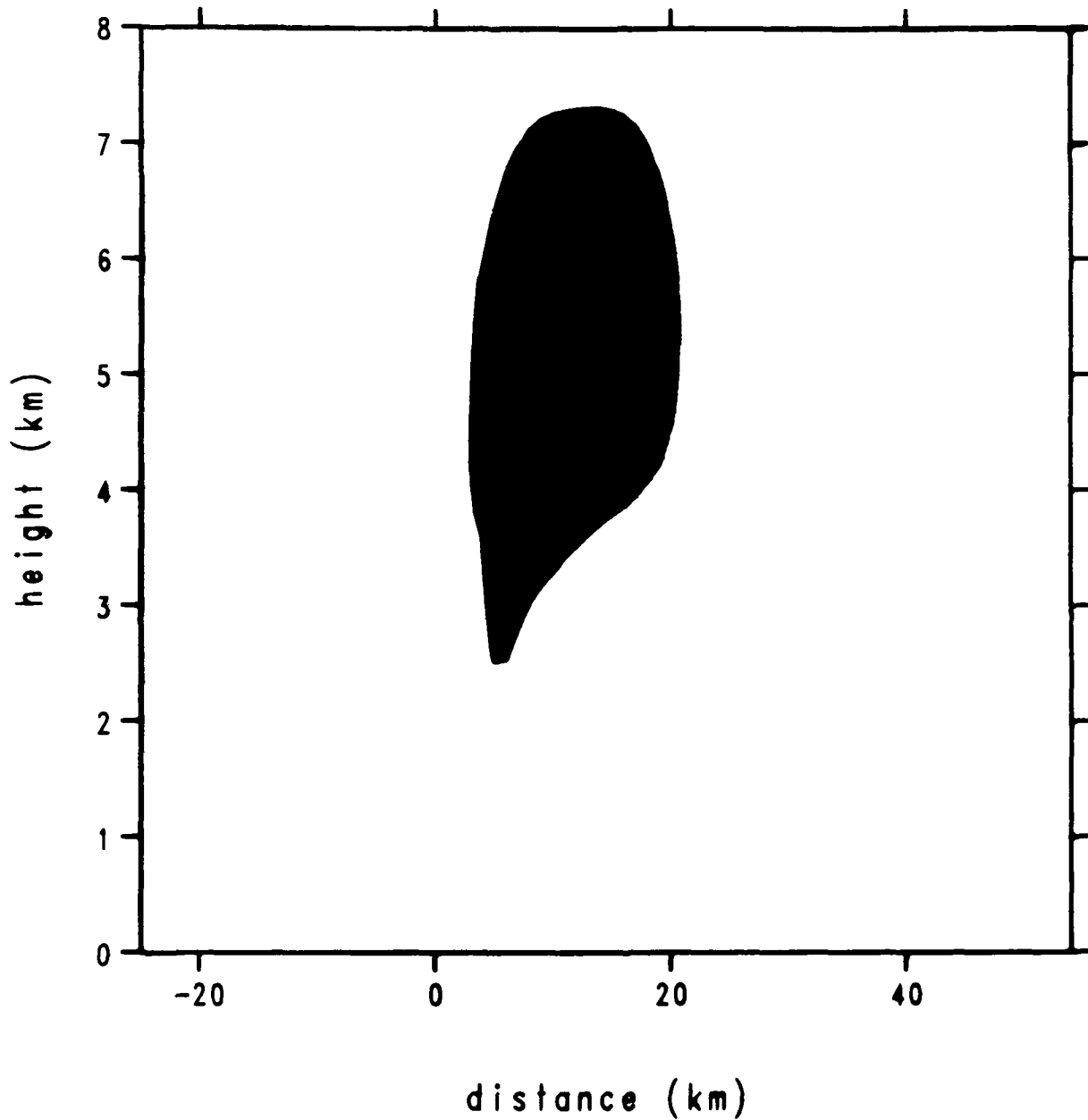


minimum value= 0. at x= -25. km and z= 0.2 km  
maximum value = 1.2994e-07 at x= 2. km and z= 0.2 km  
contour interval = 5.0000e-09

\*\*\*\*\*02/23/8714:33:43e p. 182

SMOKE IN CLOUD WATER (g/cm\*\*3)

60 min

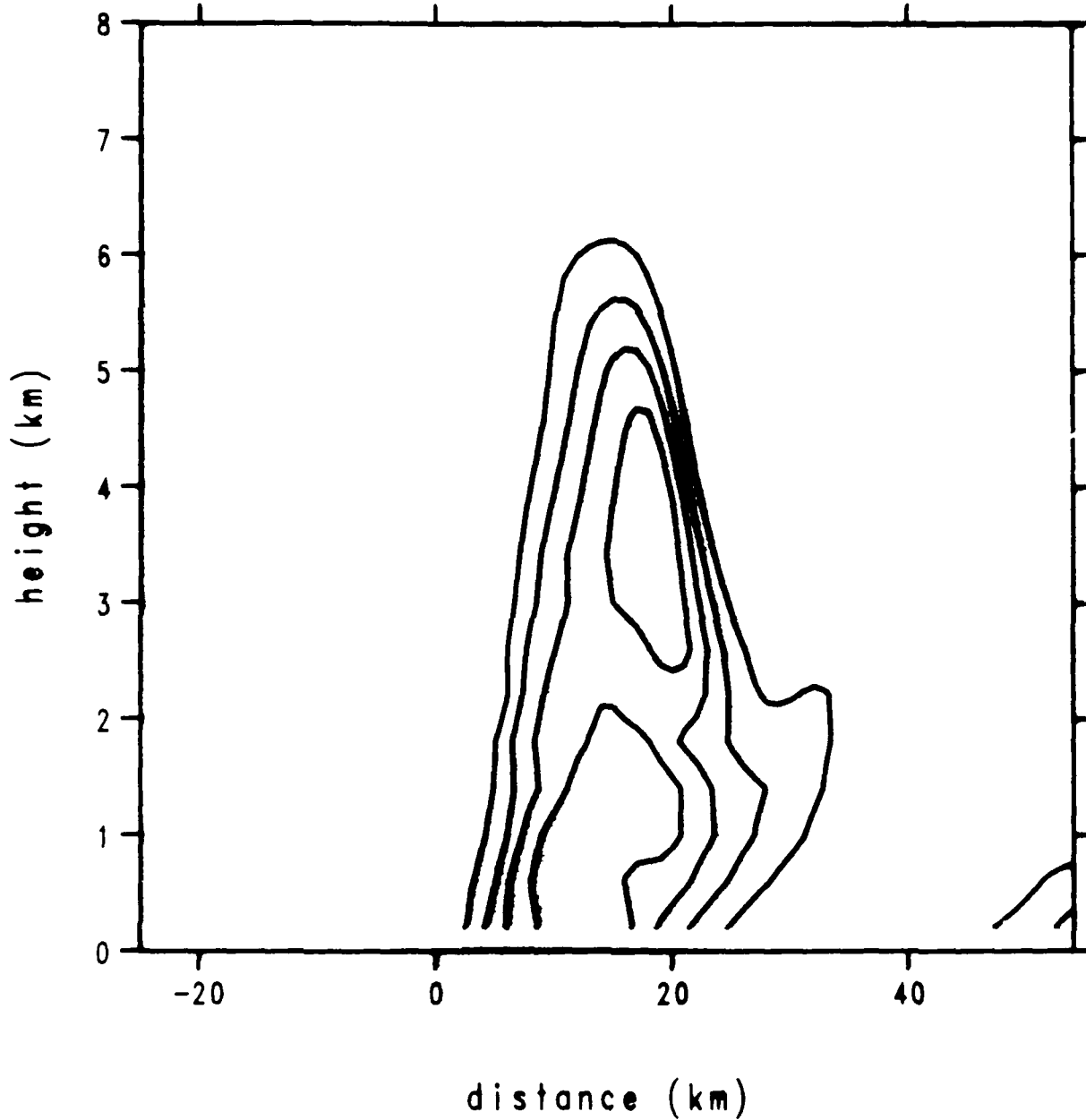


minimum value= 0. at x= -25. km and z= 0.2 km  
maximum value = 9.2953e-09 at x= 4. km and z= 4.2 km  
contour interval = 1.0000e-09

XXXXXXXXXX02/23/8714:33:43e p. 183

SMOKE IN RAINWATER (g/m\*\*\*3)

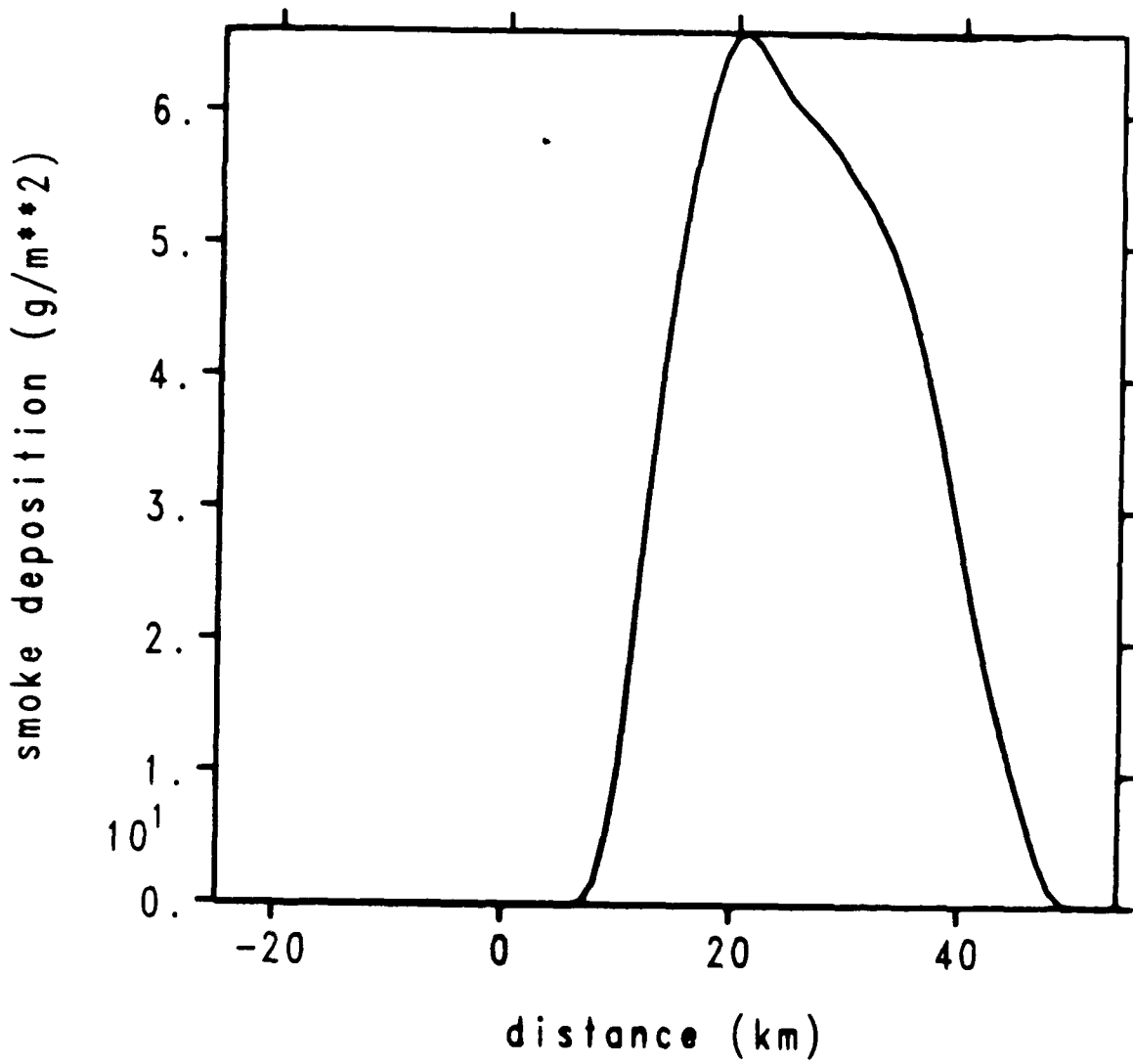
60 min



minimum value= 0. at x= -25. km and z= 0.2 km  
maximum value = 2.4044e-09 at x= 19. km and z= 3.0 km  
contour interval = 5.0000e-10

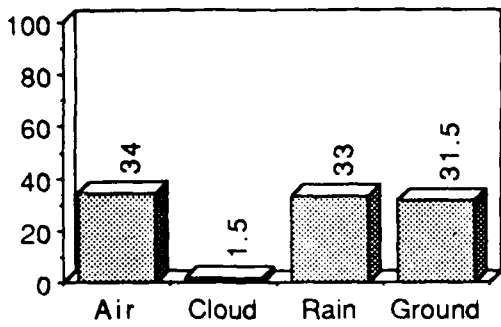
\*\*\*\*\*02/23/8714:33:43\* p. 184

# CUMULATIVE SMOKE RAINOUT

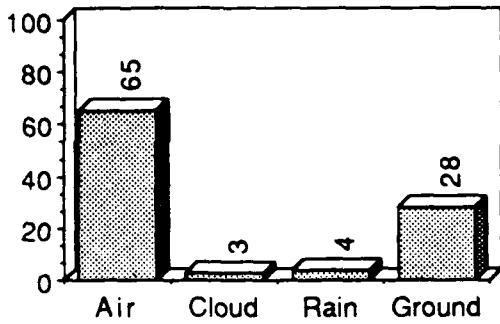
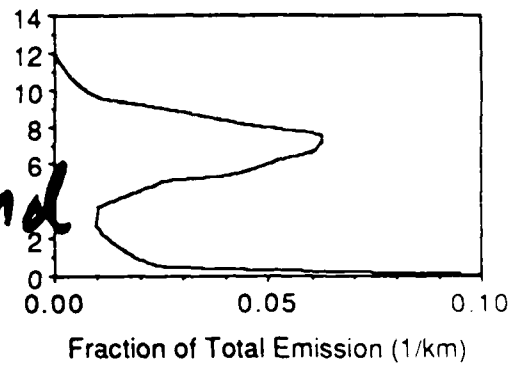




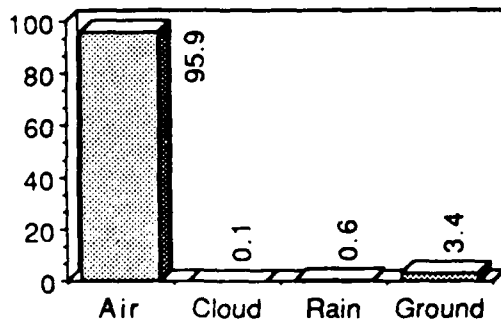
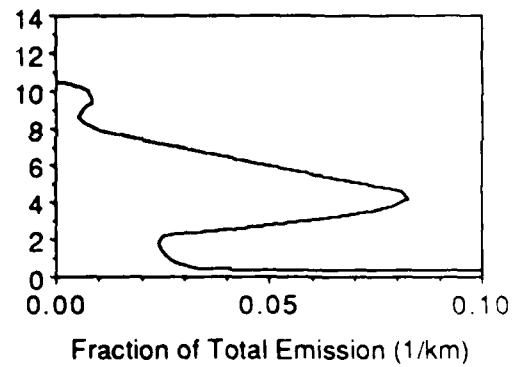
$C = 100$



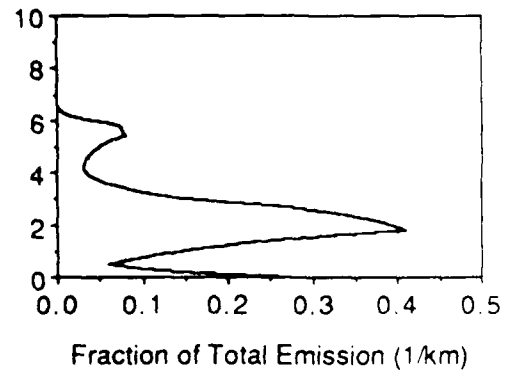
Large  
Fire  
No Wind



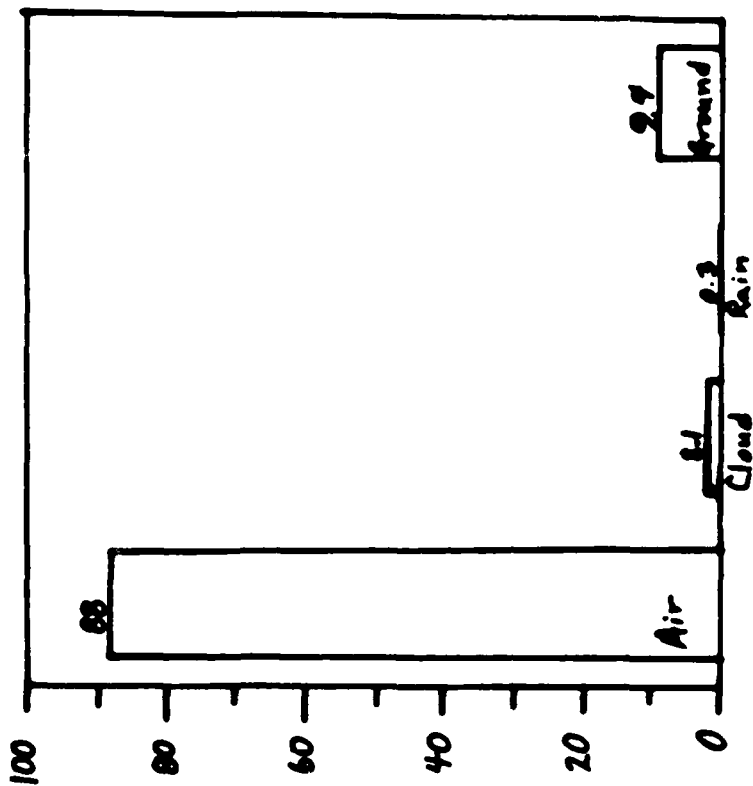
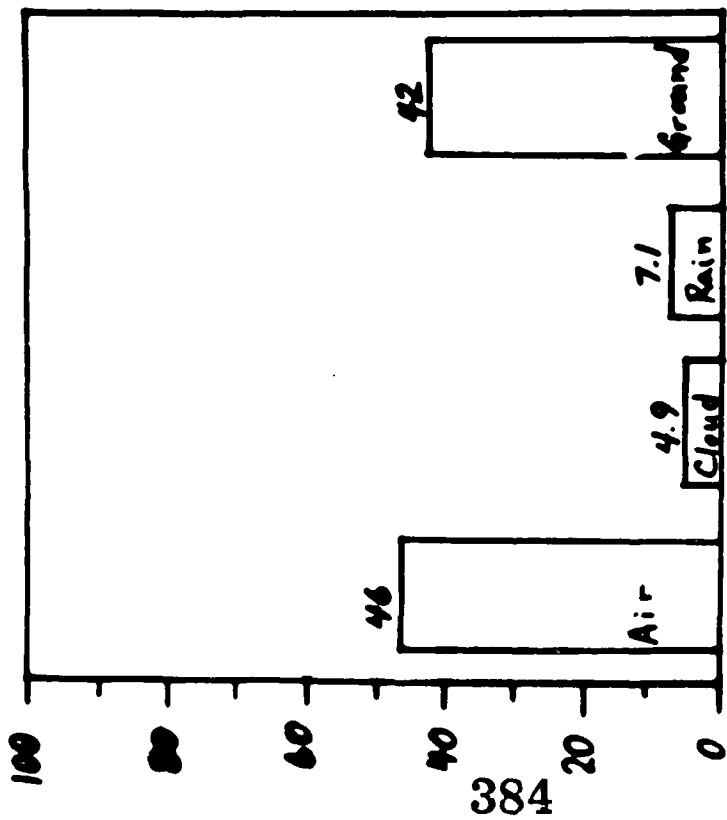
wind



Med  
Fire  
Wind!



C=225



65

3

4

28

C=100

96

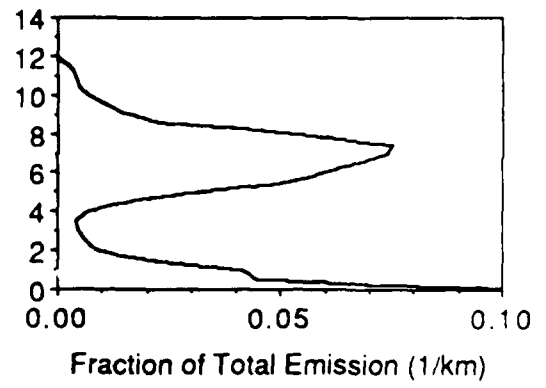
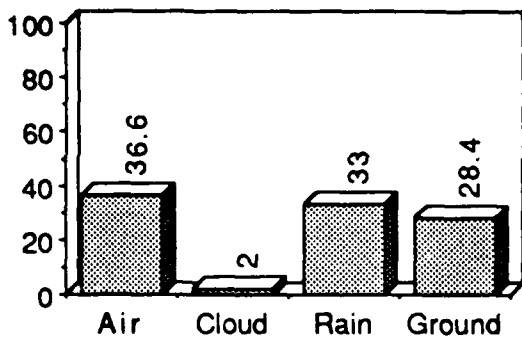
0.1

0.6

3.4

High Int.

Medium Int.



## **Conclusions**

---



- **A significant fraction of the smoke could be promptly removed by nucleation scavenging.**
- **Nucleation scavenging is most effective for intense fires and low ambient wind speeds. These are the same conditions that favor the tallest plumes.**
- **Raindrop formation by coalescence nucleation may be a viable process. If so, rain will not be suppressed by high smoke particle number concentrations.**

## **Future research**



- **Three-dimensional model**
- **Ice processes**
- **Further developement of condensation nucleation parameterization**

**A Numerical Simulation of the Smoke Plume  
Generated by a Hypothetical Urban Fire  
Near San Jose, California**

**Gregory J. Tripoli**

**Department of Atmospheric Science  
Colorado State University  
and**

**ASTeR Inc.  
Fort Collins, Colorado**

**Sang-Wook Kang**

**University of California  
Livermore, California**

**Abstract**

After a comprehensive land use study of the San Jose, California area, the Lawrence Livermore Urban Fires Code is employed to calculate the burn area, intensity and smoke output following an assumed nuclear detonation. Using these calculations as input, the Colorado State University cloud/mesoscale numerical model is employed to determine the regional atmospheric response to these fires, and the evolution of the emitted smoke plume. In doing so, a real atmospheric initial condition is used in conjunction with actual topography and land/sea interface.

The results suggest that smoke injection in the upper troposphere is only likely in a scenario where the rubble left in the immediate blast area burns robustly. In that case, heating rates reach as high as  $10 \text{ kW m}^{-2}$ . This initially produces a deep smoke plume, depositing some smoke above the tropopause. After a period of several hours, it is shown that convergence of the Earth's vorticity, leads to the formation of an inertially stable mesocyclone which lessens convergence of air mass into the burn region. As a result, the plume updraft weakens and the smoke injection height falls dramatically. This has a secondary effect of increasing precipitation efficiency and scavenging above the  $-22 \text{ C}$  temperature level.

In the case where the rubble is assumed not to burn, results indicate no significant cloud is formed because the plume fails to rise above the  $3 \text{ km}$  AGL level. The existence of surface vorticities was also predicted for this case, except that they were less intense and non-steady.

## DISTRIBUTION LIST

### DEPARTMENT OF DEFENSE

ARMED FORCES RADIOBIOLOGY RSCH INST  
ATTN: COL G IRVING

ASSISTANT TO THE SECRETARY OF DEFENSE  
ATOMIC ENERGY  
ATTN: LTCOL L MILLS

DEFENSE INTELLIGENCE AGENCY  
ATTN: N BARON  
ATTN: RTS-2B

DEFENSE NUCLEAR AGENCY  
ATTN: DFRA  
ATTN: DFSP G ULLRICH  
ATTN: RAAE K SCHWARTZ  
ATTN: RAAE L WITWERT  
ATTN: RAAE G BAKER  
ATTN: RAAE R WEBB  
ATTN: RARP D AUTON  
ATTN: SPSD LT COL E WERZ  
ATTN: SPWE M FRANKEL  
ATTN: TDTD/M FLOHR  
ATTN: TDTL COL T HAWKINS

4 CYS ATTN: TITL

DEFENSE TECH INFO CENTER  
12CYS ATTN: DD

#### DIRECTOR

ATTN: LTCOL G BETOURNE  
ATTN: R RUFFIN

NATIONAL DEFENSE UNIVERSITY  
ATTN: COL S GARDINER  
ATTN: G FOSTER  
ATTN: H ALMOND

### DEPARTMENT OF THE ARMY

U S ARMY ATMOSPHERIC SCIENCES LAB  
ATTN: R SUTHERLAND  
ATTN: SLCAS-AR-M MR RUBIO

U S ARMY CORPS OF ENGINEERS  
ATTN: DAEN-RDM R GOMEZ  
ATTN: DR CHOROMOKOS DAEN-RDM

U S ARMY CORPS OF ENGINEERS  
ATTN: L ZIEGLER  
ATTN: R BECKER

U S ARMY ENGR WATERWAYS EXPER STA  
ATTN: DR V E LAGARDE

U S ARMY MISSILE INTEL AGENCY  
ATTN: J GAMBLE

U S ARMY NATICK RSCH DEV & ENGRG CTR  
ATTN: H M EL-BISI

U S ARMY STRATEGIC DEFENSE COMMAND  
ATTN: DR J LILLY  
ATTN: G EDLIN  
ATTN: J VEENEMAN

ATTN: M CAPPS  
ATTN: R BRADSHAW

### DEPARTMENT OF THE NAVY

CNO EXECUTIVE PANEL  
ATTN: CAP L BROOKS

NAVAL RESEARCH LABORATORY  
ATTN: R JEK

NAVAL SURFACE WARFARE CENTER  
ATTN: K-44 S MASTERS

### DEPARTMENT OF THE AIR FORCE

AF/INYXC  
ATTN: LTCOL N BARRY

AIR FORCE GEOPHYSICS LABORATORY  
ATTN: D CHISHOLM  
ATTN: LS/R MURPHY  
ATTN: LSI/ H GARDINER  
ATTN: LYC/R BANTA  
ATTN: LYP H S MUENCH

AIR FORCE INSTITUTE OF TECH/EN  
ATTN: AFIT/ENP MAJ S R BERGGREN  
ATTN: DR C BRIDGEMAN

AIR FORCE OFFICE OF SCI RSCH  
ATTN: D BALL

AIR FORCE SPACE DIVISION  
ATTN: YNC CAPT K O'BRYAN

AIR FORCE TECHNICAL APPLICATIONS CTR  
ATTN: J MARSHALL

AIR FORCE WEAPONS LABORATORY  
ATTN: CAPT LEONG  
ATTN: J JANNI  
ATTN: J W AUBREY, NTEd

BALLISTIC MISSILE OFFICE  
ATTN: LT ROTHCHILD  
ATTN: MYSP/CAP TOMASZEWSKI

DEPUTY CHIEF OF STAFF/XOX  
ATTN: AFXOX

STRATEGIC AIR COMMAND/XPXF  
3 CYS ATTN: CAPT W NICHOLS  
ATTN: LT COL W GIFFORD  
ATTN: T BAZZOLI

### DEPARTMENT OF ENERGY

ARGONNE NATIONAL LABORATORY  
ATTN: H DRUCKER  
ATTN: M WESLEY

BROOKHAVEN NATIONAL LABORATORY  
ATTN: B MANOWITZ  
ATTN: E WEINSTOCK

**DASIAC TN-87-35-VI (DL CONTINUED)**

DEPARTMENT OF ENERGY  
ATTN: I NEDDOW  
ATTN: T HARRIS

DESERT RESEARCH INSTITUTE  
ATTN: J HALLETT  
ATTN: J HUDSON

LAWRENCE BERKELEY NATIONAL LAB  
ATTN: H ROSEN

LAWRENCE LIVERMORE NATIONAL LAB  
ATTN: C R MOLENKAMP  
ATTN: C SHAPIRO  
ATTN: F LUTHER  
ATTN: G BING  
ATTN: G SIMONSON  
ATTN: J PENNER  
ATTN: A GROSSMAN  
ATTN: J KNOX  
ATTN: L ANSPAUGH  
ATTN: R PERRETT  
ATTN: M MACCRACKEN  
ATTN: S GHAN

LOS ALAMOS NATIONAL LABORATORY  
ATTN: D SAPPENFIELD  
ATTN: E J CHAPYAK  
ATTN: E JONES  
ATTN: E SYMBALISTY  
ATTN: G GLATZMAIER  
ATTN: G M SMITH  
ATTN: L H AUER  
ATTN: M GILLESPIE  
ATTN: L CLOUTMAN  
ATTN: R MALONE  
ATTN: T YAMATTA

OAK RIDGE NATIONAL LABORATORY  
ATTN: D FIELDS

SANDIA NATIONAL LABORATORIES  
ATTN: B ZAK  
ATTN: R BACKSTROM  
ATTN: D DAHLGREN  
ATTN: D FORDHAM  
ATTN: D WILLIAMS  
ATTN: K D BERGERON  
ATTN: L TROST  
ATTN: M D BENNETT

**OTHER GOVERNMENT**

CENTRAL INTELLIGENCE AGENCY  
ATTN: 7E47 R NELSON

DEPARTMENT OF AGRICULTURE  
ATTN: D HAINES

DEPARTMENT OF TRANSPORTATION  
ATTN: COL M ROESCH

ENVIRONMENTAL PROTECTION AGENCY  
ATTN: R COTHERN  
ATTN: W E FALLON

FEDERAL EMERGENCY MGT AGENCY  
ATTN: B W BLANCHARD  
ATTN: J KELLETT  
ATTN: J LABARRE  
ATTN: J POWERS

GENERAL ACCOUNTING OFFICE  
ATTN: P BOLLEA  
ATTN: V BIELECKI

NASA  
ATTN: N CRAYBILL  
ATTN: W R COFER

NASA  
ATTN: D WESTPHAL  
ATTN: R HABERLE  
ATTN: O TOON  
ATTN: R PUESCHEL  
ATTN: R YOUNG  
ATTN: T ACKERMAN

NATIONAL BUREAU OF STANDARDS  
ATTN: G MULHOLLAND  
ATTN: R LEVINE  
ATTN: R REHM  
ATTN: R SCHRACK

NATIONAL BUREAU OF STANDARDS  
ATTN: H BAUM

NATIONAL CENTER ATMOSPHERIC RSCH  
ATTN: J KIEHL  
ATTN: S SCHNEIDER  
ATTN: S THOMPSON

NATIONAL CLIMATE PROGRAM OFFICE  
ATTN: A HECHT  
ATTN: M YERG

NATL OCEANIC & ATMOSPHERIC ADMIN  
ATTN: F FEHSENFELD  
ATTN: J DELUISE  
ATTN: V DERR

NATL OCEANIC & ATMOSPHERIC ADMIN.  
ATTN: B HICKS

NATIONAL RESEARCH COUNCIL  
ATTN: R DEFRIES

NATIONAL SCIENCE FOUNDATION  
ATTN: E BIERLY  
ATTN: H VIRJI  
ATTN: L HAMATY  
ATTN: R SINCLAIR  
ATTN: R TAYLOR

NUCLEAR REGULATORY COMMISSION  
ATTN: R ALEXANDER

OFFICE OF SCI AND TECH POLICY  
ATTN: B HEALY  
ATTN: MAJ HARRISON  
ATTN: T RONA



**DASIAC TN-87-35-VI (DL CONTINUED)**

OFFICE OF TECHNOLOGY ASSESSMENT  
ATTN: R WILLIAMSON

U S ARMS CONTROL & DISARMAMENT AGCY  
ATTN: B DOENGES NWC-DPA  
ATTN: G PITMAN  
ATTN: H SCHAEFFER  
ATTN: R GODESKY

U S DEPARTMENT OF STATE  
ATTN: C CLEMENT  
ATTN: S CLEARY  
ATTN: T VREBALOVICH

U S GEOLOGICAL SURVEY  
ATTN: R DECKER

U S GEOLOGICAL SURVEY  
ATTN: E SHOEMAKER

U S HOUSE OF REPRESENTATIVES  
ATTN: C BAYER  
ATTN: COMMITT ON SCI & TECH J DUGAN

U S HOUSE OF REPRESENTATIVES  
ATTN: J FREIWALD  
ATTN: M HERBST

US DEPARTMENT AGRICULTURE  
ATTN: D WARD

**DEPARTMENT OF DEFENSE CONTRACTORS**

AEROSPACE CORP  
ATTN: C RICE  
ATTN: G LIGHT  
ATTN: L R MARTIN

AMERICAN ASSN ADVANCEMENT OF SCI  
ATTN: D M BURNS

ANALYTIC SERVICES, INC (ANSER)  
ATTN: R BROFFT

APPLIED RESEARCH CORP  
ATTN: A ENDAL

AT&T DEFENSIVE SYSTEMS STUDIES  
ATTN: R JANOW

ATMOSPHERIC AND ENVIRONMENTAL RES  
ATTN: N SZE

AUDIO INTELLIGENCE DEVICES INC  
ATTN: H BAUM

AVCO CORPORATION  
ATTN: G GRANT, DEPT MGR

BALL AEROSPACE SYSTEMS DIVISION  
ATTN: B CUMMINGS  
ATTN: C BRADFORD

BDM CORP  
ATTN: J LEECH

BERKELEY RSCH ASSOCIATES, INC  
ATTN: S BRECHT

BOEING TECH & MANAGEMENT SVCS, INC  
ATTN: G HALL

C. L. CONSULTING SERVICES  
ATTN: F FEER

CALIF RESEARCH & TECHNOLOGY, INC  
ATTN: M ROSENBLATT  
ATTN: R GAJ  
ATTN: S KRUEGER

CALSPAN CORP  
ATTN: R MAMBRETTI  
ATTN: R MISSERT

CARNEGIE CORPORATION OF NEW YORK  
ATTN: D ARSENIAN

CHARLES STARK DRAPER LAB, INC  
ATTN: A TETEWski

COLORADO STATE UNIVERSITY  
ATTN: D KRUEGER  
ATTN: W COTTON

COMPUTER SCIENCES CORP  
ATTN: G CABLE

DARTSIDE CONSULTING  
ATTN: A FORESTER

DELTA RESEARCH, INC  
ATTN: L WEINER  
ATTN: M RADKE

DYNAMICS TECHNOLOGY, INC  
ATTN: D HOVE

ENW INTERNATIONAL, LTD  
ATTN: J CANE

EOS TECHNOLOGIES, INC  
ATTN: B GABBARD  
ATTN: N JENSEN  
ATTN: W LELEVIER

FACTORY MUTUAL RESEARCH CORP  
ATTN: M A DELICHATSIOS

FEDERATION OF AMERICAN SCIENTISTS  
ATTN: J STONE

GENERAL ELECTRIC CO  
ATTN: R E SCHMIDT

GENERAL RESEARCH CORP  
ATTN: B BENNETT  
ATTN: J BALTES

HORIZONS TECHNOLOGY INC  
ATTN: J AMBROSE

**DASIAC TN-87-35-VI (DL CONTINUED)**

HORIZONS TECHNOLOGY, INC  
ATTN: R W LOWEN  
ATTN: W T KREISS

HUGHES AIRCRAFT CO  
ATTN: E DIVITA

INFORMATION SCIENCE, INC  
ATTN: W DUDZIAK

INSTITUTE FOR DEFENSE ANALYSES  
ATTN: E BAUER  
ATTN: F ALBINI

JOHNS HOPKINS UNIVERSITY  
ATTN: M LENEVSKY  
ATTN: R FRISTROM  
ATTN: W BERL

KAMAN SCIENCES CORP  
ATTN: J RUSH  
ATTN: J SCRUGGS

KAMAN SCIENCES CORP  
ATTN: P GRIFFIN  
ATTN: P TRACY

KAMAN SCIENCES CORPORATION  
ATTN: D ADERSON  
ATTN: DASIAC

KAMAN TEMPO  
ATTN: B GAMBILL  
ATTN: D FOXWELL  
ATTN: DASIAC  
ATTN: E MARTIN  
ATTN: R RUTHERFORD  
ATTN: R YOUNG  
ATTN: S FIFER  
ATTN: W KNAPP

LOCKHEED MSL & SPACE CO, INC  
ATTN: J HENLEY  
ATTN: J PEREZ

LOCKHEED MSL & SPACE CO, INC  
ATTN: P DOLAN  
ATTN: W MORAN

M I T LINCOLN LAB  
ATTN: S WEINER

MARTIN MARIETTA DENVER AEROSPACE  
ATTN: D HAMPTON

MCDONNELL DOUGLAS CORP  
ATTN: T CRANOR  
ATTN: T TRANER

MCDONNELL DOUGLAS CORP  
ATTN: A MONA  
ATTN: F SAGE  
ATTN: G BATUREVICH  
ATTN: J GROSSMAN  
ATTN: R HALPRIN

ATTN: S JAEGER  
ATTN: W YUCKER

MERIDIAN CORP  
ATTN: E DANIELS  
ATTN: F BAITMAN

MIDWEST RESEARCH INSTITUTE  
ATTN: J S KINSEY

MISSION RESEARCH CORP  
ATTN: R ARMSTRONG

MISSION RESEARCH CORP  
ATTN: C LAUER  
ATTN: C LONGMIRE  
ATTN: D SOWLE  
ATTN: G MCCRATOR  
ATTN: R BIGONI  
ATTN: T OLD

MITRE CORPORATION  
ATTN: J SAWYER

MRJ INC  
ATTN: D FREIWALD

NATIONAL ADVISORY COMMITTEE  
ATTN: J ALMAZAN  
ATTN: J BISHOP

NATIONAL INST. FOR PUBLIC POLICY  
ATTN: K PAYNE

NICHOLS RESEARCH CORP, INC  
ATTN: H SMITH  
ATTN: J SMITH  
ATTN: M FRASER  
ATTN: R BYRN

NORTHROP SERVICES INC  
ATTN: T OVERTON

ORLANDO TECHNOLOGY INC  
ATTN: R SZCZEPANSKI

PACIFIC-SIERRA RESEARCH CORP  
ATTN: G ANNO  
ATTN: H BRODE, CHAIRMAN SAGE  
ATTN: M DORE  
ATTN: R SMALL

PHOTOMETRICS, INC  
ATTN: I L KOFISKY

PHOTON RESEARCH ASSOCIATES  
ATTN: J MYER

PHYSICAL RESEARCH INC  
ATTN: H FITZ

PHYSICAL RESEARCH INC  
ATTN: D MATUSKA

PHYSICAL RESEARCH INC  
ATTN: J WANG

DASIAC TN-87-35-VI (DL CONTINUED)

PHYSICAL RESEARCH, INC  
ATTN: D WESTPHAL  
ATTN: D WHITENER  
ATTN: H WHEELER  
ATTN: R BUFF  
ATTN: R DELIBERIS  
ATTN: T STEPHENS  
ATTN: W C BLACKWELL

PHYSICAL RESEARCH, INC  
ATTN: G HARNEY  
ATTN: J DEVORE  
ATTN: J THOMPSON  
ATTN: R STOECKLY  
ATTN: W SCHLUETER

PHYSICAL RESEARCH, INC  
ATTN: H SUGIUCHI

POLYTECHNIC OF NEW YORK  
ATTN: B J BULKIN  
ATTN: G TESORO

PRINCETON UNIVERSITY  
ATTN: J MAHLMAN

QUADRI CORP  
ATTN: H BURNSWORTH

R & D ASSOCIATES  
ATTN: A KUHL  
ATTN: F GILMORE  
ATTN: G JONES  
ATTN: J SANBORN  
ATTN: R TURCO

R & D ASSOCIATES  
ATTN: B YOON  
ATTN: C KNOWLES

R J EDWARDS INC  
ATTN: R SEITZ

RADIATION RESEARCH ASSOCIATES, INC  
ATTN: B CAMPBELL  
ATTN: M WELLS

RAND CORP  
ATTN: P ROMERO

ROCKWELL INTERNATIONAL CORP  
ATTN: J KELLEY

S-CUBED  
ATTN: B FREEMAN  
ATTN: K D PYATT, JR  
ATTN: R LAFRENZ

SCIENCE APPLICATIONS INC  
ATTN: R EDELMAN

SCIENCE APPLICATIONS INTL CORP  
ATTN: C HILL

SCIENCE APPLICATIONS INTL CORP  
ATTN: B MORTON

ATTN: B SCOTT  
ATTN: D SACHS  
ATTN: G T PHILLIPS  
ATTN: J BENGSTOM  
ATTN: D HAMLIN

SCIENCE APPLICATIONS INTL CORP  
ATTN: D BACON  
ATTN: DR L GOURE  
ATTN: F GIESSLER  
ATTN: J COCKAYNE  
ATTN: J GAHAN  
ATTN: J SHANNON  
ATTN: J STUART  
ATTN: M SHARFF  
ATTN: W LAYSON

SCIENCE APPLICATIONS INTL CORP  
ATTN: J SONTOWSKI

SCIENCE APPLICATIONS INTL CORP  
ATTN: T HARRIS

SCIENTIFIC RESEARCH ASSOC, INC  
ATTN: B WEINBERG

SRI INTERNATIONAL  
ATTN: C WITHAM  
ATTN: D GOLDEN  
ATTN: D MACDONALD  
ATTN: D ROBERTS  
ATTN: E UTHE  
ATTN: G ABRAHAMSON  
ATTN: J BACKOVSKY  
ATTN: W CHESNUT

STAN MARTIN AND ASSOCIATES  
ATTN: S B MARTIN

STANTON CONSULTING  
ATTN: M STANTON

SWETL, INC  
ATTN: T Y PALMER

SYSTEM PLANNING CORP  
ATTN: B GARRETT  
ATTN: C FELDBAUM  
ATTN: J SCOURAS  
ATTN: M BIENVENU  
ATTN: R SCHEERBAUM

SYSTEMS AND APPLIED SCIENCES CORP  
ATTN: M KAPLAN

TELEDYNE BROWN ENGINEERING  
ATTN: A ORTELL  
ATTN: F LEOPARD  
ATTN: J FORD

TELEDYNE BROWN ENGINEERING  
ATTN: D GUICE

TEXAS ENGR EXPERIMENT STATION  
ATTN: W H MARLOW

**DASIAC TN-87-35-VI (DL CONTINUED)**

TOYON RESEARCH CORP  
ATTN: C TRUAX  
ATTN: J GARBARINO  
ATTN: J ISE

TRW INC  
ATTN: H BURNSWORTH  
ATTN: J BELING

TRW INC  
ATTN: F FENDELL  
ATTN: G KIRCHNER  
ATTN: H CROWDER  
ATTN: J FEDELE  
ATTN: M BRONSTEIN  
ATTN: R BACHARACH  
ATTN: S FINK  
ATTN: T NGUYEN

TRW SPACE & DEFENSE, DEFENSE SYS  
ATTN: M HAAS

VISIDYNE, INC  
ATTN: H SMITH  
ATTN: J CARPENTER

WASHINGTON, UNIVERSITY OF  
ATTN: J I KATZ

**FOREIGN**

AERE ENVIRONMENTAL AND MEDICAL SC  
ATTN: S PENKETT

ATOMIC WEAPONS RSCH ESTABLISHMENT  
ATTN: P F A RICHARDS

ATOMIC WEAPONS RSCH ESTABLISHMENT  
ATTN: D L JONES  
ATTN: D M MOODY

AUSTRALIA EMBASSY  
ATTN: A TEBBS  
ATTN: AIR VICE MARSHAL B GRATION  
ATTN: DR A J BEDFORD

BRITISH DEFENCE STAFF  
ATTN: J EDMONDS

CANADIAN FORESTRY SERVICE  
ATTN: B STOCKS  
ATTN: T LYNHAM

CSIRO  
ATTN: I GALBALLY

CSIRO: ATMOSPHERIC RESEARCH  
ATTN: A PITTOCK

EMBASSY OF BELGIUM  
ATTN: L ARNOULD

ISRAEL EMBASSY  
ATTN: N BELKIND

MAX-PLANCK INSTITUTE FOR CHEMISTRY  
ATTN: P J CRUTZEN

MINISTRY OF DEFENCE  
ATTN: R RIDLEY

NATIONAL DEFENCE HEADQUARTERS  
ATTN: H A ROBITALLE

TRINITY COLLEGE  
ATTN: F HARE

**DIRECTORY OF OTHER**

ATMOS. SCIENCES  
ATTN: G SISCOE

BUCKNELL UNIVERSITY  
ATTN: O ANDERSON

CALIFORNIA, UNIVEPSITY  
ATTN: R WILLIAMSON

CALIFORNIA, UNIVERSITY OF  
ATTN: L BADASH

COLORADO, UNIVERSITY LIBRARIES  
ATTN: J BIRKS  
ATTN: R SCHNELL

DREXEL UNUVERSITY  
ATTN: J FRIEND

GEORGE MASON UNIVERSITY  
ATTN: PROF S SINGER  
ATTN: R EHRlich

GEORGE WASHINGTON UNIVERSITY  
ATTN: R GOULARD

GEORGIA INST OF TECH  
ATTN: E PATTERSON

HARVARD COLLEGE LIBRARY  
ATTN: W PRESS

HARVARD UNIVERSITY  
ATTN: G CARRIER

HARVARD UNIVERSITY  
ATTN: D EARDLEY

IOWA, UNIVERSITY OF  
ATTN: S PYNE

MARYLAND UNIVERSITY OF  
ATTN: A ROBOCK  
ATTN: A VOGELMANN  
ATTN: R ELLINGSON

MIAMI LIBRARY UNIVERSITY OF  
ATTN: C CONVEY

MIAMI UNIV LIBRARY  
ATTN: J PROSPERO

NEW YORK STATE UNIVERSITY OF  
ATTN: R CESS

OAK RIDGE ASSOCIATED UNIVERSITIES  
ATTN: C WHITTLE

SOUTH DAKOTA SCH OF MINES & TECH LIB  
ATTN: H ORVILLE

TENNESSEE, UNIVERSITY OF  
ATTN: K FOX

UNIVERSITY OF SOUTH FLORIDA  
ATTN: S YING

UNIVERSITY OF WASHINGTON  
ATTN: C LEOVY  
ATTN: L RAOKE  
ATTN: P HOBBS

VIRGINIA POLYTECHNIC INST LIB  
ATTN: M NADLER

WISCONSIN UNIVERSITY OF  
ATTN: P WANG

END

DATE

FILMED

9-88

DTIC